

NASA CR-132575-1

(NASA-CR-132575-1) ARROW-WING SUPERSONIC  
CRUISE AIRCRAFT STRUCTURAL DESIGN CONCEPTS  
EVALUATION. VOLUME 1: SECTIONS 1 THROUGH 6  
(Lockheed-California Co.) 436 p HC \$11.75

N76-28219

Unclas  
46762

CSCL 01C G3/05

SUBSTANTIATING DATA FOR

# ARROW-WING SUPERSONIC CRUISE AIRCRAFT STRUCTURAL DESIGN CONCEPTS EVALUATION

Volume 1, Sections 1 through 6

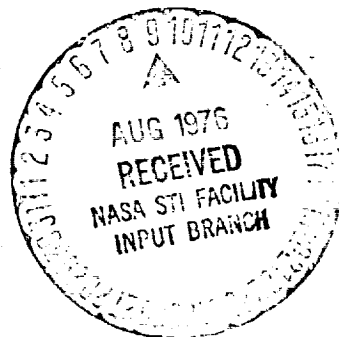
by

I. F. Sakata and G. W. Davis

Prepared under Contract No. NAS1-12288

Lockheed-California Company  
Burbank, California

for Langley Research Center



NATIONAL AERONAUTICS AND SPACE ADMINISTRATION



## TABLE OF CONTENTS

<u>Section</u>		<u>Page</u>
	Volume 1	
	Summary	iii
	Introduction	v
	Acknowledgement	xi
1	Structural Design Concepts	1-1
2	Baseline Configuration	2-1
3	Aerodynamics	3-1
4	Structural Design Criteria	4-1
5	Structural Design Loads	5-1
6	Structural Temperatures	6-1
	Volume 2	
7	Materials and Producibility	7-1
8	Basic Design Parameters	8-1
9	Structural Analysis Models	9-1
10	Vibration and Flutter	10-1
11	Point Design Environment	11-1
	Volume 3	
12	Structural Concept Analysis	12-1
13	Fatigue and Fail-Safe Analysis	13-1
14	Acoustics	14-1
	Volume 4	
15	Mass Analysis	15-1
16	Production Costs	16-1
17	Concept Evaluation and Selection	17-1
18	Design	18-1
19	Propulsion-Airframe Integration	19-1
20	Advanced Technology Assessment	20-1
21	Design Methodology	21-1





## SUMMARY

An analytical study was performed to determine the structural approach best suited for the design of a Mach 2.7 arrow-wing supersonic cruise aircraft. Results, procedures, and principal justification of results are presented in Reference 1. Detailed substantiation data are given herein. In general, each major analysis is presented sequentially in separate sections to provide continuity in the flow of the design concepts analysis effort. In addition to the design concepts evaluation and the detailed engineering design analyses, supporting tasks encompassing: (1) the controls system development (2) the propulsion-airframe integration study, and (3) the advanced technology assessment are presented.

**PRECEDING PAGE BLANK NOT FILMED**

- 
- Reference 1 Sakata, I. F. and Davis, G. W.: Evaluation of Structural Design Concepts for an Arrow-Wing Supersonic Cruise Aircraft NASA CR- 1976



## INTRODUCTION

The design of an economically viable supersonic cruise aircraft requires reduced structural mass fractions attainable through application of new materials, advanced concepts and design tools. Configurations, such as the arrow-wing, show promise from the aerodynamic standpoint; however, detailed structural design studies are needed to determine the feasibility of constructing this type of aircraft with sufficiently low structural mass fraction.

For the past several years, the NASA Langley Research Center has been pursuing a supersonic cruise aircraft research program (1) to provide an expanded technology base for future supersonic aircraft, (2) to provide the data needed to assess the environmental and economic impacts on the United States of present and especially future foreign supersonic cruise aircraft, and (3) to provide a sound technical basis for any future consideration that may be given by the United States to the development of an environmentally acceptable and economically viable commercial supersonic cruise aircraft.

The analytical study, reported herein, was performed to provide data to support the selection of the best structural concept for the design of a supersonic cruise aircraft wing and fuselage primary structure considering near-term start-of-design technology. A spectrum of structural approaches for primary structure design that has found application or had been proposed for supersonic aircraft design; such as the Anglo-French Concorde supersonic transport, the Mach 3.0-plus Lockheed F-12 and the proposed Lockheed L-2000 and Boeing B-2707 supersonic transports were systematically evaluated for the given configuration and environmental criteria.

The study objectives were achieved through a systematic program involving the interactions between the various disciplines as shown in Figures A through C. These figures present an overview of the study effort and provides a summary statement of work, as follows:

- (1) Task I - Analytical Design Studies (Figure A).- This initial task involved a study wherein a large number of candidate structure

concepts were investigated and subjected to a systematic evaluation process to determine the most promising concepts. An airplane configuration refinement investigation, including propulsion-airframe integration study were concurrently performed.

- (2) Task II - Engineering Design/Analyses (Figure B).- The most promising concepts were analyzed assuming near-term start-of-design technology, critical design conditions and requirements identified, and construction details and mass estimates determined for the Final Design airplane. Concurrently, the impact of advanced technology on supersonic cruise aircraft design was explored.
- (3) Task III - Mass Sensitivity Studies (Figure C).- Starting with the Final Design airplane numerous sensitivity studies were performed. The results of these investigations and the design studies (Task I and Task II) identified opportunities for structural mass reduction and needed research and technology to achieve the objectives of reduced structural mass.

Displayed on the figures are the time-sequence and flow of data between disciplines and the reason for the make-up of the series of sections presented in this report. The various sections are independent of each other, except as specifically noted. Results of this structural evaluation are reported in Reference 1. This reference also includes the procedures and principal justification of results, whereas this report gives detailed substantiation of the results in Reference 1. This report is bound as four separate volumes.

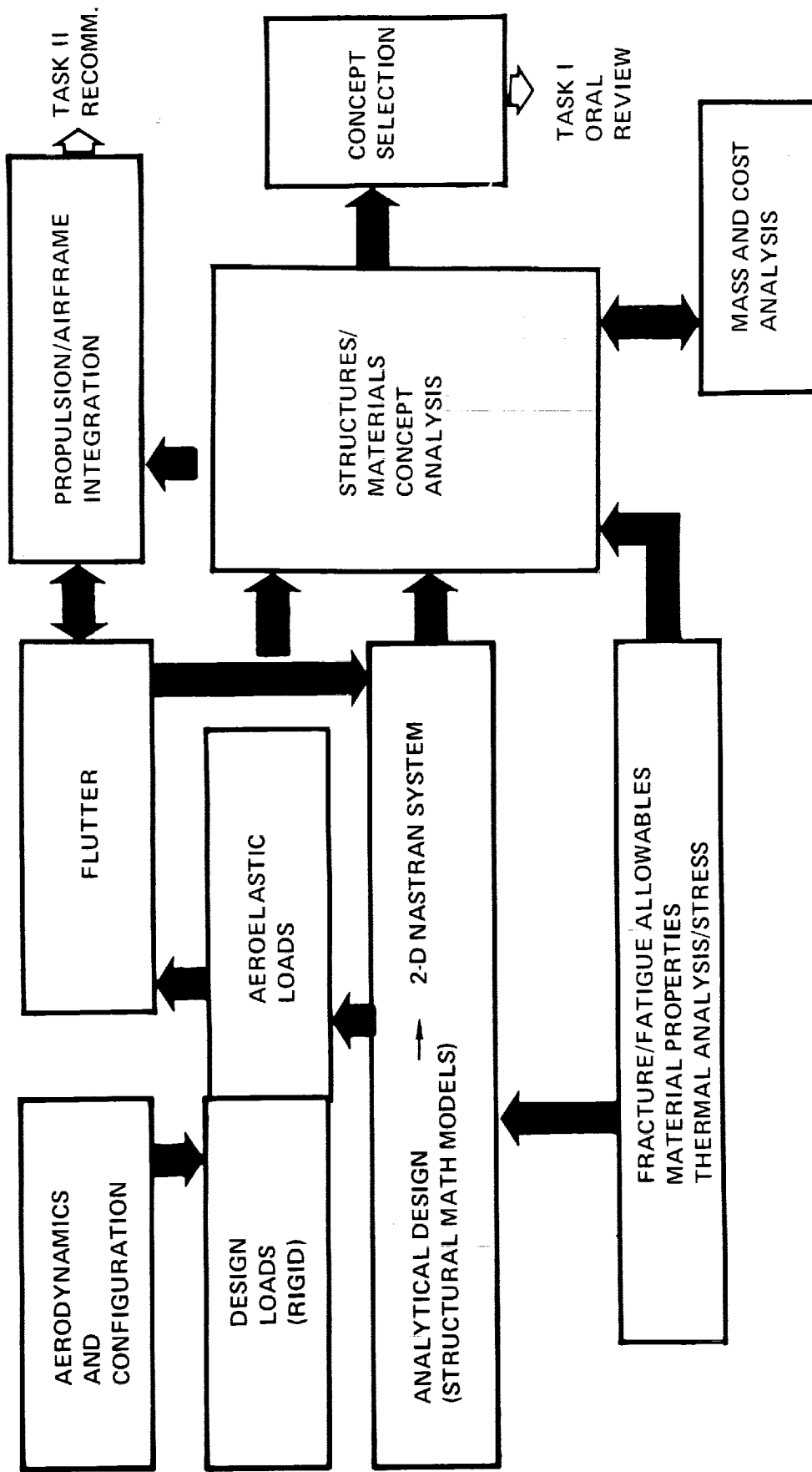


Figure A. Analytical Design Studies - Task I

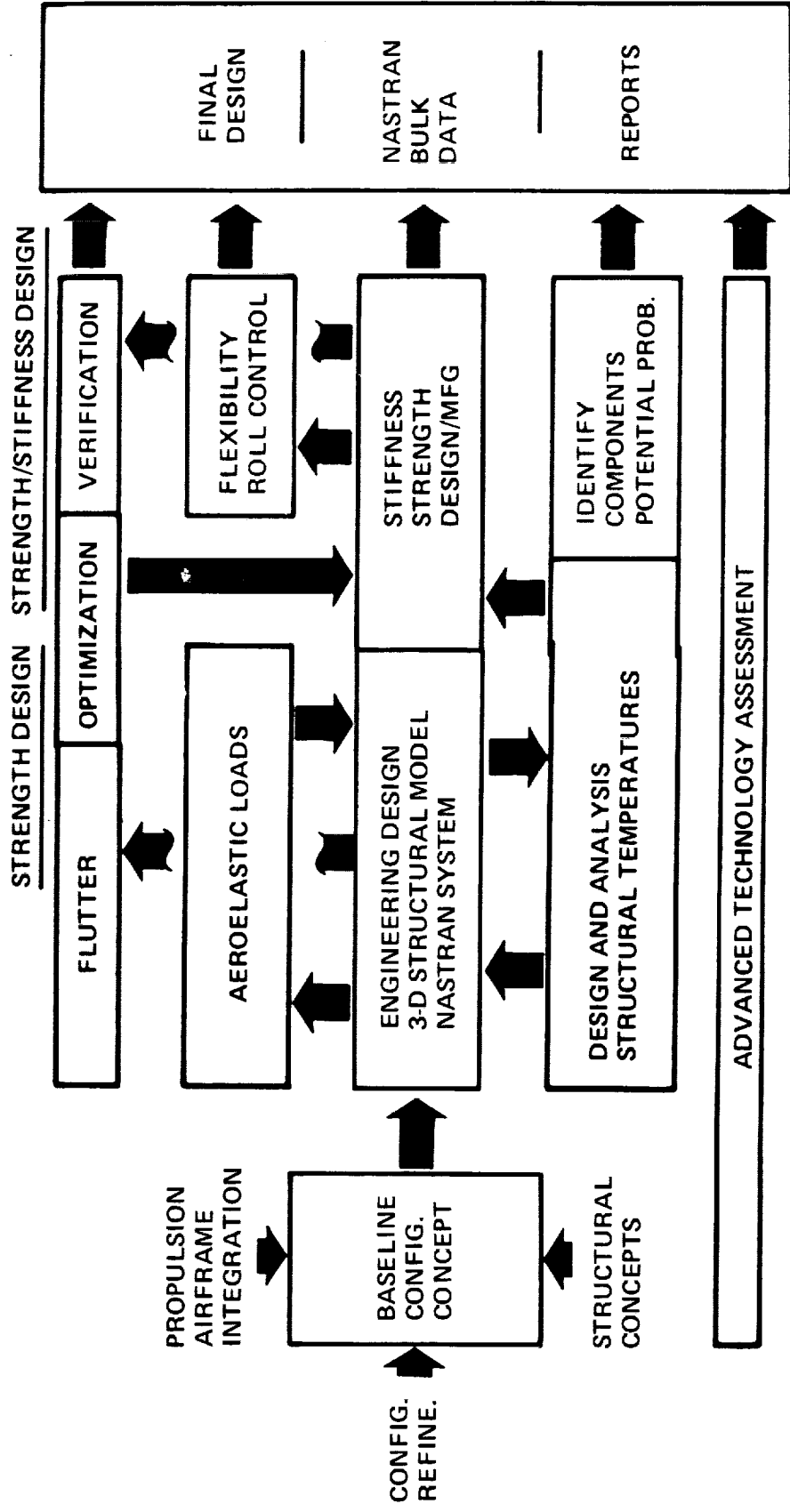


Figure B. Engineering Design and Analyses

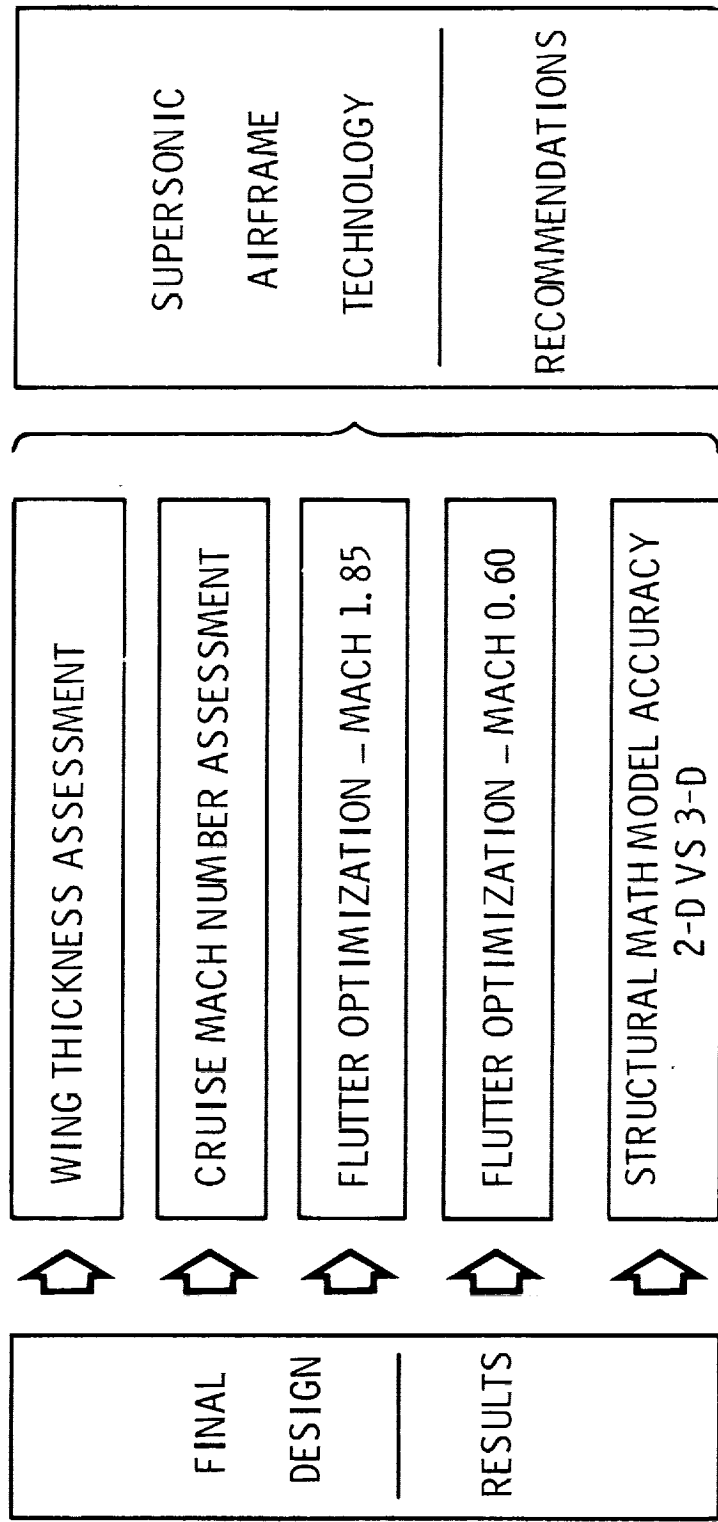


Figure C. Mass Sensitivity Studies





ACKNOWLEDGEMENT

This investigation was conducted under NASA Contract No. NAS1-12288, Study of Structural Design Concepts for an Arrow-Wing Supersonic Transport Configuration. The study was performed within the Science and Engineering Branch of the Lockheed-California Company, Burbank, California, with the participation of the Lockheed-Georgia Company in a composite design subcontract effort. I. F. Sakata was the Project Engineer, and G.W. Davis was the Lead Engineer. The other contributors to the program are acknowledged at each section.

Mr. J. C. Robinson of the Design Concepts Section, Thermal Structures Branch, and Dr. E. C. Yates, Jr., Computer Aided Methods Branch, Structures and Dynamics Division, NASA Langley Research Center, Hampton, Virginia, were the Technical Representative of the Contracting Officer (TRCO), and Alternate TRCO, respectively for the project.

**PRECEDING PAGE BLANK NOT FILMED**



SECTION 1

STRUCTURAL DESIGN CONCEPTS

BY

I. F. SAKATA



TABLE OF CONTENTS

<u>Section</u>	<u>Page</u>
INTRODUCTION	1-1
WING STRUCTURAL CONCEPTS	1-2
Monocoque	1-2
Semimonocoque - Spanwise	1-4
Semimonocoque - Chordwise	1-4
Composite Reinforced	1-6
FUSELAGE STRUCTURAL CONCEPTS	
Sandwich Shell	1-6
Skin-Stringer and Frame Shell	1-7
EVALUATION OF STRUCTURAL APPROACH	1-7

LIST OF FIGURES

<u>Figure</u>		<u>Page</u>
1-1	Wing Structural Arrangement - Monocoque	1-3
1-2	Wing Structural Arrangement - Spanwise Stiffened	1-3
1-3	Wing Structural Arrangement - Chordwise Stiffened	1-5
1-4	Wing Structural Arrangement - Composite Reinforced	1-5
1-5	Fuselage Structural Arrangement - Skin-Stringer and Frame	1-8

LIST OF TABLES

<u>Table</u>		<u>Page</u>
1-1	Evaluation of Structural Approaches - Task I	1-9





## SECTION 1

### STRUCTURAL DESIGN CONCEPTS

#### INTRODUCTION

An important facet of supersonic technology is the development of lightweight structures. To realize the full potential for structural mass reduction, a spectrum of structural approaches for an advanced supersonic cruise aircraft that fully exploits the practically attainable advantages of near-term start-of-design technology was established considering the following:

- Improved titanium alloys (beta alloys)
- Improved fatigue quality through minimizing fasteners by use of welding, bonding and brazing
- Large scale fabrication to minimize the number of joints
- Minimizing or eliminating tank sealing by use of large scale application of welding, bonding and brazing
- Selective reinforcement of metal structure with organic and metal matrix composites
- Determining the structural arrangements most efficient in coping with the interactive loading of a large flexible aircraft.

Design and manufacturing concepts studies established feasibility of the application of advanced manufacturing techniques to large scale production. These studies examined the fabrication feasibility down to the smallest sub-component level, and involved the design of structural concepts that represented both structural efficiency and applicability to advanced fabrication techniques.

Advanced materials data reported in Section 7 were used to establish design allowables for the advanced titanium alloys. Both the alpha-beta and beta alloys in the annealed and solution treated and aged conditions were considered. The advanced producibility techniques aspects are discussed in detail in

Section 8. Composite application studies, related to the structural concepts identified, were made and are reported in Section 12. Methodology and design data used in the study are also reported therein.

## WING STRUCTURAL CONCEPTS

The primary load carrying structural concepts for a supersonic cruise aircraft wing structure design are categorized as:

- (1) Monocoque - biaxially stiffened panels
- (2) Semimonocoque - uniaxially stiffened panels.

### Monocoque

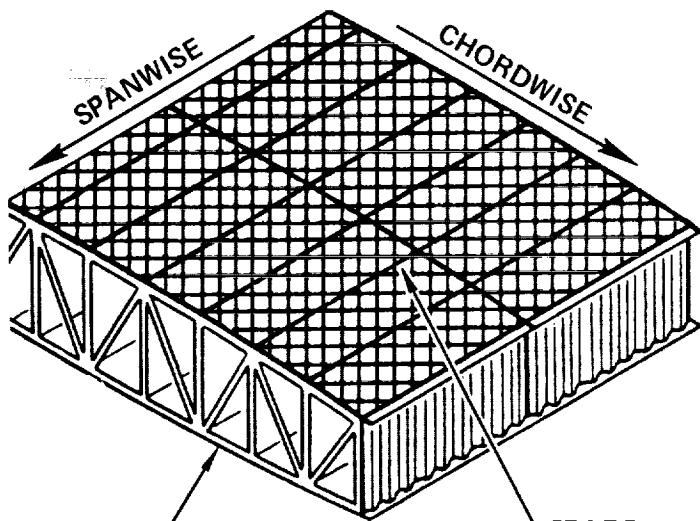
Monocoque construction consists of biaxially stiffened panels which support the principal load in both the span and chord direction as indicated in Figure 1-1. For the substructure arrangement both multirib and multispar designs are considered.

The monocoque construction has a smooth skin that results in minimum aerodynamic drag. However, thermal stresses are absorbed by the primary structural elements with minimal relief. Biaxial loading results in reduced fatigue allowables, yet criticality of other design parameters often controls minimum mass structural designs.

The biaxially stiffened panels considered are the honeycomb core and the truss-core sandwich concepts. The honeycomb core panels are assumed to be aluminum brazed (Aeronca); both diffusion bonded and welded (spot and EB) joining process are assumed for the truss-core sandwich panel configuration.

In the monocoque concept, as well as in all other primary structure concepts, circular-arc (sine-wave) corrugated webs are used for rib and spar webs at the tank closures. Truss-type webs are used for all other areas. The caps

**MONOCOQUE (BIAXIALLY STIFFENED)**



**RIBS**  
 ● TRUSS  
 ● CIRCULAR-ARC

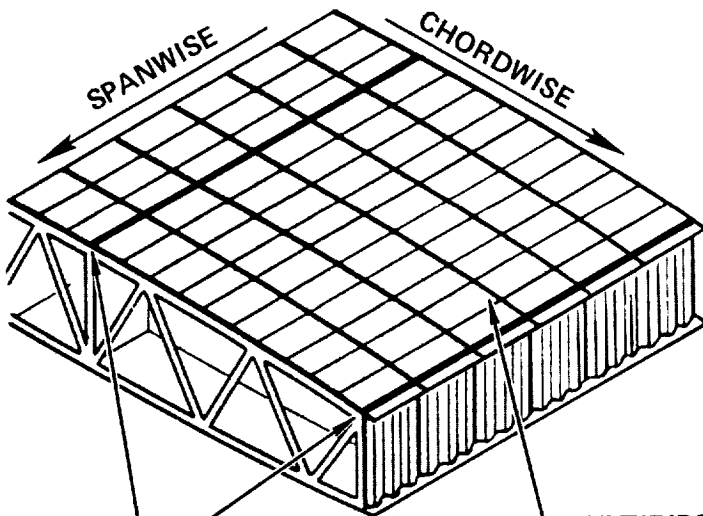
**SPARS**  
 ● TRUSS  
 ● CIRCULAR-ARC

**PANEL STRUCTURAL CONCEPTS**



FIGURE 1-1 WING STRUCTURAL ARRANGEMENT - MONOCOQUE

**SPANWISE STIFFENED**



**SPARS**  
 ● TRUSS  
 ● CIRCULAR-ARC

**MULTIRIBS**  
 ● TRUSS  
 ● CIRCULAR-ARC

**PANEL STRUCTURAL CONCEPTS**

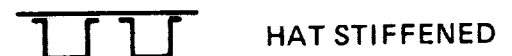
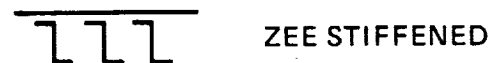


FIGURE 1-2 WING STRUCTURAL ARRANGEMENT - SPANWISE STIFFENED

of the spars and ribs are inplane with the surface panels for the monocoque concept to minimize the effect of eccentricities.

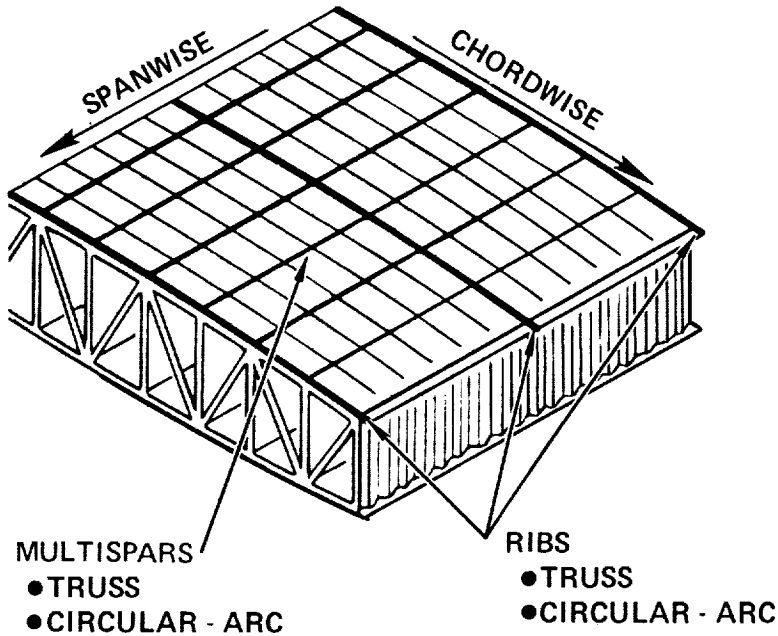
### Semimonocoque

The two types of semimonocoque concepts are (1) panels supporting loads in the spanwise direction, and (2) panels supporting loads in the chordwise direction. Both have the same type of rib and spar webs as the monocoque structure. Discrete spar and rib caps are provided for the semimonocoque concepts since the panels cannot support biaxial loads. Depending upon the stiffening arrangement, either the spar cap or the rib cap must have sufficient area to support inplane loads acting normal to the panel stiffeners.

Spanwise. - The spanwise-stiffened wing concept, including a schematic of the substructure arrangement is shown in Figure 1-2. The arrangement of the substructure is essentially a multirib design with closely spaced ribs and widely spaced spars. The surface panel configurations shown in the figure have effective load carrying capability in their stiffened direction. Smooth skins are required for aerodynamic performance, thus thickening of the skins panels is required to accommodate the chordwise thermal strains.

Chordwise. - The chordwise-stiffened panel and substructure arrangement is shown in Figure 1-3. The arrangement is essentially a multispar structure with widely spaced ribs. Submerged spar caps are provided except at panel closeouts and at fuel tank bulkheads. The submerged caps afford reduced temperatures and increased allowable stresses (strength and fatigue). The surface panel concepts for this arrangement have stiffening elements oriented in the chordwise direction. Structurally efficient beaded skin designs were explored. These efficient circular-arc sections of sheet metal construction provide effective designs when properly oriented in the airstream to provide acceptable performance as demonstrated on the Lockheed YF-12 aircraft. These shallow depressions or protrusions provide smooth displacements under

**CHORDWISE STIFFENED**



**PANEL STRUCTURAL CONCEPTS**



**CIRCULAR-ARC  
CONCAVE BEADED SKIN**



**CIRCULAR-ARC  
CONVEX BEADED SKIN**



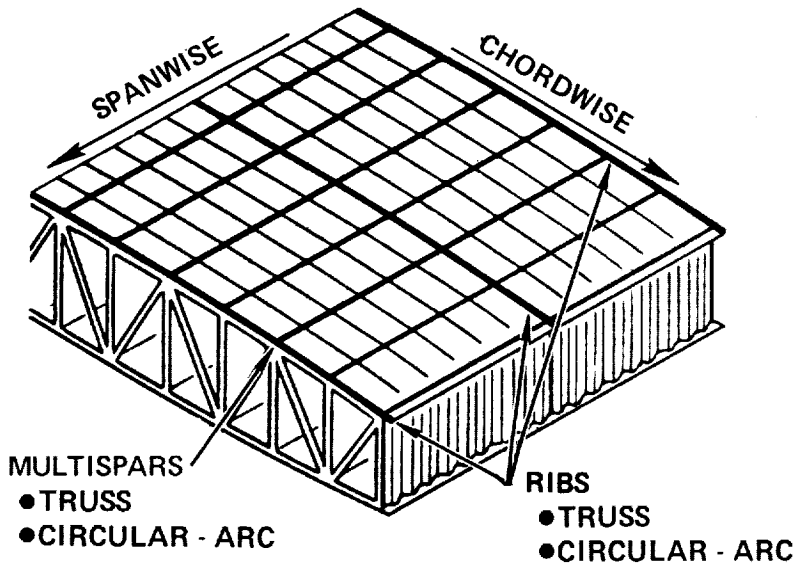
**TRAPEZOIDAL CORRUGATION  
CONCAVE BEADED SKIN**



**BEADED CORRUGATION  
CONCAVE BEADED SKIN**

**FIGURE 1-3 WING STRUCTURAL ARRANGEMENT - CHORDWISE STIFFENED**

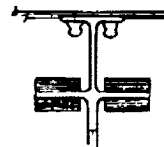
**CHORDWISE STIFFENED  
COMPOSITE REINFORCED**



**STRUCTURAL CONCEPTS**



**REINFORCED PANEL**



**REINFORCED CAPS**

**FIGURE 1-4 WING STRUCTURAL ARRANGEMENT - COMPOSITE REINFORCED**

thermally induced strains and operational loads and offer significant improvement in fatigue life. Panel spanwise thermal stresses are minimized by allowing thermal expansion (deformation) in the spanwise direction.

Composite Reinforced. - Selective reinforcement of the basic metallic structure is considered as the appropriate level of composite application for the near-term design. Furthermore, based on the principle of maximum return for minimum cost and risk, the application is directed towards unidirectional reinforcing of members carrying primary axial loads, such as spar caps, stringers and stiffeners of wing panel designs.

The chordwise stiffened arrangement described above, provides the basic approach offering the maximum mass saving potential and adopted for the application of composite reinforcing. The many unique design features are retained. In addition, structurally efficient, multi-element (fail-safe) composite reinforced spar cap designs as shown in Figure 1-4 are employed to transmit the spanwise bending moments as concentrated axial loads with minimum mass.

#### FUSELAGE STRUCTURAL CONCEPTS

The primary load carrying structural concepts for fuselage design are categorized as:

- (1) sandwich shell
- (2) skin-stringer and frame shell
- (3) composite reinforced shell.

#### Sandwich Shell

The sandwich shell design has a potential for weight savings over the more conventional skin-stringer and frame design with specific advantages with

regard to sonic fatigue resistance and reduced sound and heat transmission. Preliminary structural design and analyses were conducted to assess the potential mass savings benefit and manufacturing/design feasibility of the sandwich shell. The manufacturing complexity; and the parasitic weight which the sandwich must carry, in terms of core and bonding agent, proved to be a disadvantage, and thus was not included as part of the study.

### Skin-Stringer and Frame Shell

The basic structural arrangement for the latter two categories is a uniaxial stiffened structure of skin and stringers with supporting frames. The stringer configuration with the potential of achieving minimum weight are the zee-stiffened and the open and closed hat sections that are shown in Figure 1-5. The hat sections are also amenable to composite reinforcing. Supporting frames that merit consideration are both the fixed and floating type. The joining methods evaluated for this arrangement include mechanical fastening, welding and bonding.

### EVALUATION OF STRUCTURAL APPROACH

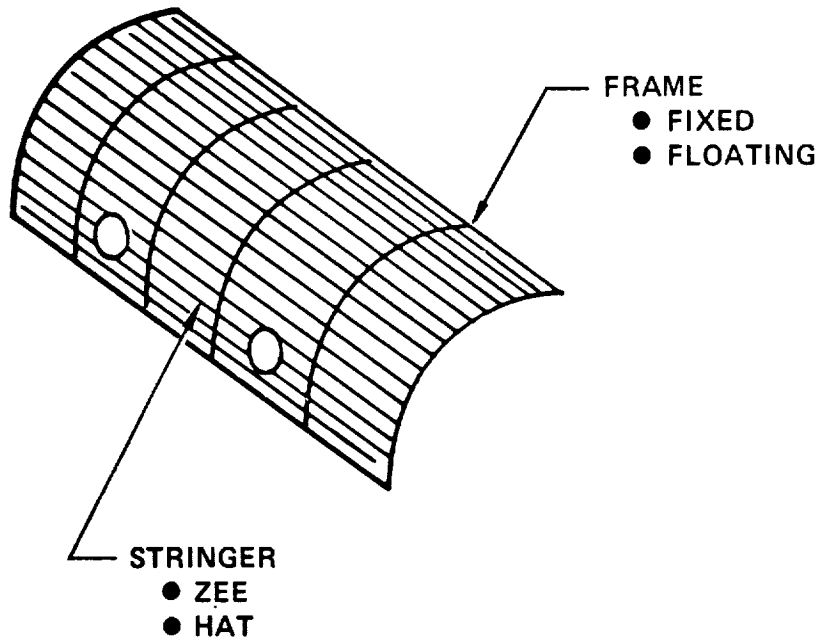
A spectrum of structural approaches for wing and fuselage application that fully exploit the practically attainable advantages of near-term (1975-1981) start-of-design were evaluated.

Both smooth-skin (spanwise, monocoque) and beaded-skin (chordwise) external surface designs were explored. Structurally efficient circular-arc sections of sheet metal construction were applied to the design. The fuselage structural arrangement is a uniaxial stiffened structure (skin-stringer) with supporting frames.

Component fabrication and subassembly consider techniques involving brazing, bonding, weld-bond, etc., as well as mechanical fasteners. Assembly joining of large assemblies encompasses both welding and mechanical fastening.

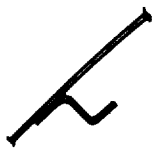
A summary of the sequence and scope for evaluating the candidate structural arrangement is presented in Table 1-1.

SKIN-STRINGER AND FRAME

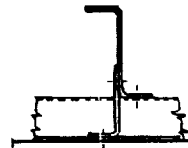


PANEL STRUCTURAL CONCEPTS

FRAME STRUCTURAL CONCEPTS



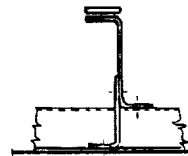
ZEE STIFFENED



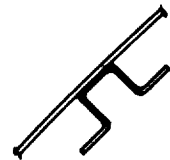
FLOATING ZEE  
W/SKIN SHEAR TIE



CLOSED-HAT



FLOATING ZEE  
W/SKIN SHEAR TIE  
COMPOSITE  
REINFORCED



OPEN-HAT



CLOSED-HAT  
COMPOSITE  
REINFORCED

FIGURE 1-5 FUSELAGE STRUCTURAL ARRANGEMENT - SKIN - STRINGER AND FRAME



TABLE 1-1 EVALUATION OF STRUCTURAL APPROACHES - TASK I

MACH 2.7 - NEAR TERM START OF DESIGN

MATERIALS	STRUCTURAL ARRANGEMENTS	FABRICATION AND/OR ASSEMBLY	FABRICATION AND STRUCTURAL ARRANGEMENT TRADE-OFF	DESIGN GUIDELINE AND EVALUATION DATA	EVALUATION AND SELECTION
<ul style="list-style-type: none"> <li>● METALS</li> <li>● TI-6AL4V</li> <li>● BETA C</li> <li>● COMPOSITES</li> <li>● GRAPHITE POLYIMIDE</li> <li>● BORON POLYIMIDE</li> <li>● BORON ALUMINUM</li> <li>● BORSIC ALUMINUM</li> </ul>	<p>STRUCTURAL CONCEPTS</p> <ul style="list-style-type: none"> <li>● SPARS</li> <li>● RIBS</li> <li>● COVERS</li> <li>● FRAMES</li> </ul>	<p>WELDED</p>	<ul style="list-style-type: none"> <li>● BI-AXIALLY STIFFENED</li> </ul>	<p>IMPORTANCE OF:</p> <ul style="list-style-type: none"> <li>● FATIGUE QUALITY</li> <li>● TANK SEALING</li> <li>● DAMAGE TOLERANCE</li> <li>● STRUCTURAL APPROACH</li> <li>● ARRANGEMENT</li> <li>● COVER, RIB, SPAR AND FRAME CONCEPTS</li> <li>● WING-BODY INTERFACE</li> <li>● THERMAL STRESSES</li> <li>● CONTROL SYSTEM</li> <li>● FLUTTER</li> <li>● STATIC AERO-ELASTICITY</li> <li>● FUEL VOLUME REQ'D</li> <li>● MATERIAL SELECTION</li> <li>● METALS</li> <li>● COMPOSITES</li> </ul> <p>COST</p> <ul style="list-style-type: none"> <li>● EASE OF FABRICATION AND ASSEMBLY</li> <li>● MATERIAL AND FABRICATION COST</li> <li>● MAINTAINABILITY AND SERVICEABILITY</li> </ul>	<p>IDENTIFY:</p> <p>STRUCTURAL APPROACHES BEST SUITED FOR WING AND FUSELAGE</p> <p>CONCEPTS MERITING FURTHER DETAILED DESIGN &amp; ANALYSIS</p>
	<ul style="list-style-type: none"> <li>● BI-AXIALLY STIFFENED</li> <li>● SPANWISE STIFFENED</li> <li>● CHORDWISE STIFFENED</li> <li>● CHORDWISE STIFFENED, SELECTIVE COMPOSITE REINFORCED</li> <li>● FUSELAGE SKIN, STRINGER FRAME</li> </ul>	<p>FASTENERS</p>	<ul style="list-style-type: none"> <li>● WELDING VS FASTENERS</li> <li>● ALL BRAZED Ti HONEY COMB.</li> <li>● FATIGUE QUALITY</li> <li>● TANK SEALING (FASTENERS) VS WELDED</li> <li>● BI-AXIAL VS SPANWISE VS CHORDWISE STIFFENING</li> <li>● ALL METAL VS COMPOSITE REINFORCED METAL</li> <li>● ALL METAL VS COMPOSITE REINFORCED METAL</li> </ul>		

The steps in the procedure are as follows: (1) establish the material system and fabrication and/or assembly method for the candidate concepts, (2) perform fabrication and structural trade studies, (3) define the detail mass and cost evaluation of each concept in accordance with the design guidelines, and (4) evaluate and select the most promising arrangement for further detailed study.

Both metallic and composite material systems were considered. The prime emphasis was placed on the metallic system with composite application being limited to selective reinforcement of basic metallic structure. The materials considered were:

- Titanium alpha-beta and beta alloys
- Boron and graphic polyimide organic matrix composites
- Boron and BORSIC aluminum metal matrix composites.

The manufacturing techniques were based on the assembly of large components by fasteners and welding, and sub-assemblies by welding, spot weld bonding, spot brazing, braze and fasteners.

Five structural approaches were considered. These structural approaches were designed to provide, through analyses and trade-offs, a basis for quantitative evaluation of the full structural mass saving potential available to the Mach 2.7 Arrow-Wing configuration. The five approaches are listed below. The first four share a common fuselage approach, skin/stringer/frame. The fuselage approach for the fifth is skin/stringer/frame, selectively composite reinforced.

- Approach 1 - Biaxially Stiffened - Welded
- Approach 2 - Biaxially Stiffened - Mechanically Fastened
- Approach 3 - Spanwise Stiffened - Mechanically Fastened
- Approach 4 - Chordwise Stiffened - Mechanically Fastened
- Approach 5 - Chordwise Stiffened - Selective Composite Reinforced, Mechanically Fastened.

Each of these structural concepts was analyzed, screened, and the arrangement geometry defined in terms of minimum mass. Design guidelines were established to assist in the assessment of the relative importance of such design parameters as: fatigue quality, tank sealing, damage tolerance, structural approach, etc., on the candidate arrangements.

The evaluation and selection of candidate structural approaches were performed on the basis of direct operating cost (DOC), which includes such factors as mass, production cost, maintainability, and fuel consumption. Simplified cost-benefit studies were performed to provide additional basis for decision.



SECTION 2

BASELINE CONFIGURATION

BY

I. F. SAKATA, D. M. URIE, C. W. LINDBLOM, R. N. JENSEN



## CONTENTS

<u>Section</u>	<u>Page</u>
INTRODUCTION	2-1
REFERENCE CONFIGURATION	2-1
CONFIGURATION REFINEMENTS	2-7
Design Changes	2-7
Low Speed Longitudinal Characteristics	2-10
Airframe Design Recommendations	2-20
Engine Recommendations	2-21
BASELINE CONFIGURATION - TASK I	2-26
General Arrangement	2-26
Basic Dimensions	2-27
Fuel Tank Arrangement	2-28
Interior Arrangement	2-30
Airplane Mass Properties	2-42
BASELINE CONFIGURATION - TASK II	2-47
General Arrangement	2-48
Basic Dimensions	2-48
Fuel Tank Arrangement	2-49
Interior Arrangement	2-49
Airplane Mass Properties	2-50
Mass Moment of Inertia	2-52
Center of Gravity Travel	2-52
REFERENCES	2-65

## LIST OF FIGURES

<u>Figure</u>		<u>Page</u>
2-1	Arrow-Wing Supersonic Cruise Aircraft Configuration	2-2
2-2	Baseline Configuration Development Rationale	2-2
2-3	SCAT 15F Variations	2-3
2-4	NASA Data Deck Airplane Concept	2-5
2-5	Fuselage Cross Section	2-9
2-6	Fuselage Area Ruling	2-9
2-7	Main Landing Gear Configuration - NASA Data	2-11
2-8	Advanced Main Landing Gear Concept	2-13
2-9	Low Speed Longitudinal Characteristics	2-16
2-10	Computer Graphics Console - Low Speed Pitch Up Analysis	2-16
2-11	Computer Program Logic	2-18
2-12	Arrow-Wing Pitch Up Characteristics	2-18
2-13	Pitch Up Study Results	2-19
2-14	Tail Size Criteria	2-19
2-15	Baseline Configuration/Longitudinal Controls	2-23
2-16	Duct Burning Turbofan Engine - Mach 2.7	2-23
2-17	Nacelle Dimensions and Scaling Data - BSTF 2.7-2	2-24
2-18	Preliminary Nacelle	2-24
2-19	General Arrangement - Task I	2-31
2-20	Basic Dimensions - Task I	2-33
2-21	Fuselage Dimensional Data - Task I	2-35
2-22	Fuel Tank Arrangement - Task I	2-37
2-23	Interior Arrangement - Task I	2-39
2-24	Center of Gravity Diagram - Task I	2-46
2-25	General Arrangement - Task II	2-53
2-26	Basic Dimensions - Task II	2-55
2-27	Fuselage Dimensional Data - Task II	2-57
2-28	Fuel Tank Arrangement - Task II	2-59
2-29	Interior Arrangement - Task II	2-61
2-30	Aircraft Moment of Inertia - Task II	2-63
2-31	Center of Gravity Diagram - Task II	2-64



LIST OF TABLES

<u>Table</u>		<u>Page</u>
2-1	Engine Cycle Description - BSTF 2.7-2	2-22
2-2	Propulsion System Parameters	2-25
2-3	Estimated Group Mass and Balance Statement	2-43
2-4	Airplane Mass Moment of Inertia	2-45
2-5	Estimated Group Mass and Balance Statement - Task II	2-51



## SECTION 2

### BASELINE CONFIGURATION

#### INTRODUCTION

The supersonic cruise aircraft configuration shown in Figure 2-1 is a discrete wingbody airplane with a low wing that is continuous under the fuselage. The baseline configurations for the study effort (Task I and Task II) were developed using the technical information for the Arrow-Wing Supersonic Cruise Aircraft provided by NASA and the applicable data from the Supersonic Cruise Aircraft Research and Technology Assessment Studies (Reference 1). Figure 2-2 presents the primary configuration concept differences and development rationale.

The numerical definition of the basic NASA 15F airplane concept was provided to Lockheed by the NASA-Langley Research Center (NASA-LaRC) as a computer card deck (identified as 733-336C follow-on, April 1973). In addition to the geometric data, a series of working papers (Figure 2-3) which contained wind tunnel data for various modifications of this basic concept were also provided. The data, coupled with the NASA computer programs which allowed theoretical calculations of many of the aerodynamic drag characteristics to be determined, were used to adjust the aerodynamic data so as to reflect design changes made by Lockheed. This collection of information provides a solid data base to permit aerodynamic and airframe refinements to be made.

#### REFERENCE CONFIGURATION

The external shape of the airplane concept defined by NASA was based on the Boeing 969-336C airplane. The airplane does not incorporate a canard or in-board wing leading edge devices. Only a horizontal tail was provided for pitch control and trim. The fuselage was also moved aft approximately 17-1/2 feet

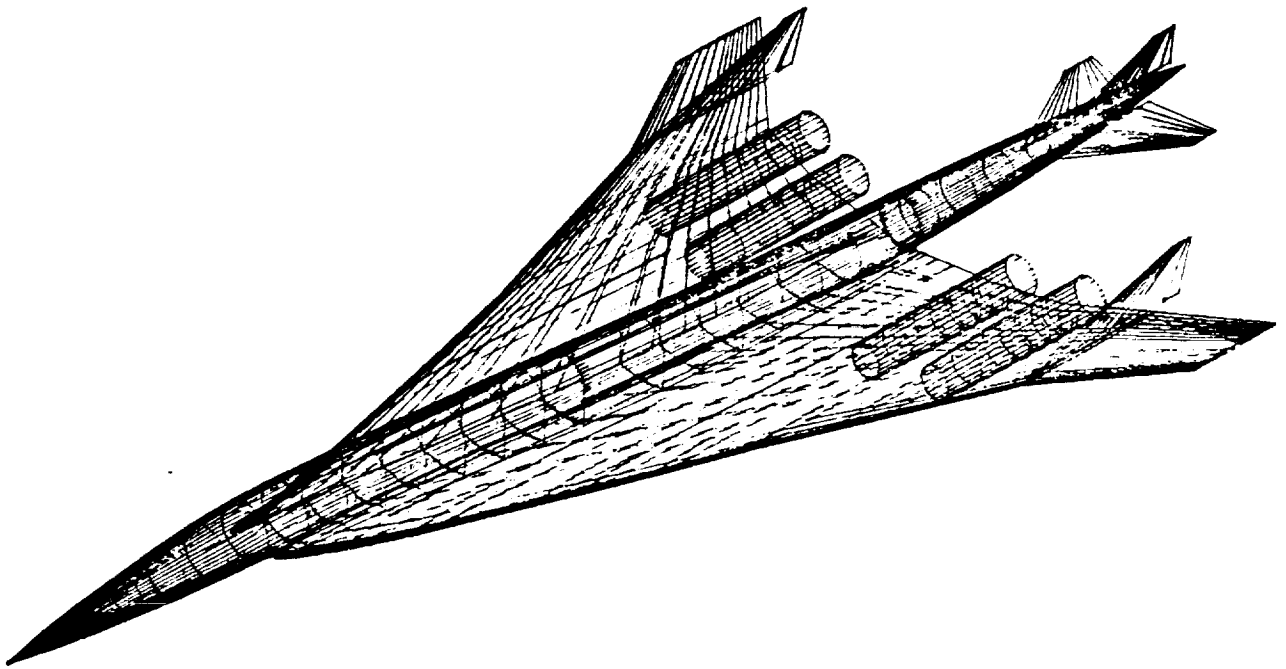


Figure 2-1. Arrow-Wing Supersonic Cruise Aircraft Configuration

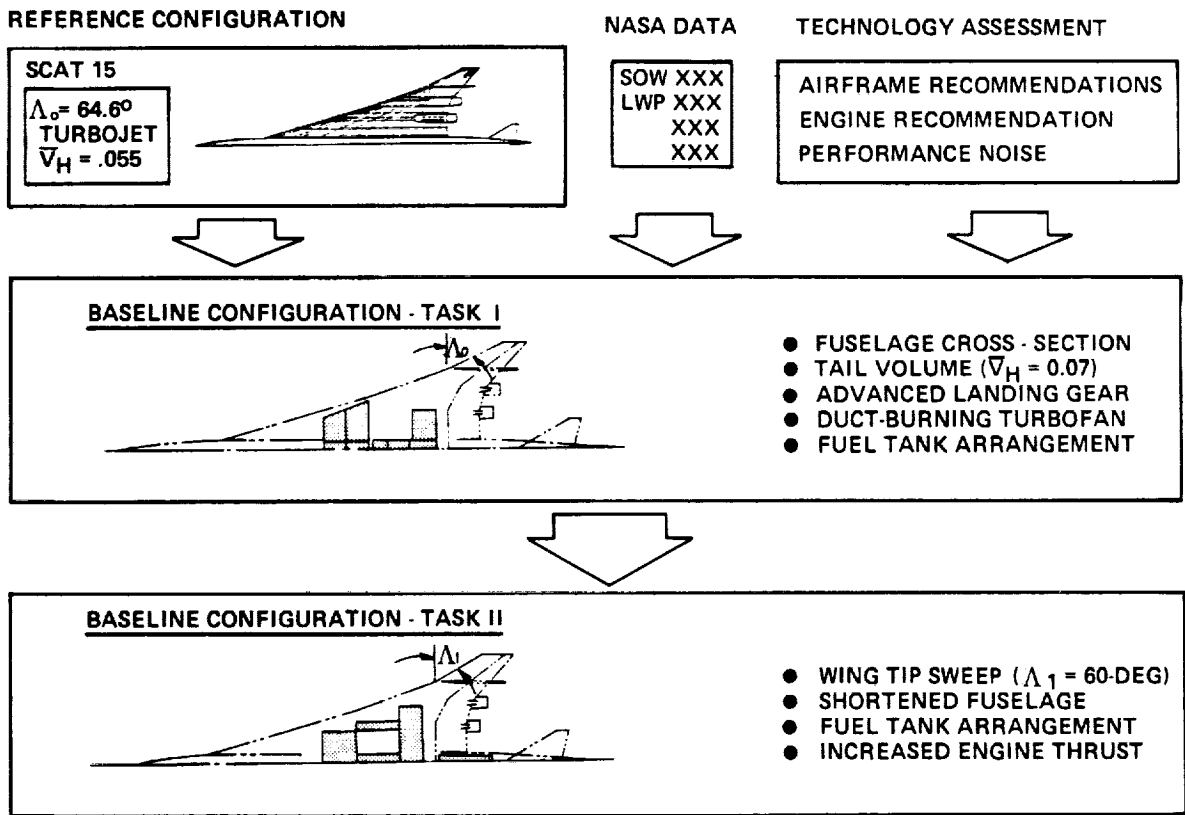


Figure 2-2. Baseline Configuration Development Rationale

(TWELVE LANGLEY WORKING PAPERS)

<u>COMPONENT</u>	<u>NO. OF VARIATIONS</u>	<u>DIFFERENCES</u>
WING	9	LEADING EDGE RADIUS, DROOP, PLANFORM, TIP SWEEP
BODY	8	FOREBODY SHAPES, AFTBODY SHAPES, LOCATION ON WING
HORIZONTAL TAIL	4	TAIL SIZE
VERTICAL TAIL	15	TAIL SIZE, ARRANGEMENT, LOCATION, VENTRALS
HIGH LIFT DEVICES	22	INBOARD AND OUTBOARD LOCATION, LEADING AND TRAILING EDGE POSITION, SHAPE, PLAIN AND SLOTTED.
CANARD	3	POSITION ON FUSELAGE
GROUND PLANE		HEIGHT ABOVE GROUND

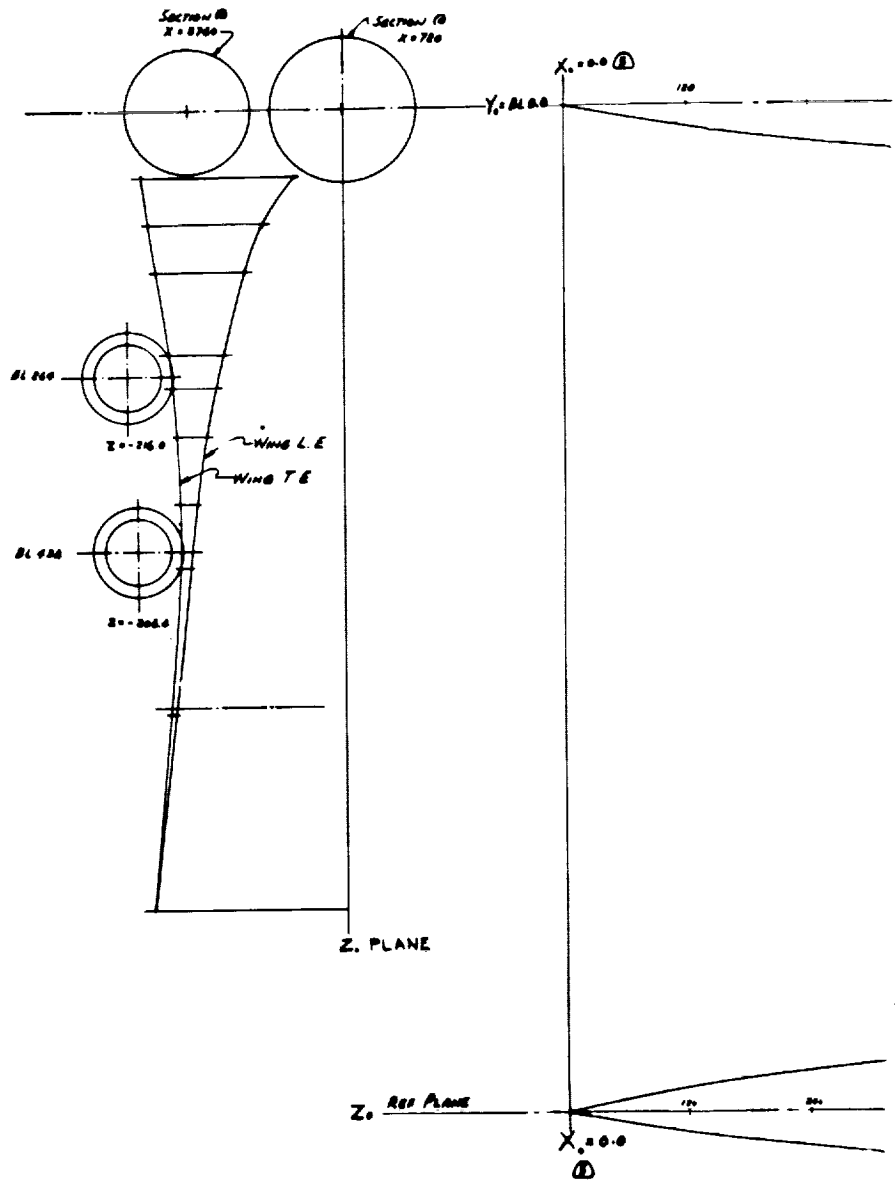
Figure 2-3. SCAT 15F Variations

with reference to the -336C. The NASA data deck airplane concept is shown in Figure 2-4. Note that the nacelles and the fixed vertical fins are shown on butt line (BL) locations and that all dimensional data is given relative to X, Y, and Z axes.

Regarding the basic NASA 15F concept there were three areas of particular concern to Lockheed. One was the adequacy of the fuselage and the passenger accommodations provided, in terms of comfort, baggage stowage, cargo, and passenger services. Further, was the forebody shape of the fuselage adequate to meet the space and visibility requirements for a commercial transport flight station? Did the design provide adequate fuel stowage, and could the landing gear be suitably stowed into the wing or fuselage? Although a few significant changes appear to be necessary, in general, the concept is close to being a practical commercial transport design. This situation exists because of the close working relationship which developed between the airplane manufacturers and NASA during the first generation SST development program conducted in the late 1960's.

A second concern regarding the 15F concept relates to arrow-wing low speed longitudinal characteristics. This type of planform with conventional leading edge geometry inherently produces pitch-up characteristics at high airplane attitudes. The seriousness of this problem can become aggravated because of (1) limited control power, (2) wing flexibility because of thin airfoil shapes, (3) need to minimize control surface sizes to reduce airplane weight, and drag, and (4) high pitch inertia characteristics of long slender heavy airplanes. NASA-Langley has been aware of these problems and numerous means of alleviating the situation have been examined in the wind tunnel.

The third 15F concept problem relates to its lift capabilities which are inherently poor because of the highly swept leading edge. In order to achieve reasonable lift coefficients needed for airport operations high airplane pitch attitudes are called for. Studies of this problem and practical solutions were investigated in the Langley working papers. Included are data involving both leading edge and trailing edge high lift devices in combination



ORIGINAL PAGE IS  
OF POOR QUALITY

MOLDOUT FRAME /





X DISTANCE IN Z<sub>0</sub> PLANE →

BL 67° 0

74° (100°)

X = 742.7  
Z = -48.84

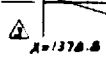
Y Y

V V

E E



BL 257.1



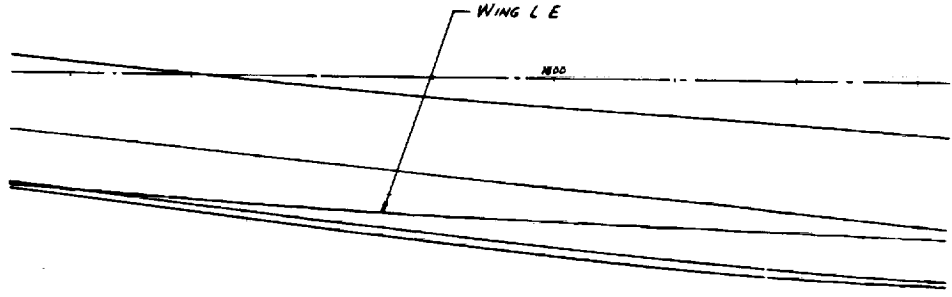
MAC - 1387.0

BL 311.2

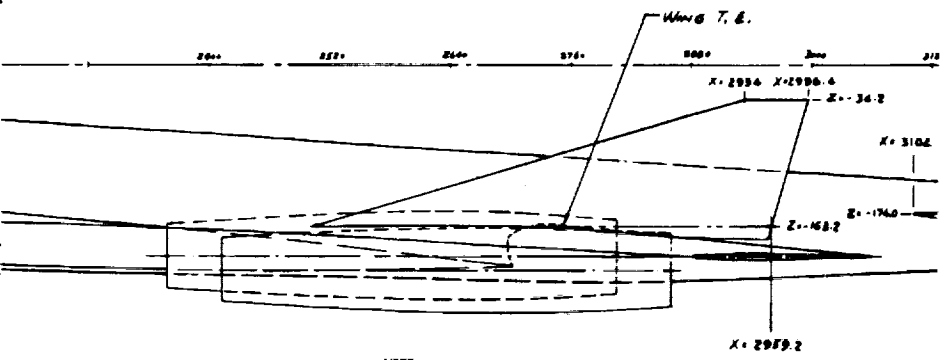
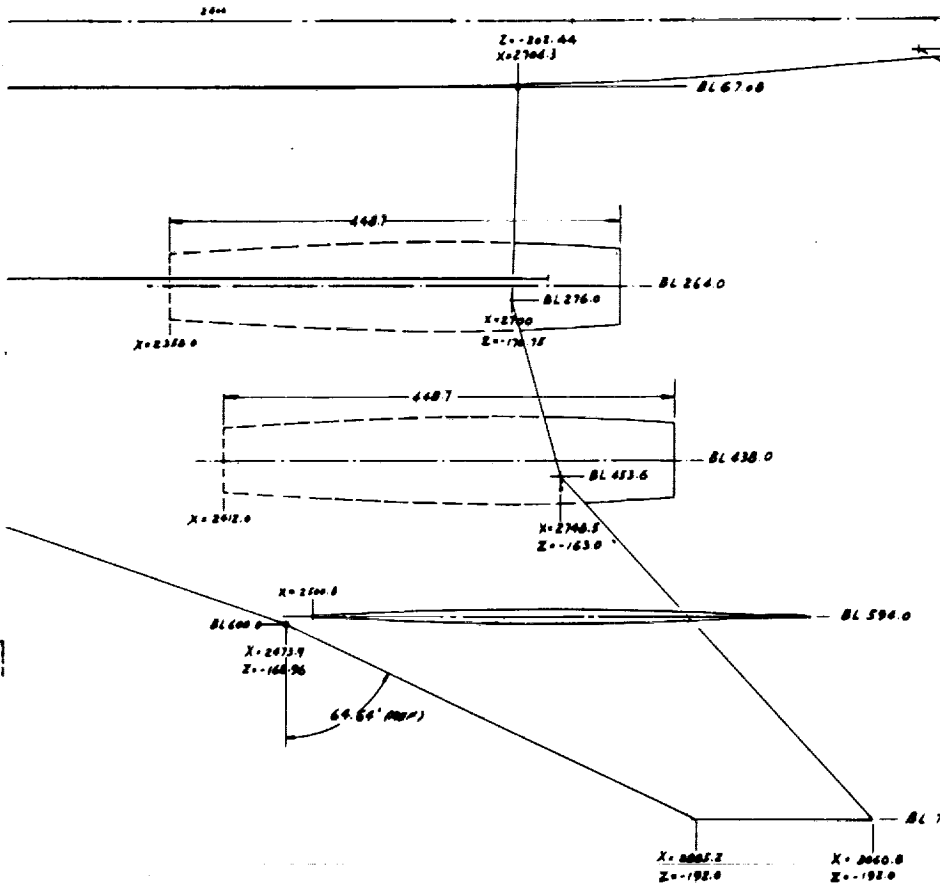
X=1873.1  
Z=1692.24

70.84' (REF)

WING CONTOUR @ BL 6708



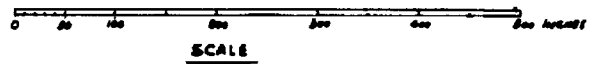
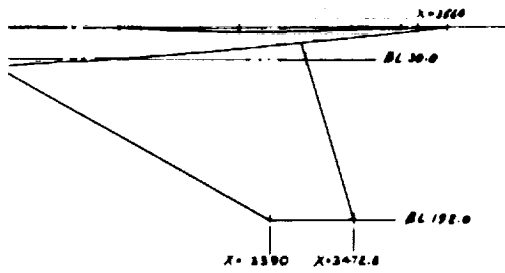




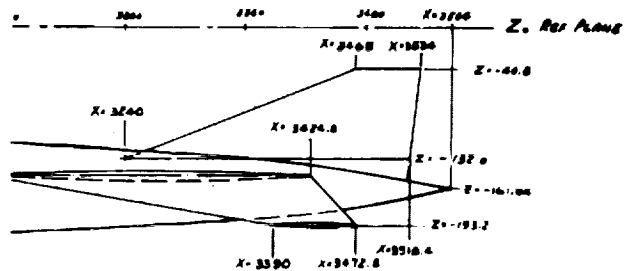
NOTE  
 X DISTANCES IN Z. PLANE →

6  
 5  
 4  
 3  
 2  
 1  
 C  
 A  
 NO7





192.0



ALL DIMS IN X-Y-Z COORDINATES.  
 ORIGIN OF X-DISTANCES TAKEN AS O.O AT NOSE.  
 SEE SHEET 2 FOR SECTIONS.  
 NOT PRINTOUT DATA.  
 DIMENSIONS IN INCHES & DEGREES.  
 CONFIGURATION PER NASA FURNISHED DECK,  
 MODEL 733-336C FOLLOW-ON 0.5% LER.  
 'E

Figure 2-4. NASA Data Deck Airplane Concept





with auxiliary trimming surfaces (canards and horizontal tails). These surfaces provide various schemes for supplementing the lift characteristics of the arrow planform.

### CONFIGURATION REFINEMENTS

The configuration refinements made to the NASA 15F concept in regards to the three areas of concern are highlighted in the following paragraphs. Appropriate changes were adopted for the respective tasks, consistent with the objectives of the planned effort.

#### Design Changes

One of the major objectives when laying out an airplane design is the efficient use of all volume within the airplane. Related to this design goal is the interior layout of the fuselage in the passenger accommodations area, for cruise drag places heavy emphasis on minimizing the fuselage cross-sectional area. From a passenger comfort standpoint, however, it is necessary to provide head room and have a cabin width which will allow for wide seats and sufficient aisle widths. Below-the-floor-volume is needed for cargo and baggage.

The contour adopted is compared with the cross-sectional area of the NASA 15F concept as defined by the NASA-Langely computer deck in Figure 2-5. This comparison shows the marginal head room which is given in the NASA configuration. It is felt that for a practical commercial transport with adequate passenger comfort the head room more like that shown and as developed for the Lockheed L-2000 is required.

This additional head room can be obtained in two ways. It can be obtained by increasing the fuselage diameter as suggested by the sketches in Figure 2-5. The alternative means would be to provide a depression in the floor between the seats in the passenger aisle thereby granting head room while walking fore and aft in the cabin and providing a step-up to the seats on either side of the

aisle. It is not believed that this is a practical arrangement from an emergency passenger evacuation standpoint, nor is it an efficient structural design. The depression will create kick loads in the wing beams which will introduce weight penalties. For these reasons, then, in the region critical to the wing design in the rear part of the passenger cabin the Lockheed basic concept design adopts the larger head room arrangement rather than the floor depression scheme. The effect of this change to the fuselage cross-sectional area and drag at the design cruise Mach number is shown in Figure 2-6. The distribution of fuselage cross-sectional area with fuselage length is shown for the NASA reference configuration as well as the fuselage that would have full head room for the entire length of the passenger compartment. It is seen that the full head room configuration increases the maximum frontal area from approximately 125 to 137 square feet. Also shown on Figure 2-6 is a compromise concept which would provide the full head room in the aft cabin, but in the forward passenger compartment adopt the idea of the depressed floor along the aisle so as to permit a reduced fuselage cross-section area in the forward portion of the fuselage.

The total airplane wave drag coefficient for the three configurations is noted on the figure. With the reduced frontal area associated with the NASA reference concept the wave drag is .00223. The intermediate concept increases the wave drag coefficient approximately six tenths of a drag count and the full head room arrangement increases the wave drag 1.4 drag counts. Until more detailed fuselage design and analysis is made to study the total impact of the floor depression in the forward cabin, i.e., what it might do to the structural design of the beams in the forward part of the wing and allow an analysis of the weight penalty for that depression, the full-head-room passenger compartment arrangement was adopted.

A second design consideration which received attention was the design of the main landing gear. The design of a gear for a supersonic transport presents a challenge because of the high gross weight of the aircraft (approximately 750,000 pounds). This puts the airplane in the same class as the four stick landing gear design of the 747 airplane.

# FUSELAGE CROSS SECTION

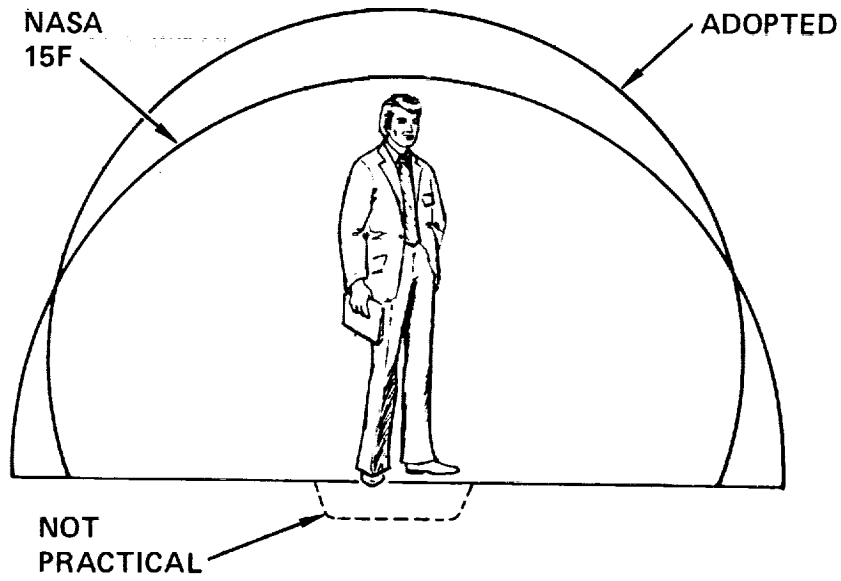


Figure 2-5. Fuselage Cross Section

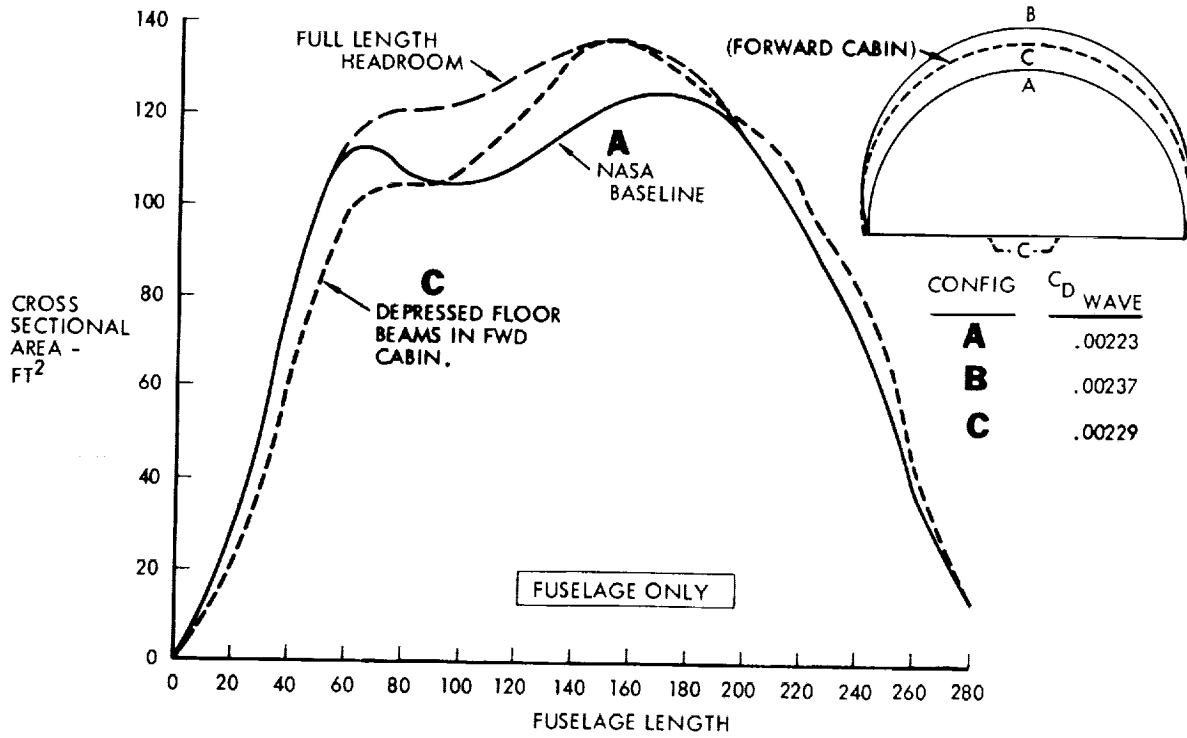


Figure 2-6. Fuselage Area Ruling

Landing gear design concepts were examined to establish feasibility of concepts which avoided external contour deviations as required by the NASA supplied data. A wing-stowed, forward retracting main landing gear (MLG) having 12 tires per strut is shown in Figure 2-7. The hump required in the upper surface above the stowed wheels is also shown. This hump involves not only a drag penalty but also an increase in complexity and weight of the upper surface.

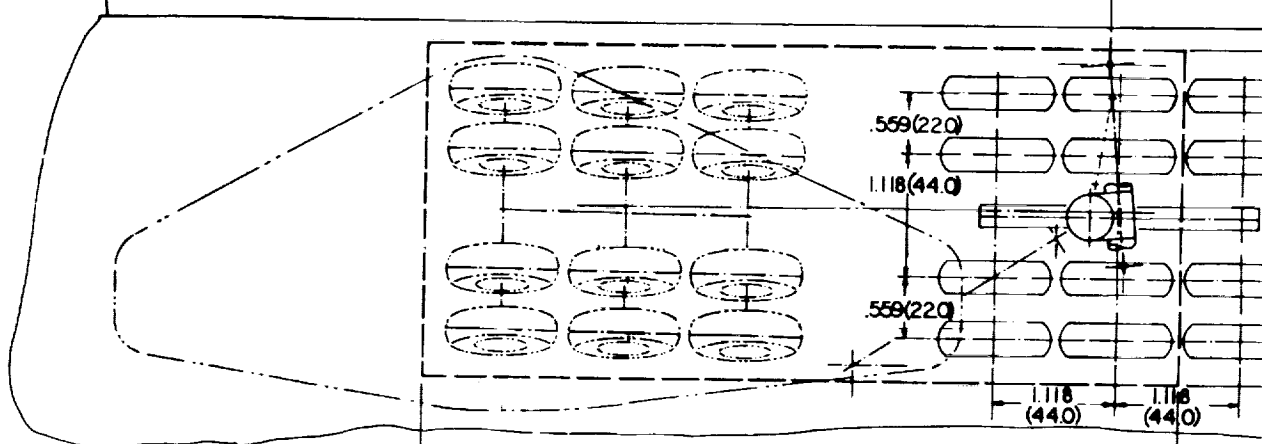
A brief study was made to review the design considerations relating to pavement stress, number of wheels, number of gear struts, the general arrangement and retraction mechanism of gear. This effort resulted in the development of the design shown in Figure 2-8. The design utilizes three tires per wheel, or 18 tires per strut, to reduce the tire diameter and eliminate the hump in the wing surface. This design improvement is accomplished while retaining the same size wheel well and very nearly the same MLG geometry as the 12 tire/wheel design depicted in Figure 2-7.

#### Low Speed Longitudinal Characteristics

The arrow-wing concept requires careful attention with regard to its low speed longitudinal characteristics. Compared to today's swept wing airplanes the planform shape provides extremely low lift curve slopes. Therefore added emphasis must be placed on the need for high lift devices. One means for achieving additional lift is to operate the arrow-wing at higher angles of attack. However, this introduces the problem of pitch-up which is caused by wing tip stall at moderate angles of attack. As angle of attack is increased, the tips stall before the remainder of the wing and there is a tendency for the airplane to want to nose-up further and aggravate the flow breakdown situation.

Figure 2-9 outlines the considerations with regard to geometry and design that were considered in order to arrive at an arrow-wing concept that displays

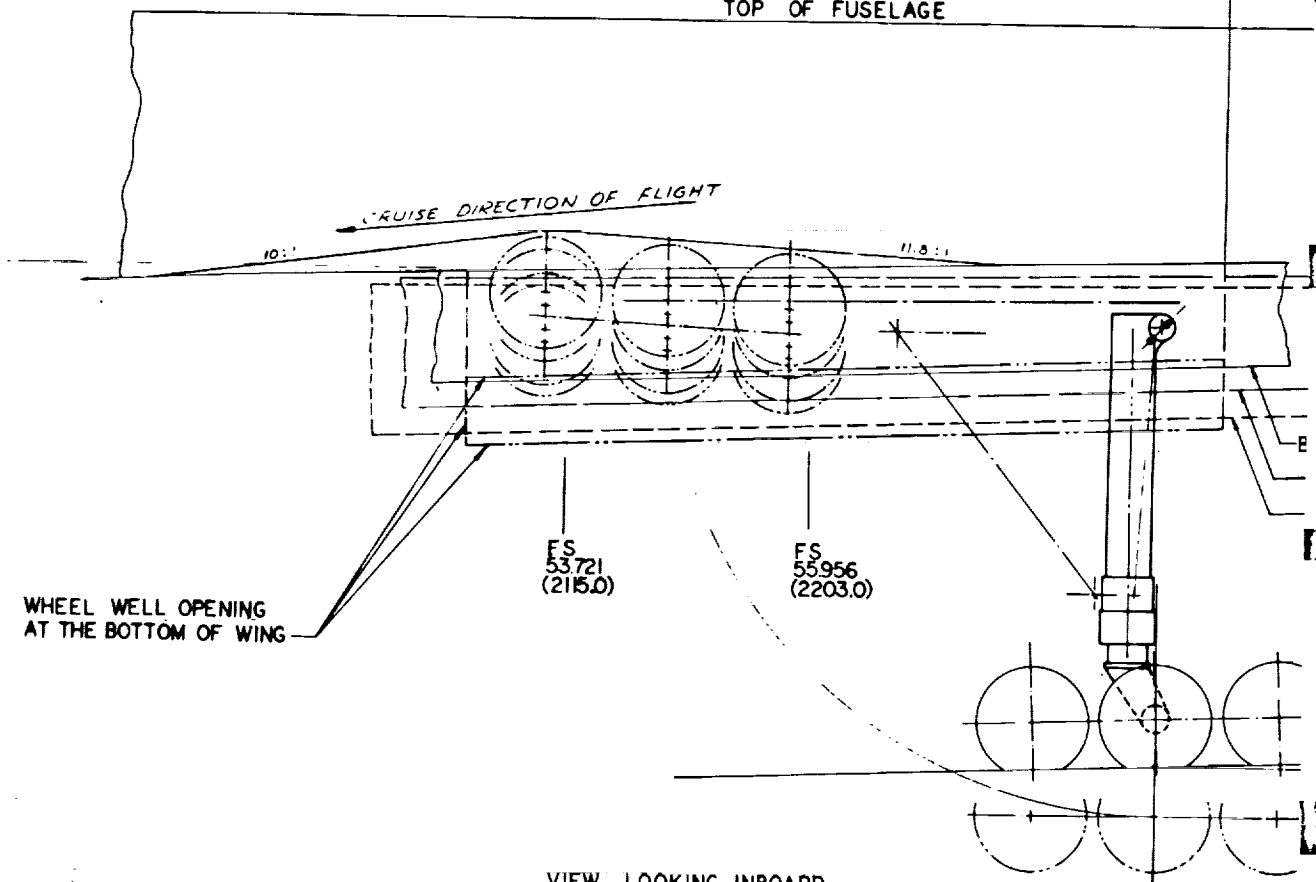
BL 0.0



FS 52 807 (2079.0)

FS 59 715 (2351.0) REF

TOP OF FUSELAGE



WHEEL WELL OPENING AT THE BOTTOM OF WING

FS 53.721 (2115.0)

FS 55.956 (2203.0)

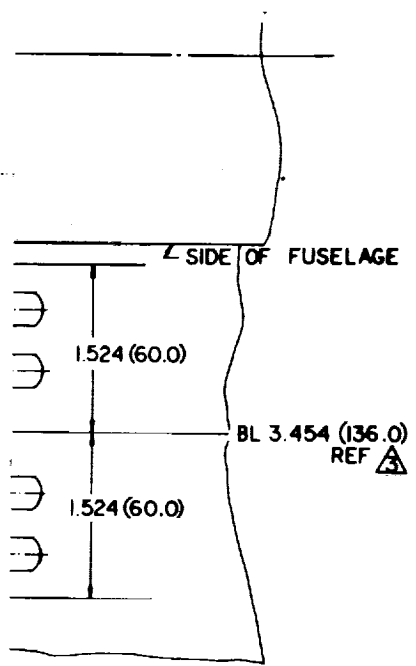
VIEW LOOKING INBOARD

FS 59 1637 (2329.28) REF

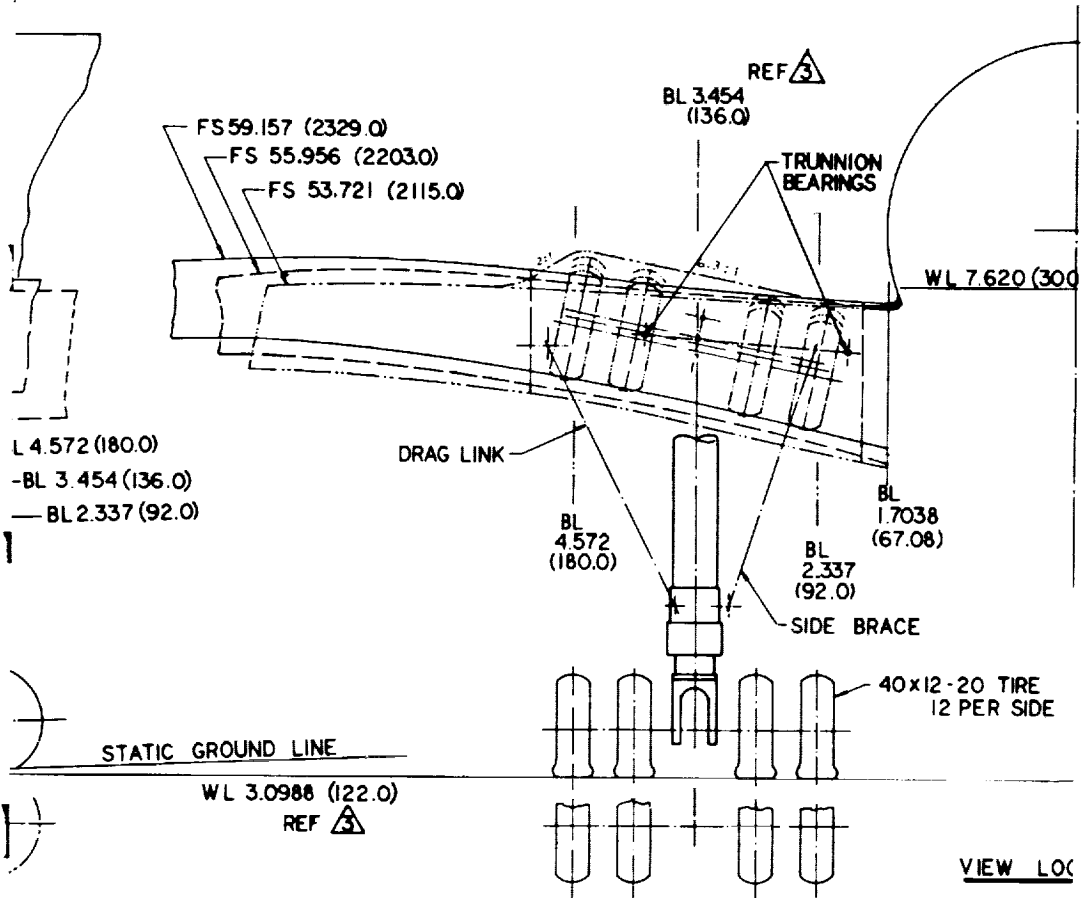
ORIGINAL PAGE IS OF POOR QUALITY

(FOLDOUT FRAME)





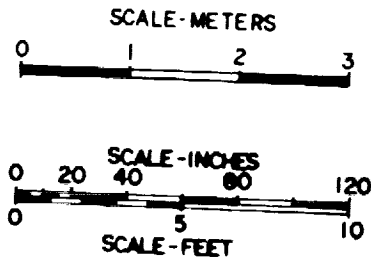
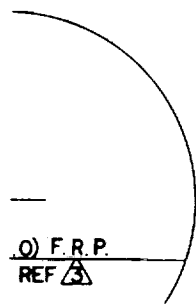
REF 3



VIEW LOC





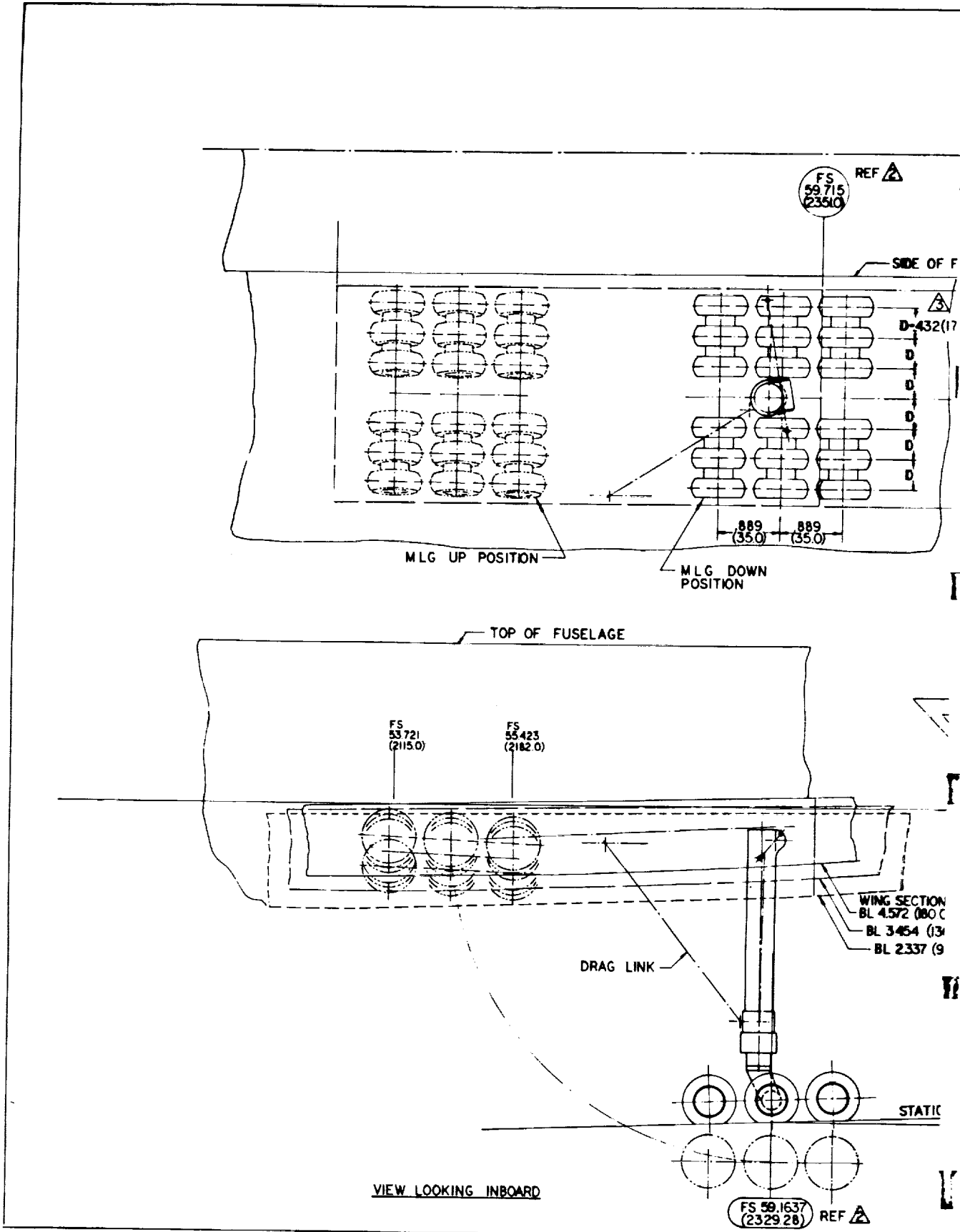


3 SEE DWG CL1606-3-3.  
2. M.L.G. CONFIGURATION PER DATA FURNISHED BY NASA.  
1. DIMENSIONS IN METERS (INCHES).  
NOTE

WORKING FORWARD

Figure 2-7. Main Landing Gear Configuration - NASA Data

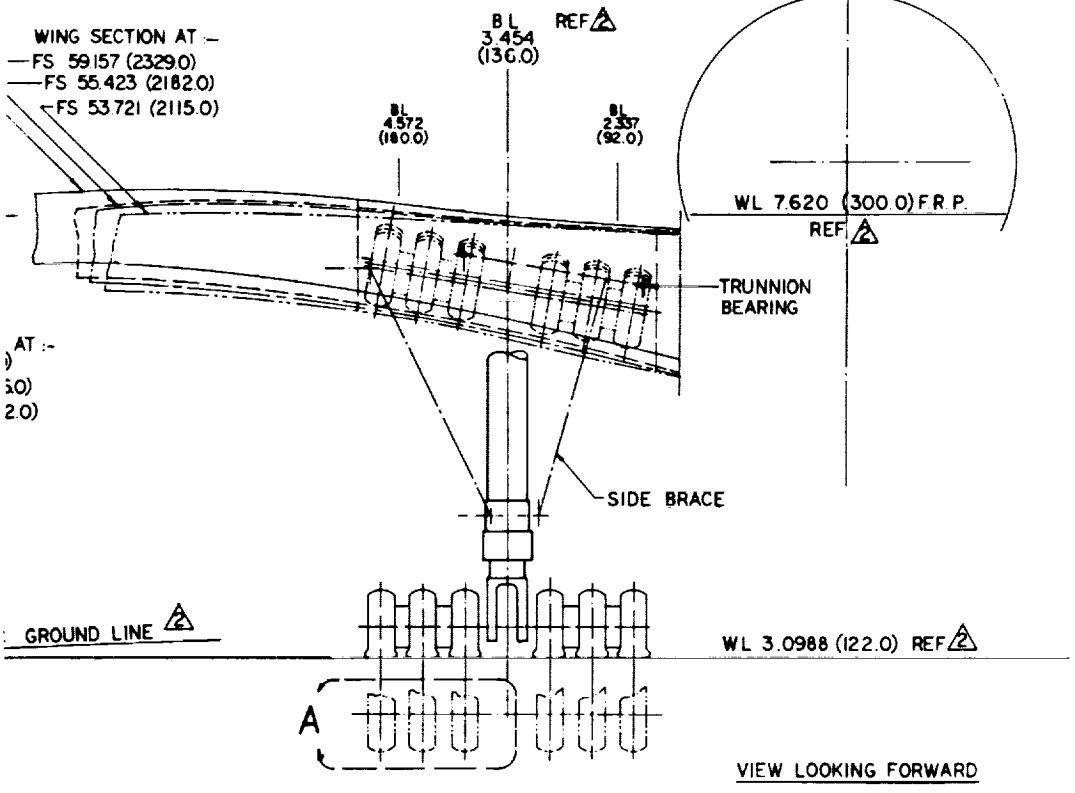
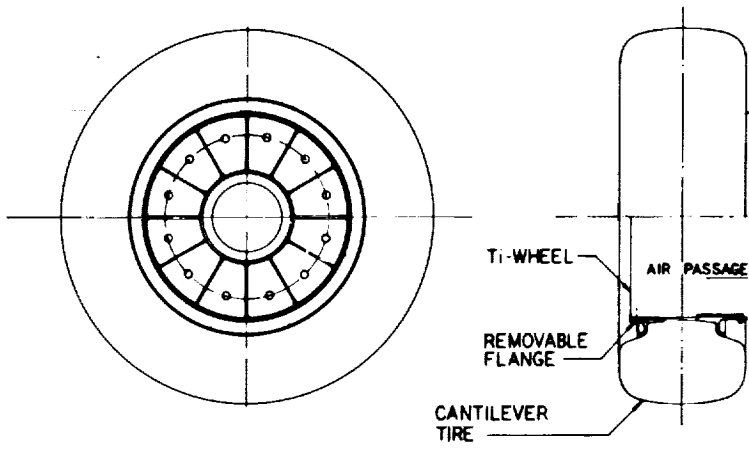
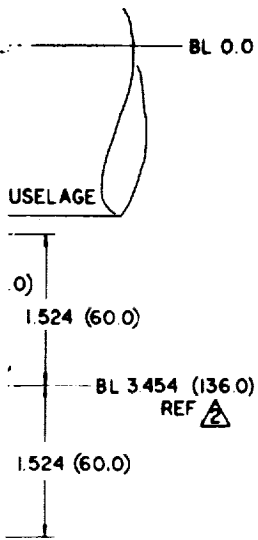




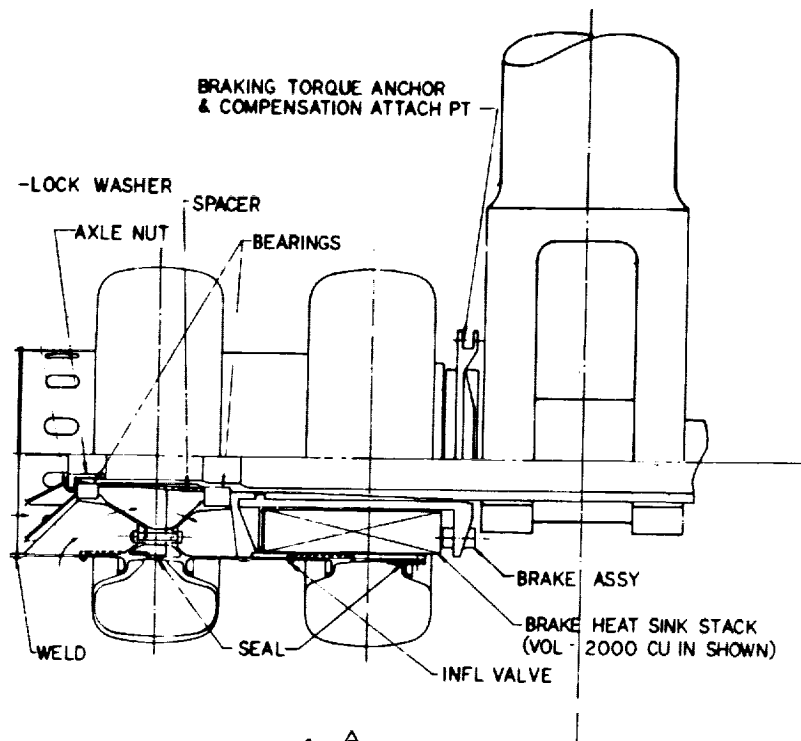
PRECEDING PAGE BLANK NOT FILMED


FOLDOUT FRAME / ORIGINAL PAGE IS OF POOR QUALITY

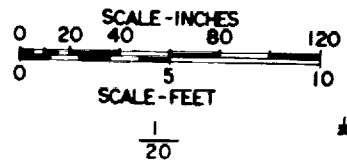
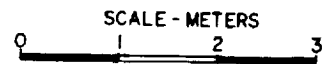









DETAIL A   
 SCALE - 1/4



4 FOR MLG PER NASA DATA,  
 SEE DWG CL 1606-3-9.

 LOCKHEED ADV DES CONFIGURA-  
 TION - NOT NASA FURNISHED

 SEE DWG CL 1606-3-3.  
 1 DIMENSIONS IN METERS (INCHES)

NOTE

Figure 2-8. Advanced Main Landing Gear Concept





satisfactory handling quality characteristics. With regard to design, the configuration development considered the trades offered by either a canard or an aft tail arrangement. Various trailing edge devices and leading edge devices were explored with regard to lift enhancement and pitch stability improvement. Fences, notches, and other controls that provide added improvements in lift characteristics and the control of the pitch-up were also analyzed. Related to these studies of various control surfaces and devices, the balance characteristics of the airplane were also investigated. Balance involves the fuel system and its related tankage arrangement, the loadability of the airplane which relates back to the location of the fuselage passenger compartment and its relationship to the airplane's center of gravity, and the desirable stability and control and trim drag characteristics that must be considered. Takeoff and landing attitudes were established as the analysis involved basic wing lift characteristics, and trailing edge flap effectiveness.

A low speed handling quality study was conducted to examine the low speed pitch characteristics of the arrow-wing. To assist in this analysis, the computer graphics set-up shown in Figures 2-10 and 2-11 were employed. This is an in-house facility which was developed during the L-1011 program and has been modified with regard to input data so that it can be used to simulate the behavior of a typical advanced supersonic transport design. The arrangement has the capability of displaying in real time in graphic form on the cathode ray tube the behavior of the airplane longitudinal characteristics in response to control disturbances which are applied and monitored by the operator. Computer set-up allows the operator not only to vary the disturbance inputs into the airplane analysis but also to vary the characteristics of the airplane as well. As shown in Figure 2-11 the weight or inertia of the airplane and the center of gravity location can be changed so that the static stability margin is varied or an unstable airplane characteristic can be investigated. Different horizontal tail sizes can be included to examine the impact of variations in control power on the behavior of the airplane. The use of the aft tail with various levels of pitch trim gain and lead can be examined to establish

15F PLANFORM

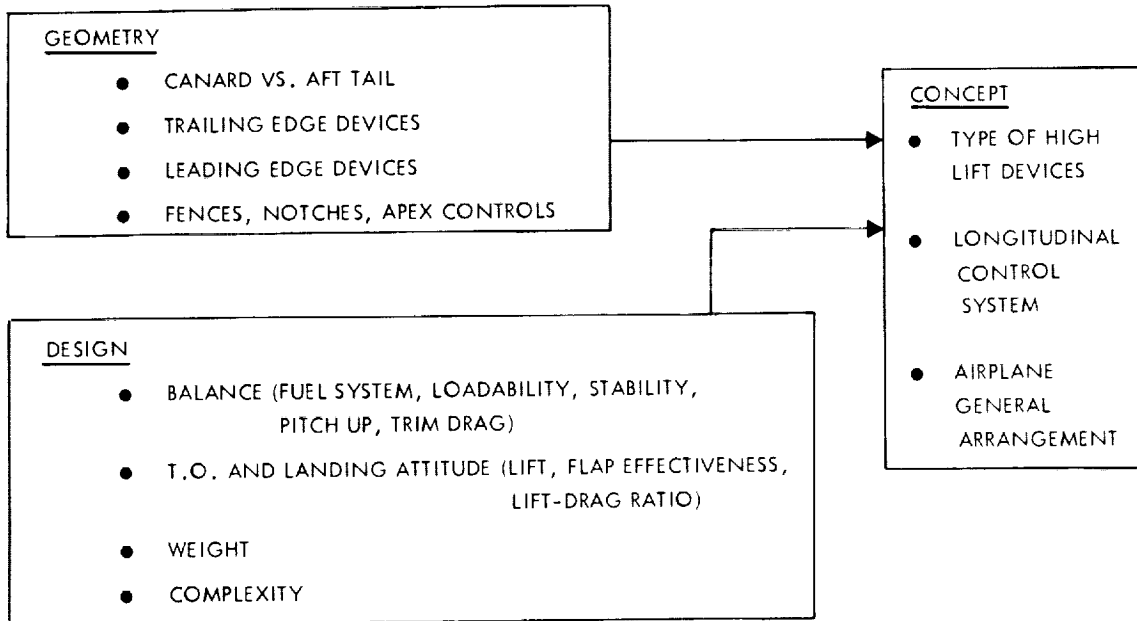


Figure 2-9. Low Speed Longitudinal Characteristics

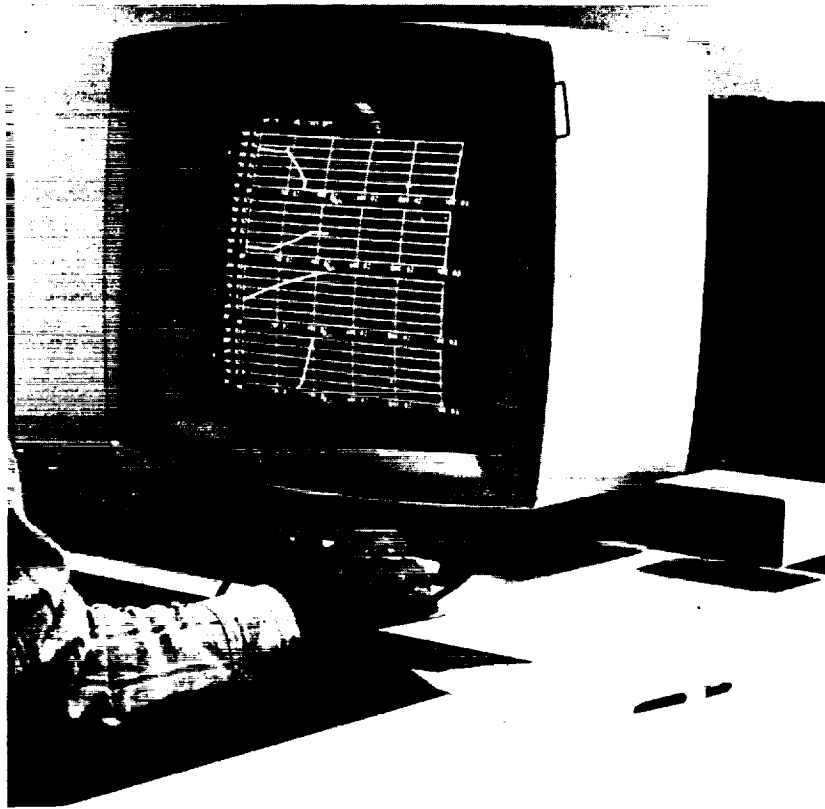


Figure 2-10. Computer Graphics Console — Low Speed Pitch Up Analysis

the use of the empennage as a pitch limiter control. This arrangement provides a design tool that allows the operator to quickly examine many design parameters and get a quick intuitive feeling regarding whether he is making improvements or degrading the characteristics of the airplane. He can rapidly zero in on a proper combination of design parameters.

Figure 2-12 presents typical low speed pitch characteristics for an arrow-wing concept without inboard leading edge treatment for control of pitch up tendencies. For the data shown, a leading edge device is assumed for the wing outer panels only, and wing trailing edge flaps are employed. Noted on the figures are desired levels of  $C_L$  needed for acceptable values of  $V_{MIN}$ ,  $V_{TO}$ , and  $V_{APPROACH}$ . It is seen that operation at or near  $V_{MIN}$  will place the airplane lift needs in the vicinity of the pitch up region.

Studies were run to assess the feasibility of using the horizontal tail as a pitch limiter to provide satisfactory longitudinal control while operating into the pitch up arena. The aforementioned graphic computer program was set up to examine various levels of  $V_{MIN}$ , stall entry rate, airplane weight, tail size, c.g. position, and pitch control rate and gain. Typical curves for various tail sizes are shown in Figure 2-13. If adequate control authority is provided, it is possible to provide automatic pitch limiting capability and satisfactorily provide good handling qualities for an aircraft having the pitch characteristics of Figure 2-12. Two requirements must be met: there are definite tail size and center of gravity relationships that must be met. The pitch limiter system must be fail operative.

Figure 2-14 summarizes the study findings as they relate to the horizontal tail size and balance. Shown are the tail size and center of gravity position relationships that must be observed for various flight conditions. On the basis of these data, a tail volume coefficient of .07 is the minimum desired; the airplane balance should be set so that the center of gravity is at 55-percent MAC.

A planview of the airplane adopted and the identification of the control sur-

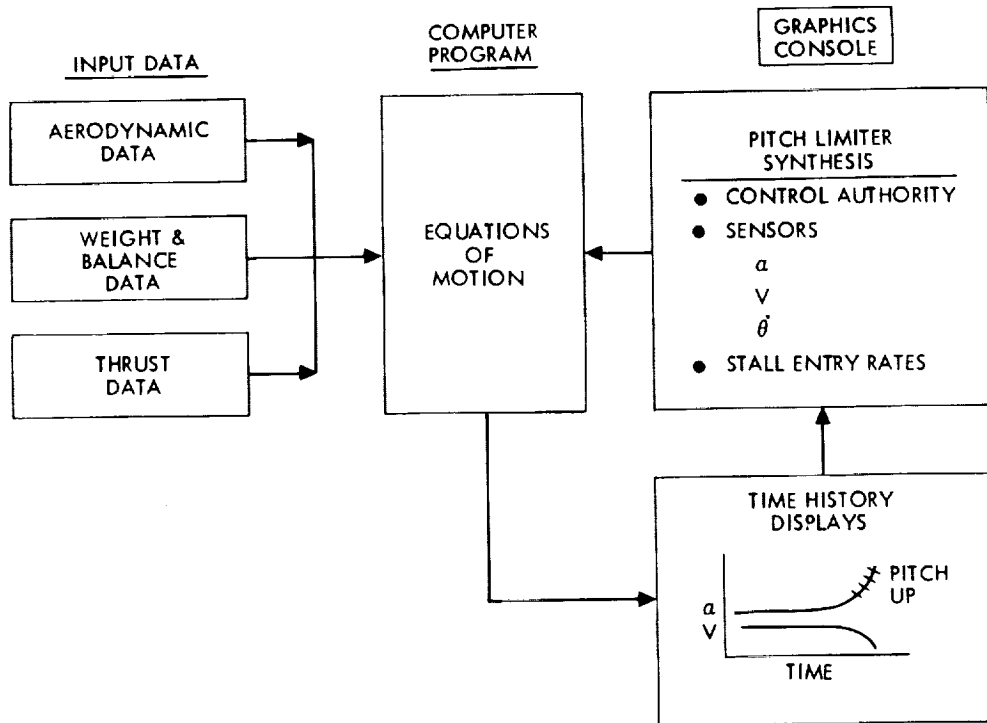


Figure 2-11. Computer Program Logic

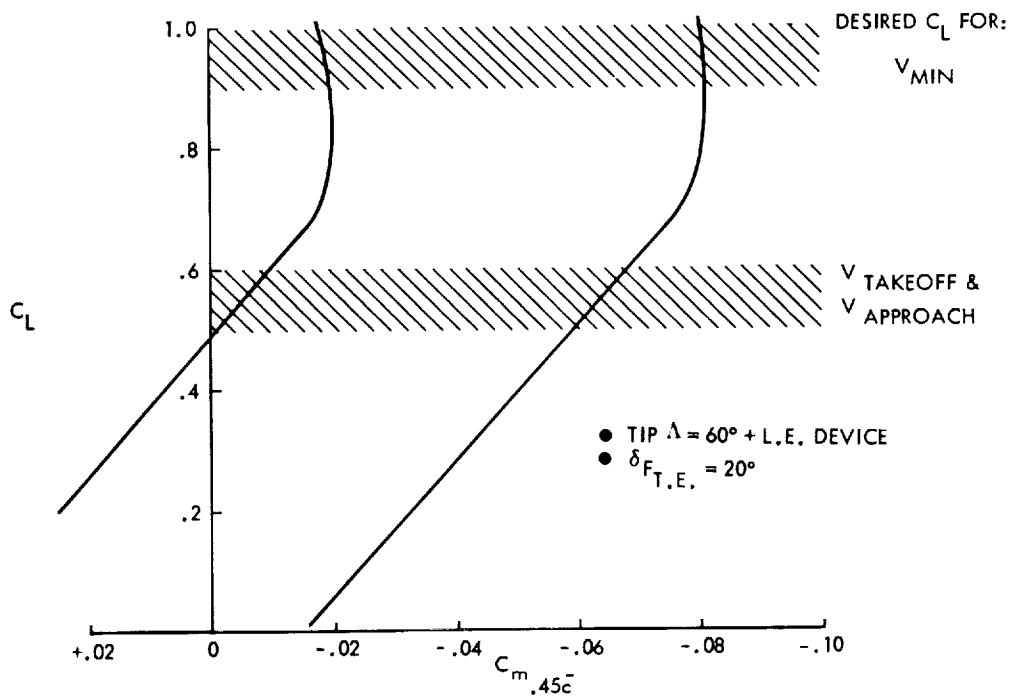


Figure 2-12. Arrow-Wing Pitch Up Characteristics

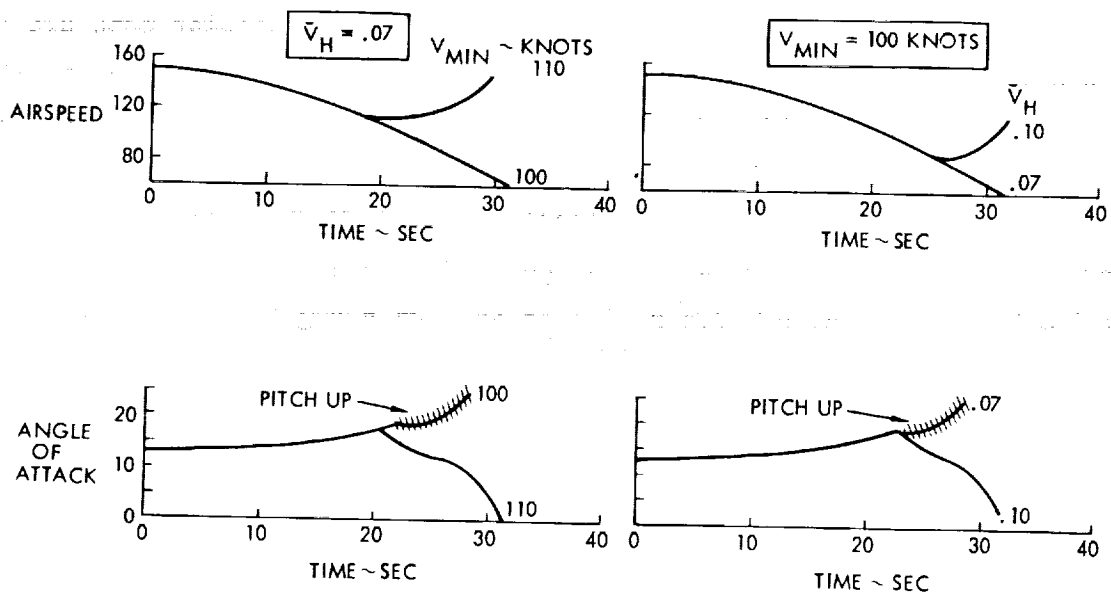


Figure 2-13. Pitch Up Study Results

MAX LANDING WT.

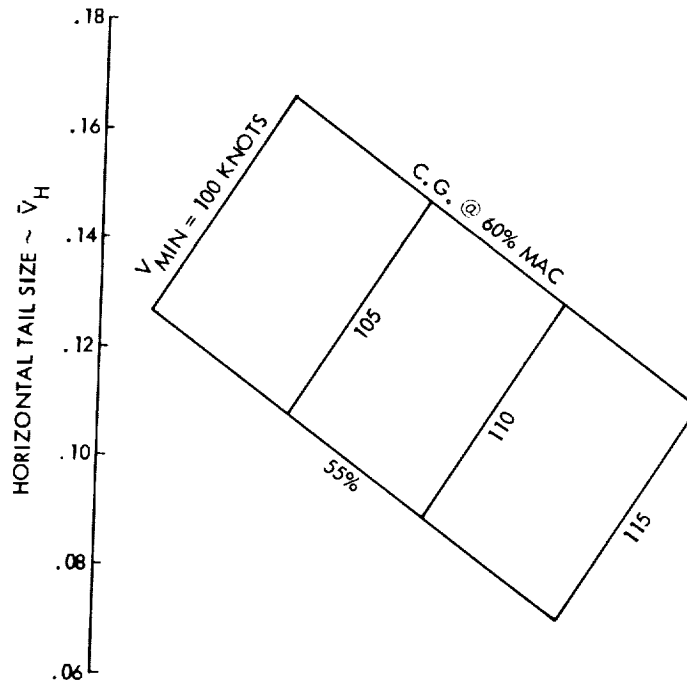


Figure 2-14. Tail Size Criteria

faces on that airplane are shown in Figure 2-15. Of particular note are the following: the wing adopts wing trailing flaps in three elements along the inboard span on either side of the rear mounted engines. Leading edge devices are employed only outboard of the two vertical fins on the wing outer panels. The wing planform adopts a leading edge sweep back angle of 74-degree inboard, 71-degree in the mid-span region, and 60-degree on the outer portion. A one-half percent leading edge radius is adopted along the leading edge. An all movable, geared elevator horizontal tail is employed to provide longitudinal control. This was preferred over that of a large forward canard to provide control and trim because of the need to retract the canard in high speed flight. If the canard were not to be retracted in high speed flight then there would be an undesirable interference of the canard flow on the wing which would degrade the cruise drag efficiency of the arrow-wing concept. As noted on the figure, however, a small canard will probably be required on the forebody to provide ride quality control but the details of this control have not been investigated. It is to be noted that the 15F concept fuselage has been shortened 119 inches. This came about during the balance exercises that were conducted to obtain a manufacturer's empty weight c.g. location at 60-percent of the mean aerodynamic chord.

Some consideration was given to using leading edge flaps inboard on the wing. The available wind tunnel data indicates that the use of wing leading edge flaps provides a means for controlling the pitch-up problem of the arrow-wing. They also provide a small increase in lift-drag ratio at low speeds. However, they also introduce weight and added complexity to the design and operation of the airplane. It was felt that if it could be shown that the leading edge flaps were not necessary to alleviate the pitch-up tendency on the airplane, then their overall value would probably be questionable. A philosophy was therefore adopted to size a proper control system and balance the airplane so that these flaps will not be necessary.

#### Airframe Design Recommendations

As a result of this brief airframe analysis the following design recommendations were adopted.

- The SCAT 15F fuselage should be increased in cross-section area throughout the passenger compartment length so as to provide adequate head room.
- The horizontal tail size of the 15F concept should be increased to provide a tail volume coefficient of .07.
- The fuselage should be shortened 119 inches to reduce fuselage weight and airplane drag.
- A baseline concept should employ the three wheel axle design so as to permit a gear stowage within wing contours.

#### Engine Recommendations

The engine characteristics for the structural study were adopted from the results of the NASA/Lockheed Technology Assessment Studies (Ref. 1). The engine (Figure 2-16), designated BSTF2.7-2, is a duct-burning turbofan with bypass ratio of 3.26, a fan pressure ratio of 3.0, and an uninstalled sea level static thrust of 78,000 pounds. The other relevant engine cycle parameters which are used in the BSTF2.7-2 duct-burning turbofan engine performance are shown in Table 2-1. The basic configuration and dimensions of the BSTF2.7-2 engine, including the methods used for dimensional and weight parametric scaling are presented in Figure 2-17. The maximum engine diameter is 90 inches with an overall inlet and engine lengths of 444.3 inches. An axisymmetric mixed compression inlet is used (Figure 2-18) with a variable convergent-divergent nozzle. The nozzle is rotated 4-degree 15-minutes relative to the engine centerline to permit proper orientation of the nacelles relative to the wing.

The initial studies (Task I) were conducted using the foregoing data which represented a scale-one (1.0) or reference engine. As the study progressed, additional thrust was required for the performance of the aircraft. The en-

TABLE 2-1. ENGINE CYCLE DESCRIPTION - BSTF2.7-2

Uninstalled Sea Level Static Std Day

Maximum thrust		78000
Corrected airflow		1039
Fan pressure ratio		3.0
Compressor pressure ratio		5.0
Overall pressure ratio		15.0
Bypass ratio		3.26
Thrust/Wt ratio		7.0
Fan adiabatic efficiency		0.863
Compressor adiabatic efficiency		0.860
Peak fan polytropic efficiency		0.90
Peak compressor polytropic efficiency		0.90
High pressure turbine adiabatic efficiency		0.91
Low pressure turbine adiabatic efficiency		0.90
Primary burner efficiency		1.00
Duct burner efficiency		0.97
Maximum turbine inlet temperature	°F	2800
Maximum duct burning temperature	°F	1700
Primary burner pressure loss ratio		0.05
Duct burner pressure loss ratio		0.04 - 0.02
Primary nozzle pressure loss ratio		0.005
Nozzle velocity coefficient		.981
Turbine cooling airflow ratio		0.10



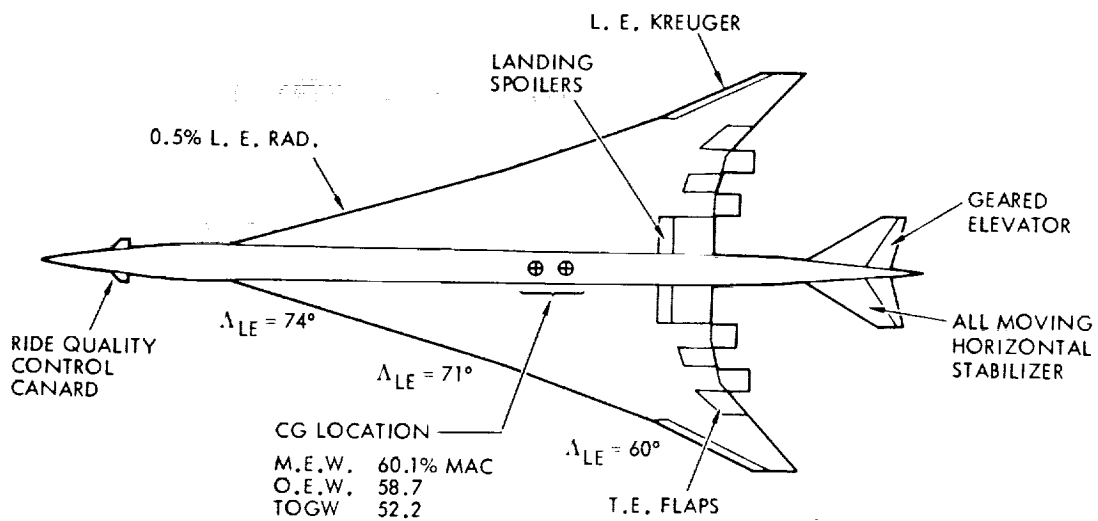


Figure 2-15. Baseline Configuration/Longitudinal Controls

**CONCEPTUAL GAS PATH SCHEMATIC  
FAN PRESSURE RATIO = 3.0**

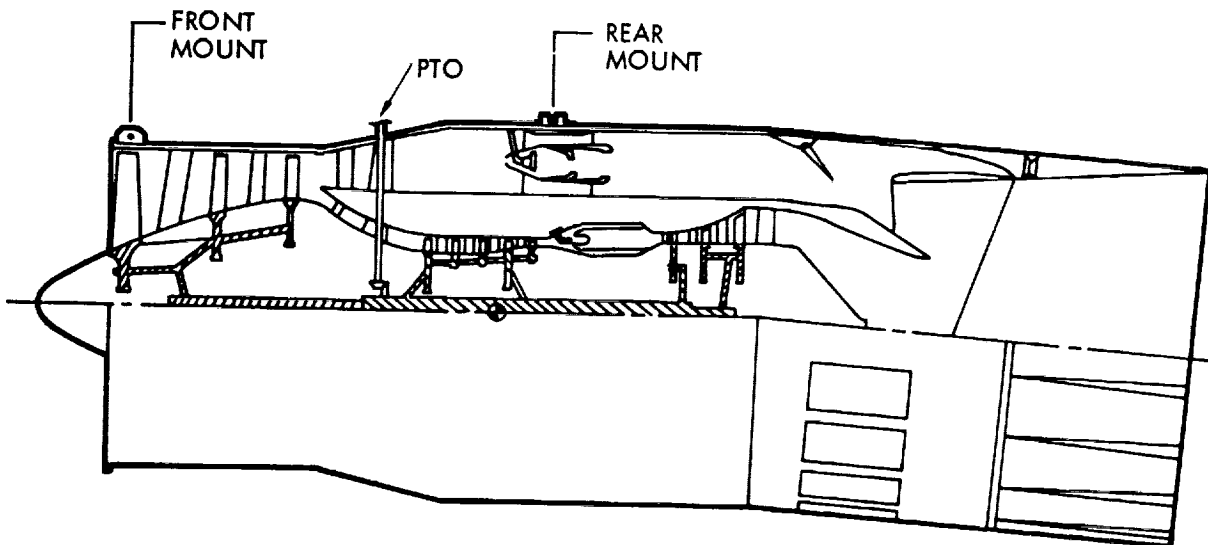


Figure 2-16. Duct Burning Turbofan Engine - Mach 2.7

MACH 2.7 DUCT BURNING TURBOFAN ENGINE

PARAMETER	REFERENCE VALUE
FNSLS MAX	78000 †
F <sub>N</sub> L.O.	59250 *
A <sub>C</sub> , FT <sup>2</sup>	33.1
D <sub>COMP</sub> , IN	79.4
D <sub>MAX</sub> , IN	90.0
D <sub>NOZ</sub> , IN	90.0
L <sub>ENG</sub> , IN	255.0
L <sub>INLET</sub> , IN	189.3
WEIGHT, LB	11143
D <sub>CAP</sub> , IN	77.9

$$DIA = DIA_{REF} \left( \frac{FNSLS}{FNSLS_{REF}} \right)^{0.5}$$

$$LENG = LENG_{REF} \left( \frac{FNSLS}{FNSLS_{REF}} \right)^{0.35}$$

$$L_{INLET} = 2.43 \times D_{CAP}$$

$$WEIGHT = WEIGHT_{REF} \left( \frac{FNSLS}{FNSLS_{REF}} \right)$$

† SLS UNINSTALLED STD DAY  
 \* 0.3 MACH MAX PWR STD + 27F DAY

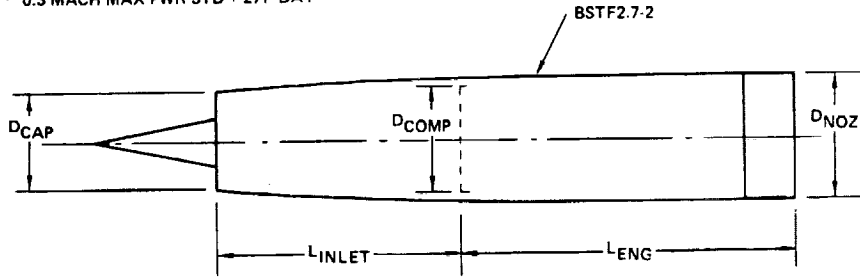


Figure 2-17. Nacelle Dimensions and Scaling Data — BSTF 2.7-2

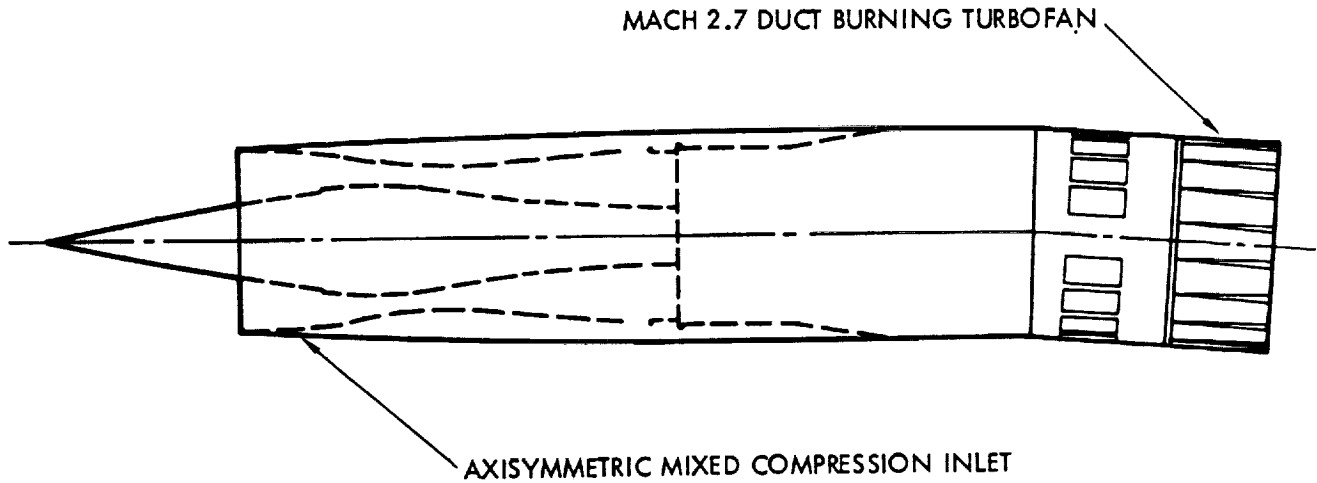


Figure 2-18. Preliminary Nacelle

gine designated BSTF2.7-2/scale-1.147 with an uninstalled sea level static thrust of 89,466 pounds was adopted for the Task II effort. The engine parameters for this larger engine are shown in Table 2-2.

The installed engine performance data for the BSTF2.7-2 duct-burning turbofan are presented in Reference 1. Engine data are provided for a standard + 14.4 F hot day and for a full range of Mach numbers (0 to 2.62) and altitudes (sea level to 80,000 feet). Takeoff data is also provided for a standard + 27 F hot day, static to Mach 0.6 and sea level to 6,000 feet altitude. The data are also available as an engine performance card deck for use in both the ASSET and Aerodynamic Mission Program.

TABLE 2-2. PROPULSION SYSTEM PARAMETERS

Engine:	BSTF 2.7-2 duct burning turbofan	
Number of engines:	4	
Noise suppression:	FAR 36-5	
Inlet/nozzle:	Axisymmetric/variable convergent-divergent	
Thrust/weight - (lift off):	0.36	
Lift of Speed:	Mach 0.30	
Scale Factor:	1.0 (Ref.)	1.147
Net thrust, lb. (A)	78,000	89,466
Engine weight, lb. (B)	11,143	12,781
ACAP, ft <sup>2</sup>	33.1	38.0
DMAX, in.	90	96.4
DCOMP, in.	79.4	85.0
DNOZ, in.	90	96.4
LENG, in.	255	267.5
LINLET, in.	189.3	203.9
Study Application	Task I	Task II

(A) SLS, Max. Power, uninstalled

(B) Includes reverser and suppressor

## BASELINE CONFIGURATION - TASK I

The airframe and engine recommendations adopted for defining the Baseline Configuration for Task I include only those refinements to the NASA 15F concept that would have primary influence on the study objectives:

- To assess the relative merits of the various structural design concepts and
- To identify the importance of the interactive parameters that influence the design of a supersonic cruise aircraft.

The configuration refinements that were adopted and impacted the NASA 15F configuration concept include:

- Fuselage cross section refinements to provide adequate head room
- Advanced main landing gear concept to avoid external contour deviations
- Horizontal tail volume ( $\bar{V}_H$ ) to provide pitch control power for envelope limiting requirements
- Duct burning turbofan engine, designated BSTF2.7-2/1.0, with an uninstalled sea level static thrust of 78,000-pounds.

The other recommended refinements and the results of the Stability and Control Analysis and Propulsion-Airframe Integration subtasks were used to define the Baseline Configuration for Task II.

### General Arrangement

The configuration shown in Figure 2-19 is a discrete wing-body airplane with a low wing that is continuous under the fuselage. For initial design purposes, the airplane has a taxi mass of 340,000 kilograms (750,000 pounds), a landing mass of 191,000 kilograms (420,000 pounds), a design range of 7800 kilometers (4200 n. miles), and a payload of 22,000 kilograms (49,000 pounds). Overall dimensions include a length of 90.5 meters (296.93 feet) and a wing span of 40.4 meters (132.55 feet).

The configuration is modified from the NASA configuration deck with respect to the fuselage external shape, cant of the engines and wing fins, and size of the horizontal and fuselage mounted vertical tails.

A preliminary definition of the primary control surfaces are indicated. An all moving horizontal stabilizer with a geared elevator is used for pitch control. For yaw control, a fuselage mounted all moving vertical tail is provided. The tail volumes for the horizontal stabilizer ( $\bar{V}_H$ ) and vertical tail ( $\bar{V}_V$ ) are 0.07 and 0.024, respectively. The inboard trailing edge panels are used as lift flaps at low speed. Leading edge flaps are provided on the outer wing for subsonic and transonic speeds, and ailerons on the trailing edge for low speed.

The wing mounted main landing gear retracts into a well just outboard of the body. Four duct-burning turbofan engines, each with 346,770 newtons (78,000 lbs.) of uninstalled thrust, are mounted in underwing pods having axisymmetric inlets and thrust reversers aft of the wing trailing edge. The engines are sized to provide a takeoff thrust-to-weight ratio of 0.36.

Dimensional data in the NASA data deck are given with respect to X, Y, and Z axes. However, most fuselage frames, wing spars and other structural elements are located in planes which are normal to the main cabin floor. Therefore, a coordinate system: fuselage station (FS), waterline (WL) and butt line (BL), was established designating the top of the main cabin floor as WL 300. The main cabin floor is a flat plane which is approximately 0.152 meters (0.50 feet) above the upper wing surface. Figure 2-19 shows the correlation of the  $Z_0$  and WL planes.

#### Basic Dimensions

Significant dimensional data are defined in the basic dimensions drawing (Figure 2-20). As noted previously, all dimensional data are given in fuselage station (FS), waterline (WL) and butt line (BL) coordinates, rather than the

X, Y, Z coordinates used in the NASA data deck, because fuselage frames, wing spars and most other structural elements will be located in FS planes which are normal to the main cabin floor.

The external configuration of Figure 2-20 is identical to that of the Reference Configuration except for the refinements adopted and as previously discussed. The fuselage nose reference is established at F.S. 160.

To ensure coordination, the basic dimensions drawing was used as the master reference for all subsequent drawings prepared for the Task I Analytical Design Studies effort.

A fuselage dimensional data drawing (Figure 2-21) was prepared to supplement the basic dimensions data. A comparison of the fuselage configuration for the Reference Configuration and the Baseline Configuration - Task I is presented. Note the contour refinements adopted at the nose landing gear region, the significant changes at FS 1234, and the Floor Reference Plane (FRP) at W.L. 300.

#### Fuel Tank Arrangement

Based on previous studies relating to fuel containment and management requirements for supersonic cruise aircraft, it was elected to stow a significant portion of the total fuel within the wing center section, between the sides of the fuselage. In this location, the upper surface of the wing tanks (the wing upper surface) is exposed to the cooled and controlled environment of the fuselage cabin while the wing lower surface (the bottom wall of the tanks) is shielded from the outside air stream by a fairing extending below, and separated from, the wing lower surface. Stowage of the maximum amount of fuel in this "protected" location permits the fuel to be most effectively used as a heat sink. The efficient use of the heat sink capacity of the fuel is considered highly desirable because the use of alternate cooling provisions could require significant effects relative to weight, cost and volume. A pre-

vious study for the L-2000-7A airplane demonstrated the high effectiveness of using the fuel as a heat sink.

The fuel tank arrangement (Task I) developed is one of several alternates considered and is based on the following design objectives:

- A maximum amount of fuel in "protected" stowage in the wing center section while still allowing adequate baggage stowage space in the bottom of the fuselage between the nose gear and the fuel.
- A "dry bay" (no fuel) completely around the main landing gear (MLG) compartment to isolate fuel stowage from the MLG support structures.
- Stowage of fuel in the inboard (deeper) portion of the wing whenever possible to minimize the ratio of exposed tank area to stowage volume.
- A minimum number and compact arrangement of tanks to minimize fuel system plumbing and components as well as tank sealing problems.

In the tank arrangement of Figure 2-22, no fuel is stowed outboard of the MLG. This approach minimizes the structural weight penalties associated with the large fuel loads and the cutout in the lower surface for the MLG. Another reason is a desire to have the capability of routing functional systems from the engines forward through the wing as well as inboard along the rear beam. This approach minimizes the access door requirements in the heavily loaded wing box aft of the MLG cutout.

Tanks 1 through 4 in Figure 2-22 are separate feed tanks of very nearly equal capacity. A fifth tank in the center section was established because it was not possible to obtain four equal tanks in the fuselage while reserving a 34-inch wide strip for the ECS components at the forward end of the MLG cutout. Fuel tanks are configured to utilize existing locations of structural elements, i.e., fuel tank walls are positioned at rib and spar locations already estab-

lished as needed for other purposes.

Fuel was not stowed in the forward apex of the wing with this space reserved for a ballast tank which might be found necessary as a result of subsequent evaluations. The tank arrangement provides stowage for 181,391 kilograms (399,900 lbs.) of usable fuel, 37-percent of which is in the protected center section. Usable capacity is taken as 90-percent of the gross volume of the tanks. Surge spars and ribs, as well as tank access doors, are provided within tanks.

Fuel management scheduling for airplane center-of-gravity (c.g.) control is specifically planned to maximize the available heat sink capacity of the fuel by emptying the exposed outboard tanks as early as possible in the flight. Additional considerations include fuel usage to permit the aircraft to cruise with a minimum of trim drag penalty. The landing and reserve fuel is located in the protected fuselage area.

Fuel stowage in the center section, below the fuselage, is considered acceptable from the standpoint of safety. This is based on precedents such as the L-2000-7A, the DC-10 and various other aircraft with fuel stowage in the center section below the fuselage. Adequate design features, such as vapor barriers, obviously are required. In addition, the fairing below the fuselage is separated from the wing lower surface and contains a keel for energy absorption and protection of the tanks in the event of ground contact. Also, the nacelles provide some protection during a "belly-landing".

The major portion of the lower fuselage is used for fuel and baggage stowage, with baggage and other requirements establishing the forward limit of fuel stowage. Forward of the fuel stowage area, the wing does not extend through the fuselage.

#### Interior Arrangement

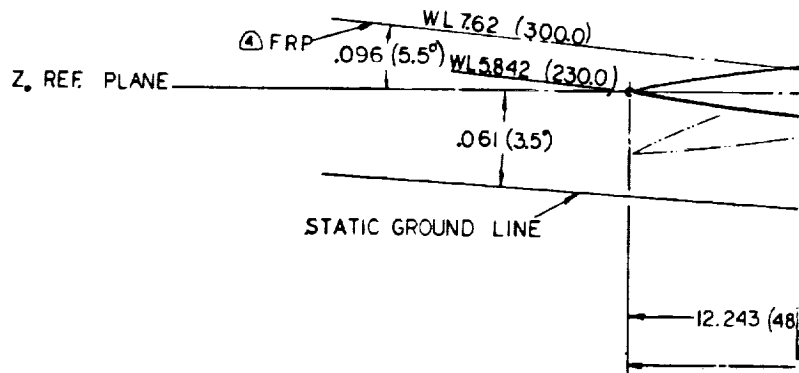
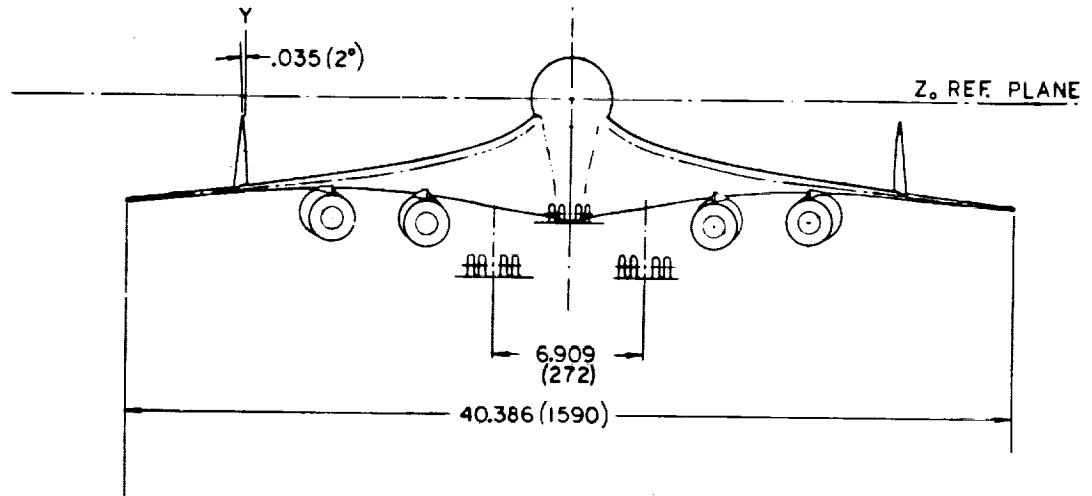
Definition of the major interior details are shown in Figure 2-23 to provide a



# CHARACTERISTICS

POWER PLANT - DUCT BURNING TURBO FAN  
 UNINSTALLED THRUST - 346,770 NEWTONS (77,957 LBS) SLS  
 TAXI MASS - 340,000 KILOGRAMS (750,000 LBS)

	WING	HORIZ TAIL	FUS VERT TAIL	WING VERT TAIL (EACH)
AREA - M <sup>2</sup> (FT <sup>2</sup> )	1005.4 (10,822)	73.868 (795)	26.94 (290)	21.65 (233)
ASPECT RATIO	1.62	1.707	0.517	0.495
TAPER RATIO	0.08	0.225	0.23	0.136
SPAN - M (IN)	40.386 (1590)	11.217 (441.6)	3.719 (146.4)	3.277 (129.0)
ROOT CHORD - M (IN)	55.766 (2195.5)	10.739 (422.8)	11.737 (462.1)	11.643 (458.4)
TIP CHORD - M (IN)	4.460 (175.6)	2.416 (95.1)	2.70 (106.3)	1.585 (62.4)
MAC - M (IN)	34.488 (1357.8)	7.455 (293.5)	8.161 (321.3)	7.889 (310.6)
LE SWEEP	(1.292 (74°)	1.058 (60.64°)	1.190 (68.2°)	1.281 (73.42°)
RADIANS (DEGREES)	1.236 (70.84°)	(1.128 (64.64°)		



ORIGINAL PAGE IS  
 OF POOR QUALITY

FOLDOUT FRAME



E

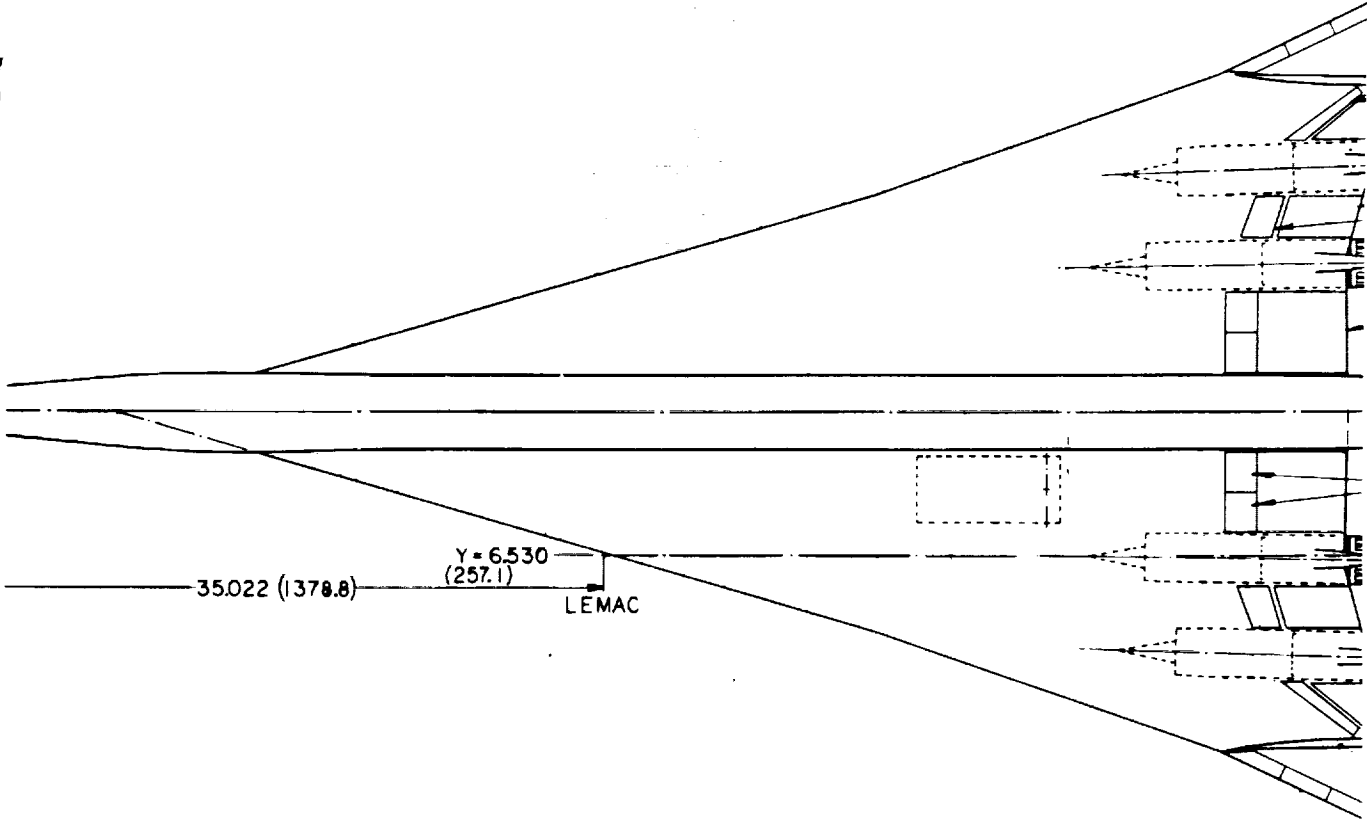
I

E

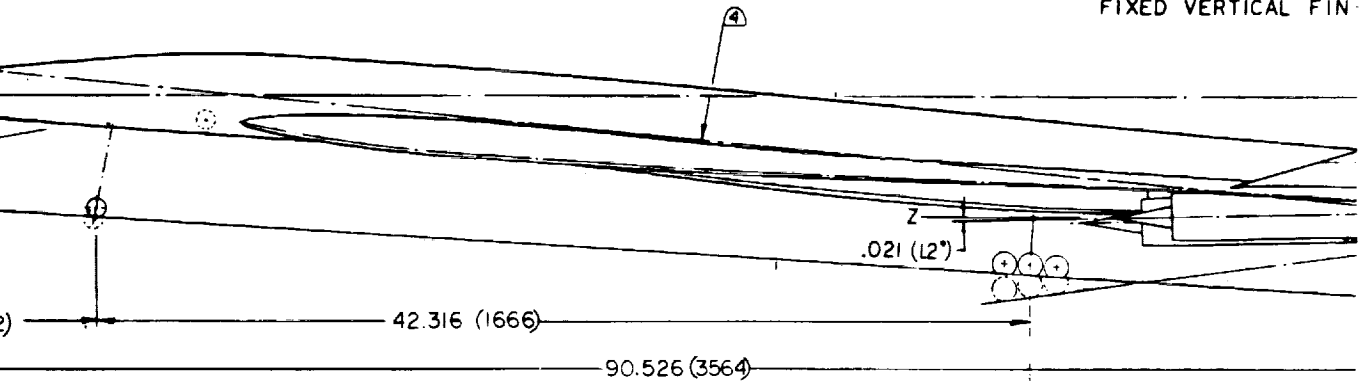
I

U

I



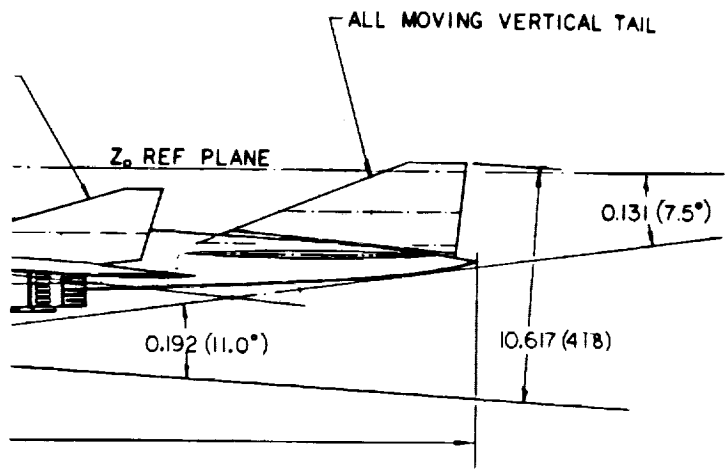
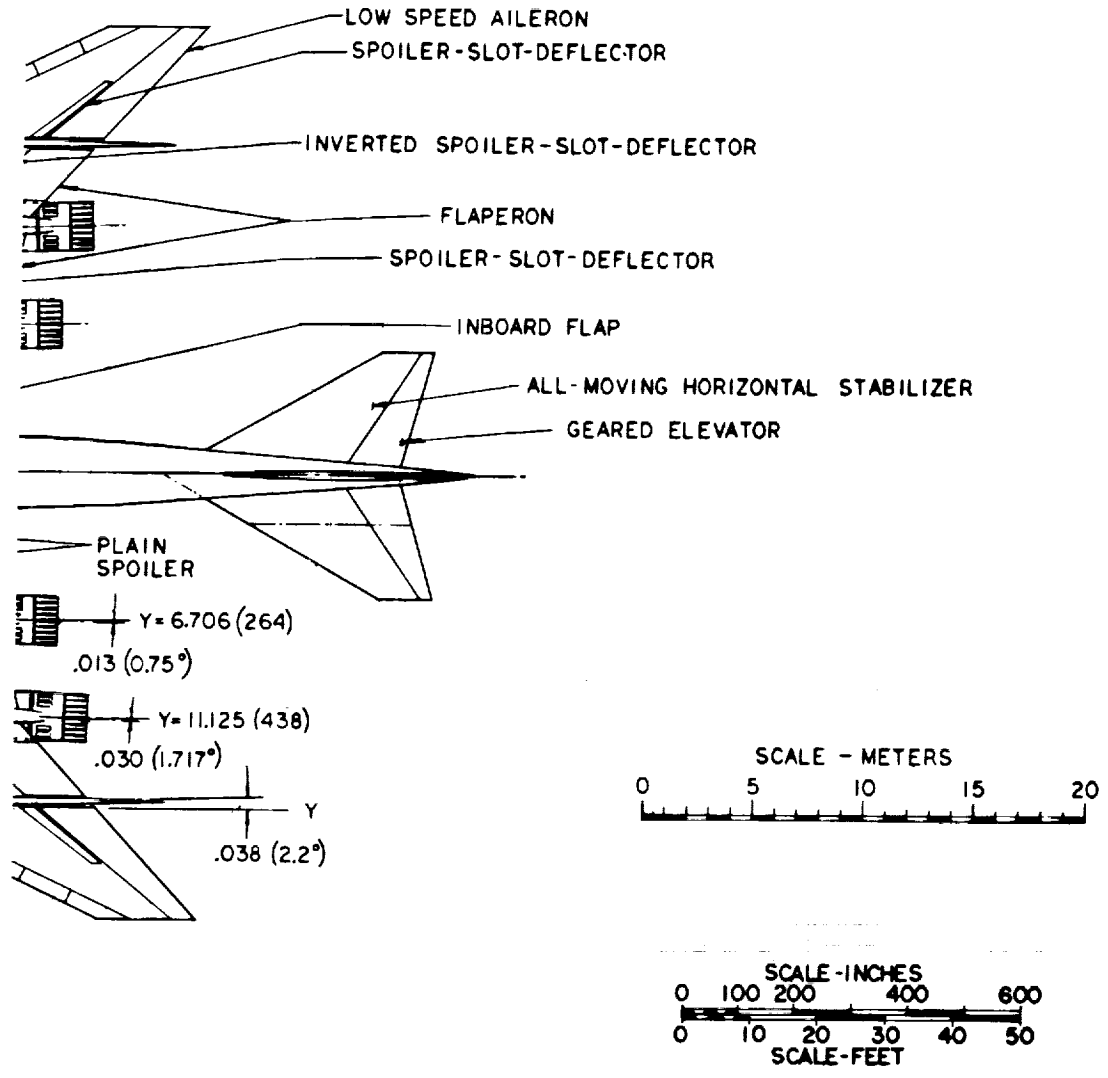
FIXED VERTICAL FIN



U

FOLDOUT FRAME 2





- ④ FLOOR REF PLANE (FRP) IS TOP OF FLOOR.
  - 3. ALL DIMS IN X-Y-Z COORDINATES.
  - 2. CONFIGURATION BASED ON ORIGINAL RELEASE OF DWG CL1607-5-1.
  - 1. DIMENSIONS IN SI (ENGLISH) UNITS.
- NOTE

Figure 2-19. General Arrangement - Task I

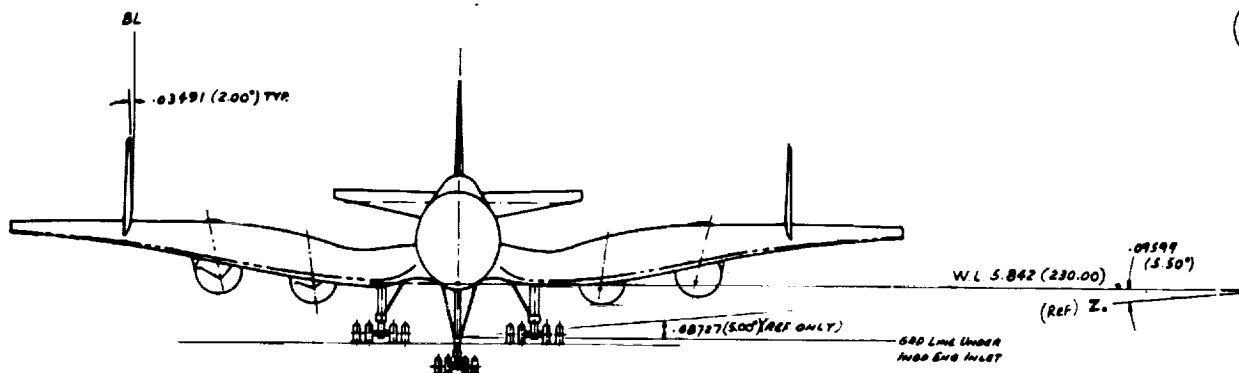


BL 0.00



SCALE

$\frac{1}{100}$



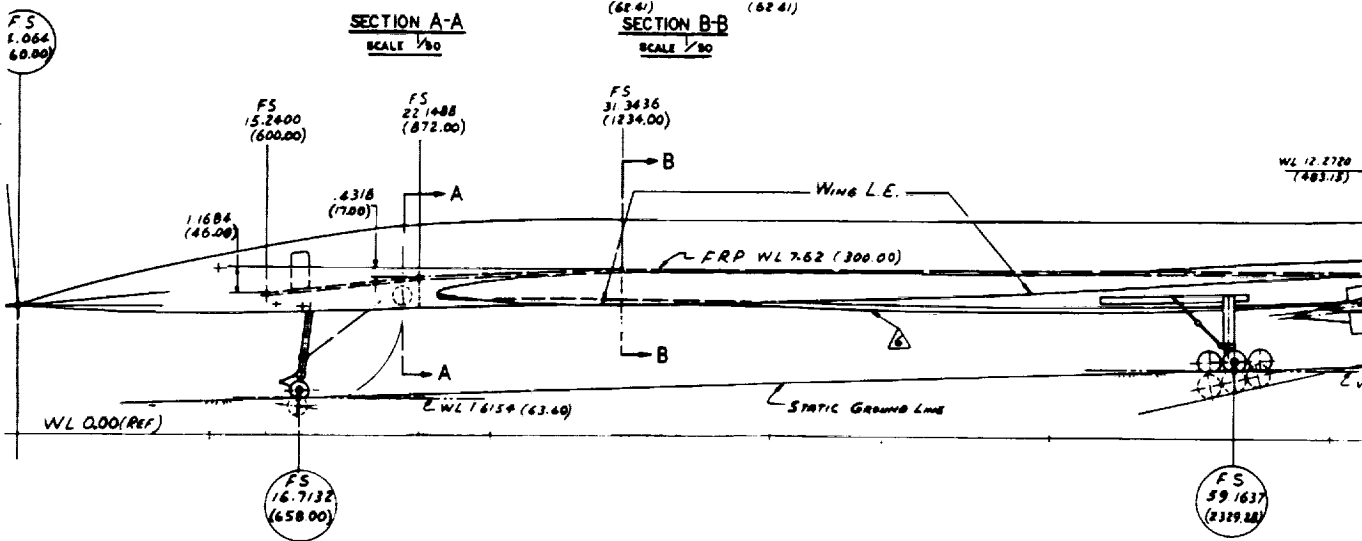
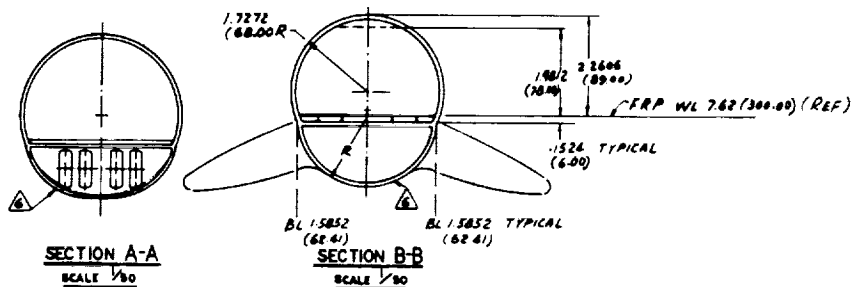
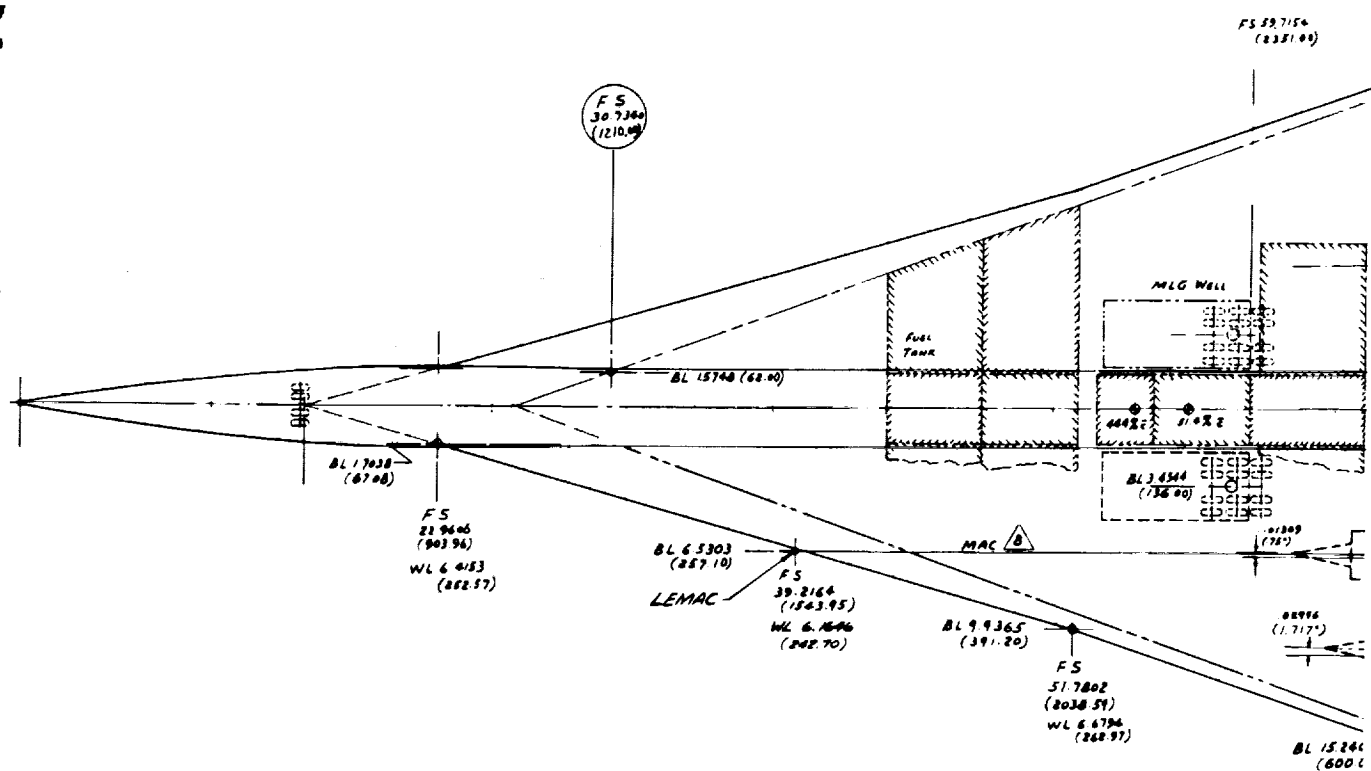
ORIGINAL PAGE IS  
OF POOR QUALITY

PRECEDING PAGE BLANK NOT FILMED

FOLDOUT FRAME /





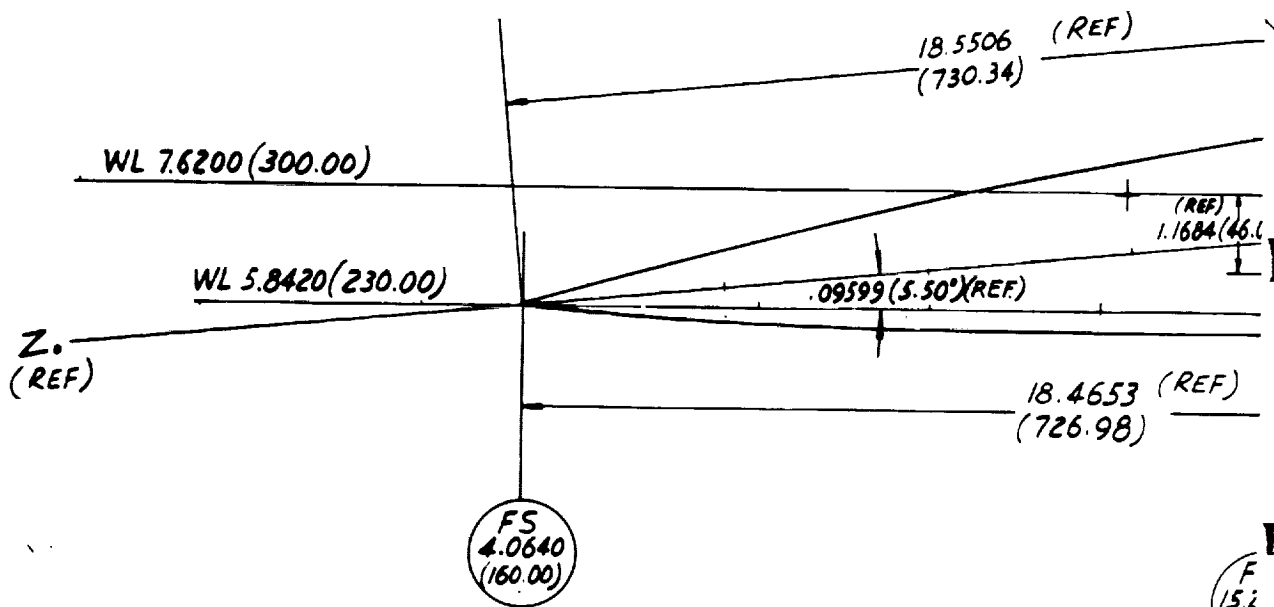


FOLDOUT FRAME 2







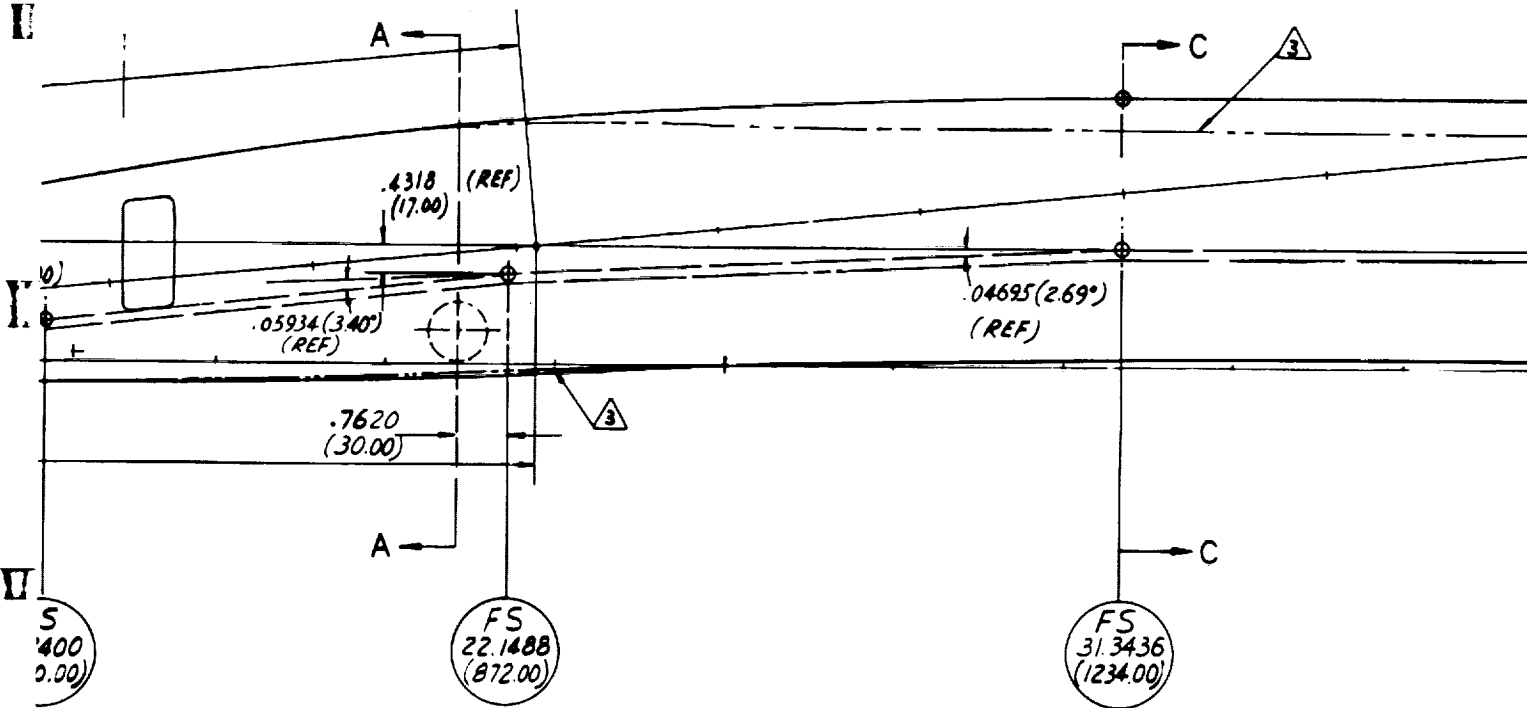
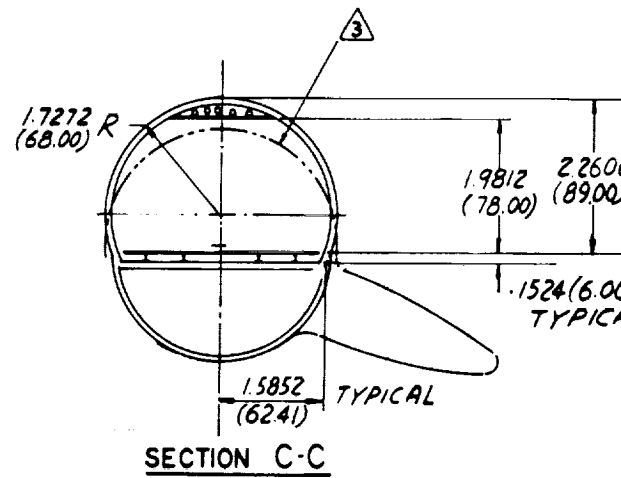
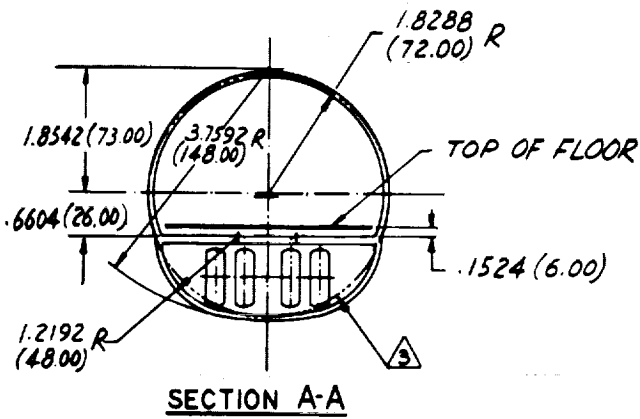


ORIGINAL PAGE IS  
OF POOR QUALITY

PRECEDING PAGE BLANK NOT FILMED

FOLDOUT FRAME )





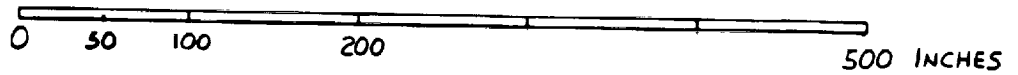
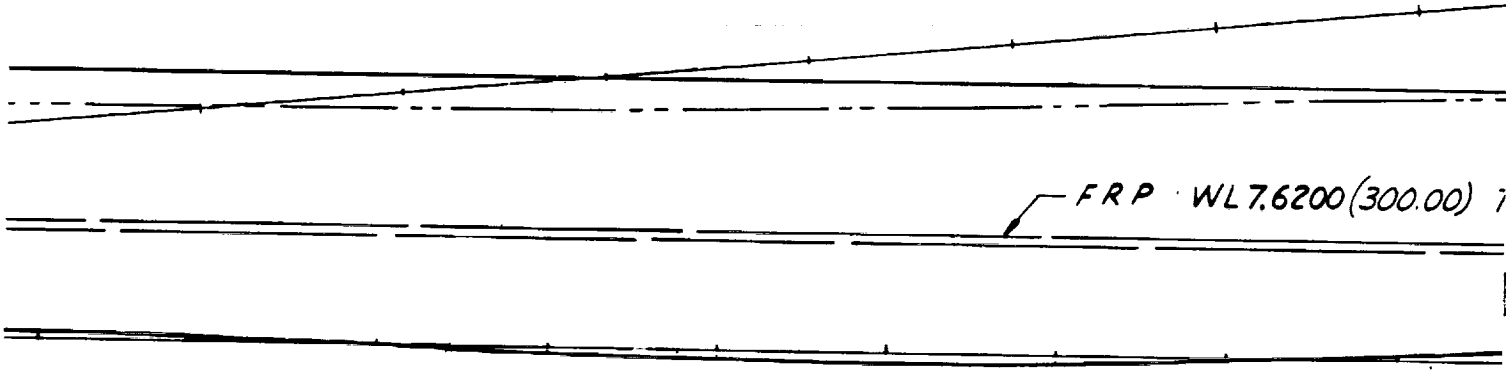
FOLDOUT FRAME 2





TYPICAL  
FROM FS 31.3436 (1234.00) TO FS 64.8970 (2555.00)

└ FRP WL 7.6200 (300.00)

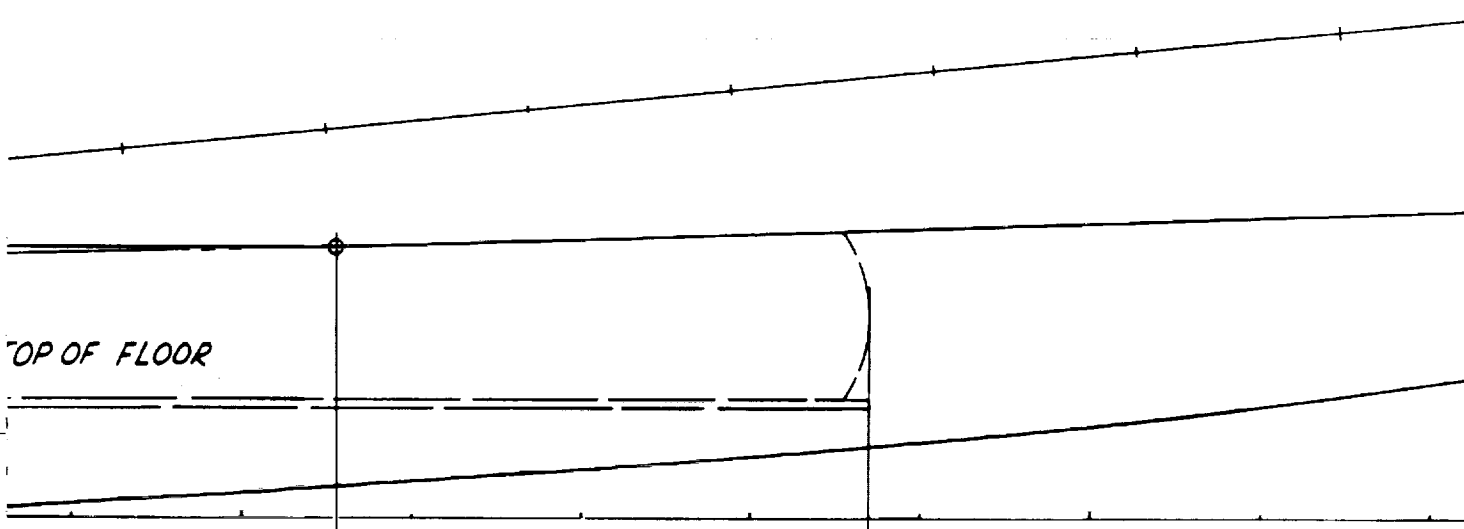


SCALE  $\frac{1}{50}$

BOLYOUT FRAME 3



E  
E  
E  
E  
E  
E  
E  
E  
E  
E  
E



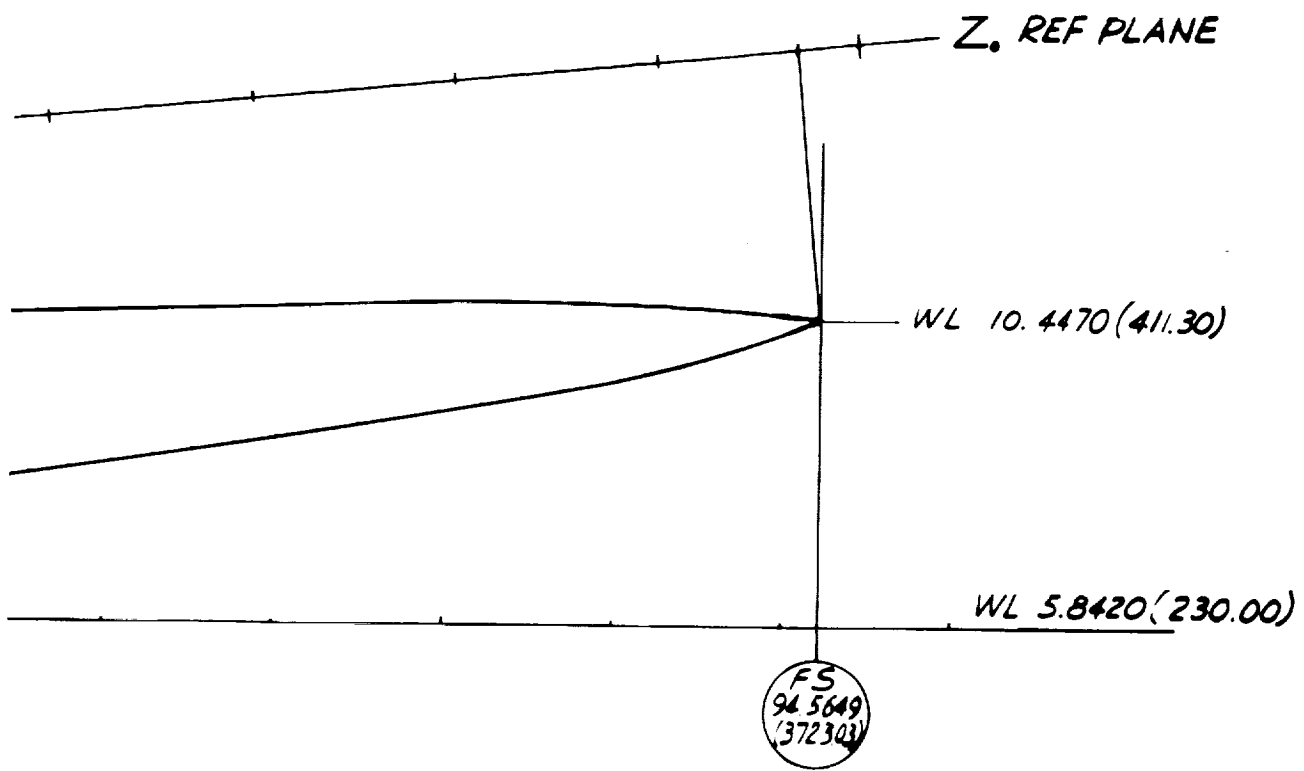
FS  
64.8970  
(2555.00)

FS  
72.8980  
(2870.00)

3. -----  
2. FOR C  
CONF  
1. DIMEN  
NOTE

OUT FRAME 4

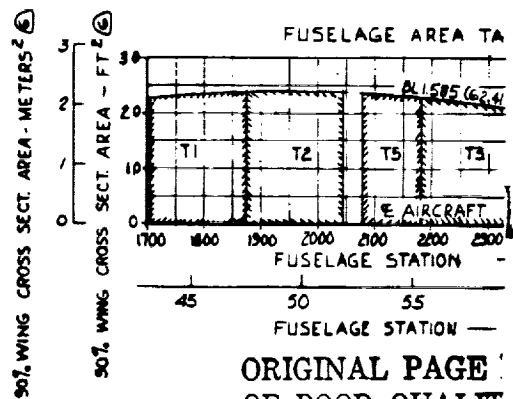
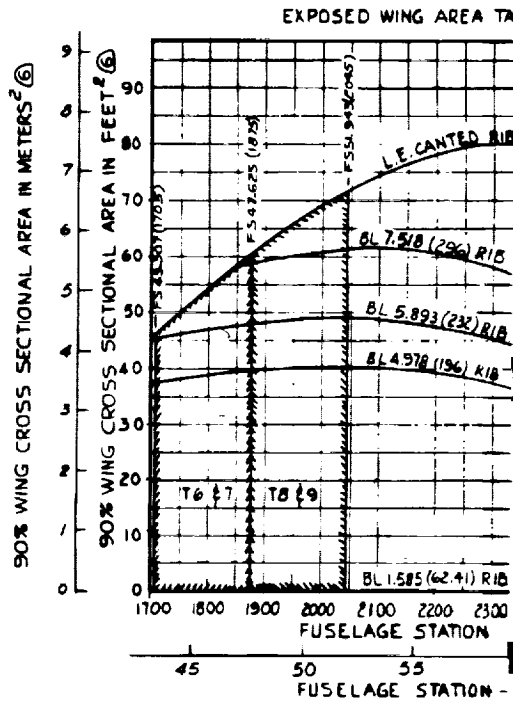
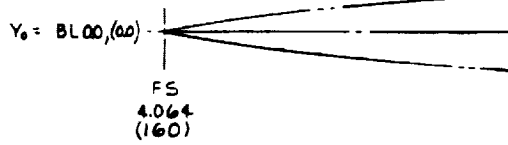




CONFIGURATION PER NASA DATA DECK.  
 COMPLETE NASA DATA DECK  
 DURATION, SEE DWG CL1606-3-5.  
 UNITS IN METERS (IN.) & RAD (DEG).

Figure 2-21. Fuselage Dimensional Data - Task 1





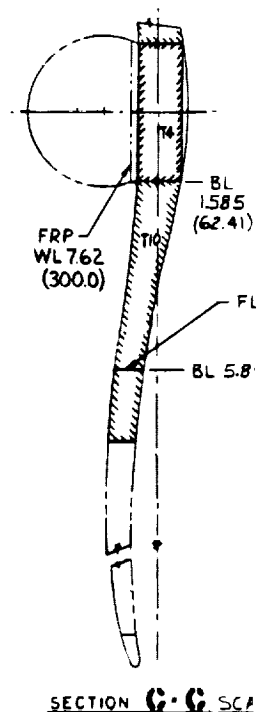
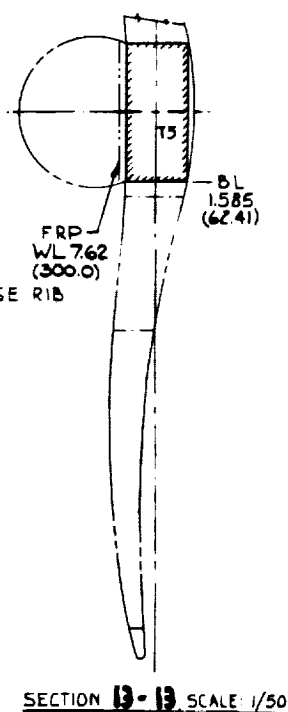
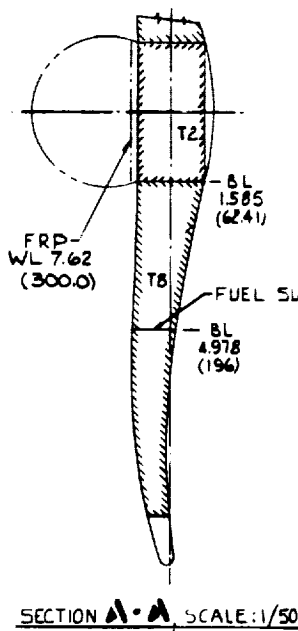
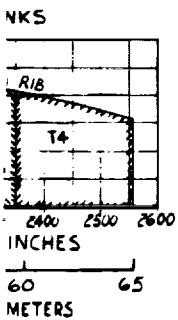
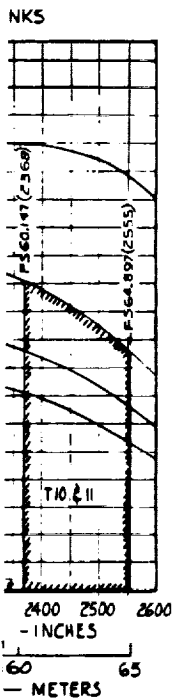
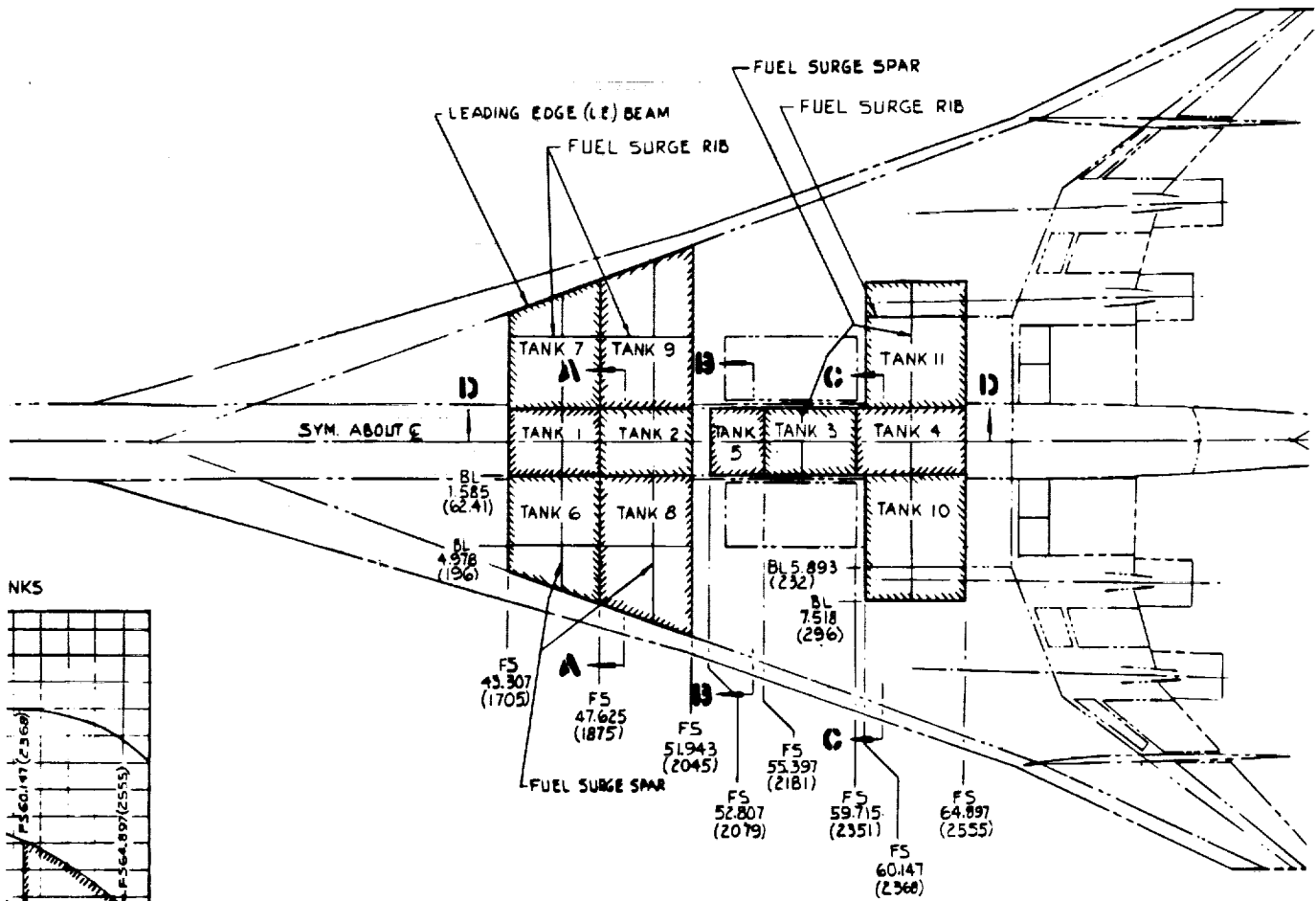
ORIGINAL PAGE OF POOR QUALITY

PRECEDING PAGE BLANK NOT FILMED

FOLDOUT FRAME |



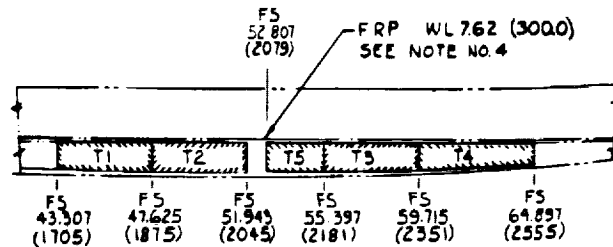
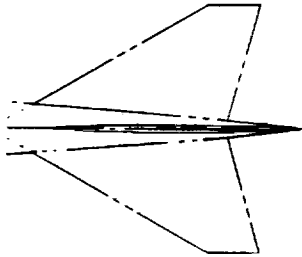






FUEL CAPACITY @  
(NASA CARD DECK COLD)

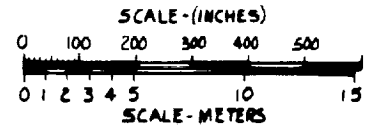
TANK NO.	QUANTITY		MASS	
	LITERS	GALLONS	KILOGRAMS	POUNDS
1	18,700	4,940	15,014	33,100
2	19,097	5,045	15,332	33,800
3	17,685	4,672	14,198	31,300
4	17,908	4,731	14,379	31,700
5	11,299	2,985	9,072	20,000
6	21,637	5,716	17,373	38,300
7	21,637	5,716	17,373	38,300
8	26,838	7,090	21,546	47,500
9	26,838	7,090	21,546	47,500
10	22,148	5,851	17,781	39,200
11	22,148	5,851	17,781	39,200
TOTAL	225,940	59,687	181,397	399,900



SECTION D-D

FUEL SURGE RIB

33 (232)



- ① NET USABLE FUEL CAPACITY FIGURED AT 90% OF GROSS VOLUME.
- ② FUEL FIGURED AT .803 KILOGRAMS/LITER OR 6.7 LBS/GALLON.
- ③ FOR BASIC DIMENSIONS OF AIRCRAFT SEE DRAWING CL1606-3-3 & FOR BASIC PROFILE CUTS SEE DRAWING 1606-3-5.
- ④ [Hatched Box] INDICATES FUEL TANK BOUNDARIES.
- ⑤ DIMENSIONS ARE METERS (INCHES).
- ⑥ FUEL CAPACITY BASED ON NASA ARROW-WING 733-336 C FOLLOW-ON CARD DECK WITHOUT ANY CHANGES.

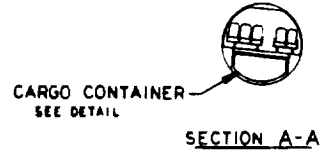
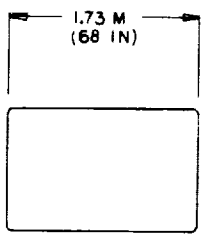
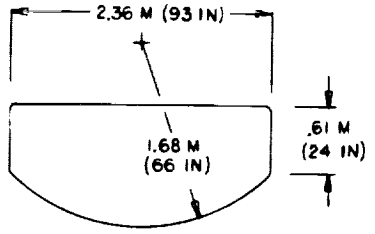
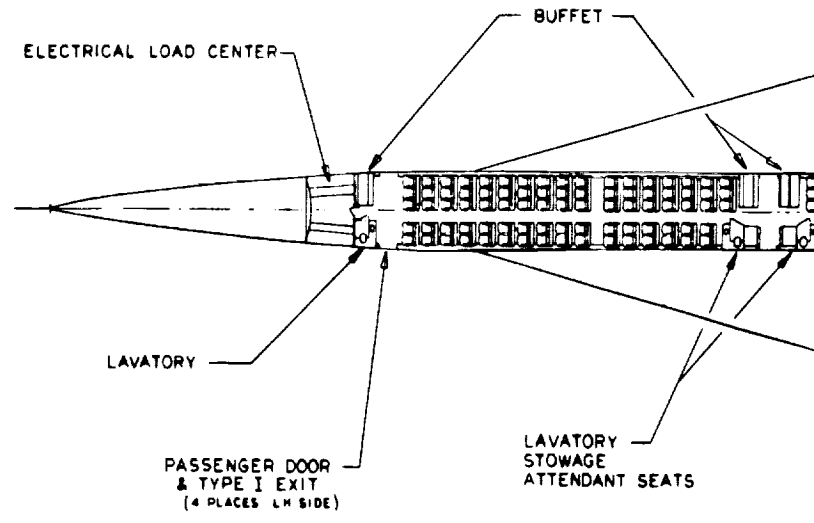
SCALE: 1/50

NOTES:

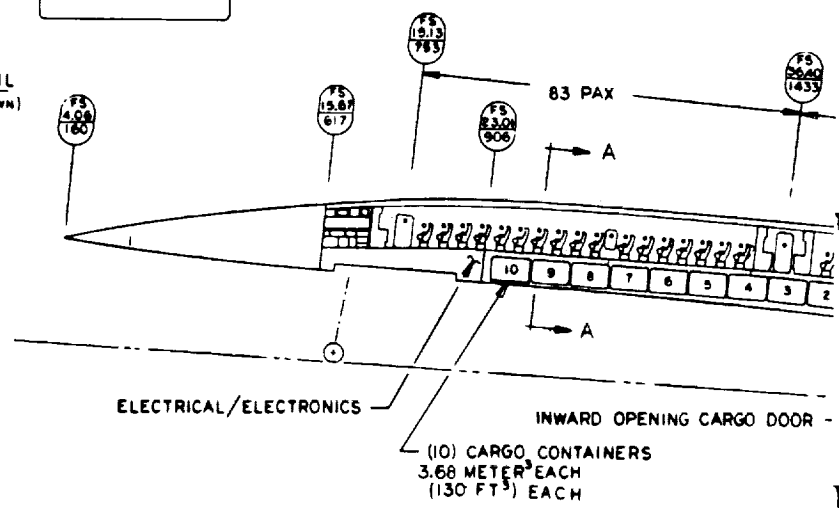
FOLDOUT FRAME

Figure 2-22. Fuel Tank Arrangement - Task I





CONTAINER DETAIL  
(OUTSIDE DIMS SHOWN)

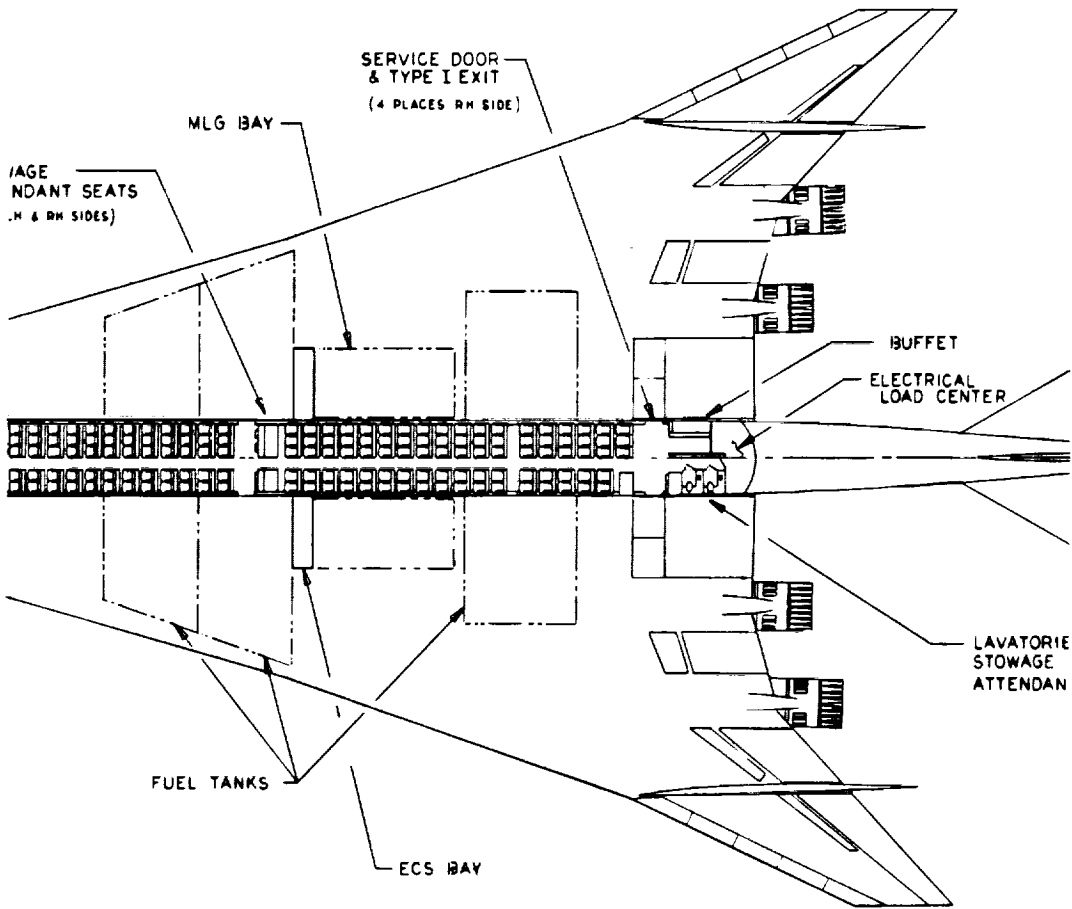


ORIGINAL PAGE IS  
OF POOR QUALITY

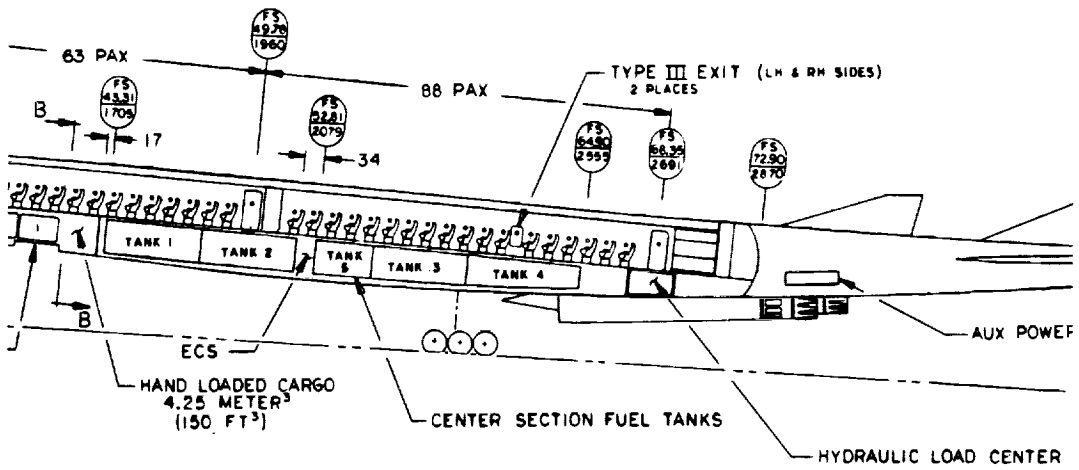
PRECEDING PAGE BLANK NOT FILMED

FOLDOUT FRAME )





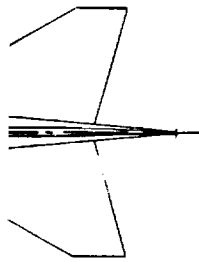
SECTION B-B



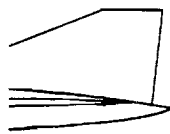
NOTE



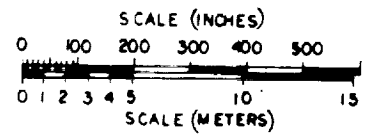





5  
T SEATS



UNIT



2. FUS STA INDICATED BY   
 1. PAYLOAD = 22000KG (49000 LBS)

FOLDOUT FRAME 2

Figure 2-23. Interior Arrangement - Task I



realistic and representative study aircraft. Space allocation for 22,000 kilograms (49,000 pounds) of payload is provided considering the specific requirements including:

- Establishment of the pressurized area of the fuselage
- Location of passengers, baggage and equipment for use in c.g. and weight distribution calculations.
- Determination of entry doors, exits and access doors for use in studies of the fuselage and wing structure
- Space allotment required for the routing of functional systems

The seating layout is based on 234 passengers at 5-abreast seating and a seat pitch of 34 inches. The cabin has a constant cross section shape over much of the central fuselage and thus provides for an efficient seating arrangement as well as cost reduction through reduced metal forming and the multiple usage of many parts.

Baggage and fuel stowage utilize the major portion of the fuselage below the floor. Baggage is stowed as far forward as possible to maximize the fuselage fuel carried in the center section. The baggage loading door is located near the aft end of the compartment so that an internally stowed door can be used along with 10-equal-sized containers with a capacity of 3.68 cubic meters (130 cu. ft.) each. Bulk cargo space of 4.25 cubic meters (150 cu. ft.) is provided just aft of the baggage loading door. For maximum space utilization, a baggage container is stowed above the access door.

The location of major service centers as well as the space contingency allowed between the baggage and fuel stowage areas are also shown. Just forward of the MLG well, a 34-inch wide strip of wing and fuselage is reserved for installation of ECS units. An Auxiliary Power Unit (APU) is located in the lower aft fuselage to minimize the exhaust problem potentially associated with this unit.

An 85-inch wide space between the rear beam and the aft wing tanks is reserved for functional system routing in the wing. In addition, no fuel is stored

outboard of the MLG well so that systems also can be routed forward through the wing to enter the fuselage around the MLG well. Further, some limited system space is available aft of the rear beam. This space is limited since the inboard flap and plain spoiler extends forward to the rear beam. As shown in the figure, an aft-retracting nose landing gear (NLG) is used even though the free-fall capability of a forward-retracting design is attractive. The aft-retracting arrangement is selected because this allows the NLG to be mounted farther forward, thus permitting the baggage stowage area to extend closer to the nose. This, in turn, enables the stowage of more fuel in the protected wing center section.

#### Airplane Mass Properties

Estimated Group Mass and Balance Statement - An Estimated Group Mass and Balance Statement is presented on Table 2-3 for the Baseline Configuration. It has a taxi mass of 340,000 kilograms (750,000 pounds), and a range of 7800 kilometers (4200 n. miles), with a payload of 22,000 kilograms (49,000 pounds).

The primarily titanium wing has a total planform area of 1,005 sq. m. and an aspect ratio of 1.62. Its mass includes the center section carry-through structure under the floor, aerodynamic control surfaces and secondary structure. The horizontal, and body mounted vertical tails are all movable. There are also fixed fins outboard on the wing. The body is 90.5 meters long, and will accommodate 234 passengers in five (5) abreast seating. The under floor baggage compartment is located between the nose landing gear and the wing carry-through structure.

The wing mounted main landing gear retracts into a well just outboard of the body. The axisymmetric inlets and duct burning turbofan engines are under the wing with the thrust reversers just aft of this wing trailing edge. The engines are sized to provide a takeoff thrust to weight ratio of 0.36.

The mass estimates for the systems and equipment reflect composite material

TABLE 2-3 ESTIMATED GROUP MASS AND BALANCE STATEMENT

ITEM	% MAC	MASS		HORIZONTAL X-ARM	
		(kg)	(lb)	(m)	(in)
WING		49,713	109,600	58.42	2,300
TAIL - FINS ON WING		1,270	2,800	75.69	2,980
TAIL - FIN ON BODY		1,043	2,300	89.66	3,580
TAIL - HORIZONTAL		2,830	6,240	87.63	3,450
BODY		18,597	41,000	47.55	1,872
LANDING GEAR - NOSE (UP)		1,361	3,000	17.53	690
LANDING GEAR - MAIN (UP)		12,428	27,400	58.32	2,296
AIR INDUCTION		8,074	17,800	67.56	2,660
NACELLES		2,223	4,900	71.55	2,817
PROPULSION - T/F ENGINE INBD.		10,115	22,300	70.87	2,790
PROPULSION - T/F ENGINE OUTBD.		10,115	22,300	72.31	2,847
PROPULSION - SYSTEMS		3,175	7,000	58.42	2,300
SURFACE CONTROLS		3,856	8,500	60.76	2,392
INSTRUMENTS		558	1,230	36.14	1,423
HYDRAULICS		2,585	5,700	58.65	2,309
ELECTRICAL		2,064	4,550	52.10	2,051
AVIONICS		862	1,900	24.64	970
FURNISHINGS & EQUIPMENT		5,216	11,500	43.36	1,707
ECS		3,765	8,300	47.98	1,889
TOLERANCE & OPTIONS		898	1,980	50.80	2,000
MEW	57.7	140,748	310,300	58.98	2,322
STD. & OPER. EQ.		4,887	10,700	43.18	1,700
OEW	56.1	145,635	321,000	58.45	2,201
PAYLOAD		22,000	49,000	42.11	1,658
ZFW	49.9	167,635	370,000	56.29	2,216
FUEL		172,365	380,000	53.01	2,087
TAXI MASS	45.1	340,000	750,000	54.64	2,151

NOSE = 4.064m (160 in.)

MAC = 34,4881 m. (1357.7964 in.) LEMAC X = 39.0855 m. (1538.7961 in.)

ORIGINAL PAGE IS  
OF POOR QUALITY

application. Standard and operating equipment includes the crew, unusable fuel, and passenger service items.

Mass Moment of Inertia - Airplane mass moments of inertia were determined for the aeroelastic studies. The data for takeoff gross weight, operational weight empty and two intermediate flight conditions are summarized in Table 2-4.

Center of Gravity Travel - The center of gravity travel is tailored to permit the airplane to cruise with a minimum trim drag penalty. This is accomplished by sequencing the fuel tanks. The forward body and forward wing tanks are used for climbing and accelerating to cruise Mach number. The remaining wing tanks and midbody tanks are used during cruise. The last two body tanks contain the landing and reserve fuel.

The interior is configured for 234 passengers in five (5) abreast seating with a seat pitch of .86 meters. The baggage is loaded aft of the nose landing gear. Loadability studies indicate unrestricted passenger seating and small curve deviation from the straight payload line. This is primarily due to the low passenger mass to taxi mass fraction.

The fuel tank center of gravities are based on a fuel density of .803 kilogram/liter. The usable fuel volumes are calculated on the basis of 90-percent of the gross contour cross sectional area to allow for structure, systems and unusable fuel.

The center of gravity travel shown in Figure 2-24 was used for the Task I - Analytical Design Studies. The results of the design, stability and control, and weight and balance studies during Task I were reflected in a new travel diagram for the Engineering Design Study of Task II.

TABLE 2-4 AIRPLANE MASS MOMENT OF INERTIA

WEIGHT CONDITION	WEIGHT (LB)	X (IN)	Z (IN)	PITCH	ROLL	YAW
				10 <sup>6</sup> SLUG-FT <sup>2</sup>		
TAKE OFF GROSS	750,000	2151	—	40.8	6.51	47.3
OPER. WT. EMPTY	321,000	2301	—	27.7	4.68	32.2
INTERMEDIATE 1	699,300	2177	-141	39.9	6.36	46.2
● ZERO FUEL	370,000	2216	-128			
● FUEL (A)	329,000	2133	-155			
INTERMEDIATE 2	455,950	2212	-133	35.2	4.75	39.9
● ZERO FUEL	370,000	2216	-128			
● FUEL (B)	85,950	2196	-157			

NOTES: (A) TANKS NOS. 2-5, 8-11 PLUS: 50 PERCENT OF NOS. 1, 6 & 7.  
 (B) TANKS NOS. 2 & 4 PLUS 50 PERCENT OF NOS. 3 & 5.

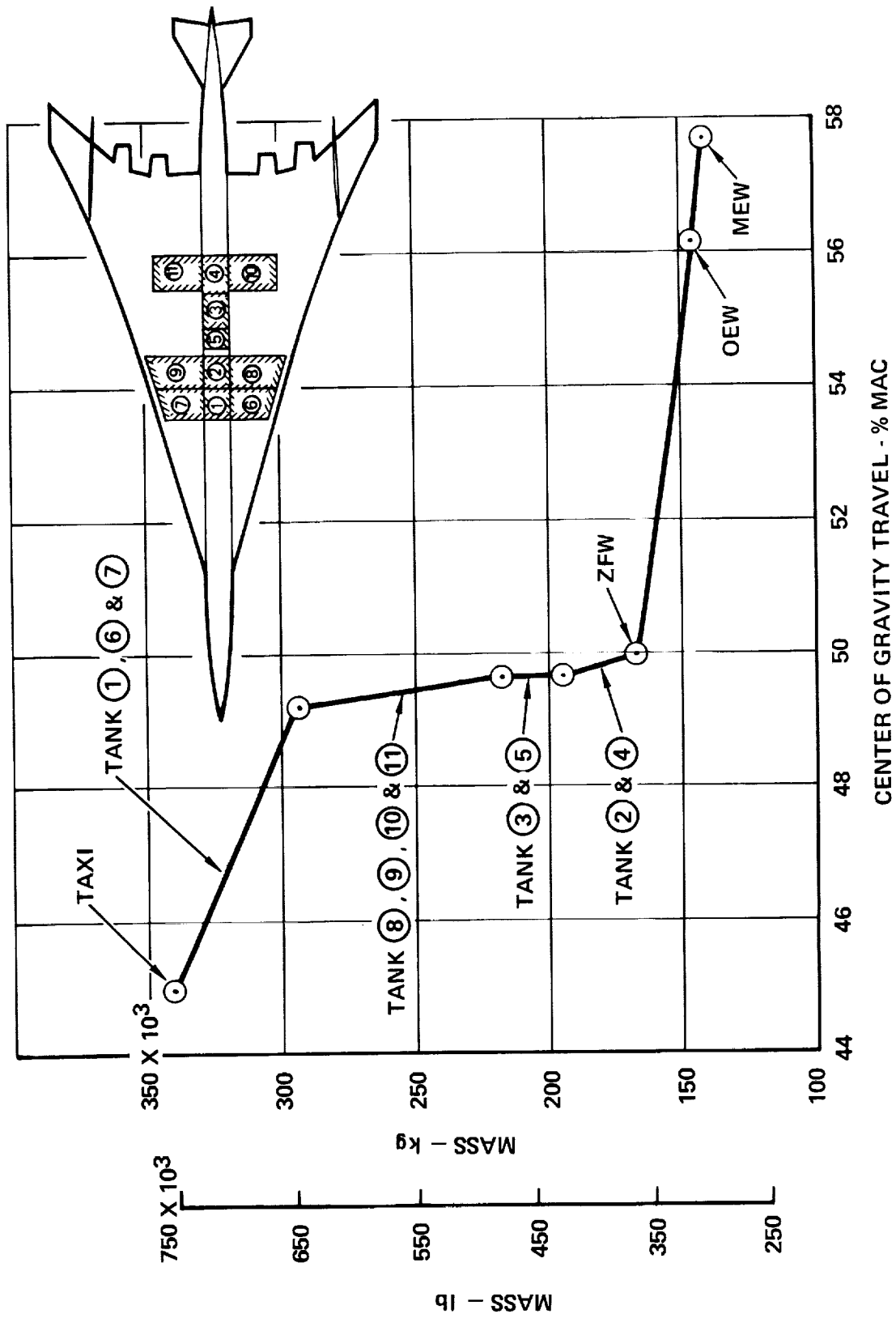


Figure 2-24. Center of Gravity Diagram - Task I



## BASELINE CONFIGURATION - TASK II

The Analytical Design Studies of Task I focused attention on assessing the relative merits of the various structural design concepts and identifying the importance of the interactive parameters that influence the design of a supersonic cruise aircraft. Only those configuration refinements that would have primary influence of the aforementioned objectives were adopted.

The development of the Baseline Configuration for the Task II effort focused attention on adapting all the recommendations made in regards to the three areas of concern and incorporating these findings in the NASA 15F concept. In addition, the results of the Stability and Controls Analysis and the Propulsion-Airframe Integration Study were applied. These additional refinements include:

- Shortening of the fuselage (119 inches) to reduce weight and drag
- Adopting the 60-degree tip sweep (in lieu of the 64.6-degree) to delay pitch up tendency at high angles of attack
- Increasing the low speed aileron area for improved cross-wind landing capability
- Providing a larger vertical tail area to correct the low speed lateral directional stability and control deficiency
- Adopting the duct burning turbofan engine, designated BSTF2.7-2/1.147, with an uninstalled sea level static thrust of 89,466 pounds for aircraft performance
- Adopting longitudinal and lateral constraints of the propulsion-airframe integration study
- Adopting center of gravity limits established as the results of the stability and control analysis
- Relocating fuel tanks to meet the center of gravity limits established

## General Arrangement

The general arrangement drawing incorporating the configuration refinements on the 15F concept is shown in Figure 2-26. The airplane has a design gross mass of 340,000 kilograms (750,000 pounds), wing planform area of 1014.69 meter<sup>2</sup> (10,923 feet<sup>2</sup>), and four duct-burning turbofan engines having a sea level, static thrust of 89,500 pounds with an airflow of 1,130 pounds per second. The engines are mounted on the wing lower surface in individual pods with axisymmetric inlets. The engine exhausts are positioned aft of the wing trailing edge. An inlet fence is provided to prevent unstart due to mutual interference. The overall lengths of the airplane is 87.48 meters (287.0 feet) and has a wing span of 40.4 meters (132.5 feet). The fuselage cross-section area has been increased to provide adequate head room. The tail volumes for the horizontal stabilizer ( $\bar{V}_H$ ) and the vertical tail ( $\bar{V}_V$ ) are 0.07 and 0.027, respectively.

## Basic Dimensions

The dimensional data for the configuration refinements adopted for the Task II effort are shown in Figure 2-27. All dimensional data are defined in the fuselage station (FS), waterline (WL) and butt line (BL) coordinates. The  $Z_0$  plane is indicated for reference. The fuselage nose reference is established at FS 279 reflecting the shortened forebody. Other refinements include:

- Aft relocation of main landing gear for adequate clearance for the engine exhaust nozzle and horizontal tail anhedral
- Wing tip and vertical tail planform changes
- Aft relocation of the nose landing gear

The basic dimensions drawing is used as the master reference for subsequent drawings including the structural arrangement and the detailed design studies of Task II.

The fuselage dimensional data drawing (Figure 2-28) shows the specific refine-

ments made to the fuselage of the NASA 15F concept. As indicated in the figure, a 119 inch section was removed aft of FS 1353 and the forward section moved aft along the floor reference plane (WL 300) and refaired with the centerbody shell. Note also the aft relocation of the pressure bulkhead to FS 3000.

#### Fuel Tank Arrangement

The fuel tanks were relocated for the Task II effort to meet the center of gravity limits established by the stability and control analysis. The tank arrangement developed (Figure 2-28) provides for a fuel storage capacity of 178,537 kilograms (393,600 pounds). The capacity of each tank is also tabulated on the figure. The 16-tank fuel storage system is designed to take advantage of the "protected-volume" of approximately 43 percent of the total storage capacity. The landing and reserve fuel is located in the protected fuselage area. Fuel management scheduling for airplane center of gravity control is specifically planned to maximize the available heat sink capacity of the fuel by emptying the exposed outboard tanks as early as possible in the flight. Additional considerations include fuel usage to permit the aircraft to cruise with a minimum of trim drag penalty.

The fuel capacity is calculated on the basis of honeycomb sandwich wing construction less 4-percent for additional structure, equipment, etc. The fuel mass and center of gravities are based on a fuel density of 0.803 kilograms/liter (6.7 lbs/gallon).

#### Interior Arrangement

The 234 passenger interior arrangement at 5-abreast seating is shown in Figure 2-29. The pressure bulkhead is moved aft (F.S. 3000) relative to the Task I arrangement (F.S. 2870) to provide passenger space in the shortened fuselage.

Baggage and fuel storage utilizes the major portion of the fuselage below the floor. The baggage is stowed in the more lightly loaded forward region with the fuel carried in the centerbody wing carry through region. Cargo loading

is accomplished through the forward located door and moved aft sequentially. The hand loaded cargo is located immediately aft of the nose landing gear (NLG).

A free-fall, forward retracting NLG is utilized in the Task II baseline configuration and the ECS units are relocated to a bay forward of the fuel tanks. To afford functional system routing in the wing, the space between the rear beam and aft wing tanks, and outboard of the main landing gear well is retained.

### Airplane Mass Properties

Estimated Group Mass and Balance Statement - The airplane mass and balance data of Table 2-5 represent the various configurations evaluated during the Task II effort. The data reflect the configuration refinements adopted to the NASA 15F concept. All data are for a fixed sized aircraft with a takeoff gross mass of 340,000 kilograms (750,000 pounds) and payload of 22,000 kilograms (49,000 pounds).

- Task IIA Configuration Refinement Data - The Task I mass data (Table 2-3) were adjusted aft to reflect the effect of the configuration changes. The mass of each item was assumed invariant. The taxi mass is at the 52-percent MAC and the zero fuel weight (ZFW) is at the 53.9-percent MAC.
- Task IIB Baseline Data - The data is representative of the configuration changes adopted and the minimum mass wing and fuselage structural approach selected for the Task II effort. The engines have been resized to reflect an uninstalled sea level static thrust of 89,466 pounds per engine and appropriate mass changes for the larger air induction system and nacelles are indicated. The initial mass data does not include allowance for flutter suppression. The taxi mass is 340,000 kilograms (750,000 pounds) with the center of gravity located at the 52.5-percent MAC.

TABLE 2-5. ESTIMATED GROUP MASS AND BALANCE STATEMENT - TASK II

ITEM	TASK IIA			TASK II					
	% MAC	CONFIG. REFINED DESIGN (LBS.)	FUS. STA. (IN.)	% MAC	BASELINE DESIGN (LBS)	STRENGTH DESIGN (LBS)	FUS. STA. (IN.)	FINAL DESIGN (LBS)	FUS. STA. (IN.)
WING		109,000	2,370		89,770	87,660	2,393	90,584	2,409
TAIL - FINS ON WING		2,800	2,991		2,800	2,800	2,991	2,800	2,991
TAIL - FINS ON BODY		2,300	3,522		2,600	2,600	3,522	2,600	3,522
TAIL - HORIZONTAL		6,240	3,449		7,950	7,950	3,449	7,950	3,449
BODY		41,000	1,923		32,100	42,122	1,923	42,122	1,923
LANDING GEAR - NOSE (UP)		3,000	915		3,000	3,000	915	3,000	915
LANDING GEAR - MAIN (UP)		27,400	2,273		27,400	27,400	2,273	27,400	2,273
AIR INDUCTION		17,800	2,667		19,760	19,760	2,626	19,760	2,626
NACELLES		4,900	2,824		5,140	5,137	2,733	5,137	2,783
PROPULSION - T/F ENGINE INBD.		22,300	2,813		25,560	25,562	2,790	25,562	2,790
PROPULSION - T/F ENGINE OUTBD.		22,300	2,870		25,560	25,562	2,834	25,562	2,834
PROPULSION - SYSTEMS		7,000	2,347		7,000	7,007	2,347	7,007	2,347
SURFACE CONTROLS		8,500	2,445		8,500	8,500	2,445	8,500	2,445
INSTRUMENTS		1,230	1,433		1,230	1,230	1,433	1,230	1,483
HYDRAULICS		5,700	2,433		5,700	5,700	2,433	5,700	2,433
ELECTRICAL		4,550	2,132		4,550	4,550	2,132	4,550	2,132
AVIONICS		1,900	1,085		1,900	1,900	1,085	1,900	1,085
FURNISHING & EQUIPMENT		11,500	1,842		11,500	11,500	1,842	11,500	1,842
ECS		8,300	2,009		8,300	8,300	2,009	8,300	2,009
TOLERANCE & OPTIONS		1,980	2,000		1,980	1,980	2,000	1,980	2,000
MEW	60.9	310,300	2,372	62.2	302,300	300,220	2,389	303,144	2,394
STD & OPER. EQ.		10,700	1,819		10,700	10,700	1,819	10,700	1,819
OEW	59.6	321,000	2,353	60.8	313,000	310,920	2,369	313,844	2,374
PAYLOAD		49,000	1,776		49,000	49,000	1,771	49,000	1,771
ZFW	53.9	370,000	2,277	54.8	362,000	359,920	2,288	362,844	2,293
FUEL		380,000	2,226		388,000	390,080	2,228	387,156	2,223
TAXI MASS	52.0	750,000	2,251	52.5	750,000	750,000	2,257	750,000	2,257

LEMAR = FS 1548.2 MAC = 1351.06

X ARM = DISTANCE FROM FUSELAGE STATION (F.S.) 0

FUS. NOSE AT F.S. 279

ORIGINAL PAGE IS OF POOR QUALITY

- Task IIB Final Data - The primary mass change is reflected by the increase in wing mass to include the requirements to suppress flutter. A trade off with fuel (Tank No. 16) is made to achieve the same center of gravity location as for the baseline data.

#### Mass Moment of Inertia

Airplane mass moment of inertia were computed and plotted in Figure 2-30. The data is similar to that shown in Table 2-4 for the Task I airplane. The pitch moment of inertia is slightly less due to the shortened fuselage while that roll moment of inertia is greater due to the heavier propulsion packages. These data are used for the aeroelastic studies reported in Section 5 and 10.

#### Center of Gravity Travel

The fuel management scheduling for airplane center of gravity control is shown in Figure 2-31. The sequencing of fuel is planned to (1) permit the airplane to cruise with a minimum of trim drag penalty and (2) maximize the heat sink capability of the fuel by emptying the outboard wing tanks as early as possible in the mission.

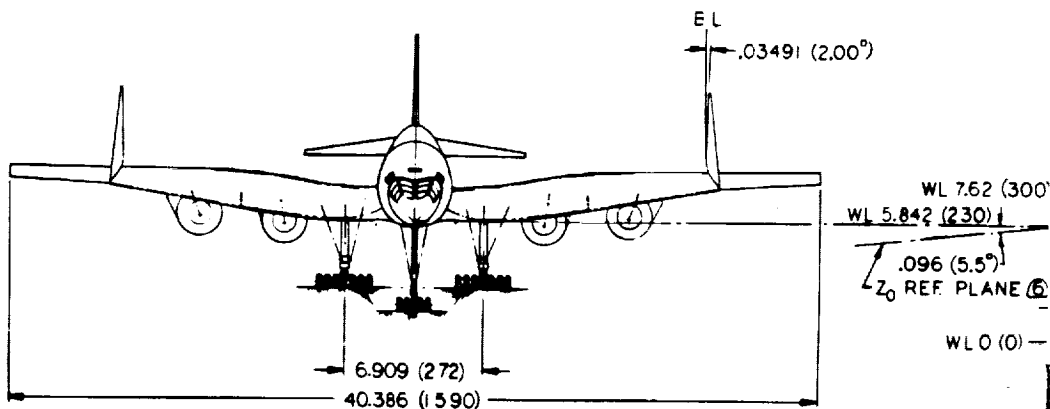
Tanks 1 through 4 are engine feed tanks and are kept full until all other tanks are empty. The usable fuel mass are based on a fuel density of 0.803 kilogram/liter (6.7 pound/gallon) and 90 percent of the gross volume to allow for structure, systems and unusable fuel. The forward limit for flight (51 percent MAC) and the aft limit for takeoff and landing are indicated at 53.5 percent MAC and 55 percent MAC, respectively.

## CHARACTERISTICS

POWER PLANT - DUCT BURNING TURBOFAN  
 UNINSTALLED THRUST - 397,964 NEWTONS, (89,466 LBS) SLS  
 TAXI MASS - 340,000 KILOGRAMS (750,000 LBS)

	WING (5)	HORIZ. TAIL (4)	FUS. VERT. TAIL (5)	WING VERT. TAIL (EACH) (5)
AREA - M <sup>2</sup> (FT <sup>2</sup> )	1014.69 (10,923)	73.868 (795)	30190 (325)(8)	2165 (233)
ASPECT RATIO	1.607	1.707	0.517	0.495
TAPER RATIO	0.1135	0.225	0.230	0.136
SPAN - M (IN)	40.386 (1590)	11.217 (441.6)	3.941 (155.55)	3.277 (129.0)
ROOT CHORD - M (IN)	55.766 (2195.5)	10.739 (422.8)	12.426 (489.22)	11.643 (458.4)
TIP CHORD - M (IN)	6.330 (249.192)	2.416 (95.1)	2.858 (112.521)	1.585 (62.4)
MAC - M (IN)	34.317 (1351.067)	7.455 (293.5)	8.640 (340.174)	7.889 (310.6)
LE SWEEP	1.292 (74°)	1.058 (60.64°)	-1.190 (68.2°)	1.281 (73.42°)
RADIAN (DEGREES)	1.236 (70.84°)	1.047 (60.00°)		
DIMEDRAL, RELATIVE TO Z PLANE	-1.745 (-10°)			

- (8) EXPOSED AREA
  - (7) ABOVE Z - 41.45 (-163.20)
  - (5) AS GIVEN IN NASA DATA DECK.
  - (5) DATA FIGURED RELATIVE TO Z<sub>0</sub> PLANE PER NASA DATA DECK
  - (4) DIMENSIONS PROJECTED INTO Z<sub>0</sub> PLANE.  
3 VIEWS SHOWN IN FS, BL & WL COORDINATES.
  - 2 LINEAR DIMENSIONS IN METERS (INCHES)  
ANGLES IN RADIAN (DEGREES).
  - 1 DIMENSIONS IN SI (ENGLISH) UNITS
- NOTE:

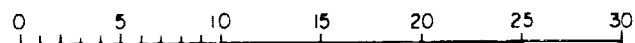
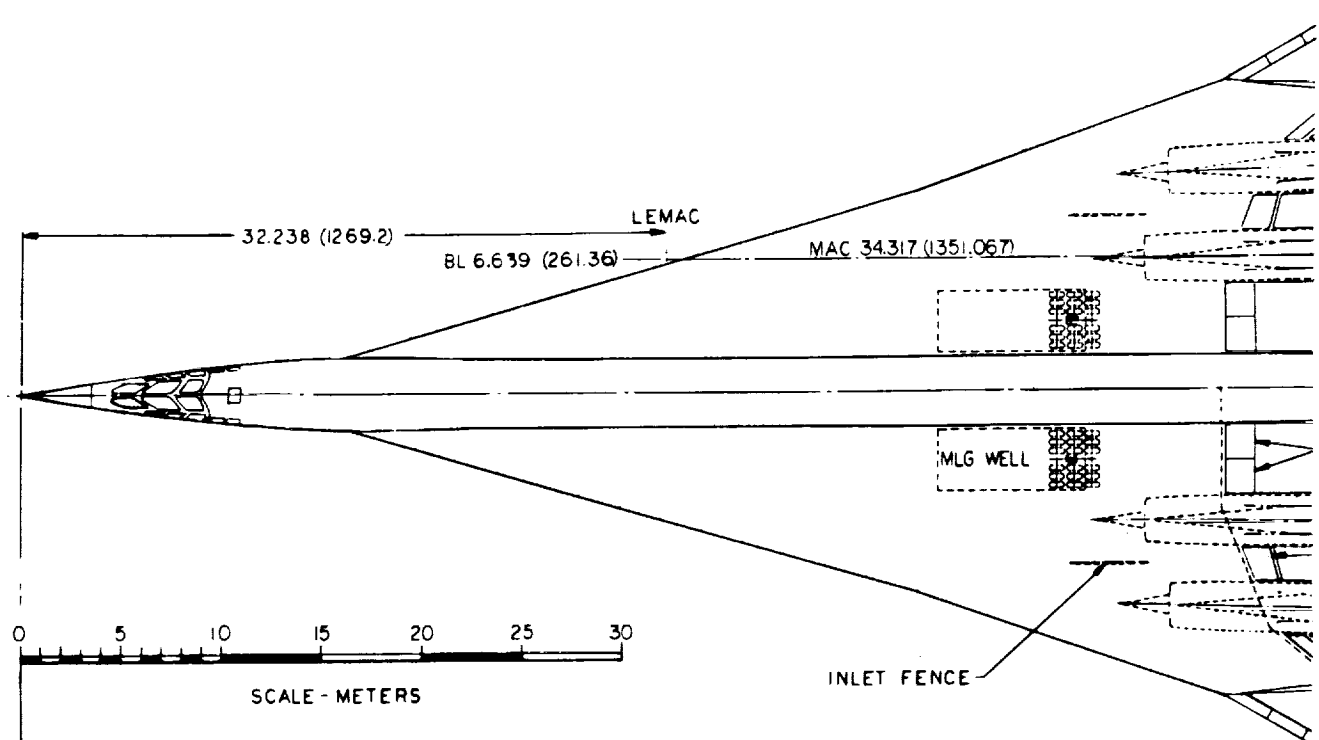


ORIGINAL PAGE IS  
 OF POOR QUALITY

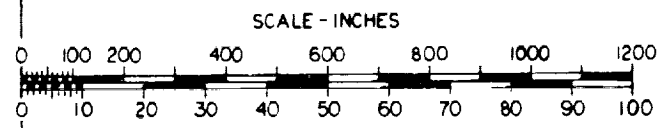
FOLDOUT FRAMES (







SCALE - METERS

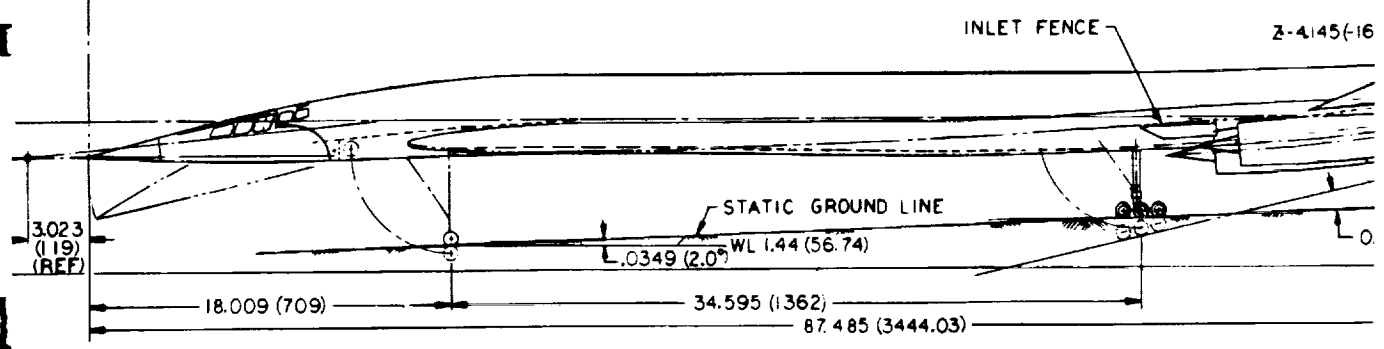


SCALE - INCHES

SCALE - FEET

FS  
7087  
(279)

FIXED VERTICA



FOLDOUT TABLE 2



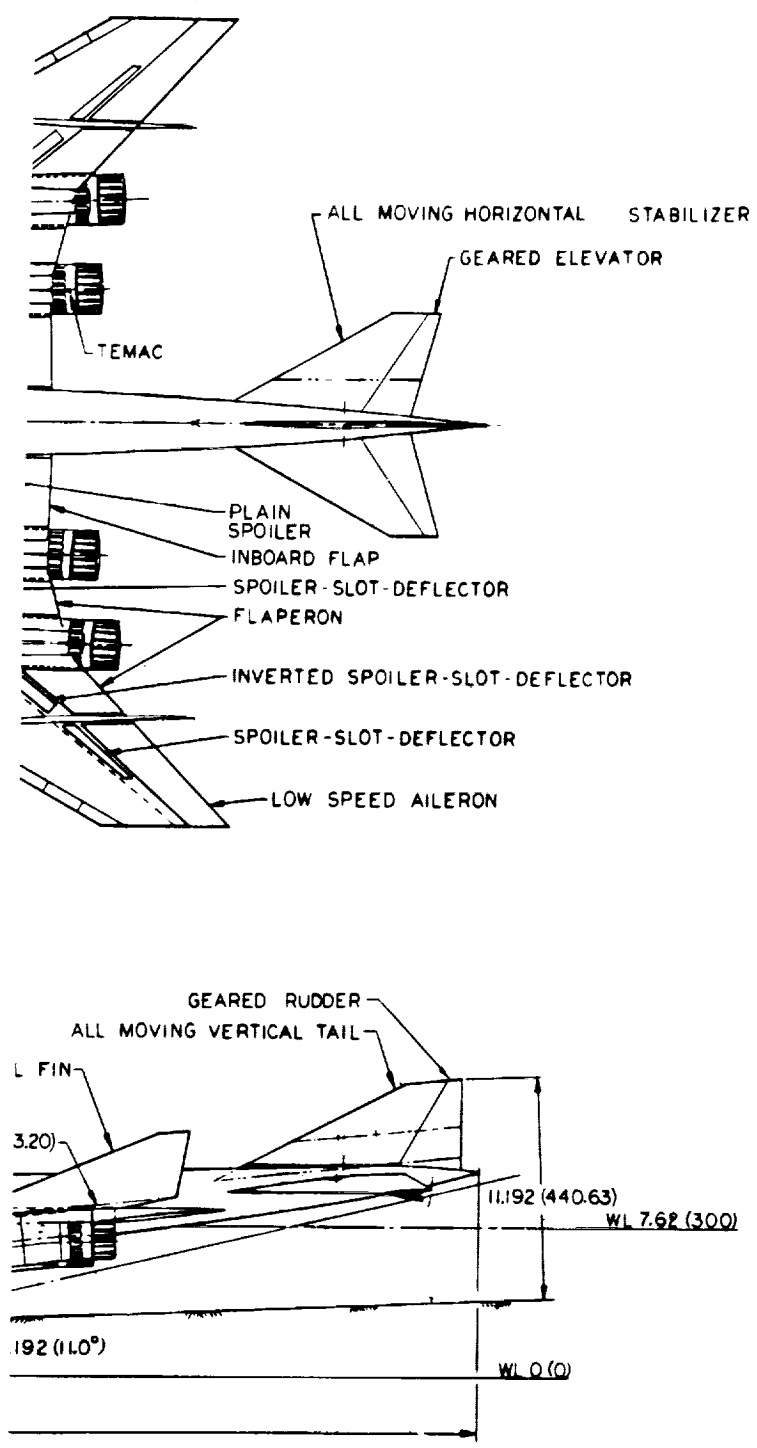
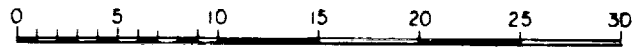


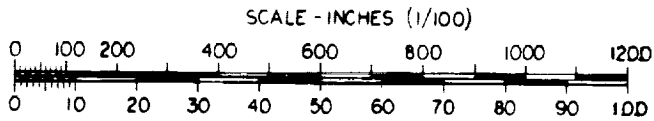
Figure 2-25. General Arrangement - Task II

FOLDOUT 13

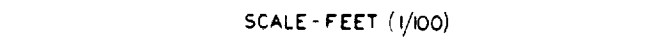




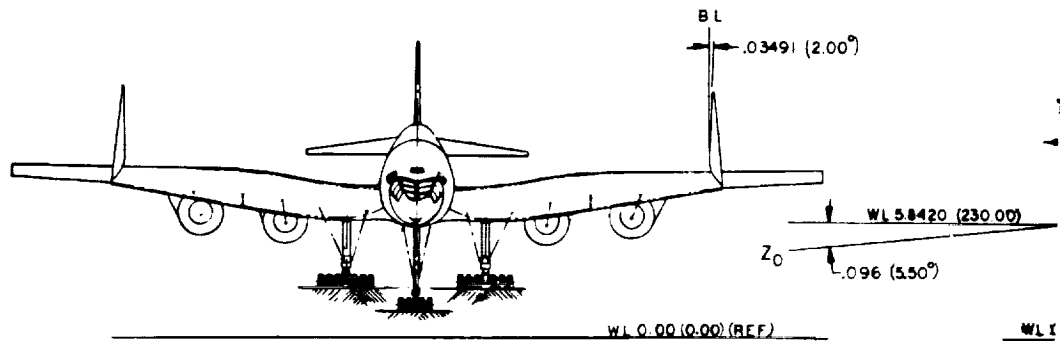
SCALE - METERS (1/100)



SCALE - INCHES (1/100)



SCALE - FEET (1/100)

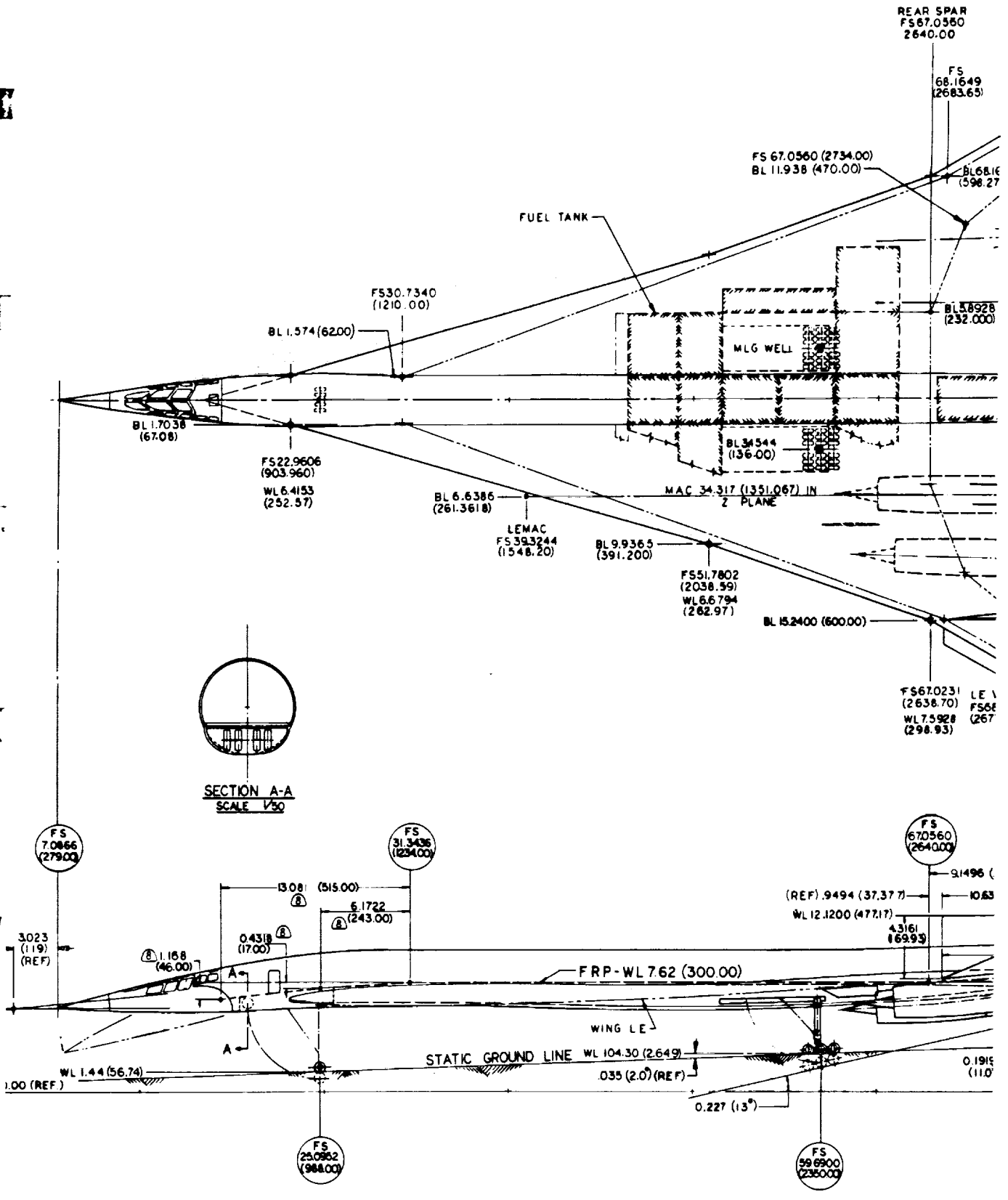


FOLDOUT FRAME)

ORIGINAL PAGE IS  
OF POOR QUALITY

PRECEDING PAGE BLANK NOT FILMED

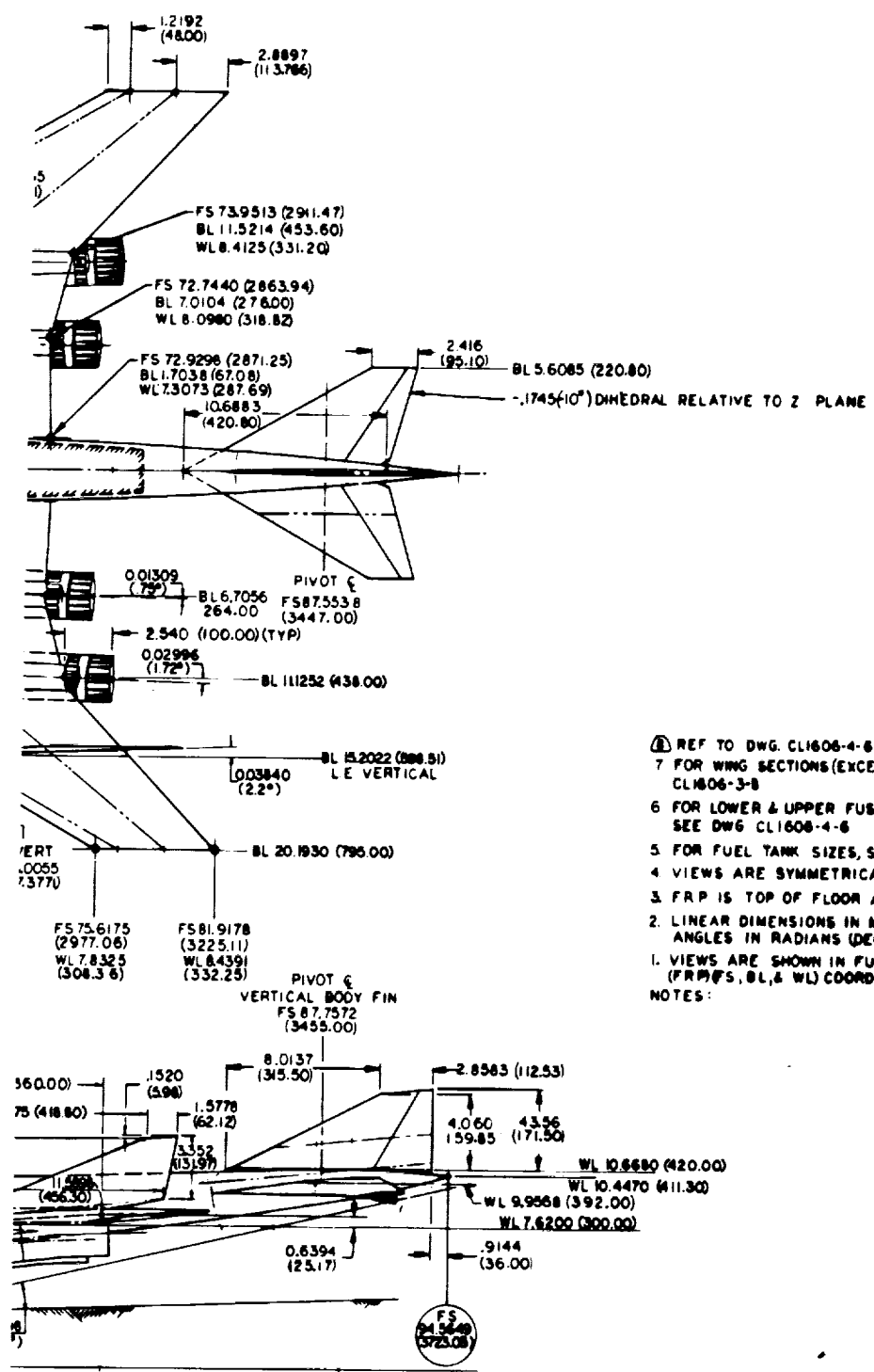




FOLDOUT FRAME 2



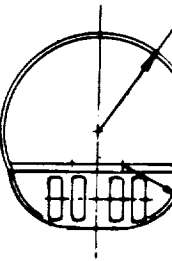




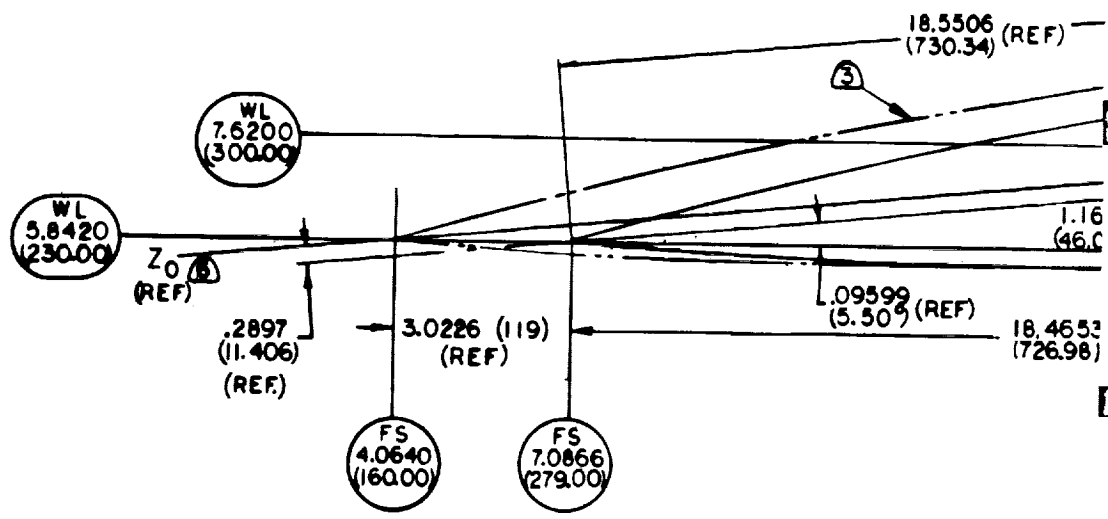
- ④ REF TO DWG. CL1606-4-6  
 7 FOR WING SECTIONS (EXCEPT TIP) SEE DWGS CL1606-3-3 & CL1606-3-8  
 6 FOR LOWER & UPPER FUSELAGE CONTOUR, SEE DWG CL1606-4-6  
 5 FOR FUEL TANK SIZES, SEE DWG CL1606-4-4.  
 4 VIEWS ARE SYMMETRICAL ABOUT BL 0.00.  
 3 FRP IS TOP OF FLOOR AT WL 7.62 (300.00).  
 2. LINEAR DIMENSIONS IN METERS (INCHES) ANGLES IN RADIAN(S) (DEGREES).  
 1. VIEWS ARE SHOWN IN FUSELAGE PLANE (FRP) (FS, BL, & WL) COORDINATES.
- NOTES:

Figure 2-26. Basic Dimensions - Task II





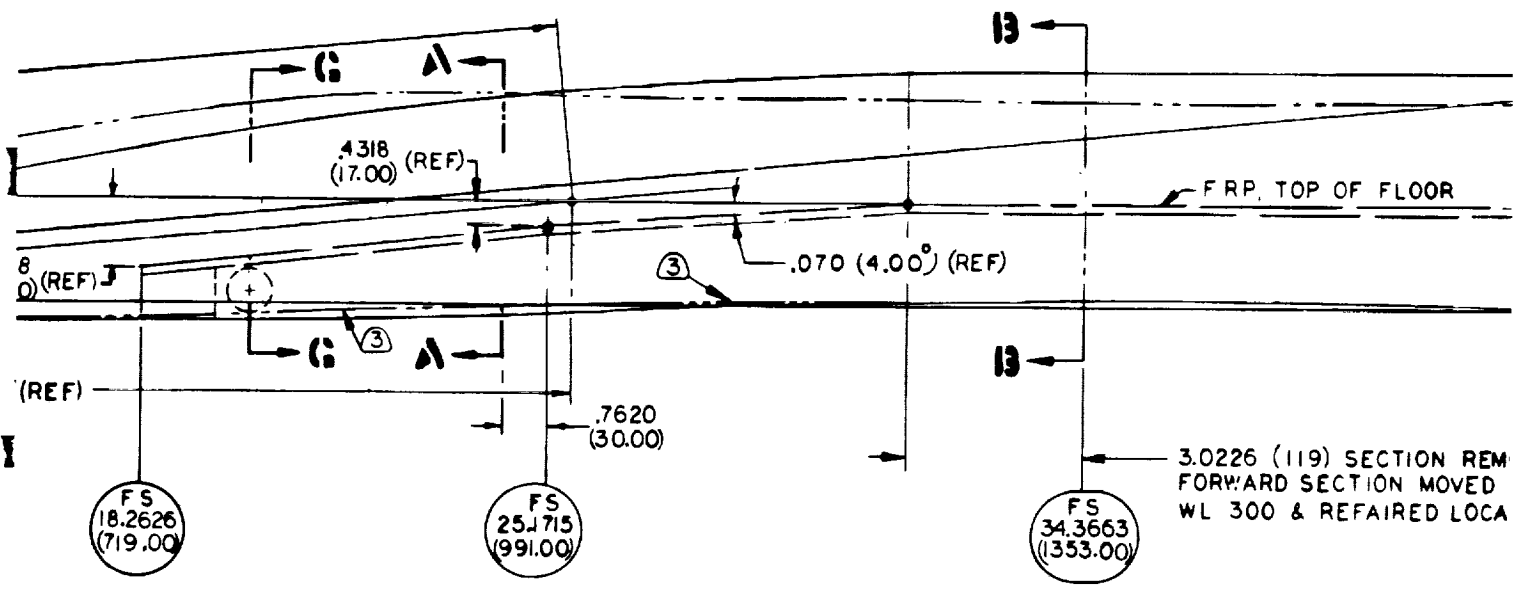
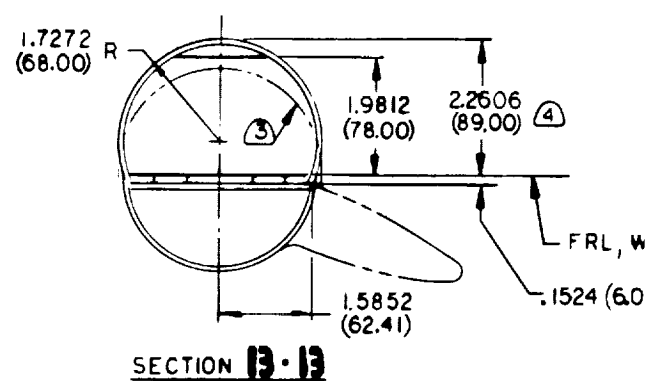
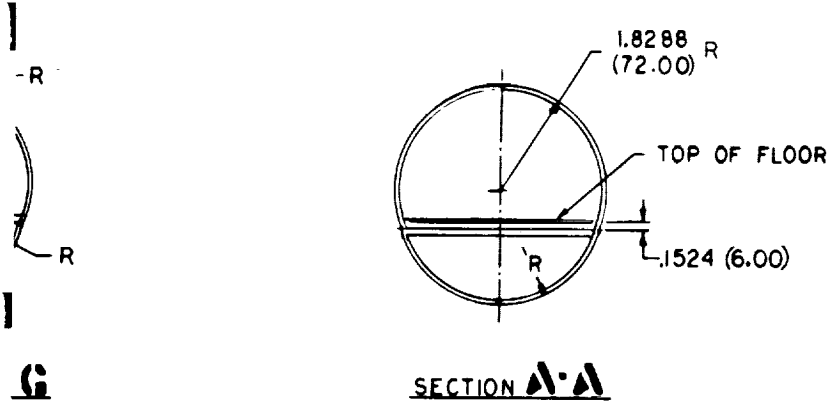
SECTION G



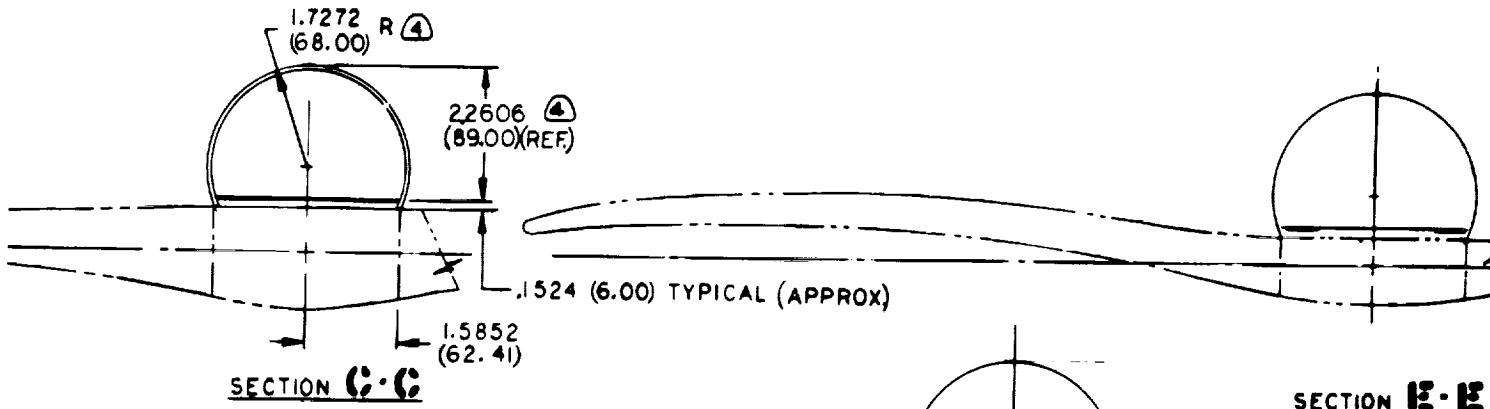
FOLDOUT FRAME /

PRECEDING PAGE BLANK NOT FILMED

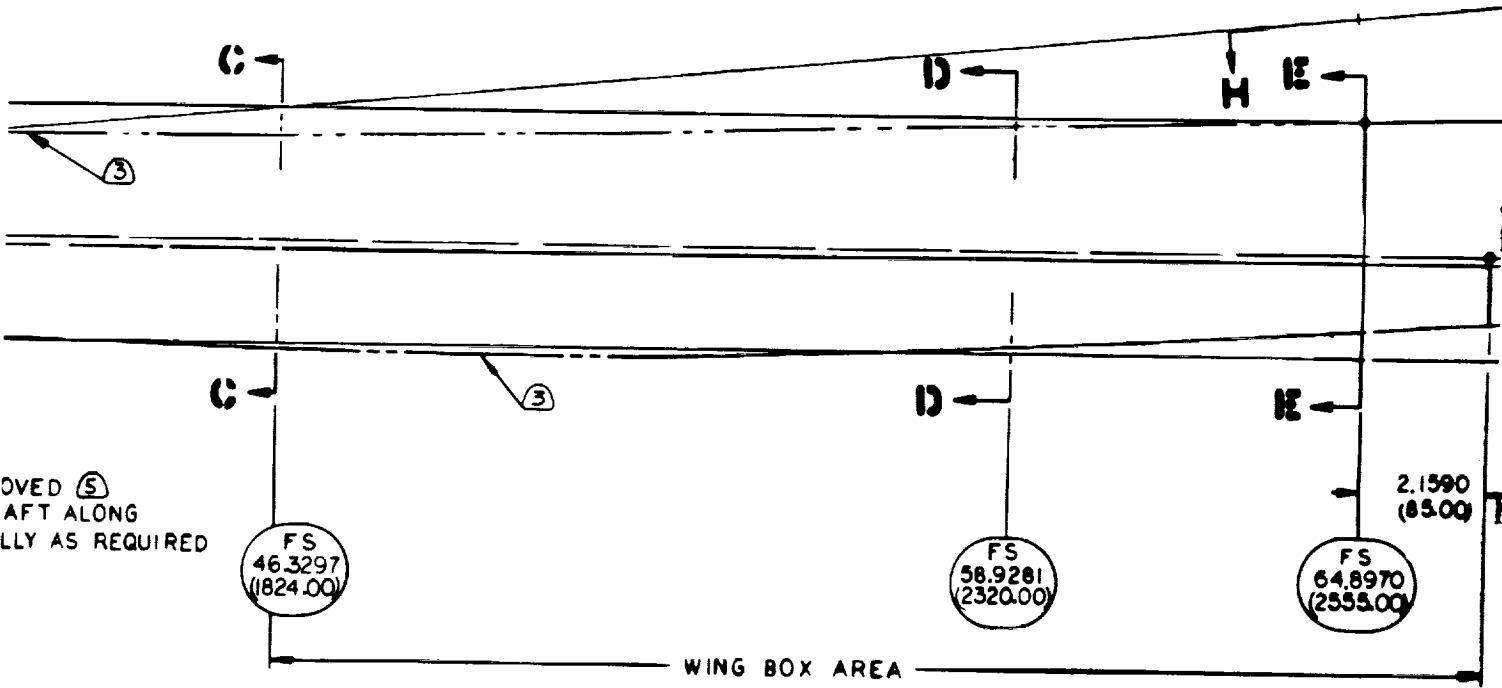








L 7.6200 (300.00)  
O(REF)



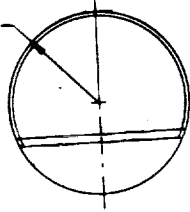
FOLDOUT FRAME 3





E

1.5494  
(61.00) R  
(REF.)



SECTION I-I

F

G

FUSELAGE

VIEW H-H

H

I-I

1.9050 R  
(75.00)

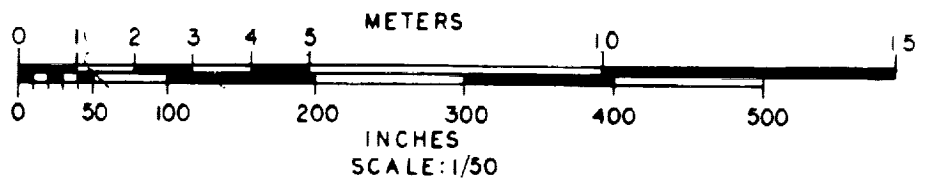
.6394  
(25.17)

J-J

K

FS  
76.2002  
(3000.00)

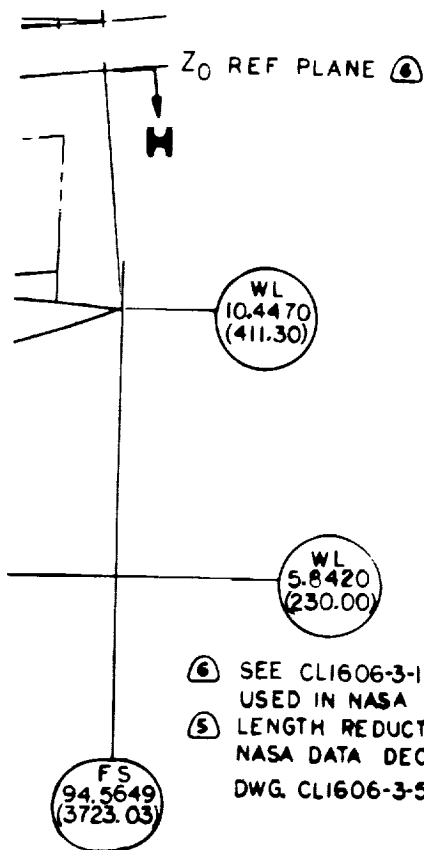
L



M

FOLIOUT FRAME 4





- ⑥ SEE CL1606-3-1 FOR LOC. OF Z<sub>0</sub> REF. PLANE USED IN NASA DATA DECK
- ⑤ LENGTH REDUCTION IS RELATIVE TO NASA DATA DECK CONFIG. IN DWG. CL1606-3-5 (SHT. 1)

④ TYPICAL FROM FS 34.3663 (1353.00) TO FS 64.8970 (2555.00)

③ \_\_\_\_\_ CONFIGURATION PER NASA DATA DECK.

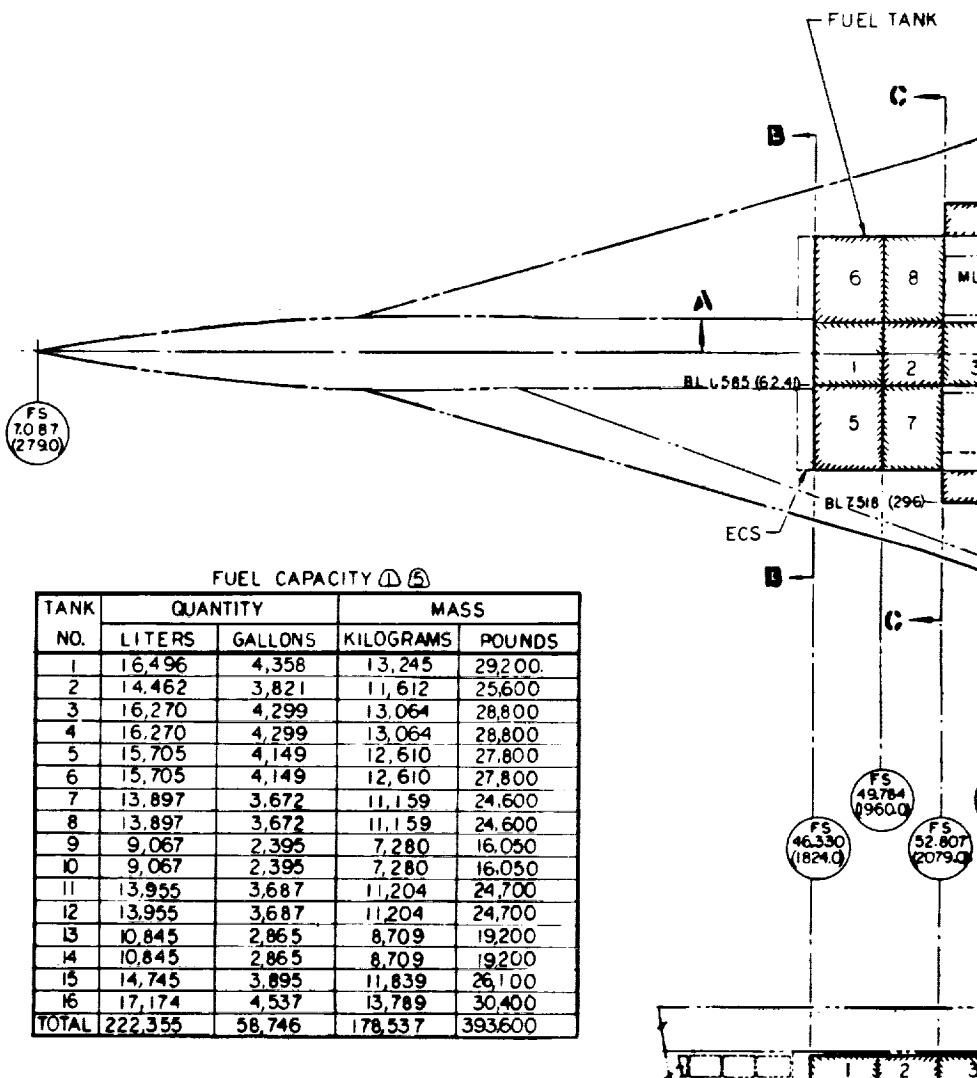
2 DIMENSIONS IN METERS (INCHES) & RADIAN (DEG)

1 FOR UNMODIFIED NASA DATA DECK CONFIGURATION, SEE DWG CL1606-3-5

NOTE:

Figure 2-27. Fuselage Dimensional Data - Task II





FUEL CAPACITY (A) (B)

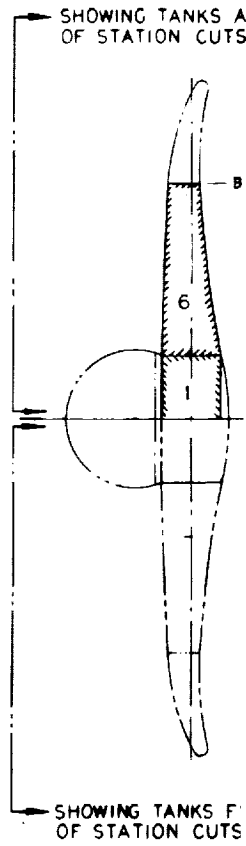
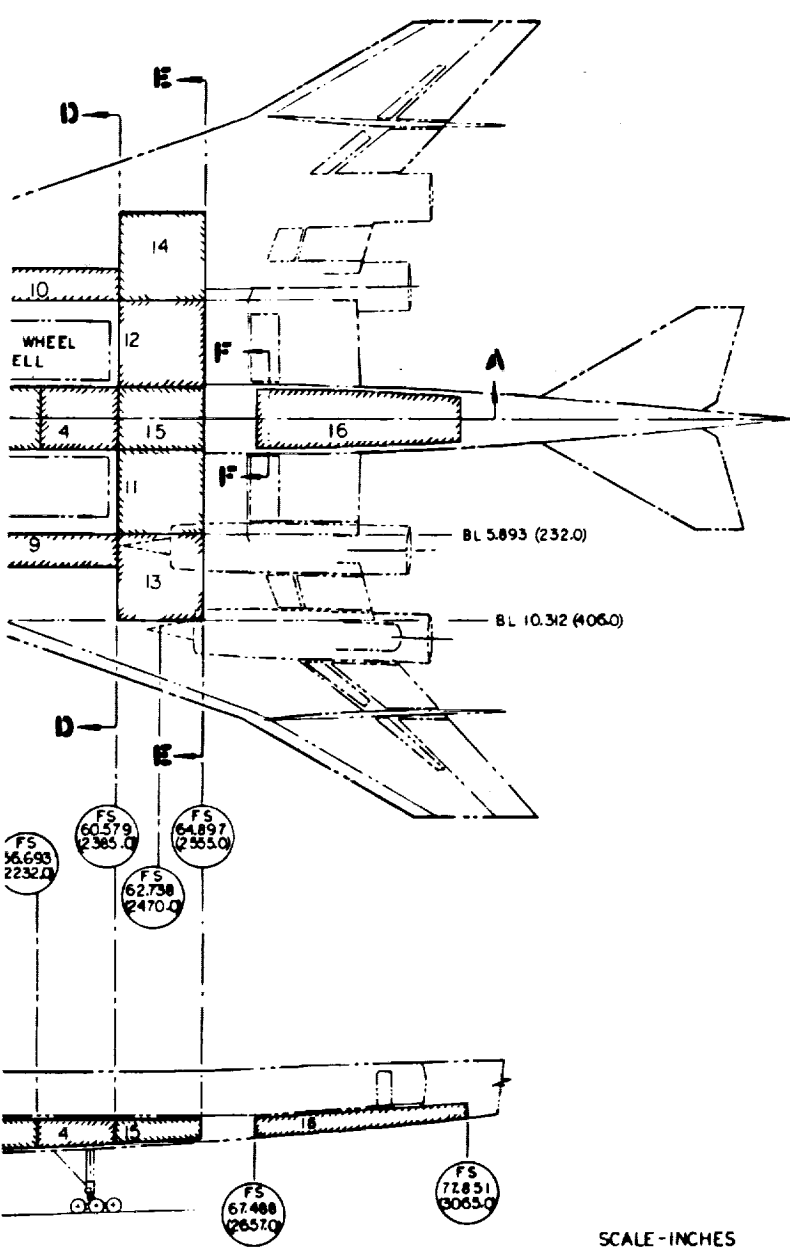
TANK NO.	QUANTITY		MASS	
	LITERS	GALLONS	KILOGRAMS	POUNDS
1	16,496	4,358	13,245	29,200
2	14,462	3,821	11,612	25,600
3	16,270	4,299	13,064	28,800
4	16,270	4,299	13,064	28,800
5	15,705	4,149	12,610	27,800
6	15,705	4,149	12,610	27,800
7	13,897	3,672	11,159	24,600
8	13,897	3,672	11,159	24,600
9	9,067	2,395	7,280	16,050
10	9,067	2,395	7,280	16,050
11	13,955	3,687	11,204	24,700
12	13,955	3,687	11,204	24,700
13	10,845	2,865	8,709	19,200
14	10,845	2,865	8,709	19,200
15	14,745	3,895	11,839	26,100
16	17,174	4,537	13,789	30,400
TOTAL	222,355	58,746	178,537	393,600

FS 49784 (19600)  
 FS 46330 (18240)  
 FS 52807 (20790)

FOLDOUT FRAME / ORIGINAL PAGE IS OF POOR QUALITY  
 PRECEDING PAGE BLANK NOT FILMED

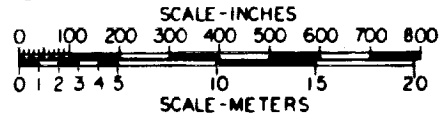
C 12





SECTION B-B  
SCALE: 1/50

SECTION A-A



- ⑤ FUEL (HONEY)
- 4 PER
- 4 FUEL (6.7 LI)
- 3 [hatched pattern]
- 2 DIMEN
- △ FUEL (733-3)
- NOTES:





## Jig Shape Definition

The aerodynamic shape of the aircraft changes during flight due to aerothermoelastic and inertia effects. This is a result of in-flight variations in dynamic pressure, Mach number, gross weight, and weight distribution; the latter two result from fuel consumption.

The governing aerodynamic shape serving as the analytical starting point, is the shape providing the optimum performance characteristics in one-g mid-cruise flight for a 4,200 nautical mile range. This governing shape is described by the camber and twist characteristics of the supersonic wind tunnel model.

When the airframe structure is subject to no-load (dynamic pressure, Mach number, and inertia loads all equal zero) the shape of the aircraft is different from the mid-cruise shape. This zero load shape is designed into the aircraft so when it is subjected to one-g level flight loads and to temperatures occurring in the mid-cruise environment, the airframe elastic deformations result in an aircraft that has the desired optimum aerodynamic shape. The manufacture of the aircraft will be in accordance to this zero-load shape in the jig, where the weight is supported in a manner that precludes elastic deformations.

The procedure to establish the jig shape is as follows:

1. The analytical starting point is a description (camber and twist) of the optimum performance cruising-flight shape.

[ $\alpha_C$  & T, mid-cr]

2. Analysis is performed to calculate structural deflections due to flight loads occurring during mid-cruise flight. Where the deflection matrix  $[\Delta\delta_z]$  is defined by the product of the structural influence coefficients [E] and the rigid airplane 1-g loads for the mid-cruise condition

$$[\Delta\delta_z] = [E] \left[ P_{z1-g \text{ mid-cr. rigid}} \right]$$

PRECEDING PAGE BLANK NOT FILMED

using these calculated deflections and the transform matrix  $[D\theta]$ , the incremental change in chordwise slope and deflections are defined

$$[\Delta\alpha] = [D\theta] [\Delta\delta_z]$$

3. The deflections are applied, negatively, to the mid-cruise shape to establish the jig shape.

$$[\alpha_{\text{jig shape}}] = [\alpha_{\text{C\&T, mid-cr}} - [\Delta\alpha]]$$

The airplane shape used for analytical reference and loft purposes is hereby defined.

The aeroelastic analysis for the final design (Task IIB) incorporates the above defined jig shape in the calculation of the design loads, rather than the mid-cruise shape used for the Task I external loads analysis.

#### Flexible Stability Derivatives

The fact that the airplane changes shape aerodynamically as a result of elastic deflections of the structure makes it necessary to modify wind tunnel force data which have been measured on a rigid model. This flexibility is accounted for by applying flexible/rigid ratios or flexible increments to the basic rigid body aerodynamics. The degree of change varies with Mach number, equivalent airspeed, airplane gross weight, and structural arrangement. The magnitude of the effect of aeroelasticity on stability and control characteristics for the baseline arrow-wing configuration are obtained from generalized stability derivative programs and are reported herein. The application of these data to the stability and control analyses is presented in Section 3.

#### Calculation and Application of Flexible Effects on Stability and Control

Characteristics. - The effects of airframe flexibility on stability and control derivatives were determined over a range of Mach numbers for the chordwise-stiffened and monocoque structural arrangements. The results of these analyses are presented in Figures 5-4 through 5-10.

Longitudinal: Airplane flexibility effects on lift curve slope and pitching moments are shown on Figures 5-4 and 5-5 for the chordwise-stiffened arrangement and Figures 5-6 and 5-7 for the monocoque arrangement.

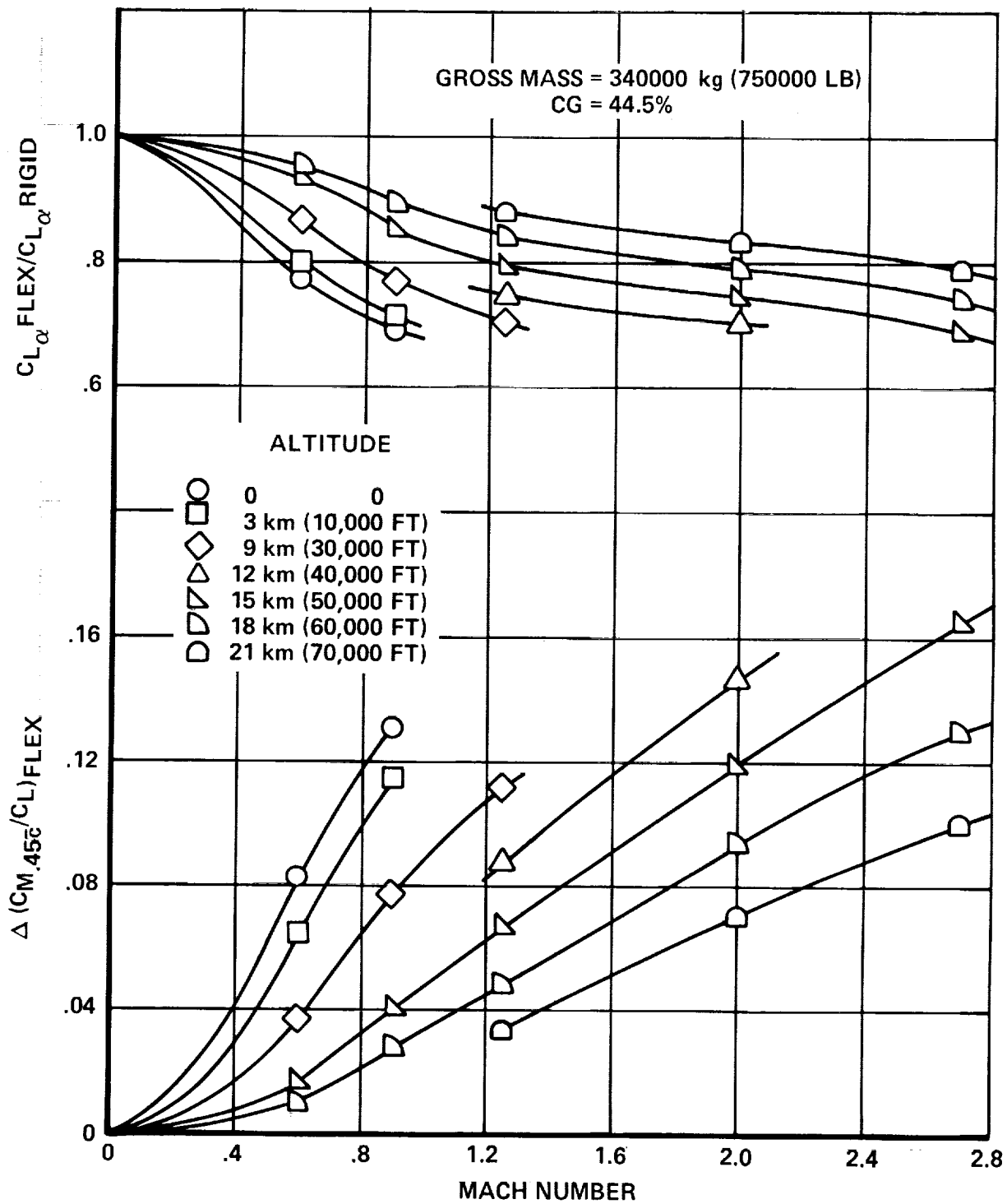


Figure 5-4. Free-Airplane Flexibility - Chordwise Stiffened Arrangement - 750,000 lb.

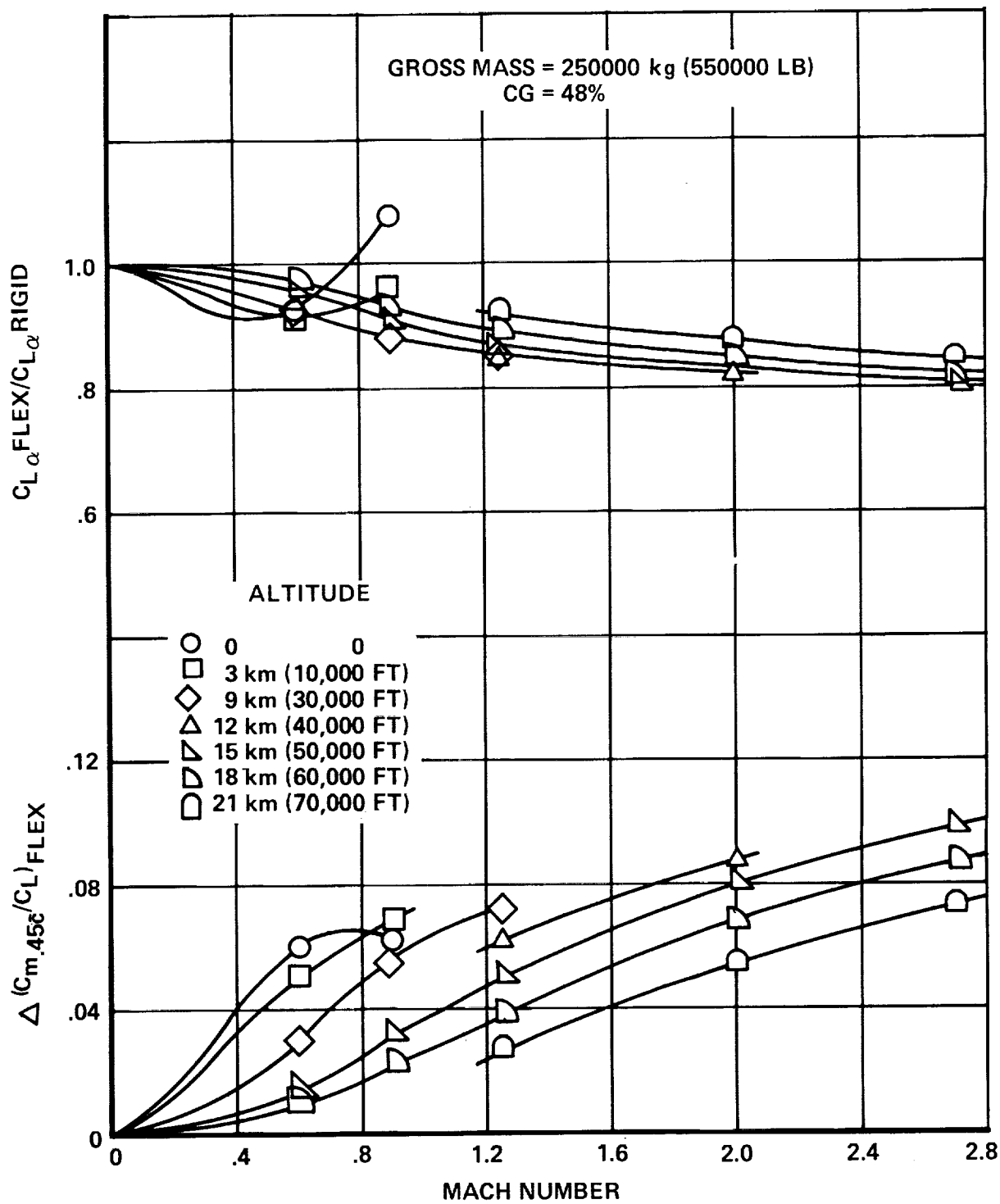


Figure 5-5. Free-Airplane Flexibility - Chordwise Stiffened Arrangement - 550,000 lb.

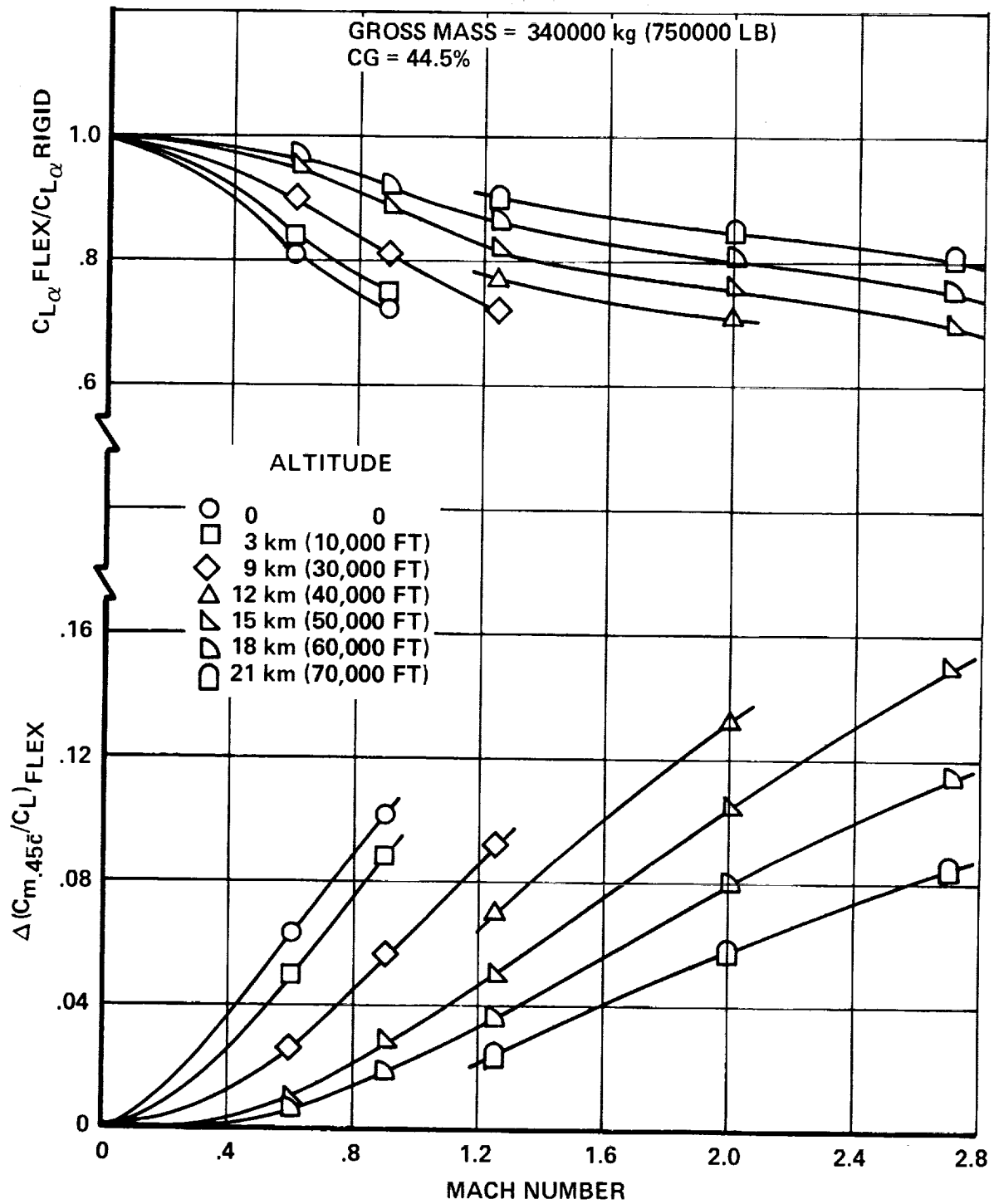


Figure 5-6. Free-Airplane Flexibility - Monocoque Arrangement - 750,000 lb.

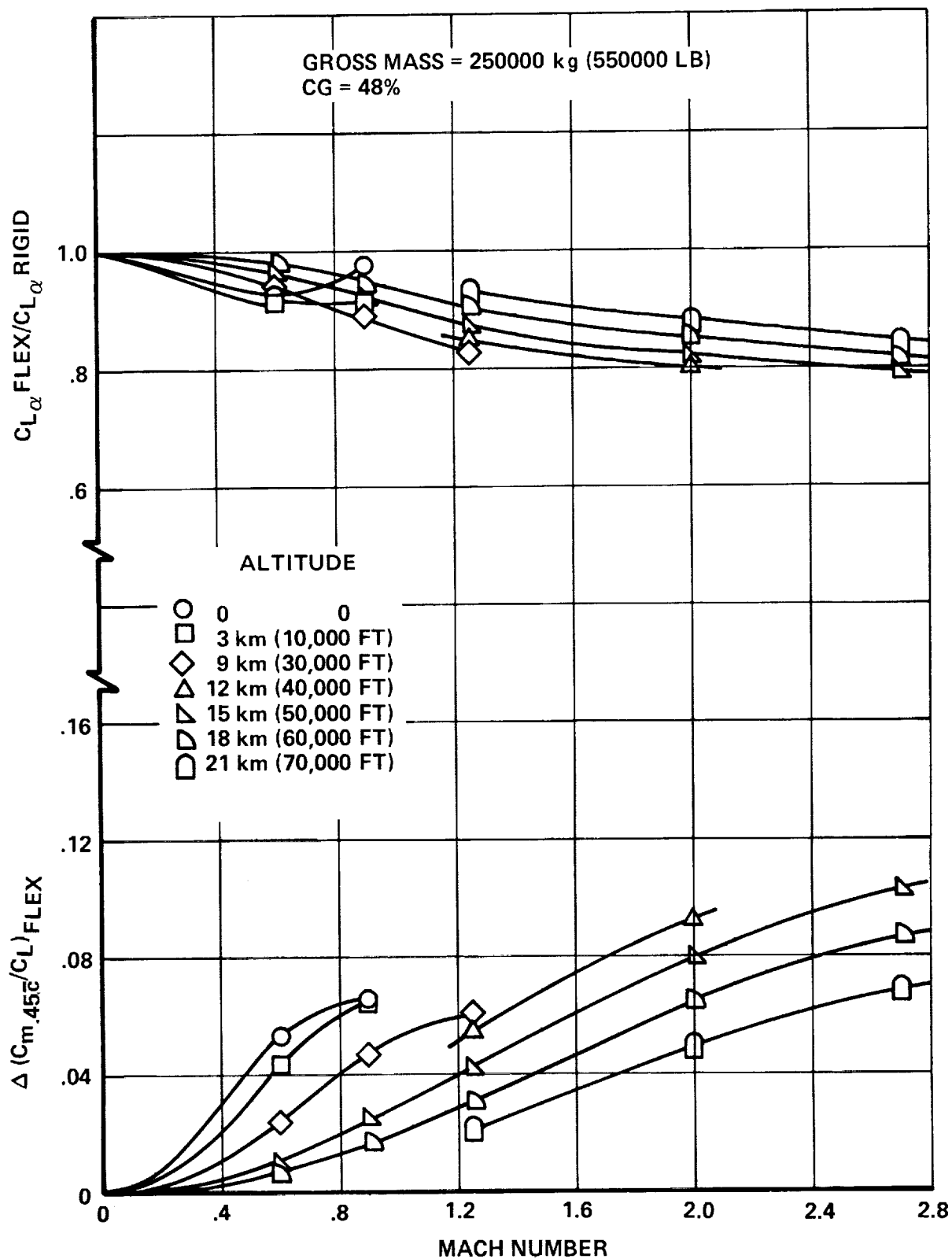


Figure 5-7. Free-Airplane Flexibility - Monocoque Arrangement - 550,000 lb.

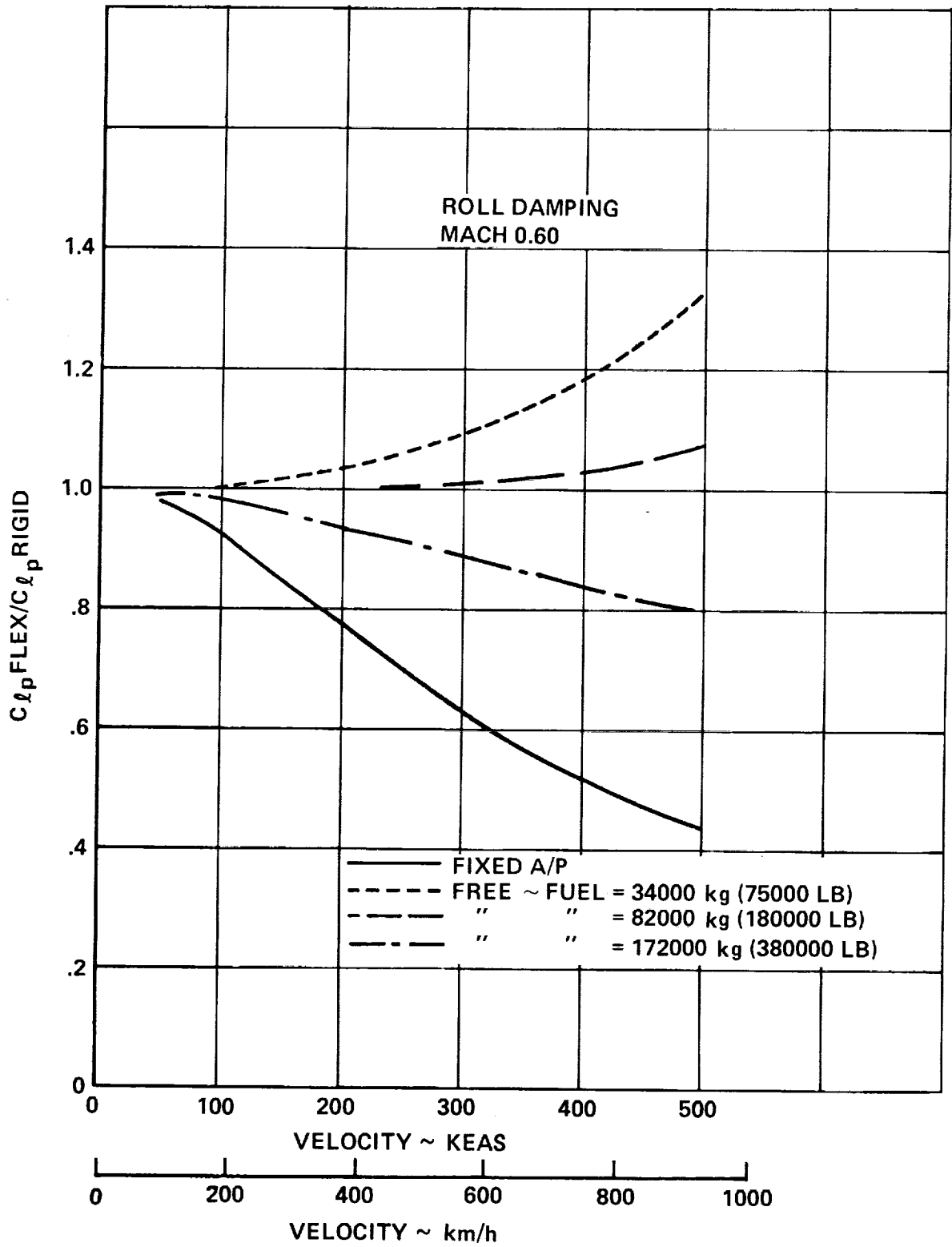


Figure 5-8. Airplane Roll Flexibility - Monocoque Arrangement - Mach 0.60

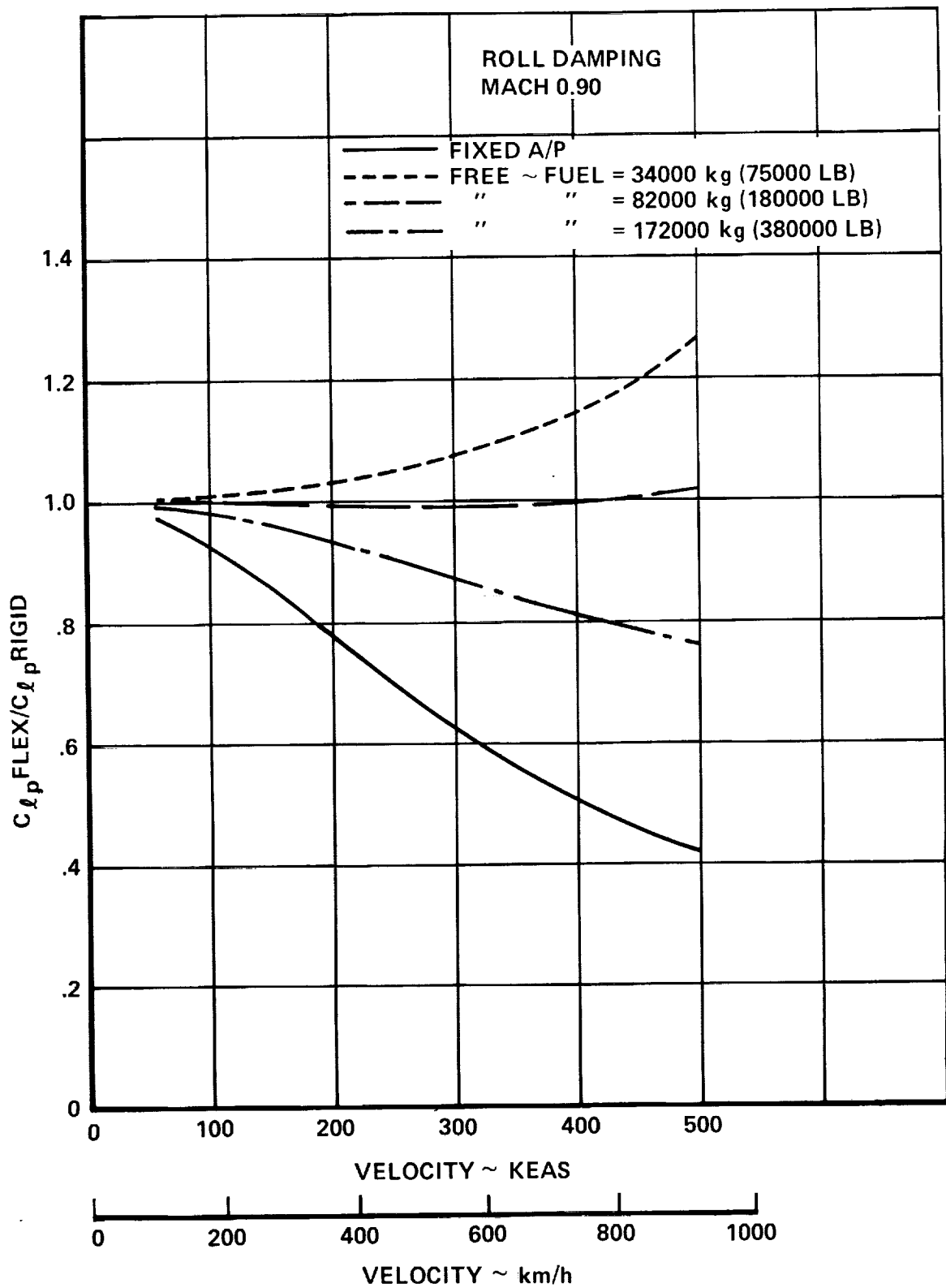


Figure 5-9. Airplane Roll Flexibility - Monocoque Arrangement - Mach 0.90



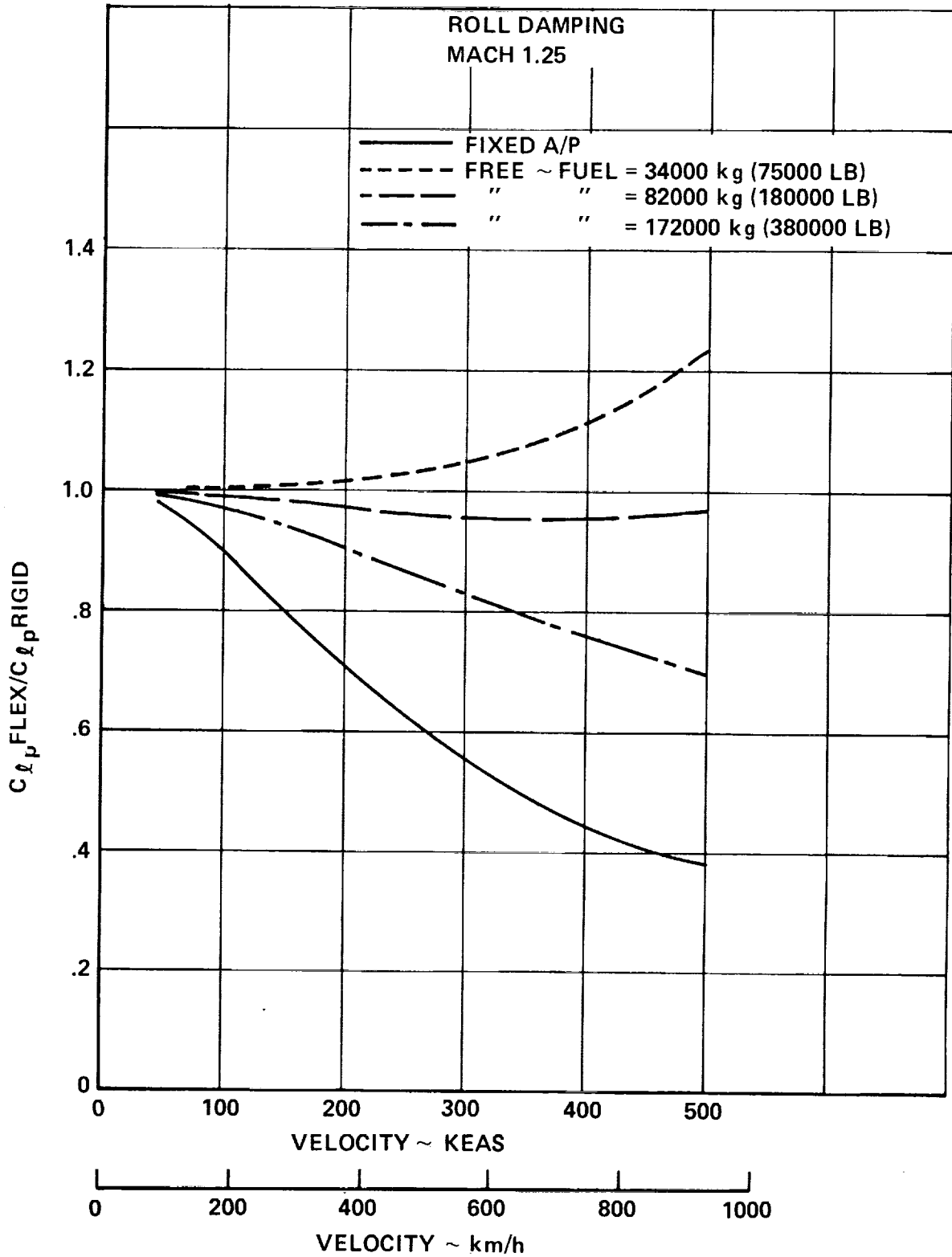


Figure 5-10. Airplane Roll Flexibility - Monocoque Arrangement - Mach 1.25

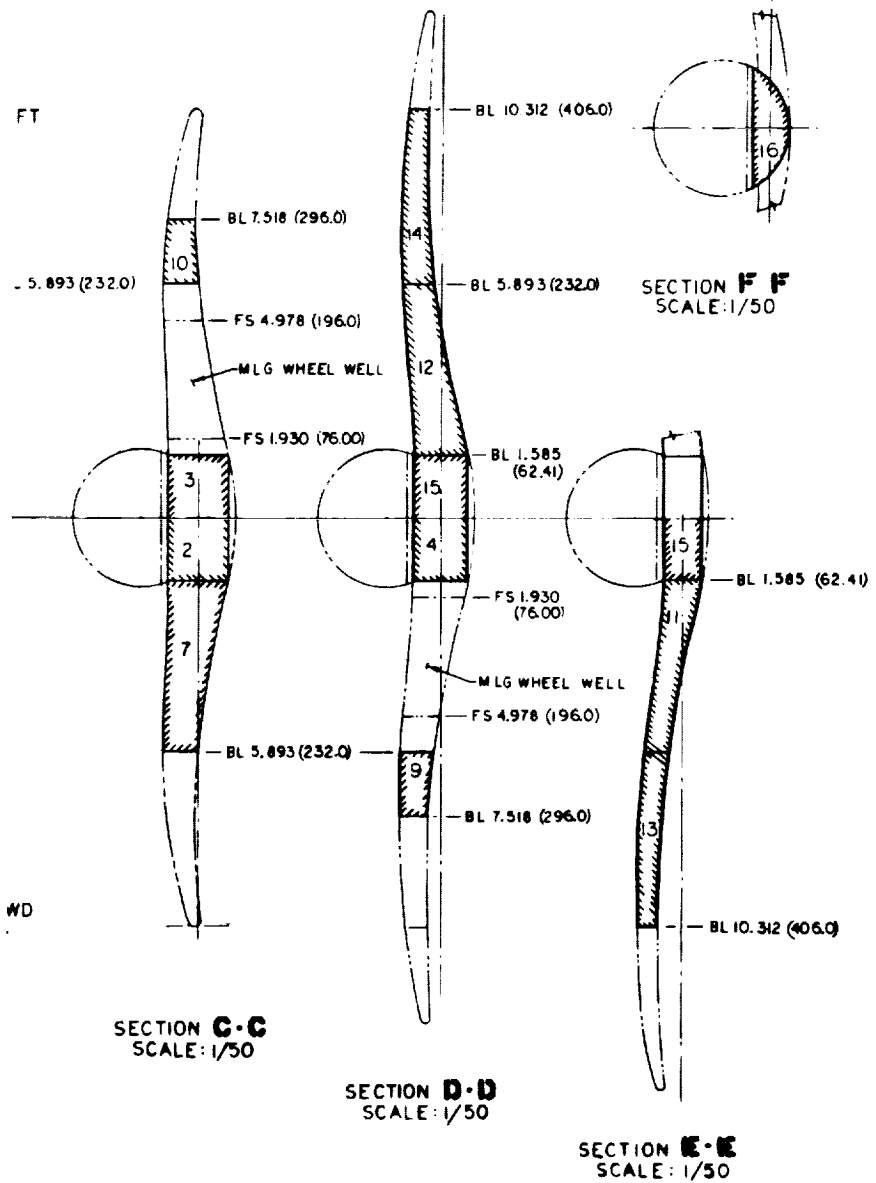
The flexible adjustments on derivatives that represent slopes such as  $(C_{l,\alpha})$  are presented in flexible-to-rigid ratio form. The adjustments to aerodynamic coefficients that represent absolute values such as  $(C_{m_0})$  are presented in the form of increments to be applied to the rigid coefficients.

The derivatives presented apply to a free-flight airplane. In the analysis, the airplane was not mathematically constrained by outside forces to establish the effects of flexibility, but was allowed to translate and rotate freely while equilibrium was maintained by inertia forces. The effect of each parameter ( $\alpha - \alpha_0$ ,  $\delta_e$ , etc.) were instantaneously applied along with representative inertia distributions. The redistribution of airloads due to airframe flexibility obtained in this manner reflects the effects of both airloads and inertia loads. The flexible derivatives thus obtained can be used directly in conventional rigid airplane equations of motion without the necessity of including aerodynamics coefficients representing inertia terms.

Airplane lift coefficient and pitching moment derivatives are presented for 2 airplane stiffnesses as defined by the chordwise-stiffened and monocoque designs. For each of the structural arrangements, 2 airplane weight cases were run: Gross weight = 750,000 lb. and 550,000 lb. Data for comparable airplane weight cases indicates negligible differences in longitudinal flexibility effects for the structural design concepts.

Rolling: Elastic lateral derivatives were determined at Mach numbers of 0.60, 0.90, and 1.25 using the AIC and SIC distributions for the chordwise-stiffened and monocoque arrangements. The resulting damping ratios, flexible-to-rigid, are shown in Figures 5-8 through 5-10 as a function of airplane velocity for the monocoque arrangement. The sensitivity of flexible-to-rigid ratio with airplane gross weight is indicated on the figures.

Figure 5-11 graphically displays the ratio of the flexible rolling moment coefficient to the rigid (wind tunnel data) coefficient obtained from Section 3. The data are for the Final Design airplane for both a low and high gross weight conditions. For the high gross weight case, the ratio is insensitive to variation in dynamic pressure. For the lightweight condition, however, the flexible-to-rigid ratio is highly sensitive to dynamic pressure



CAPACITY BASED ON BIAXIALLY STIFFENED  
COMB SANDWICH WING CONSTRUCTION LESS  
PERCENT FOR ADDITIONAL STRUCTURE, EQUIPMENT, ETC.  
FIGURED AT 803 KILOGRAMS/LITER OR  
35/GALLON.

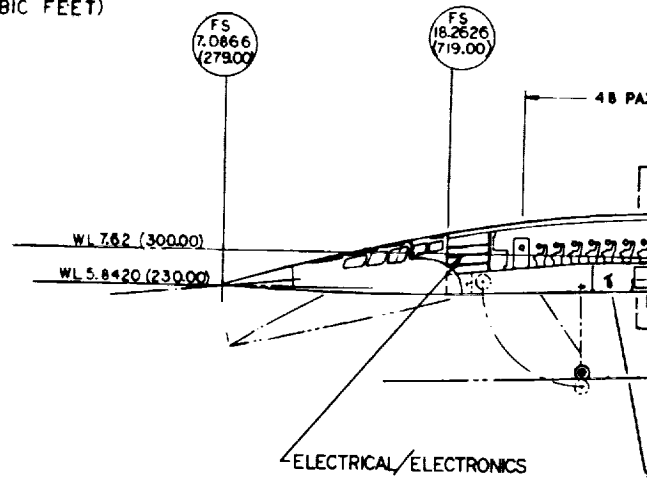
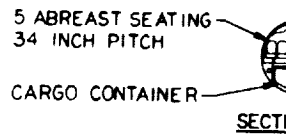
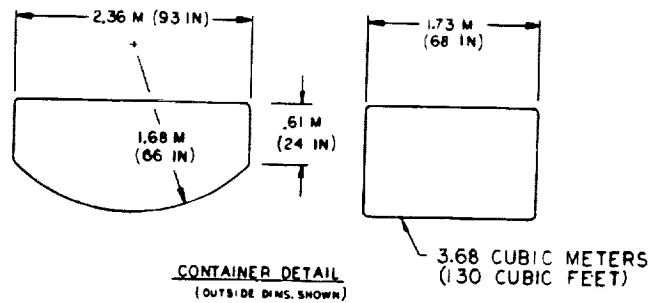
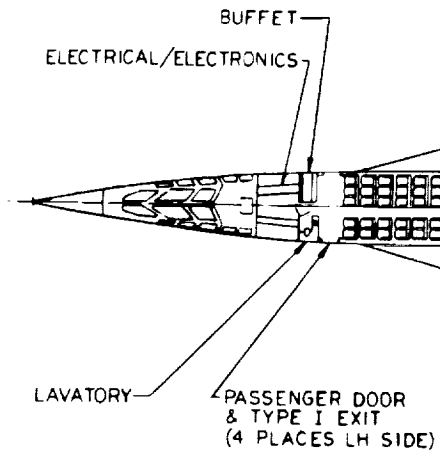
INDICATES FUEL TANK BOUNDARIES.

DIMENSIONS ARE SHOWN IN METERS (INCHES).

CAPACITY BASED ON NASA ARROW-WING  
36C FOLLOW-ON CARD DECK WITHOUT ANY CHANGES.

Figure 2-28. Fuel Tank Arrangement - Task II





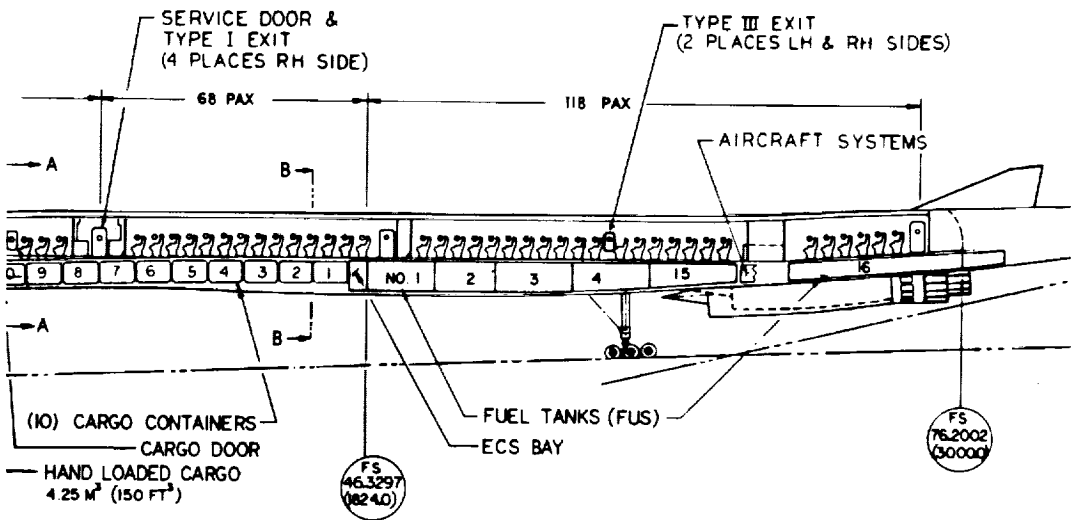
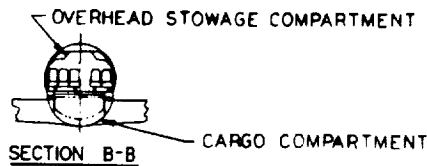
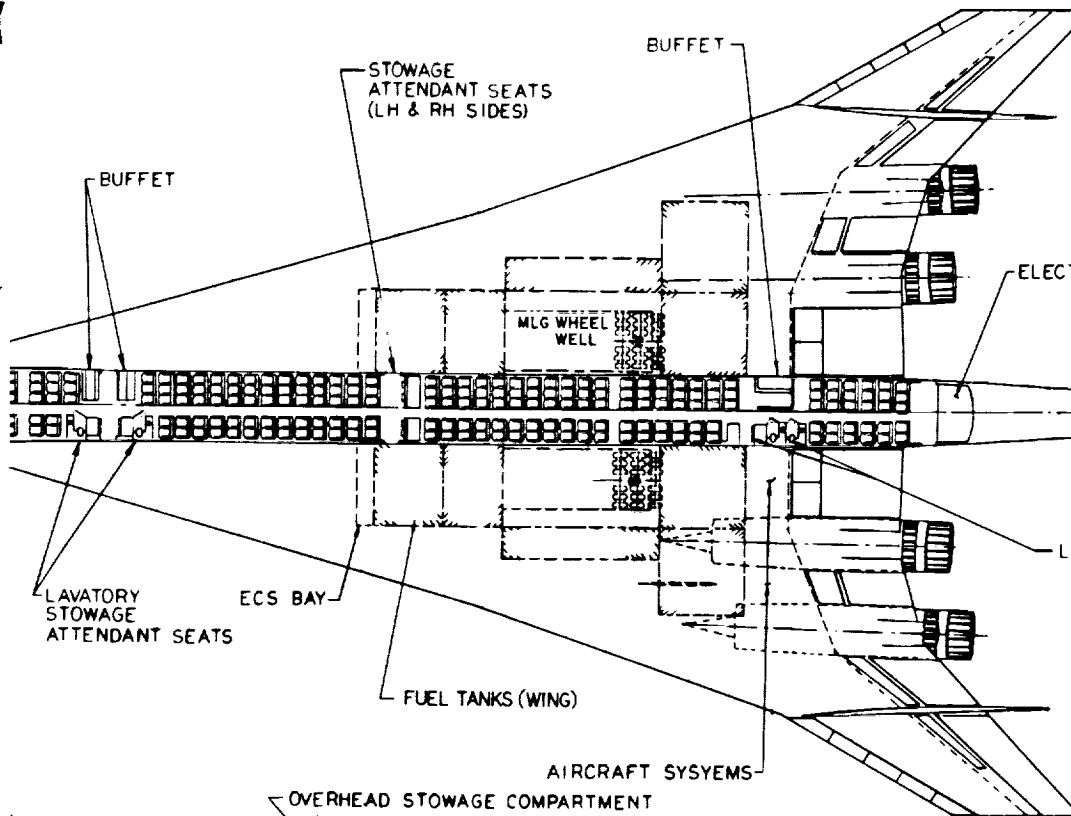
1. PAYLOAD EQUALS 22,000 KG (49,000 LBS)  
NOTE:

**ORIGINAL PAGE IS  
OF POOR QUALITY**

**PRECEDING PAGE BLANK NOT FILMED**

**FOLDOUT FRAME /**



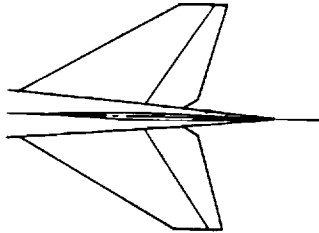






7

TRICAL LOAD CENTER



AVATORIES

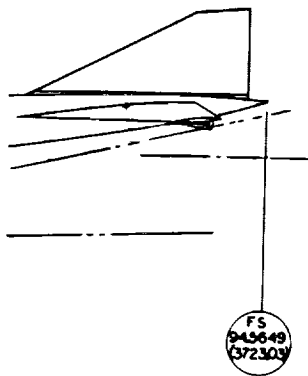
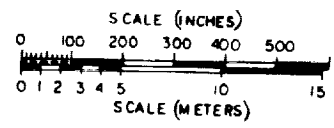


Figure 2-29. Interior Arrangement - Task II



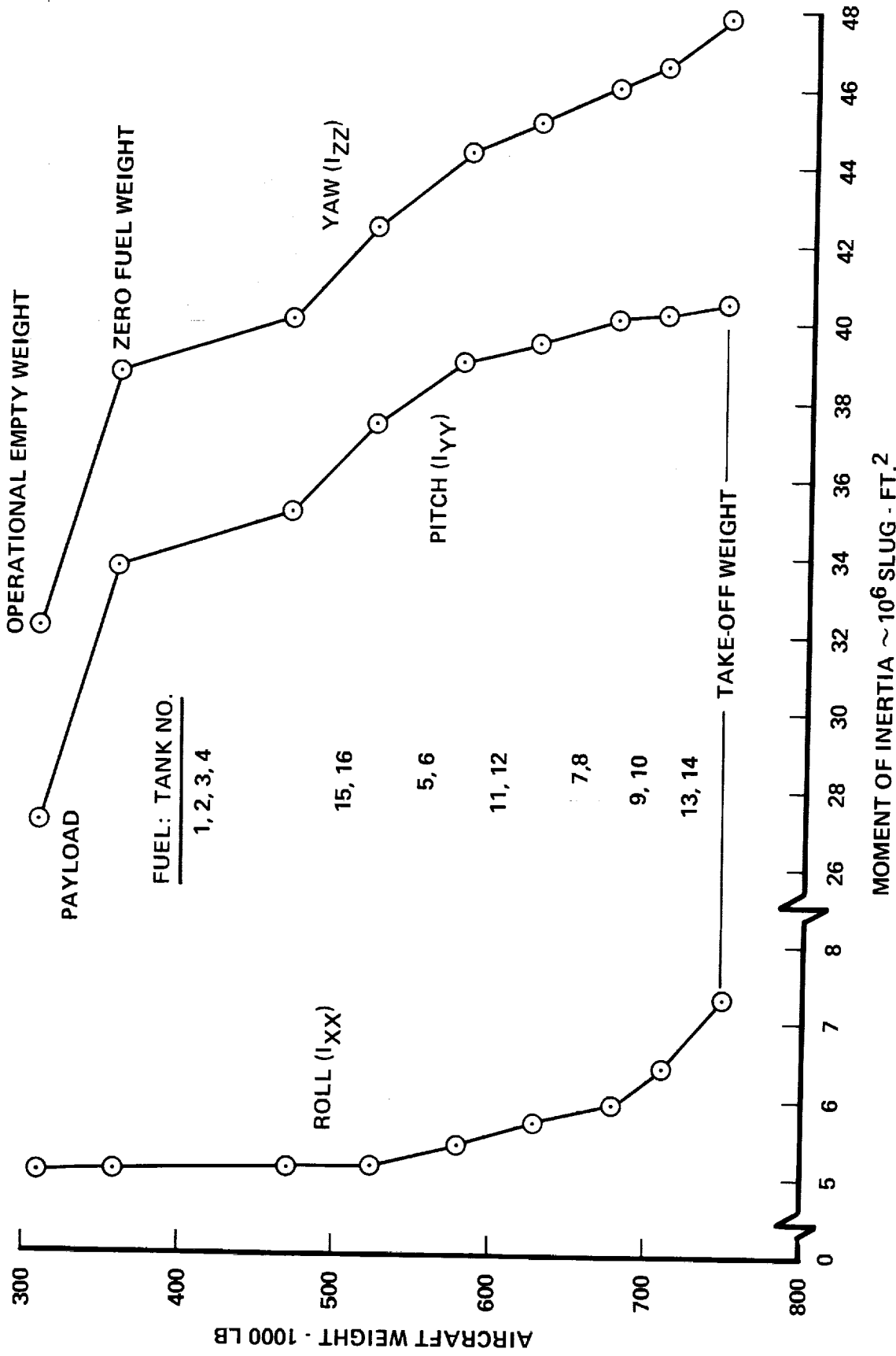


Figure 2-30. Aircraft Moment of Inertia - Task II

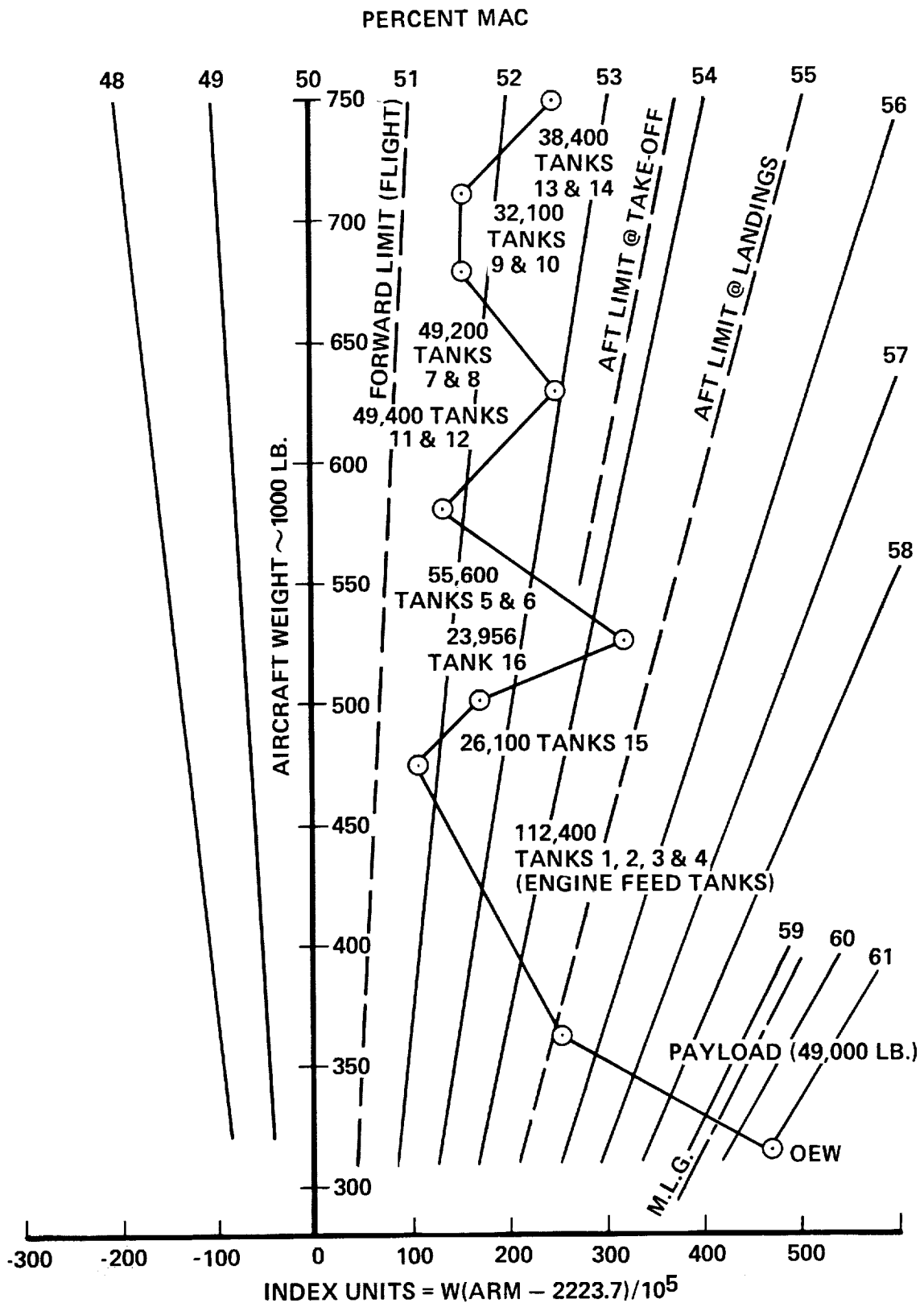
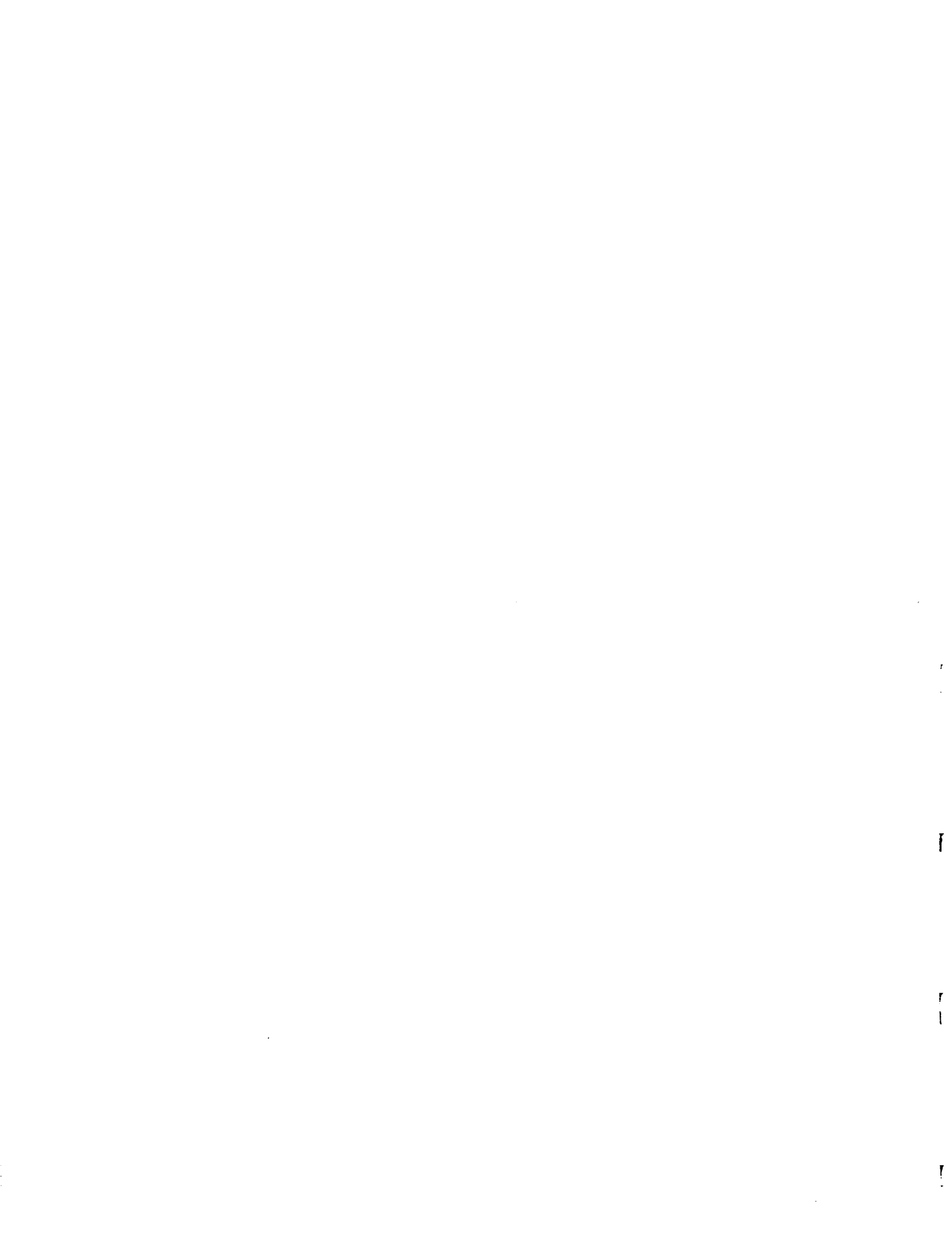


Figure 2-31. Center of Gravity Diagram - Task II

## REFERENCES

1. Foss, R.L.: Studies of the Impact of Advanced Technologies Applied to Supersonic Transport Aircraft - Task III Concept Refinement and Engine Coordination, Lockheed-California Company, LR 25827-3, 3 January 1974.



SECTION 3  
AERODYNAMICS  
BY  
D.M. URIE

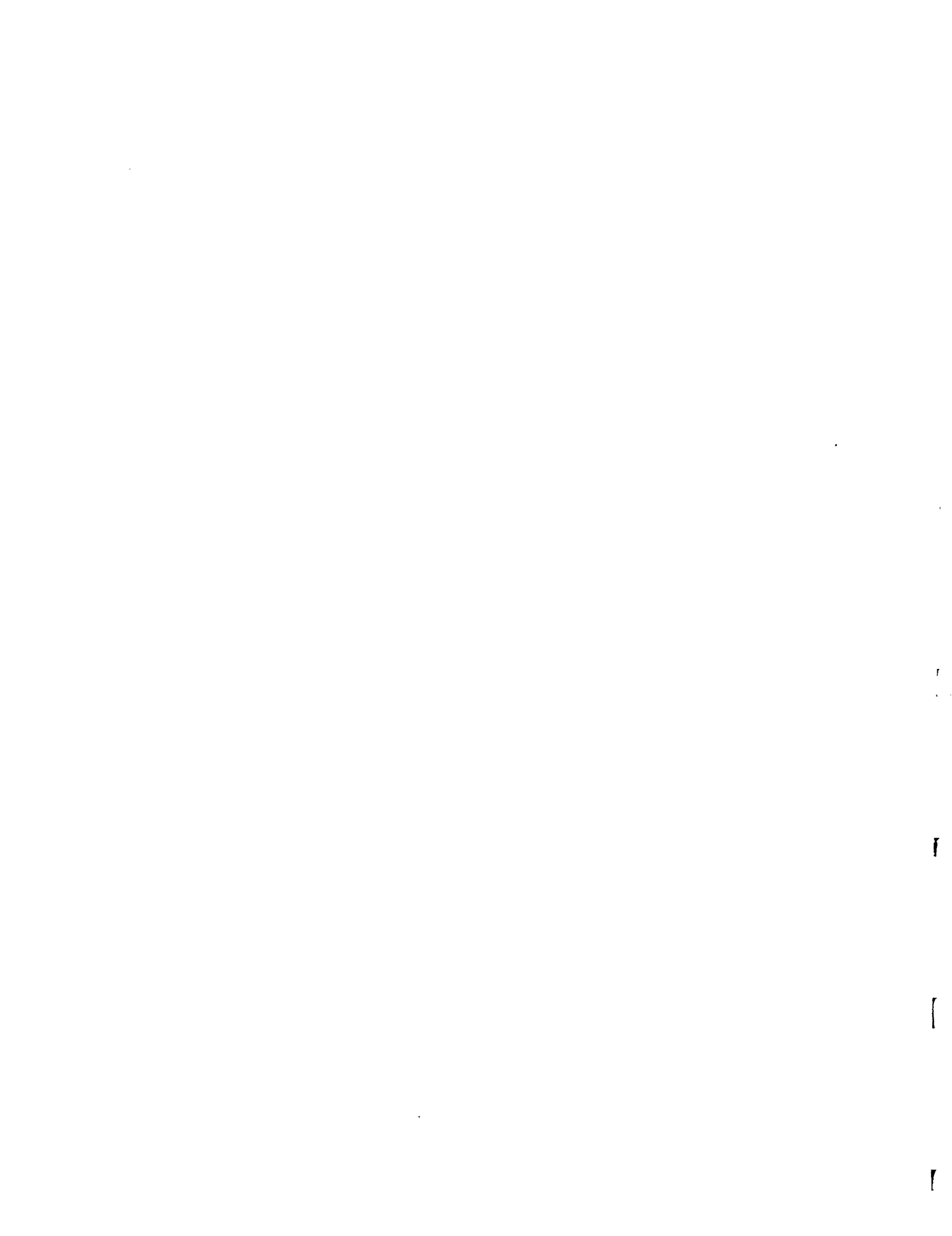




TABLE OF CONTENTS

<u>Section</u>	<u>Page</u>
INTRODUCTION	3-1
LOWSPEED DATA	3-1
HIGHSPEED DATA	3-6
AERODYNAMIC CRITERIA	3-28
CONFIGURATION CHARACTERISTICS	3-30
PERFORMANCE	3-38
STABILITY AND CONTROL	3-44
Aeroelastic Effects	3-44
Automatic Stabilization	3-44
Center-of-Gravity Limits	3-45
Operating Envelope	3-45
Takeoff Rotation	3-48
Envelope Limiting	3-48
Longitudinal Maneuvering Capability	3-50
Minimum Control Speed	3-57
Crosswind Landing	3-59
Steady Sideslip	3-59
Roll Performance	3-61
Response to Unstart	3-61

LIST OF FIGURES

<u>Figure</u>		<u>Page</u>
3-1	Baseline Configuration	3-2
3-2	Low Speed Lift Characteristic	3-2
3-3	Low Speed Pitching Moment Characteristic	3-3
3-4	Low Speed Drag Characteristics	3-3
3-5	Lift Characteristic (In Ground Effect)	3-4
3-6	Pitching Moment Characteristic (In Ground Effect)	3-4
3-7	Low Speed Drag Characteristics (In Ground Effect)	3-5
3-8	Low Speed Horizontal Tail Effectiveness	3-5
3-9	Low Speed Downwash	3-7
3-10	Low Speed Lateral-Directional Stability	3-7
3-11	Roll Control Effectiveness (Low Speed)	3-8
3-12	Low Speed Directional Control Effectiveness	3-8
3-13	Lift Characteristics, Mach 0.6	3-9
3-14	Lift Characteristics, Mach 0.9	3-9
3-15	Lift Characteristics, Mach 1.2	3-10
3-16	Lift Characteristics, Mach 2.3	3-10
3-17	Lift Characteristics, Mach 2.7	3-11
3-18	Lift Characteristics, Mach 2.95	3-11
3-19	Pitching Moment Characteristics, Mach 0.6	3-12
3-20	Pitching Moment Characteristics, Mach 0.9	3-12
3-21	Pitching Moment Characteristics, Mach 1.2	3-13
3-22	Pitching Moment Characteristics, Mach 2.3	3-13
3-23	Pitching Moment Characteristics, Mach 2.7	3-14
3-24	Pitching Moment Characteristics, Mach 2.95	3-14
3-25	High Speed Lift Characteristics	3-15
3-26	High Speed Pitching Moment Characteristics ( $-1 < n_z \leq 1$ )	3-15
3-27	High Speed Pitching Moment Characteristics ( $1 < n_z < 2.5$ )	3-16
3-28	Subsonic Cruise Polar	3-16
3-29	Transonic Cruise Polar	3-18
3-30	Off-Design Cruise Polar	3-18
3-31	Trimmed Cruise Polar	3-19
3-32	Cruise Drag Characteristics	3-19

LIST OF FIGURES (CONT'D)

<u>Figure</u>		<u>Page</u>
3-33	Pitch Rate and Angle of Attack Rate Derivatives	3-20
3-34	High Speed Horizontal Tail Effectiveness	3-20
3-35	High Speed Downwash	3-22
3-36	Transonic Lateral-Directional Stability ( $C_{n\beta}, C_{y\beta}$ )	3-22
3-37	Transonic Lateral-Directional Stability ( $C_{l\beta}$ )	3-23
3-38	Supersonic Lateral-Directional Stability	3-23
3-39	Yaw Rate Derivatives	3-24
3-40	Roll Rate Derivatives	3-24
3-41	Aileron Segment 2 Effectiveness	3-25
3-42	Aileron Segment 3 Effectiveness	3-25
3-43	Spoiler-Slot-Deflector 2 Effectiveness	3-26
3-44	Inverted Spoiler-Slot-Deflector Effectiveness	3-26
3-45	Spoiler-Slot-Deflector 4 Effectiveness	3-27
3-46	High Speed Directional Control Effectiveness	3-27
3-47	Primary Control System Layout	3-31
3-48	Take Off Speeds	3-39
3-49	Minimum Speed Relationships	3-40
3-50	Baseline Mission Profile	3-42
3-51	Trim Angle of Attack	3-43
3-52	Longitudinal Command Augmentation System	3-46
3-53	Center of Gravity Limits	3-46
3-54	Airspeed-Altitude Envelope	3-46
3-55	Minimum Demonstration Speeds	3-47
3-56	Minimum Nose Wheel Lift-Off	3-47
3-57	Airplane Nose-Up Control Power	3-49
3-58	Minimum Speed Demonstration	3-49
3-59	Horizontal Stabilizer Incidence to Trim, $\delta_F = 20^\circ$ Maximum Take-Off Weight-Aft. C.G.	3-51
3-60	Horizontal Stabilizer Incidence to Trim, $\delta_F = 20^\circ$ Maximum Take-Off Weight-Aft. C.G.	3-51
3-61	Horizontal Stabilizer Incidence to Trim, $\delta_F = 20^\circ$ Maximum Landing Weight-Fwd. C.G.	3-52
3-62	Horizontal Stabilizer Incidence to Trim, $\delta_F = 20^\circ$ Maximum Landing Weight-Aft. C.G.	3-52

## LIST OF FIGURES (CONT'D)

<u>Figure</u>		<u>Page</u>
3-63	Horizontal Stabilizer Incidence to Trim, $\delta_F = 0^\circ$ Maximum Take-Off Weight-Fwd. C.G.	3-53
3-64	Horizontal Stabilizer Incidence to Trim, $\delta_F = 0^\circ$ Maximum Take-Off Weight-Aft C.G.	3-53
3-65	Horizontal Stabilizer Incidence to Trim, $\delta_F = 0^\circ$ Maximum Landing Weight-Fwd. C.G.	3-54
3-66	Horizontal Stabilizer Incidence to Trim, $\delta_F = 0^\circ$ Maximum Landing Weight-Aft C.G.	3-54
3-67	Horizontal Stabilizer Incidence to Trim Transonic, Fwd. C.G.	3-55
3-68	Horizontal Stabilizer Incidence to Trim, Transonic, Aft. C.G.	3-55
3-69	Horizontal Stabilizer Incidence to Trim, Supersonic, Fwd. C.G.	3-56
3-70	Horizontal Stabilizer Incidence to Trim, Supersonic, Aft. C.G.	3-56
3-71	Ground Minimum Control Speed	3-58
3-72	Air Minimum Control Speed	3-58
3-73	Cross-Wind Landing	3-60
3-74	Engine Out Steady Sideslip	3-60
3-75	Roll Performance-Landing Approach	3-62
3-76	Roll Performance-Climb Configuration, $V_{MO}$	3-62
3-77	Supersonic Roll Power for Stiffened Wing	3-63
3-78	Response to Inlet Unstart	3-64

LIST OF TABLES

<u>Table</u>		<u>Page</u>
3-1	Airplane Dimensional Data	3-32
3-2	Primary Control System	3-37

1

2

3

4

5

## LIST OF SYMBOLS

A	aspect ratio
b	span
BL	buttock line
$\bar{c}$ , MAC	mean aerodynamic chord
$C_D$	drag coefficient, $\frac{\text{Drag}}{q S_{REF}}$
C.G.	center of gravity location
$C_L$	lift coefficient, $\frac{\text{Lift}}{q S_{REF}}$
$C_{L_H}$	$\frac{\text{Lift of horizontal tail}}{q S_H}$
$C_{L_q}$	rate of change of lift coefficient with pitch rate
$C_{L\dot{\alpha}}$	rate of change of lift coefficient with angle-of-attack rate
$C_l$	rolling moment coefficient, $\frac{\text{Rolling moment}}{q S_{REF} b}$
$C_{l_p}$	rate of change of rolling moment coefficient with roll rate
$C_{l_r}$	rate of change of rolling moment coefficient with yaw rate
$C_{l\beta}$	rate of change of rolling moment coefficient with sideslip angle
$C_{l\delta_a}$	rate of change of rolling moment coefficient with aileron deflection
$C_{l\delta_v}$	rate of change of rolling moment coefficient with vertical tail deflection
$C_{m_{.45\bar{c}}}$	pitching moment coefficient, $\frac{\text{Moment about } .45\bar{c}}{q S_{REF} \bar{c}}$

**PRECEDING PAGE BLANK NOT FILMED**

$C_{m_0}$	Zero lift pitching moment coefficient
$C_{m_{q.45c}}^{\bar{}}$	rate of change of pitching moment coefficient with pitch rate
$C_{m_{\dot{\alpha}.45c}}^{\bar{}}$	rate of change of pitching moment coefficient with angle-of-attack rate
$C_n$	yawing moment coefficient, $\frac{\text{yawing moment}}{q S_{REF} b}$
$C_{n_p}$	rate of change of yawing moment coefficient with roll rate
$C_{n_r}$	rate of change of yawing moment coefficient with yaw rate
$C_{n_\beta}$	rate of change of yawing moment coefficient with sideslip angle
$C_{n_{\delta_a}}$	rate of change of yawing moment coefficient with aileron deflection
$C_{n_{\delta_v}}$	rate of change of yawing moment coefficient with vertical tail deflection
$C_r$	root chord
$C_t$	tip chord
$C_Y$	side force coefficient, $\frac{\text{Side Force}}{q S_{REF}}$
$C_{Y_p}$	rate of change of side force coefficient with roll rate
$C_{Y_r}$	rate of change of side force coefficient with yaw rate
$C_{Y_\beta}$	rate of change of side force coefficient with sideslip angle
$C_{Y_{\delta_a}}$	rate of change of side force coefficient with aileron deflection
$C_{Y_{\delta_v}}$	rate of change of side force coefficient with vertical tail deflection



$h$	height above ground of $.45\bar{c}$ point on water line 300
$l$	control surface arm from moment reference
$n_z$	normal load factor $\sim g$ 's
$q$	free stream dynamic pressure
$q_H$	dynamic pressure at the horizontal tail
$S$	surface area
$S_H$	total area of horizontal tail
$S_{REF}$	wing reference area
$S_W$	total wing area
$\bar{V}$	control surface volume coefficient
$\alpha_{LO}$	zero lift angle-of-attack
$\alpha_{WRP}$	angle-of-attack of wing reference plane
$\beta$	sideslip angle
$\Gamma$	dihedral angle
$\delta_a$	aileron deflection
$\delta_F, \delta_{F_{TE}}$	wing trailing edge flap deflection
$\delta_{ISSD}$	inverted spoiler-slot-deflector deflection
$\delta_{SSD}$	spoiler-slot-deflector deflection
$\delta_V$	vertical tail deflection
$\epsilon$	downwash angle at the horizontal tail
$\epsilon_o$	zero lift downwash at the tail
$\eta$	$\frac{q_H}{q}$
$\Lambda_{LE}$	leading edge sweepback angle

$\lambda$	taper ratio
$\phi$	bank angle
$\frac{dC_L}{d\alpha}$	rate of change of lift coefficient with angle-of-attack
$\frac{dC_{m.45c}}{dC_L}$	rate of change of pitching moment coefficient with lift coefficient
$\frac{dC_{m.45c}}{d\delta_e}$	rate of change of pitching moment coefficient with elevator deflection
$\frac{dC_{m.45c}}{d\delta_H}$	rate of change of pitching moment coefficient with horizontal tail deflection
$\frac{d\epsilon}{d\alpha}$	rate of change of downwash at the tail with wing angle-of-attack

## SECTION 3

### AERODYNAMICS

#### INTRODUCTION

The aerodynamic data presented herein are intended to represent the Baseline Configuration Concept - Task II (Figure 3-1) which is described in detail in Section 2. These data were developed from the results of NASA wind tunnel tests of the Arrow-Wing Configuration. The test results are unpublished but have been collected in working papers and in the form of data packages from several tests.

Appropriate corrections have been applied to the data to account for differences in wing planform geometry, tail volume coefficients, and surface arrangements between wind tunnel models and the baseline airplane controls.

#### LOW SPEED DATA

The longitudinal data for Mach numbers below 0.6 are shown in Figures 3-2 through 3-4 for zero and twenty-degrees trailing edge flap deflection. Trailing edge flaps are Panels 1, 2 and 3. The lift data is shown as a function of wing reference plane (WRP) angle of attack. Pitching moment data is referred to the 45-percent point of the mean aerodynamic chord (MAC), where the mean aerodynamic chord is calculated on the basis of total wing area. The ground effect was obtained from wind tunnel tests with ground plane and is shown in Figures 3-5 and 3-7 for the 20-degrees trailing edge flap position only. This flap angle is assumed for both take-off and landing configurations.

Low speed horizontal tail effectiveness is shown on Figure 3-8 as a set of lines representing various elevator deflections. The tail lift curve slope for the various elevator deflections are constant as indicated by the parallel

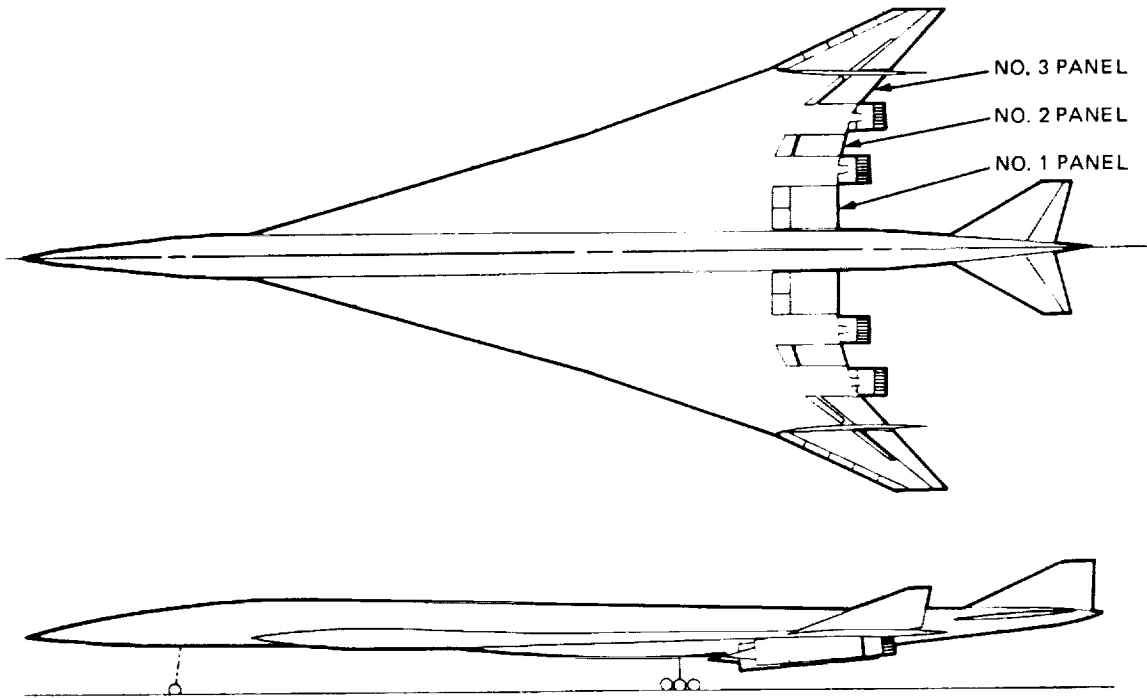


FIGURE 3-1. BASELINE CONFIGURATION

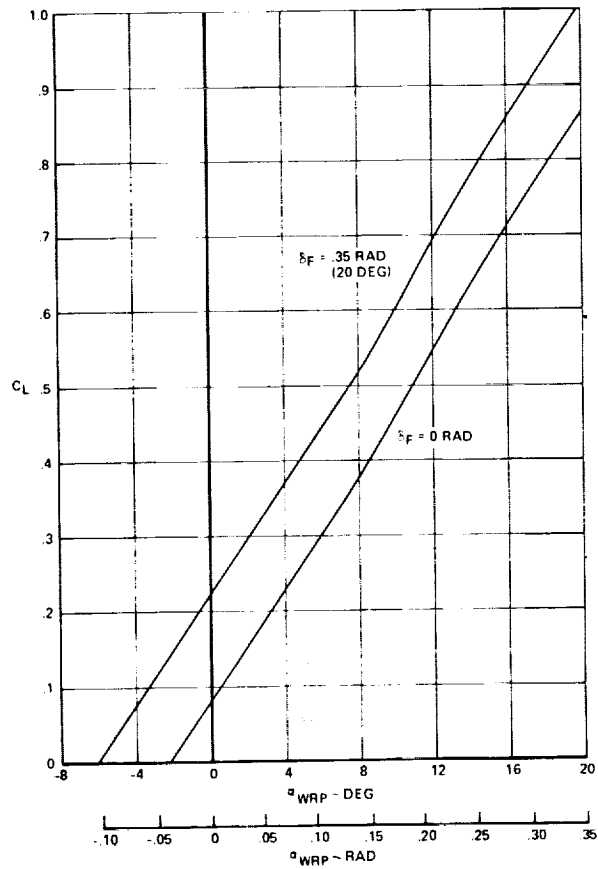


FIGURE 3-2. LOW SPEED LIFT CHARACTERISTIC

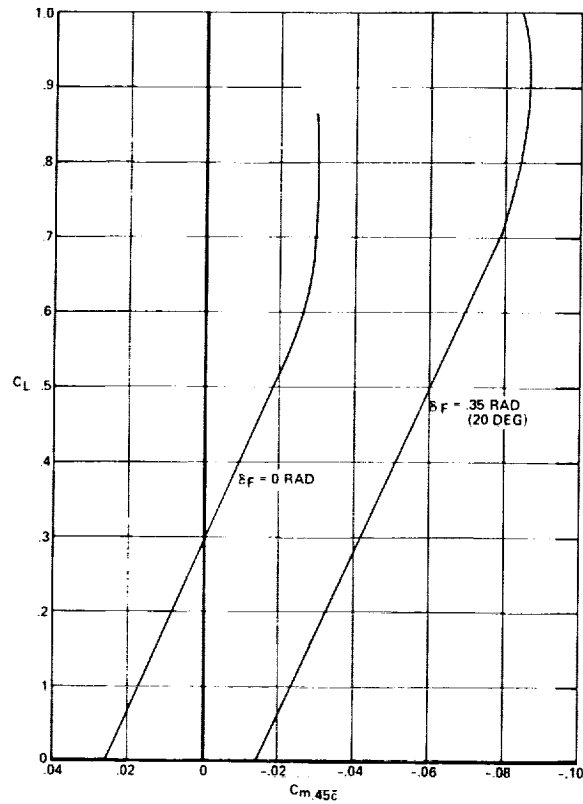


FIGURE 3-3. LOW SPEED PITCHING MOMENT CHARACTERISTIC

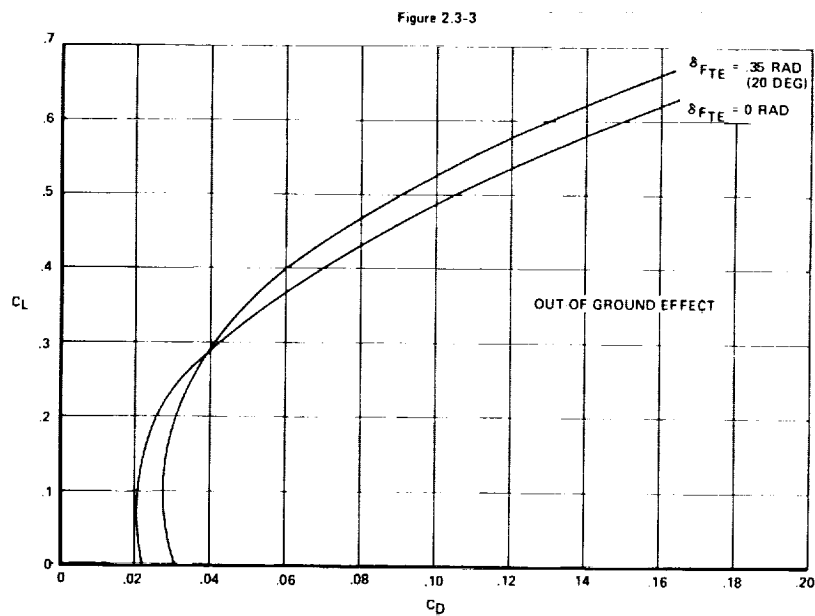


FIGURE 3-4. LOW SPEED DRAG CHARACTERISTICS

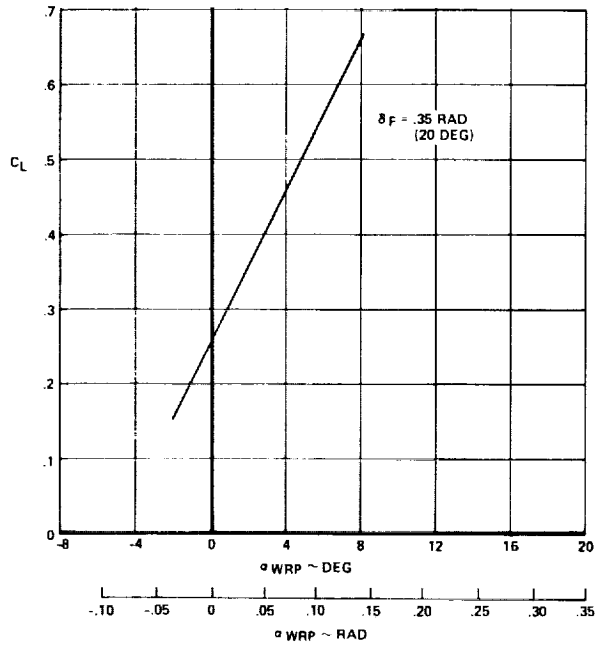


FIGURE 3-5. LIFT CHARACTERISTIC (IN GROUND EFFECT)

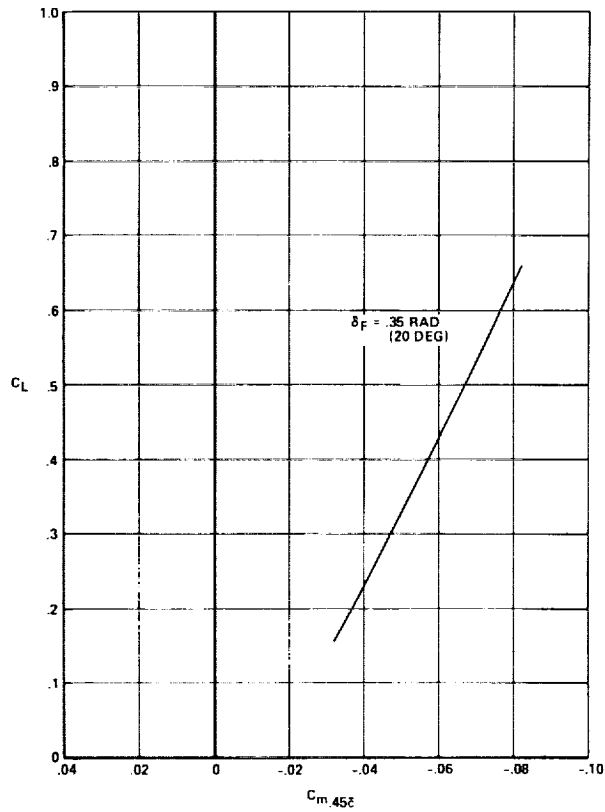


FIGURE 3-6. PITCHING MOMENT CHARACTERISTIC (IN GROUND EFFECT)

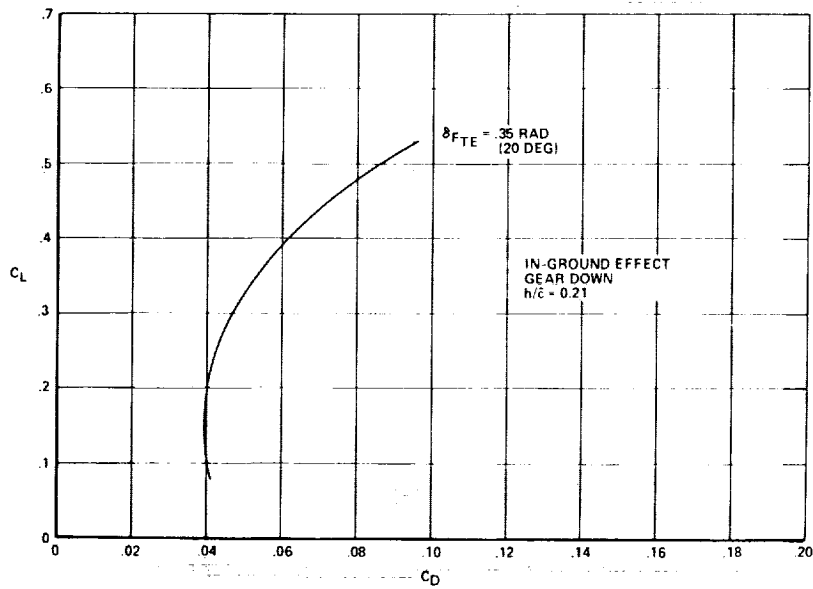


FIGURE 3-7. LOW SPEED DRAG CHARACTERISTICS (IN GROUND EFFECT)

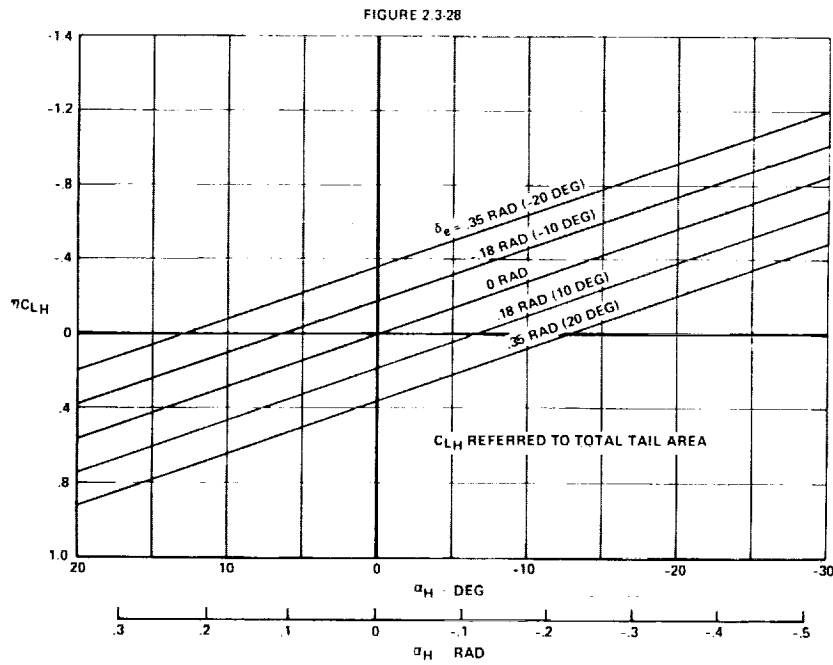


FIGURE 3-8. LOW SPEED HORIZONTAL TAIL EFFECTIVENESS

sloping lines. Low speed downwash out of the ground effect is shown as a function of angle of attack in Figure 3-9.

The lateral directional data for the low speed case is shown in Figure 3-10 as a function of wing reference plane angle of attack. Rolling moment coefficient is referenced about water line 300 and the yawing moment coefficient is referred to the 45 percent MAC.

The low speed aileron effectiveness data are shown as linearized derivatives in Figure 3-11. The effectiveness of all three panels used as ailerons (Number 2 flaperon panel, and Number 3&4 Aileron Panels) are shown versus angle of attack linearized over  $\pm 60$ -degree total aileron where total aileron is right side deflection minus left side deflection.

Low speed directional control power is shown in Figure 3-12 for the vertical fin only and vertical fin with geared rudder. It is intended that the control surface consist of the vertical fin plus geared rudder. Only the yawing moment is shown for either low or high speed. The rolling moment due to vertical fin is negligibly small and the side force is shown in each figure as a factor of the yawing moment coefficient.

#### HIGH SPEED DATA

Lift and pitching moment data for Mach 0.60 up to Mach 2.95 are shown in non-linear form for specific Mach numbers in Figures 3-13 through 3-24 followed by linearized data in Figures 3-25 through 3-27 covering the entire Mach range. These data are shown for both horizontal tail-off and tail-on. The data represents the rigid airplane with the wing at the 1-g mid-cruise (Mach 2.7) shape. The pitching moment data have been linearized in two sets. One set covers the segment of the pitching moment curve at or below lift coefficients for 1-g flight and applies to trim and to negative maneuvers. The second set is linearized over lift coefficients for load factors from 1-g to 2.5-g and applies to positive maneuvers.



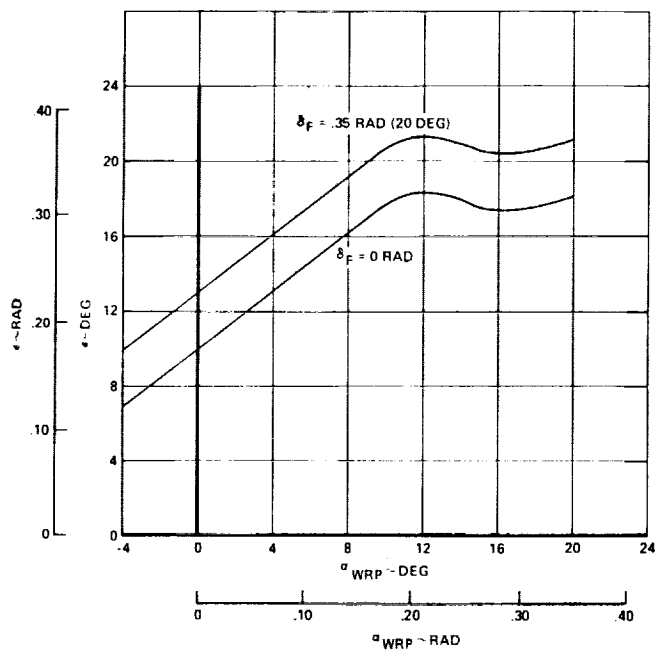


FIGURE 3-9. LOW SPEED DOWNWASH

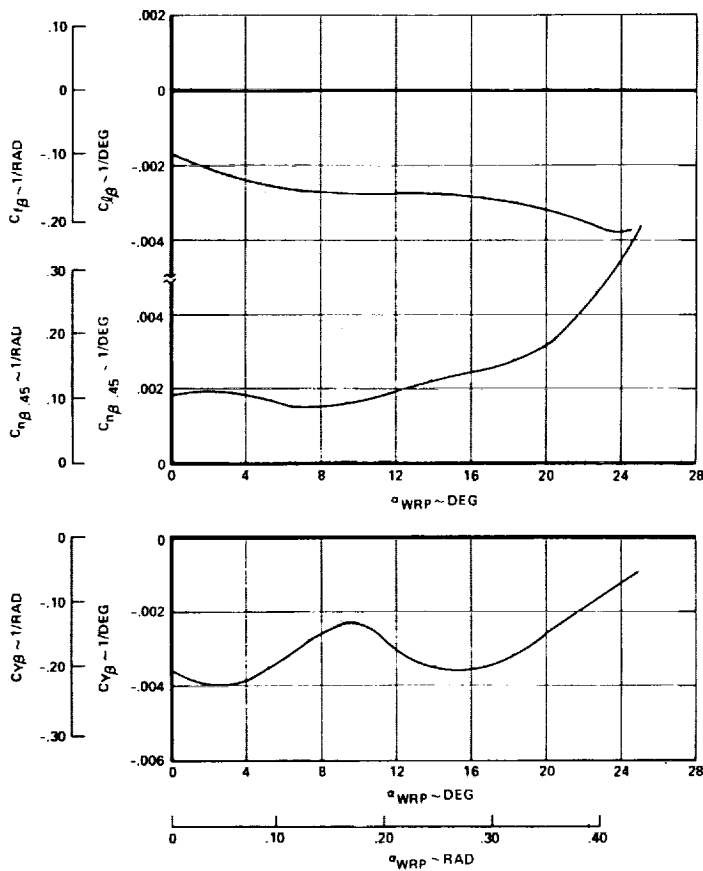


FIGURE 3-10. LOW SPEED LATERAL-DIRECTIONAL STABILITY

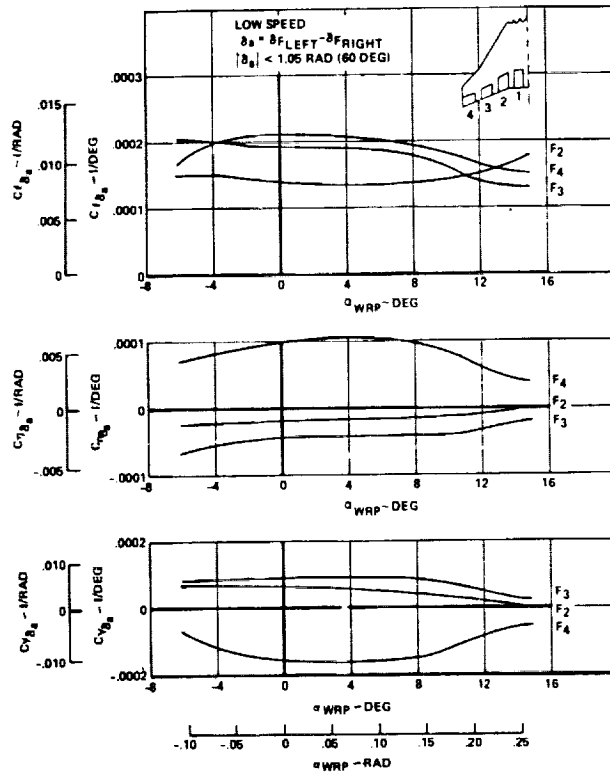


FIGURE 3-11. ROLL CONTROL EFFECTIVENESS (LOW SPEED)

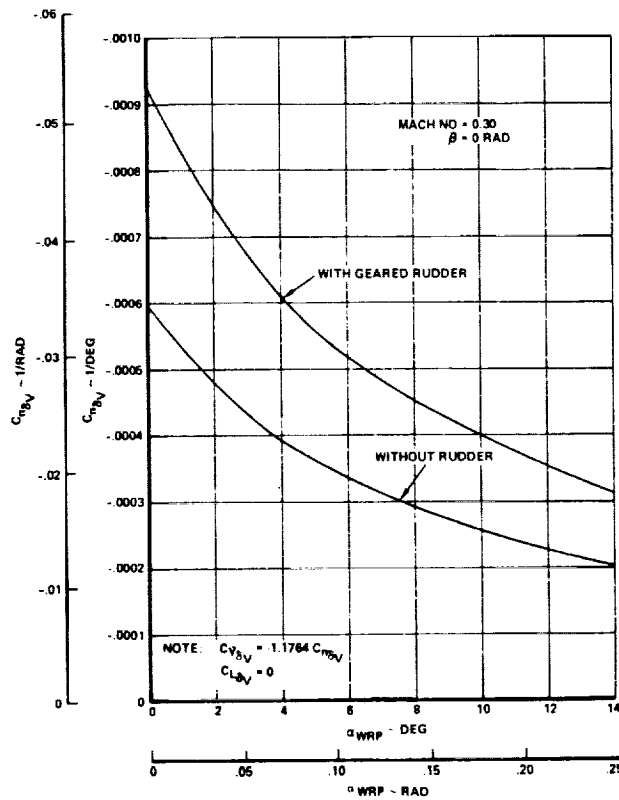


FIGURE 3-12. LOW SPEED DIRECTIONAL CONTROL EFFECTIVENESS

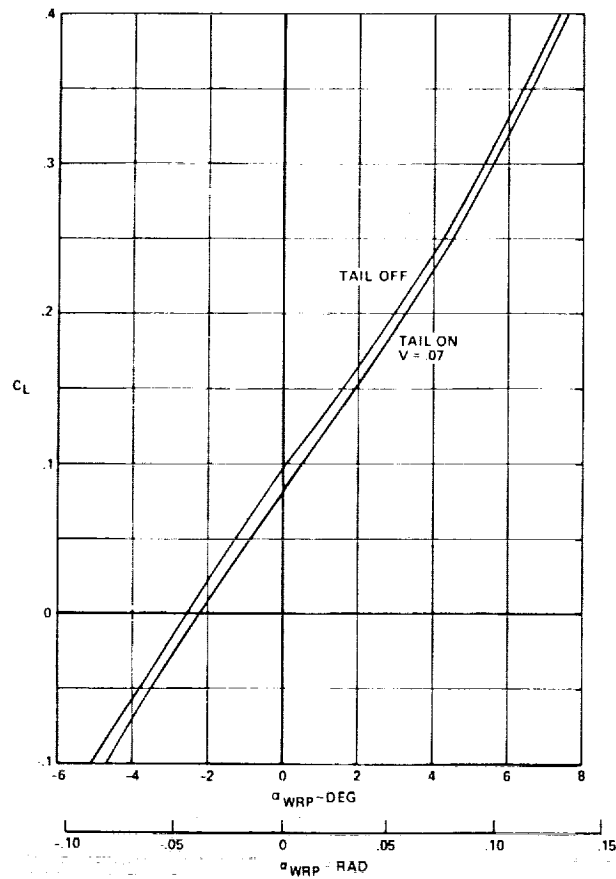


FIGURE 3-13. LIFT CHARACTERISTICS, MACH 0.6

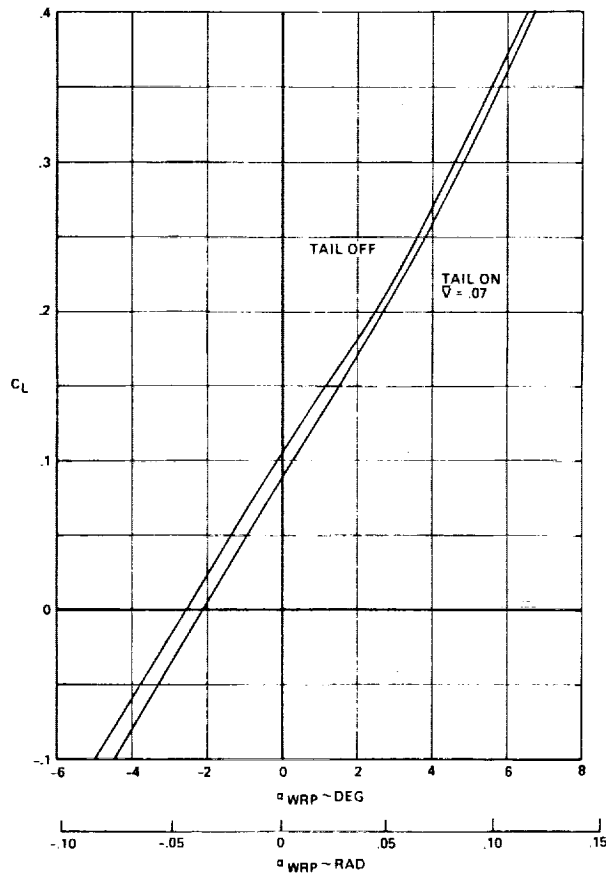


FIGURE 3-14. LIFT CHARACTERISTICS, MACH 0.9

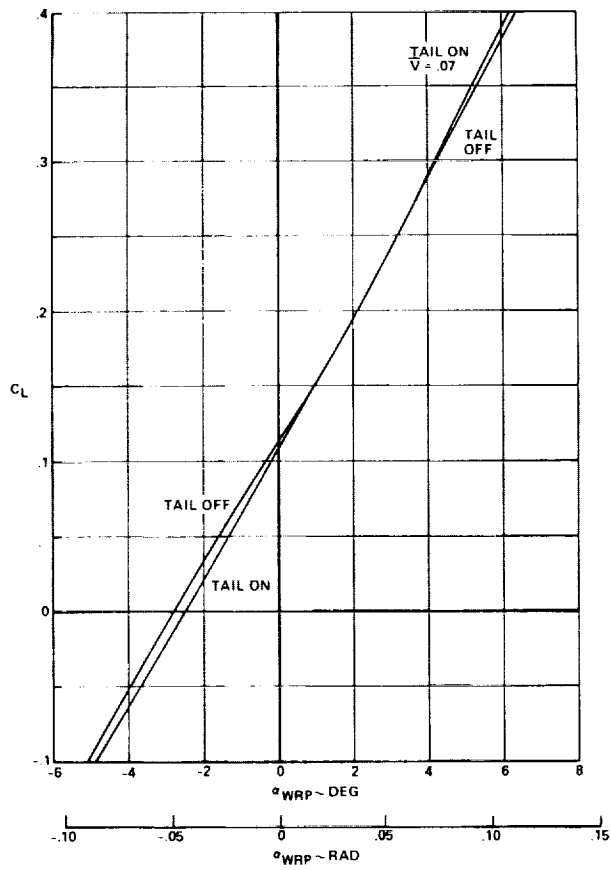


FIGURE 3-15. LIFT CHARACTERISTICS, MACH 1.2

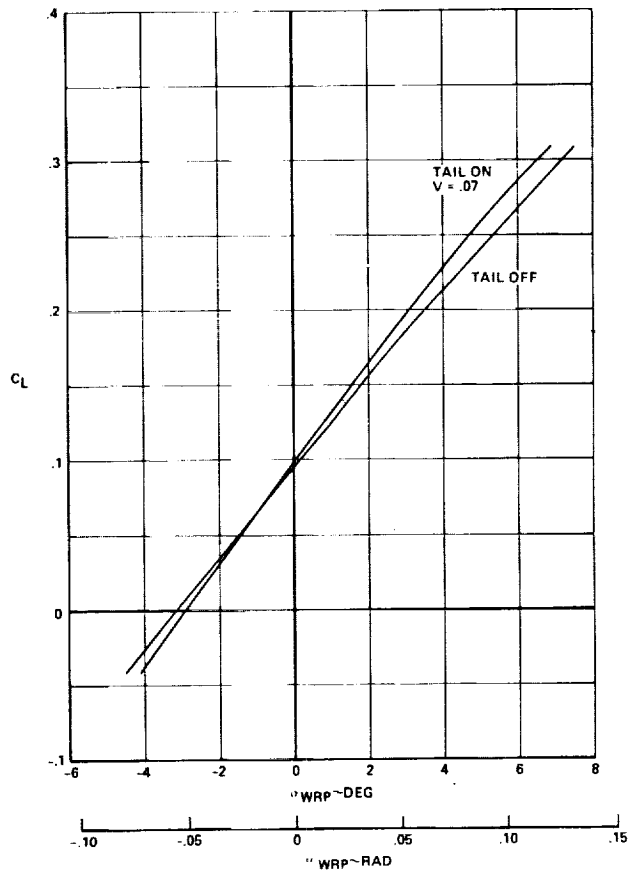


FIGURE 3-16. LIFT CHARACTERISTICS, MACH 2.3

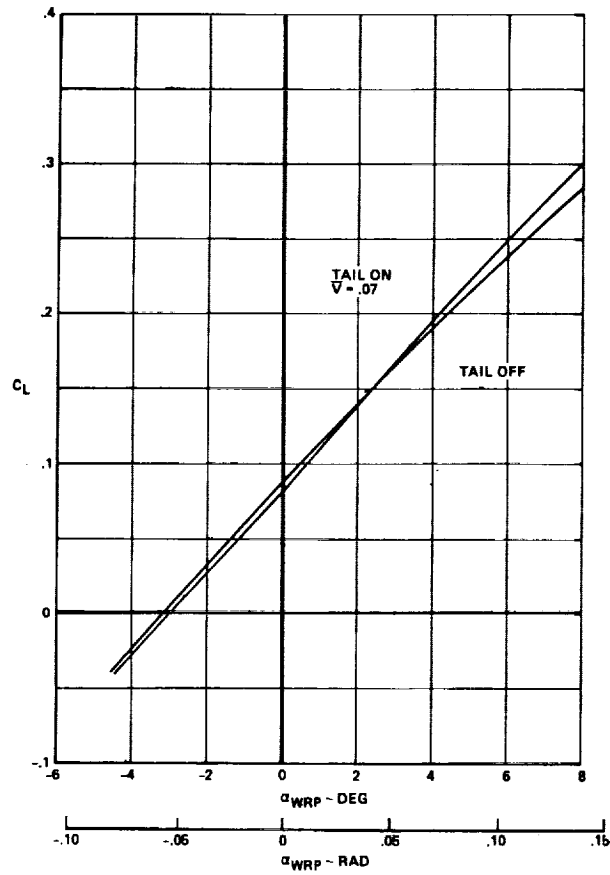


FIGURE 3-17. LIFT CHARACTERISTICS, MACH 2.7

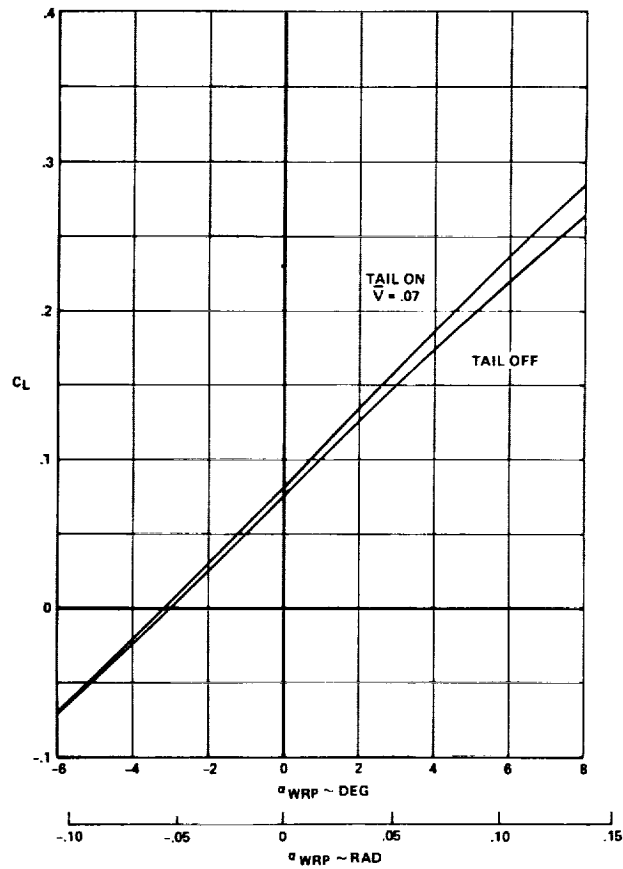


FIGURE 3-18. LIFT CHARACTERISTICS, MACH 2.95

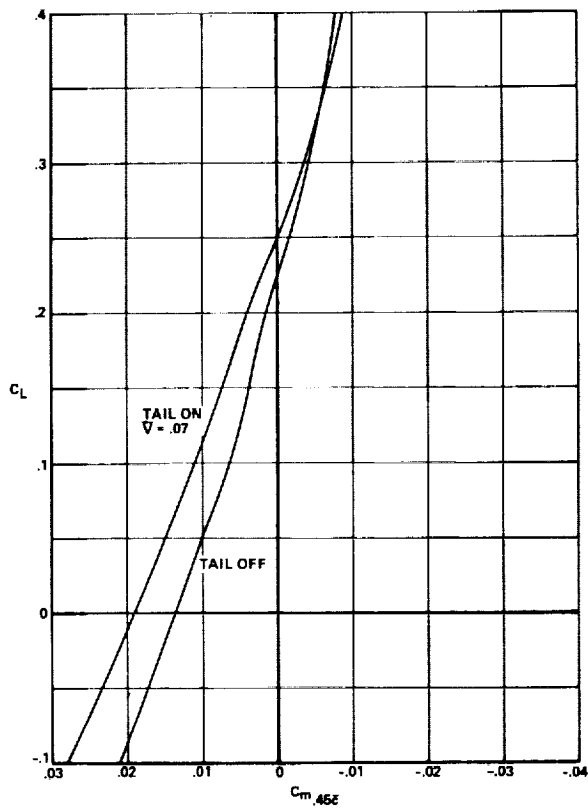


FIGURE 3-19. PITCHING MOMENT CHARACTERISTICS, MACH 0.6

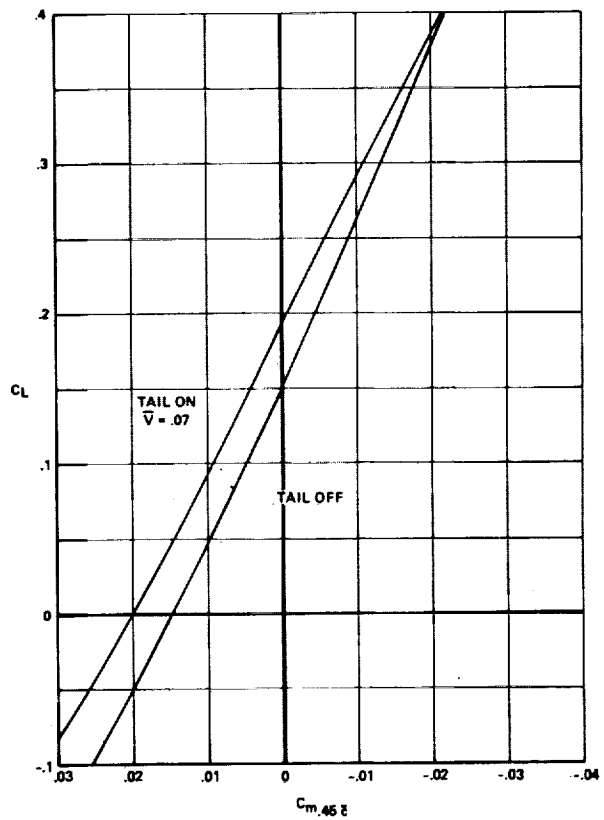


FIGURE 3-20. PITCHING MOMENT CHARACTERISTICS, MACH 0.9

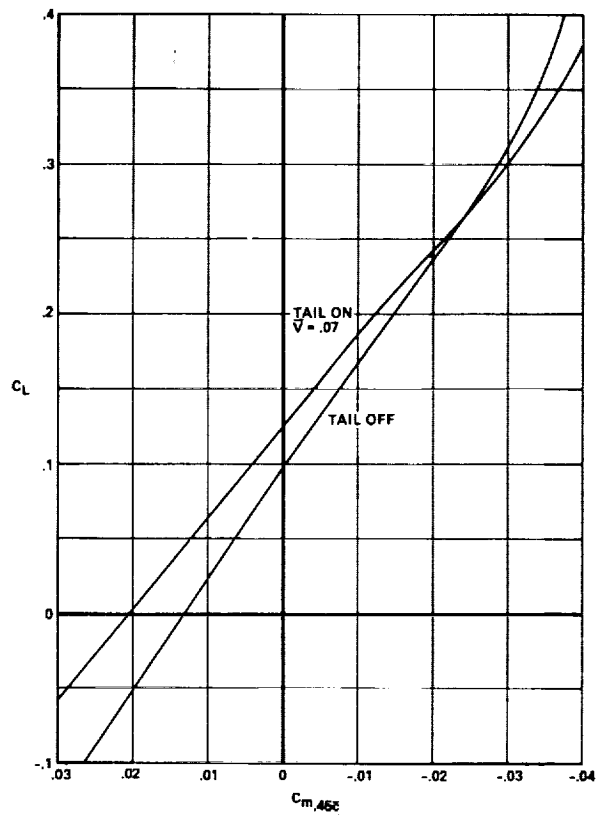


FIGURE 3-21. PITCHING MOMENT CHARACTERISTICS, MACH 1.2

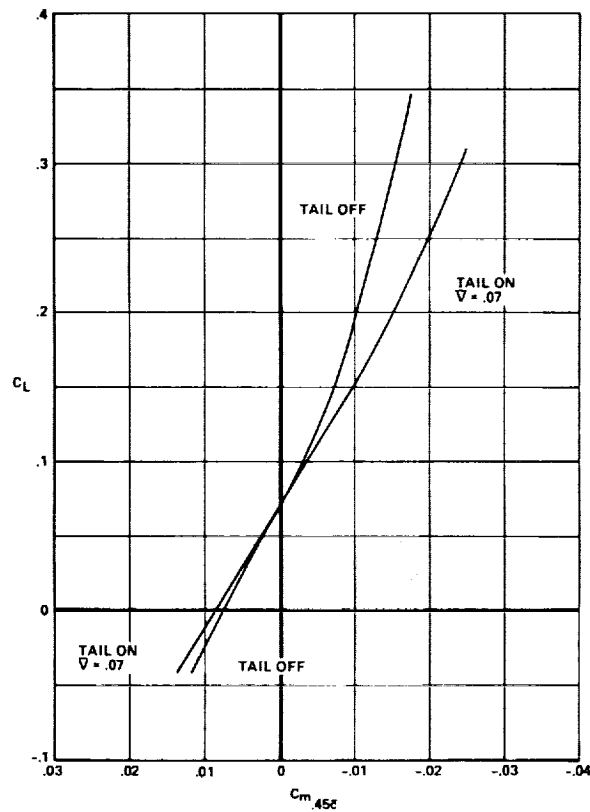


FIGURE 3-22. PITCHING MOMENT CHARACTERISTICS, MACH 2.3

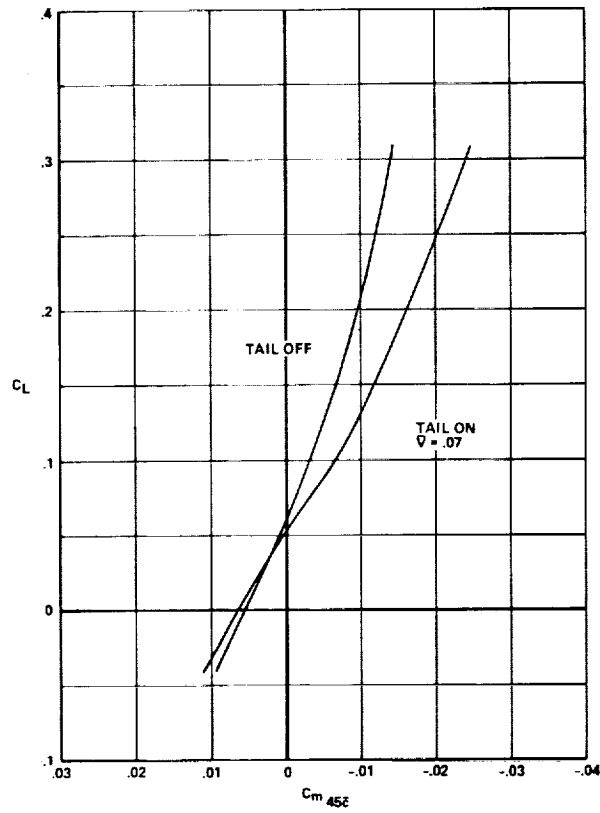


FIGURE 3-23. PITCHING MOMENT CHARACTERISTICS, MACH 2.7

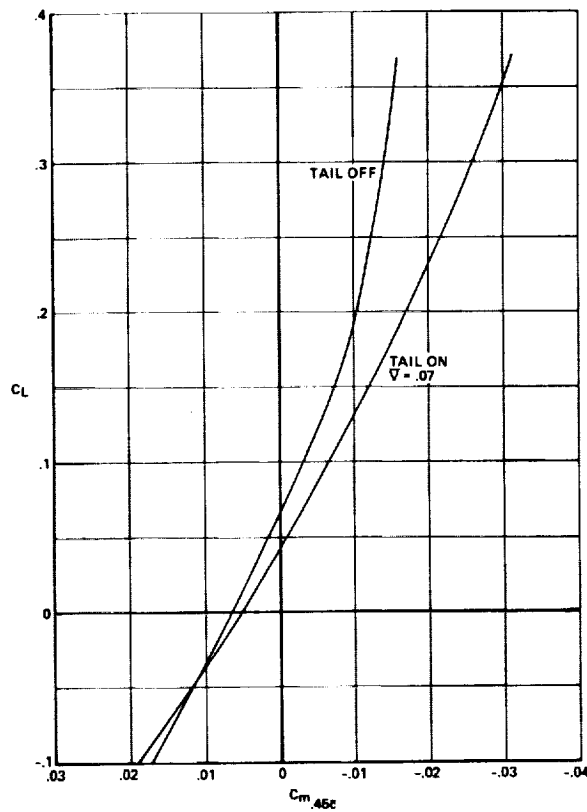


FIGURE 3-24. PITCHING MOMENT CHARACTERISTICS, MACH 2.95



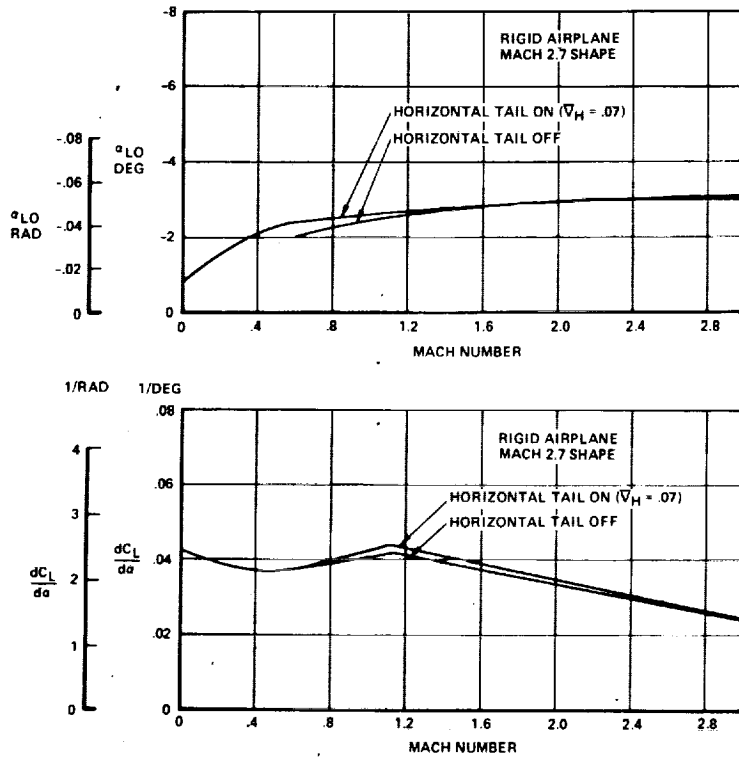


FIGURE 3-25. HIGH SPEED LIFT CHARACTERISTICS

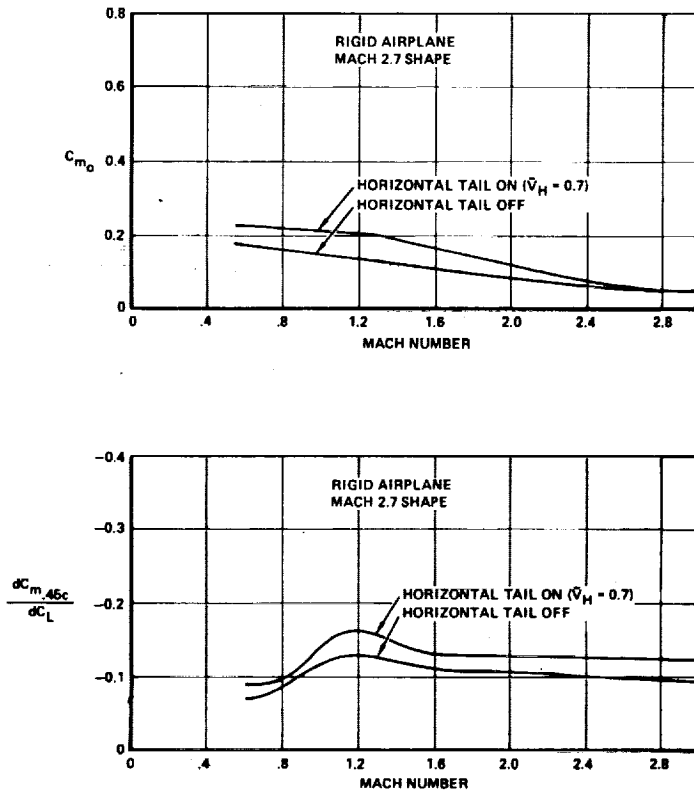


FIGURE 3-26. HIGH SPEED PITCHING MOMENT CHARACTERISTICS ( $-1 < n \leq 1$ )

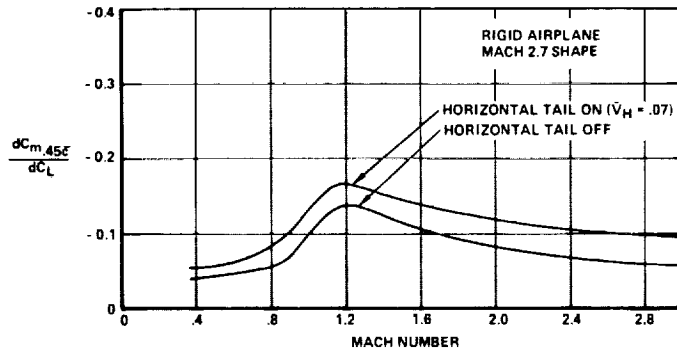
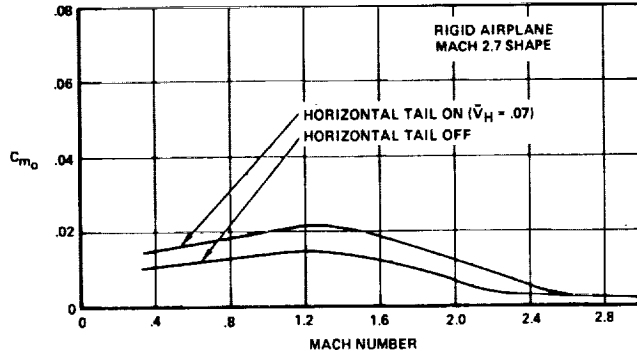


FIGURE 3-27. HIGH SPEED PITCHING MOMENT CHARACTERISTICS ( $1 < n_z < 2.5$ )

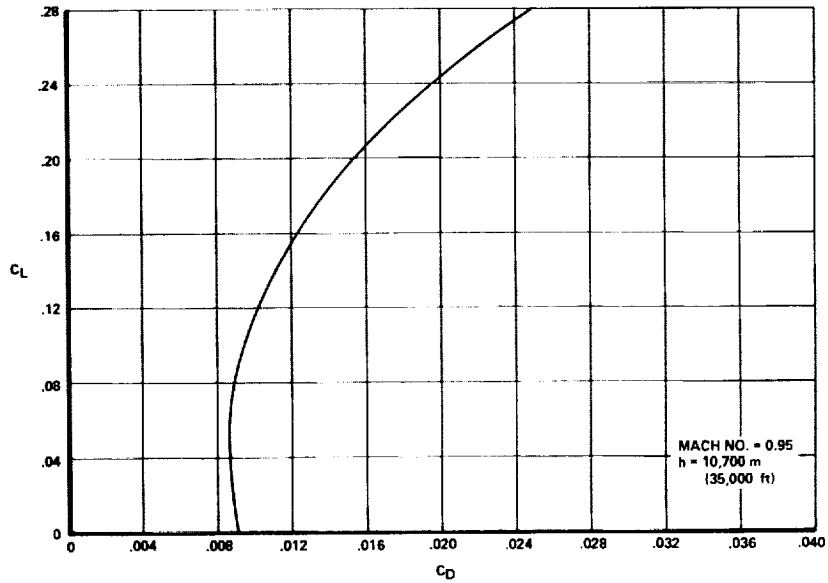


FIGURE 3-28. SUBSONIC CRUISE POLAR

Drag polars at transonic climb and supersonic cruise conditions are shown in Figures 3-28 through 3-31. Drag data are corrected to full scale by the following procedure:

1. Tail-off polars were obtained from wind tunnel data.
2. Data were corrected to baseline airplane reference area.
3. Wave drag was computed for the wind tunnel model and the full scale airplane.
4. Skin friction drag was computed for the wind tunnel model and the full scale airplane.
5. Roughness drag was computed for the airplane.
6. Data were corrected to full scale to account for difference in skin friction and wave drag.
7. Drag of the horizontal tail, at zero incidence was added.
8. Full scale polars were trimmed to the forward c.g. (51% MAC).

Drag data at cruise Mach number are shown in Figure 3-32. The data presents drag coefficient versus pitching moment coefficient about the 45-percent MAC as a function of total airplane lift coefficient (the coefficient based on total wing area) and of tail lift coefficient where the tail lift coefficient is based on horizontal tail area. It is apparent in Figure 3-32 that minimum drag occurs where the tail lift is positive and this is at a point where there is a negative pitching moment about the 45-percent chord. Obviously the airplane must be balanced well aft of 45-percent chord in order to have the correct lift coefficient on the tail as well as the wing to optimize cruise trim drag.

High speed tail effectiveness is shown in Figure 3-34 as a function of Mach number. High speed downwash in Figure 3-35 shows a negative slope of  $d\epsilon/d\alpha$  of Mach numbers above 2.0.

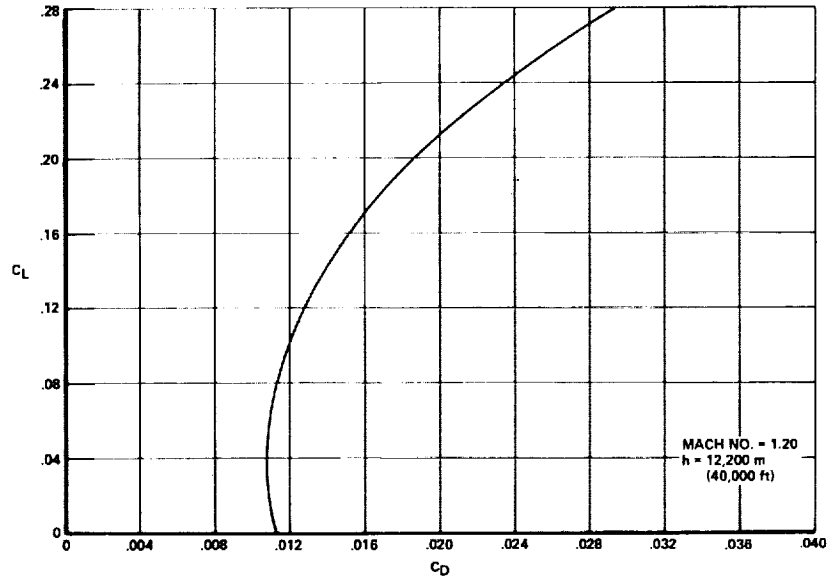


FIGURE 3-29. TRANSONIC CRUISE POLAR

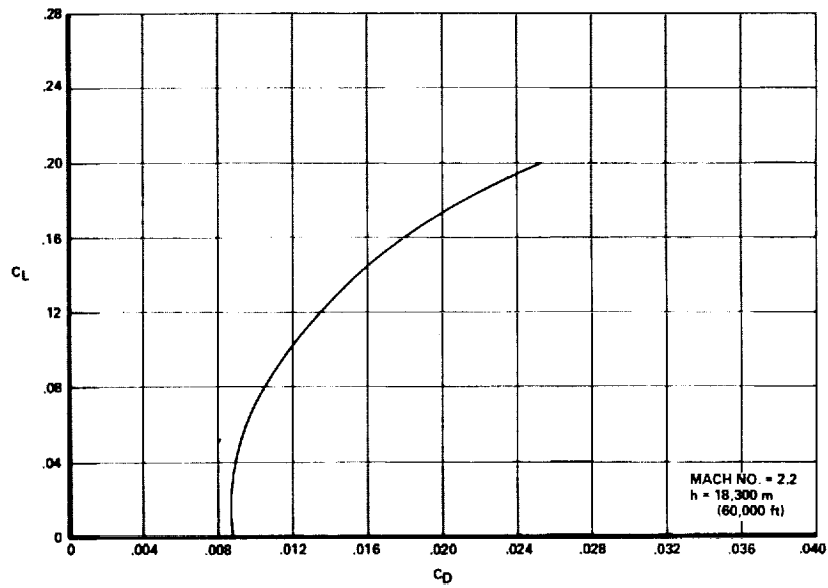


FIGURE 3-30. OFF-DESIGN CRUISE POLAR

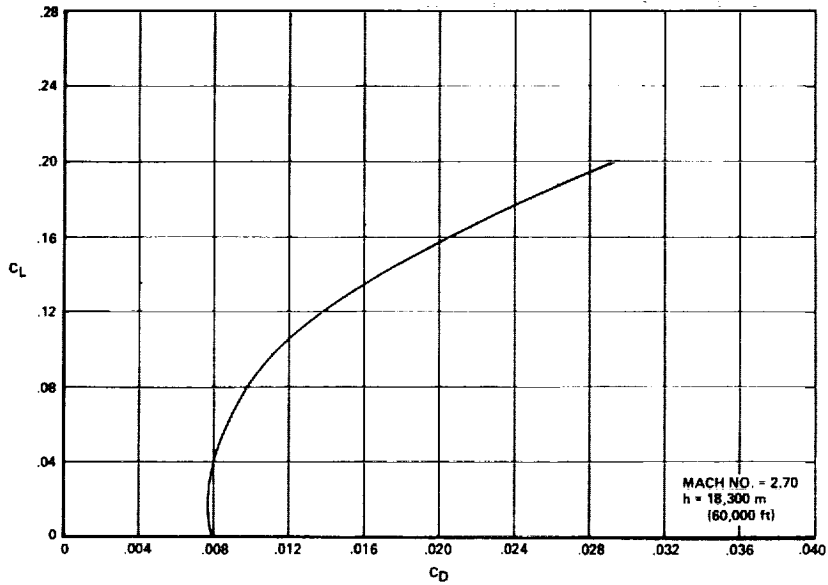


FIGURE 3-31. TRIMMED CRUISE POLAR

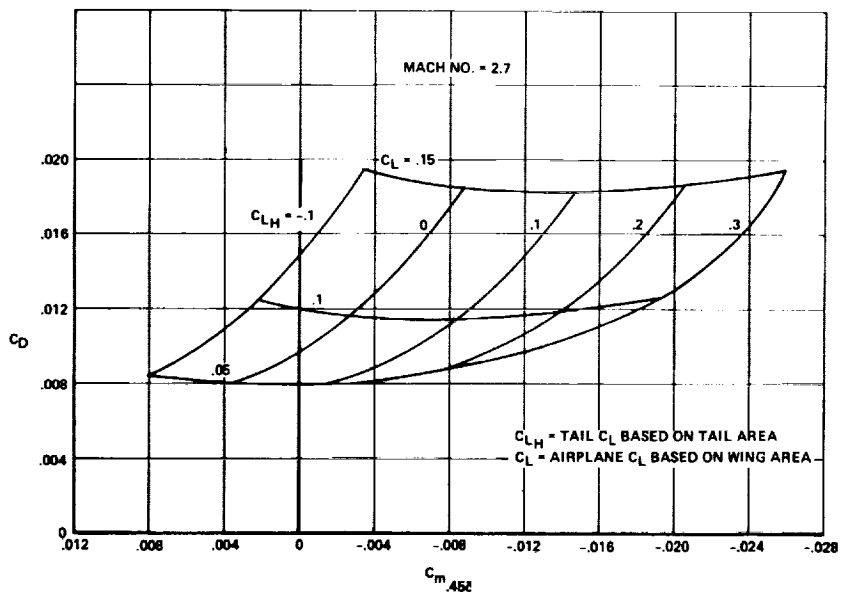


FIGURE 3-32. CRUISE DRAG CHARACTERISTICS

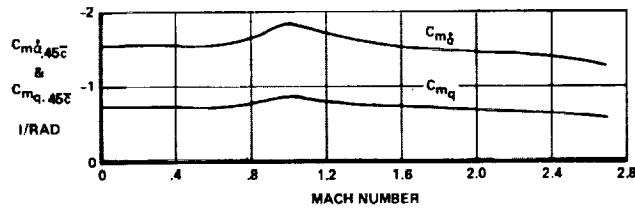
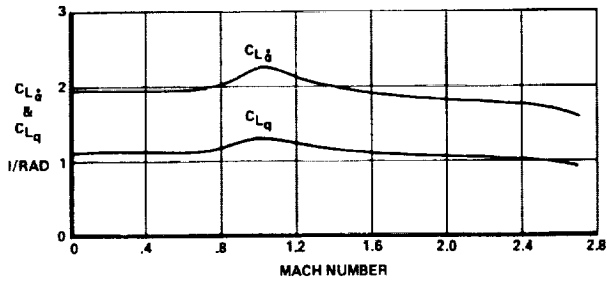


FIGURE 3-33. PITCH RATE AND ANGLE OF ATTACK RATE DERIVATIVES

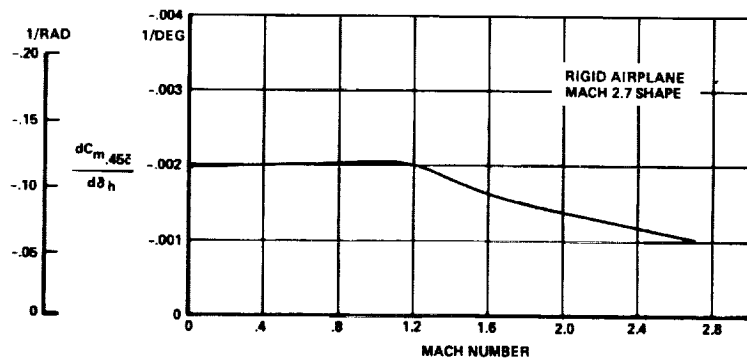
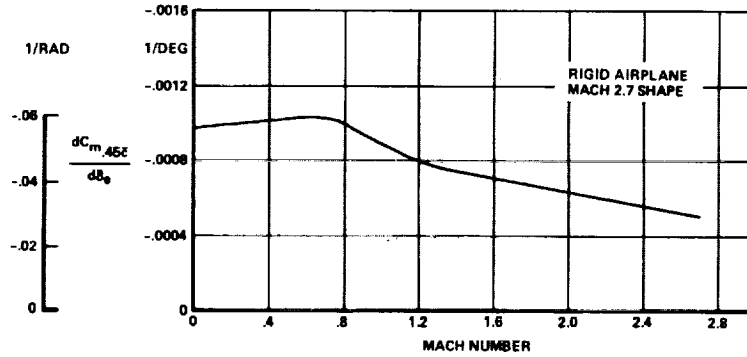


FIGURE 3-34. HIGH SPEED HORIZONTAL TAIL EFFECTIVENESS

Lateral directional data at only four Mach numbers 0.60, 0.95, 1.2 and 2.7 are presented in Figures 3-36 through 3-38. The yaw, side force and rolling moment coefficients are shown against wing reference plane angle of attack.

The dynamic derivatives in the pitch plane are shown on Figure 3-33,  $C_{L\dot{\alpha}}$ ,  $C_{Lq}$ ,  $C_{m\dot{\alpha}}$ , and  $C_{mq}$ , are plotted versus Mach number. The lateral directional rate derivatives of Figures 3-39 and 3-40 are shown as a function of Mach number and where necessary as a function of lift coefficient as well.

The high speed aileron data are shown at several angles of attack versus Mach number for Panels 2 and 3 in Figures 3-41 and 3-42, respectively. Panel 4 is locked out at Mach number equal to 0.40 and only low speed values are required.

The spoiler-slot-deflector at location 2 (ahead of Trailing Edge Panel No. 2) is shown in Figure 3-43 as incremental rolling moment and yawing moment coefficient for 30- and 60-degree deflection. The upper and lower panels deflect an equal amount so that the 60-degree data represent the coordinated deflection to 60-degree of both upper and lower panels. These data were obtained at low angles of attack but it can be assumed that the data are valid for the entire maneuvering angle of attack range for this study. The inverted-spoiler-slot-deflector Panel Number 3 is shown in Figure 3-44 only for 30-degree deflection. Spoiler-slot-deflector Panel 4, although it is locked out at a fairly low Mach number, is still shown over the whole Mach range in Figure 3-45.

High speed yaw effectiveness of the vertical fin with and without a geared rudder is shown in Figure 3-46.

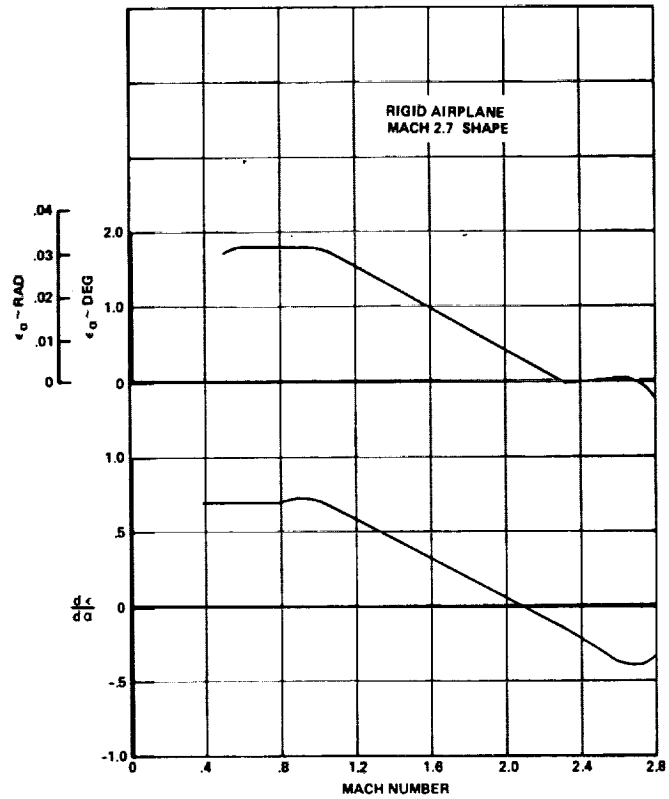


FIGURE 3-35. HIGH SPEED DOWNWASH

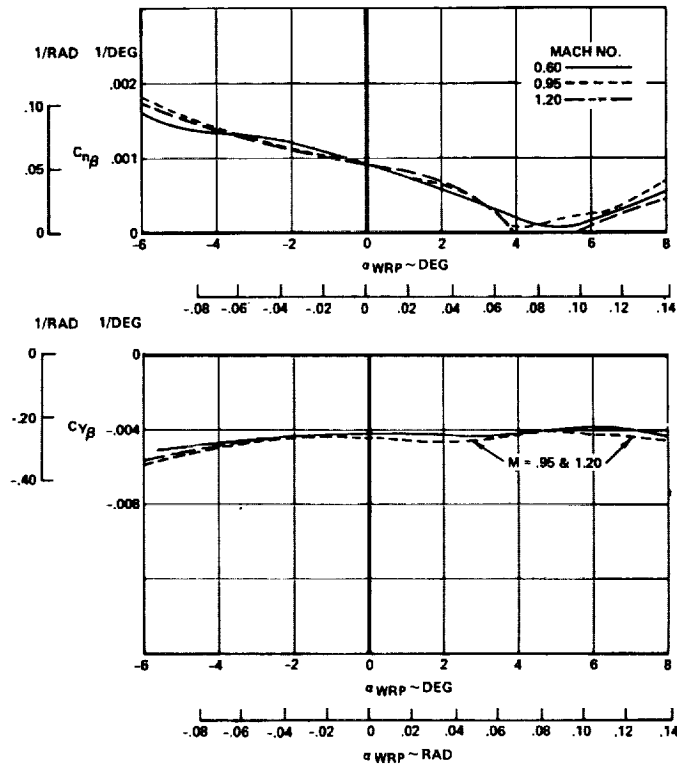


FIGURE 3-36. TRANSONIC LATERAL-DIRECTIONAL STABILITY ( $C_{n\beta}, C_{y\beta}$ )



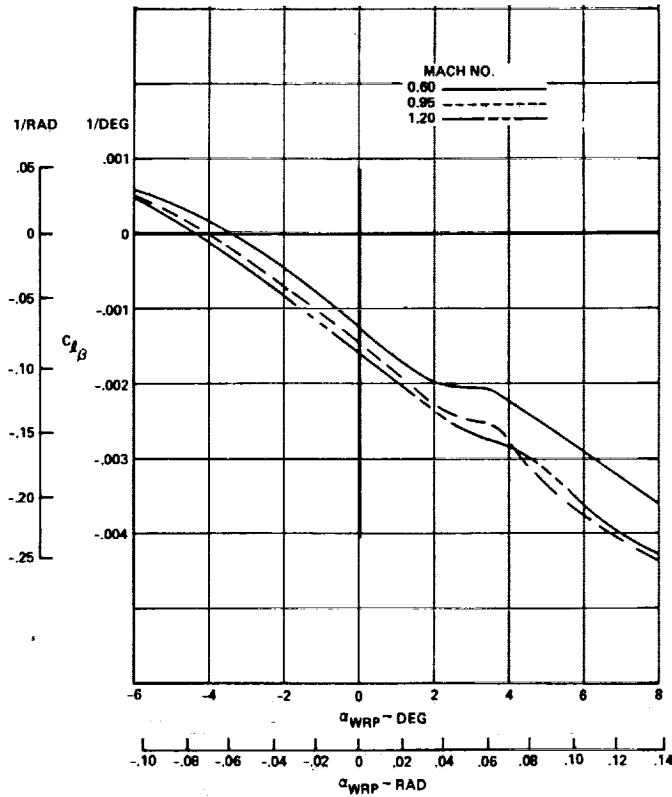


FIGURE 3-37. TRANSONIC LATERAL-DIRECTIONAL STABILITY ( $C_{l\beta}$ )

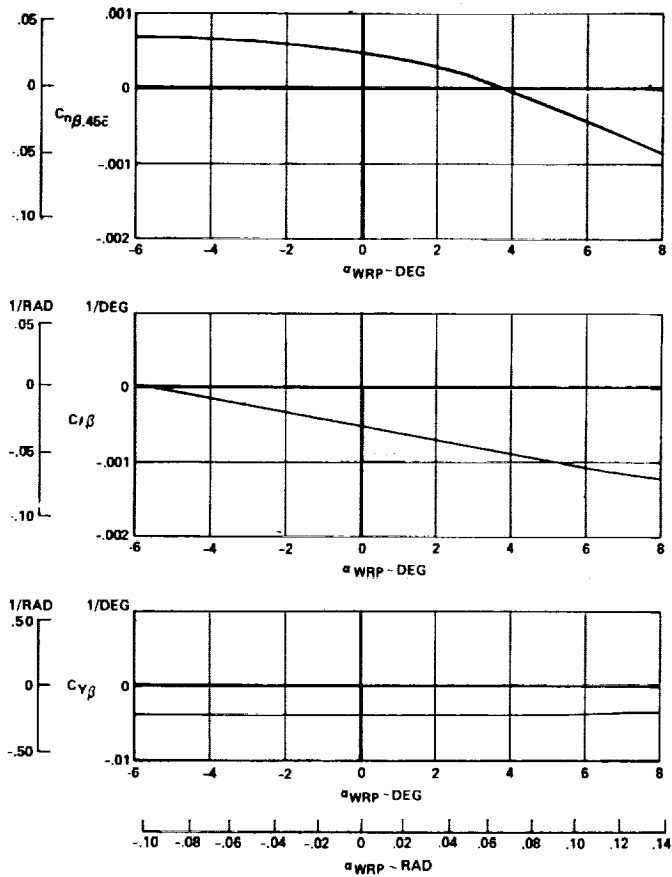


FIGURE 3-38. SUPERSONIC LATERAL-DIRECTIONAL STABILITY

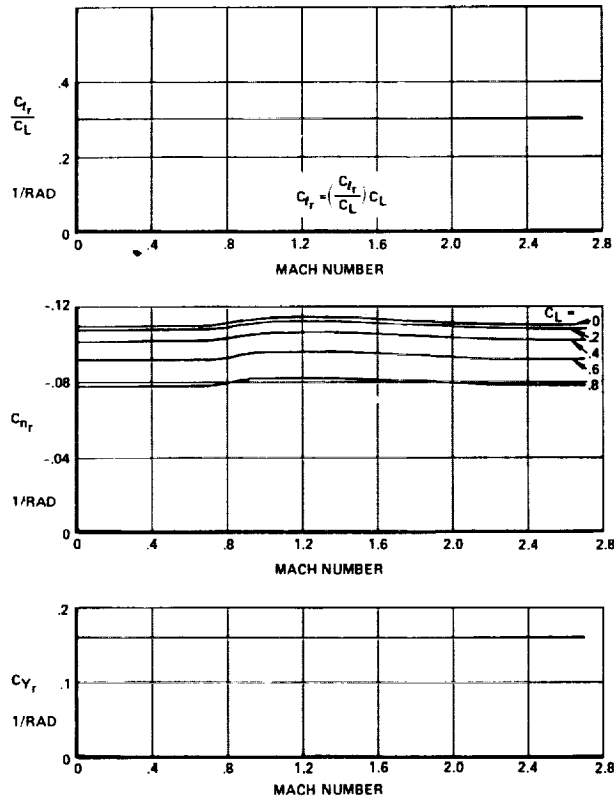


FIGURE 3-39. YAW RATE DERIVATIVES

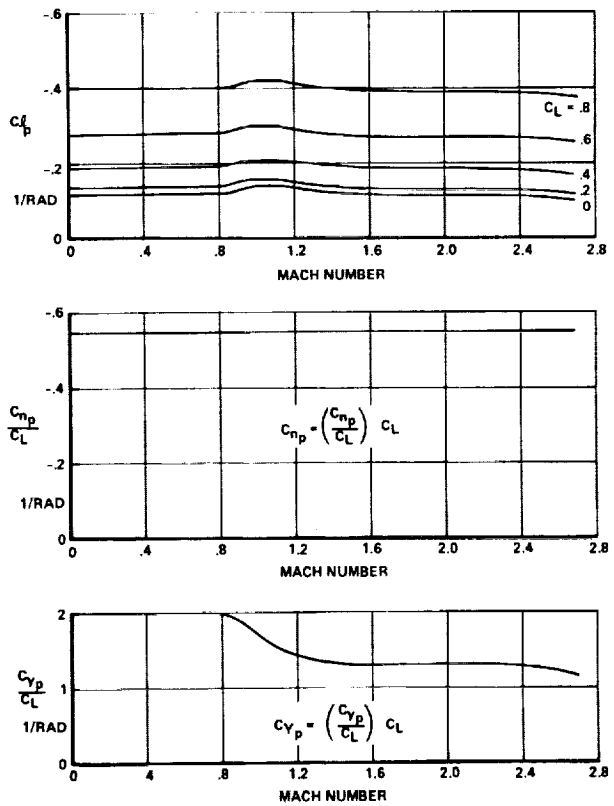


FIGURE 3-40. ROLL RATE DERIVATIVES

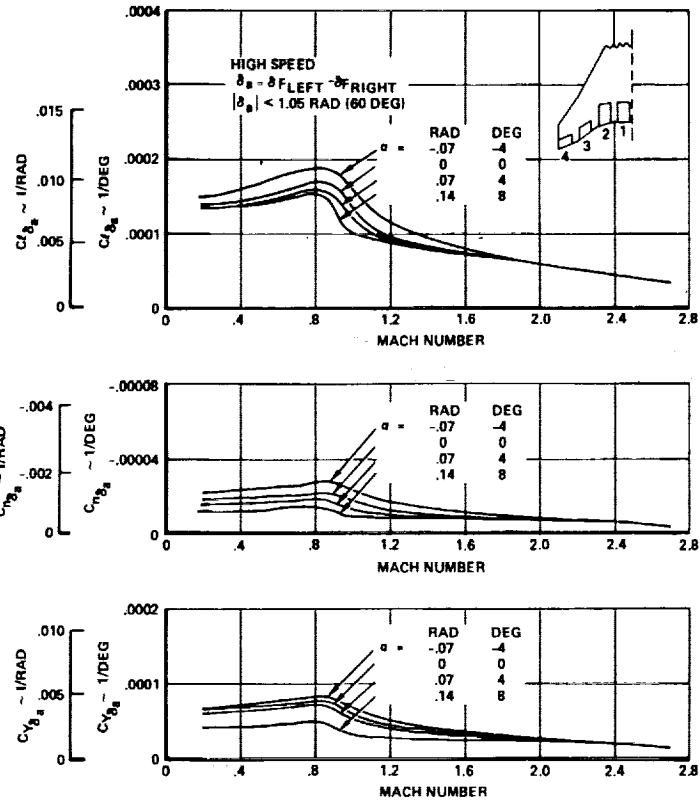


FIGURE 3-41. AILERON SEGMENT 2 EFFECTIVENESS

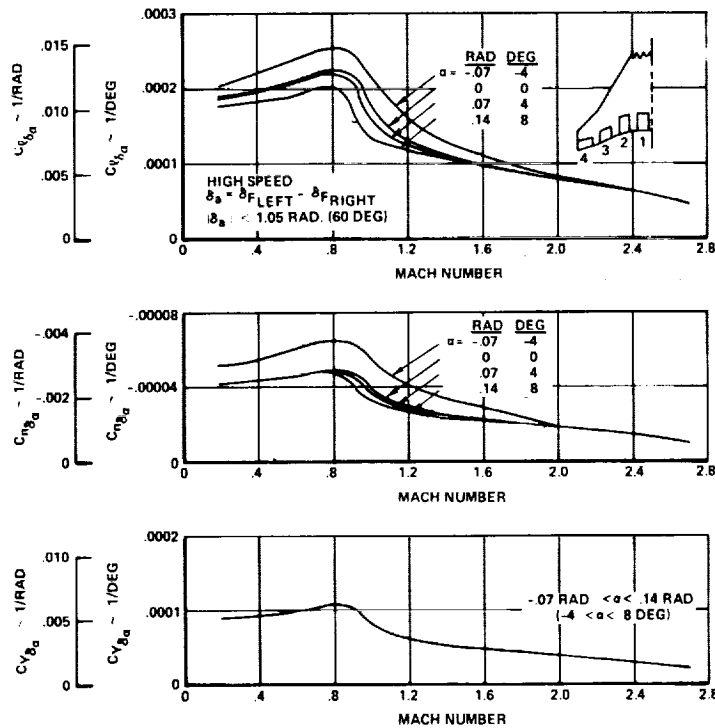


FIGURE 3-42. AILERON SEGMENT 3 EFFECTIVENESS

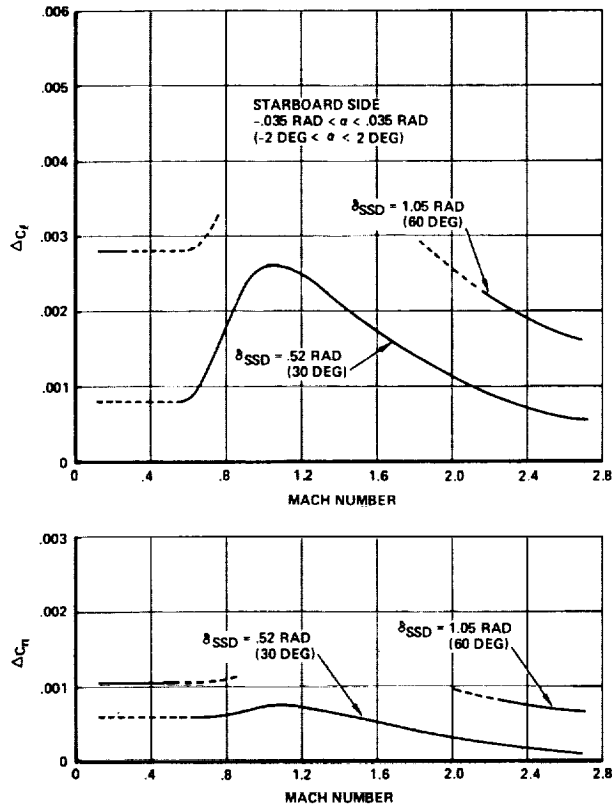


FIGURE 3-43. SPOILER-SLOT-DEFLECTOR 2 EFFECTIVENESS

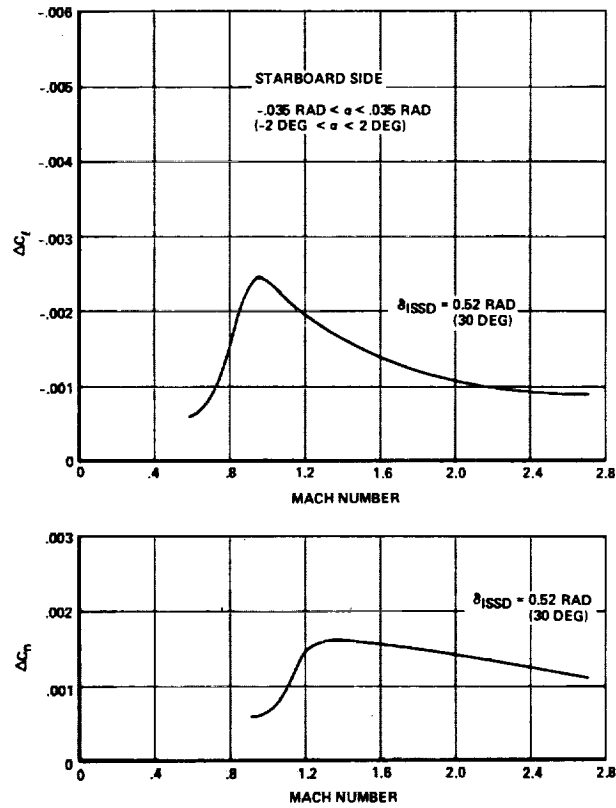


FIGURE 3-44. INVERTED SPOILER-SLOT-DEFLECTOR EFFECTIVENESS

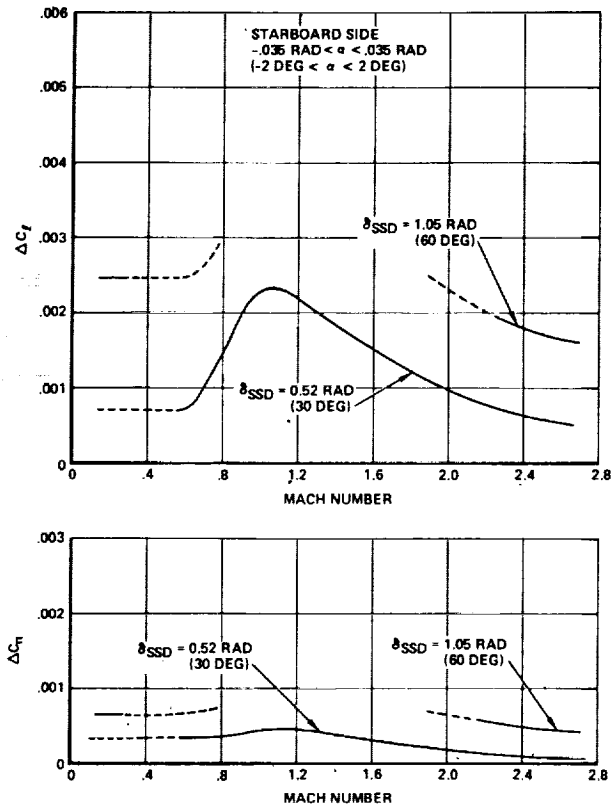


FIGURE 3-45. SPOILER-SLOT-DEFLECTOR EFFECTIVENESS

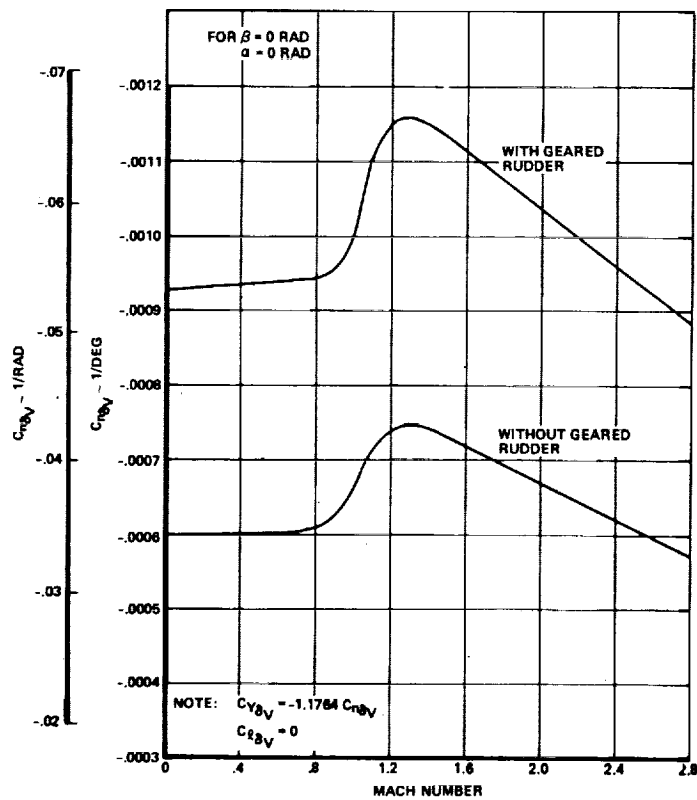


FIGURE 3-46. HIGH SPEED DIRECTIONAL CONTROL EFFECTIVENESS

## AERODYNAMIC CRITERIA

The baseline aircraft must satisfy the Federal Aviation Regulations Part 25 and the Special Conditions 25-43-EU-12 for SNIA/BAC Concorde Model Airplane. In order to establish specific design objectives assuring compliance with the regulations, these stability and control criteria are adopted.

### I LONGITUDINAL STABILITY AND CONTROL CRITERIA

#### I.1 Takeoff

- I-1.1 Rotation speed low enough to attain performance objectives
- I-1.2 Control to geometry limit in full ground effect
- I-1.3 No lock-in
- I-1.4 Maneuver to 0.5-g (incremental) at and above  $1.2 V_{MIN}$

#### I.2 Landing

- I-2.1 Maneuver to 0.5-g (incremental) at and above  $1.2 V_{MIN}$
- I-2.2 No lock-in
- I-2.3 Satisfactory flare characteristics
- I-2.4 Control to geometry limit in full ground effect

#### I-3 Pitch-Up

During a maximum pull-up maneuver hold full nose-up control for 1.0 sec after warning and recover without the velocity going below  $V_S$ .

#### I-4 Flaps-Up

- I-4.1 Apparent maneuver stability margin of 1.5 percent  $C_{ref}$  for all flight conditions bounded by  $1.2 V_S$  and  $V_{MO}/M_{MO}$  and by  $\alpha$  limit or limit load factor
- I-4.2 Maneuver to 1.0-g (incremental) from  $1.2 V_{MIN}$  to  $V_{MO}/M_{MO}$
- I-4.3 Maneuver to 0.5-g (incremental) from  $V_{MO}/M_{MO}$  to  $V_D/M_D$

### II LATERAL-DIRECTIONAL STABILITY AND CONTROL CRITERIA

#### II-1 General

Negative roll due to sideslip is required from  $1.2 V_{MIN}$  to  $V_D/M_D$

- II-2      Cross-Wind Landing  
 Land in a 30 knot cross-wind with no more than 4-degree crab using 2/3 of total rudder control (1/3 remains for control in gusts and turbulence).
- II-3      Roll Response
- II-3.1      Landing approach - attain a bank angle,  $\phi$ , of 30-degrees (0.52 rad) in 2.0 sec
- II-3.2      Cruise configuration -  $V_{MO}/M_{MO}$  - Roll 30-degrees (0.52 rad) to 30-degrees (0.52 rad) in 7 sec  
 $V_D/M_D$  - Roll 30-degrees (0.52 rad) to 30-degrees (0.52 rad) in 11 sec
- II-3.3      Roll rate reversals are not acceptable
- II-3.4      Only 75 percent wheel for full rudder sideslip
- II-4      Minimum Speeds
- II-4.1       $V_{MCG}$  - include the effect of a 7 knot (12.95 km/h) adverse cross-wind. Control outboard engine failure with a deviation from the runway centerline of less than 25 ft (7.64m) with a pilot reaction time of 0.6 sec
- II-4.2       $V_{MCG}$  less than or equal to  $V_1$   
 1.05  $V_{MCA}$  less than or equal to  $V_R$   
 1.1  $V_{MCA}$  less than or equal to  $V_2$
- II-5      Tameness  
 Control shall be maintained using wheel-control only following any inlet-engine failure not classified extremely remote.
- III      PERFORMANCE CRITERIA
- III-1      Mission
- III-1.1      Carry 49,000 lb (22,000 kg) payload, 4200 n. mi. (7,780 km)
- III-1.2      Cruise at Mach 2.7
- III-1.3      Fuel reserves as specified in FAR 121.648
- III-2      Aircraft Performance
- III-2.1      FAR balanced field length - 10,500 ft (3200 m)
- III-2.2      Approach speed - 150 keas (277.5 km/h)

## CONFIGURATION CHARACTERISTICS

The configuration characteristics of the baseline airplane are defined in this section. The planform and elevation views of the configuration with control surfaces identified are shown in Figure 3-47. Descriptive dimensional data for the wing and control surfaces are listed in Table 3-1.

There are no leading edge devices on the wing between the fuselage and the outer wing break at BL 600 (15.24m) . Outboard from the break to the wingtip are Kreuger flaps which are deflected 45-degrees (0.785 rad) to improve the pitching moment characteristic at low speed and 25-degrees (0.436 rad) to increase the transonic lift to drag ratio. The wing trailing edge is divided into four plain flap panels. Panels 1 through 3 are deflected 20-degrees (0.349 rad) trailing edge down to increase the lift coefficient for takeoff and landing performance. Plain spoilers ahead of Panel 1 are used as ground speed brakes.

An all moving horizontal tail is used for longitudinal trim, maneuver control and active stabilization. Directional control is provided by an all moving vertical tail on the fuselage centerline. A 25-percent chord geared elevator is provided to increase the stabilizer effectiveness. Similarly, the moving vertical tail has a 25-percent chord geared rudder.

Two fixed vertical fins on the wings provide additional directional stability at high Mach numbers.

Roll control is provided by ailerons, spoiler-slot-deflectors, and inverted spoiler-slot-deflectors. Trailing edge flap Panels 2 and 3 serve as ailerons as well as flaps. When deployed as lift flaps they are capable of differential deflection in response to roll commands. Trailing Edge Panel Number 4 acts as an aileron only. Spoiler-slot-deflectors are located ahead of the hinge lines of Panels 2 and 4. In front of Panel 3 is an inverted spoiler-slot-deflector. The use of these devices is scheduled as a function of Mach number as specified in Table 3-2.



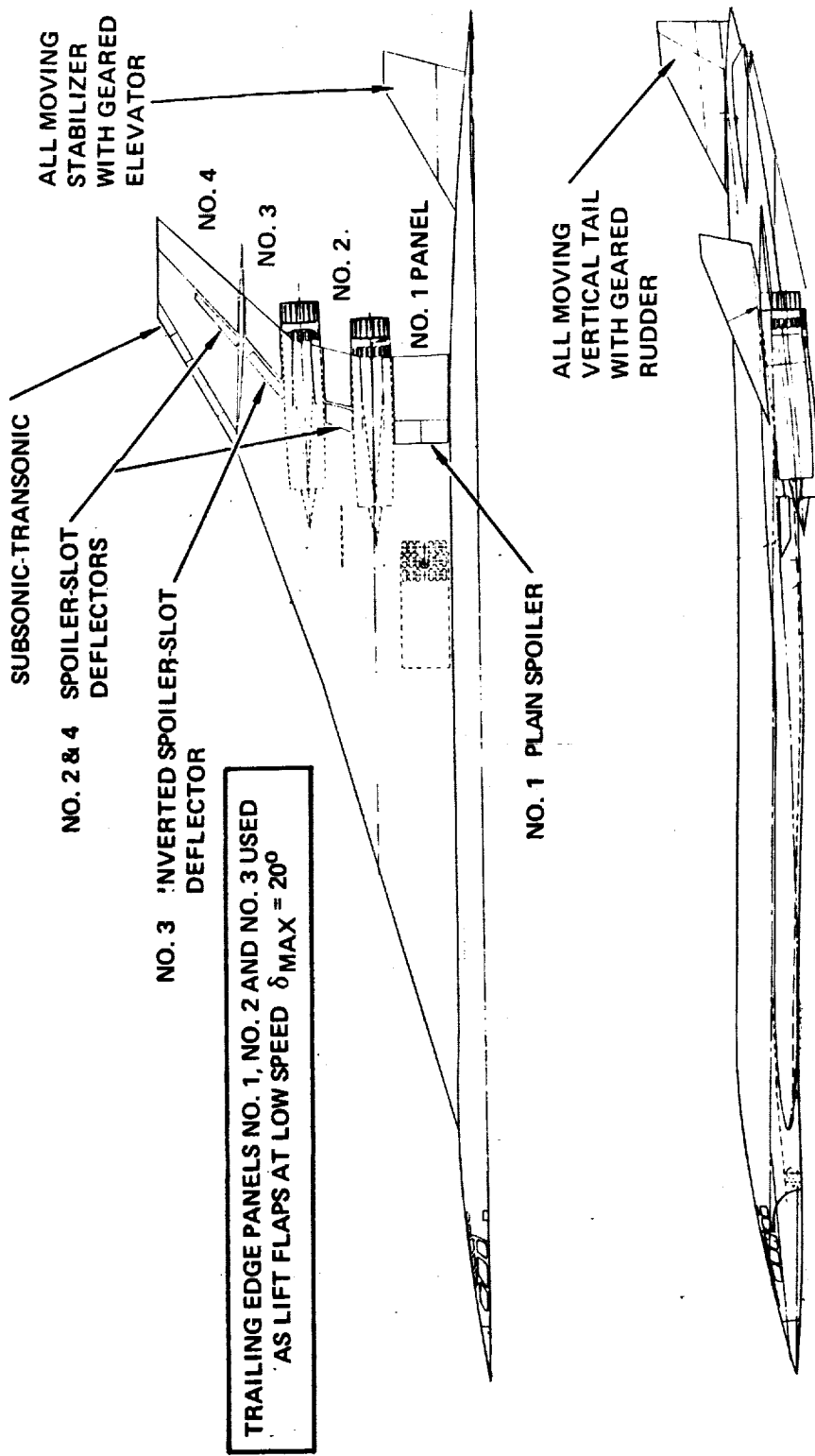


FIGURE 3-47. PRIMARY CONTROL SYSTEM LAYOUT

TABLE 3-1

## AIRPLANE DIMENSIONAL DATA

<u>WING</u>		
$S_W$	10923 ft <sup>2</sup>	1014.69 m <sup>2</sup>
$S_{REF}$	10500 ft <sup>2</sup>	975.45 m <sup>2</sup>
$\bar{A}$	1.607 ft <sup>2</sup>	
$\lambda$	.1135 ft <sup>2</sup>	
b	1590.0 in	40.386 m
$C_r$	2195.5 in	55.766 m
$C_t$	249.2 in	6.330 m
$\bar{c}$	1351.1 in	34.317 m
$\alpha_{LE}$ (to BL 391.2)	74 deg (to BL 9.94)	1.292 rad
(to BL 600 )	70.84 deg (to BL 15.24)	1.236 rad
(to Tip )	60 deg (to Tip )	1.047 rad

TRAILING EDGE PANEL #1 (LIFT FLAP)

S	152.5 ft <sup>2</sup> (per side)	14.16 m <sup>2</sup>
$C_r$	165.0 in	4.19 m
$C_t$	160.0 in	4.06 m
$BL_r$	72.0 in	1.83 m
$BL_t$	207.0 in	5.26 m

TRAILING EDGE PANEL #2 (Flaperon)

S	57.6 ft <sup>2</sup> (per side)	5.35 m <sup>2</sup>
$C_r$	132.0 in	3.35 m
$C_t$	132.0 in	3.35 m
$BL_r$	314.0 in	7.98 m
$BL_t$	378.0 in	9.61 m

TABLE 3-1 (continued)

TRAILING EDGE PANEL #3 (Flaperon)

S	71.4 ft <sup>2</sup> (per side)	6.63 m <sup>2</sup>
C <sub>r</sub>	126.0 in	3.20 m
C <sub>t</sub>	105.0 in	
BL <sub>t</sub>	487.0 in	
BL <sub>r</sub>	576.0 in	

TRAILING EDGE PANEL #4 (Aileron)

S	121.7 ft <sup>2</sup>	11.30 m <sup>2</sup>
C <sub>r</sub>	102.0 in	2.59 m
C <sub>t</sub>	76.0 in	1.93 m
BL <sub>r</sub>	598.0 in	15.19 m
BL <sub>t</sub>	795.0 in	20.19 m

SPOILER #1 (Plain)

S	54.5 ft <sup>2</sup> (per side)	5.06 m <sup>2</sup>
C <sub>r</sub>	58.0 in	1.47 m
C <sub>t</sub>	58.0 in	1.47 m
BL <sub>r</sub>	72.0 in	1.83 m
	207.0 in	5.26 m

er-Slot-Deflector)

S	21.8 ft <sup>2</sup> (per side)	2.02 m <sup>2</sup>
C <sub>r</sub>	52.0 in	1.32 m
C <sub>t</sub>	46.0 in	1.17 m
BL <sub>r</sub>	314.0 in	7.98 m
BL <sub>t</sub>	378.0 in	9.60 m

TABLE 3-1 (continued)

SPOILER #3 (Inverted Spoiler-Slot-Deflector)

S	21.0 ft <sup>2</sup> (per side)	1.95 m <sup>2</sup>
C <sub>r</sub>	36.0 in	.915 m
C <sub>t</sub>		.15 m
BL <sub>r</sub>	487.0 in	.9 m
BL <sub>t</sub>	576.0 in	14.64 m

SPOILER #4 (Spoiler-Slot-Deflector)

S	14.2 ft <sup>2</sup> (per side)	1.32 m <sup>2</sup>
C <sub>r</sub>	26.0 in	.66 m
C <sub>t</sub>	14.0 in	.36 m
BL <sub>r</sub>	598.0 in	15.19 m
BL <sub>t</sub>	700.0 in	17.78 m

KRUEGER FLAP

S	59.0 ft <sup>2</sup> (per side)	5.48 m <sup>2</sup>
C <sub>r</sub>	44.0 in	1.12 m
C <sub>t</sub>	44.0 in	1.12 m
BL <sub>r</sub>	602.0 in	15.20
BL <sub>t</sub>	795.0 in	20.

HORIZONTAL STABILIZER (Total)

S	795 ft <sup>2</sup>	73.868 m <sup>2</sup>
A	1.707	
λ	.225	
b	441.6 in	11.217 m
C <sub>r</sub>	422.8 in	10.739 m
C <sub>t</sub>	95.1 in	2.416 m
$\bar{C}_H$	293.5 in	7.455 m
$\Lambda_{LE}$	60.64 deg	1.058 rad

TABLE 3-1 (continued)

HORIZONTAL STABILIZER (Total)  
(Continued)

$l_H$ (.45 $\bar{c}$ to .5 $\bar{c}_H$ )	1292.9 in	32.85 m
$\bar{v}_H$	.07	
$\Gamma$	-10 deg	- .1745 rad

ELEVATOR

s	85.25 ft <sup>2</sup>	7.91 m <sup>2</sup>
b	198.0 in	5.04 m
$c_r$	98.0 in	2.49 m
$c_t$	26.0 in	.66
$c/c_H$	.25	

FUSELAGE VERTICAL FIN

S (Total)	325 ft <sup>2</sup>	30.190 m <sup>2</sup>
R	.517	
$\lambda$	.23	
b	155.55 in	3.941 m
$c_r$	489.22 in	12.426 m
$c_t$	112.521 in	2.858 m
$\bar{c}_{VF}$	340.174 in	8.640 m
$\Lambda_{LE}$	68.2 deg	1.190 rad
$l_{VF}$ (.45 $\bar{c}$ to .5 $\bar{c}_{VF}$ )	1362.8 in	34.605 m
$\bar{v}_{VF}$	.0267	

RUDDER

s	79.2 ft <sup>2</sup>	7.36 m <sup>2</sup>
b	155.0 in	3.94 m

TABLE 3-1 (continued)

RUDDER

(Continued)

$C_r$	120.0 in	3.05 m
$C_t$	28.0 in	.71 m
$C/C_{VF}$	.25	

WING VERTICAL FINS

$S$	233 ft <sup>2</sup> (Each)	21.65 m <sup>2</sup>
$R$	.495	
$\lambda$	.136	
$b$	129.0 in	3.277 m
$C_r$	458.4 in	11.643 m
$C_t$	62.4 in	1.585 m
$\bar{c}_{VW}$	310.6 in	7.889 m
$\Lambda_{LE}$	73.42 deg	1.281 rad
$l_{VW}$ (.45 $\bar{c}$ to .50 $\bar{c}_{VW}$ )	846.8 in	21.52 m
$\bar{v}_{VW}$	.0118 (Each)	

TABLE 3-2 AIRPLANE DIMENSIONAL DATA

CONTROLLED DEGREE OF FREEDOM	MACH	SURFACE	DEFLECTION					
			LIMIT			RATE		
			RAD	DEG	RAD/SEC	RAD/SEC	(DEG/SEC)	
PITCH	ALL	ALL MOVING STABILIZER ( $\bar{V}_H = .07$ )	+52 -35	+30 -20	±.87 ±.70	±.87 ±.70	±50	
	ALL	GEARED ELEVATOR ( $C_e/C_H = .25$ )	±.35	±20	±.70	±.70	±40	
	YAW	$M \leq .4$	ALL MOVING VERTICAL TAIL ( $\bar{V}_V = .027$ )	±.44	±25	±.87	±.87	±50
$M \leq .4$		GEARED RUDDER ( $C_r/C_v = .25$ )	±.44	±25	±.87	±.87	±50	
$M > .4$		ALL MOVING VERTICAL	±.22	±12.5	±.44	±.44	±25	
$M > .4$		GEARED RUDDER	±.22	±12.5	±.44	±.44	±25	
ROLL	$M \leq .4$	WING T.E. PANEL #4	±.61	±35	±.61	±.61	±70	
	$M \leq .8$	WING T.E. PANEL #3	±.35 WITH RESPECT TO FLAP ANGLE	+20 WITH RESPECT TO FLAP ANGLE	±.70	±.70	±40	
	$M \leq 1.2$	WING T.E. PANEL #2	UPPER PANEL -1.05 LOWER PANEL -.70	UPPER PANEL -60 LOWER PANEL -40	±.70	±.70	±40	
	$.4 < M \leq .8$	SPOILER SLOT- DEFLECTOR AT NO. 4	UPPER PANEL -1.05 LOWER PANEL -.70	UPPER PANEL -60 LOWER PANEL -40	FULL DEFLECTION IN ONE SECOND			
	$M > .8$	INVERTED SPOILER- SLOT-DEFLECTOR AT NO. 3	UPPER AND LOWER PANEL -.70	UPPER AND LOWER PANEL -40	FULL DEFLECTION IN ONE SECOND			
	$M > 1.2$	SPOILER SLOT- DEFLECTOR AT NO. 2	UPPER PANEL -1.05 LOWER PANEL -.70	UPPER PANEL -60 LOWER PANEL -40	FULL DEFLECTION IN ONE SECOND			

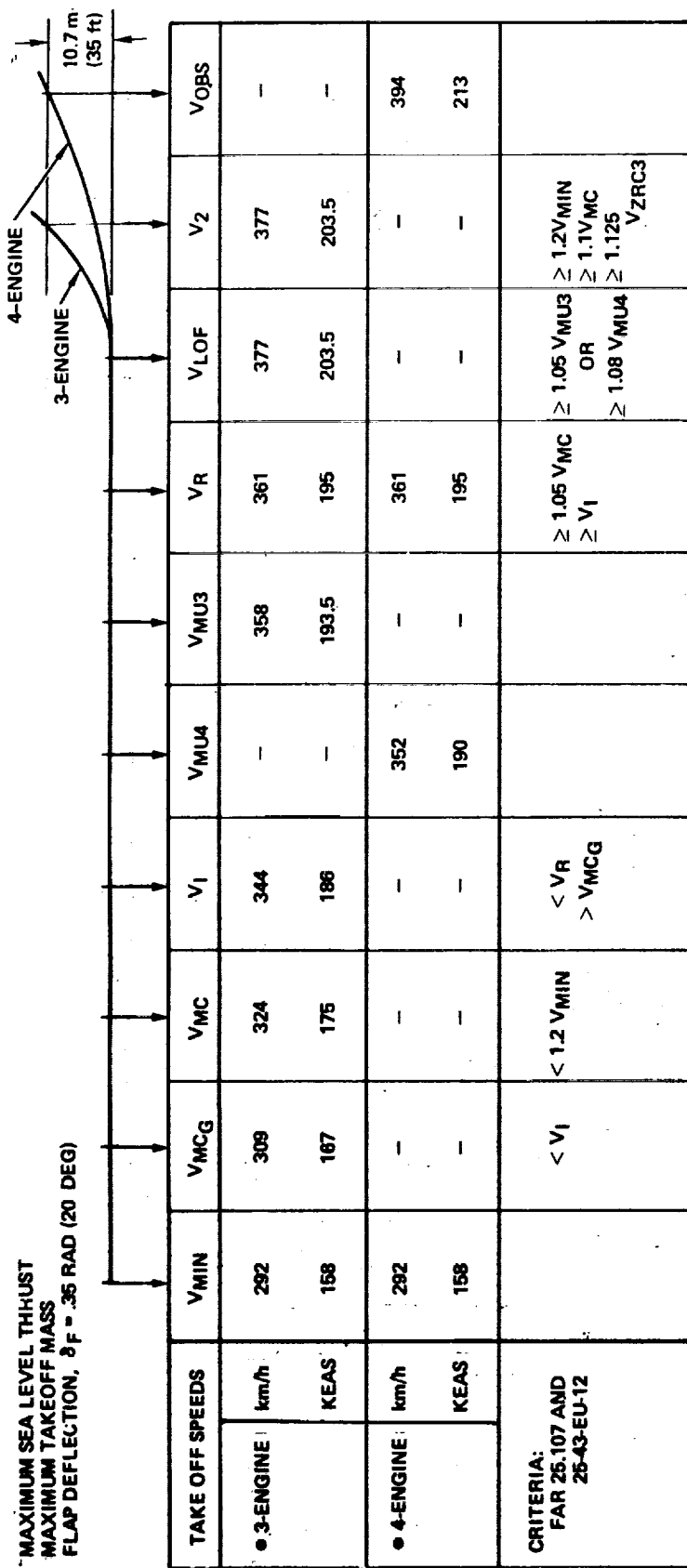
## PERFORMANCE

The performance capability of the baseline airplane is presented. The data documents the ability of the airplane to perform the design mission of 7780 kilometers (4200 n. miles) with a payload of 22,000 kg (49,000 lb). Takeoff and landing performance are designed to give a 3,200 meter (10,500 ft) balanced field length. Takeoff and landing configurations are the same using 0.349 rad (20-degree) trailing edge flaps. There are no leading edge devices inboard of the wing vertical fins. Outboard of the fins there are Krueger flaps which are deflected 0.785 radians (45-degree). These do not enhance low speed lift capability to a measurable extent, but do provide some relief from pitchup tendency. Deflected 0.436 radians (25-degree) during transonic climb, these Kruegers improve the lift-to-drag ratio over that segment.

The speeds referred to in the Federal Aviation Regulations Part 25, pertaining to takeoff are portrayed in Figure 3-48. The sequence are of reference speeds marked along a takeoff acceleration run in equivalent airspeed. The appropriate 3 or 4 engine takeoff conditions and the required relationships between these speeds are also indicated. In addition to Part 25 of the FAR, special conditions 25-43-EU-12 for the SNIA/BAC Concorde have been incorporated. The use of minimum demonstration speed ( $V_{MIN}$ ) rather than stall speed ( $V_S$ ) results from these special conditions. Also, an added requirement on  $V_2$  speed is that it be equal to or greater than 1.125 times the zero rate of climb speed with one engine inoperative.

Figure 3-49 compares  $V_{MIN}$  and the minimum unstick speed with 4 engines operating ( $V_{MU4}$ ) for 0- and 20-degree trailing edge flap deflection. It is noted that the minimum demonstration speed is relatively unaffected by flap position. This implies that the stall speed with and without flap deflection is essentially the same. Minimum unstick speed is reduced by approximately 20 KEAS with 20-degrees of flap, while the minimum demonstration speeds are only 2 KEAS apart.





V <sub>MIN</sub>	-	MINIMUM DEMONSTRATION SPEED	V <sub>MU3</sub>	-	MINIMUM UNSTICK SPEED (3-ENG)
V <sub>MCG</sub>	-	GROUND MINIMUM CONTROL SPEED	V <sub>R</sub>	-	ROTATION SPEED
V <sub>MC</sub>	-	MINIMUM CONTROL SPEED (AIR)	V <sub>LOF</sub>	-	LIFTOFF SPEED
V <sub>I</sub>	-	REFUSAL SPEED	V <sub>2</sub>	-	SPEED AT 36 FT HEIGHT - ONE ENGINE INOPERA.
V <sub>MU4</sub>	-	MINIMUM UNSTICK SPEED (4-ENG)	V <sub>OBS</sub>	-	SPEED AT 36 FT HEIGHT - ALL ENGINES OPERATING

FIGURE 3-48. TAKE-OFF SPEEDS

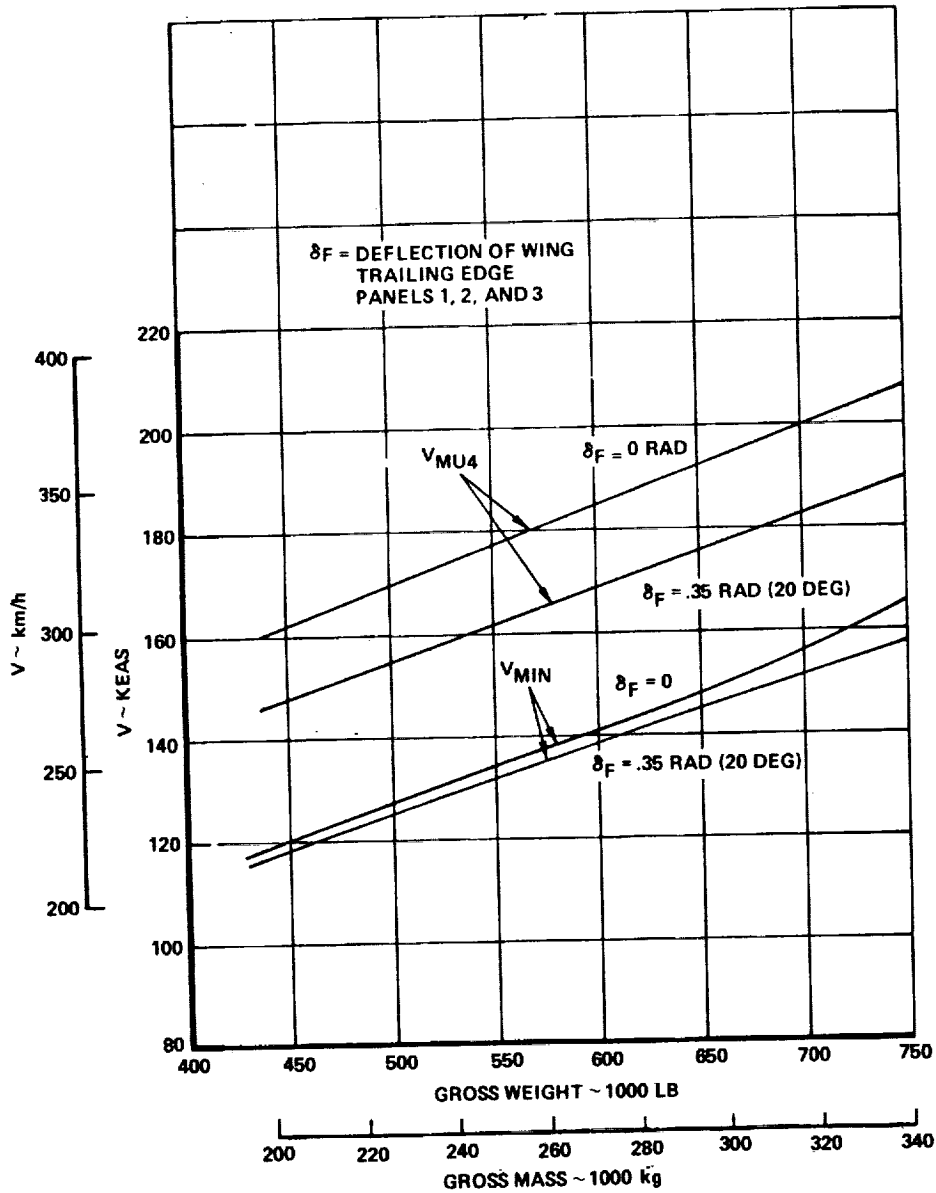
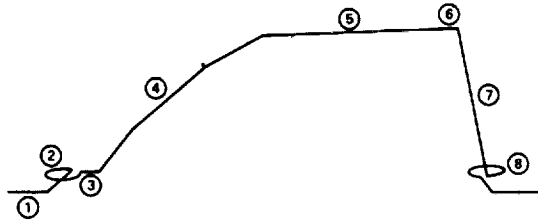
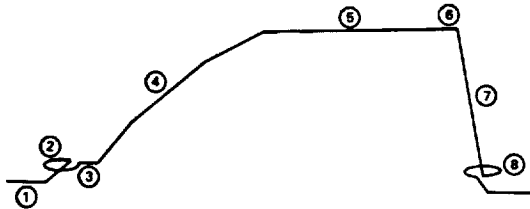


FIGURE 3-49. MINIMUM SPEED RELATIONSHIPS

The international baseline mission is described in Figure 3-50 with a sketch showing the mission segments. The segments are identified with the fuel used during each segment and the distance covered during each segment. Block fuel and range are totaled and the relevant takeoff and landing weights are indicated. Time history of wing reference plane angle of attack and a Mach time history are shown in Figure 3-51 over the mission profile. The design mission was run for a standard day plus 8° K to be conservative in terms of the engine output and fuel consumption.



SEGMENT	SEGMENT FUEL (Lb)	SEGMENT DIST. (N.Mi.)
① Ground Maneuver T.O. & Climb to 5000 Ft.	17,540 Lb.	10
② Loiter @ 5000 Ft. for 4 Min.	3,910	0
③ Accelerate to 325 KEAS	1,741	1
④ Climb to Optimum Altitude	77,500	346
⑤ Cruise @ M = 2.62 (Hot Day)	219,668	3,714
⑥ Decelerate to 325 KEAS	5	1
⑦ Descent to 5000 Ft. @ 325 KEAS	1,415	191
⑧ Loiter @ 5000 Ft. for 5 Min.	2,506	0
BLOCK FUEL = 324,285 Lb.		RANGE = 4,263 N. Mi.
Dispatch Wt.	750,000 Lb.	
Landing Wt.	426,074 Lb.	
Reserve Fuel	64,074 Lb.	
Payload Wt.	49,000 Lb.	



SEGMENT	SEGMENT FUEL (kg)	SEGMENT DIST. (km)
① Ground Maneuver T.O. & Climb to 1526 m	7,900 kg	18.5
② Loiter @ 1526 m for 4 min.	1,772	0
③ Accelerate to 602 km/hr	790	1.85
④ Climb to Optimum Altitude	35,150	640
⑤ Cruise @ M = 2.62 (Hot Day)	99,500	6,870
⑥ Decelerate to 602 km/hr	2	1.85
⑦ Descent to 1526 m @ 602 km/hr	641	353.5
⑧ Loiter @ 1526 m for 5 Min.	1,138	0
BLOCK FUEL = 147,893 kg		RANGE = 7,885.7 km
Dispatch Wt.	340,000 kg	
Landing Wt.	192,107 kg	
Reserve Fuel	29,000 kg	
Payload Wt.	22,200 kg	

FIGURE 3-50. BASELINE MISSION PROFILE

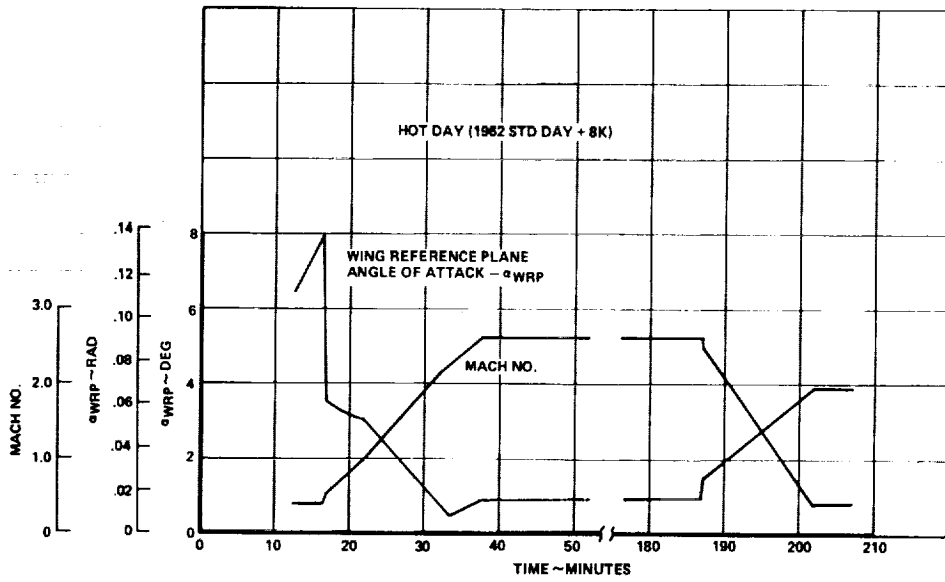


FIGURE 3-51. TRIM ANGLE OF ATTACK

## STABILITY AND CONTROL

The analysis presented herein substantiates the ability of the baseline airplane to meet the stability and control criteria outlined. Much of the analysis was accomplished using a Continuous Systems Modeling Program interactive computer graphics technique for simulating real time responses. This technique was used to verify control power and set center of gravity limits. It was essential to the selection and demonstration of a satisfactory stability augmentation concept. The results presented here are limited to summary presentations showing specific compliance with the criteria. However, additional maneuvers typical of those employed in flight testing for subjective pilot evaluation have been modeled. These time histories show that the baseline airplane with augmentation performs the maneuvers smoothly and accurately at rates appropriate for a transport airplane of this size.

### Aeroelastic Effects

The effects of aeroelasticity are included in the stability and control analysis. The aeroelastic effects are detailed in Section 4. These effects are limited to the airframe lift coefficient and pitching moment derivatives, the roll control effectiveness and roll damping. In the longitudinal plane the difference in stiffness between the candidate structural design concepts is negligible. The relative wing stiffness of the structural concepts is felt primarily in roll control effectiveness and to a lesser extent in roll damping. The roll performance implicit in the lateral-directional analysis is based on the stiffness of the strength designed monocoque structure. Of the structural designs considered, this concept afforded the least degradation in roll performance.

### Automatic Stabilization

The baseline airplane is assumed to be equipped with a three axis stability augmentation system (SAS) which will be required to function at all times.

No SAS off responses are shown because it is assumed that the system will have adequate redundancy so that it will always be in operation. A schematic diagram of the longitudinal augmentation loop is shown in Figure 3-52. In a feed forward loop the pilot stabilizer input command signal is lag-conditioned and then compared with the airframe pitch rate feedback. A gain is applied to that net signal and it is then summed with the pilot input to drive the stabilizer servo. Similar rate command augmentation loops around the yaw and roll axes are also employed.

#### Center of Gravity Limits

The center of gravity limits on Figure 3-53 show the forward limit at 51-percent for all weights and flight conditions. Although, after takeoff, a center of gravity position more forward than this could be tolerated, for the sake of efficient cruise the forward limit has been defined as 51-percent at all times.

#### Operating Envelopes

A summary of the baseline configuration speed altitude capability is shown in the envelope of Figure 3-54. The equivalent airspeed and Mach number limits are shown as a function of pressure altitude. The maximum operating speeds ( $V_{MO}$ ,  $M_{MO}$ ) and the design dive speeds ( $V_D$ ,  $M_D$ ) are consistent with structural design limits and are in accordance with Federal Aviation Regulations, Part 25.335.

The estimated minimum demonstration speeds for the clean airplane and for the 20-degree flap configuration are shown in Figure 3-55. These speeds are obtained from time histories of minimum speed demonstration maneuvers with a forward c.g. and an entry rate of 1 deg/sec (0.01745 rad/sec). This entry rate was chosen in lieu of being able to satisfy the usual entry rate of 1 knot/sec (0.5144 m/sec). The minimum speed shown is the speed at which recovery from the demonstration was initiated. Strong nose down pitching moment

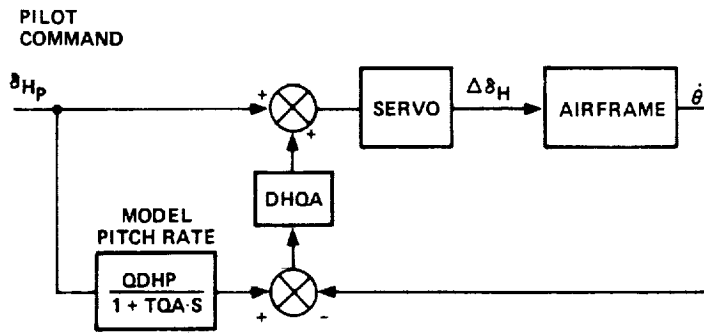


FIGURE 3-52. LONGITUDINAL COMMAND AUGMENTATION SYSTEM

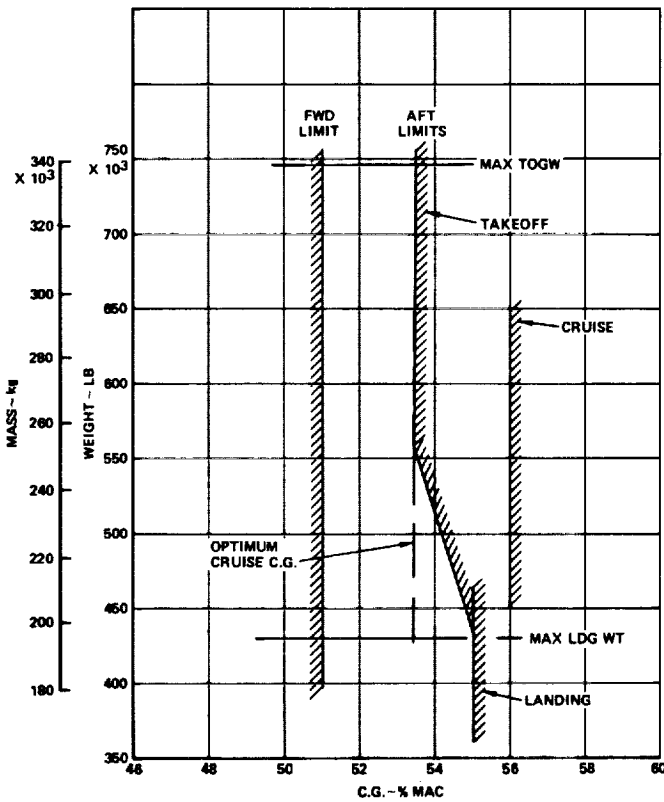


FIGURE 3-53. CENTER OF GRAVITY LIMITS

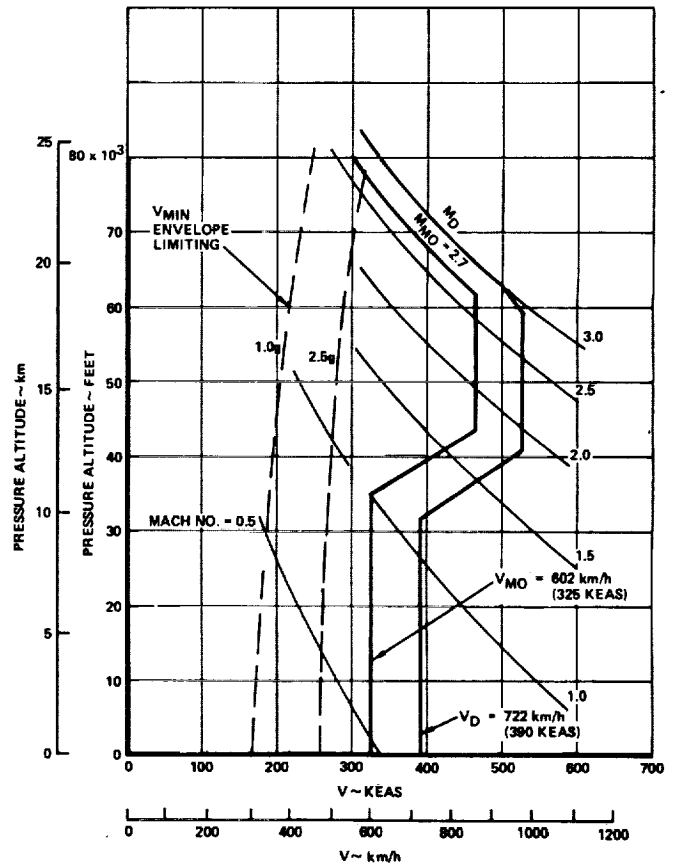


FIGURE 3-54. AIRSPEED-ALTITUDE ENVELOPE



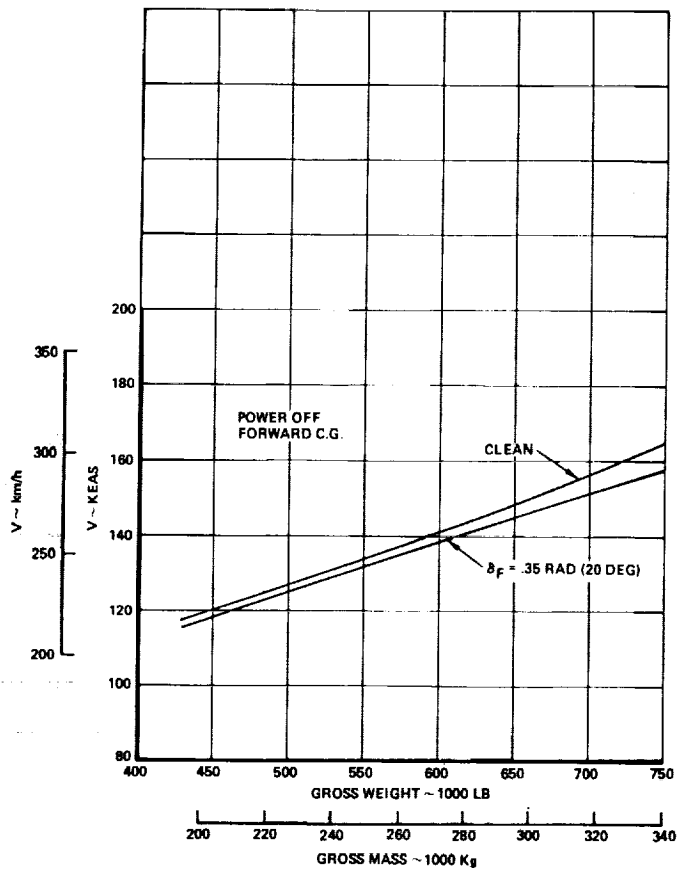


FIGURE 3-55. MINIMUM DEMONSTRATION SPEEDS

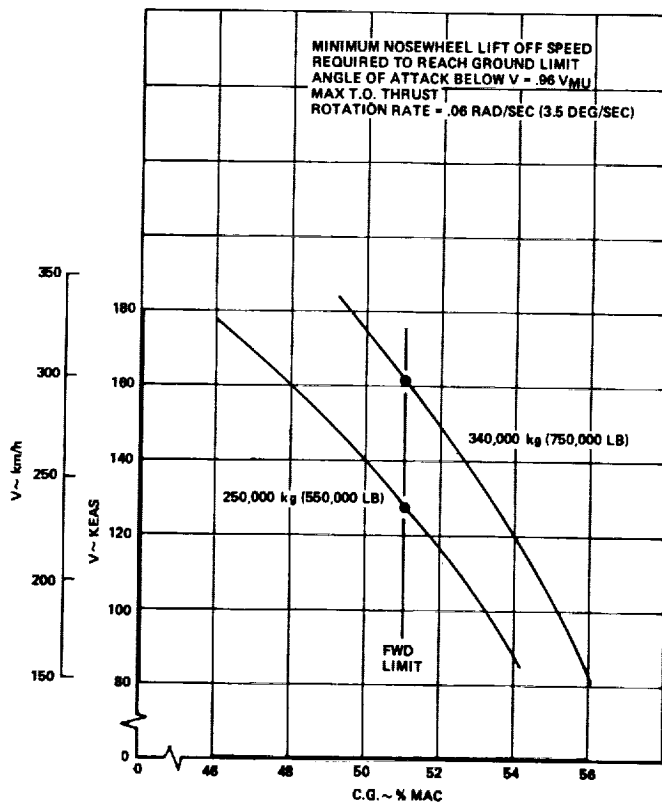


FIGURE 3-56. MINIMUM NOSE WHEEL LIFT-OFF

occurs at angles of attack above the angle for minimum speed through the action of the envelope limiting mode of the longitudinal SAS.

#### Takeoff Rotation

Minimum nose wheel liftoff speeds as a function of c.g. position have been computed for two weights as shown on Figure 3-56. The c.g. position that will give the maximum nose wheel lift off speed and yet qualify as geometry limited is shown. In order to be geometry limited, the angle of attack for ground scrape must be attained at a speed equal to or less than 0.96 times the minimum unstick speed. The nose wheel must lift earlier by an interval which depends on the acceleration down the runway and the rotation rate. Dynamic takeoff studies have shown that the rate of rotation for takeoff should not be greater than 4-degrees per second or excessive tail strike loads will result. Assuming a rotation rate of 3.5-degrees per second, the required minimum speeds are calculated for nose wheel lift off. These are shown for two weights. At both weights the center of gravity which corresponds to the required minimum speed occurs at 51-percent MAC. Thus, there is no dependence of forward limit on takeoff gross weight. Nose up control power in ground effect is indicated by Figure 3-57 where the pitch characteristic is shown for zero stabilizer incidence and full airplane nose up stabilizer. The forward c.g. line is shown. It is seen that the control power is more than adequate (1-1/2 times what is required) at the scrape angle and the rotational acceleration at static ground altitude is quite high.

#### Envelope Limiting

An example of the minimum speed demonstrated maneuver is shown in Figure 3-58. This is the trace of a CSMP Graphics modeling of the airplane at maximum landing weight with an aft c.g. The airplane nose down stabilizer input for envelope limiting is applied at a speed of 214 km/h (115.5 keas). This speed is the minimum speed required in order to give a landing approach reference speed ( $1.3 V_{MIN}$ ) of 278 km/h (150 keas). The speed decreases somewhat below the stick actuation speed but this undershoot is not considered in establishing the minimum speed. Minimum speed is identified as the lowest speed at which

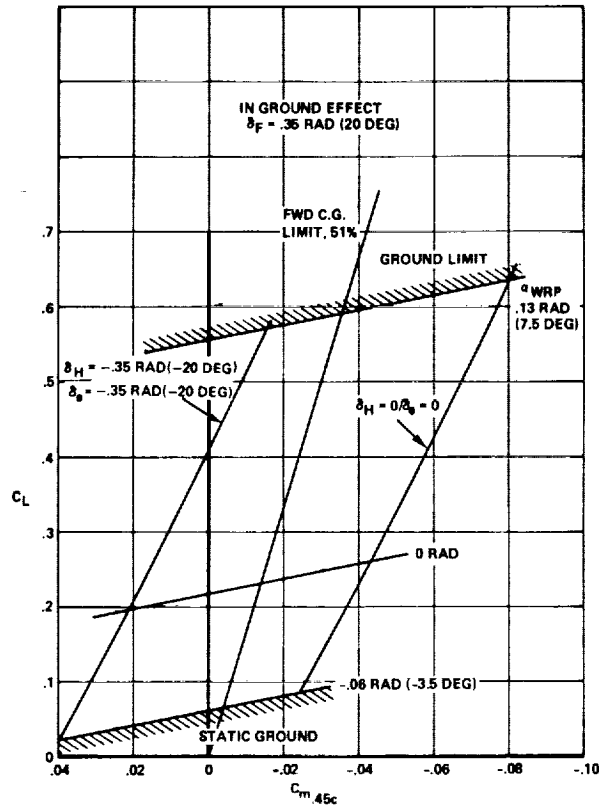


FIGURE 3-57. AIRPLANE NOSE-UP CONTROL POWER

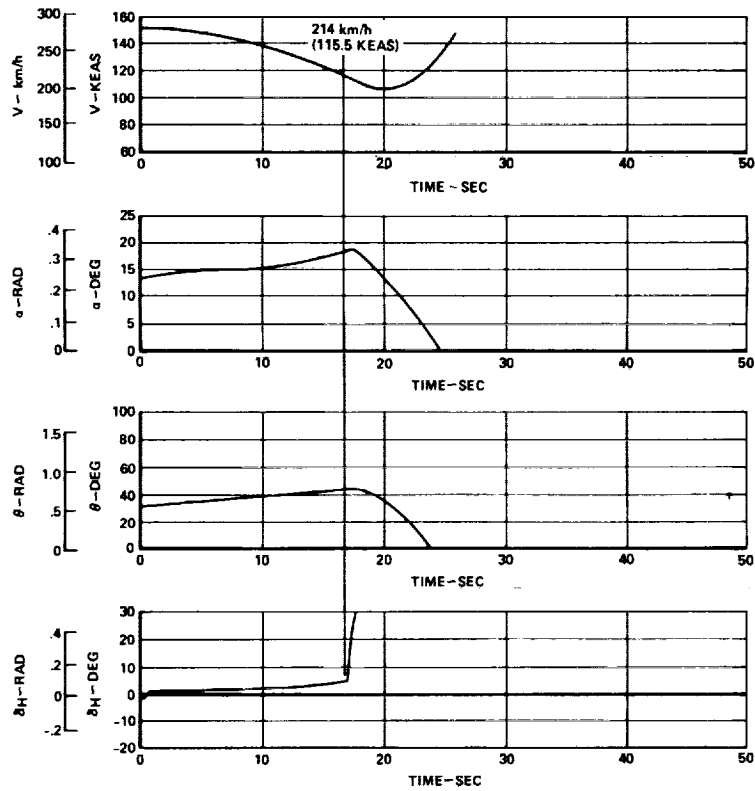


FIGURE 3-58. MINIMUM SPEED DEMONSTRATION

normal recovery techniques could be successfully applied. That would be the speed immediately before the automatic pitch limiting system is actuated at 214 km/h (115.5 keas), so that is used as the minimum speed in lieu of stall speed. Similar studies were conducted for other weights and these studies produced the aft c.g. limit line for low speed which is shown on the center of gravity limits (Figure 3-53).

#### Longitudinal Maneuver Capability

With the advent of fail-operational active controls apparent maneuver stability margin is diminished as a useful criterion. Therefore criterion I-4.1 has been discarded and no analysis responding directly to it is included in this report.

A set of longitudinal stabilizer incidence settings for trim and maneuver are shown in Figures 3-59 through 3-70 for conditions at sea level, and at altitudes of 9160 m (30,000 ft) and 21,360 m (70,000 ft). Data shown on these figures demonstrate that adequate longitudinal control is available throughout the flight envelope to attain the maneuver g-levels established by criteria I-1.4, I-2.1, I-4.2 and I-4.3. Both flaps down and flaps up configurations are presented.

Aeroelastic effects have been included in arriving at the incidence angles shown in the transonic and supersonic charts. The free airplane shape is represented for the chordwise stiffened wing at the correct altitude and Mach number. For the transonic curves a fully loaded wing at 750,000 lb is used to represent a climb condition. For the supersonic curves the mid-cruise weight of 550,000 lb is used.

An angle of attack limit line showing the speed-load factor boundary set by the actuation of the automatic envelope limiting system is also shown. It can be seen that at the lowest normal operating speed of  $1.2 V_{MIN}$  at  $\pm .5$ -g maneuvering capability exists for conditions at sea level and aft c.g. at 9160 m (30,000 ft). At cruise altitudes the envelope limiting does not restrict maneuvers. The stabilizer deflections are more positive for aft c.g. because the airplane is statically unstable. The location of the aerodynamic center (a.c.) at cruise for the rigid airplane is 55-percent MAC. With 8-percent destabilizing effect of aeroelasticity at cruise Mach number,

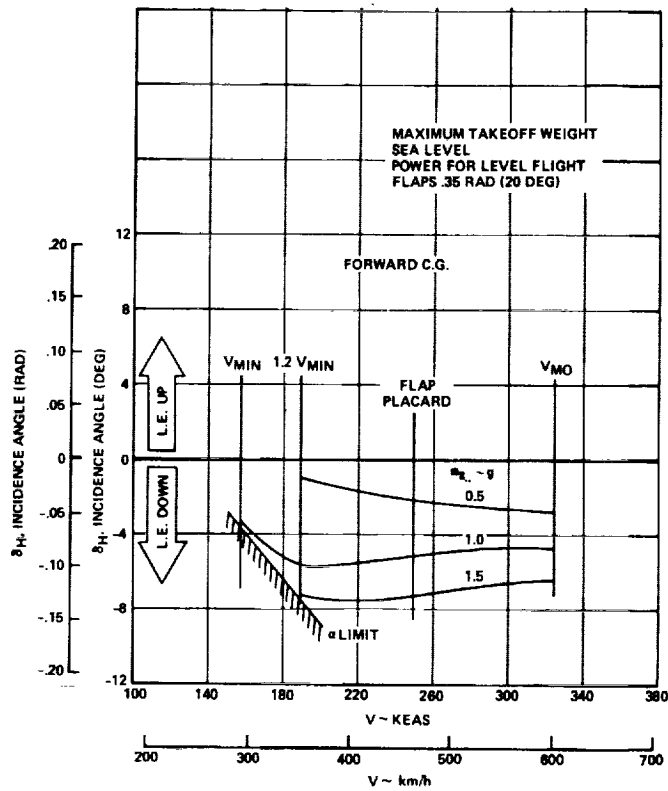


FIGURE 3-59. HORIZONTAL STABILIZER INCIDENCE TO TRIM,  $\delta_F = 20$ -DEG.  
MAXIMUM TAKE-OFF WEIGHT- FWD C.G.

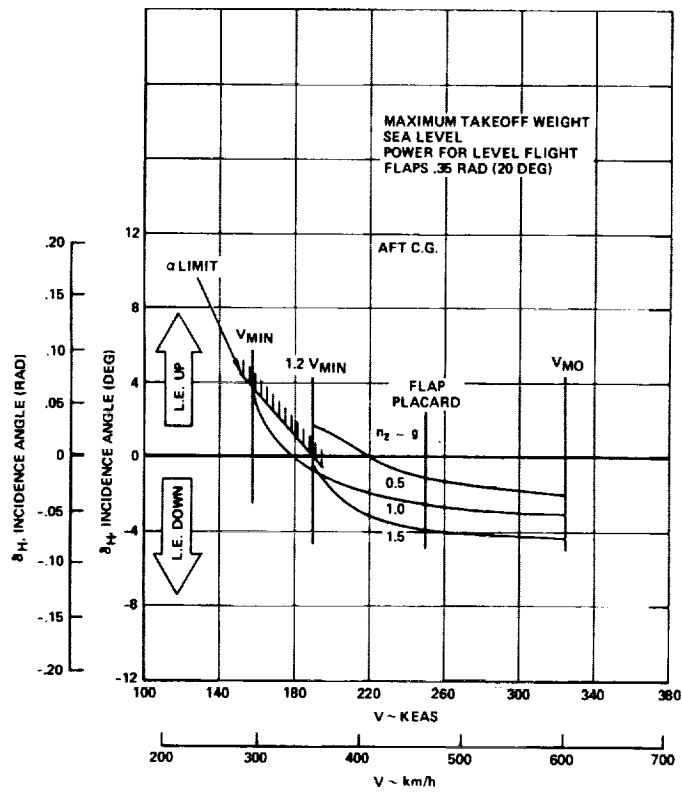


FIGURE 3-60. HORIZONTAL STABILIZER INCIDENCE TO TRIM,  $\delta_F = 20$ -DEG.  
MAXIMUM TAKE-OFF WEIGHT-AFT. C.G.

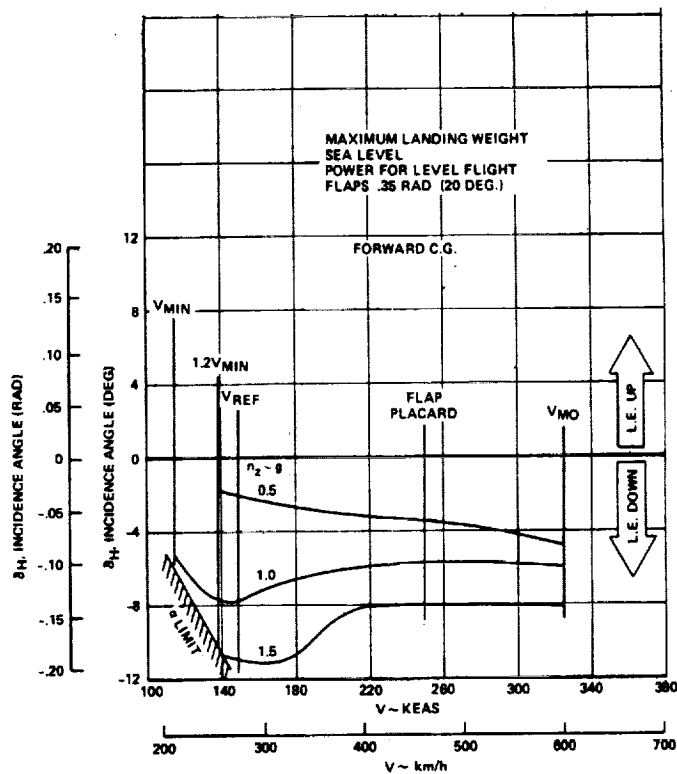


FIGURE 3-61. HORIZONTAL STABILIZER INCIDENCE TO TRIM,  $\delta_F = 20$ -DEG.  
MAXIMUM LANDING WEIGHT-FWD C.G.

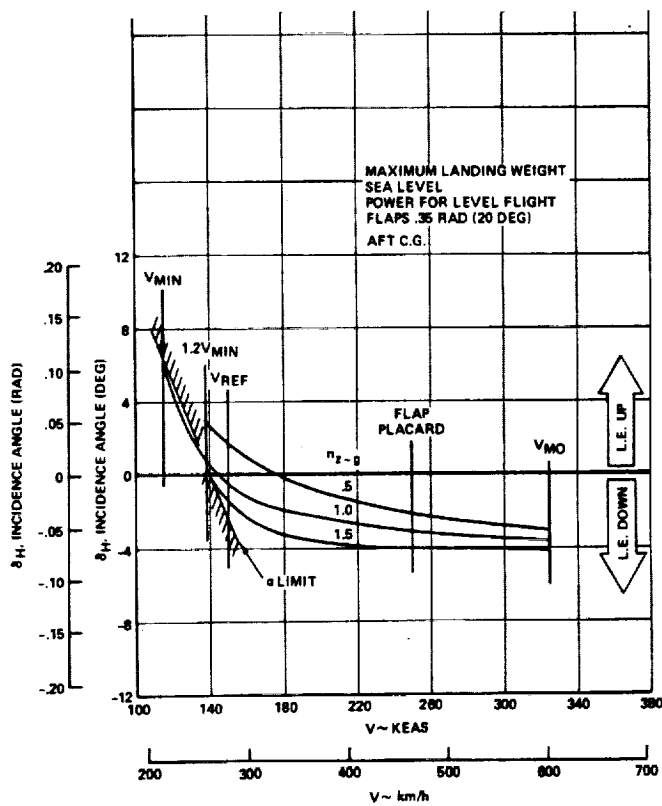


FIGURE 3-62. HORIZONTAL STABILIZER INCIDENCE TO TRIM,  $\delta_F = 20$ -DEG.  
MAXIMUM LANDING WEIGHT-AFT C.G.

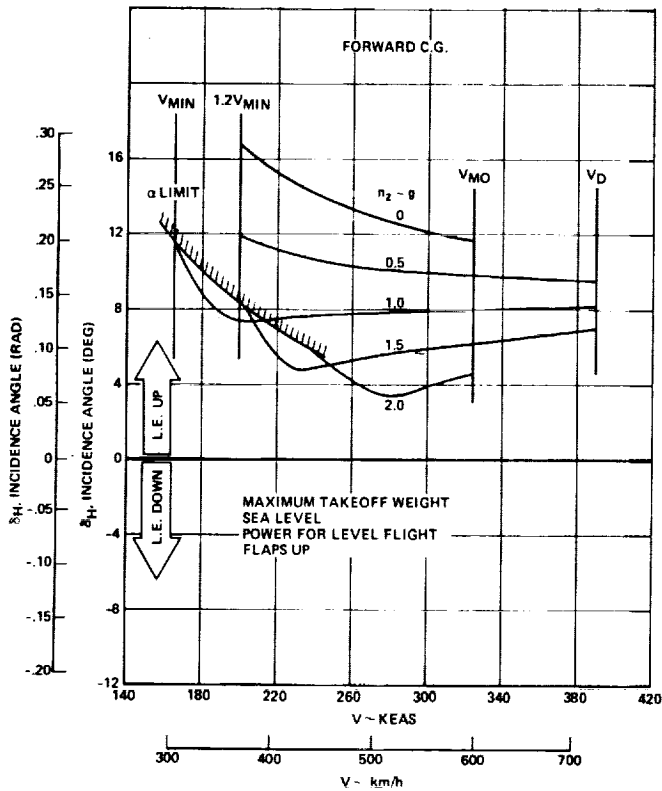


FIGURE 3-63. HORIZONTAL STABILIZER INCIDENCE TO TRIM,  $\delta_F = 0$ -DEG  
 MAXIMUM TAKE-OFF WEIGHT-FWD. C.G.

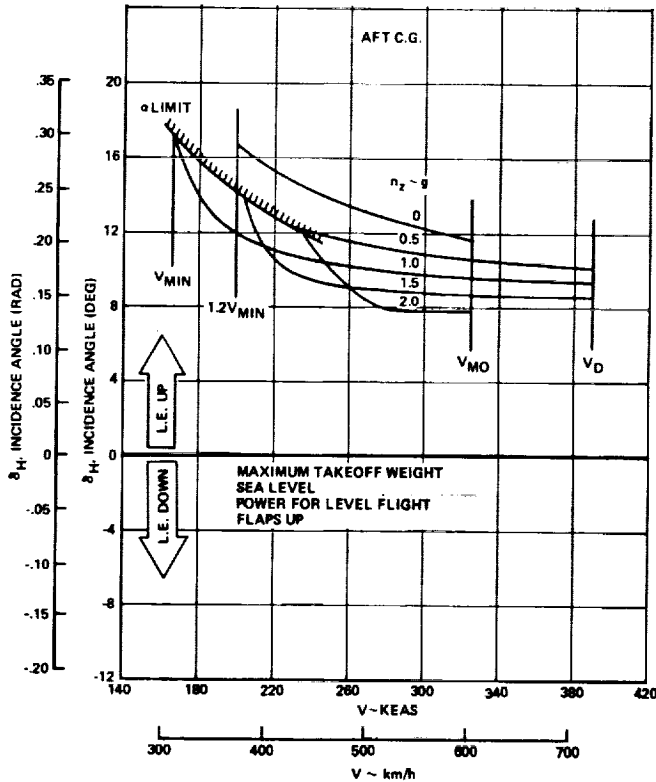


FIGURE 3-64. HORIZONTAL STAB LIZER INCIDENCE TO TRIM,  $\delta_F = 0$ -DEG.  
 MAXIMUM TAKE-OFF WEIGHT-AFT. C.G.

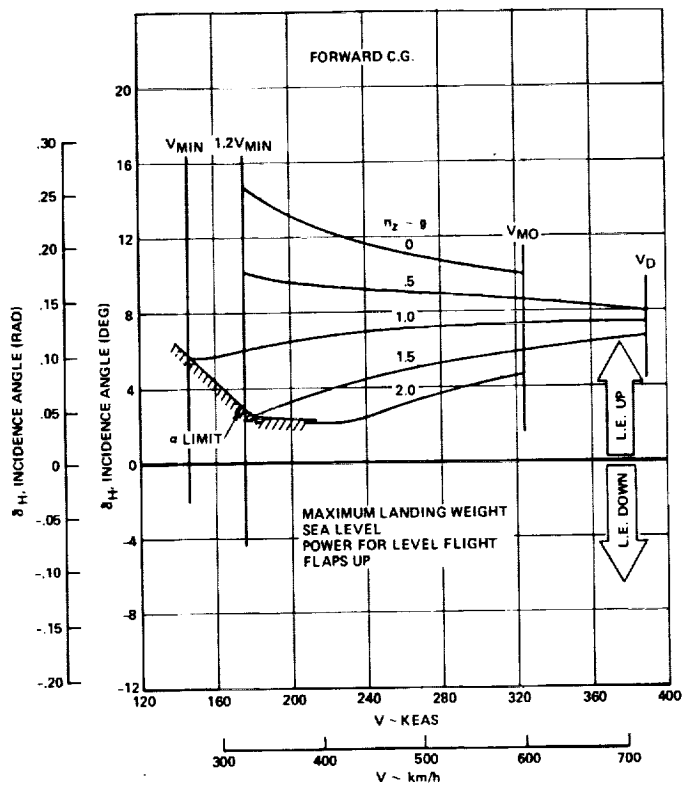


FIGURE 3-65. HORIZONTAL STABILIZER INCIDENCE TO TRIM,  $\delta_F = 0$ -DEG. MAXIMUM LANDING WEIGHT-FWD. C.G.

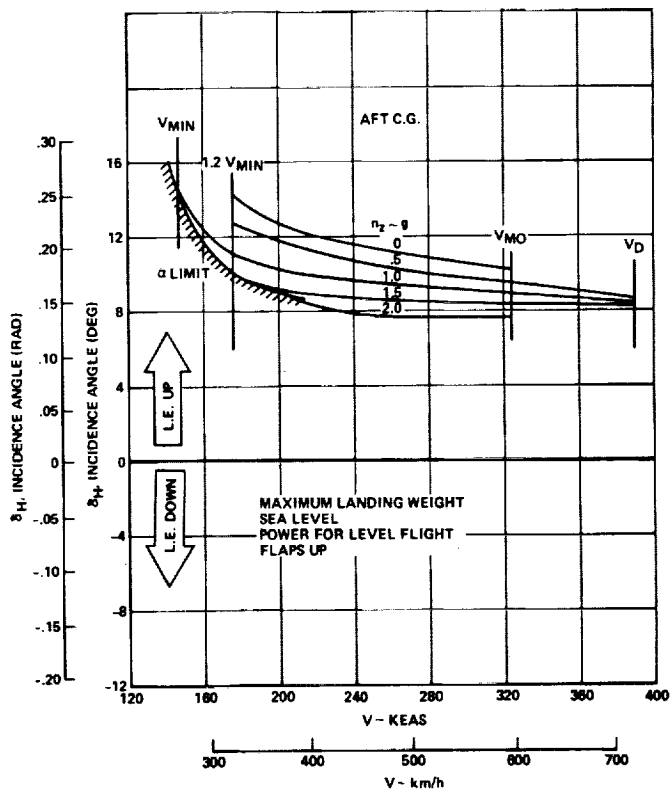


FIGURE 3-66. HORIZONTAL STABILIZER INCIDENCE TO TRIM,  $\delta_F = 0$ -DEG. MAXIMUM LANDING WEIGHT-AFT. C.G.



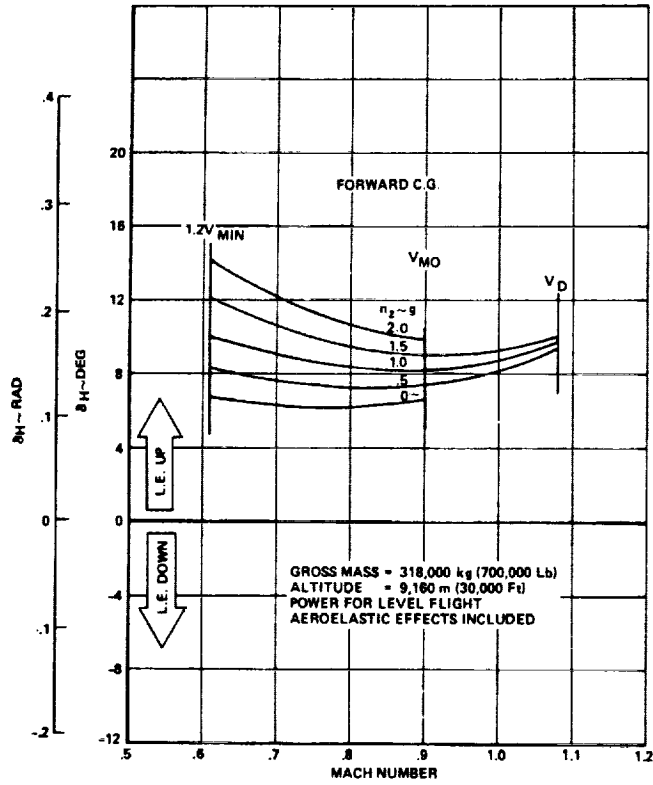


FIGURE 3-67. HORIZONTAL STABILIZER INCIDENCE TO TRIM, TRANSONIC, FWD. C.G.

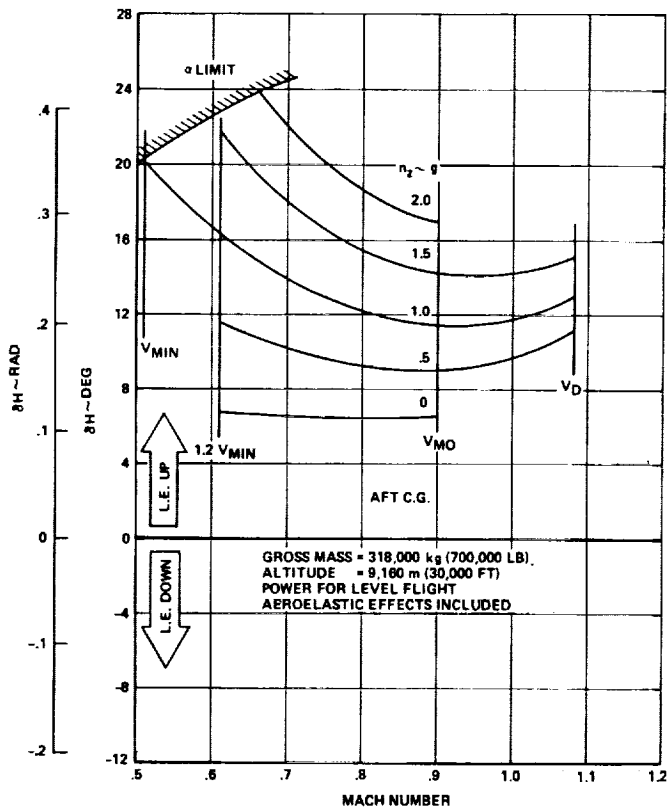


FIGURE 3-68. HORIZONTAL STABILIZER INCIDENCE TO TRIM, TRANSONIC, AFT. C.G.

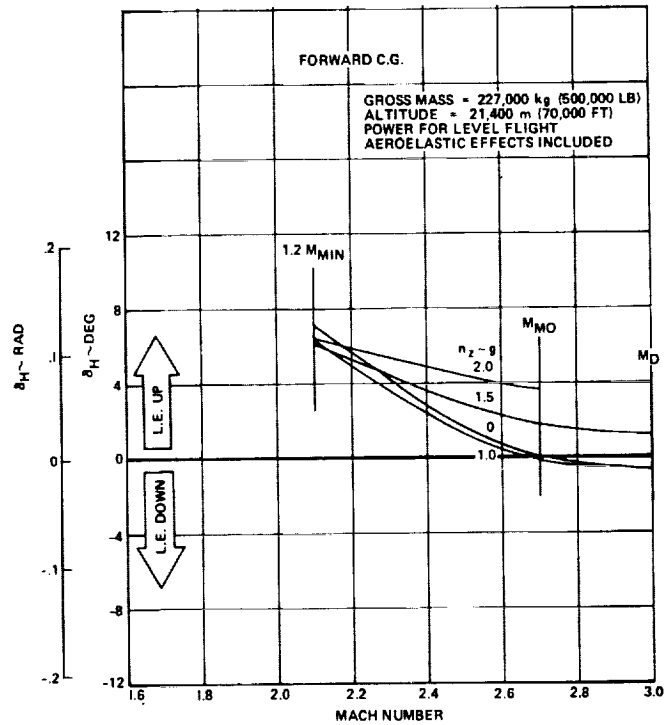


FIGURE 3-69. HORIZONTAL STABILIZER INCIDENCE TO TRIM, SUPERSONIC, FWD. C.G.

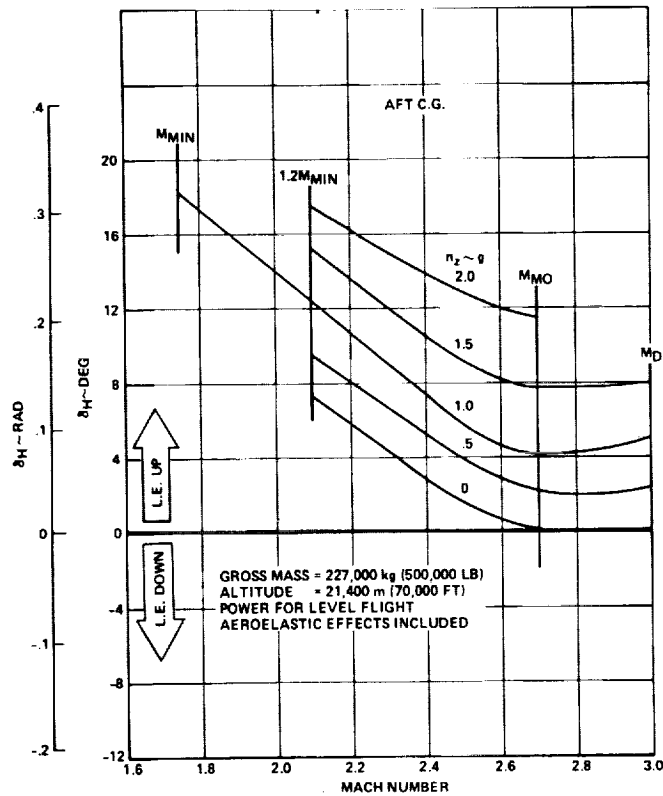


FIGURE 3-70. HORIZONTAL STABILIZER INCIDENCE TO TRIM, SUPERSONIC, AFT C.G.

altitude and midcruise weight, the flexible airplane a.c. is at 47-percent. The c.g. envelope is 51-percent to 55-percent so the airplane is always unstable. The farther aft the c.g. the more positive tail incidence is required for trimming and for positive maneuvers. For the forward c.g. where the airplane is near neutral stability the lines are compressed indicating that the tail incidence for trim and maneuver differ slightly if at all. The active stabilization system will accommodate this and provide the proper angle to achieve or maintain the commanded pitch rate.

Minimum speed for each weight and altitude condition is established for the aft c.g. case. This is the most positive tail incidence required to trim. The minimum speed occurs when the incidence to trim for 1-g flight is equal to the total leading edge up stabilizer minus the tail deflection required to provide the airplane nose down pitch acceleration needed at that speed and altitude. Dynamic time history studies of pitch envelope limiting recovery show that a residual pitch capability at the recovery initiation must be adequate to provide a  $-.1 \text{ rad/sec}^2$  nose down acceleration.

#### Minimum Control Speed

The minimum control speed on the ground ( $V_{MCG}$ ) was determined using aerodynamic control alone. Nosewheel steering or landing gear resistance was not included. A seven-knot (13 km/h) adverse crosswind has been included. The minimum speed is shown in Figure 3-71 as 167 keas (309 km/h). The Federal Aviation Regulations, Part 25, requires that the takeoff decision speed  $V_1$  be greater than  $V_{MCG}$ . Decision speed necessary for meeting the performance objective of 10,500 ft (3200 m) balanced field length is 186 keas (344 km/h). Thus the FAR requirement is easily met with no constraint on performance.

Air minimum control speed ( $V_{MCA}$ ) as shown on Figure 3-72 was determined for two flight conditions. For both conditions one fourth of the available roll control power has been retained for handling gusts.

The first condition is takeoff with one outboard engine failed and the others at maximum takeoff thrust. This condition defines the minimum control speed for meeting FAR takeoff speed requirements. Criterion II-4.2 summarizes these

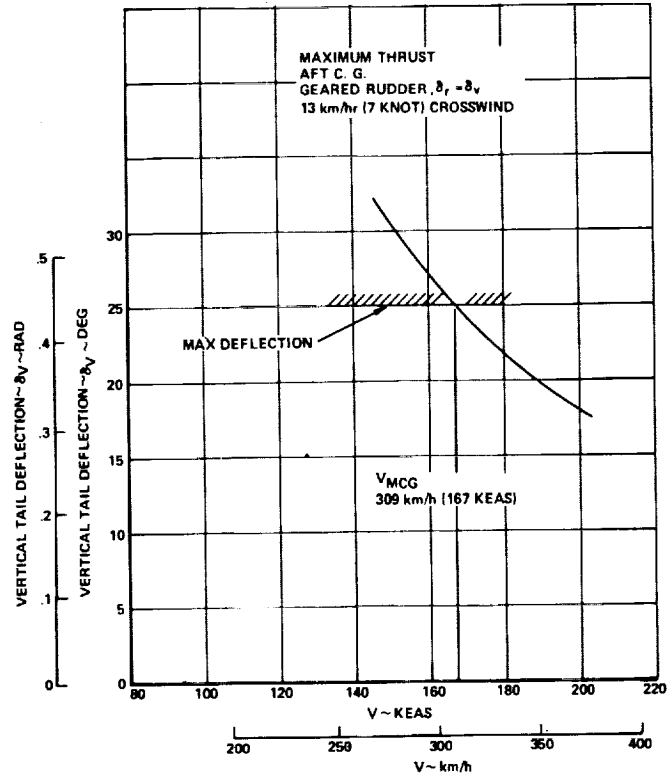


FIGURE 3-71. GROUND MINIMUM CONTROL SPEED

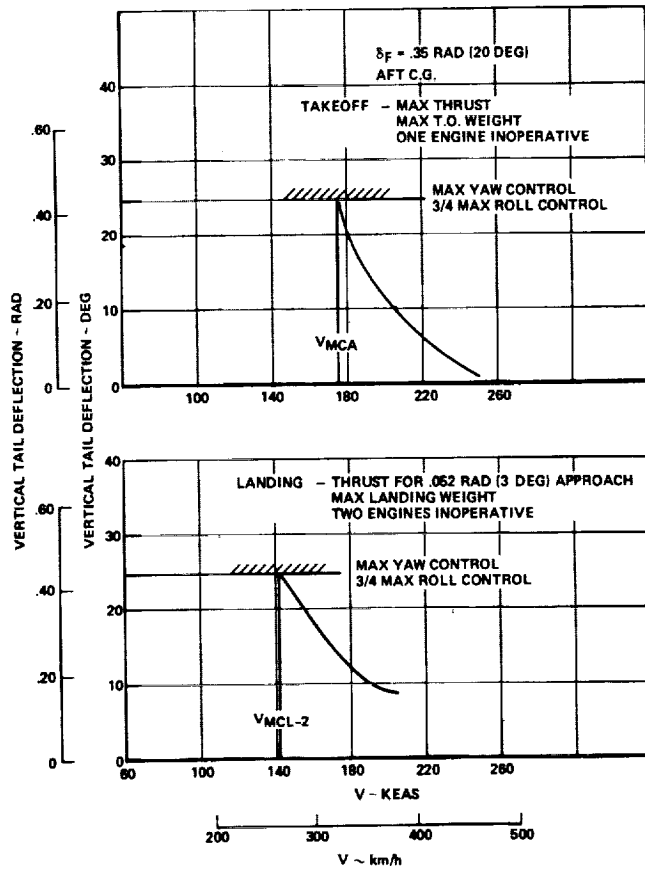


FIGURE 3-72. AIR MINIMUM CONTROL SPEED

as:  $1.05 V_{MCA}$  must be less than or equal to rotational speed ( $V_1$ ) and  $1.1 V_{MCA}$  must be less than or equal to  $V_2$ . Reference to Figure 3-48 shows that this criterion is met.

The second flight condition is landing with two engines failed. Power for maintaining a 3-degree approach is retained on the remaining engines. Landing minimum control speed with 2 engines out ( $V_{MCL-2}$ ) was introduced as a criterion by the Concorde special conditions. They require that approach speed ( $V_{APP}$ ) be less than or equal to  $1.05 V_{MCL-2}$ . This is satisfied with  $V_{MCL-2} = 142$  keas and  $V_{APP} = 150$  keas.

### Crosswind Landing

The maximum crosswind that can be controlled by the lateral directional control system assuming a 4 degree (0.0698 rad) crab angle and no bank is presented in Figure 3-73. Criterion II-2 requires that 2/3 of the maximum yaw control be employed retaining 1/3 for control of gusts. It is seen that a  $1.3 V_{MIN}$  which is the landing reference speed that a 90-degree (1.57 rad) crosswind of 22 keas (40.7 km/h) can be controlled and in this condition less than full roll control capability is employed. The limiting crosswind speed is recorded when the roll control is saturated and in this condition at  $1.3 V_{MIN}$  at 27 keas (50 km/h) can be handled. Less than full yaw control is used here retaining some margin for gusts. The intent of the criterion in retaining some margin of yaw control is met by this capability. The roll control limited crosswind landing capability is considered to be meeting the criterion within 10-percent. If any amount of de-crab capability is supplied by the landing gear there should be no difficulty in landing with a 30 knot (55.5 km/h) crosswind.

### Steady Sideslip

A steady state sideslip at  $V_{APP}$  in landing configuration with all engines operating is shown in Figure 3-74. With full directional control input ( $\delta_v = 25$  deg) the roll control required is less than three fourths of the

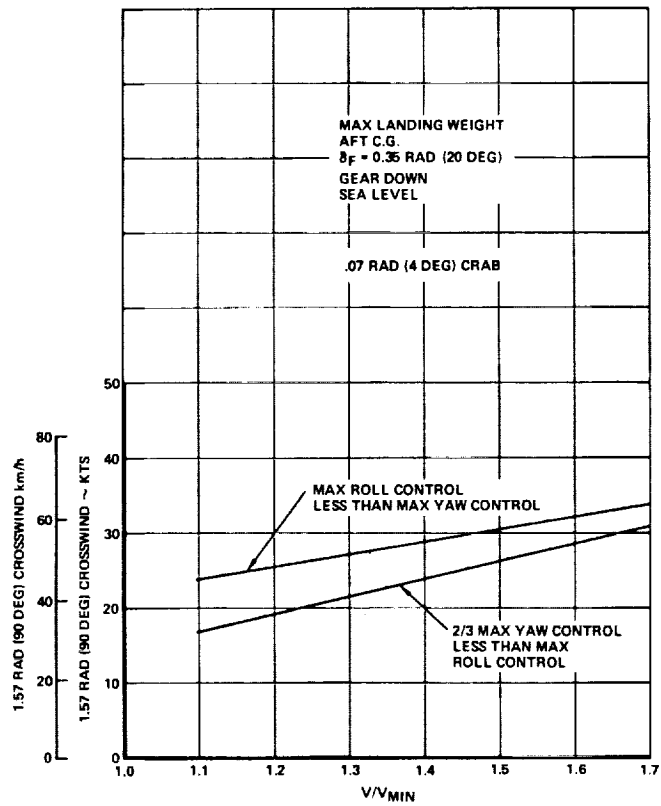


FIGURE 3-73. CROSS-WIND LANDING

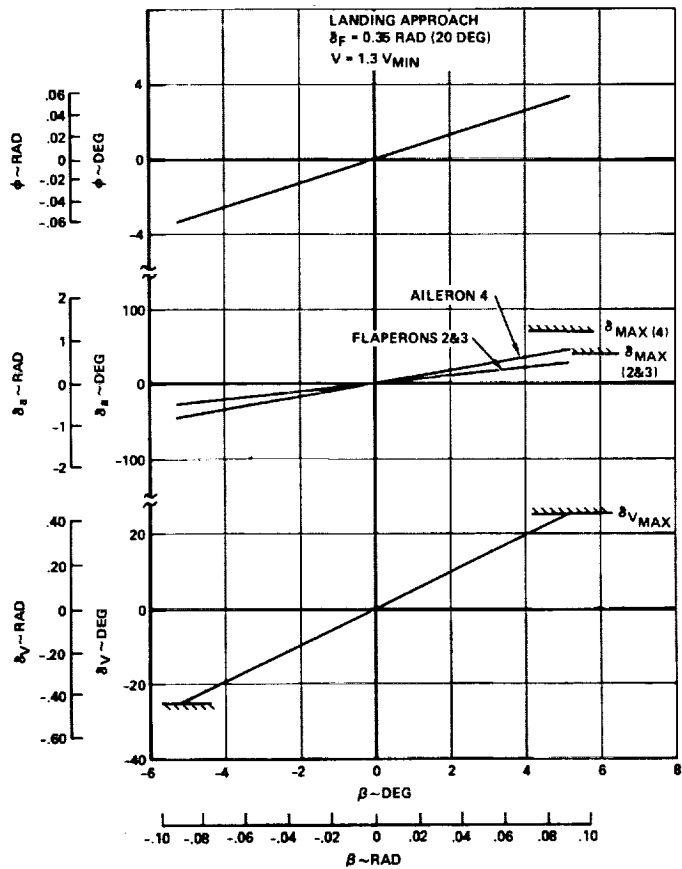


FIGURE 3-74. ENGINE OUT STEADY SIDESLIP

control available thus satisfying criterion II-3.4. At full directional control the sideslip angle is 5.1 degree and bank angle is 3.3-degree. The landing approach condition is presented because it is among the most critical and it is a condition where the sideslip maneuver may be expected to occur in operational practice. At higher speed flight conditions directional control authority may be limited while for the landing approach and takeoff full authority may be available.

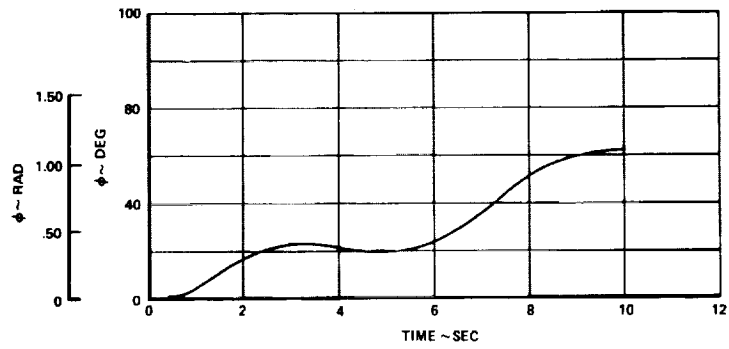
### Roll Performance

Roll performance time histories are shown for two flight conditions in Figures 3-75 and 3-76. The two conditions are landing approach and transonic cruise-climb. Full roll control is applied at initiation and held throughout the time interval shown. No yaw damping is employed. It is obvious from both cases that active yaw stability augmentation is required to damp out the severe Dutch roll tendency. Criteria II-3.1, II-3.2 and II-3.3 cannot be met without active controls on the yaw axis. Roll rate reversal occurs in both cases and in neither is the objective roll angle acquired within the desired time. Maximum roll rates on the order of 20 degrees (0.349 rad) per second in the initial phase of the maneuver show that adequate roll control power is available but roll performance cannot be realized without yaw rate damping.

Figure 3-77 presents a measure of roll capability of the Final Design airplane at supersonic speeds. The results were obtained by executing a one-degree of freedom steady state roll using spoiler-slot deflector 2 and inverted spoiler-slot deflector 3. The results indicate a 20-degree per second roll rate capability at supersonic speeds for a flexible supersonic cruise transport.

### Response to Unstart

Experience with YF-12 type aircraft shows that unstart of an engine inlet can be one of the most severe hazards of supersonic cruise flight for multi-engine aircraft. This phenomena has engendered the existence of tameness criteria such as Criterion II-5. Meeting this criterion without using hardened SAS would require a vertical stabilizer much larger than has been provided on the



0.35 RAD (20 DEG) FLAPS, 1.3  $V_{MIN}$   
 MAX. LANDING MASS, AFT C.G.  
 FULL ROLL CONTROL  
 NO AUGMENTATION

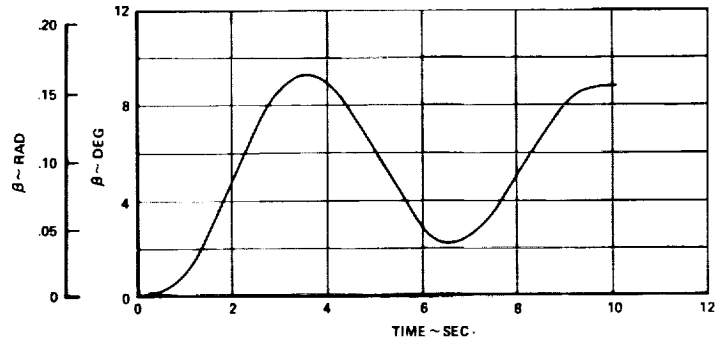
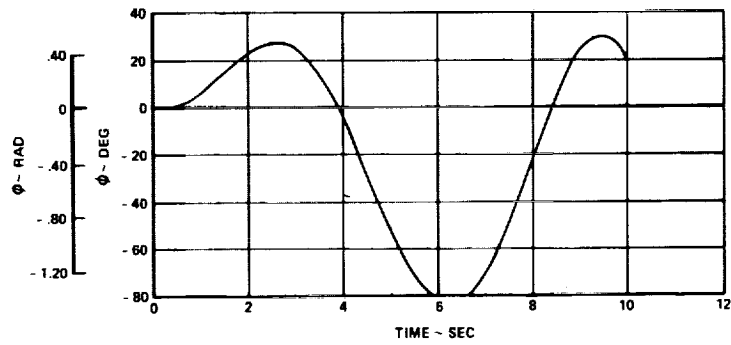


FIGURE 3-75. ROLL PERFORMANCE-LANDING-APPROACH



CLEAN CONFIGURATION,  $M = 9$   
 MASS = 318,000 kg (700,000 LB) AFT C.G.  
 9180m (30,000 ft.), FULL ROLL CONTROL  
 NO AUGMENTATION

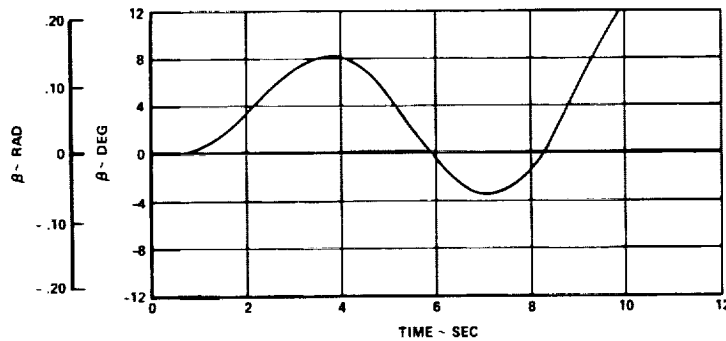


FIGURE 3-76. ROLL PERFORMANCE-CLIMB CONFIGURATION,  $V_{MO}$



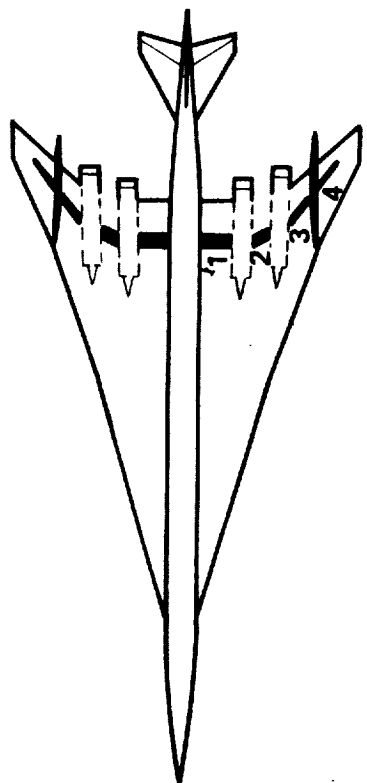
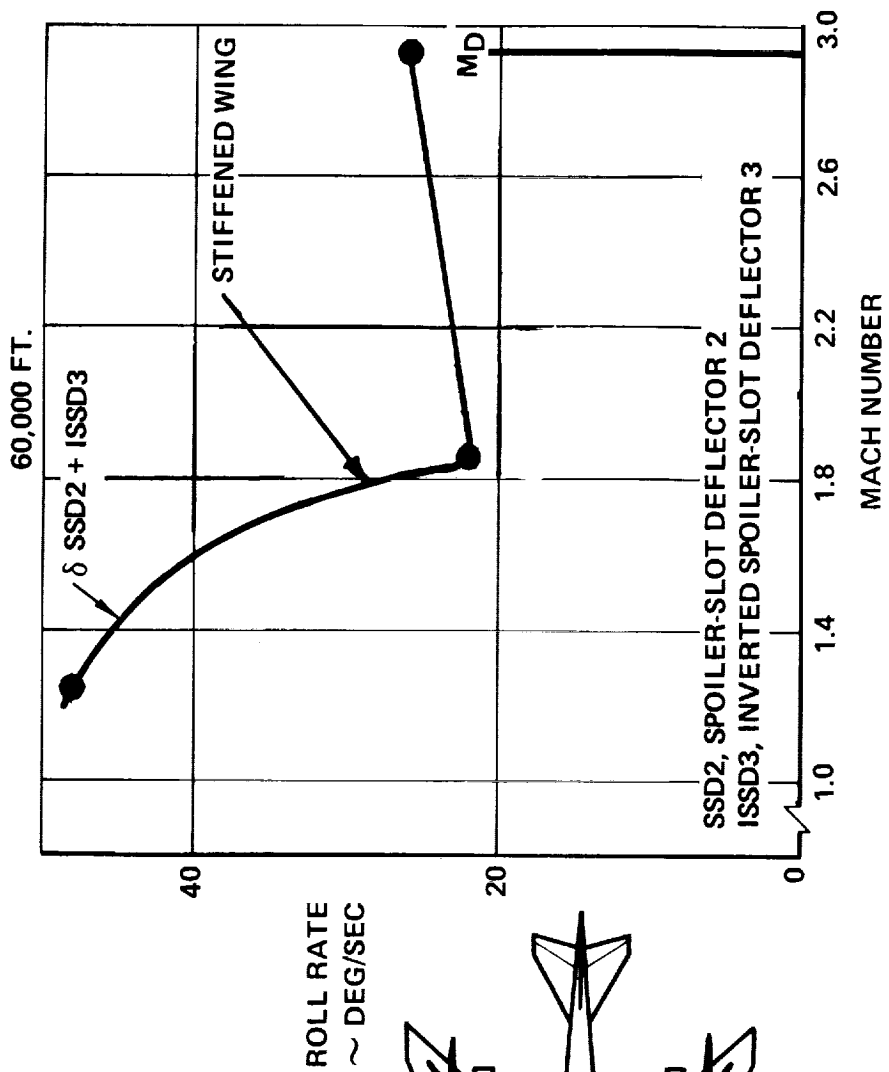


Figure 3-77. Supersonic Roll Power for Stiffened Wing

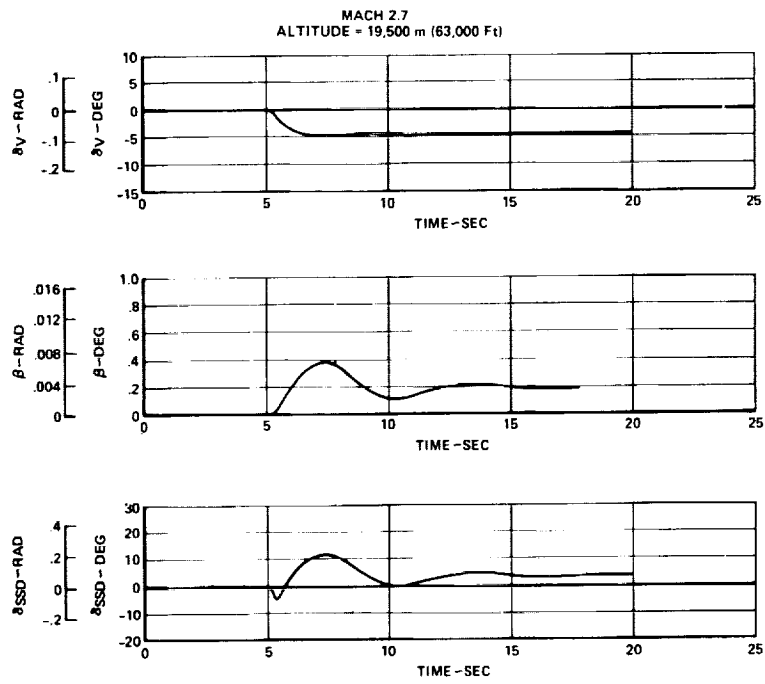
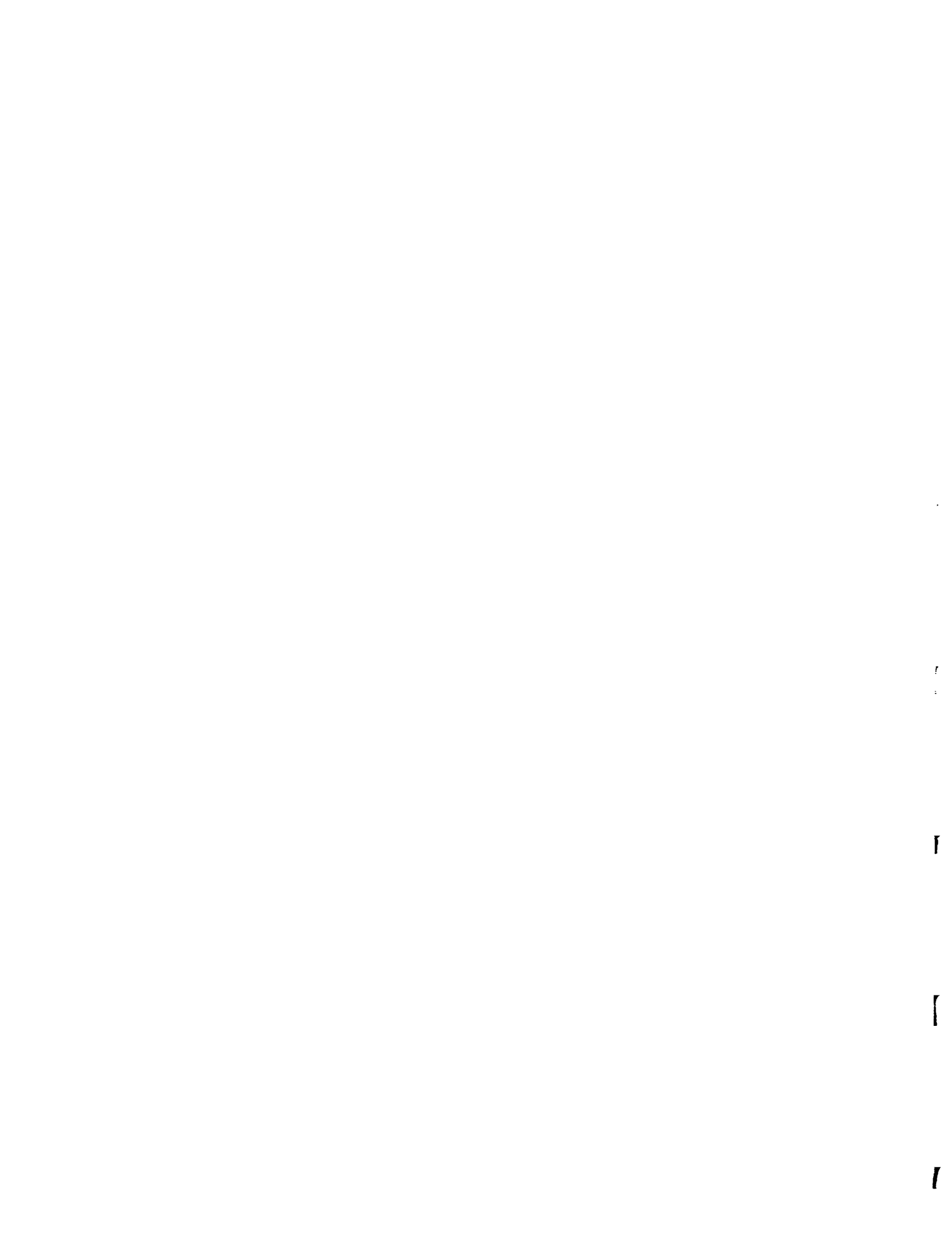


FIGURE 3-78. RESPONSE TO INLET UNSTART

aircraft as defined for this study. Use of active stabilization on all axes allows fully automatic response to the effects of unstart. Figure 3-78 shows the time history of sideslip and control deflection following an unstart at a time of 5 seconds. No pilot action is assumed. Command augmentation loops on both roll and yaw axes respond to the non-zero roll and yaw rates induced by the instantaneous effects of the unstart and the more gradual thrust asymmetry.

The peak sideslip angle attained is less than one-half degree (0.00872 rad) because of the quick response of the automatic system. Relying on pilot action with human sensory and motor lags would permit greater excursions which could cause injuries to many passengers in a transport aircraft. The small response allowed by the actively stabilized system should be tolerable and argues the necessity for hardened stability augmentation. The use of this same roll and yaw command augmentation should produce vastly improved roll performance which was shown to be deficient in the preceding section.



SECTION 4

STRUCTURAL DESIGN CRITERIA

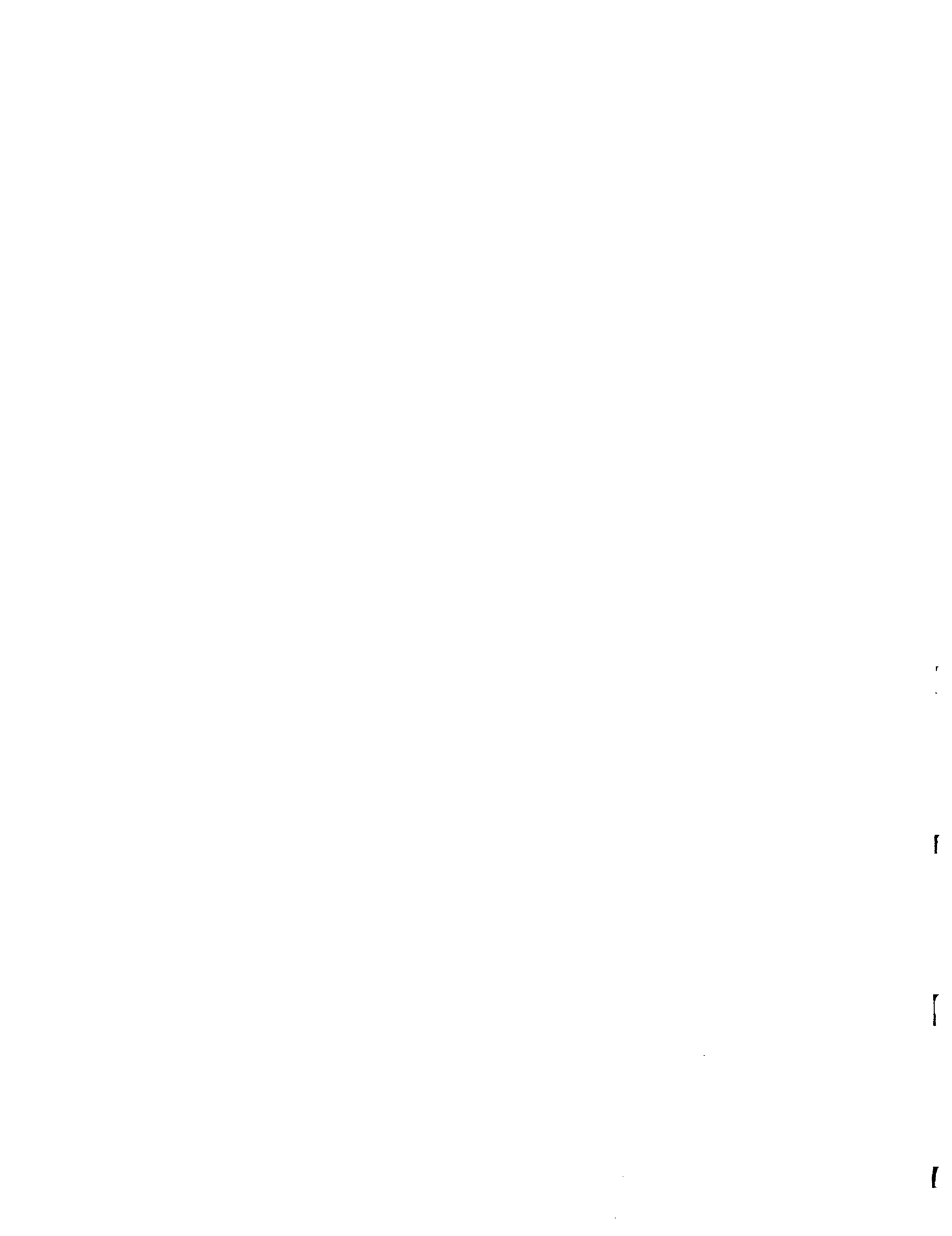
BY

B. C. WOLLNER AND I. F. SAKATA



## CONTENTS

<u>Section</u>	<u>Page</u>
INTRODUCTION	4-1
DESIGN MASS	4-1
DESIGN SPEEDS	4-4
DESIGN FLIGHT PROFILE	4-10
STRUCTURAL DESIGN TEMPERATURE CRITERIA	4-10
MANEUVERING FLIGHT CRITERIA	4-13
GROUND HANDLING CRITERIA	4-14
LANDING CRITERIA	4-15
FUEL TANK PRESSURES	4-15
EMERGENCY LANDING CRITERIA	4-16
FATIGUE AND FAIL-SAFE LOADS CRITERIA	4-16
MINIMUM GAGE CRITERIA	4-17
PRESSURIZED CABIN LOADS CRITERIA	4-20





LIST OF FIGURES

<u>Figure</u>		<u>Page</u>
4-1	Airplane Mass Variation with Altitude - Task I	4-3
4-2	Airplane Mass Variation with Center of Gravity - Task I	4-3
4-3	Airplane Mass Variation with Center of Gravity - Task II	4-5
4-4	Design Flight Profile - International Mission (Mach 2.62 Cruise)	4-5
4-5	Structural Design Speeds	4-6
4-6	Variation of Mach Numbers with Ambient Conditions	4-7
4-7	Angle of Attack Limits for Structural Design	4-9
4-8	Baseline Mission Profile - International Mission (Mach 2.62 Cruise)	4-9
4-9	Loading Spectra C	4-18
4-10	Tolerance Applied to Nominal Differential Pressure to Establish Limit Design Differential Pressure	4-21
4-11	Cabin Pressure Structural Design Envelope	4-21

**PRECEDING PAGE BLANK NOT FILMED**



LIST OF TABLES

<u>Table</u>		<u>Page</u>
4-1	International Mission - Mach 2.62 Cruise (4200 n.mile)	4-11
4-2	International Mission - Mach 2.62-Cruise (4166 n.mile)	4-12
4-3	Minimum Gage Criteria	4-19

**PRECEDING PAGE BLANK NOT FILMED**



## SECTION 4

### STRUCTURAL DESIGN CRITERIA

#### INTRODUCTION

The structural design criteria defined in this section have been developed to provide (1) the basis for the evaluation of the structural design concepts and (2) a level of structural safety equivalent to current transports for assessing structural mass trends resulting from application of these criteria.

The criteria are based on the structural requirements of the Federal Aviation Agency, FAR 25, and the Tentative Airworthiness Standards for Supersonic Transports, revised January 1, 1971. It is expected that, during the development of a supersonic cruise transport, areas requiring modification to existing airworthiness standards may be revealed. Several such instances are identified as the result of this study and appropriate criteria changes are discussed.

#### DESIGN MASS

##### Analytical Design Studies - Task I

The design gross mass of the baseline airplane is defined in the following paragraphs for the initial design studies:

Maximum Design Taxi Mass = 340,000 kg (750,000 lb)

- Includes mass of taxi and run-up fuel
- Used for all taxi and ground handling loads
- Maximum mass for design with full fuel and full payload (FFFP)

Maximum Design Take-Off Mass = 338,000 kg (745,000 lb)

- Excludes mass of taxi and run-up fuel

- Maximum taxi mass less 2270 kg (5000 lb) of fuel expended between dispatch and time at which sufficient speed is attained to permit performing a 2.5-g maneuver.
- Maximum mass at which in-flight loads are determined

Maximum Flight Gross Mass = Variable with altitude

- Flight design mass is variable with altitude as shown in Figure 4-1
- Determined by considering fuel required to reach each altitude along the flight profile.

Maximum Landing Gross Mass = 191,000 kg (420,000 lb)

- Operating weight empty (OWE) = 146,000 kg (321,000 lb)
- Payload = 22,000 kg (49,000 lb)
- Fuel = 23,000 kg (50,000 lb)

Maximum Zero Fuel Mass = 168,000 kg (370,000 lb)

- Equal to OWE plus payload

Minimum Flight Mass = 154,000 kg (340,000 lb)

- Equal to OWE plus 5 percent of fuel capacity

The variation of airplane mass with center-of-gravity location is shown on Figure 4-2. The ground handling and controllability limits are indicated for determination of design loads.

#### Engineering Design Studies - Task II

The airplane mass properties used for the detailed design studies are based on a fixed size and taxi mass airplane described in Section 2, Baseline Configuration Concepts. The design mass changes were affected by the wing and fuselage primary structure defined for the selected structural approach and propulsion system mass resulting from the Task I studies.

Maximum Design Taxi Mass = 340,000 kg (750,000 lb)

Maximum Design Take-Off Mass = 338,000 kg (745,000 lb)

Maximum Flight Gross Mass = Variable with Mach number or altitude

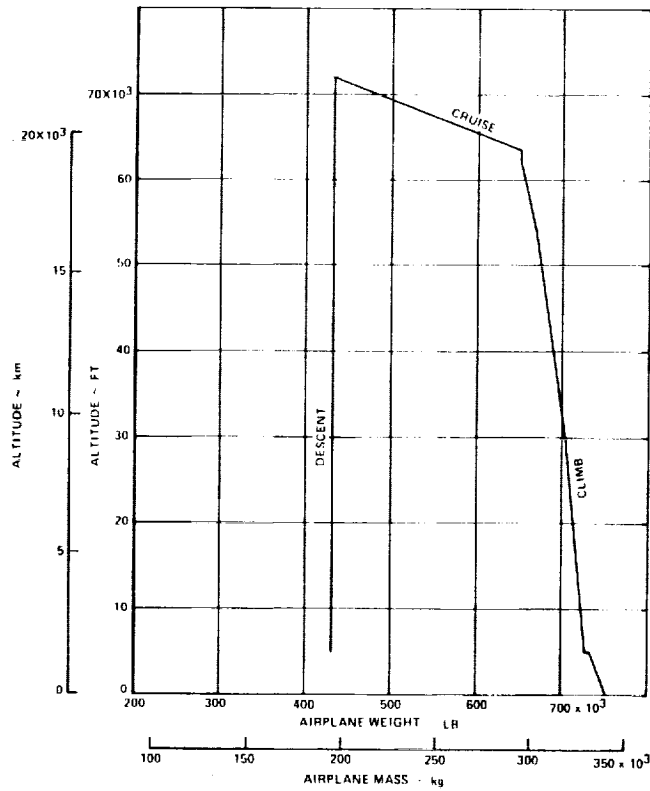


Figure 4-1. Airplane Mass Variation with Altitude - Task I

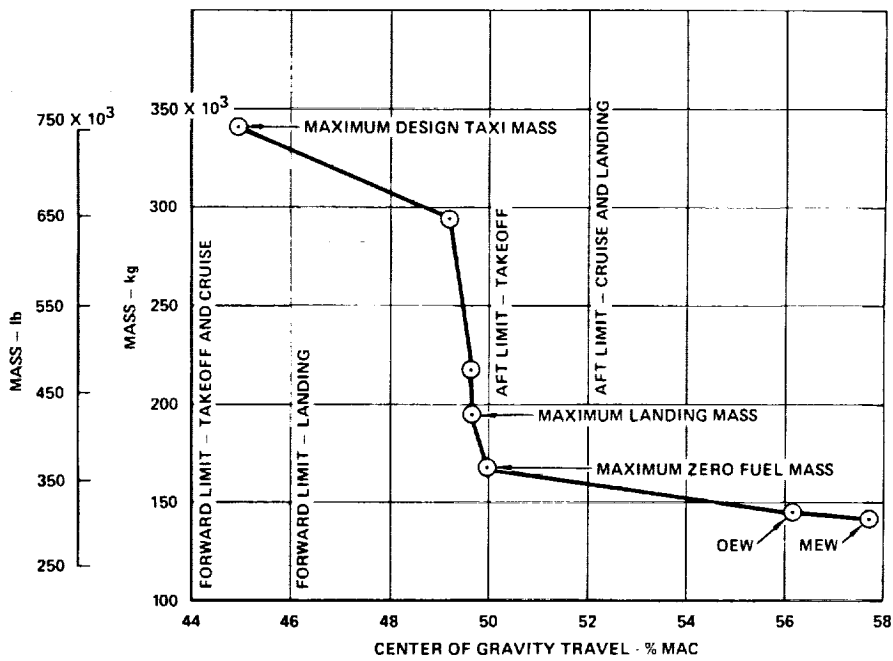


Figure 4-2. Airplane Mass Variation with Center of Gravity - Task I

<u>Maximum Landing Gross Mass</u>	= 195,000 kg (430,000 lb)
● Operating Weight Empty (OWE)	= 142,000 kg (314,000 lb)
● Payload	= 22,000 kg (49,000 lb)
● Fuel	= 30,000 kg (67,000 lb)

<u>Maximum Zero Fuel Mass</u>	= 164,000 kg (363,000 lb)
● Equal to OWE plus payload	

<u>Minimum Flight Mass</u>	= 150,000 kg (330,000 lb)
● Equal to OWE plus 5 percent of fuel capacity	

In addition to the aforementioned design mass, the following are defined and used as appropriate for the analysis in Section 10.

OWE - Strength Design	= 141,000 kg (311,000 lb)
OWE - Final Design	= 142,000 kg (314,000 lb)

The variation of airplane mass with center of gravity location is presented in Figure 4-3.

#### DESIGN SPEEDS

Design airspeeds are selected to provide an operational envelope compatible with desired flight profiles (Figure 4-4). Selected design airspeeds are expressed in terms of equivalent airspeed (EAS) in the following paragraphs.

#### Design Cruise Speed, $V_C$

The structural design cruise speed ( $V_C$ ) is selected as the planned operating speed in climb, cruise and descent. Additional margins are not included to provide tolerance for deviations from the nominal flight profile. Selection of cruise speeds for a final design should include additional margins considering such things as accuracy of the air data system and ability of the pilot or autopilot to maintain the programmed profile in climb, cruise and descent. The  $V_C$  profile in Figure 4-5 is defined as:

- A constant 325 knots equivalent airspeed from sea level to 35,300 feet
- A linear-transition from 325 knots from 35,300 feet to 460 knots at 44,000 feet.



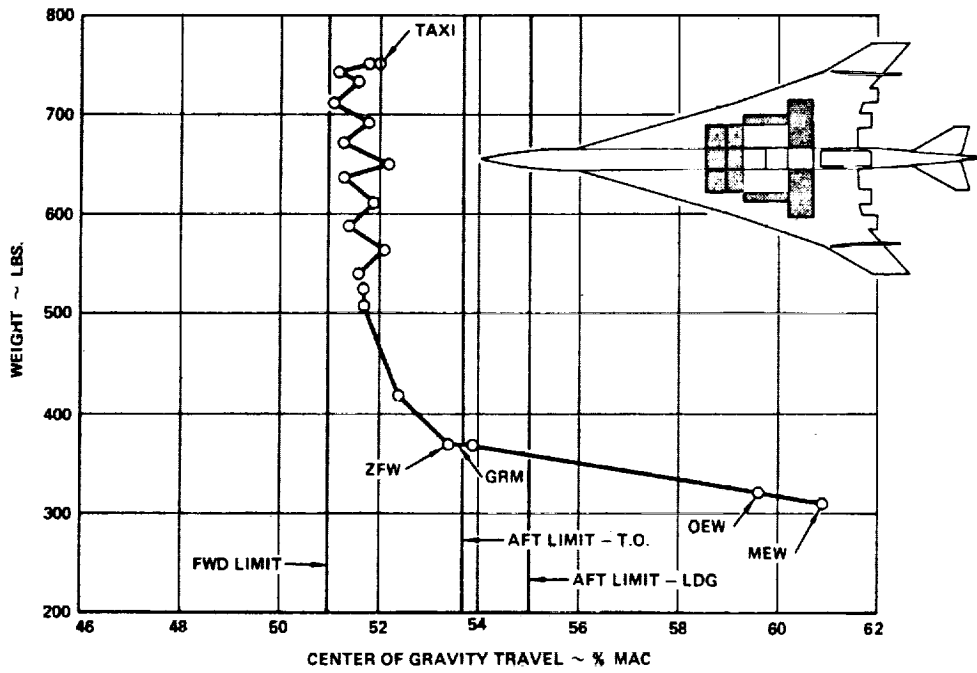


Figure 4-3. Airplane Mass Variation with Center of Gravity - Task II

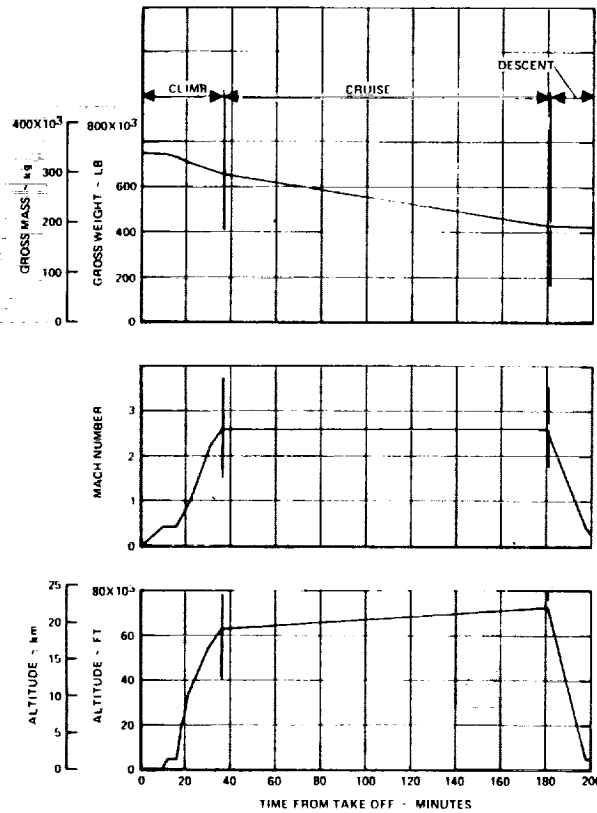


Figure 4-4. Design Flight Profile - International Mission (Mach 2.62 Cruise)

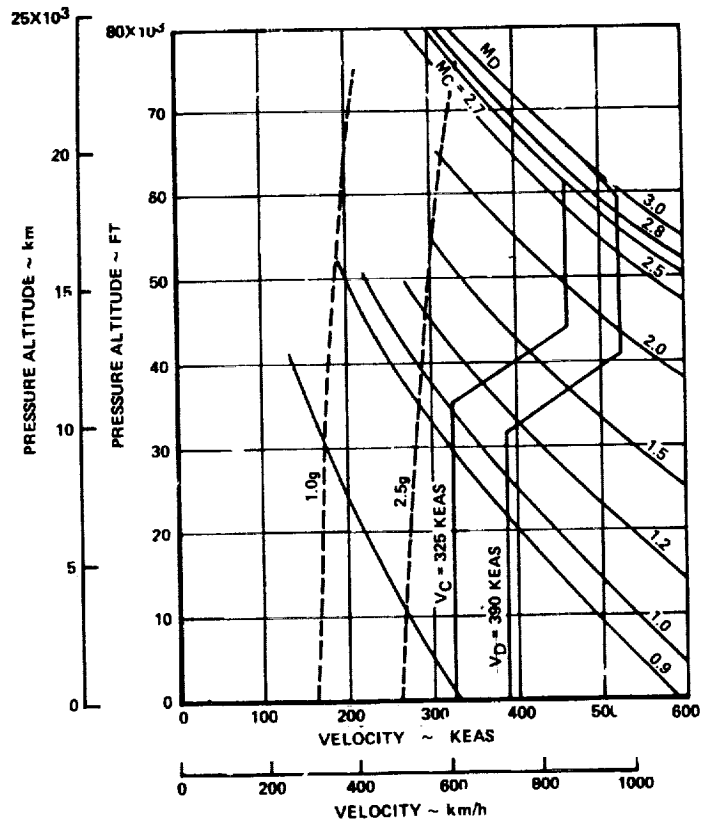


Figure 4-5. Structural Design Speeds

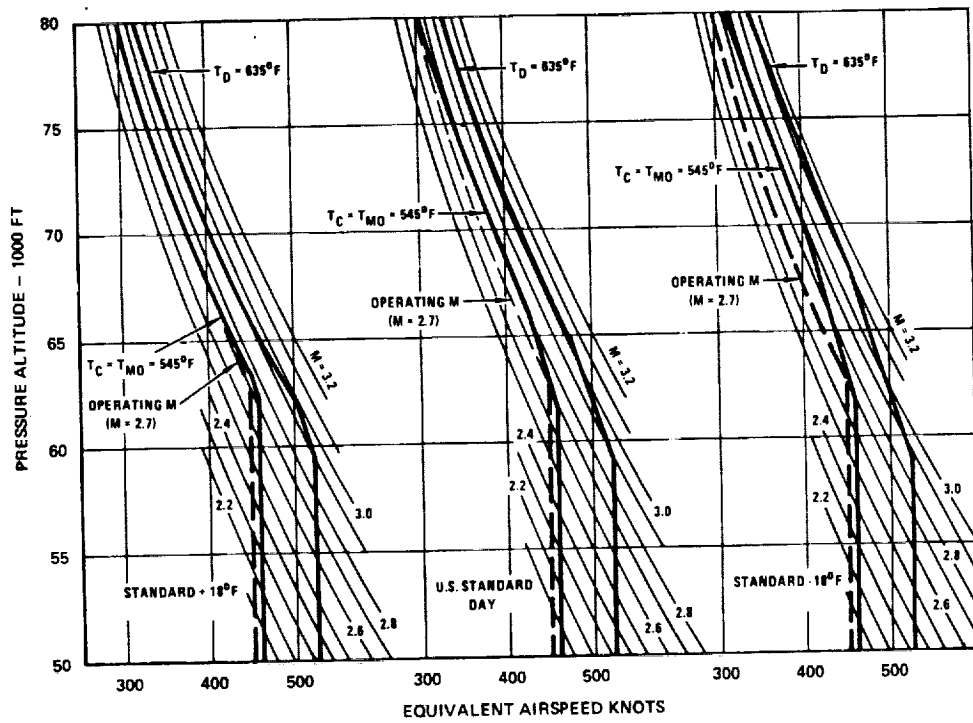


Figure 4-6. Variation of Mach Numbers with Ambient Conditions

- A constant 460 knots to 61,500 feet (Mach 2.7) with a constant cruise Mach number at higher altitudes as defined in Figure 4-5.

It is noted that this entire equivalent airspeed versus pressure altitude profile is invariant with change in ambient day condition. The ambient day condition does, however, establish the maximum altitude up to which this equivalent airspeed profile may be followed. This variable cut-off altitude is imposed by the temperature selected for structural design. Figure 4-6 illustrates the effect of a temperature limit selected for design for the L-2000-7A aircraft (i.e., Standard Day  $\pm$  18F). This maximum operating total temperature is based on providing structural adequacy in continuous flight at Mach 2.7 at pressure altitudes up to 66,000 feet on a U.S. Standard Day plus 18F. This concept of defining the maximum operating speed in the cruising altitude range provides a more meaningful criterion since total temperature integrates the thermal effect of both Mach number and ambient temperature. A single value of operating Mach number, on the other hand, does not truly establish a structural limit, unless ambient temperature is also specified. Note on the figure the change in Mach number with ambient day condition. It can be seen that the structural design and placard value of total temperature provides structural capability for a margin of  $\Delta M = 0.1$  above the operating Mach number, 2.7, on a Standard Day, and up to  $\Delta M = 0.2$  on a Standard Day -18F. On those infrequent occasions where the ambient temperature is 18F or more above Standard, the operating Mach number and the structural placard are coincident.

#### Design Dive Speed, $V_D$

The design dive speed is selected to provide a margin of safety for the inadvertent large excursions in excess of the operating speed. The  $V_D$  profile was adopted from previous comprehensive analytical studies of overspeeds resulting from a wide variety of possible conditions (Reference 1). The dive speed profile for design of the baseline configuration shown in Figure 4-5 is comprised of the following segments:

- A constant 390 knots equivalent airspeed from sea level to an altitude of 31,600 feet
- A linear transition from 390 knots at 31,600 feet to 525 knots at 41,000 feet
- A constant 525 knots to 59,000 feet altitude

- Above 59,000 feet, speeds corresponding to a maximum compressor inlet pressure of 30 psia, and/or a maximum total temperature of 635 F (Mach 2.9 on a U.S. Std. plus 18 F day). These values are compatible with limits established in the L-2000-7 design study and provide a "delta" Mach speed equal to 0.20 at supersonic Mach numbers in compliance with the tentative modification to FAR 25.335(b) contained in the Tentative Airworthiness Standards for Supersonic Transports.

Design Maneuvering Speed,  $V_A$

Design Speed for Maximum Gust Intensity,  $V_B$

Both  $V_A$  and  $V_B$  speeds are currently defined in terms of stalling speed ( $V_S$ ) with flaps retracted at each airplane mass under consideration.  $V_S$  for a supersonic transport is defined as the minimum operational speed in accordance with Tentative Airworthiness Standard 25.103 and 25.201. Minimum speed is identified as the lowest speed at which normal recovery techniques could be successfully applied. That would be the speed immediately before the automatic pitch limiting system is actuated. See Section 3 - Aerodynamics (Envelope Limiting and Longitudinal Maneuver Capability subsections). Thus, the design envelope is angle-of-attack limited rather than stall limited for the arrow-wing configuration. This definition permits establishing the design maneuvering speed as the speed corresponding to 2.5 load factor at the appropriate flight design mass and maximum usable normal force coefficient. Maximum usable normal force coefficient is defined by an angle of attack limit as a function of Mach number. Angle of attack limits in the subsonic Mach range approximate the neutral longitudinal stability boundary; at higher Mach numbers the angle of attack is sufficient to permit 2.5 load factor capability at the airplane mass/altitude combinations for cruise. Angle of attack limits for structural design are shown in Figure 4-7.

Design Flap Speed,  $V_F$

The leading edge flaps are deflected down 45-degrees during takeoff and the subsequent takeoff climb to Mach 0.4; 20-degrees deflection to Mach 1.0. Takeoff speeds are defined in Section 3, Aerodynamics.

The trailing edge flap design speeds are in accordance with FAR 25.335(e).

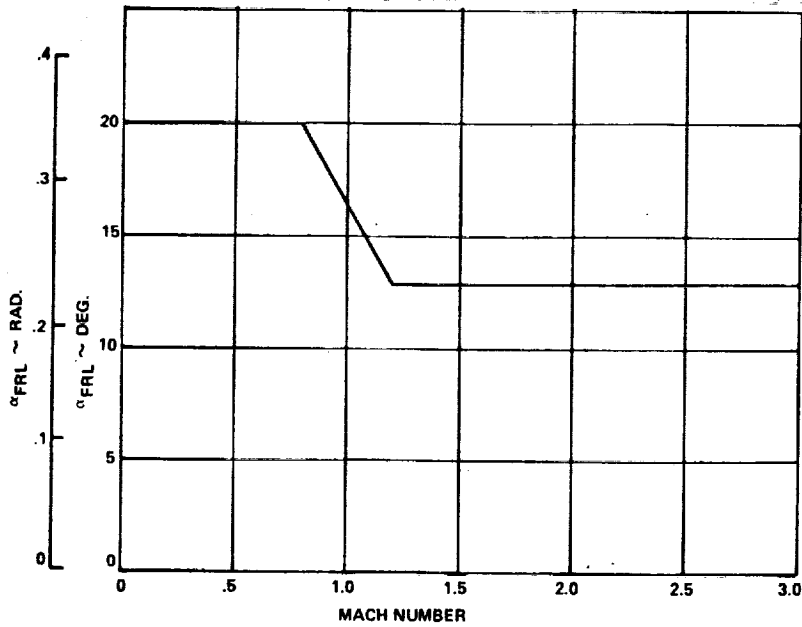
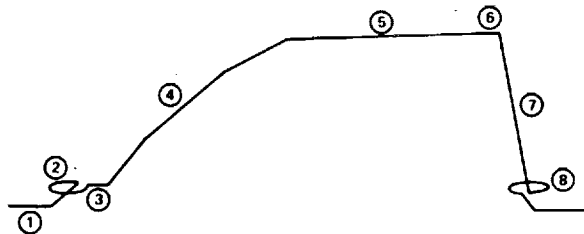


Figure 4-7. Angle of Attack Limits for Structural Design



SEGMENT	SEGMENT FUEL (Lb)	SEGMENT DIST. (N.Mi.)
① Ground Maneuver T.O. & Climb to 5000 Ft.	17,540 Lb.	.10
② Loiter @ 5000 Ft. for 4 Min.	3,910	0
③ Accelerate to 325 KEAS	1,741	1
④ Climb to Optimum Altitude	77,500	346
⑤ Cruise @ M = 2.62 (Hot Day)	219,668	3,714
⑥ Decelerate to 325 KEAS	5	1
⑦ Descent to 5000 Ft. @ 325 KEAS	1,415	191
⑧ Loiter @ 5000 Ft. for 5 Min.	2,506	0
BLOCK FUEL = 324,285 Lb.		RANGE = 4,263 N. Mi.
Dispatch Wt.	750,000 Lb.	
Landing Wt.	426,074 Lb.	
Reserve Fuel	64,074 Lb.	
Payload Wt.	49,000 Lb.	

Figure 4-8. Baseline Missions Profile - International Mission (Mach 2.62 Cruise)

## DESIGN FLIGHT PROFILE

### Analytical Design Studies - Task I

The flight profile used for limit design and in the determination of the temperatures and temperature gradients is shown in Figure 4-4. The tabulation of international mission (Table 4-1) described in the figure is further defined with a sketch, Figure 4-8, showing the mission segments. The segments are identified with the fuel used during each segment and the distance covered during each segment. The data documents the ability of the airplane to perform the design mission of 7780 kilometers (4200 n. miles) with a payload of 22,000 kilograms (49,000 lb). The international mission is approximately 3.4 hours in duration; three-quarters or 2.5 hours is at Mach 2.62 (hot day) cruise.

### Engineering Design Studies - Task II

The mission analysis results of the baseline configuration for Task II are presented in Table 4-2. As noted on the table, the dispatch mass of 340,000 kilograms (750,000 pounds) remains unchanged. However, the zero fuel mass reflects the appropriate change in structural mass resulting from the Task I analysis (Reference Section 2, Table 2-5). The data shows the ability of the airplane to perform a mission of 7700 kilometers (4166 n. miles) with a payload of 22,000 kilograms (49,000 lb). The mission duration remains essentially unchanged as indicated by the Total Time data presented.

### STRUCTURAL DESIGN TEMPERATURE CRITERIA

Structural design temperatures are based on the Mach 2.62 (hot day) international flight profile. The "hot day" condition for these analyses is defined as an ambient temperature 8K (14.4F) above U.S. 1962 Standard Day temperature. The design temperatures are determined to assure structural adequacy in selection of structural materials, establishment of material allowables, and determination of thermal stresses induced by temperature gradients. The effects of temperature on airframe stiffness properties and deflected airframe shape are also considered.

### Thermophysical Properties

Appropriate values for conductivity, specific heat, emissivity, and solar absorptivity are selected for the various materials in performing structural temperature

TABLE 4-1. INTERNATIONAL MISSION - MACH 2.62 CRUISE (4200 N. MILE)

CL-1 MISSION ANALYSIS (360-MK X)											
CL-1608-5 AST BASELINE TF 3.0 FPR ZFW											
VO/OPT/1.7 INTERNATIONAL MISSION STD DAY + 14.4 F											
SEGMENT	POWER I.D.	CONF. I.D.	INITIAL WEIGHT (LBS)	INITIAL ALTITUDE (FEET)	INITIAL MACH	SEG. TIME (MIN)	SEG. FUEL (LBS)	SEG. GRD DIST (N MI)	SEG. TOT. TIME (MIN)	TOT. FUEL (LBS)	TOT. GRD DIST (N MI)
<b>TAKEOFF</b>											
GROUND MANEUVER	0.	720.	750000.	0.	0.0	10.00	2040.	0.	10.00	2040.	0.
TAKE-OFF TO 5000	0.	720.	747500.	0.	0.415	2.55	15500.	10.	12.55	17540.	10.
LOITER-4	-97101.	720.	724500.	5000.	0.415	4.00	3704.	0.	16.55	21244.	10.
SET MACH	0.	720.	726750.	5000.	0.412	0.0	0.	0.	16.55	21244.	10.
ACCELERATE	97201.	720.	728750.	5000.	0.412	0.20	1664.	1.	16.81	22928.	11.
CLIMB	97201.	720.	727072.	5000.	0.535	1.77	6367.	12.	18.59	32659.	23.
CLIMB	97201.	720.	717360.	19000.	0.710	2.07	8690.	17.	20.66	41565.	40.
CLIMB	97201.	720.	708530.	30930.	0.920	0.68	2447.	6.	21.34	44032.	47.
CLIMB	97201.	720.	706424.	34000.	0.988	0.61	3347.	15.	30.95	77379.	62.
CLIMB	97201.	720.	673254.	54500.	2.225	3.17	15705.	124.	36.12	93084.	176.
CLIMB	97201.	720.	657584.	62500.	2.620	0.27	725.	7.	36.39	93809.	183.
CRUISE-3	-97201.	720.	656802.	63540.	2.620	14.382	220137.	3062.	180.21	321946.	3954.
DECELERATE	97501.	720.	428747.	72514.	2.620	0.55	48.	13.	180.74	321993.	4007.
DESCEND	97501.	720.	428700.	72514.	2.475	16.92	1534.	194.	197.65	323548.	4201.
LOITER-2	-97101.	720.	426442.	5000.	0.400	5.00	2147.	0.	202.65	325695.	4201.
<b>RESERVES</b>											
TPCT BK FUEL	0.	720.	424295.	5000.	0.210	0.0	22790.	-4200.	207.65	348493.	1.
ACCELERATE	97201.	720.	401490.	235.	0.210	0.16	1093.	1.	202.81	349586.	1.
CLIMB	97201.	720.	400403.	235.	0.380	0.06	570.	0.	202.80	350156.	1.
ACCELERATE	97201.	720.	399833.	1500.	0.369	0.11	744.	1.	203.00	350900.	2.
CLIMB	97201.	720.	399089.	1500.	0.505	2.03	10274.	15.	205.04	361174.	17.
CLIMB	97201.	720.	369227.	30530.	0.920	1.07	3604.	5.	206.11	364178.	26.
CRUISE-3	-97101.	720.	380330.	43815.	0.920	20.55	9298.	184.	226.66	373577.	210.
DESCEND	97501.	720.	376948.	44020.	0.920	2.12	195.	19.	228.79	373771.	226.
LOITER-2	-97101.	720.	376817.	30930.	0.920	6.10	774.	56.	236.88	374545.	284.
MISSION SUMMARY						30.00	10960.	0.	266.88	385505.	284.
<b>MISSION FACTORS</b>											
DISPATCH WEIGHT	750000.	LBS									721.
BLOCK FUEL	325695.	LBS									0.0
LANDING WEIGHT	424267.	LBS									10500.000
RESERVE FUEL	55811.	LBS									4.560
ZERO FUEL WEIGHT	364450.	LBS									14.400
MISSION RANGE	4200.	N MI									6000.000
											-4.0000
											1.0000

THE ZERO FUEL WEIGHT HAS A 0.0 LB. TOLERANCE

ORIGINAL PAGE IS OF POOR QUALITY

TABLE 4-2. INTERNATIONAL MISSION - MACH 2.62 CRUISE (4166 N.MILE)

CL-1 MISSION ANALYSIS (360-MK X)

CL-1606-4 AST BASELINE TF 3.0 FPR  
VO70PT/1.7 INTERNATIONAL MISSION STD DAY + 14.4 F

SEGMENT	PUMER I.D.	CONF. I.D.	INITIAL WEIGHT (LBS)	INITIAL ALTITUDE (FEET)	INITIAL MACH	SEG. TIME (MIN)	SEG. FUEL (LBS)	SEG. GRD DIST (N MI)	TOT. TIME (MIN)	TOT. FUEL (LBS)	TOT. GRD DIST (N MI)
<b>TAKEOFF</b>											
GROUND MANEUVER	0.	723.	750000.	0.	0.0	10.00	2040.	0.	10.00	2040.	0.
TAKE-OFF TO 5000	0.	723.	747960.	0.	0.415	2.55	19500.	10.	12.55	17540.	10.
LOITER-4	-97101.	723.	732460.	5000.	0.415	4.00	3910.	0.	16.55	21450.	10.
SET MACH	0.	723.	728550.	5000.	0.412	0.0	0.	0.	16.55	21450.	10.
ACCELERATE	97201.	723.	728550.	5000.	0.412	0.27	1741.	1.	16.82	23192.	11.
CLIMB	97201.	723.	726808.	5000.	0.539	1.87	10517.	12.	18.69	33708.	24.
CLIMB	97201.	723.	716547.	19000.	0.710	2.28	9543.	19.	20.97	43251.	43.
CLIMB	97201.	723.	707170.	30930.	0.920	0.78	2774.	7.	21.75	46025.	50.
CLIMB	97201.	723.	704432.	34000.	0.988	10.96	38119.	175.	32.71	84144.	225.
CLIMB	97201.	723.	666489.	54500.	2.225	5.10	15488.	122.	37.80	99632.	347.
CLIMB	97201.	723.	651036.	62500.	2.620	0.40	1760.	10.	38.21	100692.	357.
CRUISE-3	-97201.	723.	649985.	65022.	2.620	141.94	219468.	3617.	180.15	320360.	3974.
DECELERATE	97501.	723.	430338.	74666.	2.620	0.05	5.	1.	180.20	320365.	3975.
DESCEND	97501.	723.	430334.	74666.	2.605	15.42	1415.	191.	195.62	321779.	4166.
LOITER-2	-97101.	723.	428211.	5000.	0.400	5.00	2506.	0.	200.62	324285.	4166.
<b>RESERVES</b>											
TPCT BK FUEL	0.	723.	425705.	5000.	0.202	0.0	22700.	-4166.	200.62	346985.	0.
ACCELERATE	97201.	723.	403005.	235.	0.202	0.17	1181.	1.	200.79	348166.	1.
CLIMB	97201.	723.	401825.	235.	0.380	0.09	592.	0.	200.88	348757.	1.
ACCELERATE	97201.	723.	401233.	1500.	0.388	0.11	777.	1.	200.99	349534.	2.
CLIMB	97201.	723.	400456.	1500.	0.505	2.20	11069.	16.	203.19	360602.	18.
CLIMB	97201.	723.	389801.	30930.	0.920	1.37	3724.	12.	204.56	364327.	30.
CRUISE-3	-97101.	723.	386197.	44755.	0.920	20.09	10843.	180.	224.65	375169.	209.
DESCEND	97501.	723.	375372.	45439.	0.920	2.01	183.	18.	226.66	375353.	227.
DESCEND	97501.	723.	375043.	30930.	0.920	6.31	602.	44.	232.97	375954.	271.
LOITER-2	-97101.	723.	374019.	15000.	0.440	30.00	12404.	0.	262.97	388358.	271.
<b>MISSION SUMMARY</b>											
DISPATCH WEIGHT			750000.							724.	
BLOCK FUEL			324285.							0.0	
LANDING WEIGHT			426074.							10923.000	
RESERVE FUEL			64074.							4.560	
ZERO FUEL WEIGHT			362000.							14.400	
MISSION RANGE			4166.	N MI						6000.000	
<b>MISSION FACTORS</b>											
FRICTION DRAG											
DELTA DRAG INCREMENT											
WING AREA											
NUMBER OF ENGINES											
DELTA TEMPERATURE											
MASTER FUEL FLOW FACTOR											
THRUST INCLINATION ANGLE											
SPECIFIC RANGE FACTOR											

MISSION FACTORS

DISPATCH WEIGHT	750000.	LBS
BLOCK FUEL	324285.	LBS
LANDING WEIGHT	426074.	LBS
RESERVE FUEL	64074.	LBS
ZERO FUEL WEIGHT	362000.	LBS
MISSION RANGE	4166.	N MI
<b>MISSION FACTORS</b>		
FRICTION DRAG		
DELTA DRAG INCREMENT		
WING AREA		
NUMBER OF ENGINES		
DELTA TEMPERATURE		
MASTER FUEL FLOW FACTOR		
THRUST INCLINATION ANGLE		
SPECIFIC RANGE FACTOR		

THE ZERO FUEL WEIGHT HAS A 385.44LB. TOLERANCE  
VO70

63



analyses. A detailed discussion of values used for analysis is given in Section 6, Structural Temperatures.

#### Ultimate Strain Factor

To define the ultimate combined load/strain condition, a factor of 1.25 is applied to the thermal strains wherever applications of the factor is in a direction to increase design stresses. Limit thermal strains (no factors) are used in the fatigue and fail-safe analyses.

#### MANEUVERING FLIGHT CRITERIA

Maneuver loads analyses are based on solution of the airplane equations of motion for pilot-induced maneuvers, considering altitudes between sea level and 70,000 feet, all speeds, gross mass and center of gravity limits perviously defined.

Aerodynamic stability and control characteristics used in analyses include consideration of non-linearities determined from wind tunnel measured force data and include the effects of analytically determined airload redistribution caused by airplane flexibility.

#### Limit Maneuvering Load Factors

Design load factors comply with the requirements of FAR 25.333, 25.337, and 25.335.

Symmetrical Flight Maneuvers. - Except where limited by the maximum usable normal force coefficient or by available longitudinal control deflection, the limit symmetric maneuvering load factors are as follows:

- Positive maneuvers:  $n = 2.5$  at all design speeds
- Negative maneuvers:  $n = -1.0$  up to  $V_C$  and varies linearly to zero at  $V_D$ .
- Limit maneuvering load factors with trailing edge flaps deflected are 2.0 and zero at all speeds to  $V_F$ .

Rolling Maneuver Entry Load Factors. - Symmetrical load factors at entry into the rolling maneuvers are the following:

- Upper limit:  $n = +1.67$  at all design speeds
- Lower limit:  $n = 0$  up to  $V_C$  and varies linearly up to  $+1.0$  at  $V_D$

#### Symmetrical Flight Maneuver Balanced Condition

In accordance with FAR 25.331(b), design loads are determined for the airplane in equilibrium flight with zero pitching acceleration for all significant points on the V-n diagram defined above.

#### Symmetrical Flight Maneuver Pitching Conditions

Abrupt pitching maneuver analyses are conducted for a specified control displacement in compliance with FAR 25.331(c) (3).

At speeds up to  $V_D$  at all altitudes, the longitudinal control is abruptly displaced so as to attain the specified load factor.

Example time histories and analysis results pertinent to structural design loads are given in Section 5.

#### Rolling Maneuvers

Analyses are performed in compliance with FAR 25.349 as modified by Reference 2 at speeds up to  $V_D$  at all altitudes. The analysis results pertinent to structural design loads are given in Section 5, Structural Design Loads.

#### GROUND HANDLING CRITERIA

Structural design criteria for ground handling conditions comply with the appropriate paragraph in FAR 25. In loads analyses performed for these conditions the following general provisions apply:

- Loads analyses are considered for the maximum design taxi mass, except for conditions concerning the takeoff run, in which case the maximum gross mass is the maximum design takeoff mass.

- No wing lift is considered, except where acting to increase loads in the takeoff rotation condition.

## LANDING CRITERIA

Structural design criteria for landing conditions comply with FAR 25 as modified by Reference 2.

### Airplane Mass and Centers of Gravity (FAR 25.471)

All airplane mass from minimum flying mass to maximum takeoff mass are considered at the appropriate sinking speeds as indicated below. The critical centers of gravity within the structural design mass versus center of gravity envelope are included.

### Design Sinking Speeds (FAR 25.473)

The limit design descent velocity at the instant of main landing gear impact is 10 fps at all weights from minimum design flight mass to maximum design landing mass.

## FUEL TANK PRESSURES

The following combinations of limit fuel pressure and loads are used for structural design:

### Flight Conditions - Limit Loads

Fuel pressure = the sum of fuel head multiplied by the accelerations for the particular condition and +3.0 psig (valve tolerance).

### Handling, Taxi and Ground Handling Conditions

Fuel pressure = Fuel head multiplied by the accelerations for the particular condition.

Note: Tank pressurization is negligible for these conditions.

## Fueling and Defueling

Fuel pressure = +8.0 psig and -3.0 psig.

Note: Vent system lines are selected such that these values will not be exceeded in event of dual failure of the fueling valves.

### EMERGENCY LANDING CRITERIA

Structural design criteria for emergency landing conditions comply with FAR 25.561 as modified by Reference 2. The airplane is designed to protect the occupants under the following conditions, although the airplane itself may suffer damage.

#### Design Conditions (FAR 25.561)

The following ultimate inertia load factors are applied to occupants, to each item of mass that could injure an occupant if it came loose in a minor crash landing, and to the fuel in all tanks in quantities that might be present in landings at the Maximum Design Landing Mass:

Upward:  $n = 2.0$

Forward:  $n = 9.0$

Sideward:  $n = 1.5$

Downward:  $n = 4.5$ , or any lesser value that will not be exceeded in a wheels-up landing at Maximum Design Landing Mass at an ultimate sinking speed of 5 fps.

Each load factor is applied as an arbitrary independent condition.

### FATIGUE AND FAIL-SAFE LOADS CRITERIA

Structural design criteria with respect to fatigue and fail-safe requirements are in accordance with FAR 25.571 and 25.573. The fatigue and fail-safe design objectives and analyses are presented in Section 13, Fatigue and Fail-Safe.

No requirements are currently specified for crack growth. However, analyses are conducted to show that small cracks that are likely to be missed on a given inspection will not grow to catastrophic failure before the next inspection period which is in the order of 8000 to 12,000 flight hours.

## Fatigue Spectrum

Fatigue analysis for the baseline configuration is based upon the Lockheed Loading Spectrum "C" which was developed under "Fatigue Behavior of Materials for the Supersonic Transport," contract AF-33(657)-11640, Exhibit "B", of the SST research program sponsored by the Federal Aviation Agency. Spectrum "C", shown on Figure 4-9, represents the final iteration to provide a moderately conservative representation of loading history for supersonic cruise aircraft. Reference stress level and oscillatory flight loading are defined on the spectrum and includes representative tensile thermal stress increment and simulation of ground loadings.

## Fatigue Criteria

The basic criteria is to provide a structure that will be good for a service life of 50,000 flight hours. Appropriate multiplying factors are applied to the design life for use in establishing allowable design stresses. For structure subjected to a spectrum loading, the allowables are selected using a factor of 2 X the design life of 50,000 hours. For areas of the fuselage structure subjected to constant amplitude loading the allowable stresses are selected for 200,000 flight hours of service (50,000 X 4). A larger factor is applied to constant amplitude loading because the scatter in fatigue life is larger for this type of loading.

## Fail-Safe Design Criteria

Fail-safe design concepts are employed for the wing and fuselage structures of the baseline airplane. The fail-safe structures are capable of supporting the fail-safe design load of 100 percent limit load, as defined in the Tentative Airworthiness Standards for SST, for the damage conditions analyses in Section 13. The residual strength of the damaged structure shall be capable of withstanding these limit loads without failure if practical; in any event, the requirements of FAR 25.571 will be met.

## MINIMUM GAGE CRITERIA

The following criteria have been established in the selection of minimum gages for regions which are not designated to specific strength requirements (Table 4-3).

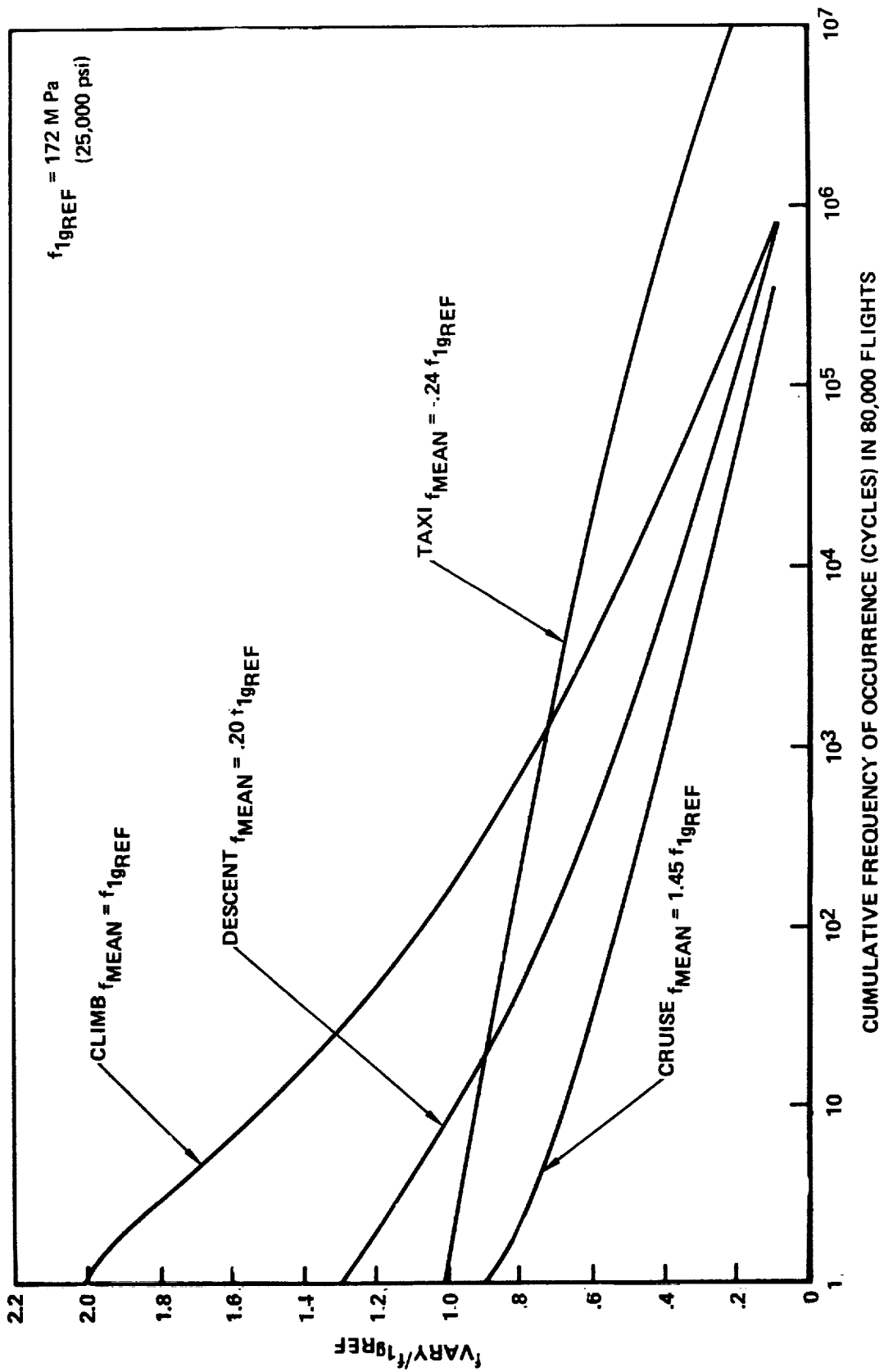


Figure 4-9. Loading Spectra C

TABLE 4-3. MINIMUM GAGE CRITERIA

<u>STRUCTURAL CONCEPT</u>	<u>ELEMENT</u>	<u>MINIMUM GAGE</u>		
		(in.)	(mm)	
<b>Monocoque Panels</b>				
● Honeycomb Core Sandwich	Skin (exterior)			
	Upper	.015	.381	
	Lower	.020	.508	
	Skin (interior)	.010	.254	
	Core	.002 (1)	.050 (1)	
● Truss-Core Sandwich	Skin (exterior)			
	Upper Surface	.015	.381	
	Lower Surface	.020	.508	
	Skin (interior)	.010	.254	
	Core	.008	.203	
<b>Spanwise Stiffened Panels</b>				
● Zee Stiffened	Skin			
	Upper Surface	.015	.381	
	Lower Surface	.020	.508	
	Stiffener	.015	.381	
● Integral Zee	Skin			
	Upper Surface	.015	.381	
	Lower Surface	.020	.508	
	Stiffener	.020	.508	
● Hat Section Stiffened	Skin			
	Upper Surface	.015	.381	
	Lower Surface	.020	.508	
	Stiffener	.015	.381	
● Integrally Stiffened	Skin			
	Upper Surface	.015	.381	
	Lower Surface	.020	.508	
	Stiffener	.020	.508	
<b>Chordwise Stiffened Panels</b>				
● Circular Arc-Concave Beaded Skin	} Skin (exterior)			
● Circular Arc-Convex Beaded Skin		Upper Surface	.015	.381
		Lower Surface	.020	.508
● Corrugation-Concave Beaded Skin		Skin (interior)	.010	.254

NOTE: (1) Brazed honeycomb minimum core foil thickness = .002 in (.050 mm)  
 Stressskin minimum gage = .0025 in (.064 mm).

The bases for selection include consideration of the structural concept employed, fabrication constraints and foreign object damage (FOD) effects.

#### PRESSURIZED CABIN LOADS CRITERIA

Criteria for design differential pressures comply with FAR 25.365. Design pressures are based on providing a 6000 ft cabin altitude at a flight altitude of 70,000 feet. These conditions produce a nominal cabin pressure of 11.8 psia, which combined with the ambient pressure at 70,000 ft altitude of 0.6 psia results in a nominal differential pressure of 11.2 psi.

Maximum design differential pressure includes a tolerance which accounts for variations in static reference, a regulator valve tolerance, and relief valve tolerances as illustrated in Figure 4-10.

An envelope of differential pressure values used to determine loads on the pressurized cabin is shown on Figure 4-11. The limits for structural design range from -0.4 psi to 11.7 psi, with intermediate values between sea level and 38,000 feet. The variation is established by considering a cabin pressure equal to sea level pressure as a limiting value.

Criteria for applying these differential pressures in structural design analyses and tests are defined below.

##### Differential Pressure for Combination with Limit Loads

A differential pressure varying from -0.4 psi to the appropriate maximum differential pressure for a particular altitude, consistent with the design envelope shown on Figure 4-11, is combined with the external air loads and other appropriate structural loads due to maneuvers or gusts.

##### Differential Pressure for Fatigue Design

The structure is evaluated for fatigue strength using the nominal differential pressure, 11.2 psi, plus the airload and other appropriate structural loads due to maneuvers and gusts.



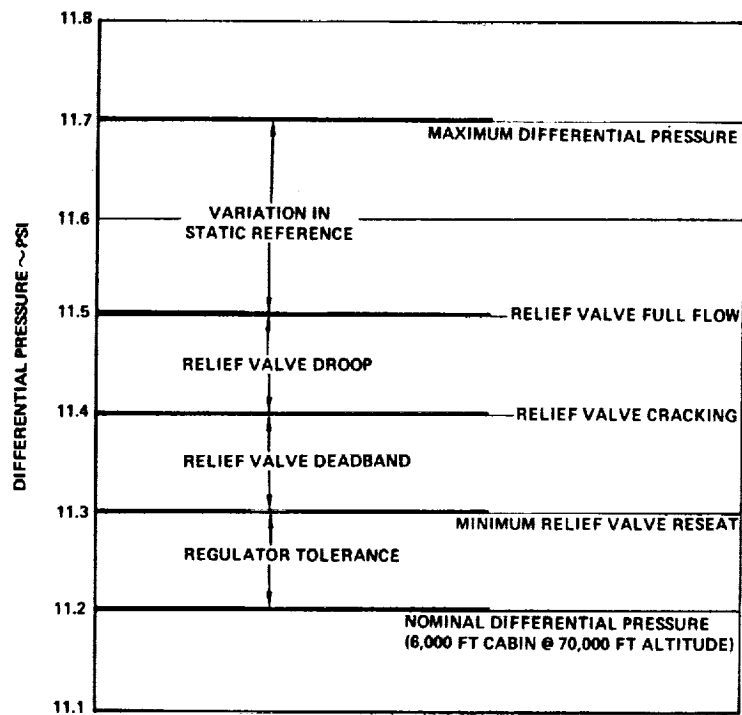


Figure 4-10. Tolerances Applied to Nominal Pressure to Established Limit Design Differential Pressure

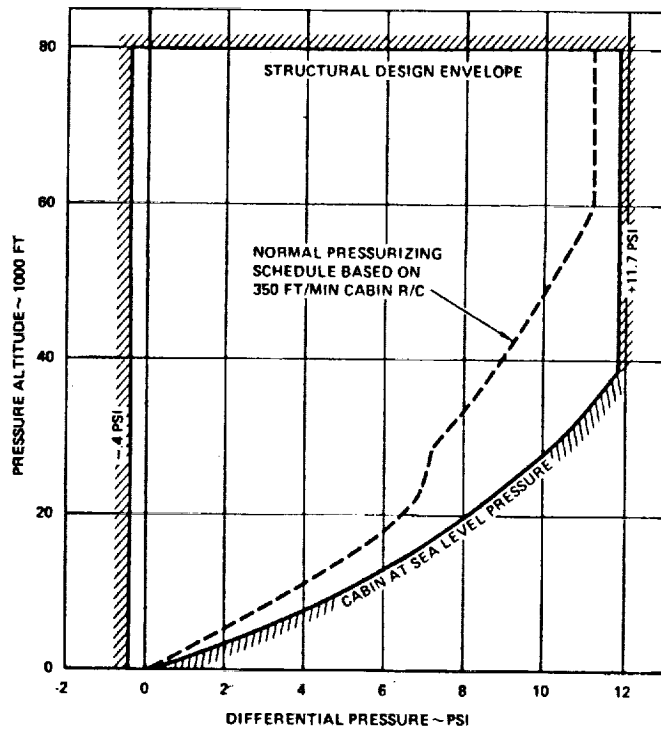


Figure 4-11. Cabin Pressure Structural Design Envelope

## Differential Pressure for Fail-safe Design

A nominal pressure regulating valve is assumed (regulator tolerance neglected). Therefore, the tolerance applied to the nominal differential pressure, 11.2 psi, is 0.4 psi (the upper three tolerance increments shown in Figure 4-10), resulting in a maximum differential pressure of 11.6 psi which is combined with appropriate external airload and the fail-safe loads defined in Section 13.

#### REFERENCES

1. Supersonic Transport Development Program (Phase III Proposal) - Airframe Design, Volume II-C, FA-SS-66-7, Lockheed-California Company, 1966.
2. FAA, Tentative Airworthiness Standards for Supersonic Transports, revised January 1, 1971.

1

2

3

4

5

SECTION 5

STRUCTURAL DESIGN LOADS

R. R. ELTZE, R. V. JENSEN, B. C. WOLLNER AND I. F. SAKATA

I

[

T

[

V

## CONTENTS

<u>Section</u>	<u>Page</u>
INTRODUCTION	5-1
STATIC AEROELASTIC ANALYSIS	5-1
Methods	5-2
Jig Shape Definition	5-11
Flexible Stability Derivatives	5-12
Roll Control Effectiveness	5-20
DESIGN LOADS - TASK I	5-30
Conditions for Design	5-30
Net Loads Summary	5-34
Net Loads Comparison	5-39
Application of Measured Data	5-46
DESIGN LOADS - TASK IIA	5-61
Net Loads Summary	5-62
Results	5-62
DESIGN LOADS - TASK IIB	5-66
Strength Design	5-66
Strength/Stiffness Design	5-71
REFERENCES	5-105

I

E

U

E

V



LIST OF FIGURES

<u>Figure</u>		<u>Page</u>
5-1	Loads Panel Grid Point System	5-3
5-2	Subsonic Aerodynamic Grid	5-5
5-3	Supersonic Aerodynamic Grid	5-9
5-4	Free-Airplane Flexibility - Chordwise Stiffened Arrangement - 750,000 lb	5-13
5-5	Free-Airplane Flexibility - Chordwise Stiffened Arrangement - 550,000 lb.	5-14
5-6	Free-Airplane Flexibility - Monocoque Arrangement - 750,000 lb.	5-15
5-7	Free-Airplane Flexibility - Monocoque Arrangement - 550,000 lb.	5-16
5-8	Airplane Roll Flexibility - Monocoque Arrangement - Mach 0.60	5-17
5-9	Airplane Roll Flexibility - Monocoque Arrangement - Mach 0.90	5-18
5-10	Airplane Roll Flexibility - Monocoque Arrangement - Mach 1.25	5-19
5-11	Airplane Roll Flexibility - Hybrid Arrangement - Mach 1.85	5-21
5-12	Primary Roll Control Schedule	5-24
5-13	Roll Control Effectiveness - Mach 0.40	5-25
5-14	Roll Control Effectiveness - Mach 0.90	5-26
5-15	Roll Control Effectiveness - Mach 1.85	5-27
5-16	Baseline Configuration Concept - Task I	5-31
5-17	Baseline Configuration/Longitudinal Controls	5-32
5-18	Airplane Longitudinal Characteristics	5-33
5-19	Critical Loading Conditions	5-37
5-20	Static Aeroelastic Loads Matrix	5-40
5-21	Wing Load Integration Axis	5-41
5-22	Wing Shears for Structural Arrangements	5-42
5-23	Wing Bending Moments for Structural Arrangements	5-43
5-24	Outer Wing Shears and Bending Moments for Structural Arrangements	5-44
5-25	Net Fuselage Shears for Structural Arrangements	5-45
5-26	Net Loads Envelope - Chordwise Stiffened - BL 62.0	5-49
5-27	Net Loads Envelope - Chordwise Stiffened - BL 470.0	5-50
5-28	Net Loads Envelope - Spanwise Stiffened - BL 62.0	5-51

LIST OF FIGURES (Continued)

<u>Figure</u>		<u>Page</u>
5-29	Net Loads Envelope - Spanwise Stiffened - BL 470.0	5-52
5-30	Net Loads Envelope - Monocoque - BL 62.0	5-53
5-31	Net Loads Envelope - Monocoque - BL 470.0	5-54
5-32	Net Integrated Wing Shears - Theoretical vs Measured	5-55
5-33	Wing Bending Moments - Theoretical vs Measured	5-56
5-34	Wing Torsion - Theoretical vs Measured	5-57
5-35	Net Integrated Fuselage Shears - Theoretical vs Measured	5-58
5-36	Span Loading Distribution - Mach 2.7	5-59
5-37	Wing Lift Coefficients - Mach 2.7	5-60
5-38	Configuration Comparison - Task I and Task IIA	5-63
5-39	Wing Shears and Bending Moments - Task IIA	5-64
5-40	Net Integrated Fuselage Shear - Task IIA	5-65
5-41	Task II Design Cycle - Strength	5-67
5-42	Design Loading Conditions - Strength	5-69
5-43	Static Aeroelastic Load Matrix	5-72
5-44	Task II Design Cycle - Strength/Stiffness	5-74
5-45	Design Loading Conditions - Strength/Stiffness	5-78
5-46	Structural Model Grid	5-79
5-47	Panel Point Loads - Final Design - Condition 8, Mach 0.90 Steady Maneuver	5-89
5-48	Panel Point Loads - Final Design - Condition 12, Mach 1.25 Steady Maneuver	5-90
5-49	Panel Point Loads - Final Design - Condition 14, Mach 1.25 <b>Negative Normal Acceleration</b>	5-91
5-50	Panel Point Loads - Final Design - Condition 16, Mach 1.25 Transient Maneuver	5-92
5-51	Panel Point Loads - Final Design - Condition 20, Mach 2.7 (Start-of-Cruise) Transient Maneuver	5-93
5-52	Panel Point Loads - Final Design - Condition 21, Mach 2.7 (Mid-Cruise) 1-g Trimmed Flight	5-94
5-53	Panel Point Loads - Final Design - Condition 23, Mach 0.90 Psuedo Gust (Positive)	5-95
5-54	Panel Point Loads - Final Design - Condition 25, Dynamic Landing	5-96
5-55	Aeroelastic Deflections - Final Design - Condition 8, Mach 0.90 Steady Maneuver	5-98

LIST OF FIGURES (Continued)

<u>Figure</u>		<u>Page</u>
5-56	Aeroelastic Deflections - Final Design - Condition 12, Mach 1.25 Steady Maneuver	5-99
5-57	Aeroelastic Deflections - Final Design - Condition 14, Mach 1.25 <b>Negative Normal Acceleration</b>	5-100
5-58	Aeroelastic Deflections - Final Design - Condition 16, Mach 1.25 Transient Maneuver	5-101
5-59	Aeroelastic Deflections - Final Design - Condition 20, Mach 2.7 (Start-of-Cruise) Transient Maneuver	5-102
5-60	Aeroelastic Deflections - Final Design - Condition 21, Mach 2.7 (Mid-Cruise) 1-g Trimmed Flight	5-103
5-61	Aeroelastic Deflections - Final Design - Condition 23, Mach 0.90 Psuedo Gust (Positive)	5-104

[

]

[

]

]

LIST OF TABLES

<u>Table</u>	<u>Page</u>	
5-1	Summary Aerodynamic Coefficient Matrices - Task I	5-7
5-2	Roll Reversal Speeds	5-28
5-3	Roll Control Effectiveness - Mach 1.85	5-29
5-4	Critical Loading Conditions	5-30
5-5	Design Loading Conditions - Chordwise Stiffened - Task I	5-35
5-6	Design Loading Conditions - Spanwise Stiffened and Monocoque - Task I	5-38
5-7	Design Loading Conditions - Task IIB Strength	5-68
5-8	Parameters for Longitudinal Conditions	5-70
5-9	Weight Cases and Output Identification	5-73
5-10	Design Loading Condition - Task IIB Strength/Stiffness	5-77
5-11	Panel Point Loads - Final Design - Condition 8, Mach 0.90 Steady Maneuver	5-81
5-12	Panel Point Loads - Final Design - Condition 12, Mach 1.25 Steady Maneuver	5-82
5-13	Panel Point Loads - Final Design - Condition 14, Mach 1.25 Negative Normal Accel	5-83
5-14	Panel Point Loads - Final Design - Condition 16, Mach 1.25 Transient Maneuver	5-84
5-15	Panel Point Loads - Final Design - Condition 20, Mach 2.7 (Start-of-Cruise) Transient Maneuver	5-85
5-16	Panel Point Loads - Final Design - Condition 21, Mach 2.7 (Mid-Cruise) 1-g Trimmed Flight	5-86
5-17	Panel Point Loads - Final Design - Condition 23, Mach 0.90 Psuedo Gust (Positive)	5-87
5-18	Panel Point Loads - Final Design - Condition 25, Dynamic Landing	5-88
5-19	Aeroelastic Deflections - Final Design - Condition 21 (Mid-Cruise)	5-97

**PRECEDING PAGE BLANK NOT FILMED**

1

2

3

4

SYMBOLS AND NOTATIONS

$\bar{c}$	Mean aerodynamic chord
$C_{L\alpha}$	Lift-curve slope
$C_{\ell p}$	Rolling moment coefficient per unit change in roll parameter, $p_b/2V$
$C_{\ell \delta a}$	Rolling moment coefficient per unit change in aileron angle
$C_{\ell \delta sp}$	Rolling moment coefficient per unit change in spoiler angle
$C_{m_0}$	Pitching moment coefficient at zero lift (positive is nose up)
$dC_{m,45} / dC_L$ or $\Delta(C_{m,45} / C_L)$	Rate of change of pitching moment coefficient with lift coefficient
$M_x$	Bending moment about the X-axis
$M_y$	Torsional moment about the Y-axis
$S_z$	Vertical shear force in the Z-axis
$P_{z_{ht}}$	Vertical tail load on the horizontal tail
$n_x$	Longitudinal inertia load factor - inertia force parallel to the airplane longitudinal reference axis divided by the weight (aft is positive)
$n_z$	Vertical inertia load factor - inertia force parallel to the airplane vertical reference axis divided by the weight (up is positive)
$\dot{\theta}$	Pitching velocity - angular velocity in pitch about the Y-axis (positive is nose up)
$\ddot{\theta}$	Pitching acceleration - angular acceleration in pitch about the Y-axis (positive is nose-up)
$\ddot{\phi}$	Rolling acceleration - angular acceleration in roll about the airplane longitudinal axis (positive is clockwise view from the aft)
$\delta_H$	Horizontal tail deflection - the angle between a line parallel to the airplane longitudinal reference axis and the deflected position (positive is trailing edge down)

PRECEDING PAGE BLANK NOT FILMED

1

2

3

4

5



## SECTION 5

### STRUCTURAL DESIGN LOADS

#### INTRODUCTION

The procedures and assumptions used in applying the criteria defined in Section 4 in the calculation of aeroelastic loads and their effects to the arrow-wing configuration supersonic cruise aircraft are described in this section. The loads calculation result in matrices of net loads over hundreds of panel points on the aircraft for every case analyzed. Reproducing these data in this report is not practical. Therefore, the Design Loads section of Task I contains bending moment and shear curves for the most severe loading condition evaluated for each structural arrangement. A net loads envelope is then presented for each arrangement at two wing locations to indicate the relative severity of the other conditions investigated.

For the Final Design airplane, stacked matrices of the critical conditions are tabulated and vector plots of the panel point loads and aeroelastic deflections are presented.

Since aeroelastic analyses are inherent in the calculation of design loads, other design data which are derived from aeroelastic loads analyses but not directly applied in strength analyses, are also included in this section. Examples of these are the effects of airframe flexibility on aerodynamic stability and control characteristics, along with related discussions on control reversal speeds.

#### STATIC AEROELASTIC ANALYSIS

The objective of the aeroelastic analysis is to reflect airframe flexibility effects in the calculation of structural design loads distributions, airframe structural deflections, and stability and control derivatives. The data generated are used: (1) to define the jig shape, (2) as input to the basic loads analysis, (3) as input to the flexible airplane performance, and (4) as input to airplane stability and control analysis.

## Methods

The aeroelastic analysis consists of combining detailed distributions of airloads, inertia loads, and airframe flexibility effects so as to result in an elastic airframe balanced in free-flight at preselected flight conditions (such as speed, altitude, acceleration, and gross weight). The detailed distributions are prepared in the form of matrices and combined by use of matrix algebra. Basic input data to the analyses consist of three parts:

- Mass Distribution
- Structural Influence Coefficient
- Airloads Distributions

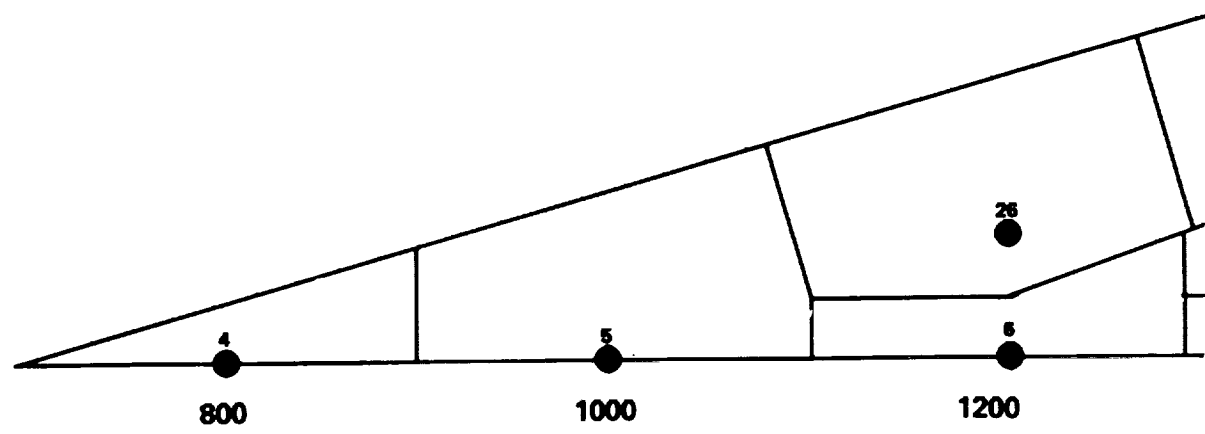
The airplane mass distribution is represented by lumped masses located at the loads panel grid point system illustrated schematically in Figure 5-1. The loads panel grid point system is coincident with the structural influence coefficient (SIC) grid described in Section 9, Structural Analyses Models.

The methods developed to calculate airload distributions use aerodynamic theories as well as wind tunnel measured force and pressure data, where available.

Theoretical Airloads Distribution. - Subsonic and supersonic airloads distribution are determined using the Discrete Load Line Element (DLLE) and the Mach Box computer programs, respectively.

Subsonic Speeds: Calculation of theoretical airload distributions at subsonic speeds is based on the Discrete Load Line Element (DLLE) method. The method is theoretically the same as the Doublet Lattice Method of Reference 1. A typical aerodynamic grid used for determination of the subsonic aerodynamics is presented in Figure 5-2. The aerodynamic influence coefficients (AIC's) are determined at the boxes and are then condensed within the computer program to the loads panel point grid system. Adjustments are also made to reflect the measured steady state lift coefficients and aerodynamic centers when required. Symmetric and antisymmetric AIC's are determined to enable calculation of lift distribution, for symmetric and asymmetric flight conditions.

600



800

1000

1200

FOLDOUT FRAME /



E

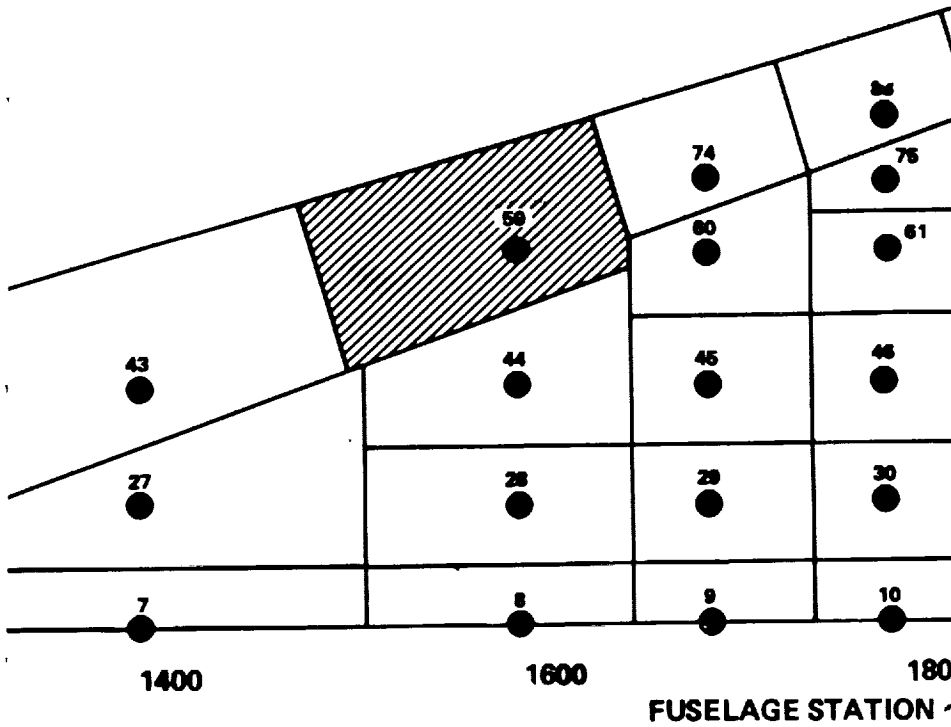
F

G

H

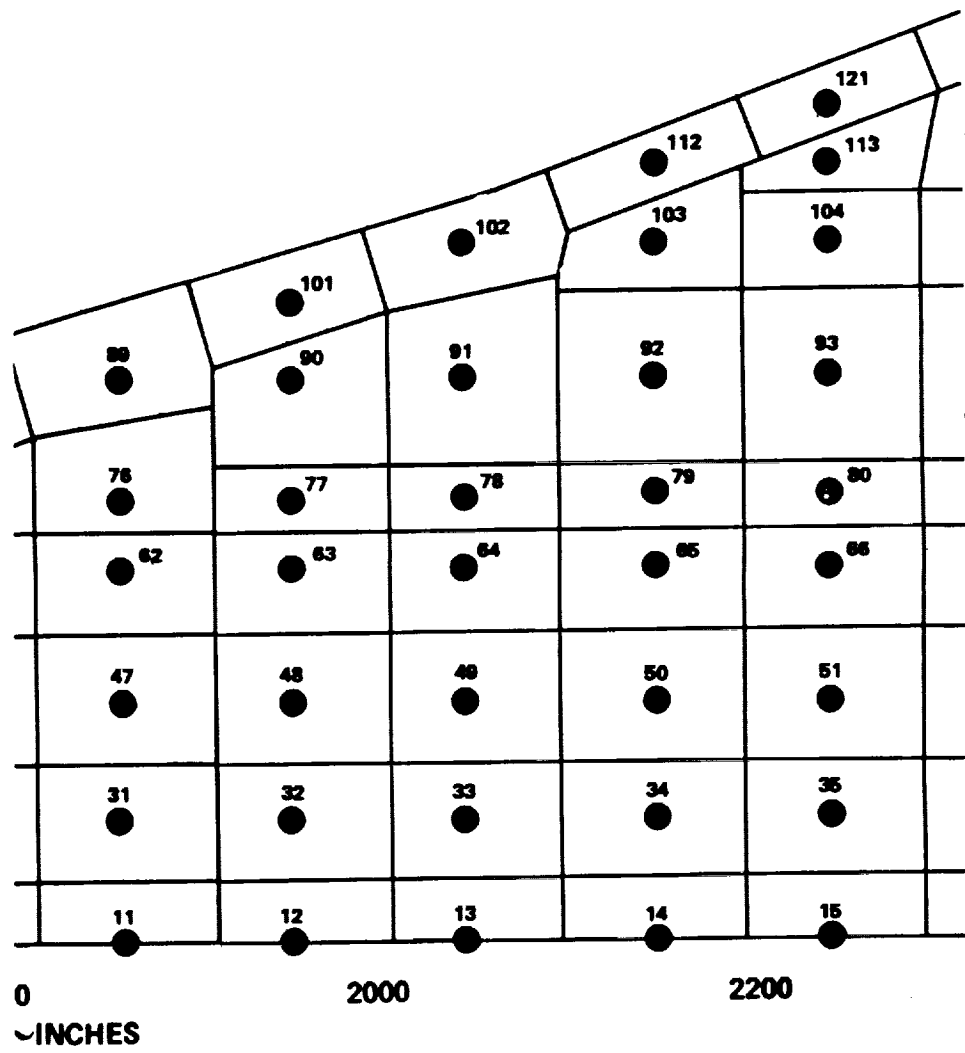
I

J



FOLDOUT FRAME 2











E E

F F

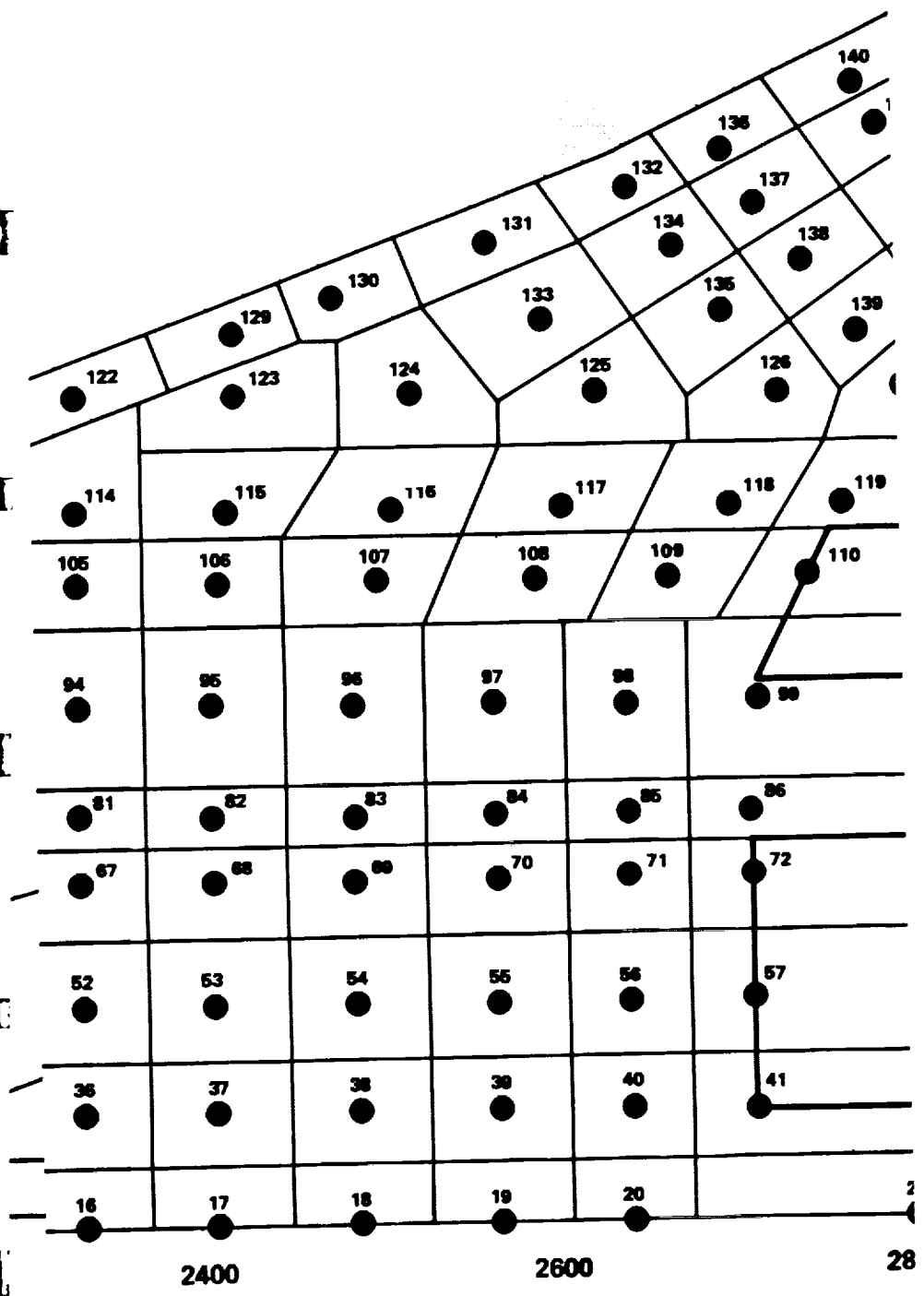
G G

H H

I I

J J

K K





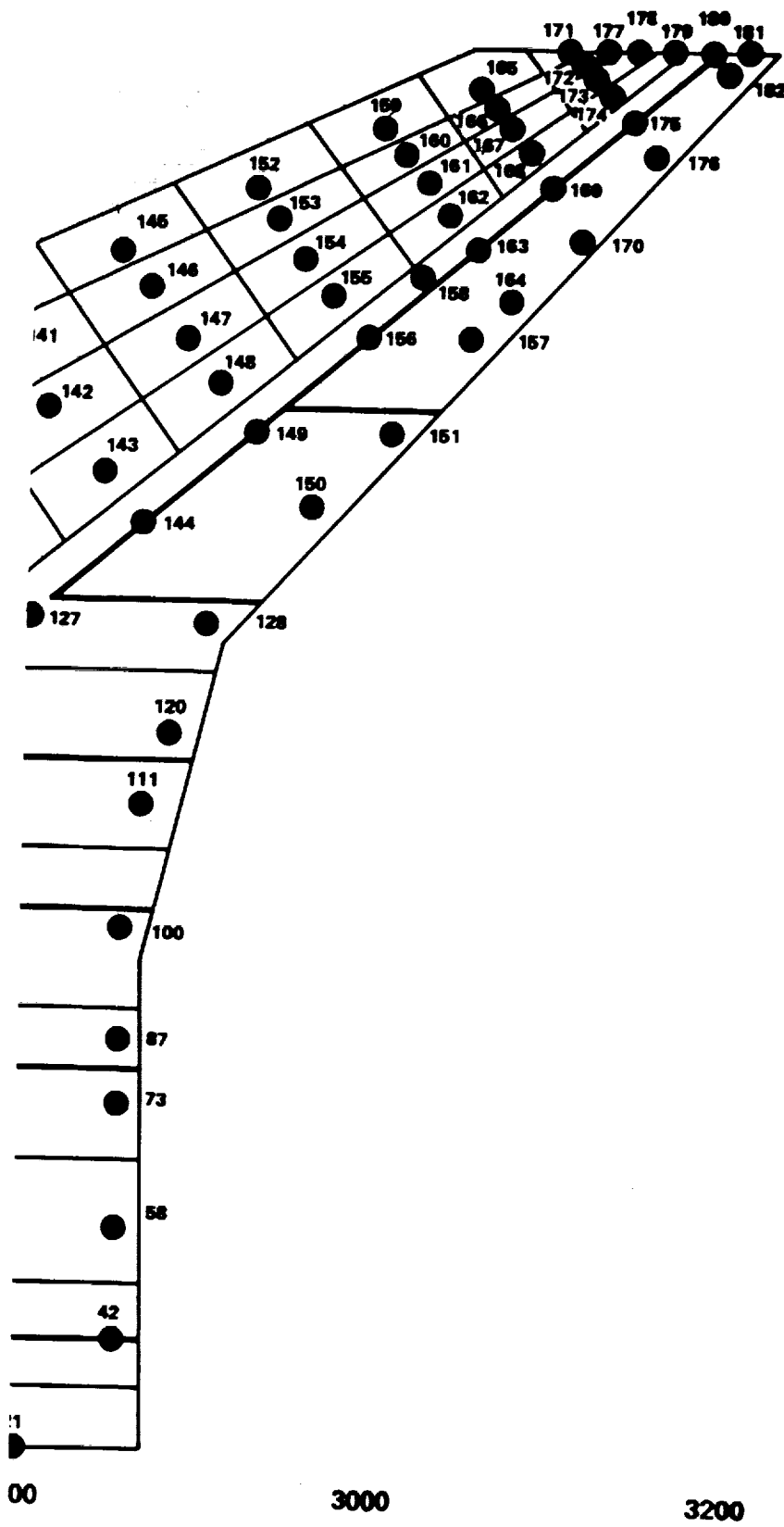


Figure 5-1. Loads Panel Grid Point System



**DOUBLE-LATTICE  
220 BOX SCHEME (INCLUDING FIN)**

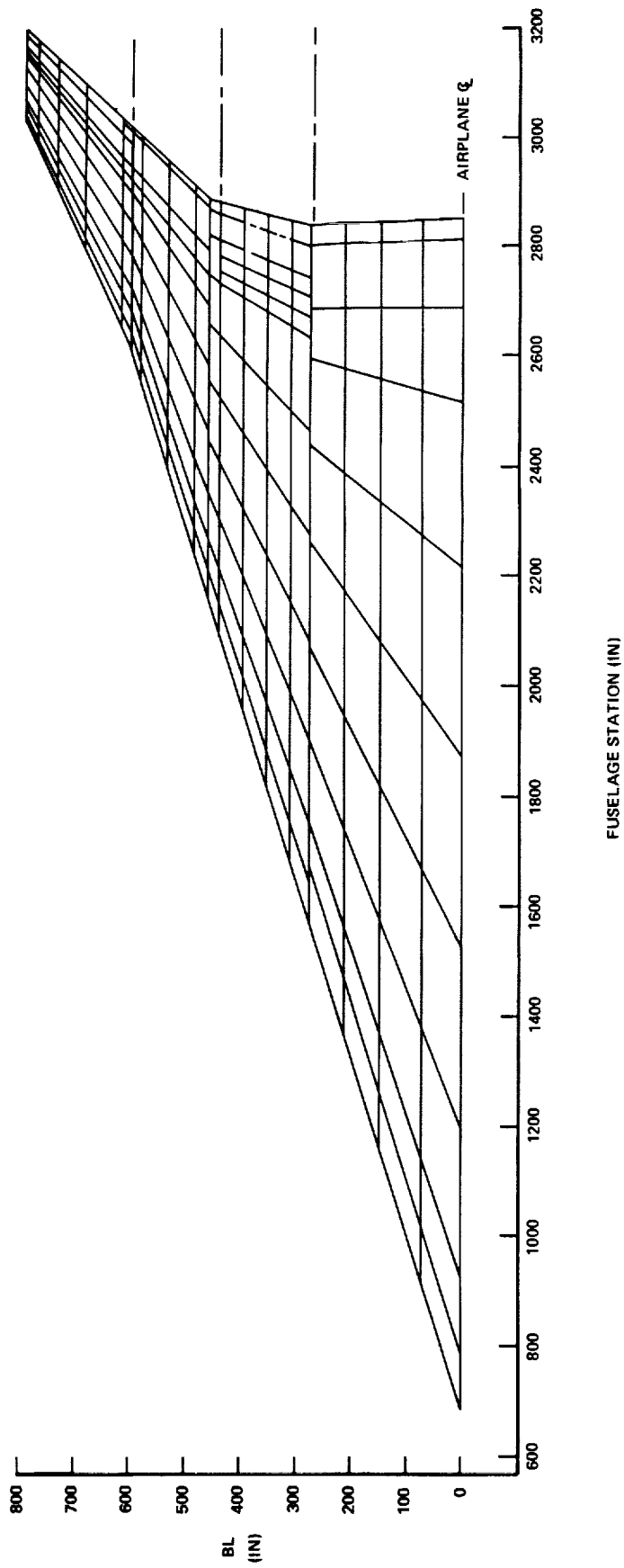


Figure 5-2. Subsonic Aerodynamic Grid

PRECEDING PAGE BLANK NOT FILMED

5-5

FOLDED FRAME |

FOLDED FRAME <



Supersonic Speeds: Theoretical airload distributions at supersonic speeds are based on the Mach Box approach. The Mach Box is an elementary rectangular area having a diagonal parallel to the Mach line as shown in Figure 5-3. The number of boxes used in the analysis varies with each Mach number and the limit is governed by the program capacity. Symmetric and antisymmetric AIC's are determined at the boxes and then condensed to the loads panel point grid system with proper adjustment of lift coefficient and aerodynamic centers.

A summary of the aerodynamic center location for subsonic and supersonic conditions and the total effective  $C_L$  (based on a reference area of 10,500 ft.<sup>2</sup>) is presented in Table 5-1. The data are consistent with the aerodynamic data presented in Section 3, Aerodynamics.

TABLE 5-1. SUMMARY AERODYNAMIC COEFFICIENT MATRICES - TASK I (k=0)

MACH NUMBER	BOUNDARY CONDITION	MATRIX SIZE	TOTAL EFFECTIVE $C_L$	LOCATION OF A. C.
0.60	Symmetric	274 x 325	2.42	FS 2324
	Antisymmetric	274 x 233		
0.90	Symmetric	274 x 325	2.58	FS2324
	Antisymmetric	274 x 233		
1.25	Symmetric	274 x 536	2.52	FS 2391
	Antisymmetric	274 x 487		
2.0	Symmetric	274 x 621	1.92	FS 2356
2.70	Symmetric	274 x 621	1.55	FS 2324

Net Flight Loads Calculations. - Panel point loads are calculated using the aforementioned data. Aerodynamic, mass, and stiffness distributions are combined with the aid of matrix algebra to formulate distributed panel loads on the airplane consistent with solution of the equations of motion for the prescribed maneuvers.

PRECEDING PAGE BLANK NOT FILMED





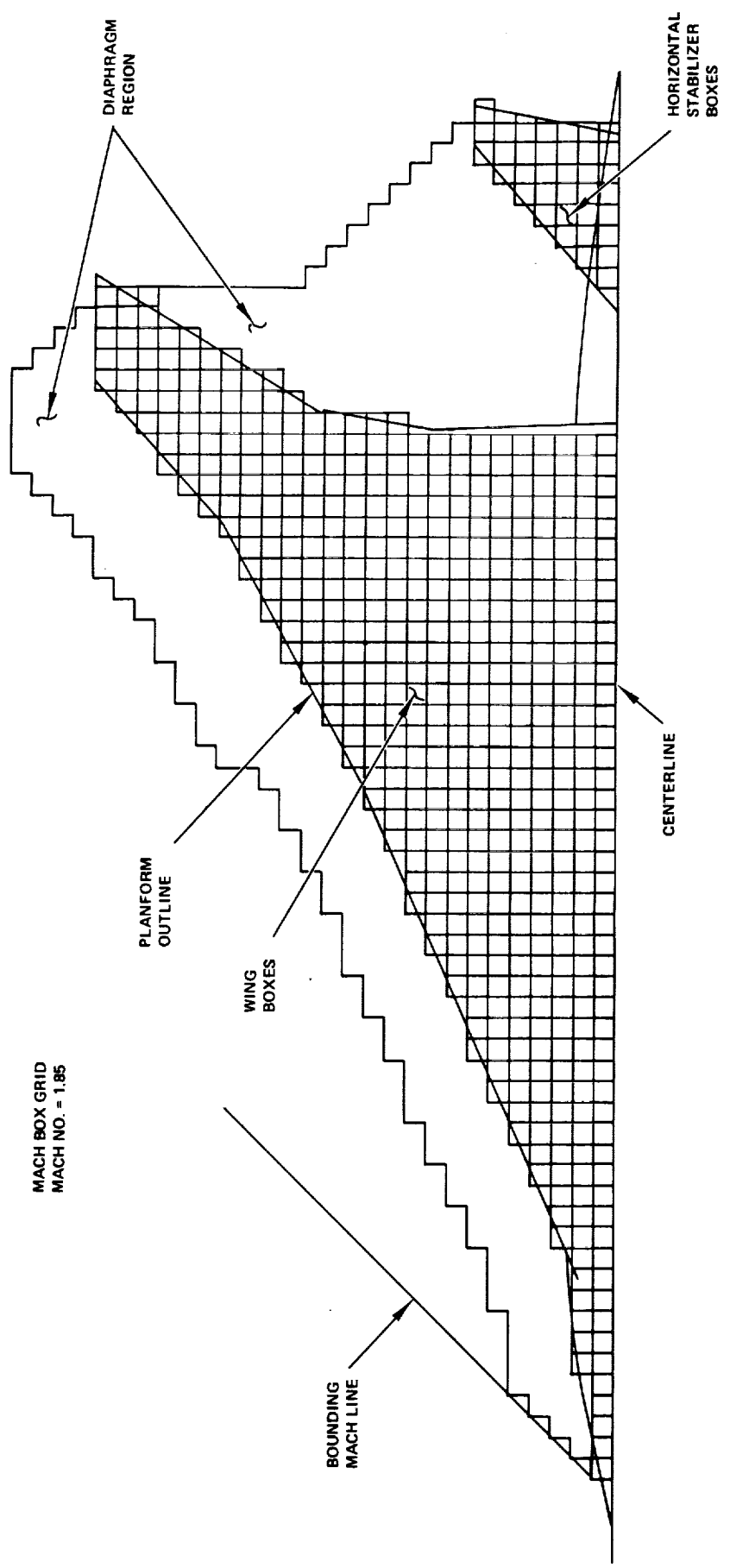


Figure 5-3. Supersonic Aerodynamic Grid

5-9

FOLDOUT FRAME 2

Fv.

PRECEDING PAGE BLANK NOT FILMED

FOLDOUT FRAME /



## Jig Shape Definition

The aerodynamic shape of the aircraft changes during flight due to aerothermoelastic and inertia effects. This is a result of in-flight variations in dynamic pressure, Mach number, gross weight, and weight distribution; the latter two result from fuel consumption.

The governing aerodynamic shape serving as the analytical starting point, is the shape providing the optimum performance characteristics in one-g mid-cruise flight for a 4,200 nautical mile range. This governing shape is described by the camber and twist characteristics of the supersonic wind tunnel model.

When the airframe structure is subject to no-load (dynamic pressure, Mach number, and inertia loads all equal zero) the shape of the aircraft is different from the mid-cruise shape. This zero load shape is designed into the aircraft so when it is subjected to one-g level flight loads and to temperatures occurring in the mid-cruise environment, the airframe elastic deformations result in an aircraft that has the desired optimum aerodynamic shape. The manufacture of the aircraft will be in accordance to this zero-load shape in the jig, where the weight is supported in a manner that precludes elastic deformations.

The procedure to establish the jig shape is as follows:

1. The analytical starting point is a description (camber and twist) of the optimum performance cruising-flight shape.

[ $\alpha_C$  & T, mid-cr]

2. Analysis is performed to calculate structural deflections due to flight loads occurring during mid-cruise flight. Where the deflection matrix  $[\Delta\delta_z]$  is defined by the product of the structural influence coefficients [E] and the rigid airplane 1-g loads for the mid-cruise condition

$$[\Delta\delta_z] = [E] \left[ P_{z1-g \text{ mid-cr. rigid}} \right]$$

PRECEDING PAGE BLANK NOT FILMED

using these calculated deflections and the transform matrix  $[D\theta]$ , the incremental change in chordwise slope and deflections are defined

$$\begin{bmatrix} \Delta \alpha \end{bmatrix} = \begin{bmatrix} D\theta \end{bmatrix} \begin{bmatrix} \Delta \delta_z \end{bmatrix}$$

3. The deflections are applied, negatively, to the mid-cruise shape to establish the jig shape.

$$\begin{bmatrix} \alpha_{\text{jig shape}} \end{bmatrix} = \begin{bmatrix} \alpha_{\text{C\&T, mid-cr}} \end{bmatrix} - \begin{bmatrix} \Delta \alpha \end{bmatrix}$$

The airplane shape used for analytical reference and loft purposes is hereby defined.

The aeroelastic analysis for the final design (Task IIB) incorporates the above defined jig shape in the calculation of the design loads, rather than the mid-cruise shape used for the Task I external loads analysis.

#### Flexible Stability Derivatives

The fact that the airplane changes shape aerodynamically as a result of elastic deflections of the structure makes it necessary to modify wind tunnel force data which have been measured on a rigid model. This flexibility is accounted for by applying flexible/rigid ratios or flexible increments to the basic rigid body aerodynamics. The degree of change varies with Mach number, equivalent airspeed, airplane gross weight, and structural arrangement. The magnitude of the effect of aeroelasticity on stability and control characteristics for the baseline arrow-wing configuration are obtained from generalized stability derivative programs and are reported herein. The application of these data to the stability and control analyses is presented in Section 3.

#### Calculation and Application of Flexible Effects on Stability and Control

Characteristics. - The effects of airframe flexibility on stability and control derivatives were determined over a range of Mach numbers for the chordwise-stiffened and monocoque structural arrangements. The results of these analyses are presented in Figures 5-4 through 5-10.

Longitudinal: Airplane flexibility effects on lift curve slope and pitching moments are shown on Figures 5-4 and 5-5 for the chordwise-stiffened arrangement and Figures 5-6 and 5-7 for the monocoque arrangement.

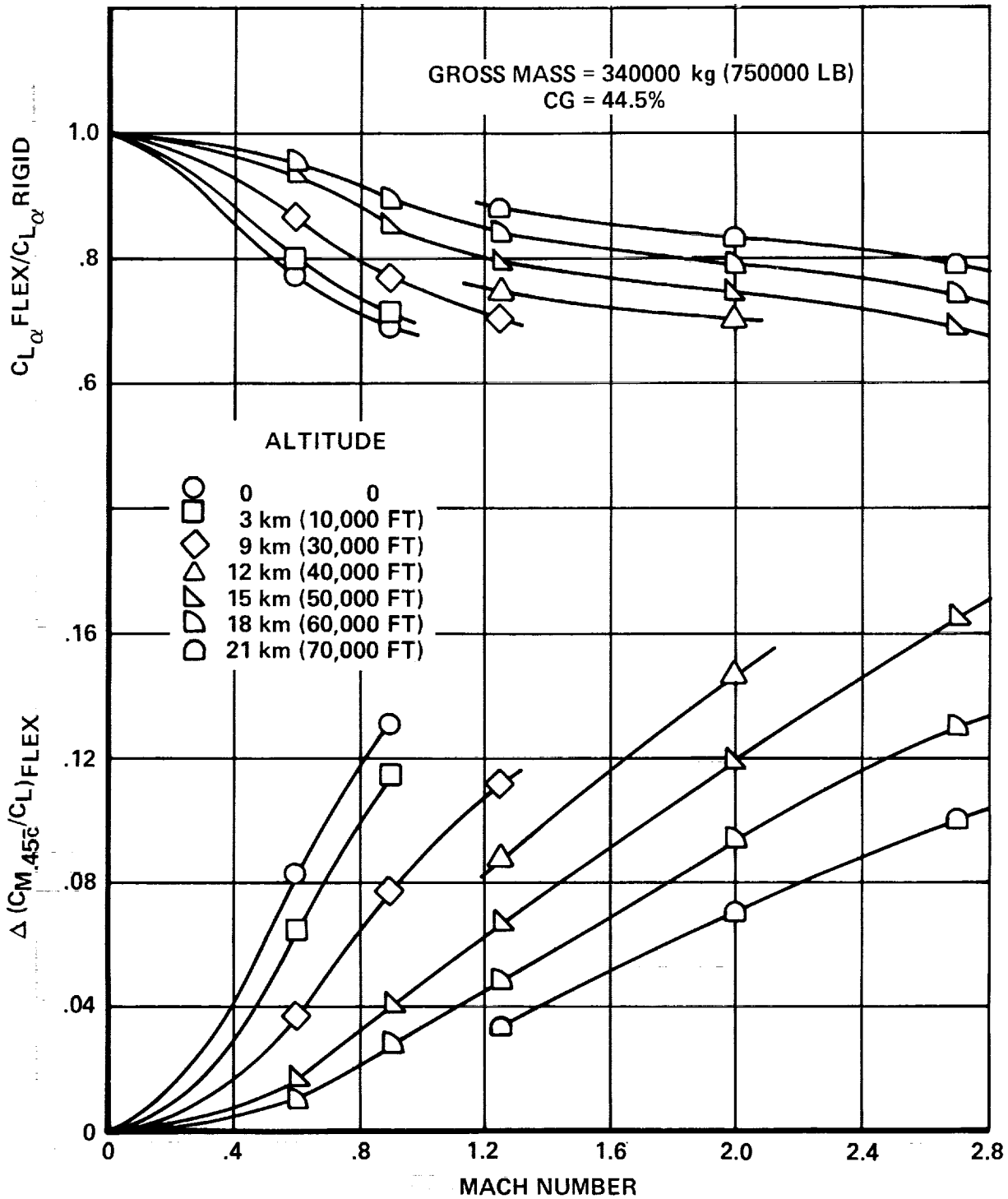


Figure 5-4. Free-Airplane Flexibility - Chordwise Stiffened Arrangement - 750,000 lb.

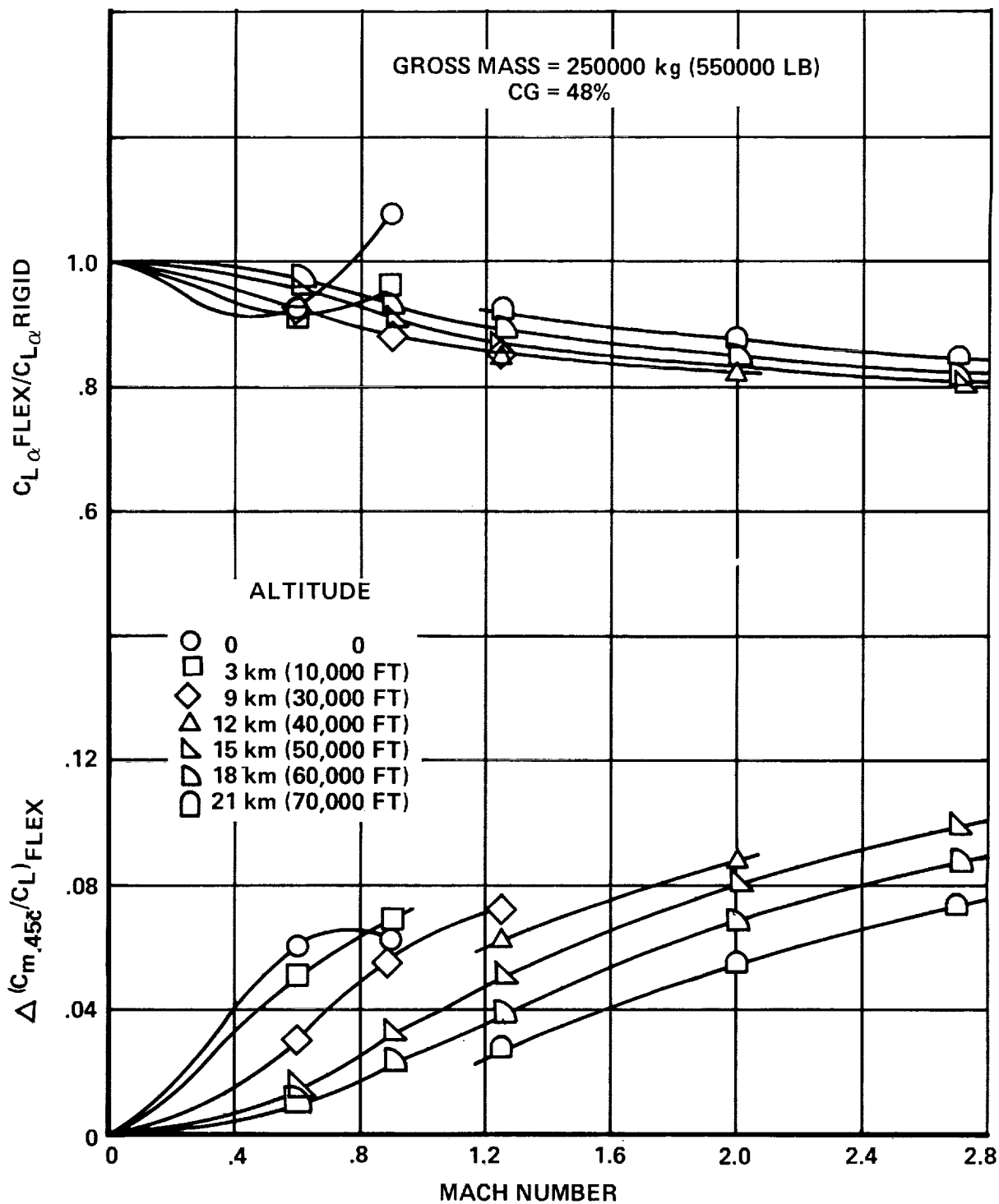


Figure 5-5. Free-Airplane Flexibility - Chordwise Stiffened Arrangement - 550,000 lb.

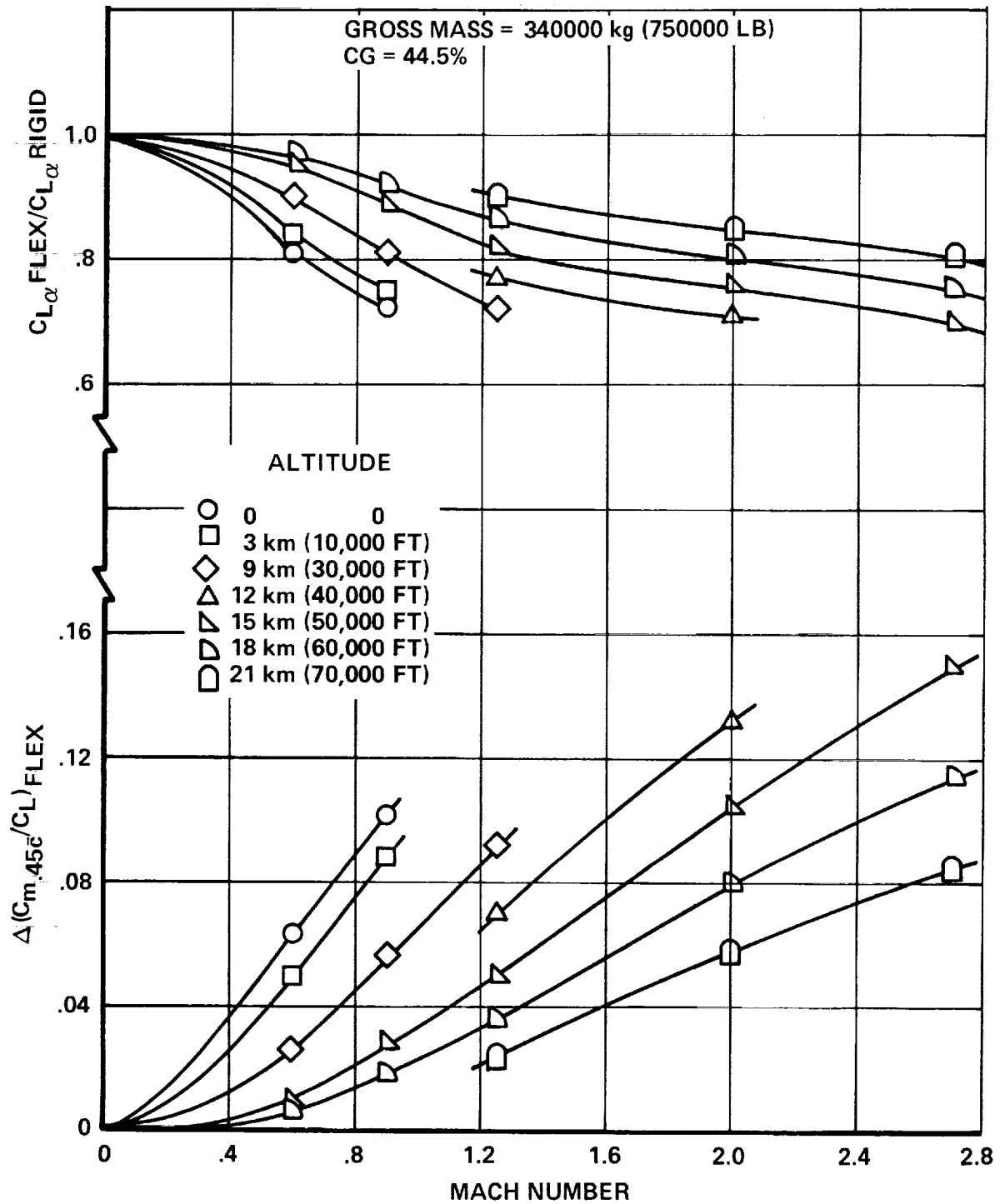


Figure 5-6. Free-Airplane Flexibility - Monocoque Arrangement - 750,000 lb.

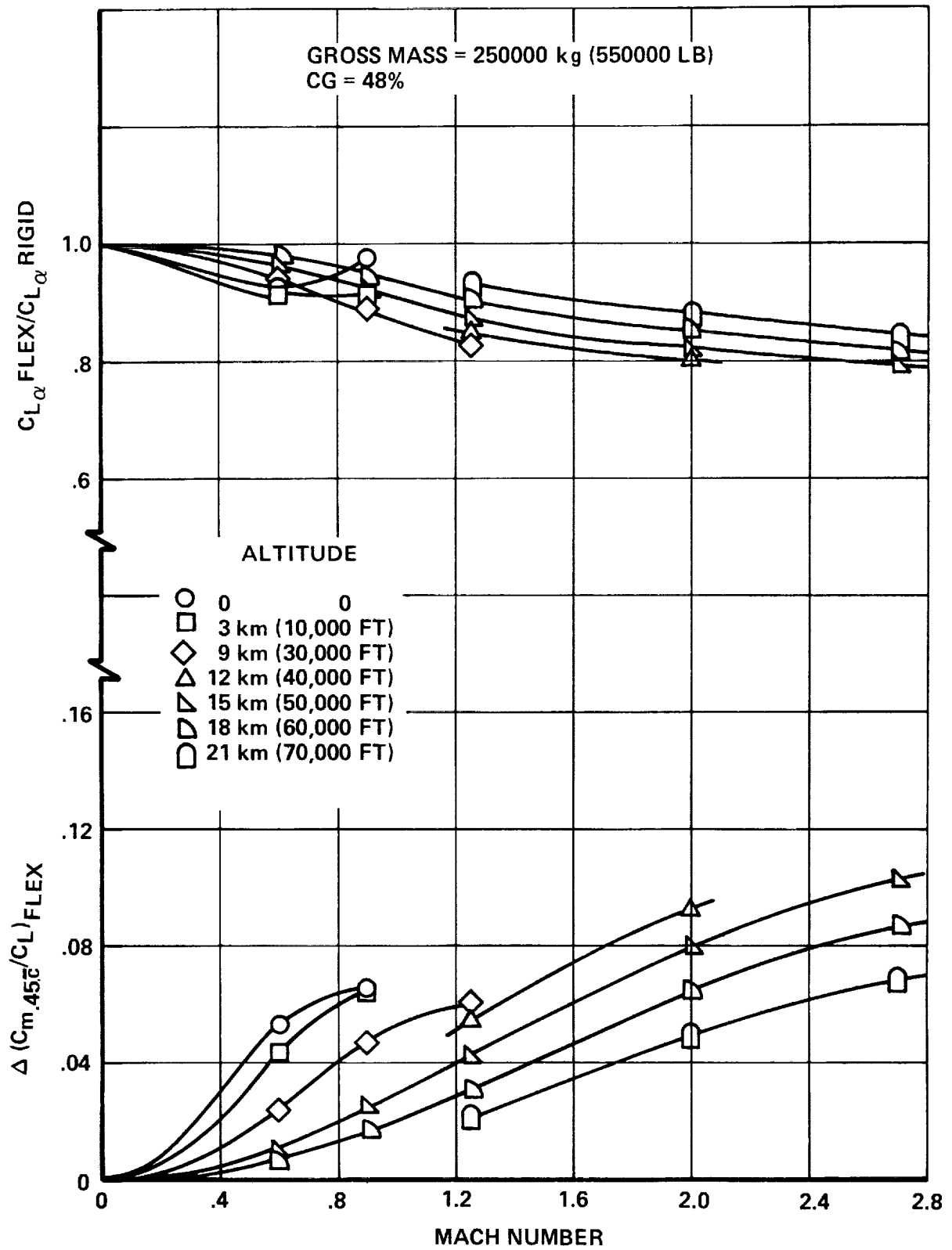


Figure 5-7. Free-Airplane Flexibility - Monocone Arrangement - 550,000 lb.



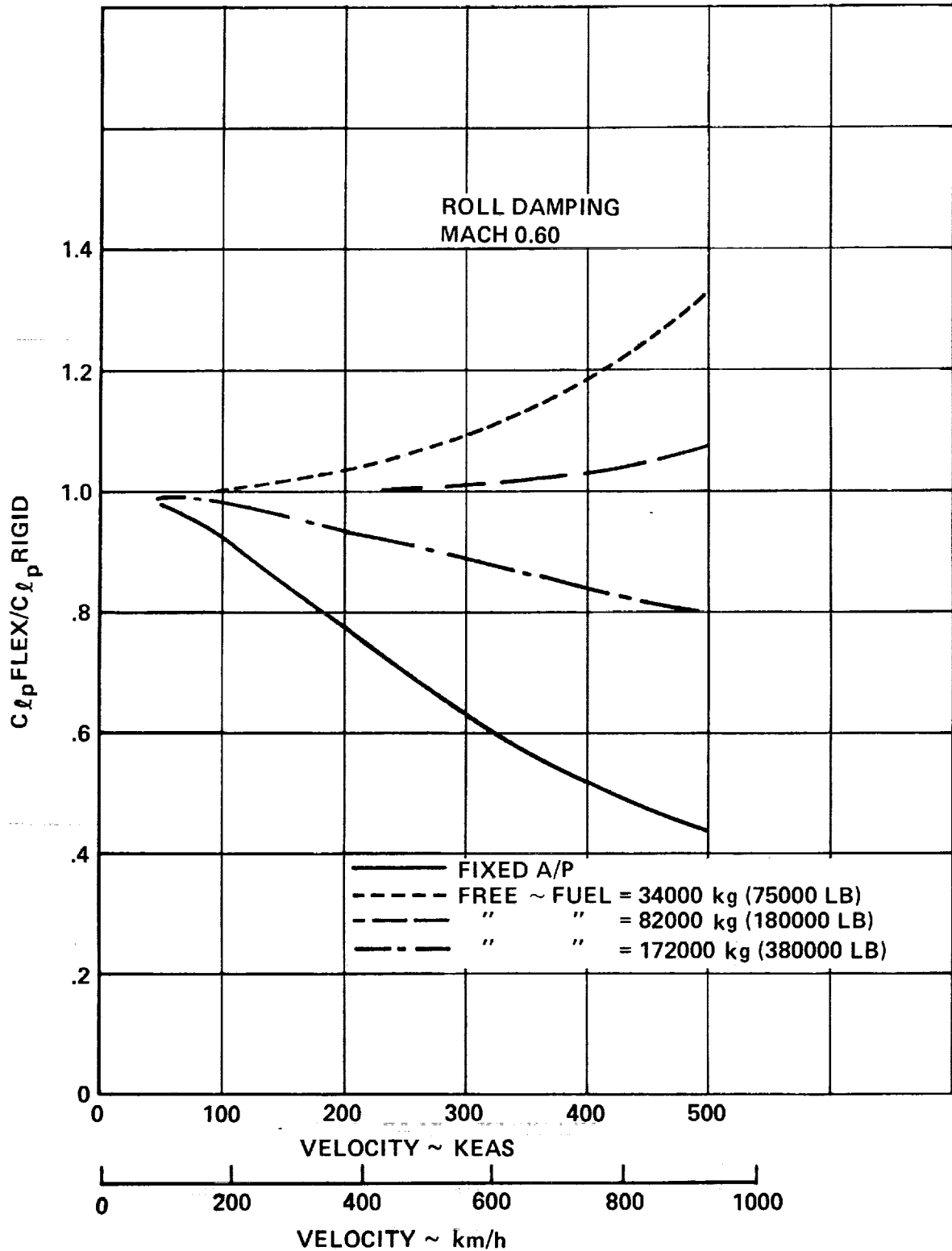


Figure 5-8. Airplane Roll Flexibility - Monocoque Arrangement - Mach 0.60

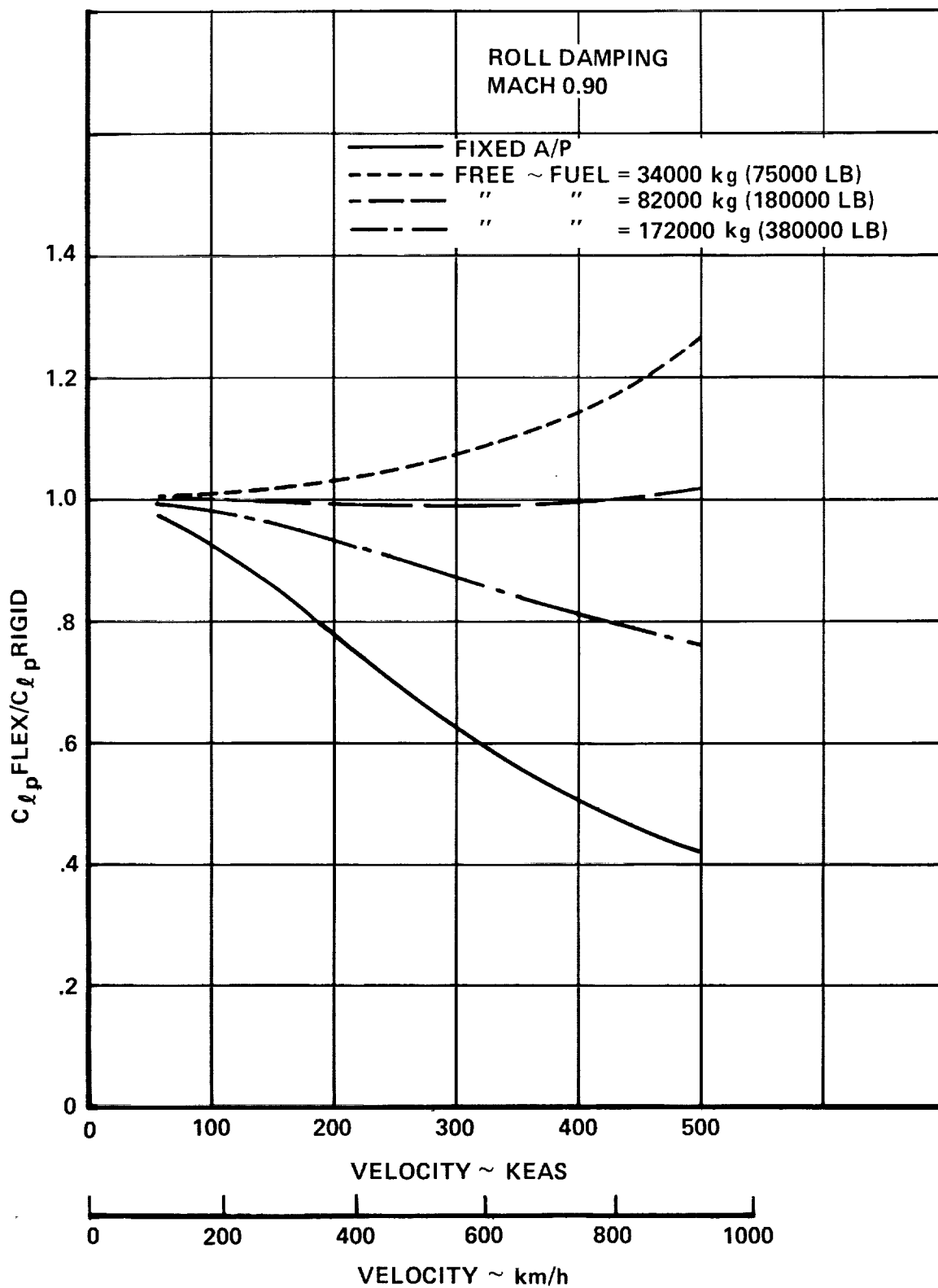


Figure 5-9. Airplane Roll Flexibility - Monocoque Arrangement - Mach 0.90

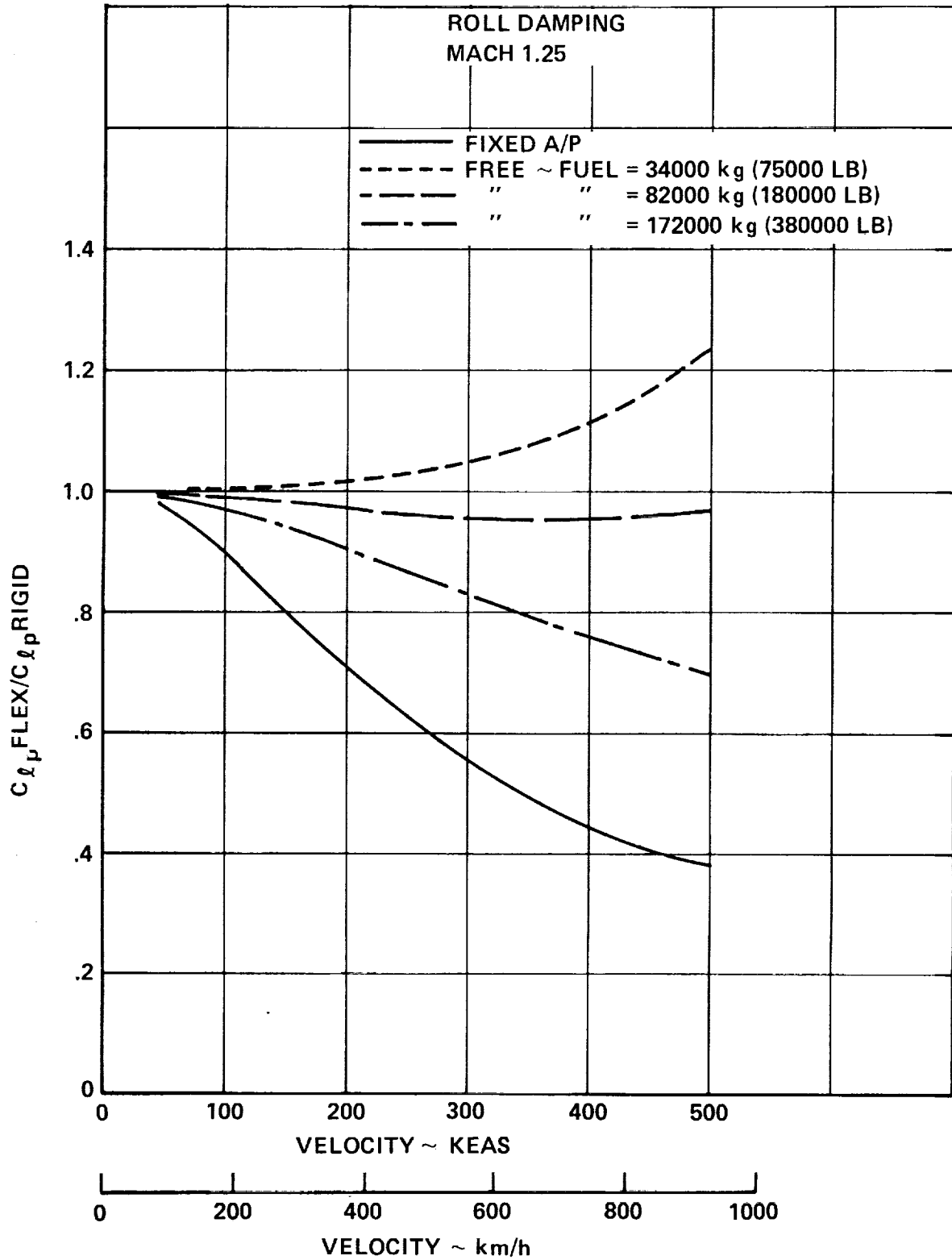


Figure 5-10. Airplane Roll Flexibility - Monocoque Arrangement - Mach 1.25

The flexible adjustments on derivatives that represent slopes such as  $(C_{l,\alpha})$  are presented in flexible-to-rigid ratio form. The adjustments to aerodynamic coefficients that represent absolute values such as  $(C_{m_0})$  are presented in the form of increments to be applied to the rigid coefficients.

The derivatives presented apply to a free-flight airplane. In the analysis, the airplane was not mathematically constrained by outside forces to establish the effects of flexibility, but was allowed to translate and rotate freely while equilibrium was maintained by inertia forces. The effect of each parameter ( $\alpha - \alpha_0$ ,  $\delta_e$ , etc.) were instantaneously applied along with representative inertia distributions. The redistribution of airloads due to airframe flexibility obtained in this manner reflects the effects of both airloads and inertia loads. The flexible derivatives thus obtained can be used directly in conventional rigid airplane equations of motion without the necessity of including aerodynamics coefficients representing inertia terms.

Airplane lift coefficient and pitching moment derivatives are presented for 2 airplane stiffnesses as defined by the chordwise-stiffened and monocoque designs. For each of the structural arrangements, 2 airplane weight cases were run: Gross weight = 750,000 lb. and 550,000 lb. Data for comparable airplane weight cases indicates negligible differences in longitudinal flexibility effects for the structural design concepts.

Rolling: Elastic lateral derivatives were determined at Mach numbers of 0.60, 0.90, and 1.25 using the AIC and SIC distributions for the chordwise-stiffened and monocoque arrangements. The resulting damping ratios, flexible-to-rigid, are shown in Figures 5-8 through 5-10 as a function of airplane velocity for the monocoque arrangement. The sensitivity of flexible-to-rigid ratio with airplane gross weight is indicated on the figures.

Figure 5-11 graphically displays the ratio of the flexible rolling moment coefficient to the rigid (wind tunnel data) coefficient obtained from Section 3. The data are for the Final Design airplane for both a low and high gross weight conditions. For the high gross weight case, the ratio is insensitive to variation in dynamic pressure. For the lightweight condition, however, the flexible-to-rigid ratio is highly sensitive to dynamic pressure

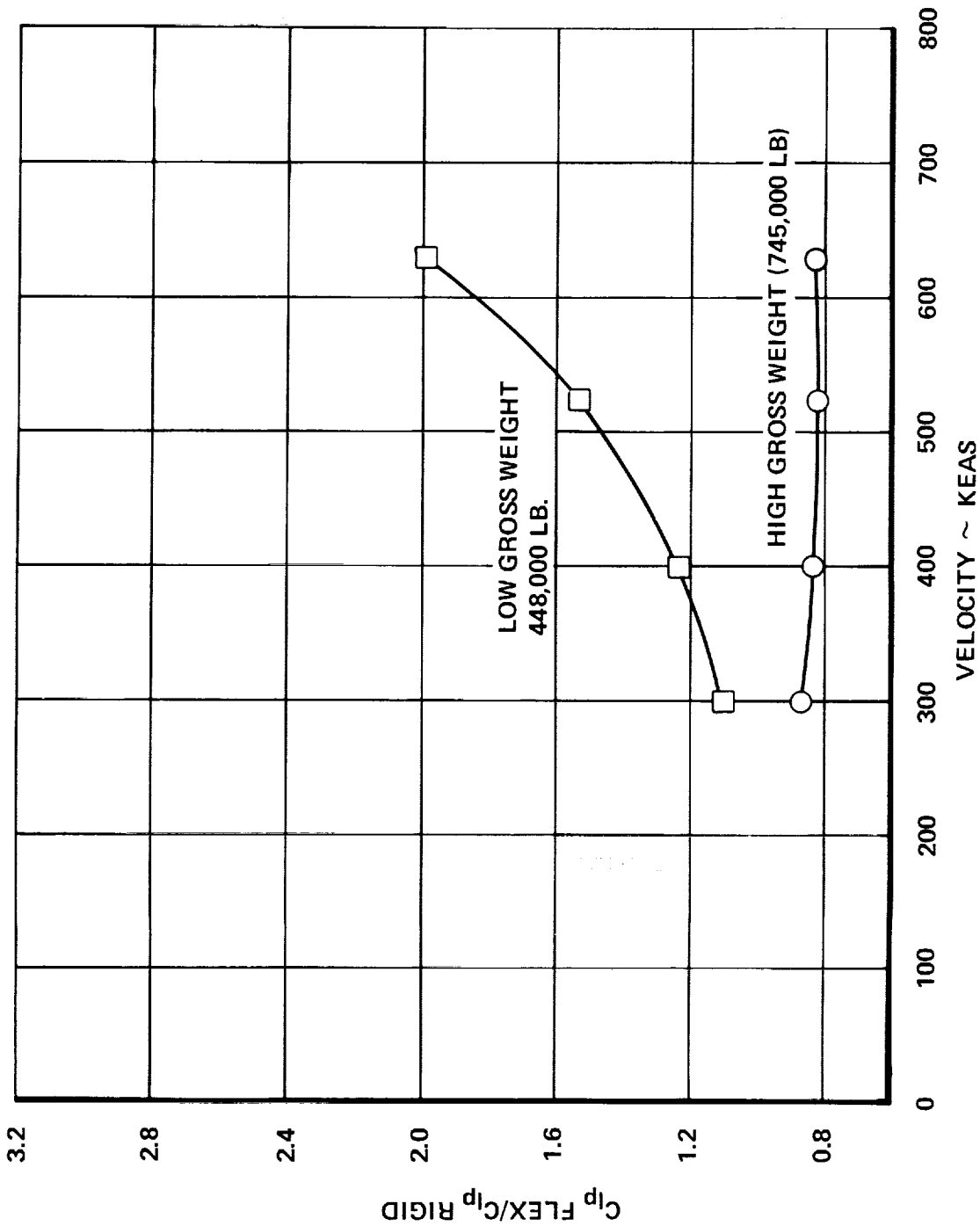


Figure 5-11. Airplane Roll Flexibility - Hybrid Arrangement - Mach 1.85

variation. For the normal operational profile, the flexible-to-rigid ratio is approximately 1.4.

Compliance with Roll Control Reversal Requirements. - The primary surfaces used for roll control at the various operational Mach numbers are shown in Figure 5-12. These data are consistent with the control surface operational schedule specified in Section 3. The subsonic control is obtained by use of the wing trailing edge panels (No. 2 through No. 4) with the low speed aileron (No. 4) locked-out above Mach 0.40 or 260 KEAS. For supersonic roll control, the spoiler-slot deflector at No. 2 and the inverted spoiler-slot deflector at No. 3 are used.

Federal Aviation Regulation 25.629(c) requires that the airplane be designed to be free from control reversal and from undue loss of longitudinal, lateral, and directional stability and control as a result of structural deformations at any speeds up to  $1.2 V_D$ . The airplane must also be shown to be free from control reversal at any speed up to  $V_D$  after any single failure or malfunction except those shown to be extremely remote.

The variation of roll effectiveness ( $C_{l\delta}$  flex) with equivalent airspeed ( $V_e$ ) for the Final Design airplane are shown in Figures 5-13 through 5-15. Separate graphical representations are displayed for the Mach numbers of 0.40, 0.90, and 1.85. Each figure presents the appropriate operational surfaces in accordance to the specified schedule (Figure 5-12) and the resulting reversal speeds.

Roll control reversal speeds are summarized in Table 5-2. Reversal speed and FAR required reversal speeds are shown for ease of comparison for both the normal scheduled surface combinations and for a selected fail-safe condition which considers the loss of a surface which has the most adverse effect on roll control reversal speed. It is noted that the outboard aileron (No. 4 panel) is locked-out at 260 KEAS; effectiveness up to 287 KEAS for the surface indicates that sufficient margin is provided for low speed operation of the ailerons. The data also shows that the control reversal requirements for normal and abnormal conditions (i.e.,  $1.2 V_D$  and  $V_D$ , respectively) are met on all surfaces and a zero margin of safety (i.e.,  $V_{\text{reversal}} = V_{\text{req'd}}$ ) for Mach 1.85. Since the control reversal speed is dependent upon the combined control effectiveness of the two surfaces involved, any relative reduction in the effectiveness of the stronger surface will result in an

adverse reduction of reversal speed. This fact, as can be identified in the detail results of the roll control study for Mach 1.85 shown in Table 5-3 for the two aircraft weight conditions (i.e., light and heavy weight), emphasizes the need for an accurate prediction of the rigid control surface effectiveness of all surfaces which make up the critical combinations.

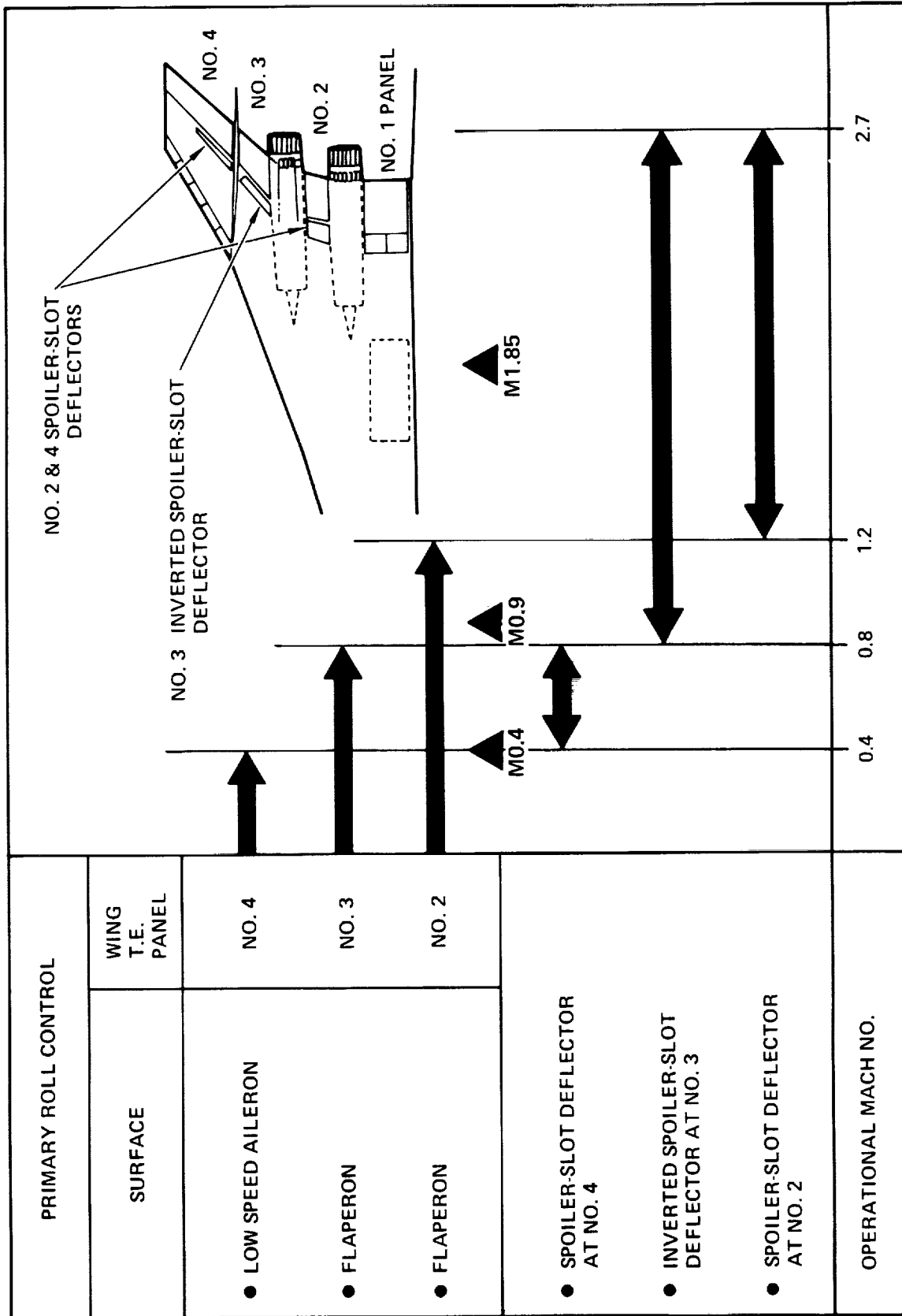


Figure 5-12. Primary Roll Control Schedule



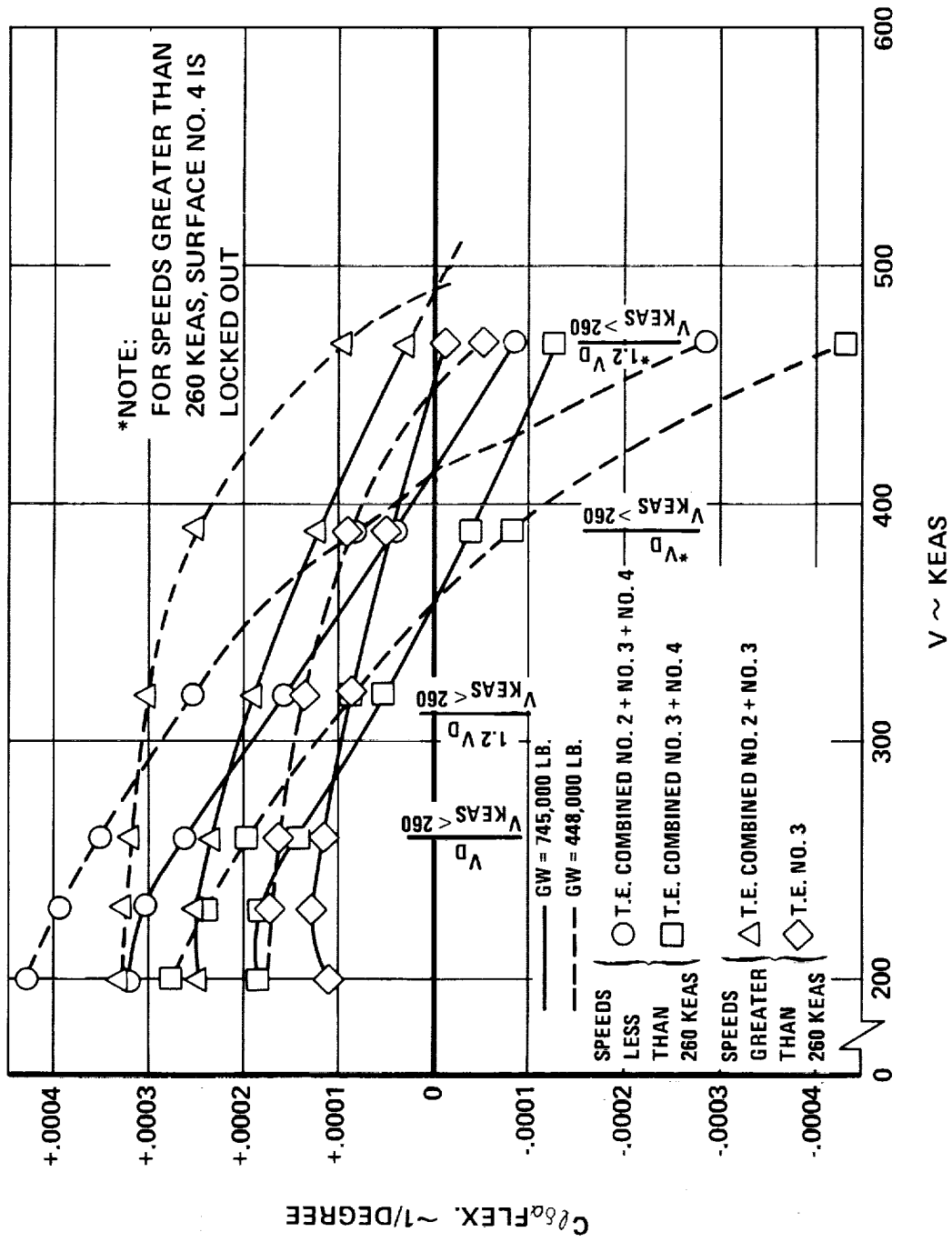


Figure 5-13. Roll Control Effectiveness - Mach 0.40

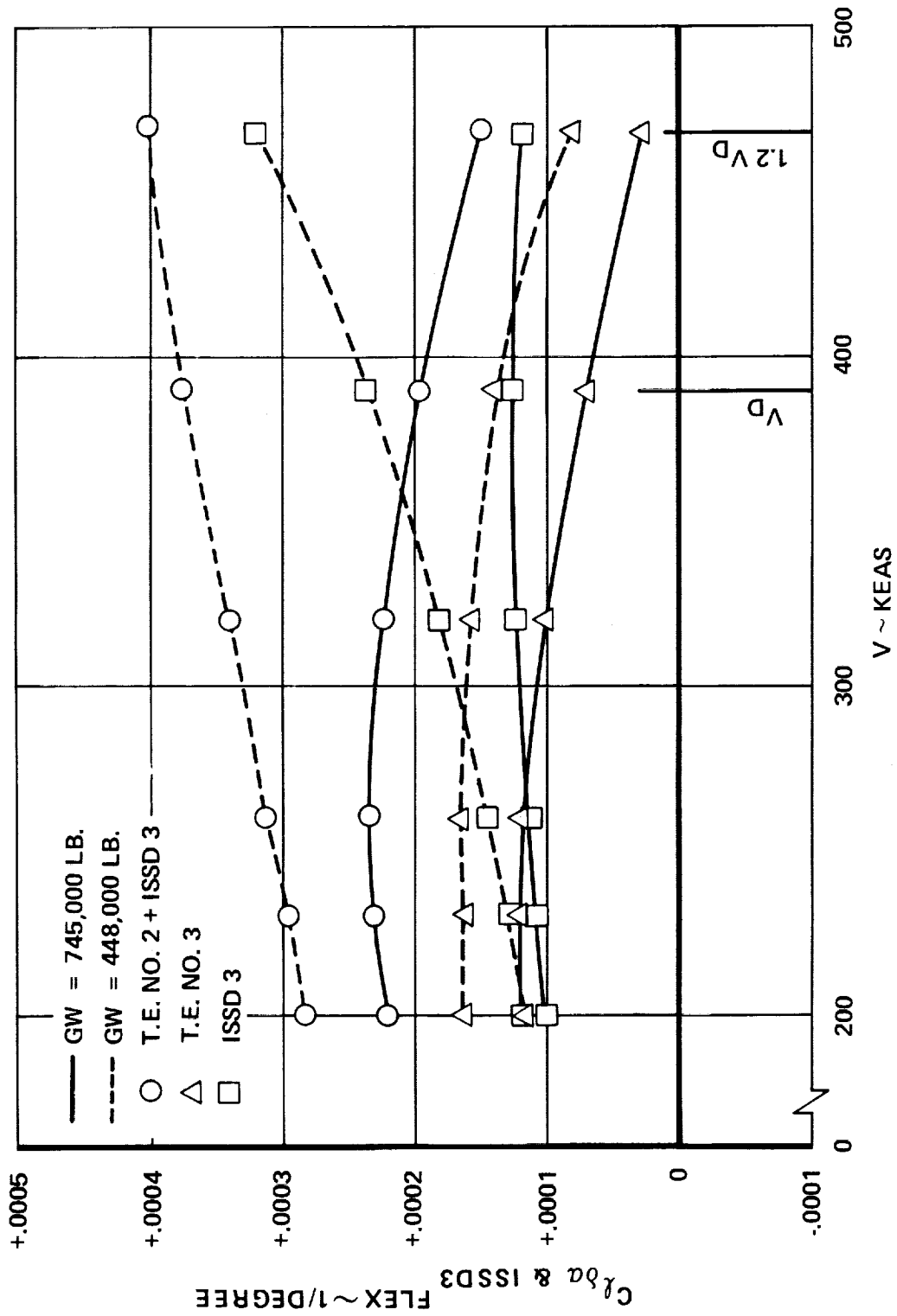


Figure 5-14. Roll Control Effectiveness - Mach 0.90

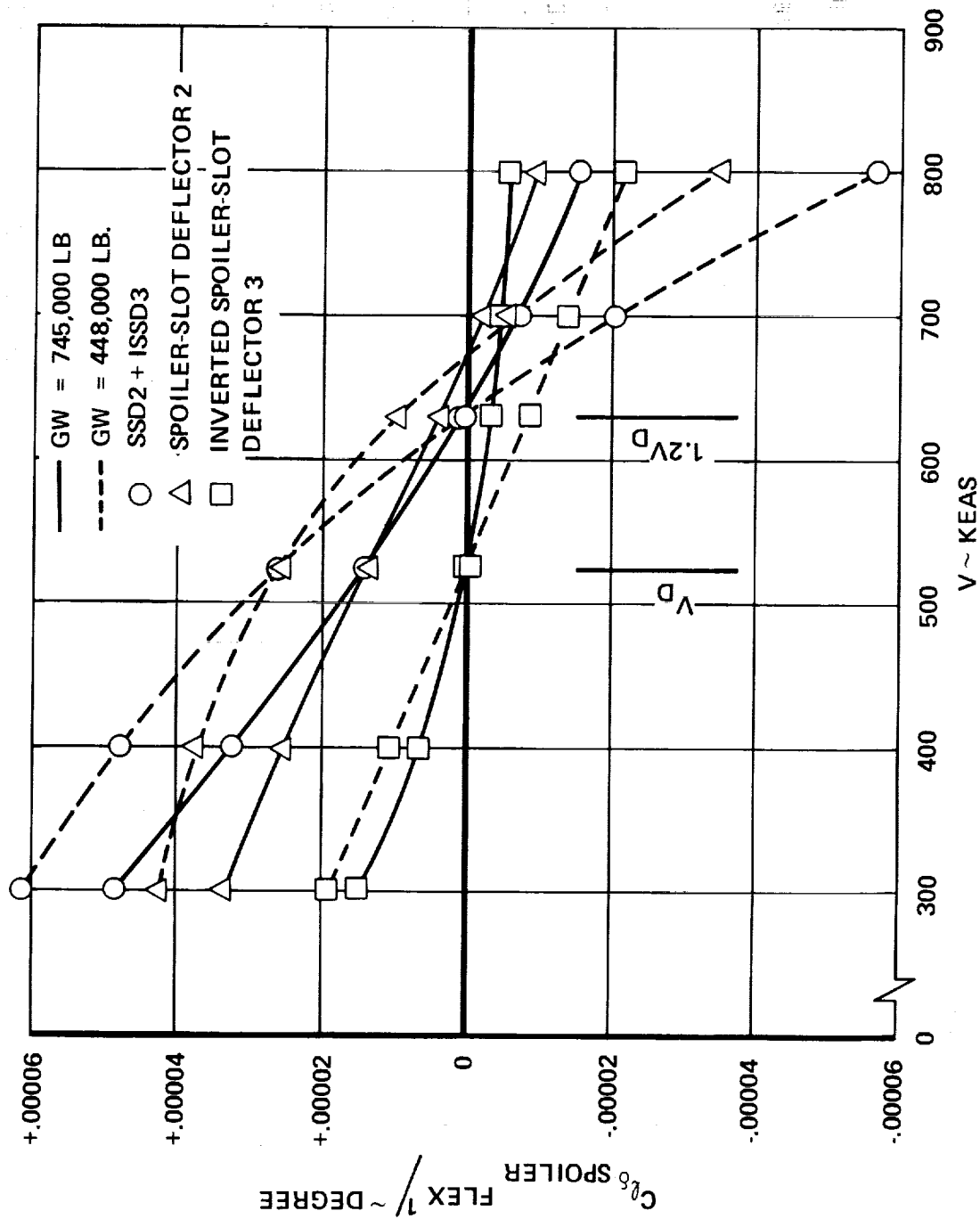


Figure 5-15. Roll Control Effectiveness - Mach 1.85

TABLE 5-2. ROLL REVERSAL SPEEDS

MACH 0.40			
SURFACE OPERATING	V REVERSAL	V REQ'D	CRITERIA
A. FOR SPEEDS LESS THAN V = 260 KEAS: (V <sub>D</sub> = 260 KEAS)			
NO. 2, NO. 3, NO. 4	410 KEAS	312 KEAS = 1.2 V <sub>D</sub>	NORMAL OPERATING COMBINATION
NO. 3, NO. 4	360 KEAS	260 KEAS = V <sub>D</sub>	ONE SURFACE INOPERATIVE
NO. 4	287 KEAS	260 KEAS = V <sub>D</sub>	LOCK-OUT SPEED
B. FOR SPEEDS GREATER THAN V = 260 KEAS - SURF. NO. 4 LOCK-OUT: (V <sub>D</sub> = 390 KEAS)			
NO. 2, NO. 3	490 KEAS	468 KEAS = 1.2 V <sub>D</sub>	NORMAL OPERATING COMBINATION
NO. 3	450 KEAS	390 KEAS = V <sub>D</sub>	ONE SURFACE INOPERATIVE
MACH 0.90			
SURFACE OPERATING	V REVERSAL	V REQ'D	CRITERIA
NO. 2 AND SPOILER NO. 3	> 1.2 V <sub>D</sub>	468 KEAS = 1.2 V <sub>D</sub>	NORMAL OPERATING COMBINATION
NO. 2	> V <sub>D</sub>	390 KEAS = V <sub>D</sub>	ONE SURFACE INOPERATIVE
SPOILER NO. 3	> V <sub>D</sub>	390 KEAS = V <sub>D</sub>	ONE SURFACE INOPERATIVE
MACH 1.85			
SURFACE OPERATING	V REVERSAL	V REQ'D	CRITERIA
SURFACE OPERATING			
SPOILER NO. 2 SPOILER NO. 3	630 KEAS	630 KEAS = 1.2 V <sub>D</sub>	NORMAL OPERATING COMBINATION
SPOILER NO. 2	675 KEAS	525 KEAS = V <sub>D</sub>	ONE SURFACE INOPERATIVE
SPOILER NO. 3	525 KEAS	525 KEAS = V <sub>D</sub>	ONE SURFACE INOPERATIVE

TABLE 5-3. ROLL CONTROL EFFECTIVENESS - MACH 1.85

Spoiler-Slot Deflector 2 and Inverted Spoiler-Slot Deflection 3

(1)	(2)	(3)	(4)	(5)	(6)	(7)	(8)	(9)	(10)	(11)	(12)
REF/OPERATION		WIND TUNNEL (A)									
q	V	$C_{l\delta}$ SSD2 f/r	$C_{l\delta}$ ISSD3 f/r	$C_{l p}$ f/r	$C_{l\delta}$ SSD2 = 60 deg 1/deg	$C_{l\delta}$ ISSD3 = 60 deg 1/deg	$C_{l\delta}$ SSD2 flex 1/deg	$C_{l\delta}$ ISSD3 flex 1/deg	$C_{l\delta}$ 2+3 flex 1/deg	$\Delta\alpha$	$\alpha$
lb/ft2	keas	-	-	(tail-off)	1/deg	1/deg	1/deg	1/deg	1/deg	deg	deg
GW = 750,000 lbs											
305	300	0.712	0.375	0.872	0.0000467	0.0000400	0.0000333	0.0000150	0.0000483	6.0	3.1
542	400	0.541	0.173	0.838	0.0000467	0.0000400	0.0000253	0.0000069	0.0000322	3.4	0.5
934	525	0.297	0.003	0.824	0.0000467	0.0000400	0.0000139	0.0000001	0.0000140	2.0	-0.9
1345	630	0.084	-0.085	0.830	0.0000467	0.0000400	0.0000039	-0.0000034	0.0000005	1.4	-1.5
1661	700	-0.048	-0.121	0.839	0.0000467	0.0000400	-0.0000022	-0.0000048	-0.0000070	1.1	-1.8
2169	800	-0.201	-0.144	0.856	0.0000467	0.0000400	-0.0000094	-0.0000058	-0.0000152	0.8	-2.1
GW = 448,000 lbs											
305	300	0.904	0.476	1.107	0.0000467	0.0000400	0.0000422	0.0000190	0.0000612	2.0	-0.9
542	400	0.798	0.255	1.237	0.0000467	0.0000400	0.0000373	0.0000102	0.0000475	1.1	-1.8
934	525	0.555	0.005	1.539	0.0000467	0.0000400	0.0000259	0.0000002	0.0000261	0.7	-2.2
1345	630	0.201	-0.203	1.981	0.0000467	0.0000400	0.0000094	-0.0000081	0.0000013	0.5	-2.4
1661	700	-0.138	-0.347	2.410	0.0000467	0.0000400	-0.0000064	-0.0000139	-0.0000203	0.4	-2.5
2169	800	-0.751	-0.541	3.202	0.0000467	0.0000400	-0.0000351	-0.0000216	-0.0000567	0.3	-2.6

NOTES: (A) REFERENCE SECTION 3, AERODYNAMICS

(B)  $\Delta\alpha = GW/C_{L\alpha} qS$

$S = 10923 \text{ ft}^2; C_{L\alpha} = 0.037/\text{deg}$

(C)  $\alpha = \Delta\alpha + \alpha_0$

$\alpha_0 = -2.9 \text{ deg}$

ORIGINAL PAGE IS OF POOR QUALITY

DESIGN LOADS - TASK I

Previous supersonic transport design studies were reviewed to identify potentially critical conditions for the baseline configuration concept. Design conditions for the SCAT-15F, Boeing 969C, and Lockheed L-2000-7 supersonic transport are summarized on Table 5-4. Loading conditions evaluated for the present study are also included on the table to indicate the scope of potentially critical loading conditions.

TABLE 5-4. CRITICAL LOADING CONDITIONS

	CONDITION	MACH NO.	$n_z$	SCAT-15F	L-2000	B-969C	ARROW WING
Flight	Symmetric	0.30	2.0	-	-	✓	✓
		0.60	2.5	✓	✓	-	✓
		0.90	2.5	✓	✓	-	✓
		1.25	2.5	-	✓	✓	✓
		2.00	2.5	-	-	-	✓
		2.70	2.5	✓	-	✓	✓
		2.90	2.5	-	-	-	✓
	Asymmetric	0.30		-	-	-	✓
		0.90	0 & 1.67	-	-	-	✓
		1.25		-	✓	-	✓
Ground	Taxi	-	2.0	-	-	✓	✓
	Rotation	-	-	-	✓	-	✓
	Landing	-	-	-	-	-	✓

Conditions for Design

Loading conditions for design of the baseline configuration for Task I (Figures 5-16 and 5-17) are evaluated at both maximum positive and maximum negative load factor and include all conditions where peak values or rapid change in aerodynamic coefficients exist as displayed in Figure 5-18. Sufficient design conditions are investigated to assure that critical design loads are included for structural analysis.

TOGW	750,000 LBS
WING AREA	10,822 FT <sup>2</sup>
LENGTH	297 FT
POWERPLANT	DUCT BURNING TURBOFAN
	1,192 LB/SEC

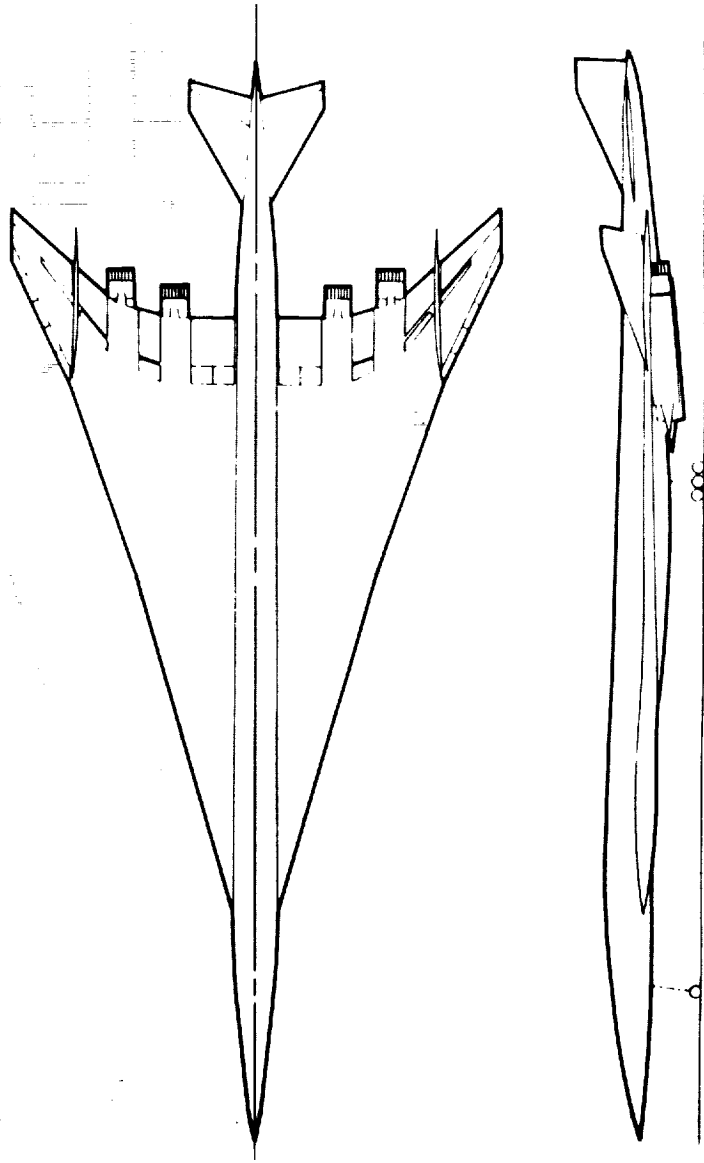


Figure 5-16. Baseline Configuration Concept - Task I

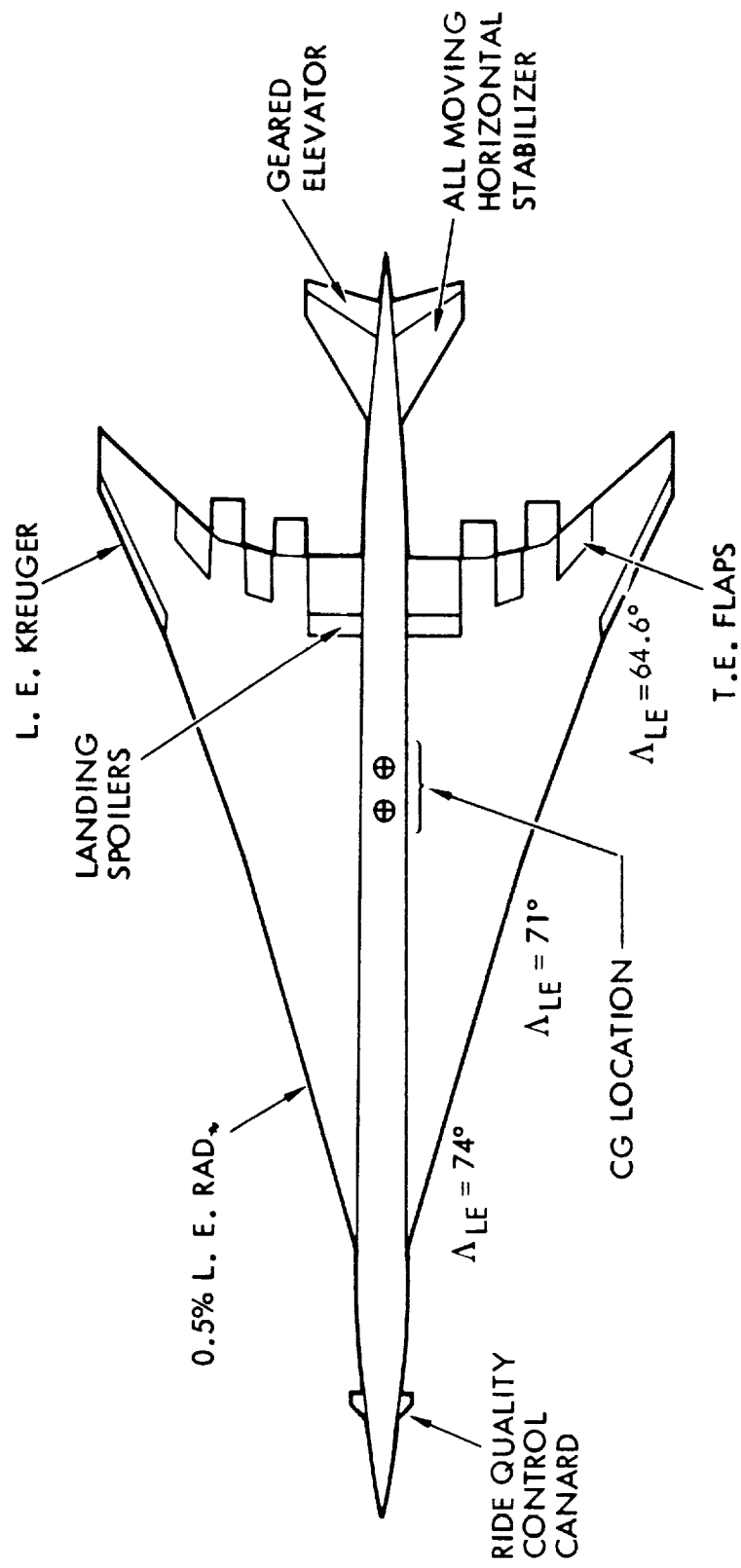


Figure 5-17. Baseline Configuration/Longitudinal Controls



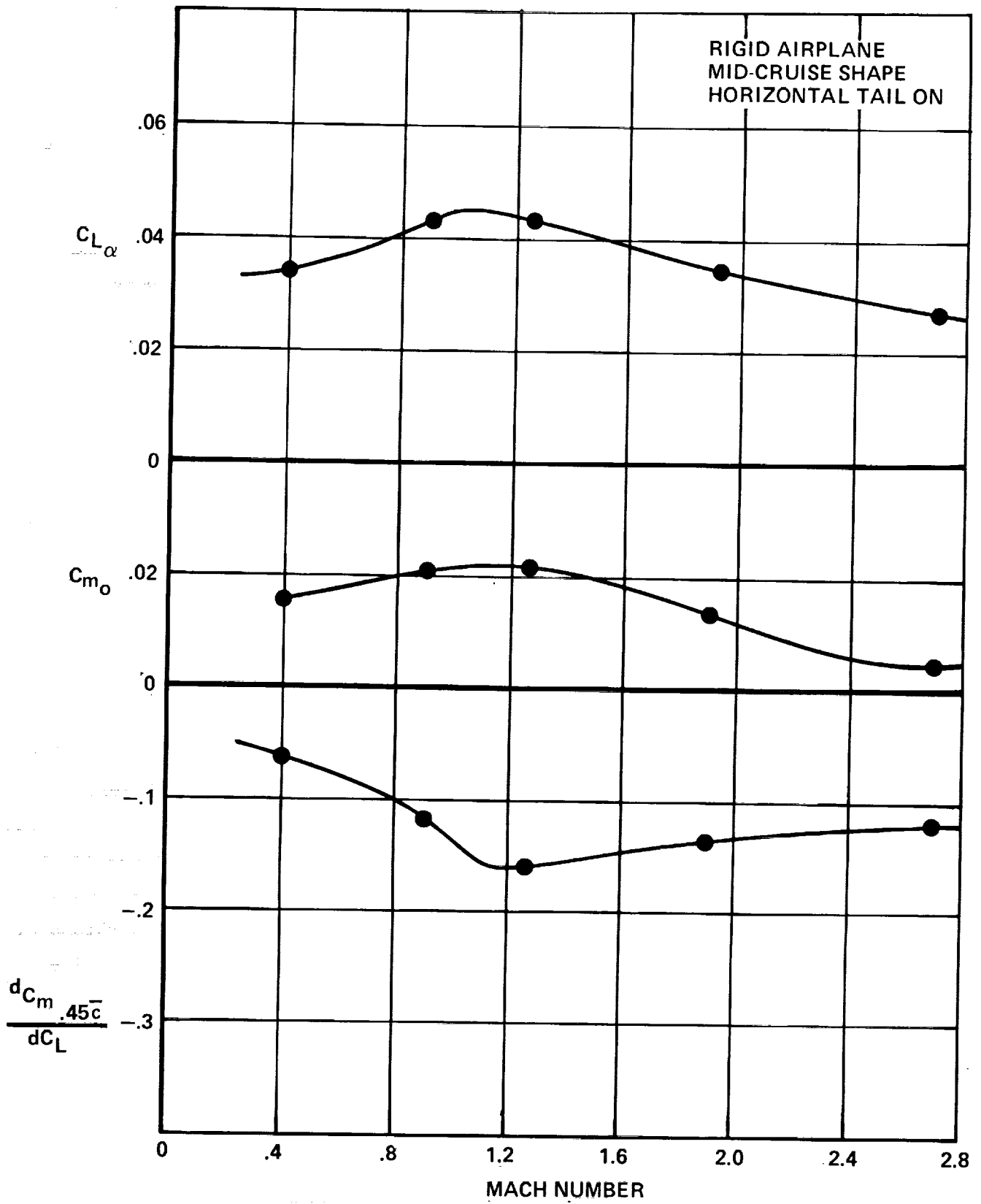


Figure 5-18. Airplane Longitudinal Characteristics

The fifty-three design conditions selected for analysis of the chordwise-stiffened wing arrangement are presented in Table 5-5. The data presented in the table include: the condition and number, airplane weight and configuration, design speed and altitude, and limit vertical load factor. The flight loads encompass level flight, steady maneuvers and transient maneuvers, as applicable. Two temperature conditions are included: Mid-cruise and start-of-cruise. The net effect of thermal loads and air loads for these conditions are obtained by superposition of the appropriate temperature condition with the design loads condition. In addition, the design loads matrix includes six ground handling, twenty-six positive symmetric flight, three negative symmetric flight and sixteen asymmetric flight conditions. The design conditions presented in Table 5-5 are further identified on the design airspeed envelope on Figure 5-19.

Table 5-6 presents the design loading conditions for the spanwise stiffened and monocoque arrangement. The ground handling conditions, loading at negative load factors and the asymmetric flight loads were determined non-critical as the result of the internal loads evaluation of the chordwise stiffened design and were not included in the load matrix.

#### Net Loads Summary

Net loads were developed for the three structural arrangements: chordwise stiffened, spanwise stiffened and monocoque. The conditions specified in Table 5-5 were included in the mix of conditions provided for design of the chordwise stiffened arrangement. This mix included the steady and accelerated roll conditions as well as the ground handling conditions. A review of the internal loads and stresses for these conditions disclosed that the aforementioned conditions did not design major portions of the structure; thus were not applied in the structural definition of the spanwise stiffened and monocoque wing designs.

Net loads for the baseline configuration were formed using a modified version of the Lockheed Static Aerolastic Loads Program - PSRL F-72. This program permits the aerodynamic influence coefficients to contain moment points and load points in directions other than vertical. Inertia loads are combined with aerodynamic loads to form aerodynamically balanced net loads using the stiffness matrices for each structural arrangement.

TABLE 5-5. DESIGN LOADING CONDITIONS - CHORDWISE STIFFENED - TASK I

	CONDITION	AIRPLANE			VELOCITY		MACH. NO.	ALTITUDE		LOAD FACTOR $n_z$	FLAP POSITION $\delta_f$
		MASS $10^3$ kg	WEIGHT $10^3$ lb	C.G. (X/C)	km/h	keas		$10^3$ km	$10^3$ ft		
TEMPERATURE CONDITIONS											
1	M2.7, MID-CRUISE										
2	M2.7, START-OF-CRUISE										
4	TAXI	340	750	-	-	-	-	-	1.0	-	-
5	LANDING	190	420	-	-	-	-	-	1.0	-	DOWN
6	T. O. ROTATION	340	750	-	-	-	-	-	1.25	-	DOWN
4F	TAIL $t=.05$ sec.	190	420	0.44	278	150	-	SL	1.0	SL	DOWN
5F	DOWN $t=.50$ sec.	190	420	0.44	278	150	-	SL	1.0	SL	DOWN
6F	LANDING $t=1.0$ sec.	190	420	0.44	278	150	-	SL	1.0	SL	DOWN
7	STEADY MAN.	338	745	0.44	407	220	0.33	SL	1.0	SL	DOWN
8	STEADY MAN.	338	745	0.44	407	220	0.33	SL	2.0	SL	DOWN
9	STEADY MAN.	338	745	0.44	407	220	0.33	SL	2.5	SL	UP
10	TRANSIENT MAN.	338	745	0.44	407	220	0.33	SL	2.5	SL	UP
9F	STEADY MAN.	338	745	0.44	482	260	0.40	SL	2.5	SL	UP
10F	TRANSIENT MAN.	338	745	0.44	482	260	0.40	SL	2.5	SL	UP
11	LEVEL FLIGHT	318	700	0.44	602	325	0.90	9.1	1.0	30.	UP
12	STEADY MAN.	318	700	0.44	602	325	0.90	9.1	2.5	30.	UP
13	TRANSIENT MAN.	318	700	0.44	602	325	0.90	9.1	2.5	30.	UP
14	LEVEL FLIGHT	313	690	0.44	689	372	1.25	11.6	1.0	38.2	UP
15	STEADY MAN.	313	690	0.44	689	372	1.25	11.6	2.5	38.2	UP
16	TRANSIENT MAN.	313	690	0.44	689	372	1.25	11.6	2.5	38.2	UP
17	LEVEL FLIGHT	311	685	0.44	852	460	1.9	14.3	1.0	47.	UP
18	STEADY MAN.	311	685	0.44	852	460	1.9	14.3	2.5	47.	UP
19	LEVEL FLIGHT	299	660	0.44	852	460	2.7	18.7	1.0	61.5	UP
20	STEADY MAN.	299	660	0.44	852	460	2.7	18.7	2.5	61.5	UP
21	LEVEL FLIGHT	249	550	0.44	803	433.6	2.7	19.5	1.0	64.	UP
22	STEADY MAN	249	550	0.44	803	433.6	2.7	19.5	2.5	64.	UP
23	LEVEL FLIGHT	249	550	0.48	803	433.6	2.7	19.5	1.0	64.	UP

TABLE 5-5. DESIGN LOADING CONDITIONS - CHORDWISE STIFFENED - TASK I (CONT'D)

CONDITION	AIRPLANE		VELOCITY		MACH. NO.	ALTITUDE		LOAD FACTOR $n_z$	FLAP POSITION $\delta_f$
	MASS $10^3$ kg	WEIGHT $10^3$ lb	C.G. (X/C)	km/h		keas	$10^3$ km		
24	202	445	0.44	732	395	2.7	20.7	68.0	UP
25	202	445	0.44	732	395	2.7	20.7	68	UP
26	299	660	0.44	972	525	2.9	18.0	59	UP
27	311	685	0.44	972	525	1.9	12.5	41	UP
28	313	690	0.44	778	420	1.25	10.4	34	UP
29	318	700	0.44	722	390	0.90	6.7	22	UP
30	318	700	0.44	722	390	0.90	6.7	22	UP
31	313	690	0.44	491	265	1.25	16.0	52.4	UP
32	313	690	0.44	491	265	1.25	16.0	52.4	UP
33	318	700	0.44	602	325	0.90	9.1	30	UP
34	338	745	0.44	407	220	0.33	SL	SL	UP
35	338	745	0.44	407	220	0.33	SL	SL	-
36	338	745	0.44	407	220	0.33	SL	SL	-
37	338	745	0.44	407	220	0.33	SL	SL	-
38	338	745	0.44	407	220	0.33	SL	SL	-
39	338	745	0.44	407	220	0.33	SL	SL	-
40	338	745	0.44	407	220	0.33	SL	SL	-
41	338	745	0.44	407	220	0.33	SL	SL	-
42	338	745	0.44	407	220	0.33	SL	SL	-
43	318	700	0.44	602	325	0.90	9.1	30	-
44	318	700	0.44	602	325	0.90	9.1	30	-
45	318	700	0.44	602	325	0.90	9.1	30	-
46	318	700	0.44	602	325	0.90	9.1	30	-
47	313	690	0.44	689	372	1.25	11.6	38.2	-
48	313	690	0.44	689	372	1.25	11.6	38.2	-
49	313	690	0.44	689	372	1.25	11.6	38.2	-
50	313	690	0.44	689	372	1.25	11.6	38.2	-

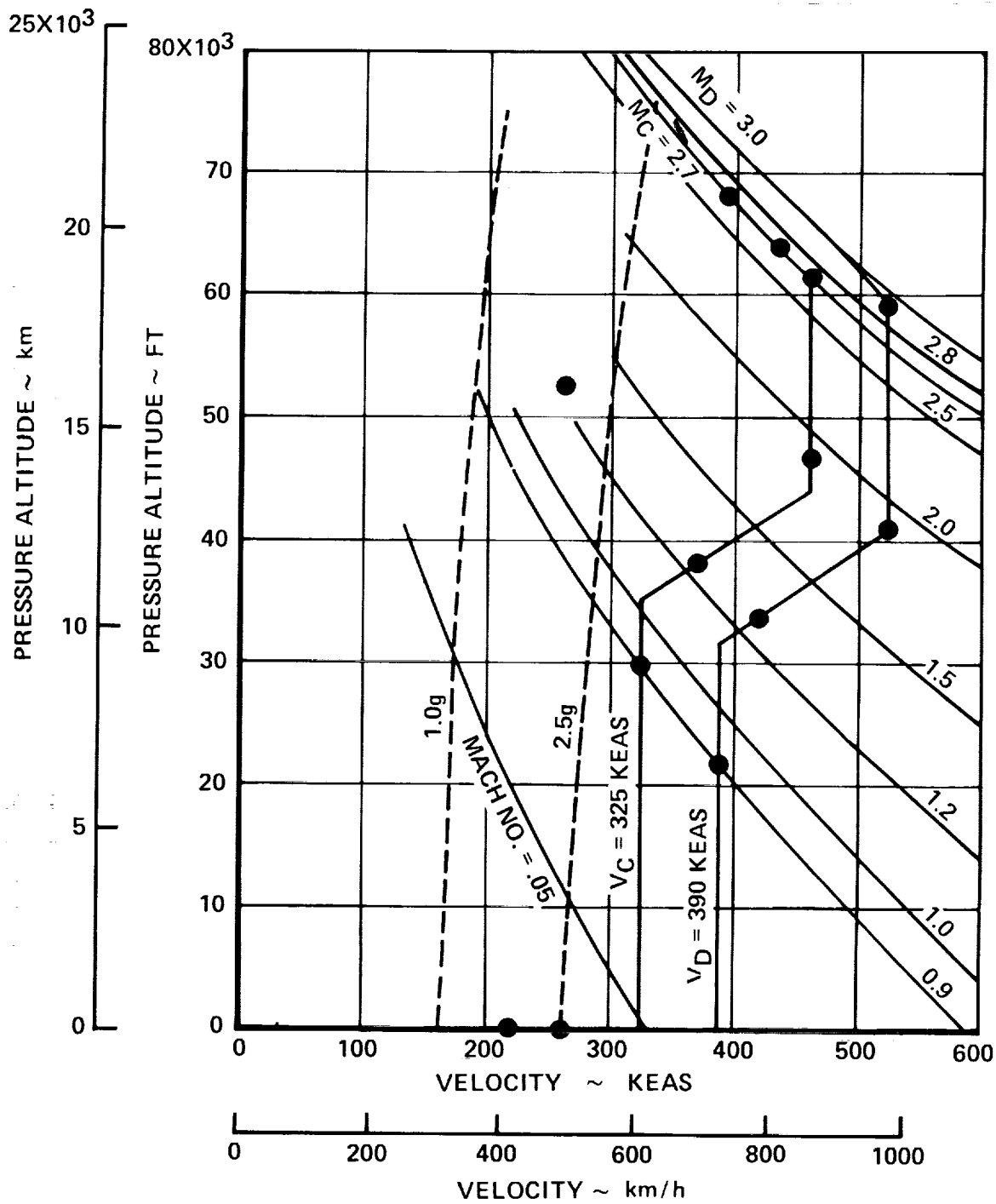


Figure 5-19. Critical Loading Conditions

TABLE 5-6. DESIGN LOADING CONDITIONS - SPANWISE STIFFENED AND MONOCOQUE - TASK I

1	CONDITION	AIRPLANE		VELOCITY		MACH NO.	ALTITUDE		LOAD FACTOR $n_z$	FLAP POSITION $\delta_f$
		MASS $10^3$ kg	WEIGHT $10^3$ lb	C.G. (X/C)	km/h		keas	$10^3$ km		
		TEMPERATURE CONDITIONS								
2	M2.7, MID-CRUISE									
7	LEVEL FLIGHT	338	745	0.44	482	260	0.40	SL	1.0	DOWN
8	STEADY MAN.	338	745	0.44	482	260	0.40	SL	2.0	DOWN
9	STEADY MAN.	338	745	0.44	482	260	0.40	SL	2.5	UP
10	TRANSIENT MAN.	338	745	0.44	482	260	0.40	SL	2.5	UP
11	LEVEL FLIGHT	318	700	0.44	602	325	0.90	9.1	1	UP
12	STEADY MAN.	318	700	0.44	602	325	0.90	9.1	2.5	UP
13	TRANSIENT MAN.	318	700	0.44	602	325	0.90	9.1	2.5	UP
14	LEVEL FLIGHT	313	690	0.44	689	372	1.25	11.6	1	UP
15	STEADY MAN.	313	690	0.44	689	372	1.25	11.6	2.5	UP
16	TRANSIENT MAN.	313	690	0.44	689	372	1.25	11.6	2.5	UP
17	LEVEL FLIGHT	311	685	0.44	852	460	1.9	14.3	1	UP
18	STEADY MAN.	311	685	0.44	852	460	1.9	14.3	2.5	UP
19	LEVEL FLIGHT	299	660	0.44	852	460	2.7	18.7	1	UP
20	STEADY MAN.	299	660	0.44	852	460	2.7	18.7	2.5	UP
21	LEVEL FLIGHT	249	550	0.44	803	433.6	2.7	19.5	1	UP
22	STEADY MAN.	249	550	0.44	803	433.6	2.7	19.5	2.5	UP
23	LEVEL FLIGHT	249	550	0.48	803	433.6	2.7	19.5	1	UP
24	LEVEL FLIGHT	202	445	0.44	732	395	2.7	20.7	1	UP
25	STEADY MAN.	202	445	0.44	732	395	2.7	20.7	2.5	UP
26	STEADY MAN.	299	660	0.44	972	525	2.9	18.	2.5	UP
27	STEADY MAN.	311	685	0.44	972	525	1.9	12.5	2.5	UP
28	STEADY MAN.	313	690	0.44	778	420	1.25	10.4	2.5	UP
29	STEADY MAN.	318	700	0.44	722	390	0.90	6.7	2.5	UP
30	STEADY MAN.	318	700	0.44	722	390	0.90	6.7	2.5	UP
31	STEADY MAN.	313	690	0.44	491	265	1.25	16.0	2.5	UP

ORIGINAL PAGE IS  
OF POOR QUALITY

Panel point loads are formed into a stacked matrix as shown in Figure 5-20 for each stiffness concept. Each condition is included twice in the antisymmetric section of the matrix. Odd numbered columns, then, include loads for positive maneuvers and even numbered columns include loads for negative maneuvers.

Longitudinal Time Histories. - Flight loads during checked and unchecked pitching maneuvers were determined by solving the linear two-degree-of-freedom flexible body equation of motion for airplane longitudinal response. Total airplane response parameters and horizontal tail airload for either steady or transient maneuvers were determined.

Lateral Time Histories. - Flexible body equations of motion for airplane lateral response were employed to obtain rolling velocity and acceleration, and control deflection angles during a roll maneuver.

#### Net Loads Comparison

The loads calculation result in matrices of net loads over hundreds of panel points on the aircraft for every case analyzed. Since it is not practical to reproduce these data, bending moment and shear curves are presented for the most severe loading condition (Condition 31, Steady Maneuver at Mach 1.25).

A sketch of the wing planform is shown in Figure 5-21 indicating reference axis for loads data presentation. All load cuts are made perpendicular to the load axis at the station indicated. The axis is skewed in the outer wing region to give a more meaningful representation of the loads.

A comparison of the net integrated loads for Condition 31 are presented in Figures 5-22 through 5-25 for the three structural arrangements. For the wing structure, the monocoque design consistently displays the highest loads and the chordwise stiffened design the lowest loads. Similar trends resulted for the fuselage as depicted by the vertical shear variation shown in Figure 5-25.

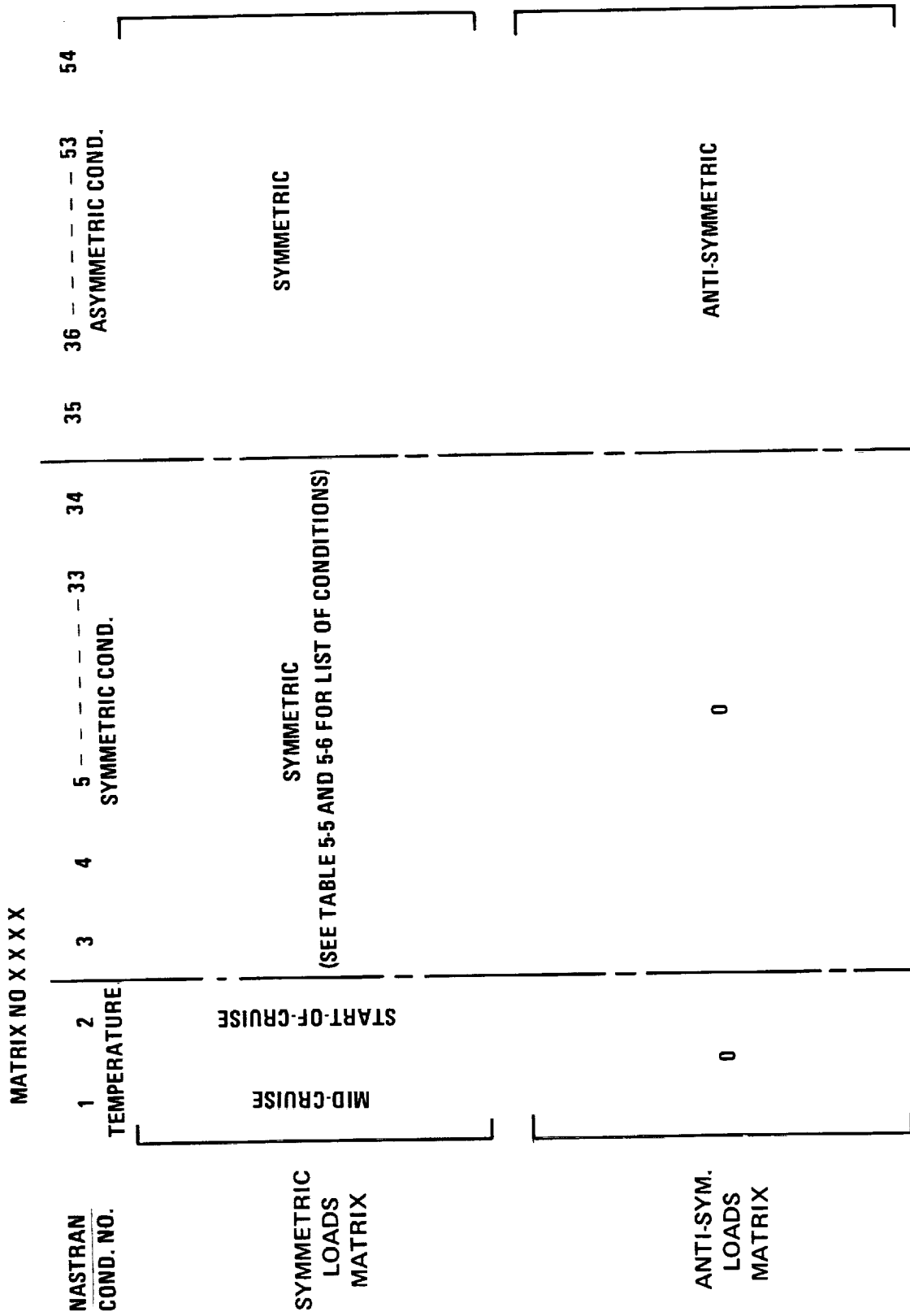


Figure 5-20. Static Aeroelastic Loads Matrix



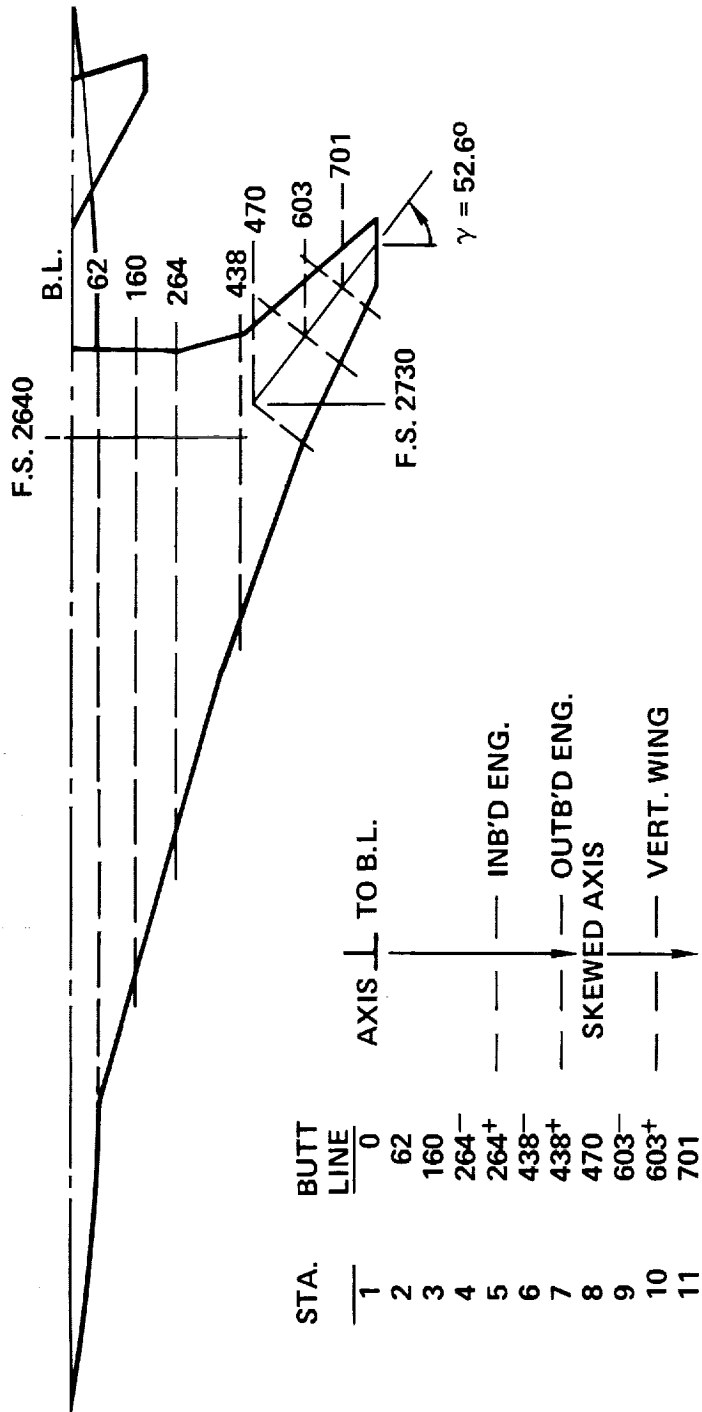


Figure 5-21. Wing Load Integration Axis

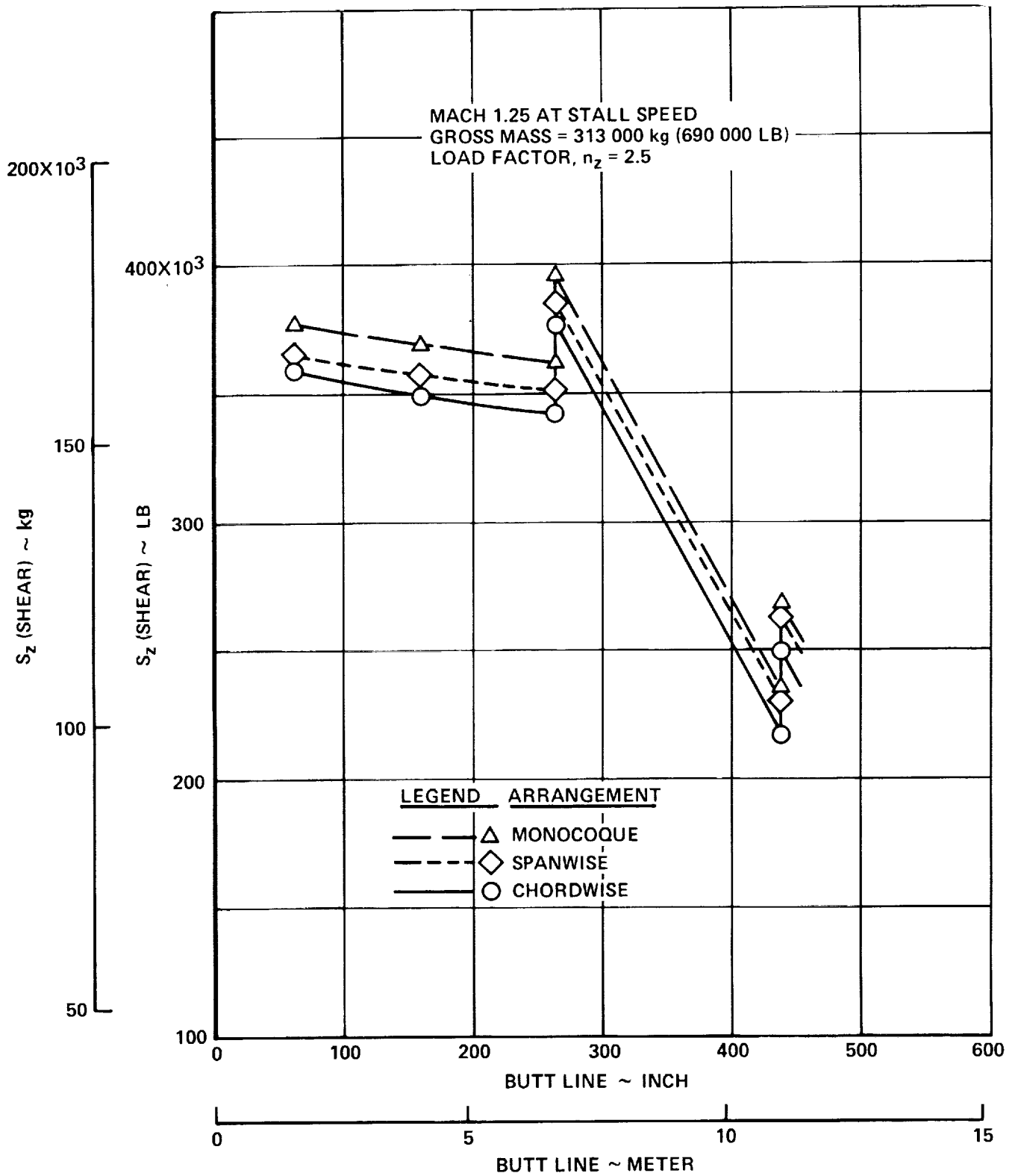


Figure 5-22. Wing Shears for Structural Arrangements

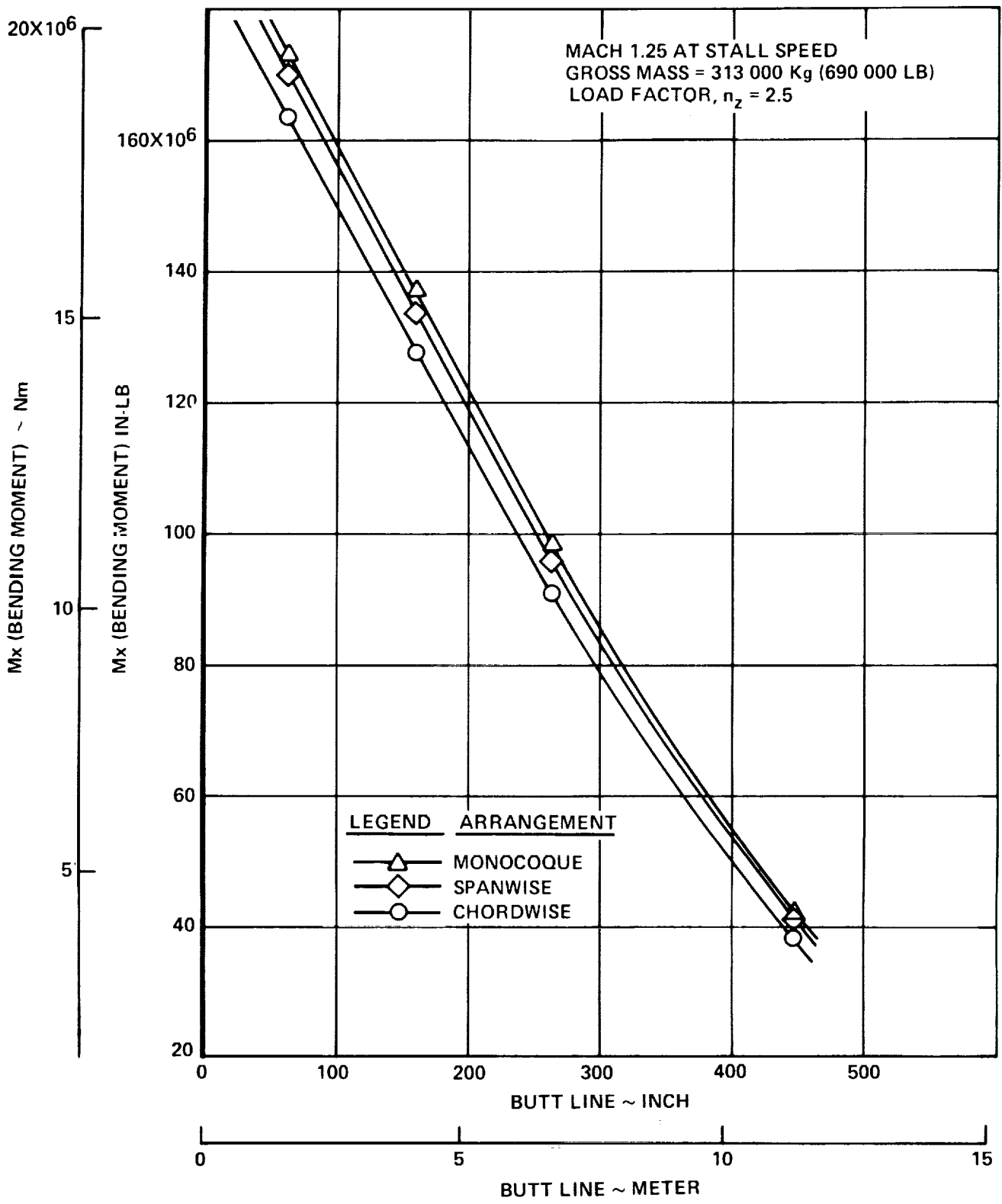


Figure 5-23. Wing Bending Moments for Structural Arrangements

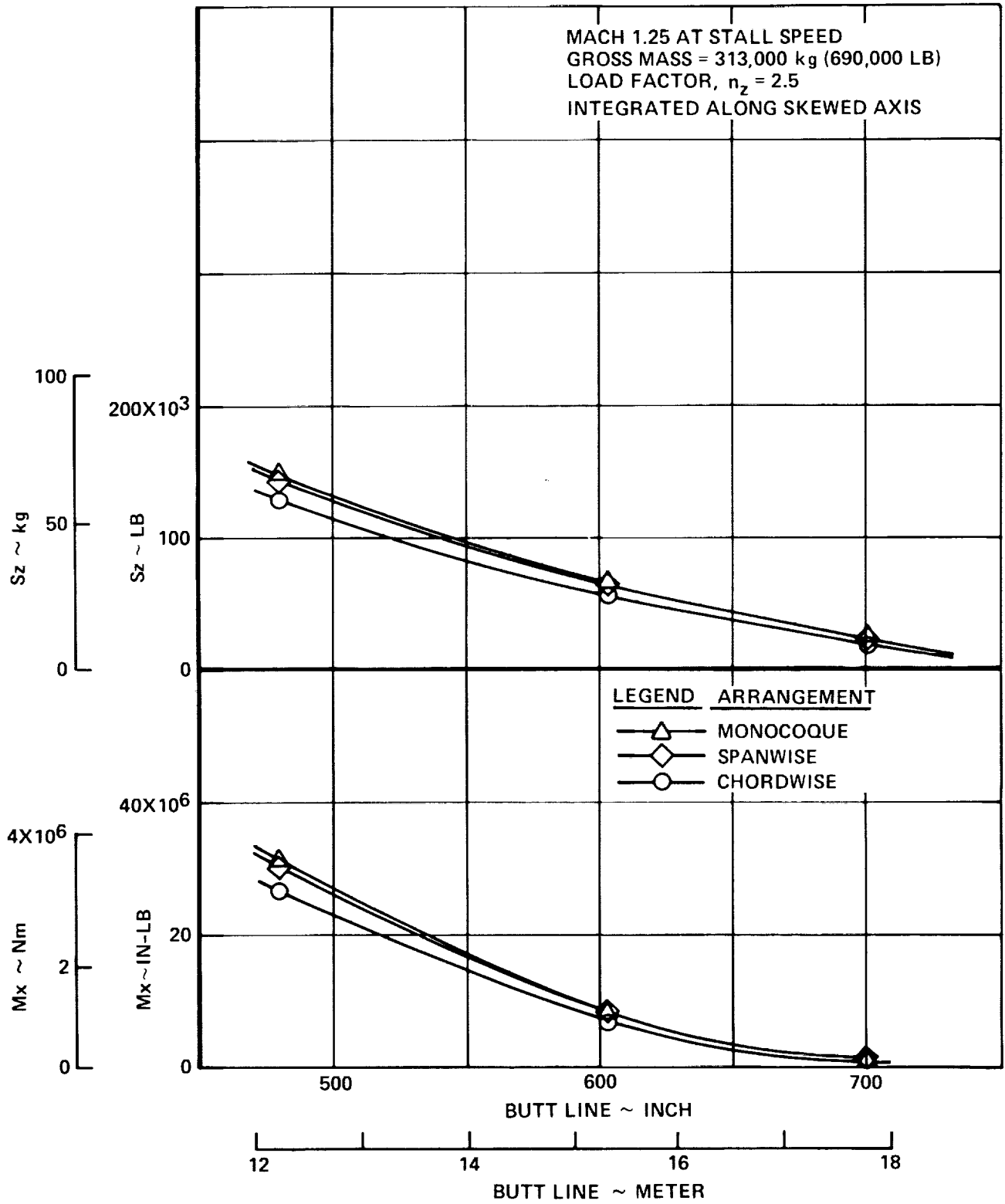


Figure 5-24. Outer Wing Shears and Bending Moments for Structural Arrangements

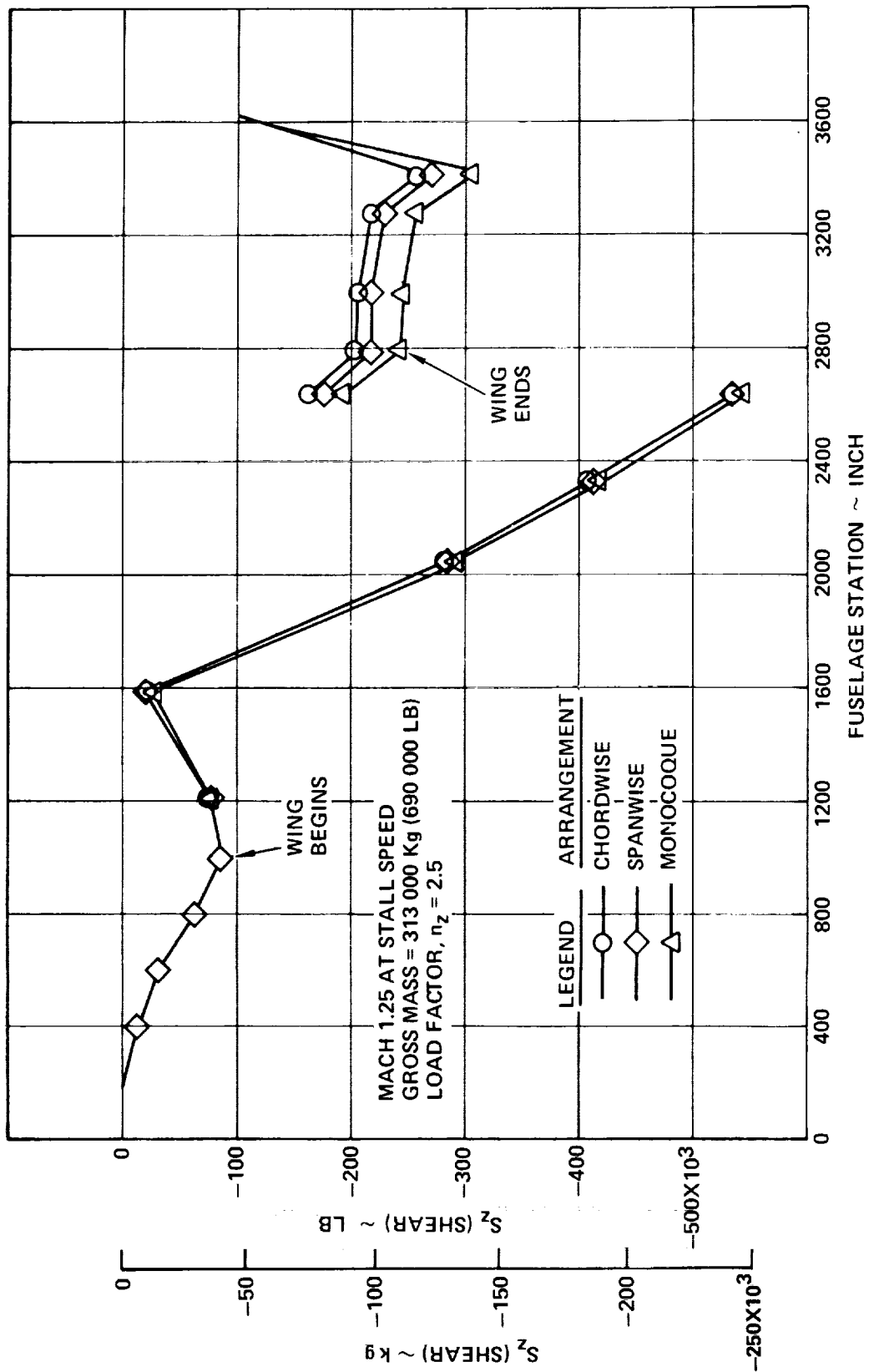


Figure 5-25. Net Fuselage Shears for Structural Arrangements

Net wing load envelopes are presented in Figures 5-26 through 5-31 for the chordwise stiffened, the spanwise stiffened and the monocoque designs. The load envelopes are for two locations on the wing structure: (1) the fuselage side at BL 62, and (2) the outer wing joint at BL 470. The data displays the relationship between the wing bending moment and torsion for the condition evaluated. A comparison of the envelope for the three structural arrangements indicates similar trends with Condition 31 yielding the maximum bending moment at both wing locations. The maximum torsional loads for the inboard location results from a steady maneuver at Mach 0.90 (Condition 30); the Mach 1.25 steady maneuver (Condition 31) results in maximum torsional loads at BL 470.

#### Application of Measured Pressure Data

Net Loads Effect. - Static aeroelastic loads were generated for a Mach 2.7 symmetrical maneuver condition using both wind tunnel measured pressure data and the theoretical distribution based on Mach Box theory. Pressure on the wing grid system were obtained by interpolation of the corrected data and factored to obtain the lift on each grid element area. The latter distributions at each angle of attack were combined into a matrix format for application to the net loads program. The data in these matrices were used to define all the airloads on the airplane due to angle of attack. Redistribution of airloads due to flexibility is computed from theoretical aerodynamic influence coefficients.

The influence of the measured pressure data on the wing and fuselage loads are shown in Figures 5-32 through 5-35. Reduced values of shear, bending moment and torsion at all span stations and reduced shears at all fuselage stations by application of the pressure data is noted.

These results occur primarily from the large reduction in tip loading by the measured data (Figure 5-32) causing a significant inboard shift of the spanwise center of pressure. Reductions in net torsion are less pronounced (Figure 5-34) in the vicinity of the fuselage due to the more forward location of the chordwise center of pressure from measured data at these inboard locations.

Span Loading Distribution. - Measured wind tunnel data were reduced and then integrated to obtain spanwise loading distributions over a wide range of angles of attack at Mach 2.7. Theoretical spanwise loading distributions were developed using the Mach Box method.

The Mach Box method, based on oscillating source-sink singularities, described a supersonic flat plate wing. The program included incidence, camber, twist, taper and sweep on a restricted set of planforms and other geometry in such combinations that the perturbation of the free stream is small.

Span loading distributions from each method are shown at two airplane angles of attack on Figure 5-36. The lower angle of attack is within the linear range of wing lift coefficient as a function of angle of attack. The wind tunnel measured data indicates a significant unloading of outboard wing stations with a high section loading near the fuselage. In comparison with the wind tunnel data, the Mach Box results display a higher loading at outer wing locations and a lower loading at inboard locations near the fuselage intersection. The Mach Box data represents a wing lift equal to that from integrated pressure data although with a more outboard center of pressure location. Available force data indicates a higher wing lift but with the same slope.

Differences between the span loading distributions beyond the linear  $C_L$  versus  $\alpha$  range are more pronounced with the relationships between the two distributions as previously described. Both force data and integrated pressure data displayed on Figure 5-37 confirm the non-linear trend of wing lift coefficient at higher angles of attack. The Mach Box method is linear and does not display this tendency.

The results of the above investigations, which were based on a limited amount of wind tunnel measured pressure data at Mach 2.7, were inconclusive concerning the choice between using the theoretical aerodynamics or wind tunnel test data for generating panel point loads. Since correlation was not obtained, the design loads for both the subsonic and supersonic flight regime were based on the applicable theoretical aerodynamics (DLLE and Mach Box) and adjusted to reflect the measured steady state lift coefficients and aerodynamic centers derived from the wind tunnel force data.





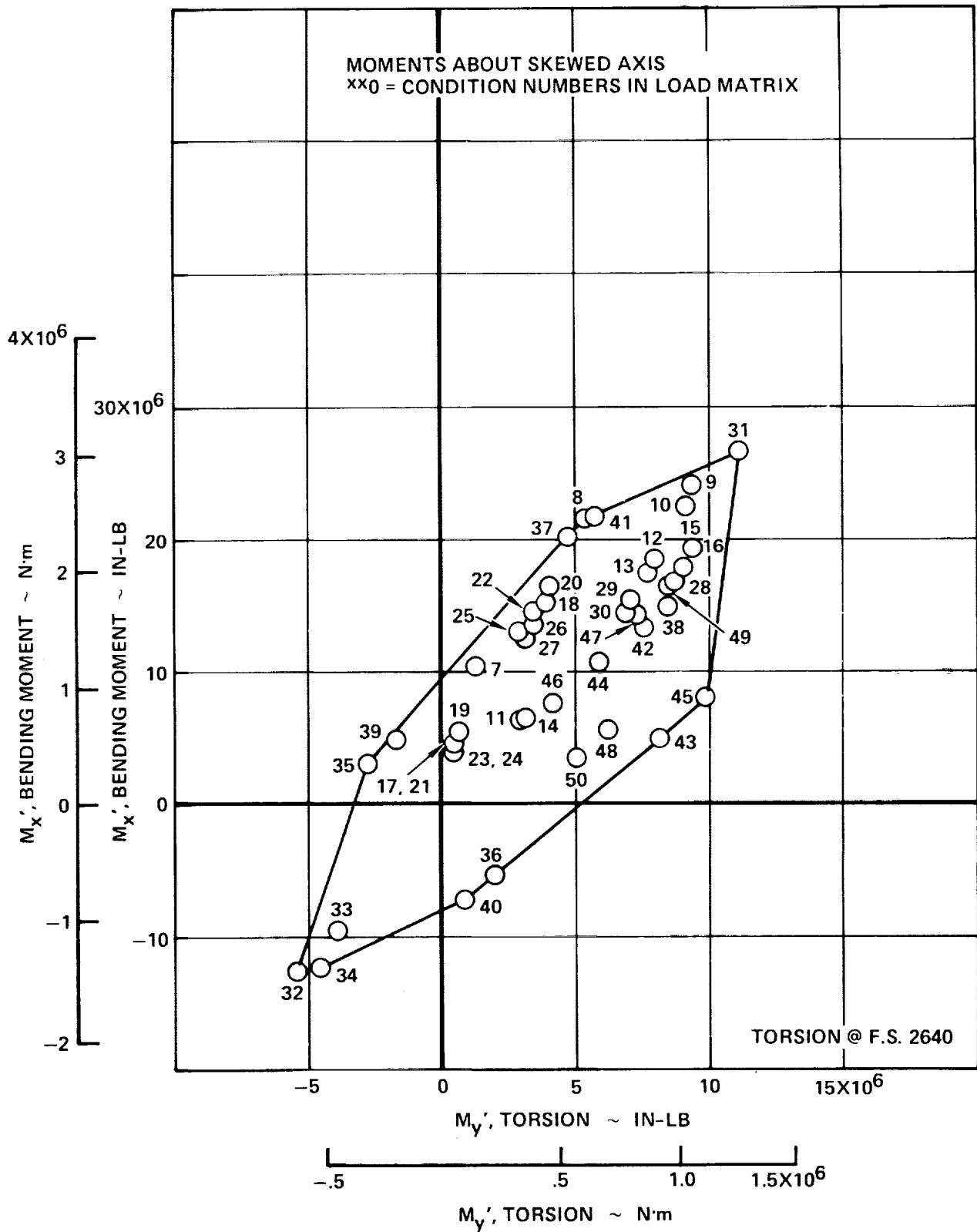


Figure 5-27. Net Loads Envelope - Chordwise Stiffened - BL 470.0

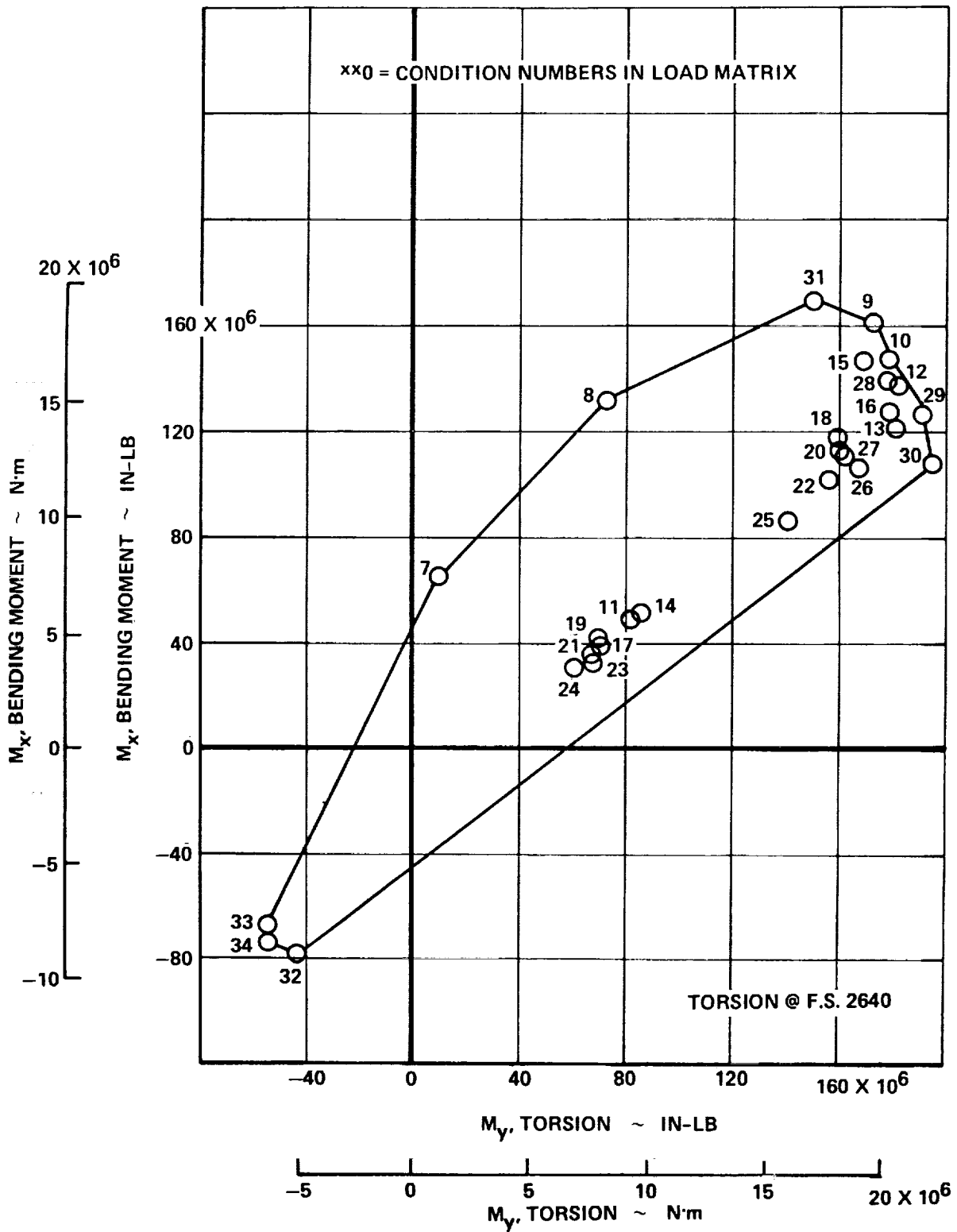


Figure 5-28. Net Loads Envelope - Spanwise Stiffened - BL 62.0

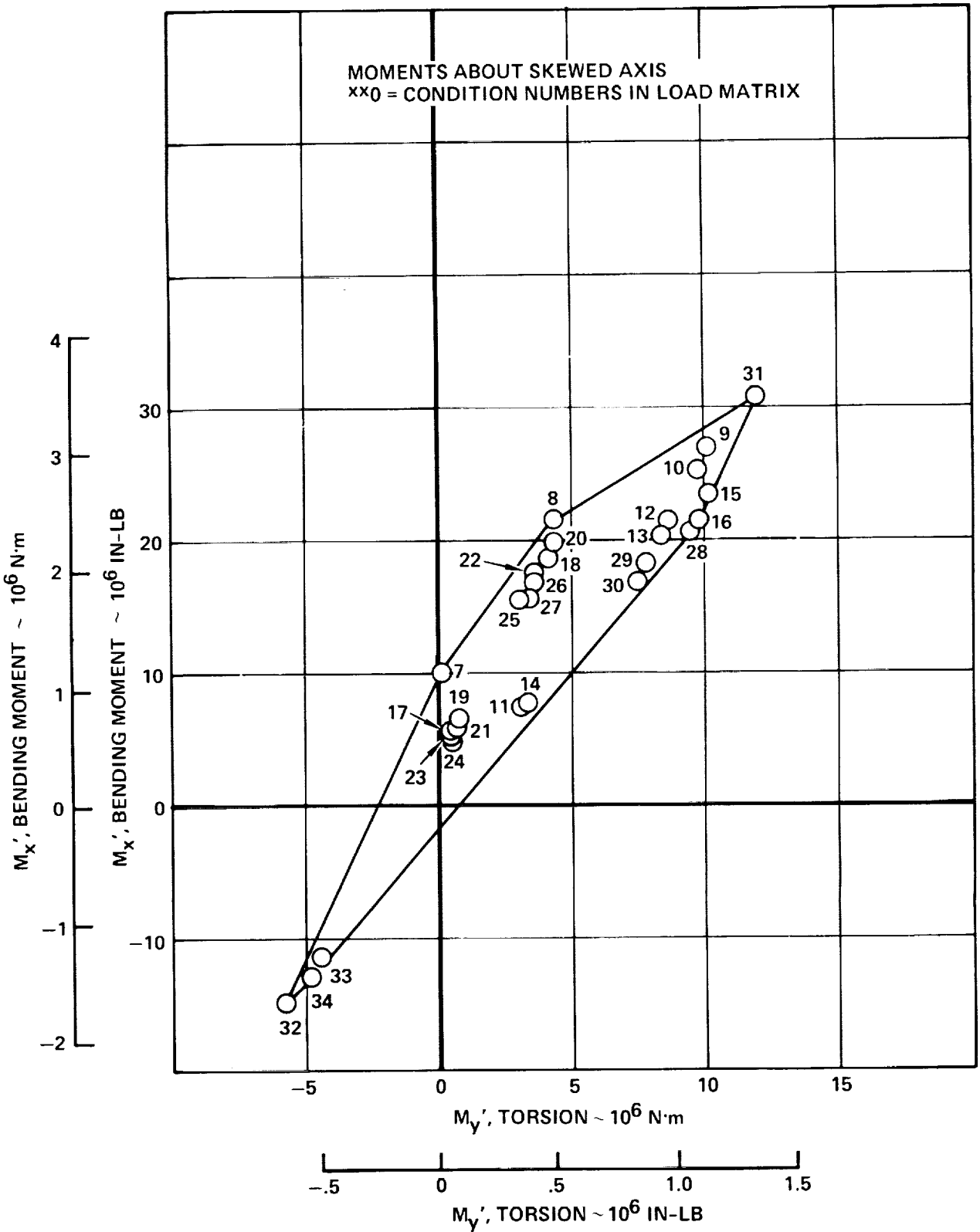


Figure 5-29. Net Loads Envelope - Spanwise Stiffened - BL 470.0

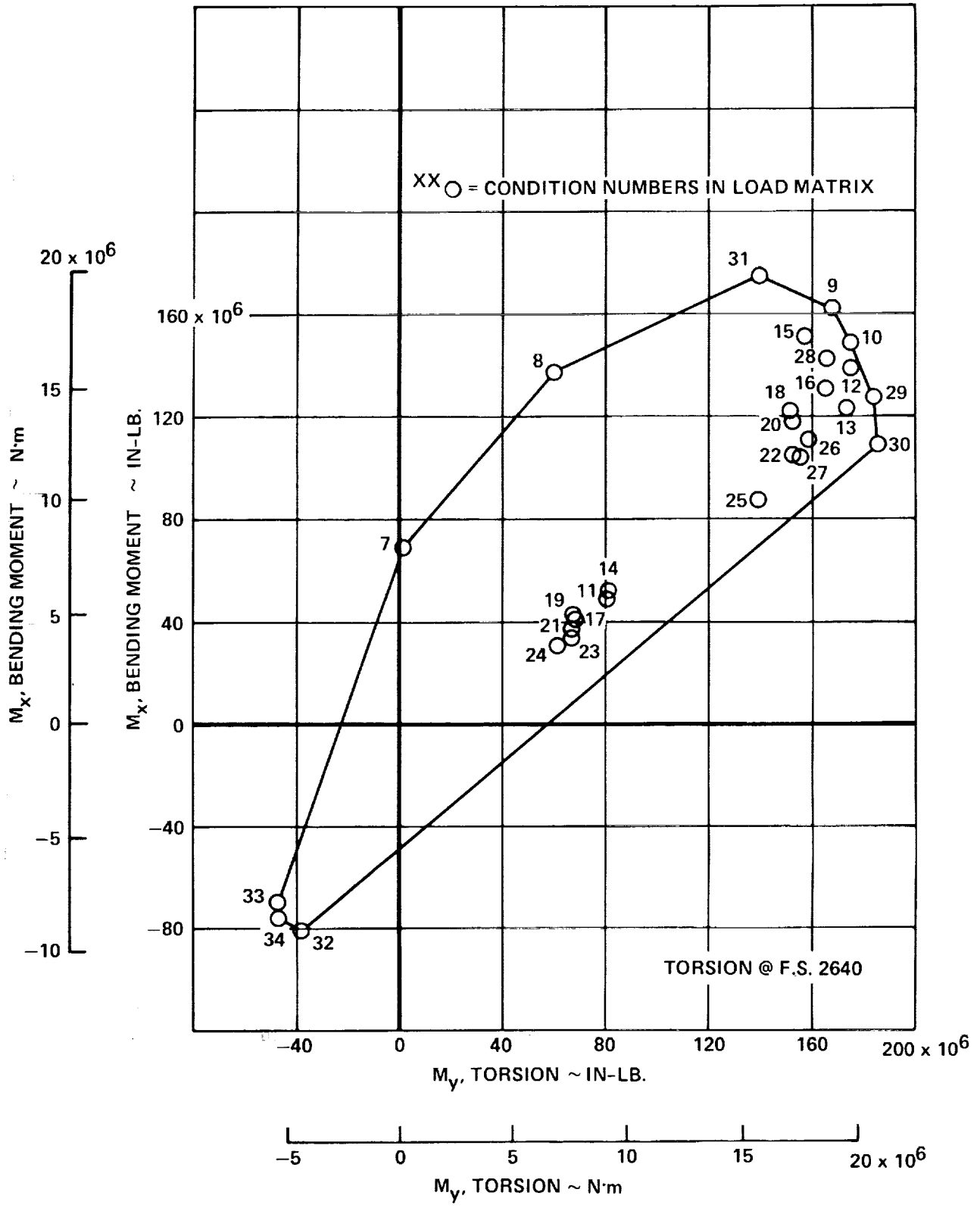


Figure 5-30. Net Loads Envelope - Monocoque - BL 62.0

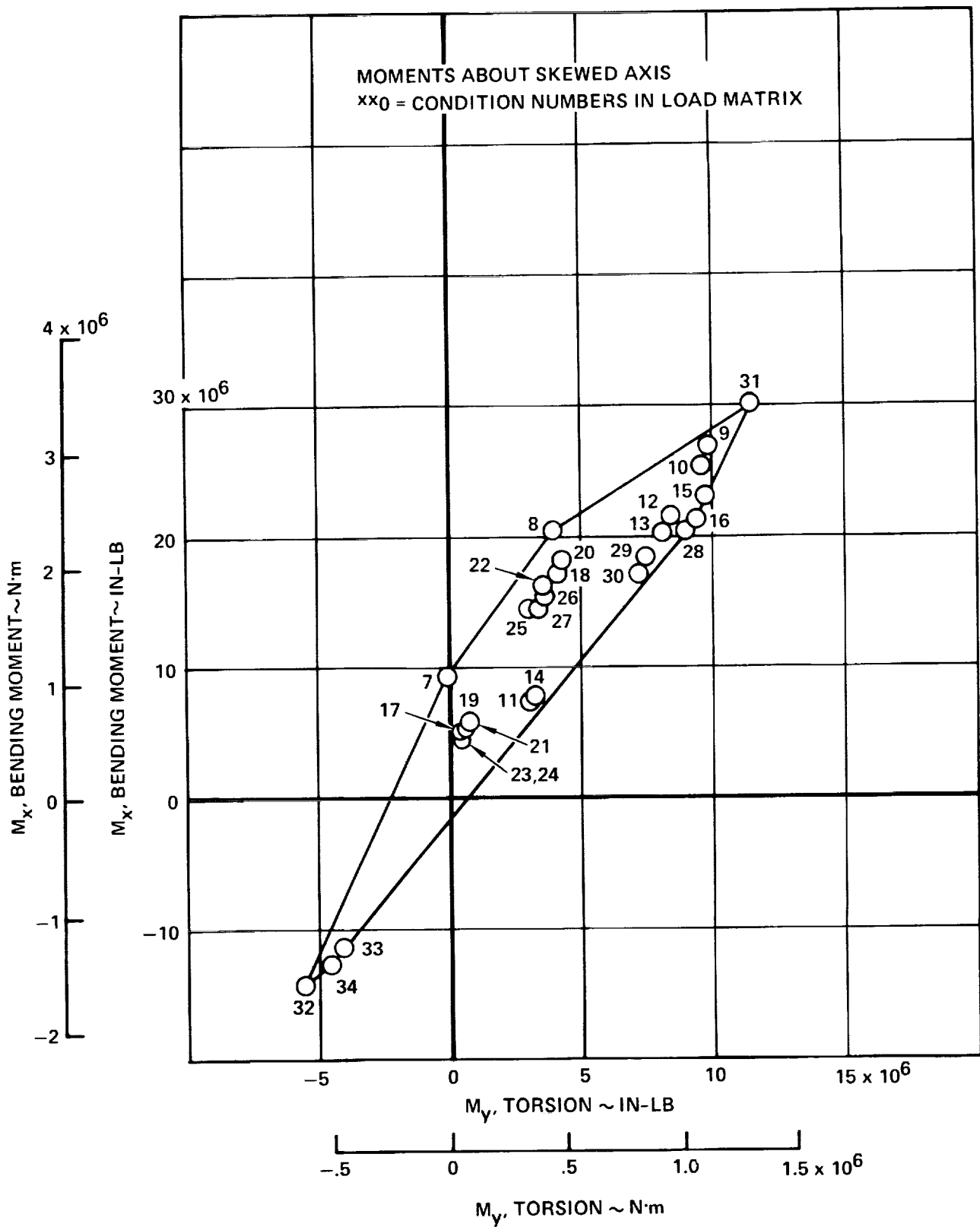


Figure 5-31. Net Loads Envelope - Monocoque - BL 470.0

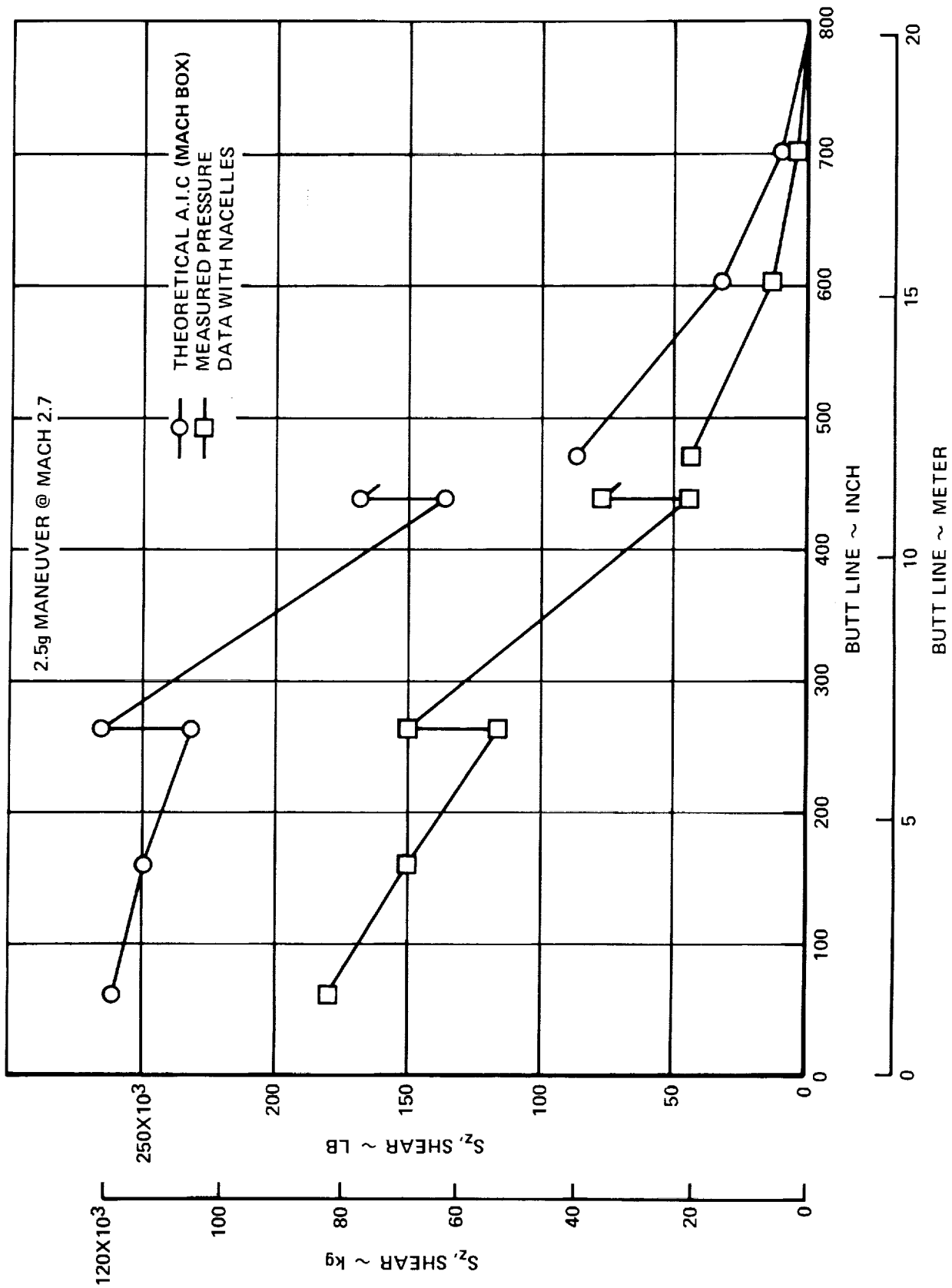


Figure 5-32. Net Integrated Wing Shears - Theoretical vs Measured

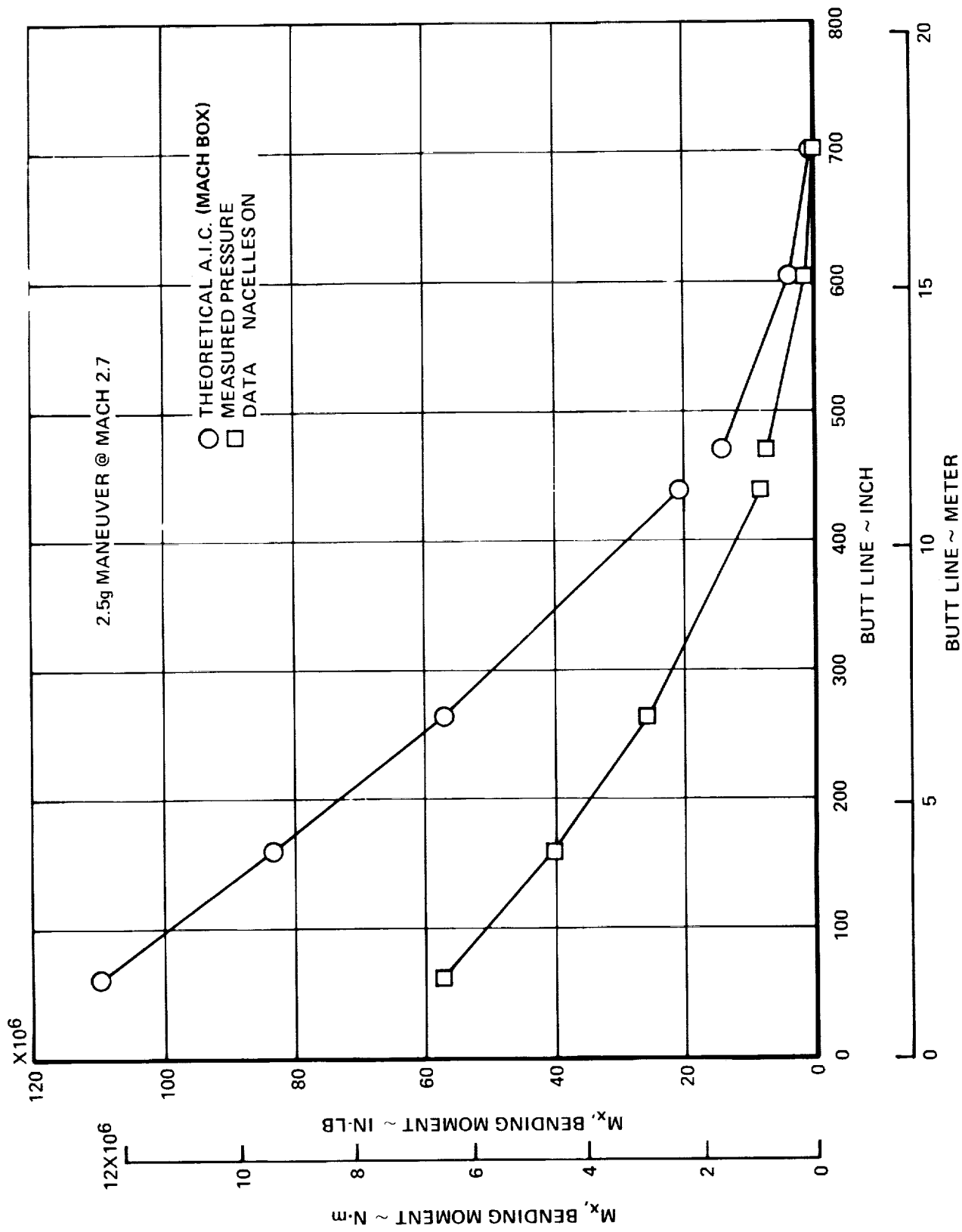


Figure 5-33. Wing Bending Moments - Theoretical vs Measured



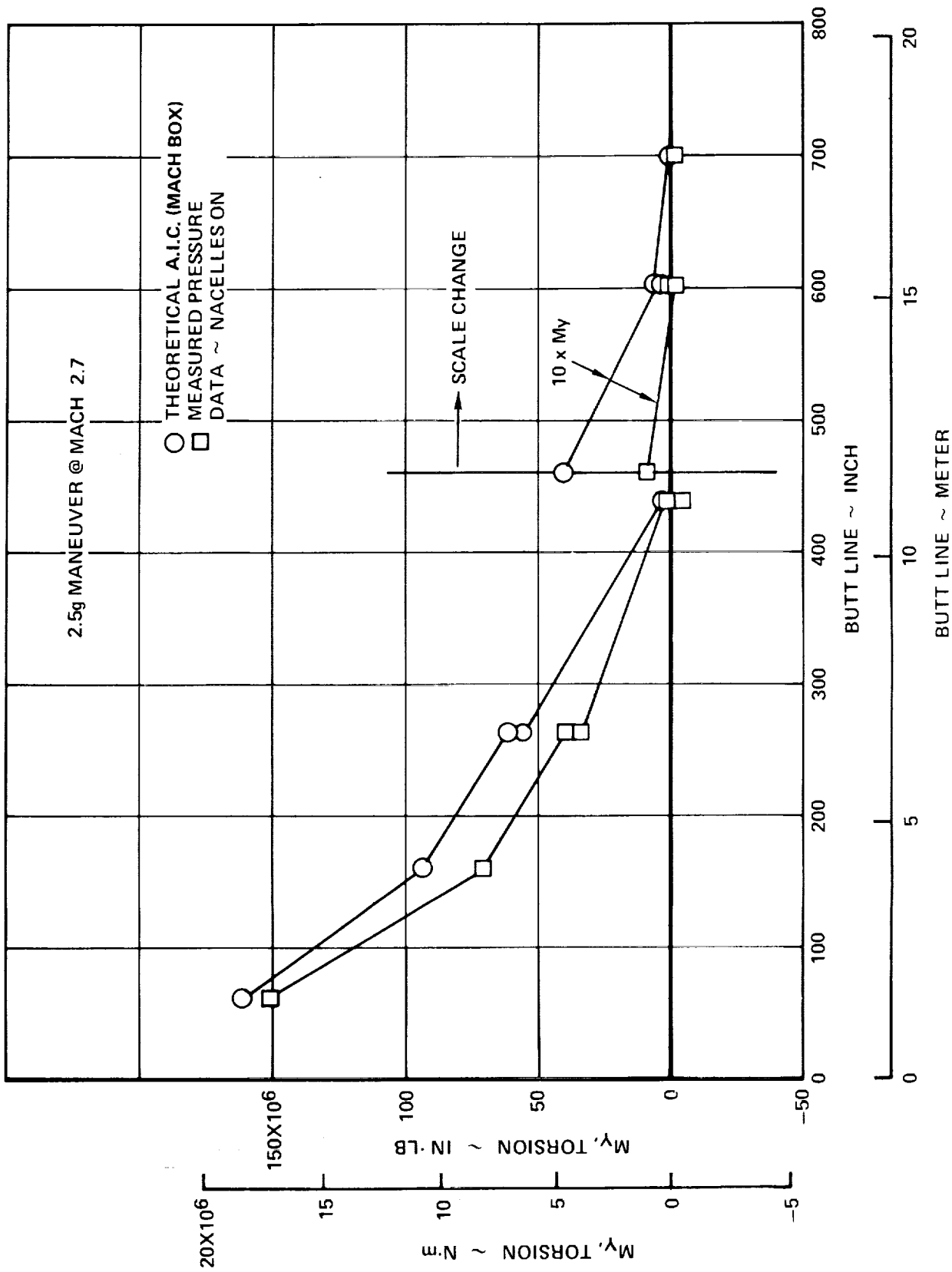


Figure 5-34. Wing Torsion - Theoretical vs Measured

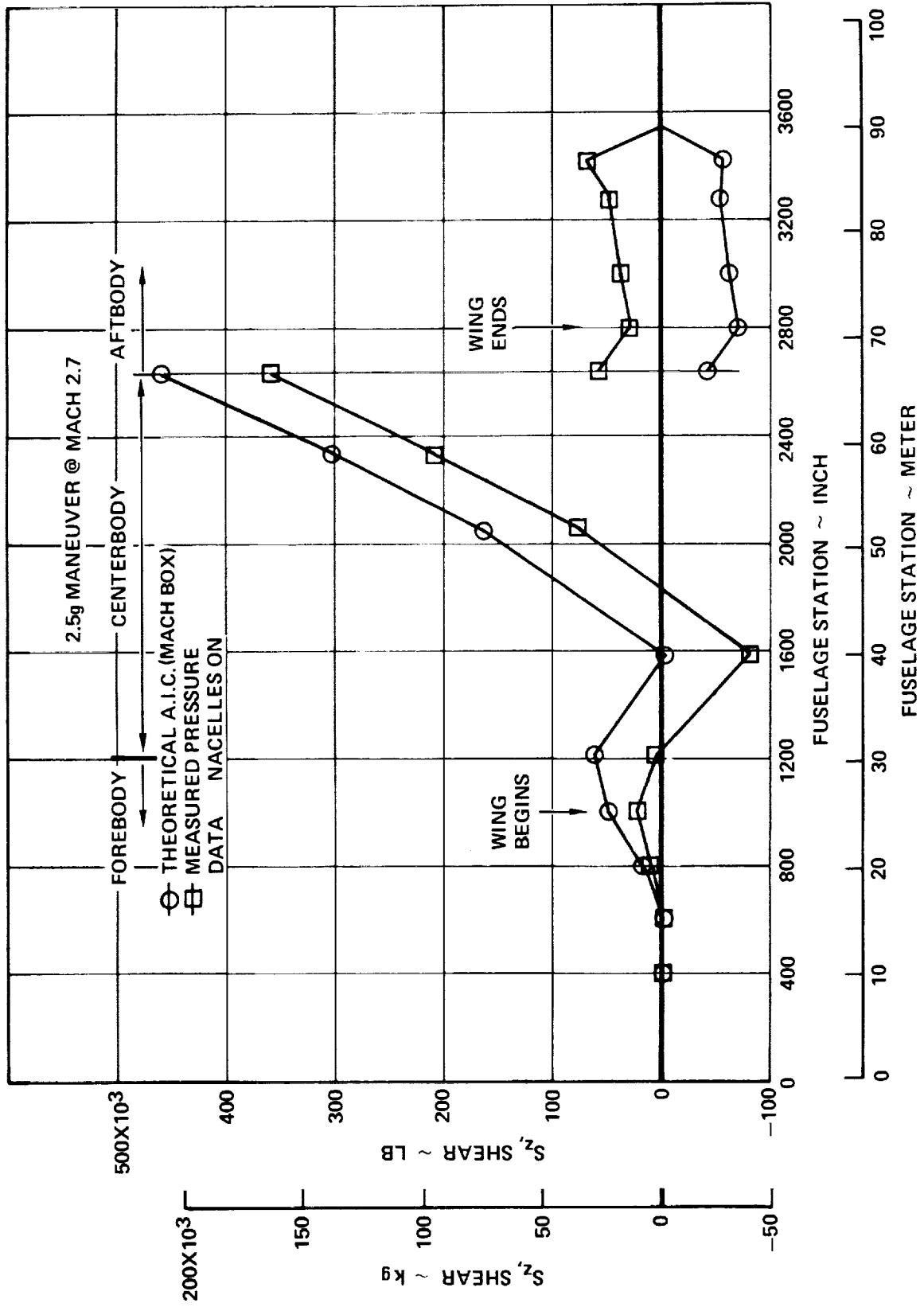


Figure 5-35. Net Integrated Fuselage Shears - Theoretical vs Measured

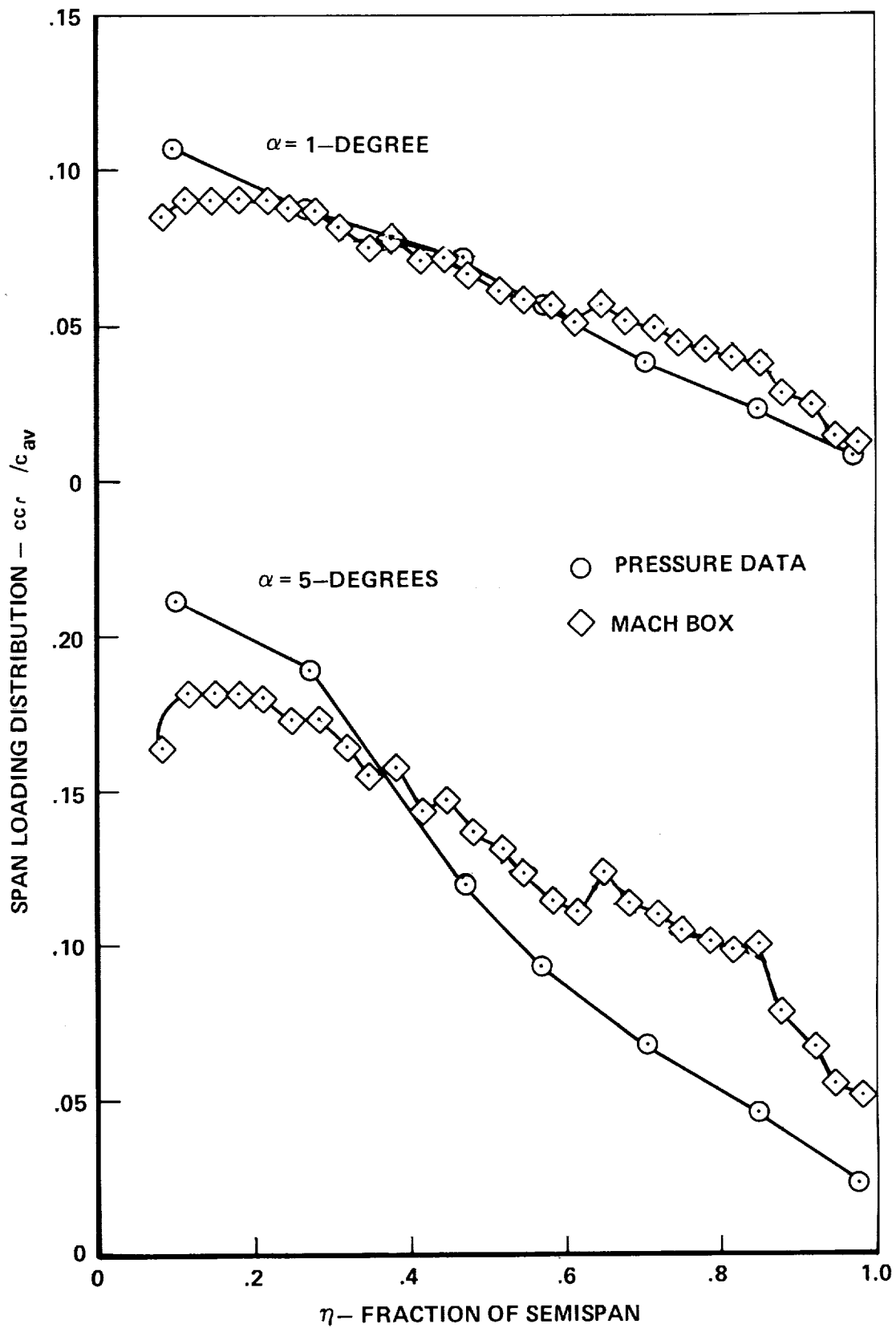


Figure 5-36. Span Loading Distribution - Mach 2.7

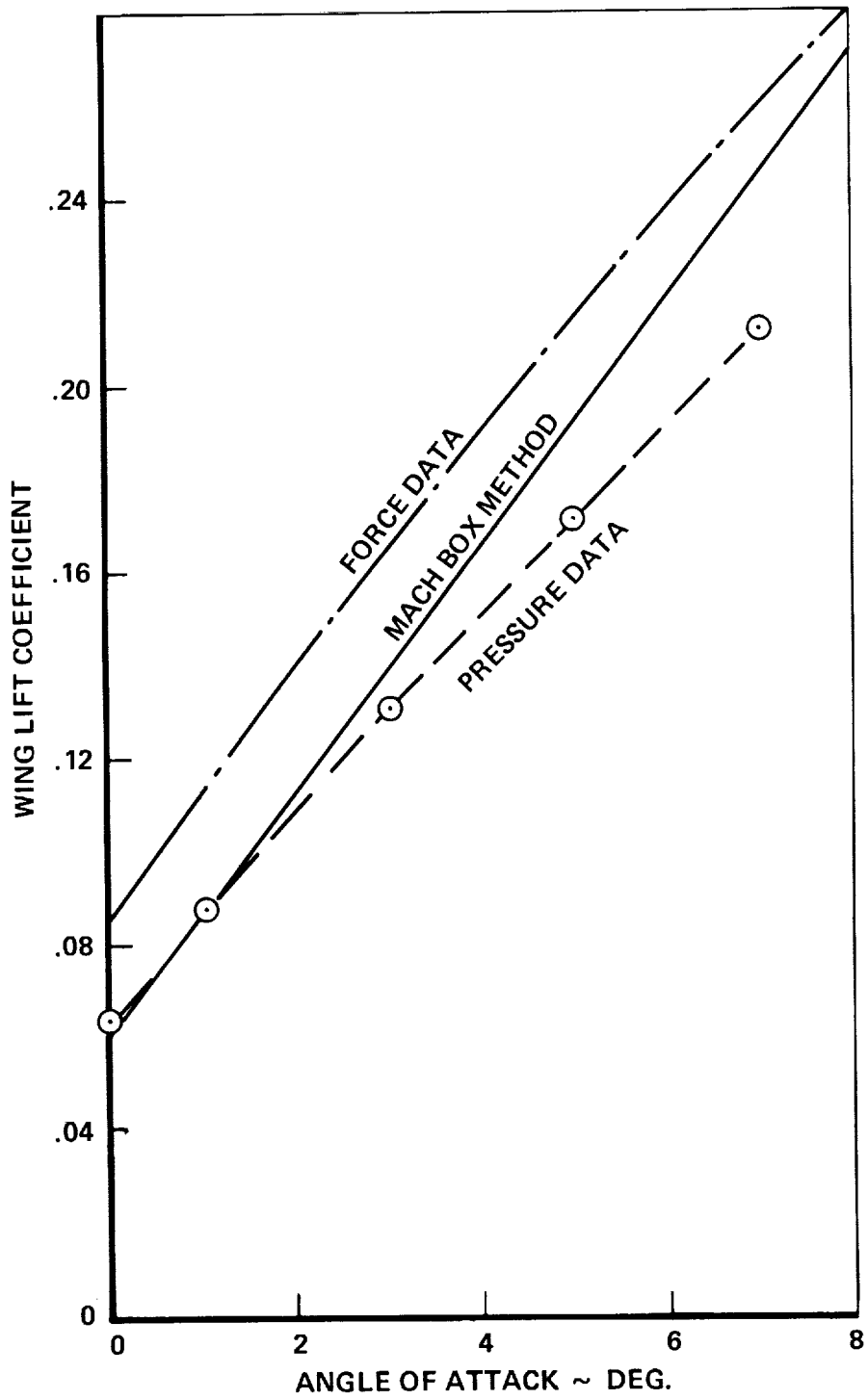


Figure 5-37. Wing Lift Coefficients - Mach 2.7

## DESIGN LOADS - TASK IIA

The Analytical Design Studies of Task I focused attention on assessing the relative merits of the various structural design concepts and identifying the importance of the interactive parameters that influence the design of a supersonic cruise aircraft. Only those configuration refinements that would have primary influence on concept selection were made. For the Task II effort, the baseline configuration adopted all recommendations made in regards to the three areas of concern delineated in Section 2, Baseline Configuration. Collectively these changes, as shown in Figure 5-38, could impact the results of the Task I significantly. Thus, to provide continuity between Task I and Task II, an abbreviated study was conducted to determine the effect of the configuration changes.

To support this investigation, a 2-D structural model was established. This model was obtained by revising the coordinates of the Task I chordwise model to reflect the airplane configuration changes:

- Fuselage shortened by 119 inches
- Tip sweep of 60-degrees in lieu of 64.6-degrees
- Added wing area resulting from the tip sweep change

In addition, the mass distribution was adjusted to correspond with the revised center of gravity travel incorporated.

A new set of aerodynamic influence coefficients (AIC's) were calculated for the Mach 0.90 subsonic flight condition. This required updating the AIC model to also reflect the configuration changes. The grid transforms (AIC to SIC) were revised and the net loads calculated for the Mach 0.90 symmetric maneuver condition. This condition included four load factors for each velocity ( $V_C$  and  $V_A$ ) investigated. The load factors were: (1) a positive 1-g, (2) a positive 2.5-g steady maneuver, (3) a 2.5-g transient maneuver and (4) a negative 1.0-g flight attitude.

## Net Loads Summary

Net loads that were developed for the 2.5-g steady maneuver at Mach 0.90 at 30,000 feet altitude (325 KEAS) are presented in Figures 5-39 and 5-40. A comparison of the integrated shears and bending moments are presented in the figures. The increase in the outer wing loading due to the increased area of the outer wing is apparent by the change in net shears outboard of BL 470. The lower magnitude of shears at the inboard locations result from the reduced balancing tail load due to the aft center of gravity shift and to the redistribution of the aeroelastic loading.

## Results

This abbreviated study indicated that the effects of configuration and mass balance changes on the structural design loads were significant. The change in planform resulted in an increase in the outer wing loading. The net wing bending loads, however, remained unchanged because of the positive balancing tail load, which in essence, reduced the net wing loads. The positive tail load, furthermore, reversed the sense of the aftbody bending moments and resulted in significant changes in the chordwise loading of the inboard wing.

The fact that the response of the structure to the externally applied loads can be logically explained enables one to interpret with confidence the Task I results into the Task IIB domain. Thus, continuity between the initial analytical task and the detailed design studies is provided.

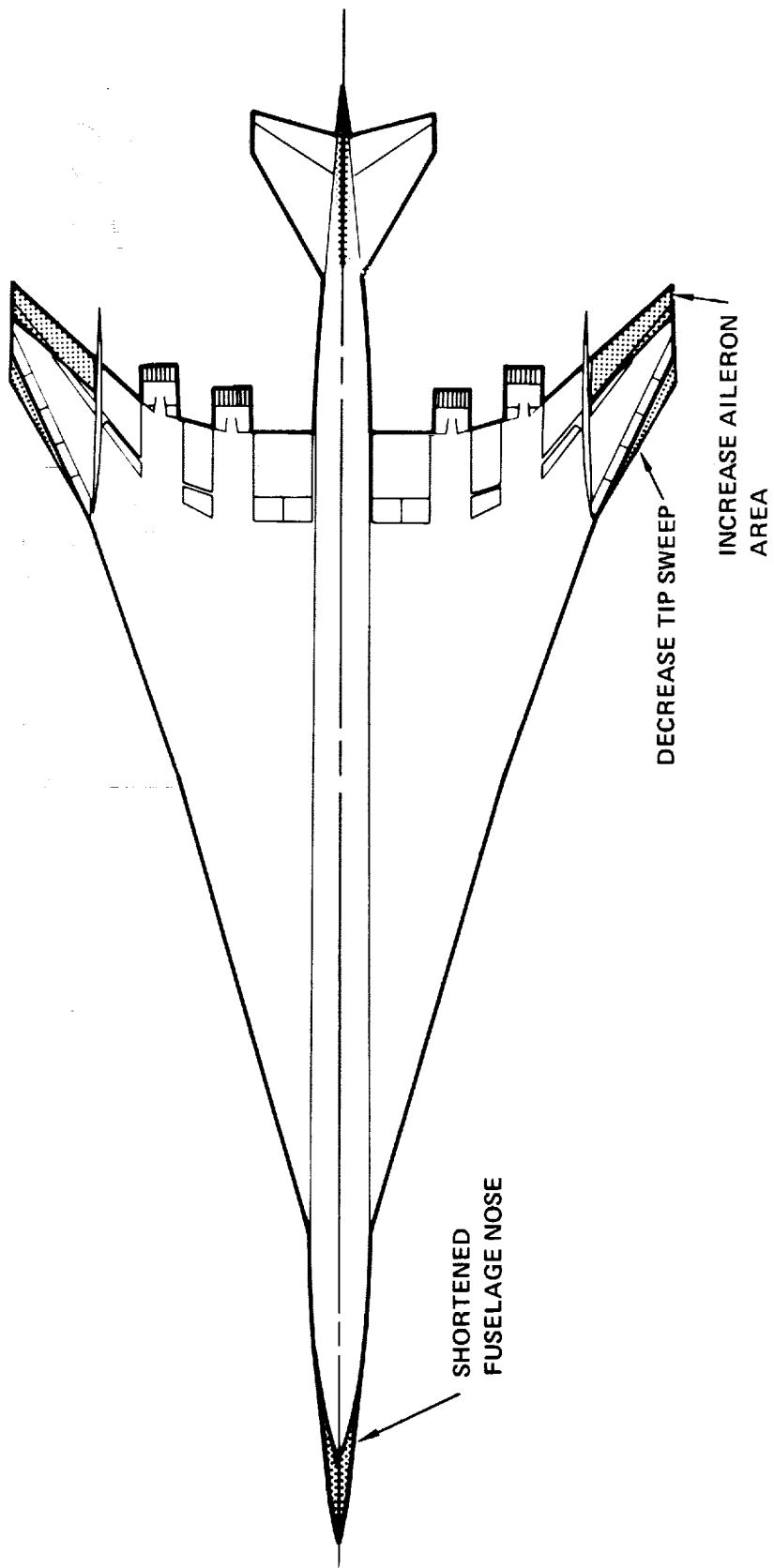


Figure 5-38. Configuration Comparison - Task I and Task IIA

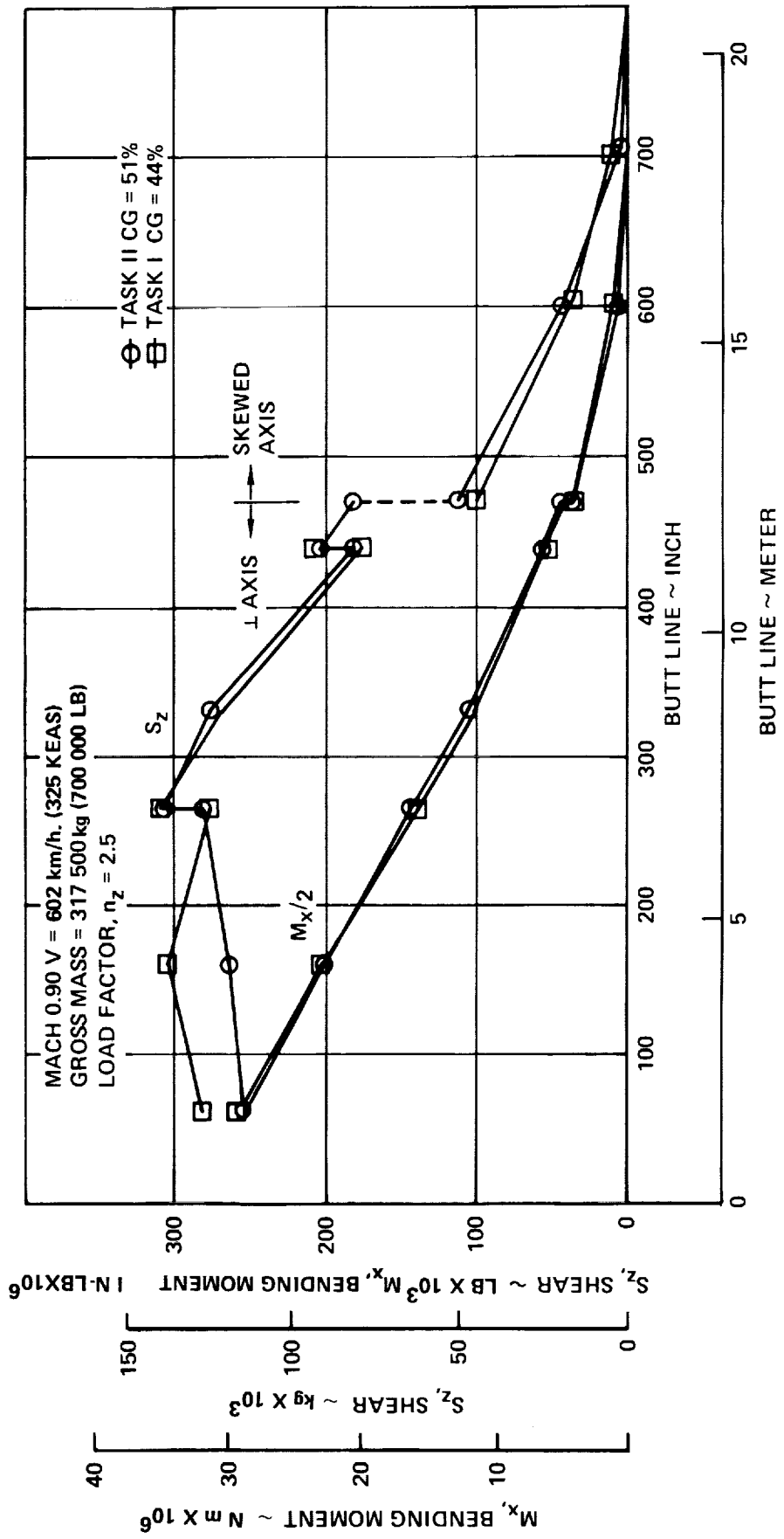


Figure 5-39. Wing Shears and Bending Moments - Task IIA



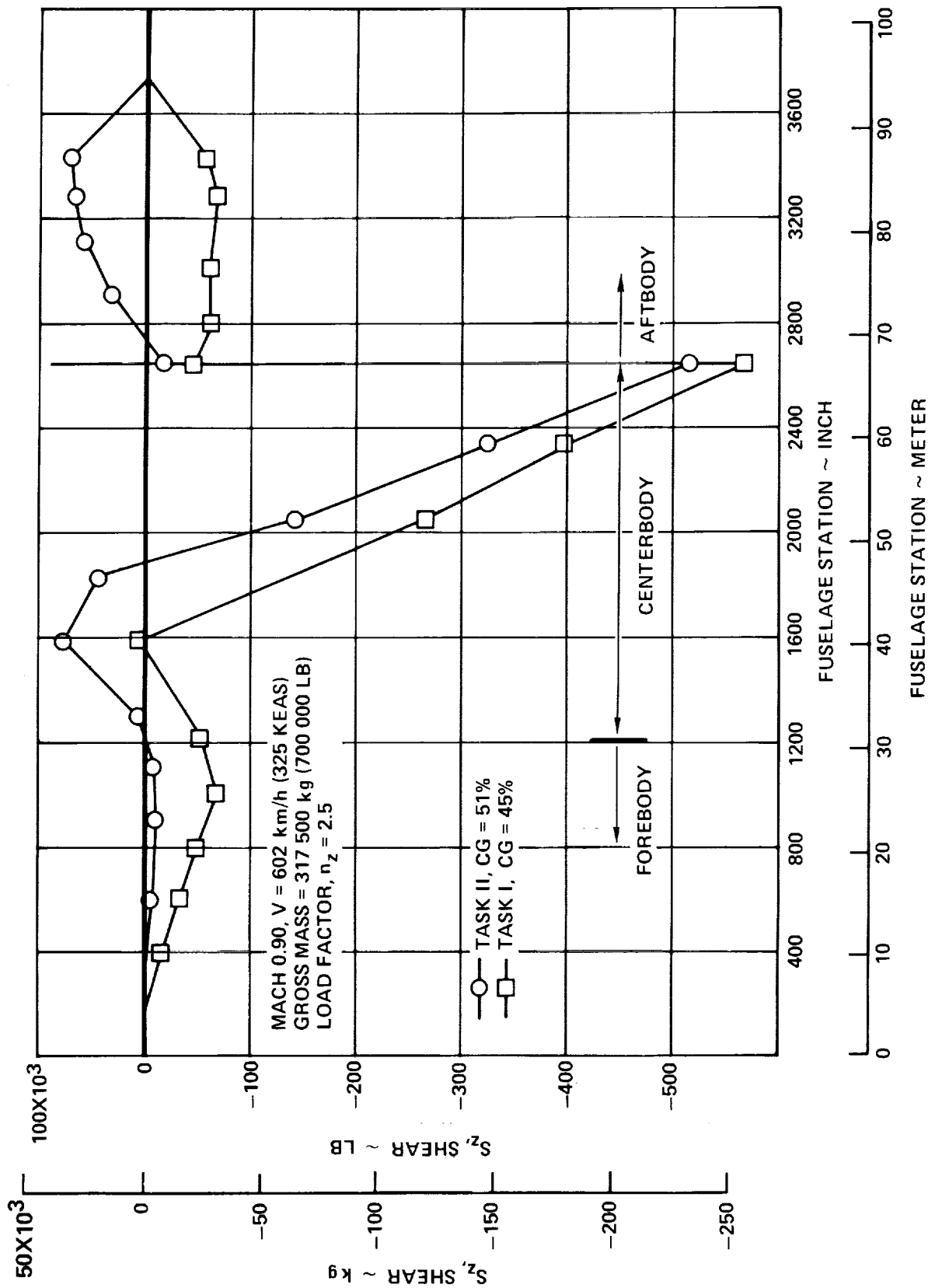


Figure 5-40. Net Integrated Fuselage Shear - Task IIA

## DESIGN LOADS-TASK IIB

The configuration refinements identified in Section 2, Baseline Configuration Concept, were adopted for the Task II detail design study. The structural approach selected for further analysis was a hybrid structural arrangement consisting of the chordwise-stiffened design for the wing structure inboard of BL 406 and the monocoque design for the stiffness critical wing tip structure. A three-dimensional (3-D) structural model, described in Section 9, Structural Analysis Model, was used with strength-designed and strength/stiffness-designed flexibilities.

### Strength Design

The scope of the structural design loads analyses for the strength-design cycle is presented in Figure 5-41. The interrelationship with the other disciplines directly involved in the design cycle are indicated on the figure. The analyses were performed (1) to calculate appropriate aerodynamic data, (2) to determine the aeroelastic loads for the critical conditions and format for NASTRAN to obtain the displacements, internal loads and stresses, and (3) to conduct a preliminary assessment of the effect of jig-shape on structural sizing and mass.

Conditions for Design. - The conditions for the loads analysis were selected following the review of the Task I results. Combinations of airplane mass and attitude that produced critical loadings on the wing components were defined following structural analysis of the previously determined loading conditions. In general, the conditions identified on Table 5-7 and shown superimposed on the design airspeed envelope on Figure 5-42, are identical to their predecessors; however, the design maneuvering speed,  $V_A$ , has been established permitting improved definition of the high angle of attack loadings. The latter conditions are redefined to reflect the angle of attack limits for structural design. The design loading conditions include both steady and transient maneuvers as indicated by the two NASTRAN condition numbers for each weight case defined on the table. The parameters for the transient conditions are shown in Table 5-8.

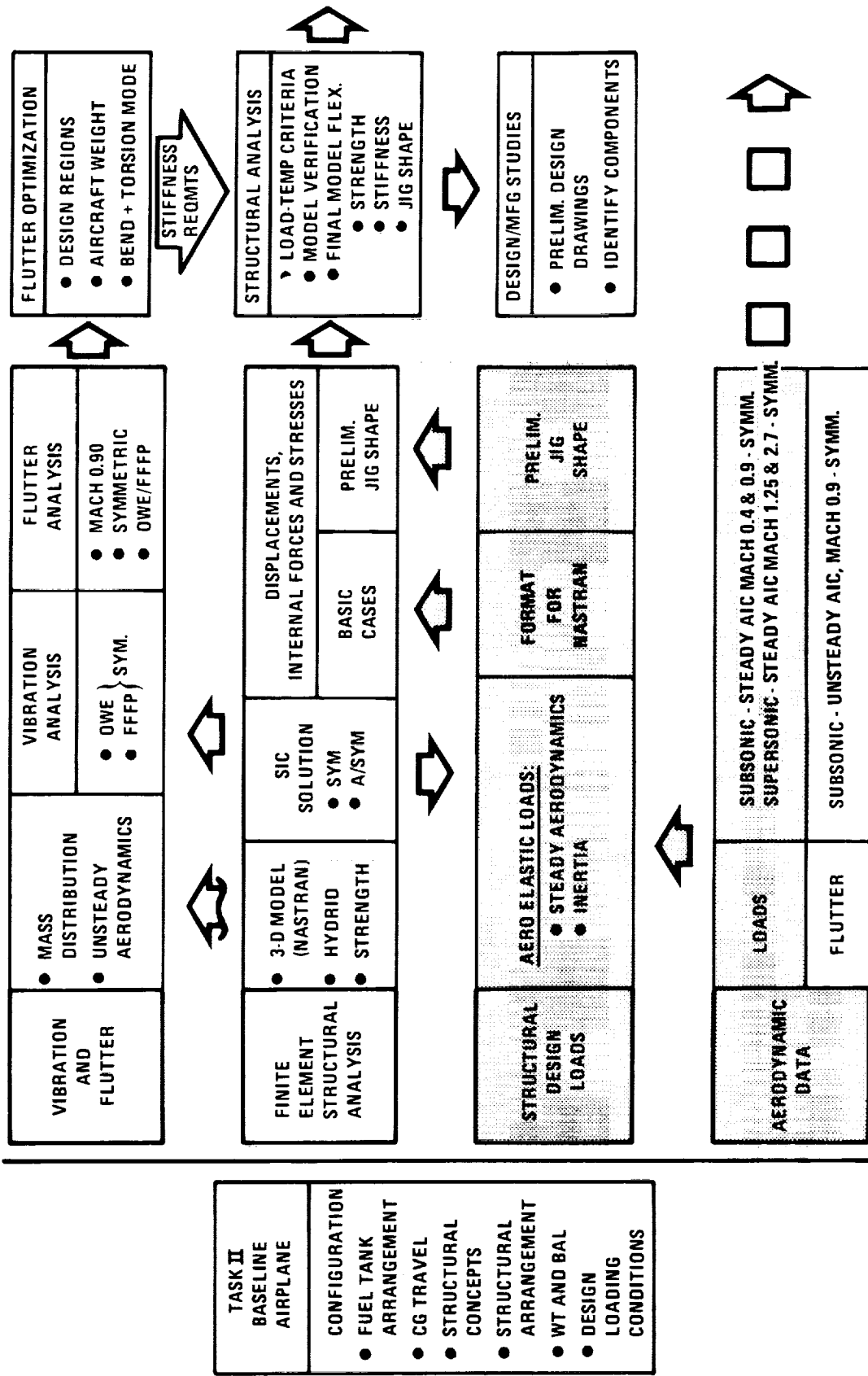


Figure 5-41. Task II Design Cycle - Strength

ORIGINAL PAGE IS  
OF POOR QUALITY

TABLE 5-7. DESIGN LOADING CONDITIONS - TASK IIB STRENGTH

NASTRAN COND. NO.	WEIGHT (1000 LB)	MACH NO.	ALTITUDE (1000 FT)	LOAD FACTOR	AIRSPEED (KNOTS)	REMARKS
4,5	745	0.40	0	2.5	264.6	STRENGTH DESIGN
6,7	700	0.90	36	2.5	282.4	STRENGTH DESIGN
8,9	700	0.90	30	2.5	325	STRENGTH DESIGN
10,11	700	0.90	22	2.5	390	STRENGTH DESIGN
* 12,13	690	1.25	48	2.5	294.3	STRENGTH DESIGN
* 14	690	1.25	48	-1.0	294.3	NEGATIVE NORM. ACCEL.
15,16	690	1.25	38.2	2.5	372	STRENGTH DESIGN
17,18	445	1.25	34	2.5	420	DESCENT - THERMAL
19,20	660	2.70	61.5	2.5	460	START OF CRUISE
21,22	550	2.70	64	1.0	433.6	MID CRUISE (JIG SHAPE)

\* PRELIMINARY JIG SHAPE STUDY

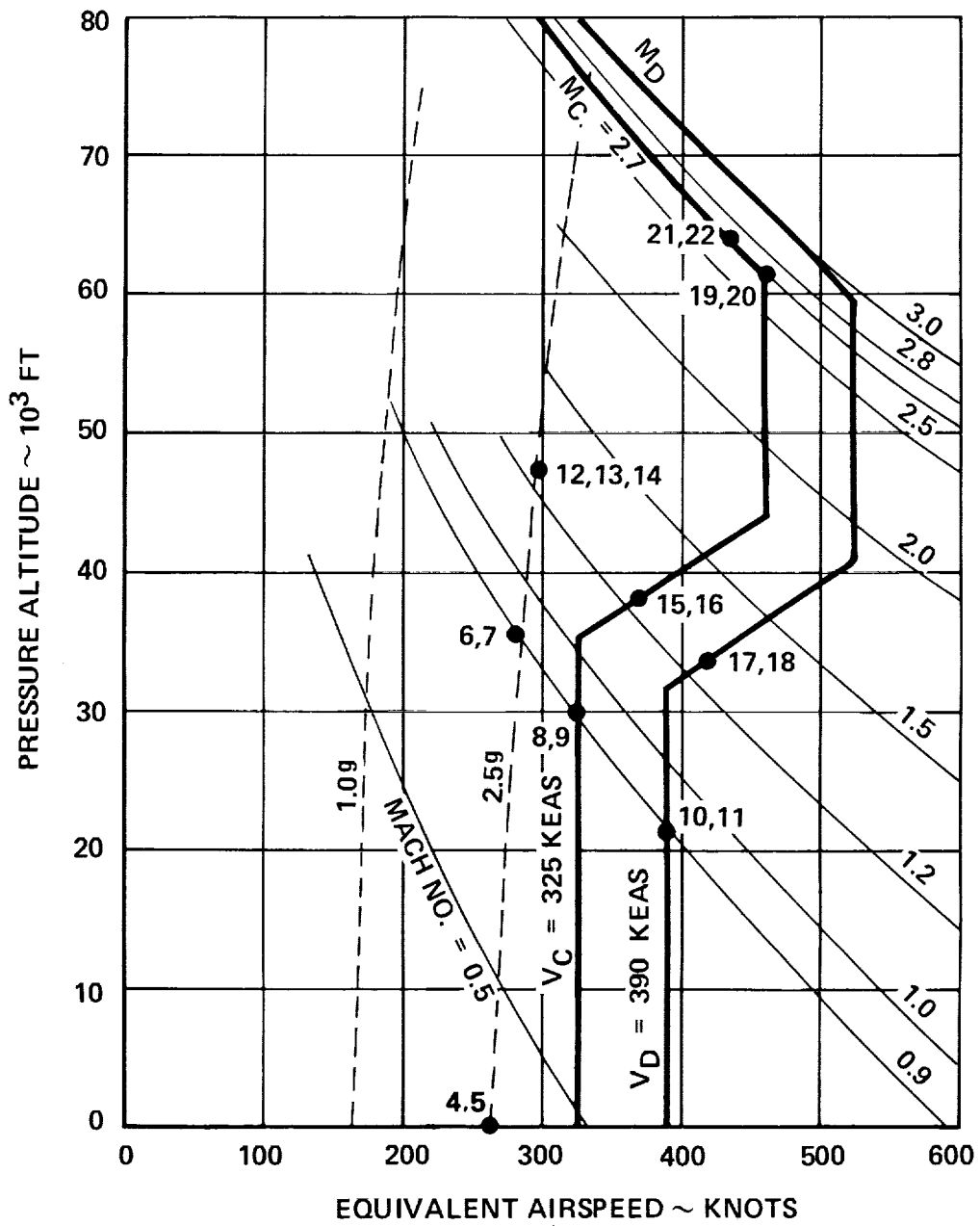


Figure 5-42. Design Loading Conditions - Strength

TABLE 5-8. PARAMETERS FOR LONGITUDINAL CONDITIONS

NASTRAN CONDITION	5	7	9	11	13	16	18	20
WEIGHT (lb x 10 <sup>-3</sup> )	745	700	700	700	690	690	445	660
C.G. (% MAC)	0.51	0.51	0.51	0.51	0.51	0.51	0.51	0.51
V <sub>e</sub> (keas)	264.6	282.4	325	390	294.3	372	420	460
MACH NO.	0.40	0.90	0.90	0.90	1.25	1.25	1.25	2.70
ALTITUDE (ft x 10 <sup>-3</sup> )	0	36	30	22	48	38.2	34	61.5
δ <sub>H</sub> (deg)	7.82	4.64	6.31	7.16	3.81	6.68	7.50	1.53
α (deg)	18.32	16.30	11.55	6.81	13.42	7.31	1.59	6.00
θ̇ (rad/sec)	0.1094	0.0712	0.0686	0.0567	0.0639	0.0691	0.0609	1.07
θ̈ (rad/sec <sup>2</sup> )	-0.0101	-0.1222	-0.0838	-0.0356	-0.1977	-0.1728	-0.1789	-0.1190
n <sub>z</sub>	2.5	2.5	2.5	2.5	2.5	2.5	2.5	2.5
n <sub>x</sub>	-0.46	-0.37	-0.27	-0.17	-0.31	-0.17	-0.02	-0.14
P <sub>z<sub>ht</sub></sub> (lb x 10 <sup>-3</sup> )	94.4	38.6	60.8	91.2	63.3	106.0	114.6	121.2

As indicated on Table 5-7, an assessment of the effect of jig shape on the aeroelastic loads were made considering the Mach 1.25 -  $V_{stall}$  condition.

Net Loads Summary. - Panel point loads were obtained directly from the net loads program and formed into stacked matrices as shown on Figure 5-43. The 274 rows of the first array contain the symmetrical portion of the net loading. Antisymmetrical loading increments are contained in the other. Each column includes net loads for a single condition. The first three columns are reserved for temperature effects, columns 4 through 34 for the symmetric conditions, and columns 35 through 54 for the asymmetric loads. Only the first 22 columns are used for the Task IIB strength-design effort.

Inertia data for use in loads analysis were obtained for airplane operating weight empty, payload, and fuel distributions. A computer program was established to obtain the combined inertia loading corresponding to each condition for which loads analysis was performed. Inertia distributions represent one-half the airplane and are compatible with the SIC grid point system. Weight cases are as listed in Table 5-9 with inertia distributions stored in the matrices corresponding to unit loadings (i.e.,  $P_z/n_z$ ,  $P_z/\ddot{\theta}$ ,  $P_z/\ddot{\phi}$ ) for each weight case. Input inertia data (per side) are contained in matrices defining (1) payload "shifter" distribution to obtain desired center-of-gravity, (2) fuselage payload distribution, (3) airplane operating weight empty distribution, (4) fuel inertia for each tank (1 through 15) and (5) factors for obtaining the desired weight case for design.

### Strength/Stiffness Design

The structural design loads analyses for the strength/stiffness design cycle is presented in Figure 5-44. The interrelationship with the structural model and the determination of the required aerodynamic data are shown. The element specifications of the strength/stiffness design reflect the changes to the airframe resulting from the strength analysis (including jig shape assessment), stiffness requirements and the associated structural weight distribution defined by the flutter optimization results, and design and manufacturing considerations. The latter includes further consideration of uniform thickness of material over a complete design region (reference Section 12, Structural Concepts Analysis).

NASTRAN COND. NO.	1	2	3	4	5	33	34	35	36	53	54
	TEMPERATURE										
	START-OF-CRUISE	MID-CRUISE	M1.25 DESCENT								
						(SEE TABLE 5-7 FOR LIST OF DESIGN CONDITIONS)					
	SYMMETRIC LOADS MATRIX										
										0	
	ANTI-SYM LOADS MATRIX										
										0	

Figure 5-43. Static Aeroelastic Load Matrix



TABLE 5-9. WEIGHT CASES AND OUTPUT IDENTIFICATION

WEIGHT CASE NO.	AIRPLANE WEIGHT 1000 LB.	AIRPLANE c.g. % c	MATRIX NUMBER		
			$P_z/n_z$	$P_z/\ddot{\theta}$	$P_z/\ddot{\phi}$
1	745	51	1624	1630	1636
2	700	51	1625	1631	1637
3	690	51	1626	1632	1638
4	660	51	1627	1633	1639
5	550	53	1628	1634	1640
6	445	51	1629	1635	1641

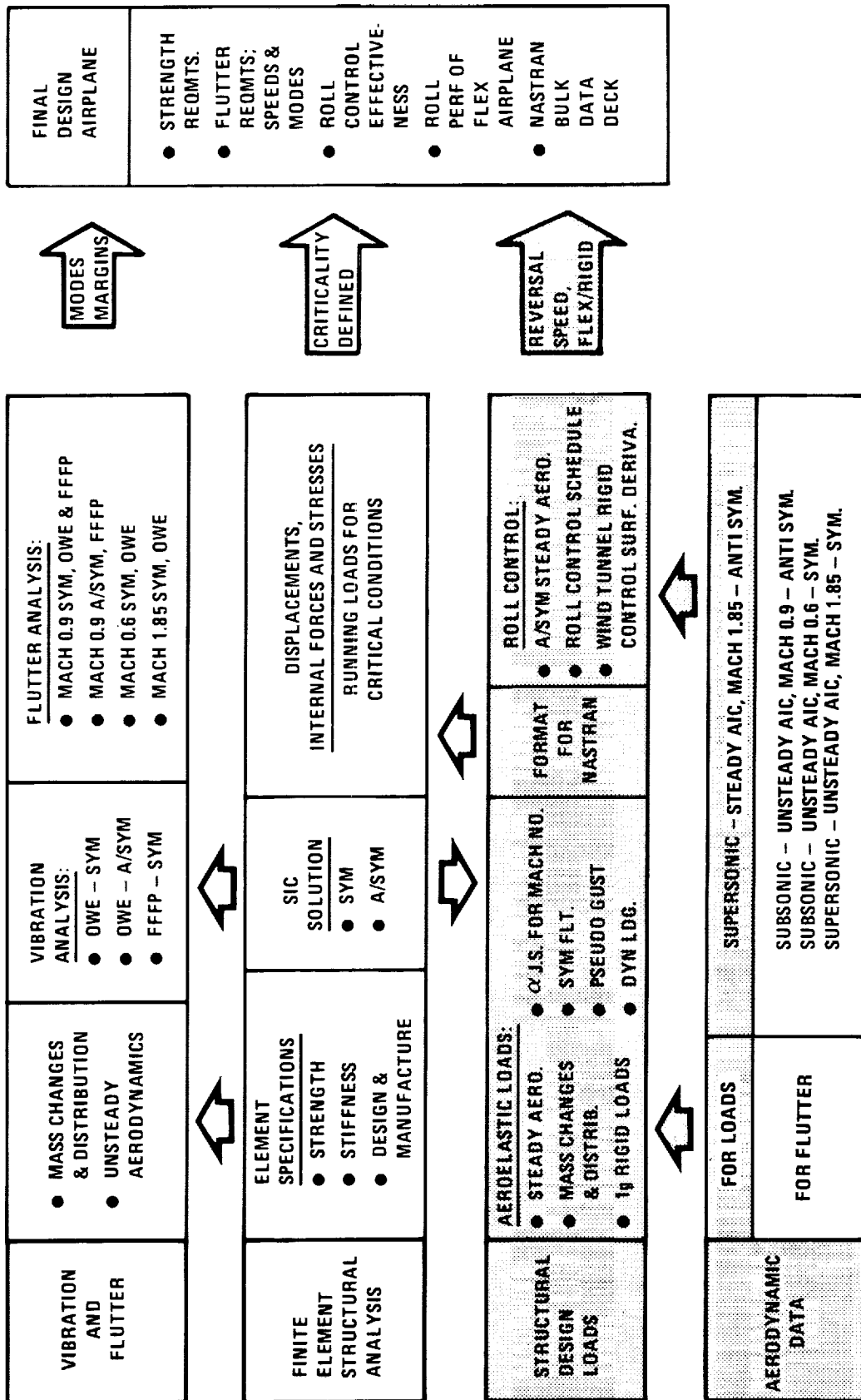


Figure 5-44. Task II Design Cycle - Strength/Stiffness

Conditions for Design. - The loading conditions for the final design cycle include 8 subsonic speed symmetric maneuvers (steady and transient); 7 low supersonic cases, including negative normal acceleration, steady and transient maneuvers at heavy and light gross weights; 4 Mach 2.7 conditions, including mid-cruise level flight and maneuver, and steady and transient maneuvers at start-of-cruise; 2 dynamic gust (pseudo) conditions at Mach 0.90 (positive and negative); and 4 dynamic landing cases, as shown in Table 5-10. These load cases, which are further identified on the design airspeed envelope of Figure 5-45, include jig shape effects considering the Final Design structural mass and flexibilities. The gust and landing cases are supplemental conditions developed for the Final Design verification effort and are selected as critical for fuselage design. The asymmetric accelerated roll condition is not included for the final loads run. The roll case results in maximum inplane loads in local regions of the strength-designed wing tip structure. However, with the added stiffness requirements in this region to suppress flutter, the condition is deleted from the list of potentially critical conditions.

Panel Point Loads. - The design loads for the Final Design airplane are presented in a grid system format previously described. These panel point loads are coincident with the SIC grid as shown in Figure 5-46 for the 3-D structural model. The Final Design loads are presented in Tables 5-11 through 5-18 for the critical conditions. The column-code on the tables refers to the NASTRAN condition number of Table 5-10. The row-code identifies the grid point number as displayed on the structural model representation of Figure 5-46.

A vector display of each of the above conditions is shown in Figures 5-47 through 5-54. The magnitude of the vector is normalized to the absolute value of the largest vector for each condition. The magnitude and location of the vectors are identified as  $P_{zG.P.XX}$  and Grid Point XX, respectively. The center line vectors are twice the values shown on the tables since the data reflects only one-half the wing.

Aeroelastic Deflections. - The aeroelastic analysis includes the calculation of airframe deflections during 1-g trimmed flight throughout a typical flight profile. These data can then be used in analytical predictions of drag polar adjustments for the flexible shapes.

A computer printout of the vertical deflections for the flexible aircraft are presented in Table 5-19 for the Mach 2.7 mid-cruise condition. These deflections are relative to the jig shape and are defined at each structural model grid point (see Figure 5-46). The underlined data defines the aeroelastic deformations at the wing tip (BL 795).

Figures 5-55 through 5-61 visually displays the limit vertical deflections for the critical conditions. The vectors represent elastic offsets relative to the jig shape and are normalized to the maximum value. In all instances the maximum deflection occurs at Grid Point 181 (wing tip).

TABLE 5-10. DESIGN LOADING CONDITION - TASK IIB STRENGTH/STIFFNESS

NASTRAN COND. NO.	WEIGHT (1000 LB)	MACH NO.	ALTITUDE (1000 FT)	LOAD FACTOR	AIRSPEED (KNOTS)	REMARKS
1						M2.7, START OF CRUISE
2						M2.7, MID-CRUISE
3						M1.25 DESCENT
TEMPERATURE CONDITIONS						
4, 5	745	0.40	0.0	2.5	264.6	STRENGTH DESIGN
6, 7	700	0.90	36.0	2.5	282.4	STRENGTH DESIGN
8, 9	700	0.90	30.0	2.5	325.0	STRENGTH DESIGN
10, 11	700	0.90	22.0	2.5	390.0	STRENGTH DESIGN
12, 13	690	1.25	48.0	2.5	294.3	STRENGTH DESIGN
14	690	1.25	48.0	1.0	294.3	NEGATIVE NORM. ACCEL.
15, 16	690	1.25	38.2	2.5	372.0	STRENGTH DESIGN
17, 18	445	1.25	34.0	2.5	420.0	DESCENT - THERMAL
19, 20	660	2.70	61.5	2.5	460.0	START OF CRUISE
21, 22	550	2.70	64.0	1.0, 2.5	433.6	MID CRUISE
23, 24	700	0.90	30.0	-	325.0	PSUEDO - GUST (POSITIVE AND NEGATIVE)
25 - 28	430	-	0.0	-	100.0	DYNAMIC LANDING CONDITIONS

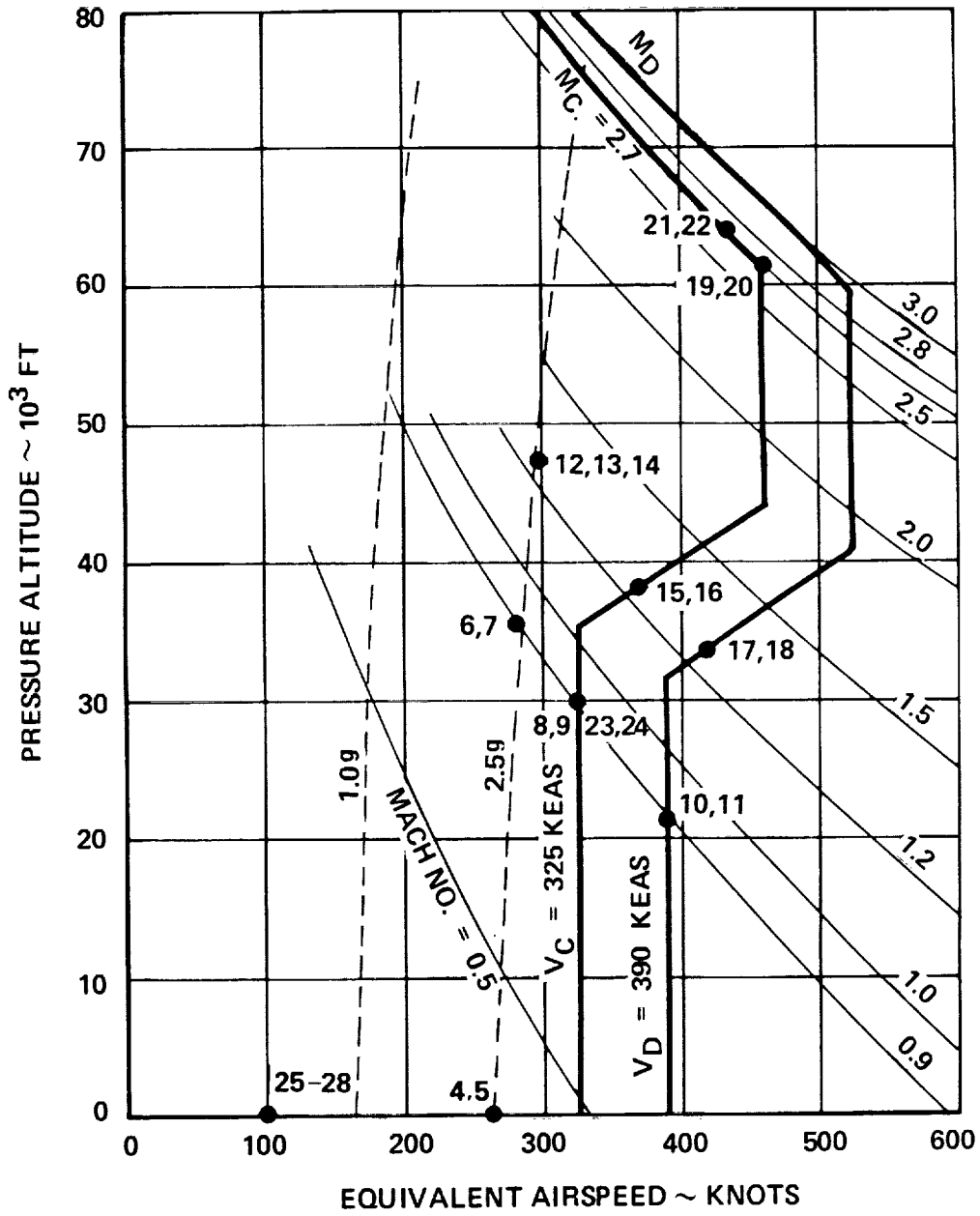
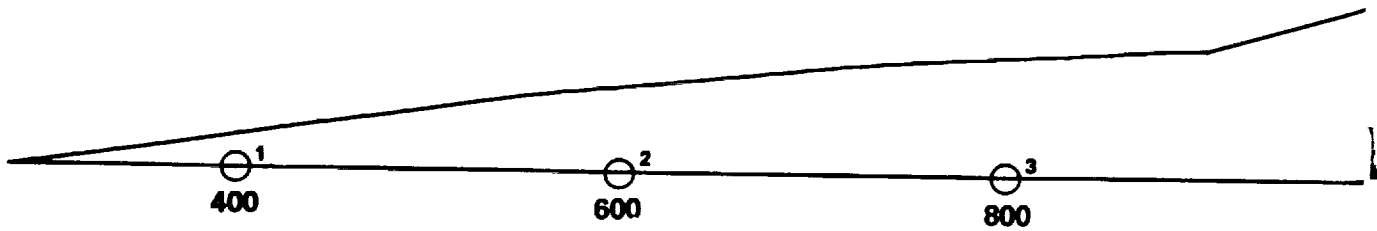
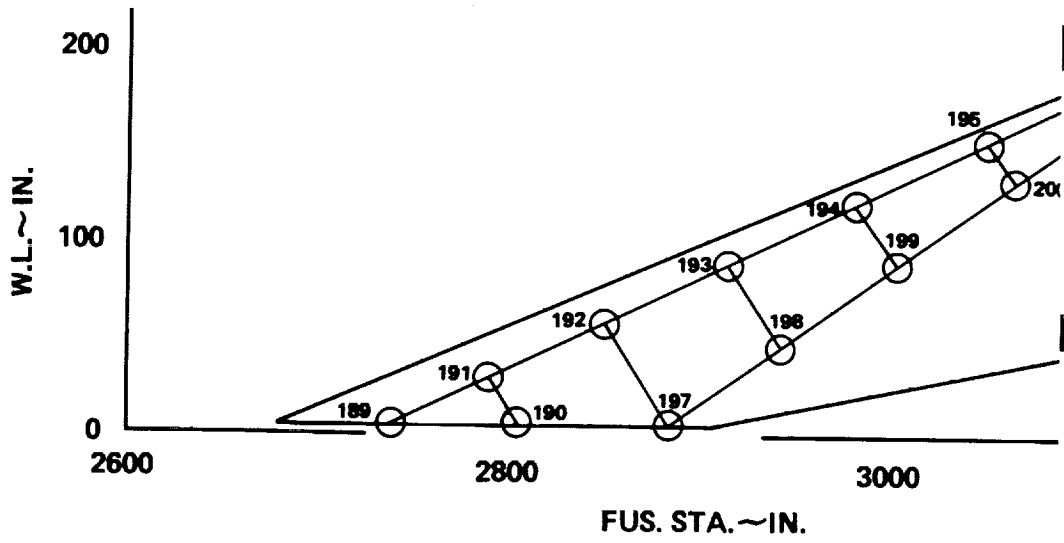


Figure 5-45. Design Loading Conditions - Strength-Stiffness



C.4 FOLDOUT FRAME 1



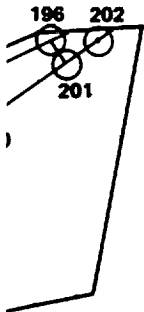




E E

E E

E E

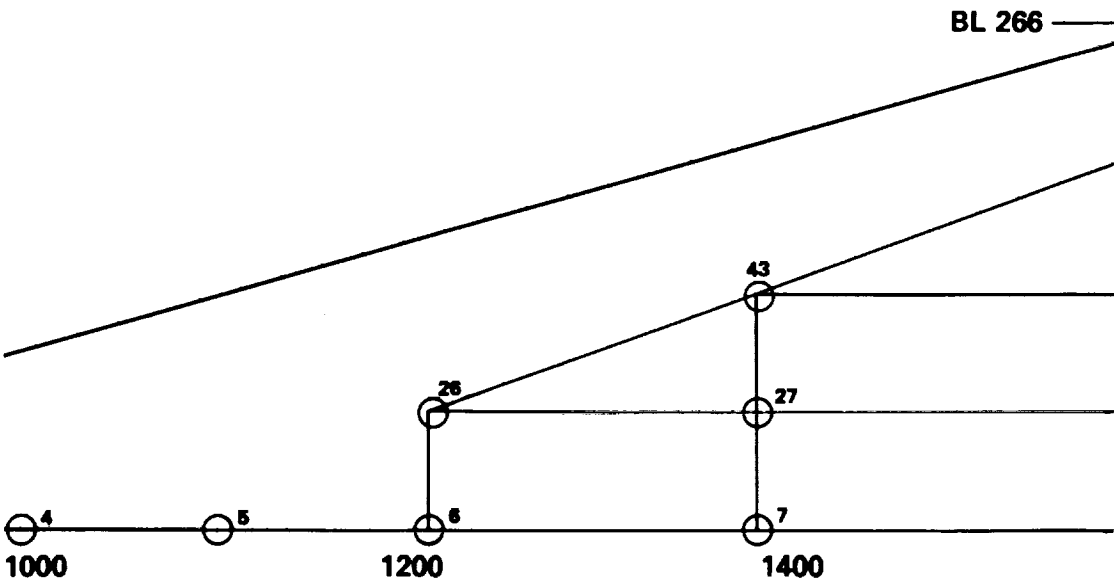


3200

E E

E E

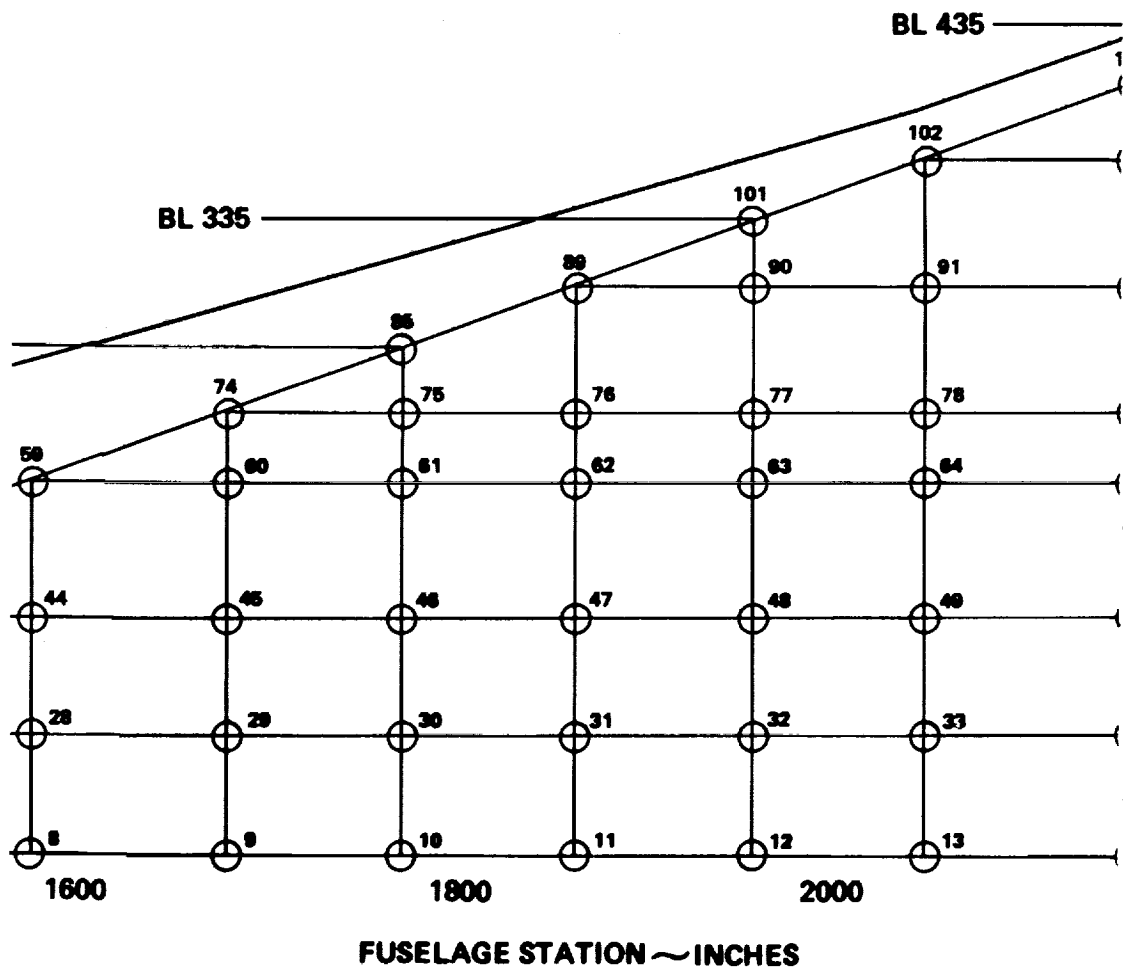
E E



E E

FOLDOUT FRAME 2





FOLDOUT FRAME 3





E E

I I

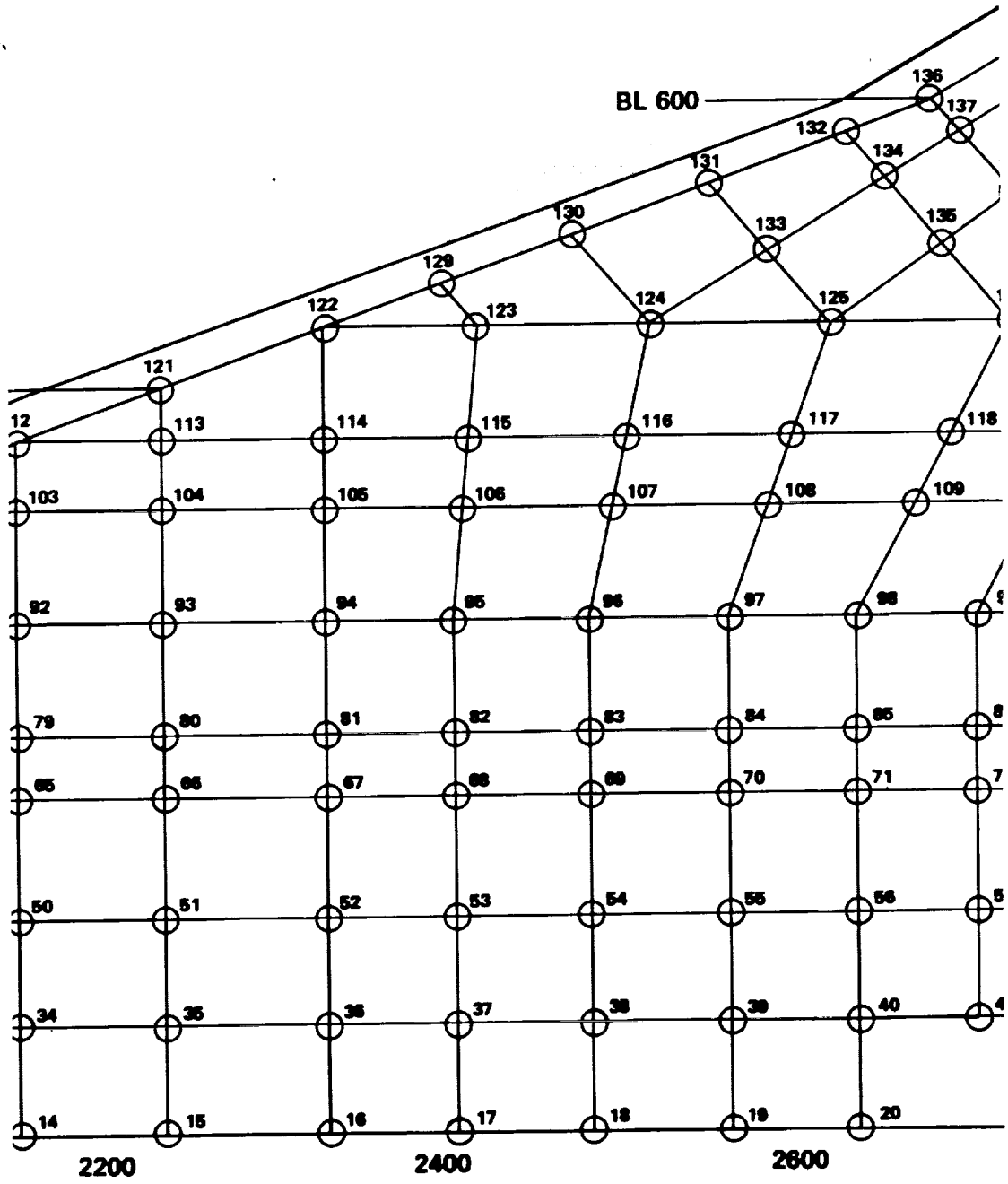
E I

I I

U U

E I

U U





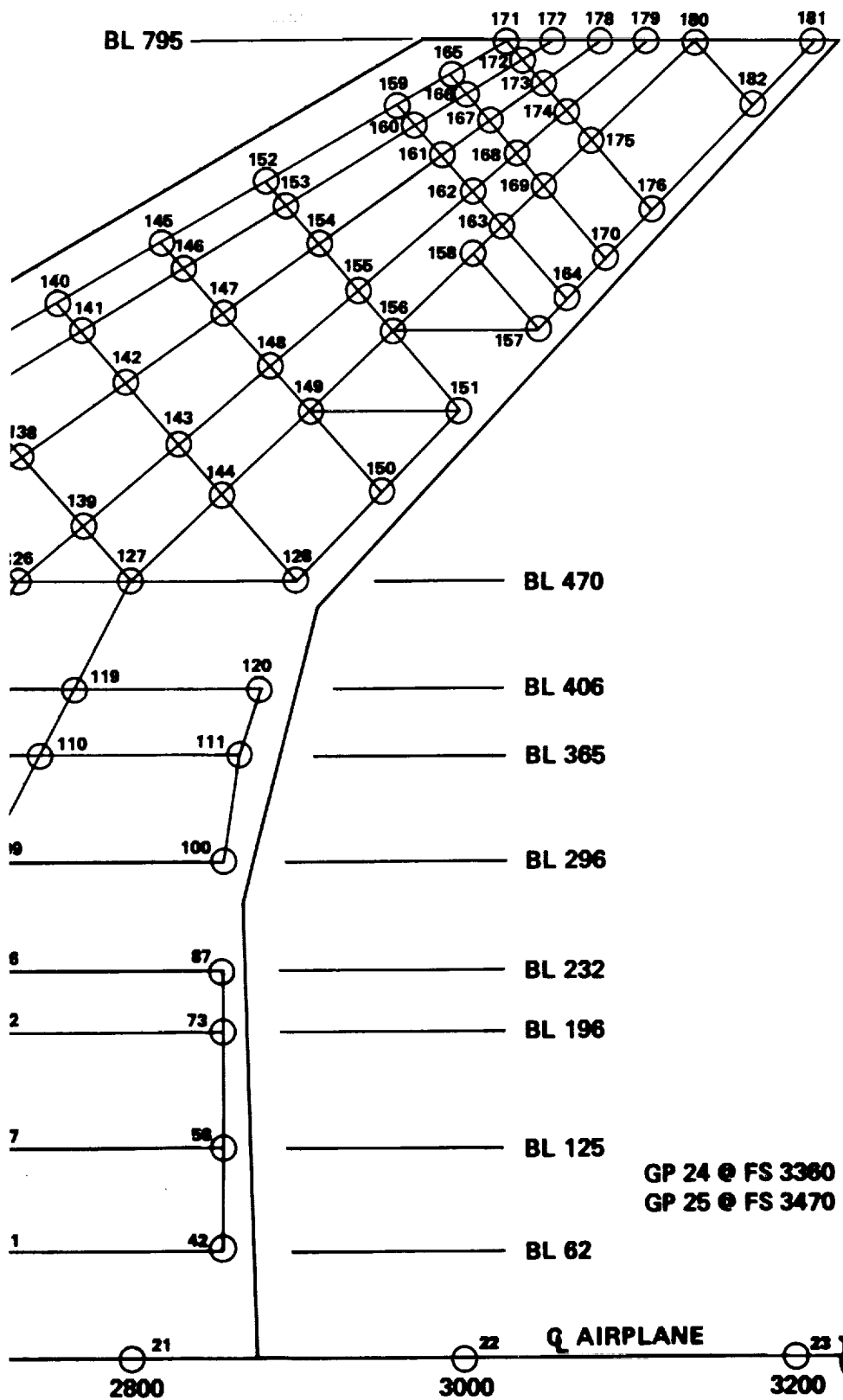


Figure 5-46. Structural Model Grid





TABLE 5-11. PANEL POINT LOADS - FINAL DESIGN - CONDITION 8, MACH 0.90 STEADY MANEUVER

STACKED LOADS

REAL	FULL	INTL. MATRIX	INDICATORS	NUM	PLW	IC	JOB	4510	SCU1	41	DATE	4/20/74	TIME	517	PAGE	4	
LUL	ALW	LUL	SUPT	PLW	PLW	NUM	PLW	PLW	PLW	PLW	NUM	PLW	PLW	PLW	PLW	PLW	
1	0.1791311	04	2	0.0422099	04	3	0.1750740	04	4	0.2544500	04	5	0.1123370	05	12	0.581980D	04
7	0.5282371	04	16	0.0000000	04	15	0.0442341	04	16	0.0000000	04	17	0.1800840	05	18	0.158942E	05
19	0.5076224	04	30	0.0117451	05	41	0.0317451	05	41	0.0317451	04	73	0.772052E	04	74	0.157219E	05
25	0.2476078	04	32	0.0114748	04	33	0.0114748	04	33	0.0114748	04	29	0.557002E	04	30	0.824485E	03
31	0.312800E	05	33	0.0206158	05	33	0.0206158	05	33	0.0206158	04	25	0.142512E	05	26	0.162170E	04
37	0.125510E	05	34	0.0206158	05	34	0.0206158	05	34	0.0206158	05	41	0.142512E	04	42	0.325678E	03
43	0.5144871	05	34	0.0101081	05	41	0.0027107	04	42	0.0077035E	04	47	0.225711E	05	48	0.139274E	05
55	0.2641571	05	35	0.0101081	05	37	0.0112121	04	37	0.0112121	04	53	0.000052E	05	54	0.133673E	05
61	0.612872E	04	62	0.0121570	05	63	0.0121570	05	64	0.0121570	05	65	0.0612450	04	66	0.837950E	04
73	0.275952E	04	68	0.019520E	05	69	0.019520E	04	70	0.019520E	04	71	0.142512E	05	72	0.268072E	04
79	0.702375E	04	74	0.021760E	05	75	0.021760E	04	76	0.021760E	04	83	0.142512E	04	84	0.185912E	04
85	0.314630E	04	80	0.027745E	05	81	0.027745E	04	82	0.027745E	04	89	0.219535E	05	90	0.543562E	04
91	0.102901E	04	92	0.041013E	03	93	0.041013E	03	94	0.041013E	05	86	0.197873E	05	87	0.788643E	04
97	0.502235E	04	94	0.025540E	04	95	0.025540E	04	96	0.025540E	04	101	0.142512E	04	102	0.91057E	04
103	0.122618E	05	104	0.011317E	05	105	0.011317E	04	106	0.011317E	04	107	0.014460E	05	108	0.268072E	04
109	0.772982E	05	110	0.017035E	05	111	0.017035E	04	112	0.017035E	05	119	0.002774E	05	120	0.640819E	04
115	0.660724E	04	116	0.067039E	04	117	0.067039E	04	118	0.067039E	05	119	0.002774E	05	120	0.230331E	04
121	0.143459E	04	122	0.042439E	05	123	0.042439E	04	124	0.042439E	04	125	0.117035E	04	126	0.627316E	05
127	0.314630E	05	128	0.0114240E	05	129	0.0114240E	05	130	0.0114240E	05	131	0.142512E	04	132	0.106181E	05
134	0.114251E	05	135	0.0117671E	05	136	0.0117671E	05	137	0.0117671E	05	137	0.005741E	04	138	0.859447E	04
139	0.231720E	04	140	0.0117671E	05	141	0.0117671E	04	142	0.0117671E	04	143	0.247511E	04	144	0.359525E	04
145	0.174457E	04	146	0.0117671E	05	147	0.0117671E	04	148	0.0117671E	04	149	0.247511E	04	150	0.217757E	04
151	0.908700E	04	152	0.0117671E	05	153	0.0117671E	05	154	0.0117671E	04	155	0.247511E	04	156	0.769630E	04
157	0.252460E	05	158	0.0055143E	05	159	0.0055143E	05	160	0.0055143E	04	161	0.329041E	04	162	0.102064E	04
163	0.412146E	05	164	0.045516E	05	165	0.045516E	04	166	0.045516E	04	167	0.116025E	01	168	0.919188E	03
169	0.225072E	05	170	0.0114491E	05	171	0.0114491E	05	172	0.0114491E	05	173	0.002655E	05	174	0.178032E	03
175	0.771215E	04	176	0.0114491E	05	177	0.0114491E	04	178	0.0114491E	04	179	0.012400E	02	180	0.202656E	03
181	0.802190E	04	182	0.0173721E	05	183	0.0173721E	05	184	0.0173721E	04	185	0.005741E	04	186	0.317309E	05
189	0.303411E	04	190	0.033111E	05	191	0.033111E	05	192	0.033111E	05	193	0.005741E	05	194	0.462242E	03
199	0.334931E	05	200	0.0127620E	02	201	0.0127620E	05	202	0.0127620E	05	194	0.005741E	05	200	0.371000E	03
207	0.115217E	05	208	0.0117551E	05	209	0.0117551E	05	210	0.0117551E	07	211	0.113675E	07	210	0.690546E	06
211	0.526248E	06	212	0.037816E	06	213	0.037816E	06	214	0.037816E	06	221	0.342519E	08	220	0.230236E	06
213	0.167504E	06	214	0.048897E	06	215	0.048897E	06	216	0.048897E	06	227	0.001195E	05	226	0.21168E	06
229	0.270200E	06	230	0.045824E	06	231	0.045824E	06	232	0.045824E	06	233	0.001195E	05	234	0.476821E	08
242	0.614723E	06	243	0.076721E	06	244	0.076721E	06	245	0.076721E	06	245	0.194335E	06	247	0.135982E	06
248	0.900503E	05	249	0.0126610E	06	250	0.0126610E	06	251	0.0126610E	06	252	0.137400E	05	253	0.009710E	05
254	0.507677E	05	255	0.032355E	05	256	0.032355E	05	257	0.032355E	05	258	0.114928E	05	259	0.191468E	06
260	0.122260E	06	261	0.033459E	04	263	0.033459E	07	264	0.033459E	07	265	0.117305E	07	266	0.127309E	07

ORIGINAL PAGE IS OF POOR QUALITY



TABLE 5-13. PANEL POINT LOADS - FINAL DESIGN - CONDITION 14, MACH 1.25 NEGATIVE NORMAL ACCEL.

STACKED LOADS

REAL	FULL	MATRIX 4175	INTL. MATRIX 16025	274 LY	INDICATORS	IC	DATE	4/26/74	TIME	517	PAGE	9
COL	RUM	COL	RUM	COL	RUM	COL	RUM	COL	RUM	COL	RUM	COL
1	0.2527790	4	0.5100110	4	0.5243390	4	0.7491410	4	0.3315310	4	0.3315310	4
7	0.2535751	5	0.3913388	5	0.6701438	5	0.7894910	5	0.5243390	5	0.5243390	5
13	0.8664121	12	0.6019071	12	0.8701438	12	0.7894910	12	0.5243390	12	0.5243390	12
19	0.7652131	21	0.6125501	21	0.8701438	21	0.7894910	21	0.5243390	21	0.5243390	21
25	0.5955481	27	0.6125501	27	0.8701438	27	0.7894910	27	0.5243390	27	0.5243390	27
31	0.1202051	32	0.1202051	32	0.1202051	32	0.1202051	32	0.1202051	32	0.1202051	32
37	0.4458671	38	0.4458671	38	0.4458671	38	0.4458671	38	0.4458671	38	0.4458671	38
43	0.1498471	44	0.1498471	44	0.1498471	44	0.1498471	44	0.1498471	44	0.1498471	44
49	0.6027001	50	0.6027001	50	0.6027001	50	0.6027001	50	0.6027001	50	0.6027001	50
55	0.2844301	56	0.2844301	56	0.2844301	56	0.2844301	56	0.2844301	56	0.2844301	56
61	0.7894910	62	0.7894910	62	0.7894910	62	0.7894910	62	0.7894910	62	0.7894910	62
67	0.1021191	68	0.1021191	68	0.1021191	68	0.1021191	68	0.1021191	68	0.1021191	68
73	0.1925181	74	0.1925181	74	0.1925181	74	0.1925181	74	0.1925181	74	0.1925181	74
79	0.4052101	80	0.4052101	80	0.4052101	80	0.4052101	80	0.4052101	80	0.4052101	80
85	0.4770071	86	0.4770071	86	0.4770071	86	0.4770071	86	0.4770071	86	0.4770071	86
91	0.2157761	92	0.2157761	92	0.2157761	92	0.2157761	92	0.2157761	92	0.2157761	92
97	0.2735381	98	0.2735381	98	0.2735381	98	0.2735381	98	0.2735381	98	0.2735381	98
103	0.4334421	104	0.4334421	104	0.4334421	104	0.4334421	104	0.4334421	104	0.4334421	104
109	0.2582231	110	0.2582231	110	0.2582231	110	0.2582231	110	0.2582231	110	0.2582231	110
115	0.4499331	116	0.4499331	116	0.4499331	116	0.4499331	116	0.4499331	116	0.4499331	116
121	0.1947911	122	0.1947911	122	0.1947911	122	0.1947911	122	0.1947911	122	0.1947911	122
127	0.1841841	128	0.1841841	128	0.1841841	128	0.1841841	128	0.1841841	128	0.1841841	128
133	0.2555431	134	0.2555431	134	0.2555431	134	0.2555431	134	0.2555431	134	0.2555431	134
139	0.4171341	140	0.4171341	140	0.4171341	140	0.4171341	140	0.4171341	140	0.4171341	140
145	0.3757171	146	0.3757171	146	0.3757171	146	0.3757171	146	0.3757171	146	0.3757171	146
151	0.1866971	152	0.1866971	152	0.1866971	152	0.1866971	152	0.1866971	152	0.1866971	152
157	0.1022441	158	0.1022441	158	0.1022441	158	0.1022441	158	0.1022441	158	0.1022441	158
163	0.3325441	164	0.3325441	164	0.3325441	164	0.3325441	164	0.3325441	164	0.3325441	164
169	0.5341251	170	0.5341251	170	0.5341251	170	0.5341251	170	0.5341251	170	0.5341251	170
175	0.4714461	176	0.4714461	176	0.4714461	176	0.4714461	176	0.4714461	176	0.4714461	176
181	0.2016501	182	0.2016501	182	0.2016501	182	0.2016501	182	0.2016501	182	0.2016501	182
187	0.3142081	188	0.3142081	188	0.3142081	188	0.3142081	188	0.3142081	188	0.3142081	188
193	0.4748121	194	0.4748121	194	0.4748121	194	0.4748121	194	0.4748121	194	0.4748121	194
199	0.5479361	200	0.5479361	200	0.5479361	200	0.5479361	200	0.5479361	200	0.5479361	200
205	0.2749361	206	0.2749361	206	0.2749361	206	0.2749361	206	0.2749361	206	0.2749361	206
211	0.2760361	212	0.2760361	212	0.2760361	212	0.2760361	212	0.2760361	212	0.2760361	212
217	0.5142691	218	0.5142691	218	0.5142691	218	0.5142691	218	0.5142691	218	0.5142691	218
223	0.1525361	224	0.1525361	224	0.1525361	224	0.1525361	224	0.1525361	224	0.1525361	224
229	0.1525361	230	0.1525361	230	0.1525361	230	0.1525361	230	0.1525361	230	0.1525361	230
235	0.2550001	236	0.2550001	236	0.2550001	236	0.2550001	236	0.2550001	236	0.2550001	236
241	0.2266901	242	0.2266901	242	0.2266901	242	0.2266901	242	0.2266901	242	0.2266901	242
247	0.2266901	248	0.2266901	248	0.2266901	248	0.2266901	248	0.2266901	248	0.2266901	248
253	0.5949001	254	0.5949001	254	0.5949001	254	0.5949001	254	0.5949001	254	0.5949001	254

ORIGINAL PAGE IS OF POOR QUALITY

TABLE 5-14. PANEL POINT LOADS - FINAL DESIGN - CONDITION 16, MACH 1.25 TRANSIENT MANEUVER

STACKED LOADS		MATRIX		INT. MATRIX		INDICATORS		DATE		TIME		PAGE	
REAL	IMAG	COL	ROW	COL	ROW	COL	ROW	DATE	TIME	DATE	TIME	PAGE	PAGE
16	1	0.182220	04	2	0.571948	04	7	0.174291	04	1	0.100380	04	0.137087
	2	0.451297	04	8	0.121760	04	11	0.119451	04	17	0.194564	04	0.128618
	14	0.194564	04	10	0.246278	04	10	0.246278	04	17	0.194564	04	0.128618
	19	0.107000	04	20	0.360429	04	23	0.254278	04	29	0.178475	04	0.229210
	20	0.107000	04	27	0.371029	04	28	0.254278	04	29	0.178475	04	0.229210
	31	0.314908	04	34	0.237028	04	35	0.237028	04	41	0.147571	04	0.213502
	37	0.182220	04	38	0.246278	04	39	0.246278	04	41	0.147571	04	0.213502
	44	0.474501	04	41	0.113193	04	42	0.103444	04	47	0.308879	04	0.113502
	53	0.174150	04	50	0.174150	04	51	0.218278	04	53	0.150558	04	0.113502
	55	0.174150	04	52	0.174150	04	53	0.218278	04	53	0.150558	04	0.113502
	61	0.349641	04	62	0.127471	04	64	0.501795	04	64	0.413077	04	0.349641
	67	0.349641	04	64	0.127471	04	64	0.501795	04	64	0.413077	04	0.349641
	73	0.112707	04	74	0.146078	04	74	0.270505	04	77	0.432471	04	0.112707
	79	0.287641	04	81	0.146078	04	82	0.146078	04	83	0.146078	04	0.112707
	85	0.524308	04	86	0.109921	04	87	0.146078	04	87	0.146078	04	0.112707
	91	0.944341	04	92	0.244731	04	94	0.944341	04	95	0.127471	04	0.112707
	97	0.151891	04	98	0.223121	04	99	0.223121	04	101	0.353091	04	0.151891
	103	0.050581	04	104	0.447431	04	105	0.974091	04	107	0.582821	04	0.050581
	109	0.050581	04	110	0.447431	04	111	0.974091	04	113	0.106312	04	0.050581
	115	0.050581	04	116	0.447431	04	117	0.974091	04	119	0.106312	04	0.050581
	121	0.335508	04	122	0.716175	04	124	0.335508	04	125	0.212155	04	0.112707
	127	0.378061	04	128	0.212155	04	130	0.212155	04	131	0.222031	04	0.378061
	133	0.564031	04	134	0.222031	04	135	0.222031	04	137	0.143077	04	0.564031
	139	0.494071	04	140	0.222031	04	141	0.222031	04	143	0.659641	04	0.494071
	145	0.571011	04	146	0.176121	04	147	0.176121	04	149	0.220851	04	0.571011
	151	0.224091	04	152	0.176121	04	154	0.224091	04	155	0.207621	04	0.224091
	157	0.224091	04	158	0.176121	04	160	0.224091	04	161	0.577021	04	0.224091
	163	0.110681	04	164	0.176121	04	165	0.176121	04	167	0.133671	04	0.110681
	175	0.110681	04	176	0.176121	04	177	0.176121	04	179	0.133671	04	0.110681
	181	0.311731	04	182	0.176121	04	183	0.176121	04	185	0.433671	04	0.311731
	187	0.311731	04	188	0.176121	04	189	0.176121	04	191	0.433671	04	0.311731
	193	0.311731	04	194	0.176121	04	195	0.176121	04	197	0.433671	04	0.311731
	201	0.151401	04	202	0.176121	04	203	0.176121	04	205	0.626091	04	0.151401
	207	0.151401	04	208	0.176121	04	209	0.176121	04	211	0.141731	04	0.151401
	213	0.151401	04	214	0.176121	04	215	0.176121	04	217	0.141731	04	0.151401
	219	0.514941	04	220	0.176121	04	221	0.176121	04	223	0.141731	04	0.514941
	225	0.514941	04	226	0.176121	04	227	0.176121	04	229	0.141731	04	0.514941
	231	0.514941	04	232	0.176121	04	233	0.176121	04	235	0.141731	04	0.514941
	237	0.514941	04	238	0.176121	04	239	0.176121	04	241	0.141731	04	0.514941
	243	0.514941	04	244	0.176121	04	245	0.176121	04	247	0.141731	04	0.514941
	249	0.514941	04	250	0.176121	04	251	0.176121	04	253	0.141731	04	0.514941
	255	0.514941	04	256	0.176121	04	257	0.176121	04	259	0.141731	04	0.514941
	263	0.110681	04	264	0.176121	04	265	0.176121	04	267	0.110681	04	0.110681

TABLE 5-15. PANEL POINT LOADS - FINAL DESIGN - CONDITION 20, MACH 2.7  
(START-OF-CRUISE) TRANSIENT MANEUVER

REAL	FULL	INDICATORS	IC	SEC1	SEC2	TIME	PAGE
20	1	0.3578290	04	7	0.1300490	04	0.7473410
	7	0.4789111	04	10	0.3400077	05	0.1560285
	13	0.1900477	05	14	0.0250071	05	0.1302222
	14	0.0001101	04	21	0.0000000	05	0.1194529
	15	0.1828004	05	21	0.0000000	04	0.1979788
	31	0.0336291	05	37	0.0705001	05	0.2536798
	37	0.0185781	05	43	0.0147001	04	0.3505131
	43	0.0445531	05	49	0.0074104	04	0.1360728
	49	0.0114000	05	50	0.0000000	05	0.1505478
	55	0.0512240	04	57	0.0116501	05	0.6372148
	61	0.0527489	04	62	0.0160001	04	0.9765141
	67	0.0504912	05	69	0.0155571	04	0.3577978
	73	0.0503519	04	74	0.0182201	05	0.3713111
	79	0.0571721	04	81	0.0330781	04	0.2875591
	85	0.0517421	05	87	0.0482481	05	0.6010391
	91	0.0540941	04	92	0.0450521	05	0.6722221
	97	0.0210041	04	98	0.0477001	04	0.1649711
	103	0.0505001	04	104	0.0517021	04	0.3842221
	109	0.0744271	05	110	0.0545001	04	0.7016051
	115	0.0744271	04	117	0.0545001	04	0.4941311
	121	0.0512581	05	122	0.0545001	04	0.3074701
	127	0.0523881	04	128	0.0570001	05	0.1003791
	133	0.0766721	04	134	0.0570001	05	0.4902311
	139	0.0766721	04	140	0.0570001	04	0.1709721
	145	0.0495001	04	146	0.0570001	04	0.5157911
	151	0.0495001	04	152	0.0570001	04	0.2421001
	157	0.0495001	04	158	0.0570001	04	0.2421001
	163	0.0495001	04	164	0.0570001	04	0.2421001
	169	0.0495001	04	170	0.0570001	04	0.1750111
	175	0.0495001	04	176	0.0570001	04	0.1367471
	181	0.0495001	04	182	0.0570001	04	0.2666721
	187	0.0495001	04	188	0.0570001	04	0.5143691
	193	0.0495001	04	194	0.0570001	04	0.4126241
	201	0.0495001	04	202	0.0570001	04	0.4769701
	217	0.0495001	04	218	0.0570001	04	0.1375931
	223	0.0495001	04	224	0.0570001	04	0.9752321
	229	0.0495001	04	230	0.0570001	04	0.1107471
	247	0.0495001	04	248	0.0570001	04	0.1107471
	253	0.0495001	04	254	0.0570001	04	0.3724051
	259	0.0495001	04	260	0.0570001	04	0.6780391
	265	0.0495001	04	266	0.0570001	04	0.1309501

ORIGINAL PAGE IS  
OF POOR QUALITY

TABLE 5-16. PANEL POINT LOADS - FINAL DESIGN - CONDITION 21, MACH 2.7  
(MID-CRUISE) 1-g TRIMMED FLIGHT

STACKED LOADS

REAL	IMAG	INT. MATRIX	INDICATORS	DATE	TIME	PAGE		
4175	10025	10025	10025	4/20/74	517	15		
REAL	IMAG	INT. MATRIX	INDICATORS	DATE	TIME	PAGE		
217	0.561477E	05	219	0.157032E	05	221	0.133740E	05
225	0.438649E	04	225	0.369471E	04	227	0.353502E	04
229	0.145794E	04	231	0.876551E	03	233	0.233104E	03
241	0.153794E	03	243	0.261750E	03	245	0.206952E	03
247	0.063559E	03	249	0.518284E	04	251	0.180413E	04
253	0.154784E	04	255	0.427431E	04	257	0.744127E	03
259	0.517420E	03	261	0.130793E	03	263	0.786600E	06
265	0.602600E	03						
2	0.370250E	04	3	0.141455E	04	7	0.524165E	04
6	0.200501E	01	9	0.152478E	03	10	0.395237E	02
10	0.545101E	04	15	0.630807E	04	16	0.623094E	04
20	0.552101E	04	21	0.971831E	03	22	0.894142E	02
25	0.894274E	04	27	0.971831E	03	28	0.794943E	03
30	0.694959E	04	33	0.551551E	04	34	0.710051E	04
38	0.402271E	04	39	0.253571E	04	40	0.710051E	04
44	0.594459E	04	45	0.215121E	04	46	0.179101E	03
50	0.781649E	03	51	0.672388E	03	52	0.557139E	04
56	0.471629E	03	57	0.258121E	03	58	0.428920E	04
61	0.151244E	03	62	0.151244E	03	63	0.149491E	04
68	0.227688E	04	69	0.227688E	04	70	0.149491E	04
74	0.227688E	04	75	0.152547E	03	76	0.789778E	03
79	0.145714E	04	81	0.305347E	03	82	0.217754E	03
85	0.101289E	04	87	0.305347E	03	88	0.232521E	04
91	0.110123E	04	93	0.181978E	04	94	0.166501E	04
97	0.110123E	04	99	0.759127E	04	100	0.168978E	04
103	0.150154E	04	105	0.191285E	04	106	0.118515E	04
109	0.172150E	03	111	0.718498E	03	112	0.134418E	04
115	0.160027E	04	117	0.834108E	03	118	0.134418E	03
121	0.105888E	04	123	0.123177E	04	124	0.211771E	02
127	0.224049E	03	129	0.123177E	04	130	0.211771E	04
133	0.181783E	04	135	0.123177E	04	136	0.115371E	03
139	0.181783E	04	141	0.123177E	04	142	0.115371E	04
145	0.186208E	03	147	0.943576E	03	148	0.528844E	03
151	0.209228E	03	153	0.135321E	03	154	0.742889E	03
157	0.133849E	04	159	0.273744E	03	160	0.435223E	04
163	0.600425E	03	165	0.116349E	03	166	0.435223E	03
169	0.447394E	03	171	0.354359E	02	172	0.354359E	03
175	0.721150E	03	177	0.307497E	01	178	0.354359E	03
181	0.721150E	03	183	0.190610E	04	184	0.135065E	03
187	0.215554E	03	191	0.453453E	03	192	0.453453E	03
193	0.215554E	03	197	0.412847E	03	198	0.515105E	03
201	0.781868E	04	213	0.058764E	03	214	0.358510E	03
217	0.561477E	05	219	0.157032E	05	221	0.133740E	05
225	0.438649E	04	225	0.369471E	04	227	0.353502E	04
229	0.145794E	04	231	0.876551E	03	233	0.233104E	03
241	0.153794E	03	243	0.261750E	03	245	0.206952E	03
247	0.063559E	03	249	0.518284E	04	251	0.180413E	04
253	0.154784E	04	255	0.427431E	04	257	0.744127E	03
259	0.517420E	03	261	0.130793E	03	263	0.786600E	06
265	0.602600E	03						

TABLE 5-17. PANEL POINT LOADS - FINAL DESIGN - CONDITION 23, MACH 0.90 PSEUDO GUST (POSITIVE)

Stacked Loads

MARKIA 4175	INT. SHELL CODE	27-17 24	JUL 4-15	SCT	41	DATE 4/29/74	TIRE 517	PAGE 17		
PIAL FULL	COL LEFT	INDICATORS	IC	ROW	COL	ROW	COL	FLW		
COL NUM	ROW	COL	ROW	COL	ROW	COL	ROW	FLW		
1	1	0.00000000	00	2	1	0.00000000	00	1	0.1357050	05
1	2	0.00000000	00	2	2	0.00000000	00	2	0.1357050	05
1	3	0.00000000	00	2	3	0.00000000	00	3	0.1357050	05
1	4	0.00000000	00	2	4	0.00000000	00	4	0.1357050	05
1	5	0.00000000	00	2	5	0.00000000	00	5	0.1357050	05
1	6	0.00000000	00	2	6	0.00000000	00	6	0.1357050	05
1	7	0.00000000	00	2	7	0.00000000	00	7	0.1357050	05
1	8	0.00000000	00	2	8	0.00000000	00	8	0.1357050	05
1	9	0.00000000	00	2	9	0.00000000	00	9	0.1357050	05
1	10	0.00000000	00	2	10	0.00000000	00	10	0.1357050	05
1	11	0.00000000	00	2	11	0.00000000	00	11	0.1357050	05
1	12	0.00000000	00	2	12	0.00000000	00	12	0.1357050	05
1	13	0.00000000	00	2	13	0.00000000	00	13	0.1357050	05
1	14	0.00000000	00	2	14	0.00000000	00	14	0.1357050	05
1	15	0.00000000	00	2	15	0.00000000	00	15	0.1357050	05
1	16	0.00000000	00	2	16	0.00000000	00	16	0.1357050	05
1	17	0.00000000	00	2	17	0.00000000	00	17	0.1357050	05
1	18	0.00000000	00	2	18	0.00000000	00	18	0.1357050	05
1	19	0.00000000	00	2	19	0.00000000	00	19	0.1357050	05
1	20	0.00000000	00	2	20	0.00000000	00	20	0.1357050	05
1	21	0.00000000	00	2	21	0.00000000	00	21	0.1357050	05
1	22	0.00000000	00	2	22	0.00000000	00	22	0.1357050	05
1	23	0.00000000	00	2	23	0.00000000	00	23	0.1357050	05
1	24	0.00000000	00	2	24	0.00000000	00	24	0.1357050	05
1	25	0.00000000	00	2	25	0.00000000	00	25	0.1357050	05
1	26	0.00000000	00	2	26	0.00000000	00	26	0.1357050	05
1	27	0.00000000	00	2	27	0.00000000	00	27	0.1357050	05
1	28	0.00000000	00	2	28	0.00000000	00	28	0.1357050	05
1	29	0.00000000	00	2	29	0.00000000	00	29	0.1357050	05
1	30	0.00000000	00	2	30	0.00000000	00	30	0.1357050	05
1	31	0.00000000	00	2	31	0.00000000	00	31	0.1357050	05
1	32	0.00000000	00	2	32	0.00000000	00	32	0.1357050	05
1	33	0.00000000	00	2	33	0.00000000	00	33	0.1357050	05
1	34	0.00000000	00	2	34	0.00000000	00	34	0.1357050	05
1	35	0.00000000	00	2	35	0.00000000	00	35	0.1357050	05
1	36	0.00000000	00	2	36	0.00000000	00	36	0.1357050	05
1	37	0.00000000	00	2	37	0.00000000	00	37	0.1357050	05
1	38	0.00000000	00	2	38	0.00000000	00	38	0.1357050	05
1	39	0.00000000	00	2	39	0.00000000	00	39	0.1357050	05
1	40	0.00000000	00	2	40	0.00000000	00	40	0.1357050	05
1	41	0.00000000	00	2	41	0.00000000	00	41	0.1357050	05
1	42	0.00000000	00	2	42	0.00000000	00	42	0.1357050	05
1	43	0.00000000	00	2	43	0.00000000	00	43	0.1357050	05
1	44	0.00000000	00	2	44	0.00000000	00	44	0.1357050	05
1	45	0.00000000	00	2	45	0.00000000	00	45	0.1357050	05
1	46	0.00000000	00	2	46	0.00000000	00	46	0.1357050	05
1	47	0.00000000	00	2	47	0.00000000	00	47	0.1357050	05
1	48	0.00000000	00	2	48	0.00000000	00	48	0.1357050	05
1	49	0.00000000	00	2	49	0.00000000	00	49	0.1357050	05
1	50	0.00000000	00	2	50	0.00000000	00	50	0.1357050	05
1	51	0.00000000	00	2	51	0.00000000	00	51	0.1357050	05
1	52	0.00000000	00	2	52	0.00000000	00	52	0.1357050	05
1	53	0.00000000	00	2	53	0.00000000	00	53	0.1357050	05
1	54	0.00000000	00	2	54	0.00000000	00	54	0.1357050	05
1	55	0.00000000	00	2	55	0.00000000	00	55	0.1357050	05
1	56	0.00000000	00	2	56	0.00000000	00	56	0.1357050	05
1	57	0.00000000	00	2	57	0.00000000	00	57	0.1357050	05
1	58	0.00000000	00	2	58	0.00000000	00	58	0.1357050	05
1	59	0.00000000	00	2	59	0.00000000	00	59	0.1357050	05
1	60	0.00000000	00	2	60	0.00000000	00	60	0.1357050	05

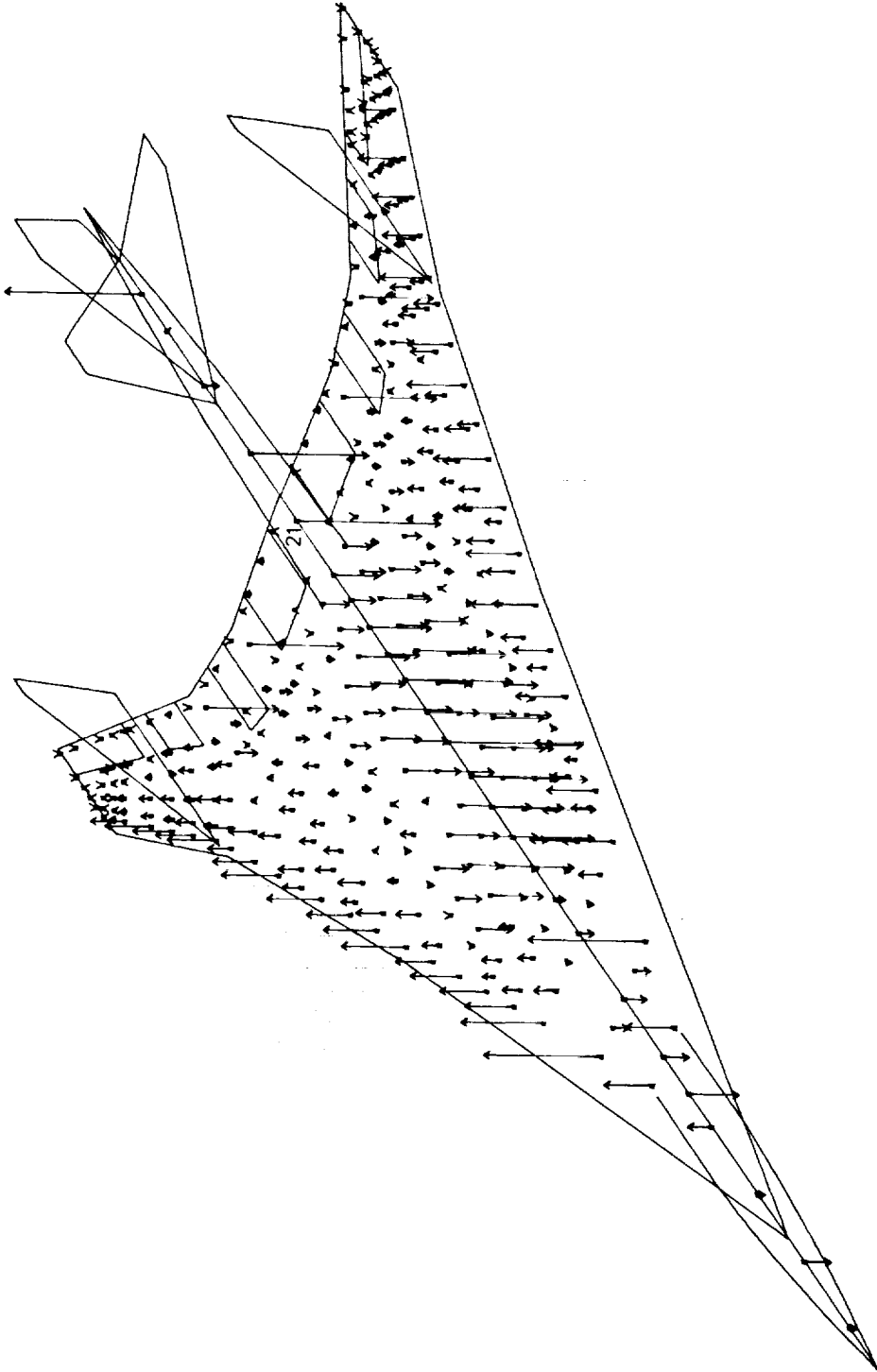
INTERNAL PAGE IS  
POOR QUALITY

TABLE 5-18. PANEL POINT LOADS - FINAL DESIGN - CONDITION 25, DYNAMIC LANDING

SLANTED LOADS

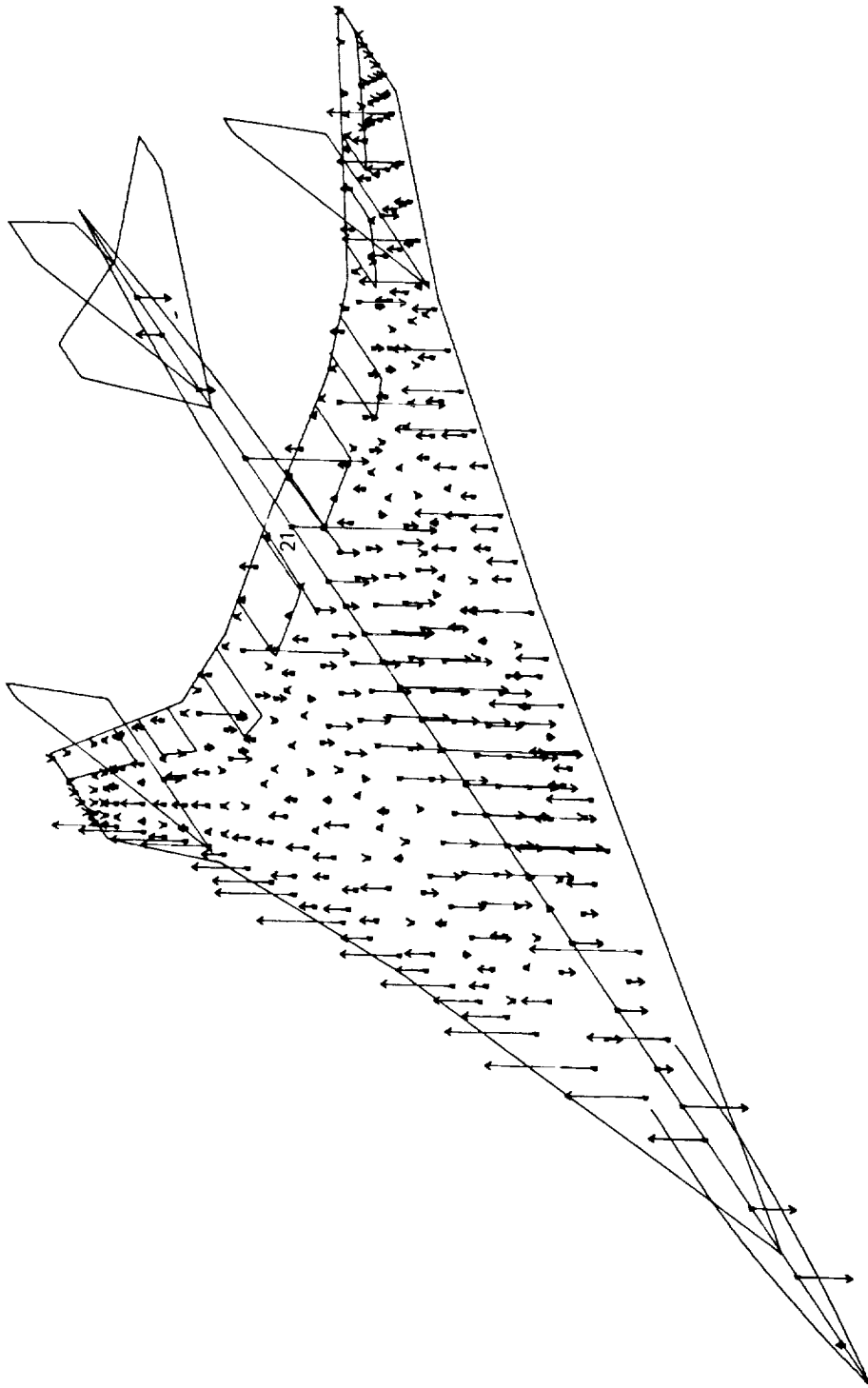
MATRIX 4175		INTL MATRIX LOADS		274 BY 14		JUL 4018		SCLT 41		LATL 4/20/74		TIML 517		PAGE 18	
REAL	FULL	CUL SMT	INDICATORS	NUM	NUM	NUM	NUM	NUM	NUM	NUM	NUM	NUM	NUM	NUM	NUM
1	-0.1901700	05	0.1307671	03	7	0.2367290	02	5	0.8528800	04	6	-0.1596920	05		
7	-0.2140416	05	-0.1067151	05	10	-0.7073517	04	11	-0.5861755	04	12	-0.6669331	04		
13	-0.2740458	05	-0.1004910	05	10	-0.7073517	04	11	-0.5861755	04	12	-0.6669331	04		
19	-0.2706816	04	-0.1524211	05	22	-0.1524211	05	22	-0.1524211	05	24	-0.4904638	04		
25	-0.2535580	05	-0.1021021	05	22	-0.1021021	05	22	-0.1021021	05	30	-0.4563476	04		
31	-0.2622700	04	-0.0731902	04	34	-0.1044102	05	34	-0.1044102	05	36	-0.2553371	05		
37	-0.2635448	04	-0.0441524	04	40	-0.0441524	04	41	-0.0441524	04	42	-0.5422606	03		
43	-0.1004471	04	-0.0427621	04	41	-0.0427621	04	41	-0.0427621	04	48	-0.3337201	04		
49	-0.1870031	04	-0.0710741	04	52	-0.0710741	04	52	-0.0710741	04	54	-0.1662471	03		
55	-0.2349111	04	-0.0461831	04	50	-0.0461831	04	50	-0.0461831	04	56	-0.1301031	04		
61	-0.2231111	02	-0.1214501	04	54	-0.1214501	04	54	-0.1214501	04	66	-0.1543471	04		
67	-0.2528701	04	-0.0825501	04	71	-0.0825501	04	71	-0.0825501	04	72	-0.1575441	03		
73	-0.2578941	04	-0.0715101	04	78	-0.0715101	04	77	-0.0715101	04	77	-0.2501360	04		
79	-0.2578941	04	-0.0715101	04	82	-0.0715101	04	85	-0.1617501	04	84	-0.5342756	04		
85	-0.2037501	04	-0.0411200	04	80	-0.0411200	04	89	-0.3234800	04	90	-0.1370350	04		
91	-0.2037501	04	-0.0411200	04	80	-0.0411200	04	89	-0.3234800	04	90	-0.1370350	04		
97	-0.2037501	04	-0.0411200	04	80	-0.0411200	04	89	-0.3234800	04	90	-0.1370350	04		
103	-0.2037501	04	-0.0411200	04	80	-0.0411200	04	89	-0.3234800	04	90	-0.1370350	04		
109	-0.2037501	04	-0.0411200	04	80	-0.0411200	04	89	-0.3234800	04	90	-0.1370350	04		
115	-0.2037501	04	-0.0411200	04	80	-0.0411200	04	89	-0.3234800	04	90	-0.1370350	04		
121	-0.2037501	04	-0.0411200	04	80	-0.0411200	04	89	-0.3234800	04	90	-0.1370350	04		
127	-0.2037501	04	-0.0411200	04	80	-0.0411200	04	89	-0.3234800	04	90	-0.1370350	04		
133	-0.2037501	04	-0.0411200	04	80	-0.0411200	04	89	-0.3234800	04	90	-0.1370350	04		
139	-0.2037501	04	-0.0411200	04	80	-0.0411200	04	89	-0.3234800	04	90	-0.1370350	04		
145	-0.2037501	04	-0.0411200	04	80	-0.0411200	04	89	-0.3234800	04	90	-0.1370350	04		
151	-0.2037501	04	-0.0411200	04	80	-0.0411200	04	89	-0.3234800	04	90	-0.1370350	04		
157	-0.2037501	04	-0.0411200	04	80	-0.0411200	04	89	-0.3234800	04	90	-0.1370350	04		
163	-0.2037501	04	-0.0411200	04	80	-0.0411200	04	89	-0.3234800	04	90	-0.1370350	04		
169	-0.2037501	04	-0.0411200	04	80	-0.0411200	04	89	-0.3234800	04	90	-0.1370350	04		
175	-0.2037501	04	-0.0411200	04	80	-0.0411200	04	89	-0.3234800	04	90	-0.1370350	04		
181	-0.2037501	04	-0.0411200	04	80	-0.0411200	04	89	-0.3234800	04	90	-0.1370350	04		
187	-0.2037501	04	-0.0411200	04	80	-0.0411200	04	89	-0.3234800	04	90	-0.1370350	04		
193	-0.2037501	04	-0.0411200	04	80	-0.0411200	04	89	-0.3234800	04	90	-0.1370350	04		
199	-0.2037501	04	-0.0411200	04	80	-0.0411200	04	89	-0.3234800	04	90	-0.1370350	04		
205	-0.2037501	04	-0.0411200	04	80	-0.0411200	04	89	-0.3234800	04	90	-0.1370350	04		





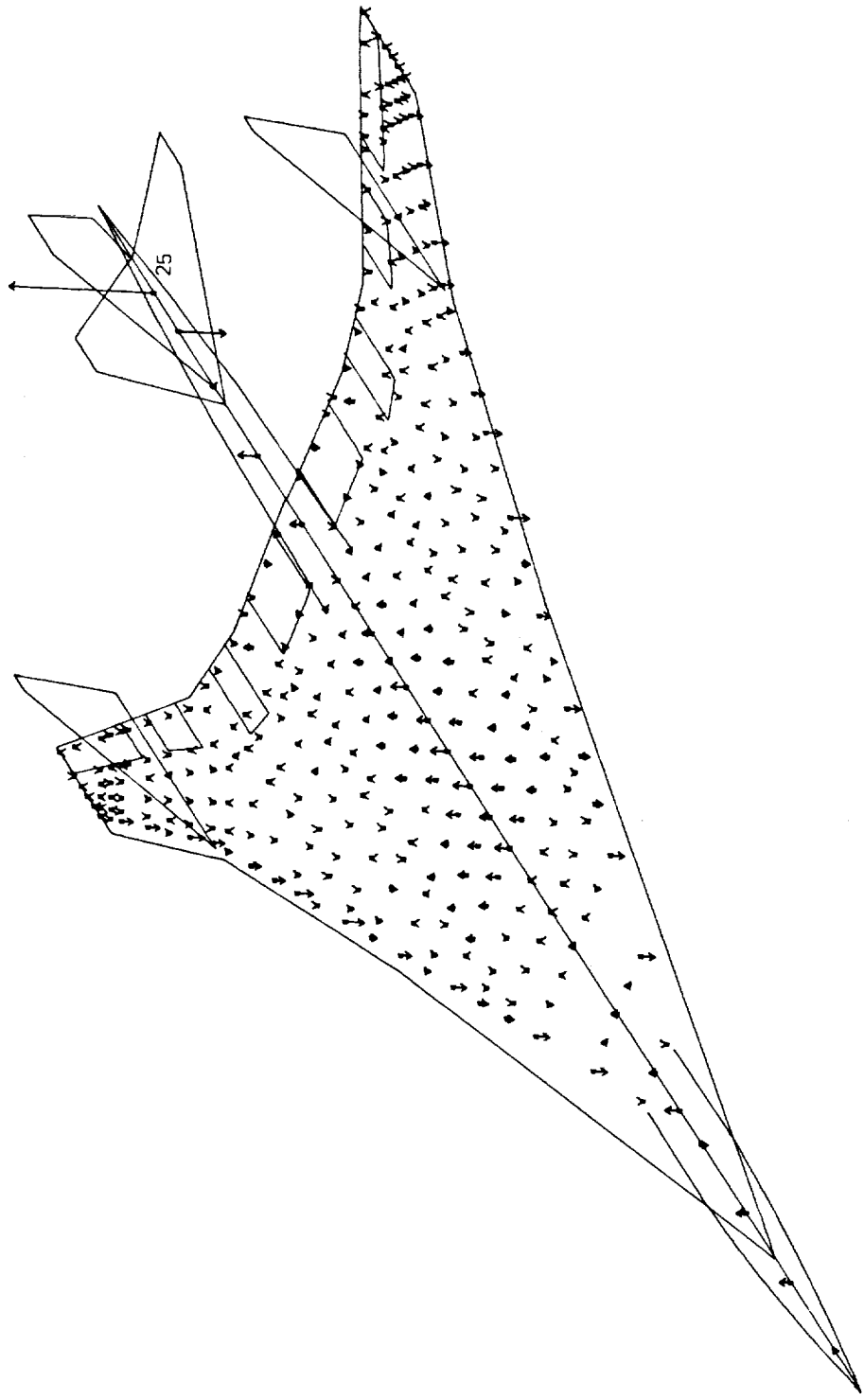
AST TASK IIB FINAL DESIGN STATIC AEROELASTIC LOAD CONDITION  $P_{Z_{GP21}} = 62.653 \text{ LB.}$

Figure 5-47. Panel Point Loads - Final Design - Condition 8, Mach 0.90 Steady Maneuver



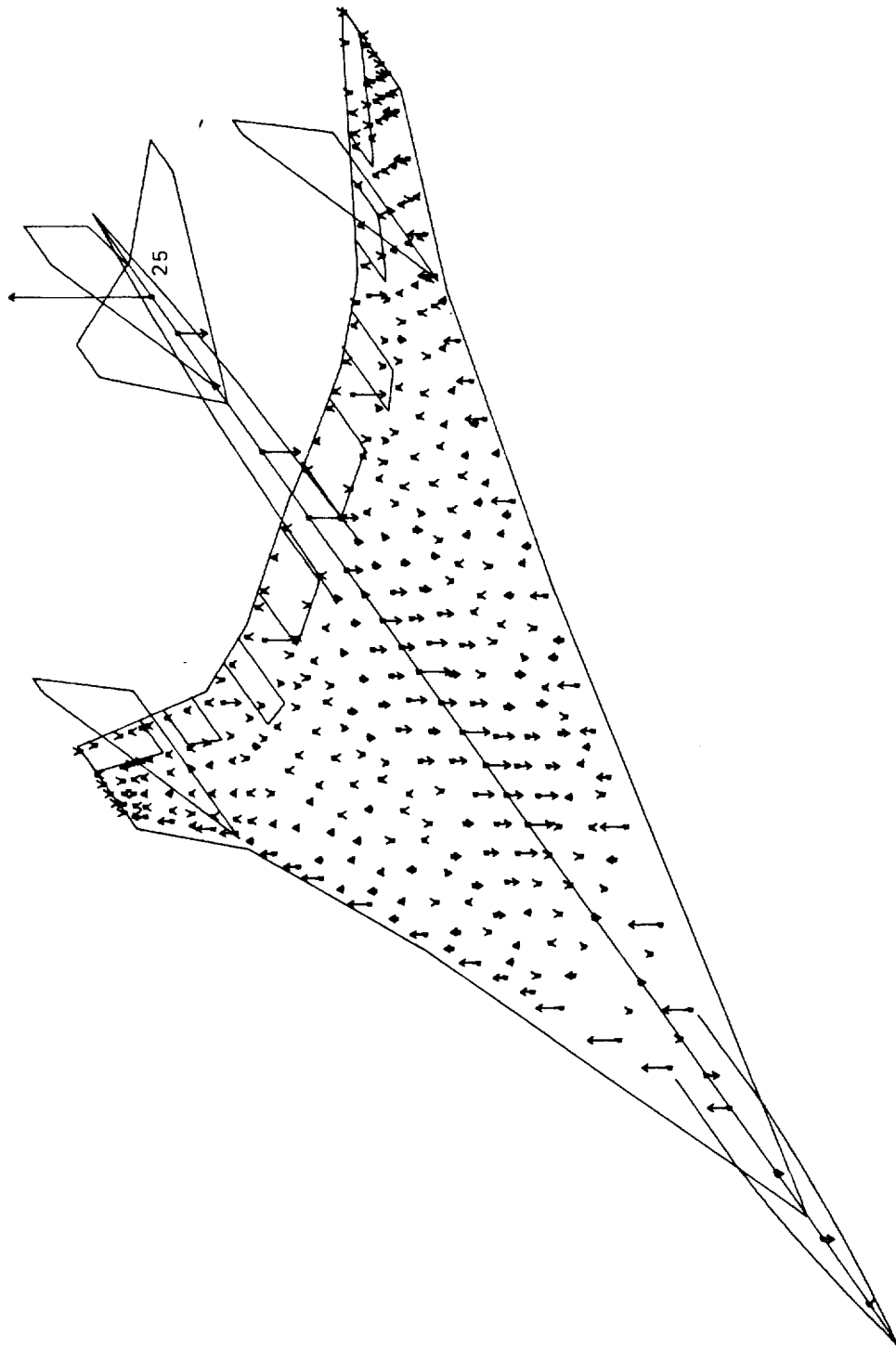
AST TASK IIB FINAL DESIGN STATIC AEROELASTIC LOAD CONDITION  $P_{Z_{GP21}} = 61,467$  LB.

Figure 5-48. Panel Point Loads - Final Design - Condition 12, Mach 1.25 Steady Maneuver



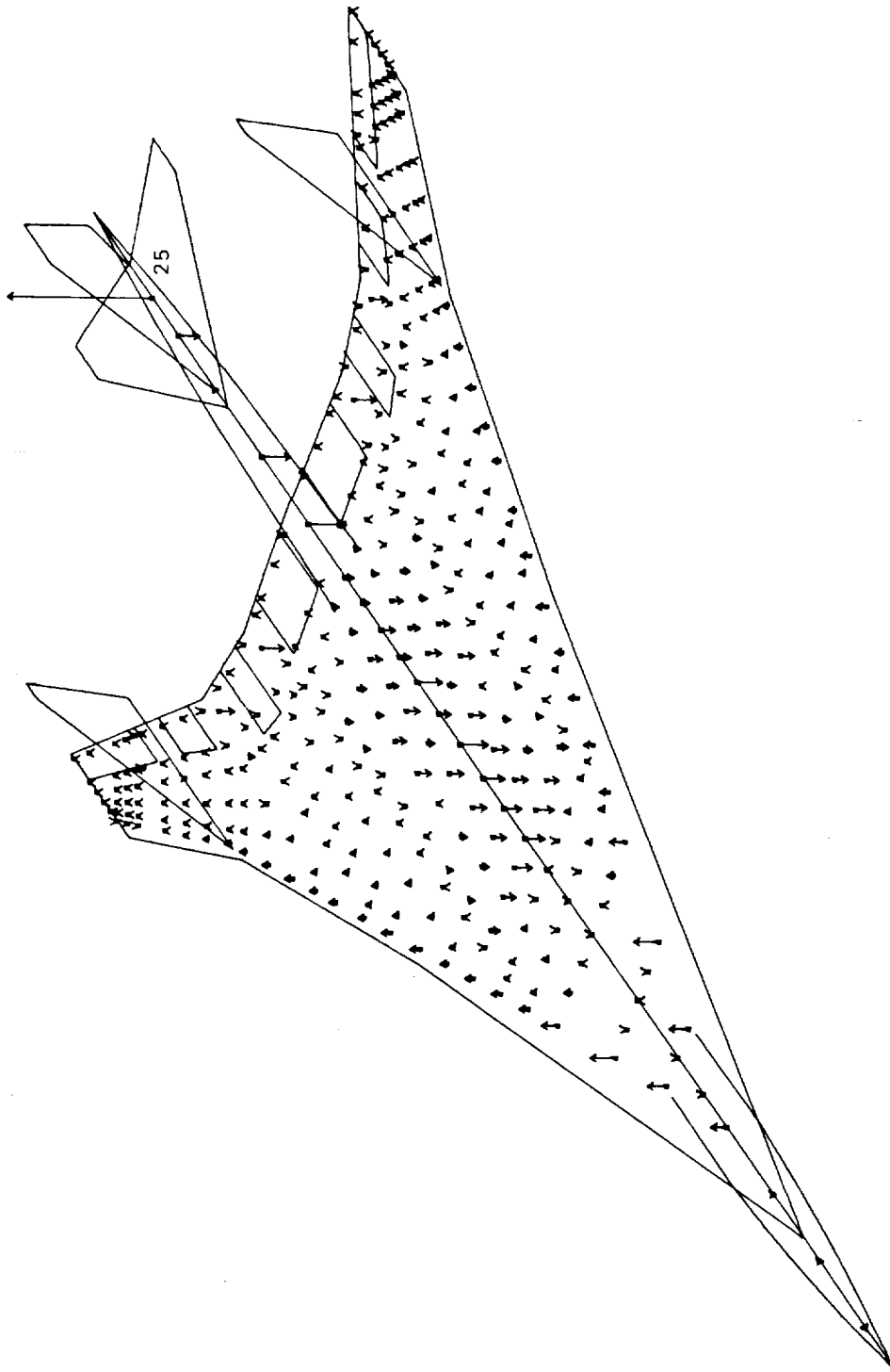
AST TASK IIB FINAL DESIGN STATIC AEROELASTIC LOAD CONDITION  $P_{ZGP25} = 139,110 \text{ LB.}$

Figure 5-57. Aeroelastic Deflections - Final Design - Condition 14, Mach 1.25 Negative Normal Accel.



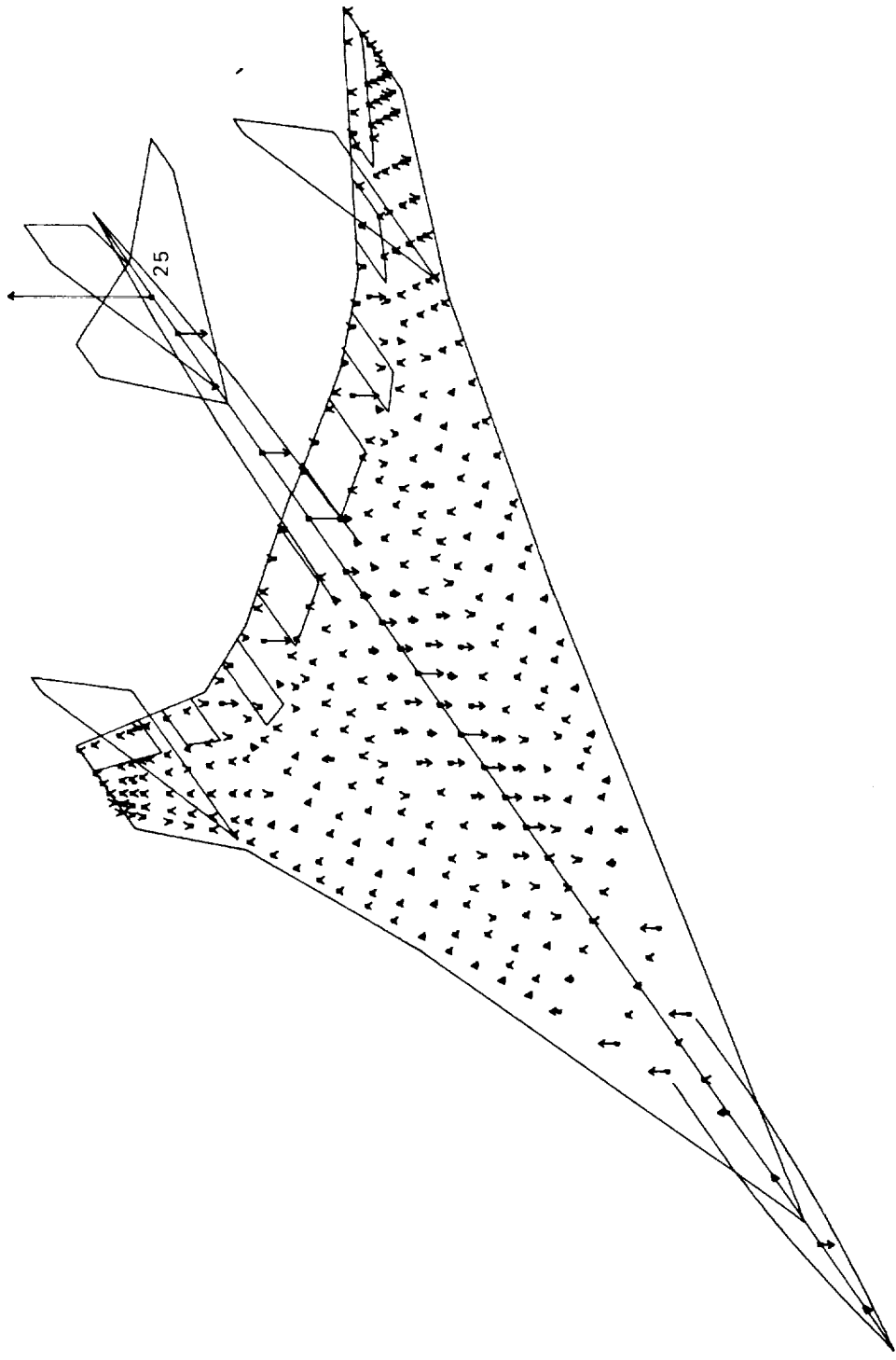
AST TASK I1B FINAL DESIGN STATIC AEROELASTIC LOAD CONDITION  $P_{ZGP25} = 216,492 \text{ LB}$

Figure 5-50. Panel Point Loads - Final Design - Condition 16, Mach 1.25 Transient Maneuver



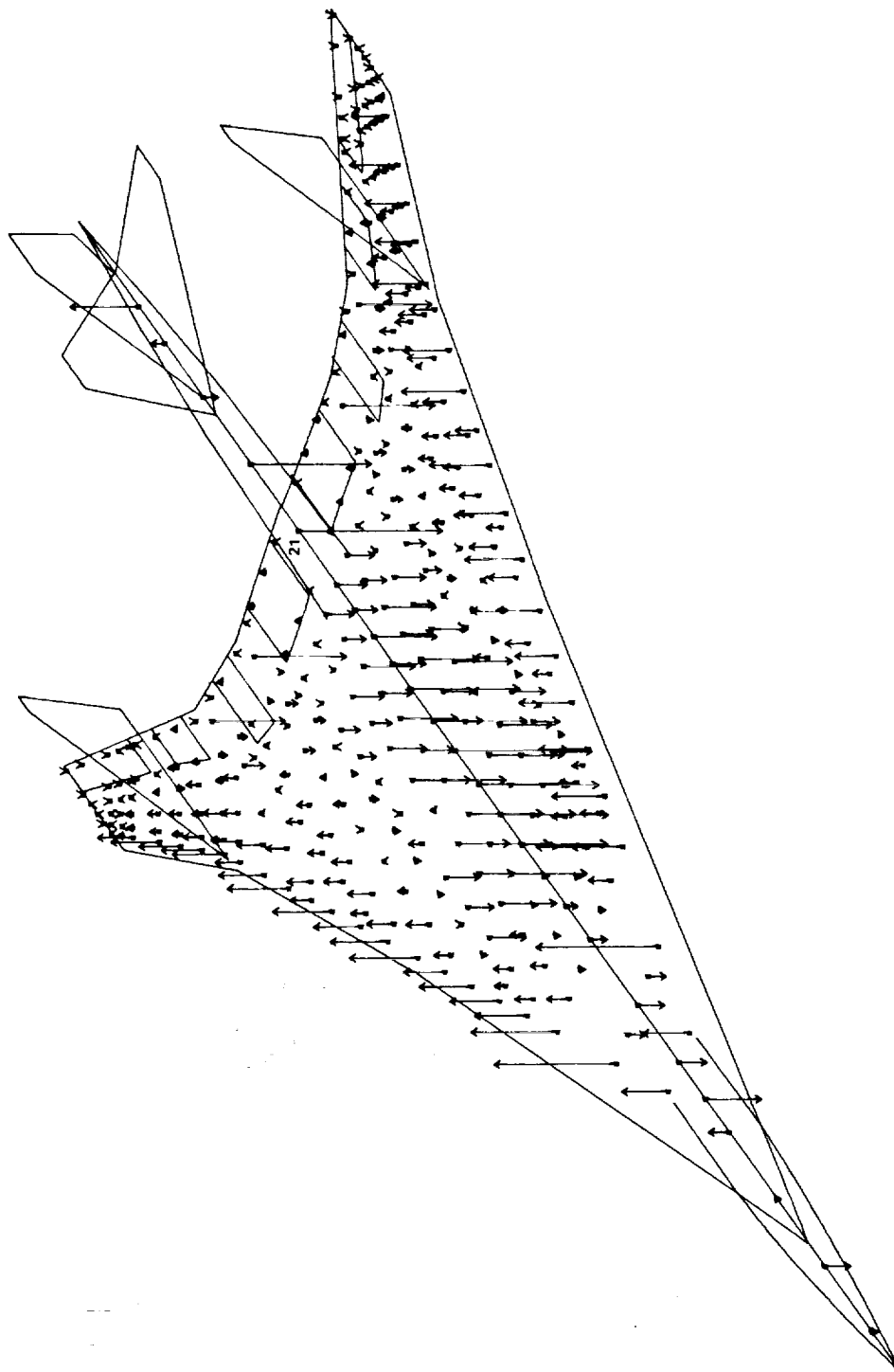
AST TASK IIB FINAL DESIGN STATIC AEROELASTIC LOAD CONDITION  $P_{ZGP 25} = 245,608 \text{ LB}$

Figure 5-51. Panel Point Loads - Final Design - Condition 20, Mach 2.7  
(Start-of-Cruise) Transient Maneuver



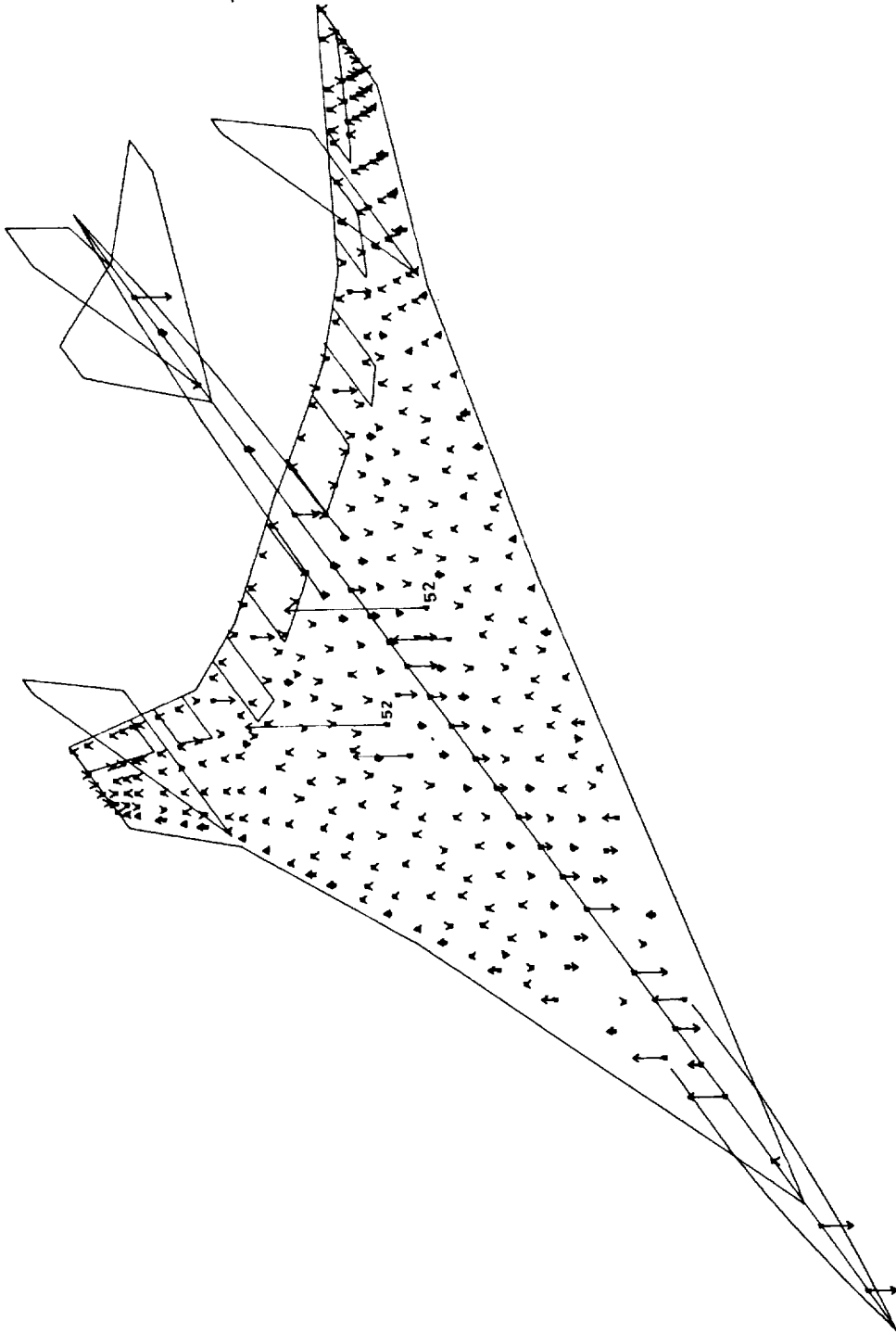
AST TASK IIB FINAL DESIGN STATIC AEROELASTIC LOAD CONDITION PZGP25 = 69,185 LB. (307,750N)

Figure 5-52. Panel Point Loads - Final Design - Condition 21, Mach 2.7  
(Mid-Cruise) 1- $\xi$  Trimmed Flight



AST TASK IIB FINAL DESIGN STATIC AEROELASTIC LOAD CONDITION  $P_{ZGP21} = .133,364 \text{ LB}$

Figure 5-53. Panel Point Loads - Final Design - Condition 23, Mach 0.90  
Pseudo Gust (Positive)



AST TASK 118 FINAL DESIGN STATIC AEROELASTIC LOAD CONDITION PZGP52 = 175,729 LB

Figure 5-54. Panel Point Loads - Final Design - Condition 25, Dynamic Landing



TABLE 5-19. AEROELASTIC DEFLECTIONS - FINAL DESIGN - CONDITION 21 (MID-CRUISE)

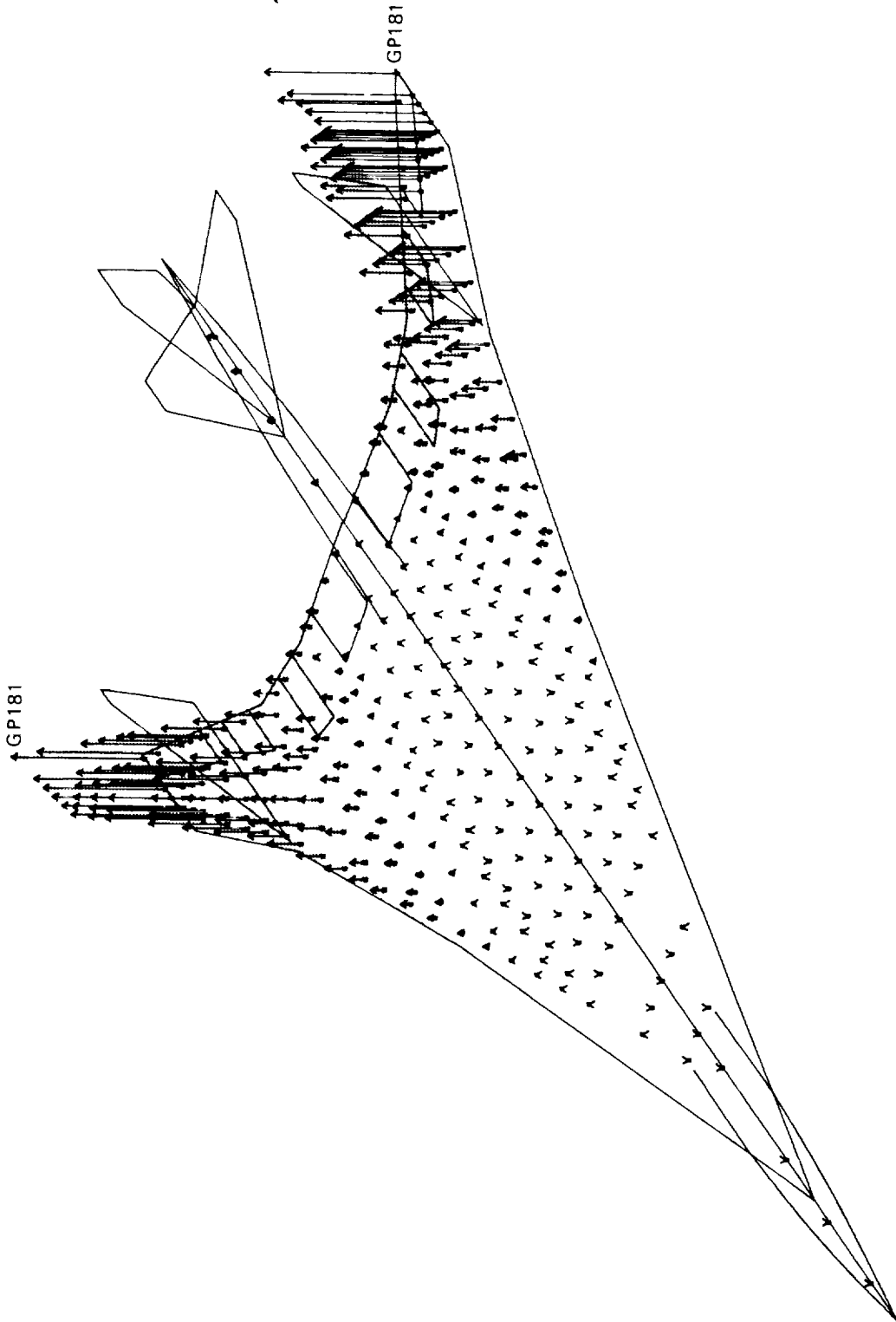
DELTA Z

MATRIX 924

MATRIX 4170 INT. MATRIX 10:22 274 BY 3 JCB 451R SECT 924 DATE 4/19/74 TIME 1240 PAGE 1

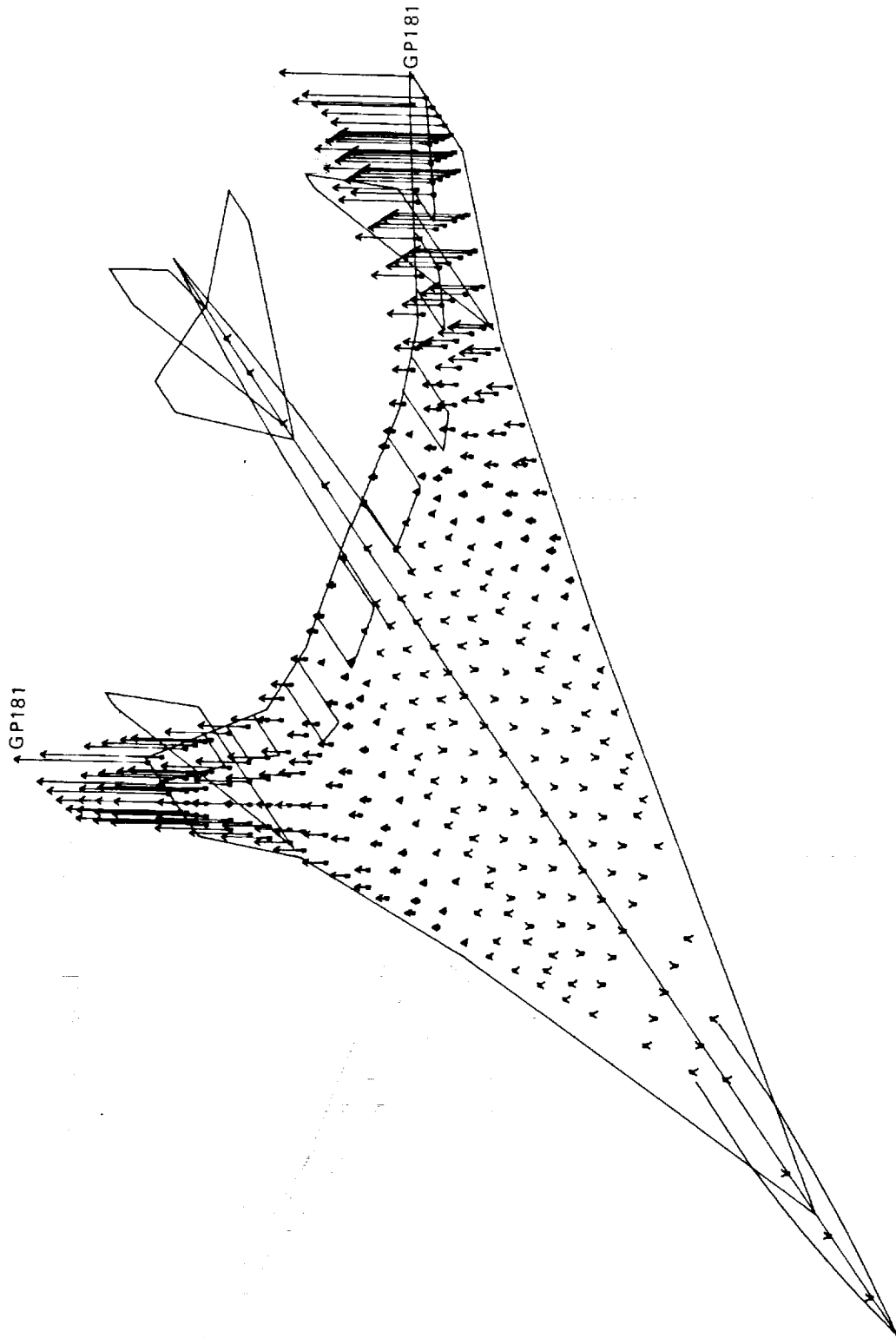
REAL	FULL	COL SORT	INDICATORS	IC	ROW	ROW	ROW	ROW	ROW	ROW	ROW	ROW	ROW	ROW	ROW
21	1	-0.182398E 01	2	-0.108162D 01	1	-0.443740E 00	5	0.112520D 00	6	0.135937D 00	7	-0.665705E-04			
8	-0.496039E 00	9	-0.758101E 00	10	-0.967442E 00	11	-0.125751E 01	12	-0.135764E 01	13	-0.130530E 01				
14	-0.114548E 01	15	-0.771010E 00	16	-0.255737E 00	17	0.222661E 00	18	0.624428E 00	19	0.150474E 01				
20	0.224408E 01	21	0.431395E 01	22	0.801047E 01	23	0.174224E 02	24	0.174224E 02	25	0.210974E 02				
26	0.192512E 00	27	-0.509266E-01	28	-0.465416E 00	29	-0.722794E 00	30	-0.963717E 00	31	-0.110331E 01				
32	-0.125876E 01	33	-0.122637E 01	34	-0.104940E 01	35	-0.750694E 00	36	-0.230327E 00	37	0.271554E 00				
38	0.861895E 00	39	0.124014E 01	40	0.224536E 01	41	0.257481E 01	42	0.262576E 01	43	0.244943E 00				
44	-0.183512E 00	45	-0.432390E 00	46	-0.687697E 00	47	-0.982859E 00	48	-0.101456E 01	49	-0.944316E 01				
50	-0.777584E 00	51	-0.218561E 01	52	-0.446635E-02	53	-0.457448E 00	54	-0.104713E 01	55	-0.162353E 01				
56	0.216550E 01	57	0.274049E 01	58	0.371858E 01	59	0.165329E 00	60	-0.254467E-01	61	-0.254104E 00				
62	-0.518419E 00	63	-0.447576E 00	64	-0.372744E 00	65	-0.750807E-01	66	0.217217E 00	67	0.552303E 00				
68	0.103378E 01	69	0.56947E 01	70	0.199484E 01	71	0.18847E 01	72	0.221832E 01	73	0.34957E 01				
74	0.209446E 00	75	0.329858E-01	76	-0.162420E 00	77	-0.127079E 01	78	0.274903E-01	79	0.243000E 00				
80	0.630264E 00	81	0.694952E 00	82	0.139599E 01	83	0.190899E 01	84	0.231534E 01	85	0.222643E 01				
86	0.253749E 01	87	0.597518E 01	88	0.342651E 00	89	0.630394E 00	90	0.604356E 00	91	0.814137E 00				
92	0.120818E 01	93	0.151232E 01	94	0.182713E 01	95	0.219629E 01	96	0.270126E 01	97	0.308454E 01				
98	0.30278E 01	99	0.254517E 01	100	0.139569E 01	101	0.116745E 01	102	0.187293E 01	103	0.225259E 01				
104	0.257358E 01	105	0.284631E 01	106	0.359428E 01	107	0.381574E 01	108	0.432689E 01	109	0.460008E 01				
110	0.440352E 01	111	0.270625E 01	112	0.245815E 01	113	0.274542E 01	114	0.259535E 01	115	0.359458E 01				
116	0.456557E 01	117	0.524392E 01	118	0.510313E 01	119	0.566801E 01	120	0.525593E 01	121	0.372194E 01				
122	0.470897E 01	123	0.523935E 01	124	0.599235E 01	125	0.692157E 01	126	0.795701E 01	127	0.921673E 01				
128	0.137441E 02	129	0.557045E 01	130	0.671291E 01	131	0.813133E 01	132	0.100041E 02	133	0.757900E 01				
134	0.566140E 01	135	0.405747E 01	136	0.116174E 01	137	0.114503E 02	138	0.109491E 02	139	0.106641E 02				
140	0.154350E 02	141	0.153105E 02	142	0.150642E 02	143	0.144436E 02	144	0.142476E 02	145	0.148573E 02				
146	0.198273E 02	147	0.196926E 02	148	0.193600E 02	149	0.193419E 02	150	0.192620E 02	151	0.248966E 02				
152	0.252570E 02	153	0.253289E 02	154	0.254154E 02	155	0.253518E 02	156	0.2544690E 02	157	0.350882E 02				
158	0.319078E 02	159	0.332265E 02	160	0.333840E 02	161	0.335537E 02	162	0.338588E 02	163	0.342490E 02				
164	0.352718E 02	165	0.368180E 02	166	0.369501E 02	167	0.372497E 02	168	0.376198E 02	169	0.380016E 02				
170	0.391371E 02	171	0.405045E 02	172	0.407148E 02	173	0.415662E 02	174	0.413391E 02	175	0.418523E 02				
176	0.430830E 02	177	0.430314E 02	178	0.428752E 02	179	0.428344E 02	180	0.4314547E 02	181	0.5426890E 02				
182	0.532455E 02	183	0.248129E 01	184	-0.463397E 01	185	0.018421E 01	186	0.0491931E 01	187	0.040000E-03				
188	0.135866E 00	189	-0.51225E-01	190	-0.690940E-01	191	-0.815944E 00	192	-0.168087E 01	193	-0.268540E 01				
194	-0.363744E 01	195	-0.444716E 01	196	-0.519871E 01	197	-0.619433E-01	198	-0.120101E 01	199	-0.247704E 01				
200	-0.365977E 01	201	-0.476628E 01	202	-0.501350E 01	203	-0.537018E-01	204	-0.178836E 00	205	-0.680177E-01				
206	0.221570E 00	208	0.885350E 00	209	0.258178E 00	210	0.459416E 00	211	0.204766E-02	214	0.240477E-02				
245	0.472840E-02	216	0.595877E-02	217	0.961342E-02	218	0.114441E-01	219	0.1378041E-01	220	0.124454E-01				
221	0.161535E-01	222	0.162334E-01	223	0.169666E-01	224	0.180723E-01	225	0.194418E-01	226	0.243008E-01				
227	0.268886E-01	228	0.357266E-01	229	0.412634E-01	230	0.459426E-01	231	0.502210E-01	232	0.549571E-01				
233	0.532443E-01	234	0.54271E-01	235	0.11397E-01	236	0.117597E-01	237	0.247094E-01	238	0.437094E-01				
240	0.572594E-02	241	0.495773E-03	242	0.113604E-02	243	0.159884E-02	244	0.117235E-02	245	0.145946E-02				
246	-0.646746E-03	247	-0.185879E-03	248	-0.336897E-02	249	-0.406688E-02	250	-0.376697E-02	251	-0.541846E-02				
252	-0.679871E-02	253	-0.880740E-02	254	-0.114523E-01	255	-0.177093E-01	256	-0.265824E-01	257	-0.4005037E-01				
258	-0.514114E-01	259	-0.638289E-01	260	-0.783435E-01	261	-0.923718E-01	262	-0.844594E-01	263	-0.140270E-01				
264	0.762883E-01	265	0.342512E-02	266	0.208349E-01	267	0.250275E-02	268	-0.345387E-02	269	0.176099E-02				
270	0.166099D-02	271	0.214510E-02	272	0.214510E-02	273	0.214510E-02	274	0.214510E-02	275	0.214510E-02				

ORIGINAL PAGE IS OF POOR QUALITY



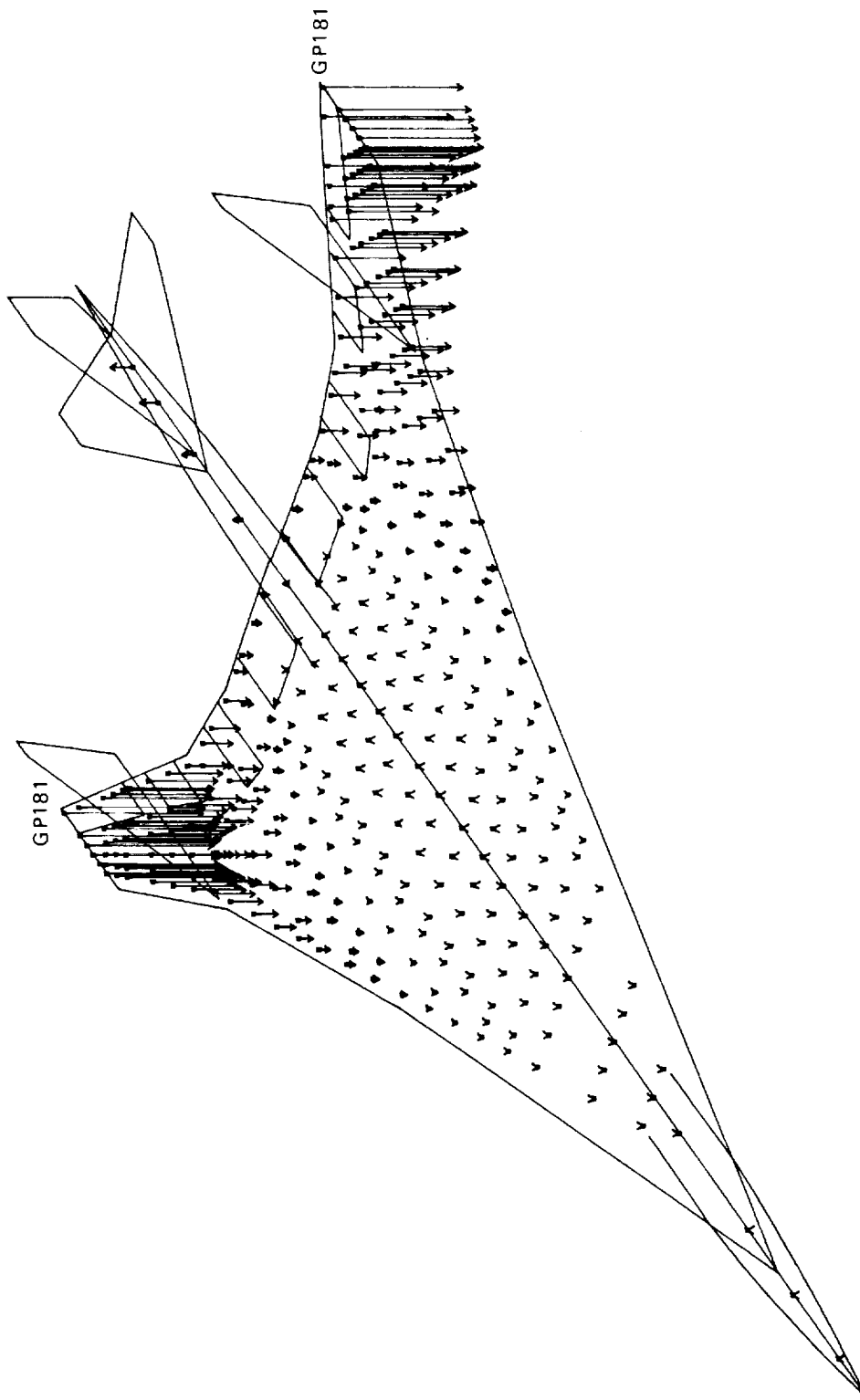
AST TASK 118 FINAL DESIGN LOAD CONDITION DEFLECTIONS - LIMIT  $\Delta Z_{GP181} = 171$  INCHES

Figure 5-55. Aeroelastic Deflections - Final Design - Condition 8, Mach 0.90 Steady Maneuver



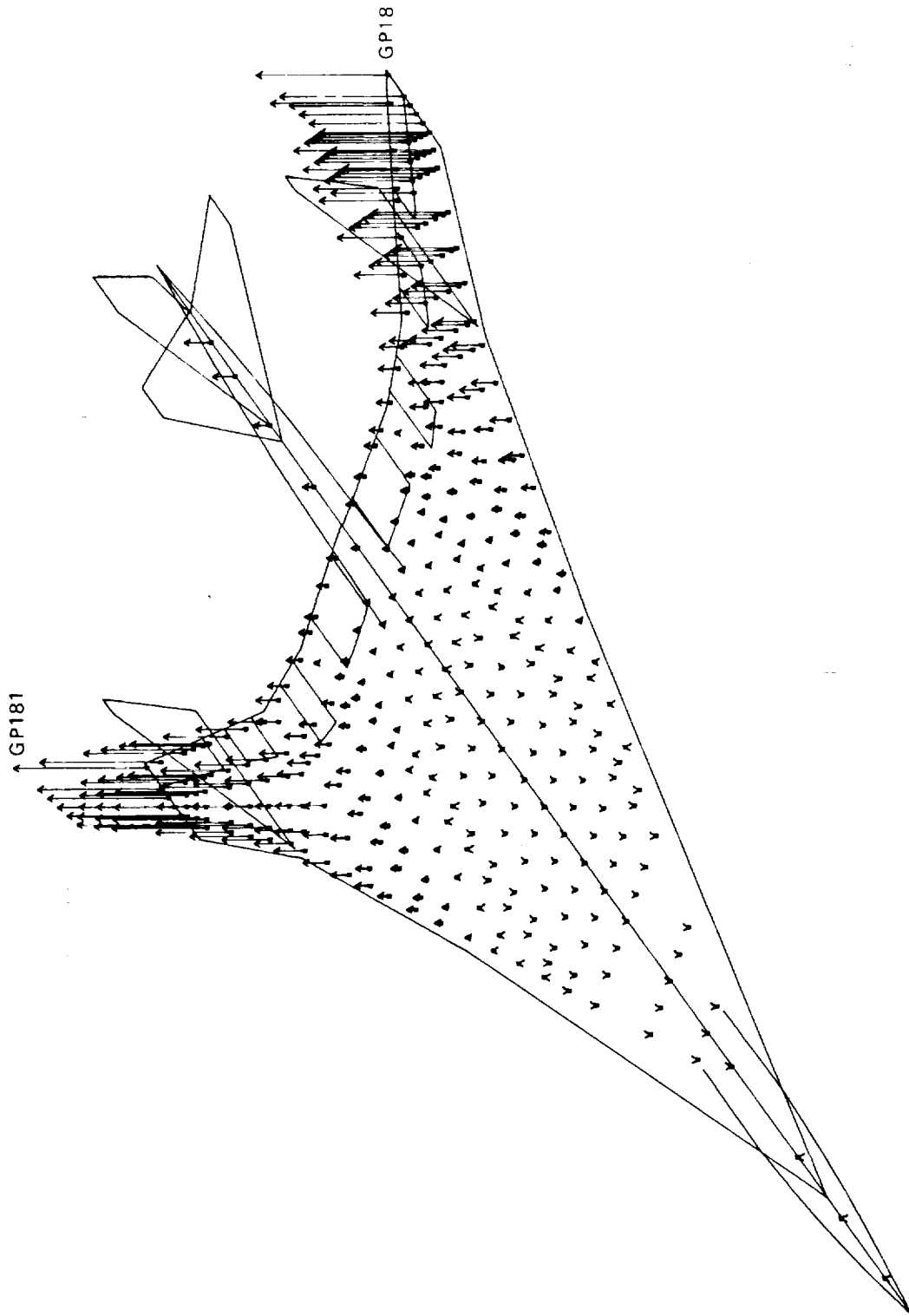
AST TASK I18 FINAL DESIGN LOAD CONDITION DEFLECTIONS - LIMIT  $\Delta Z_{GP181} = 216$  INCHES

Figure 5-56. Aeroelastic Deflections - Final Design - Condition 12, Mach 1.25 Steady Maneuver



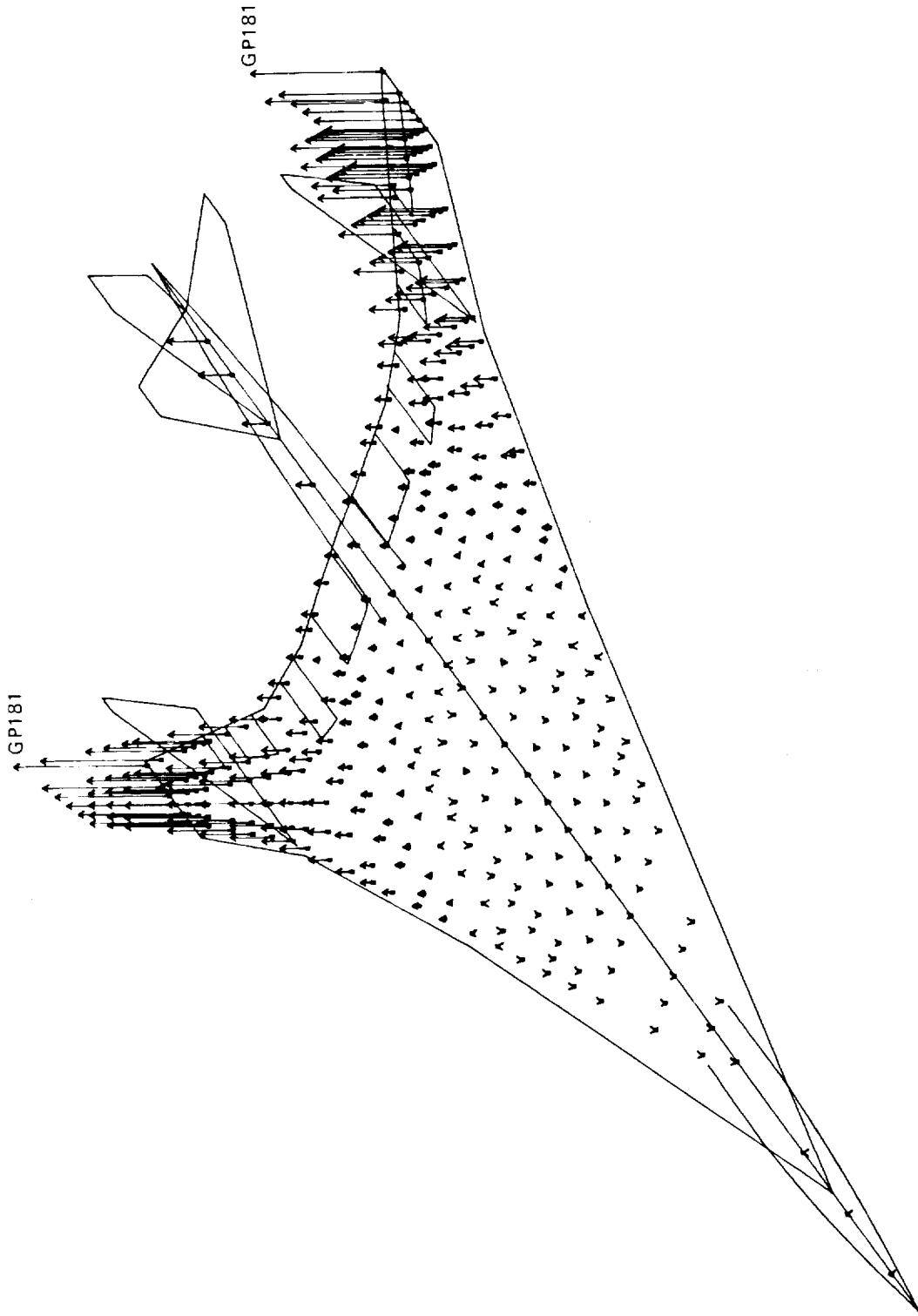
AST TASK 118 FINAL DESIGN LOAD CONDITION DEFLECTIONS - LIMIT  $\Delta Z_{GP181} = 92$  INCHES

Figure 5-49. Panel Point Loads - Final Design - Condition 14, Mach 1.25 Negative Normal Accel.



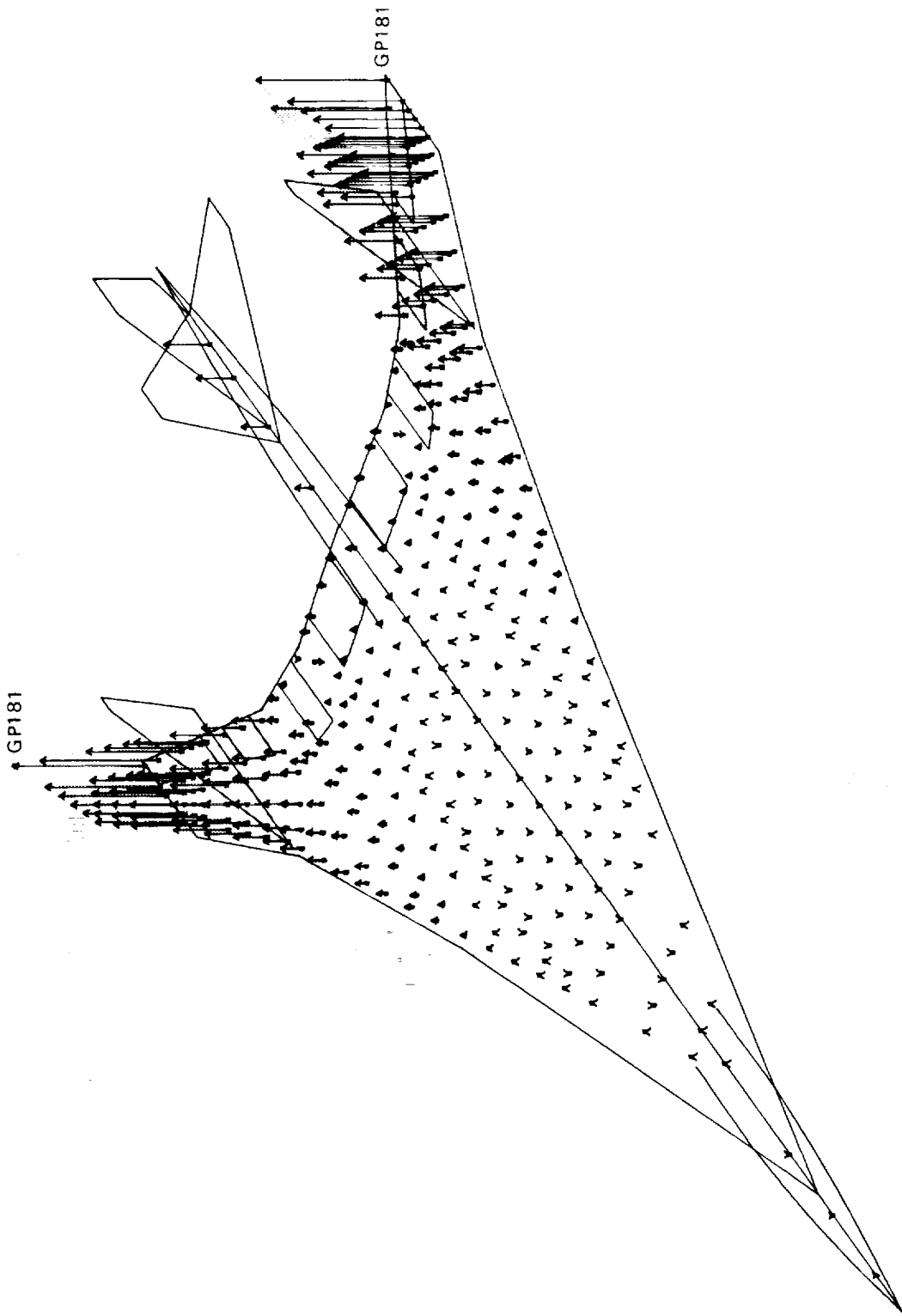
AST TASK IIB FINAL DESIGN LOAD CONDITION DEFLECTIONS - LIMIT  $\Delta Z_{GP181} = 176$  INCHES

Figure 5-58. Aeroelastic Deflections - Final Design - Condition 16, Mach 1.25 Transient Maneuver



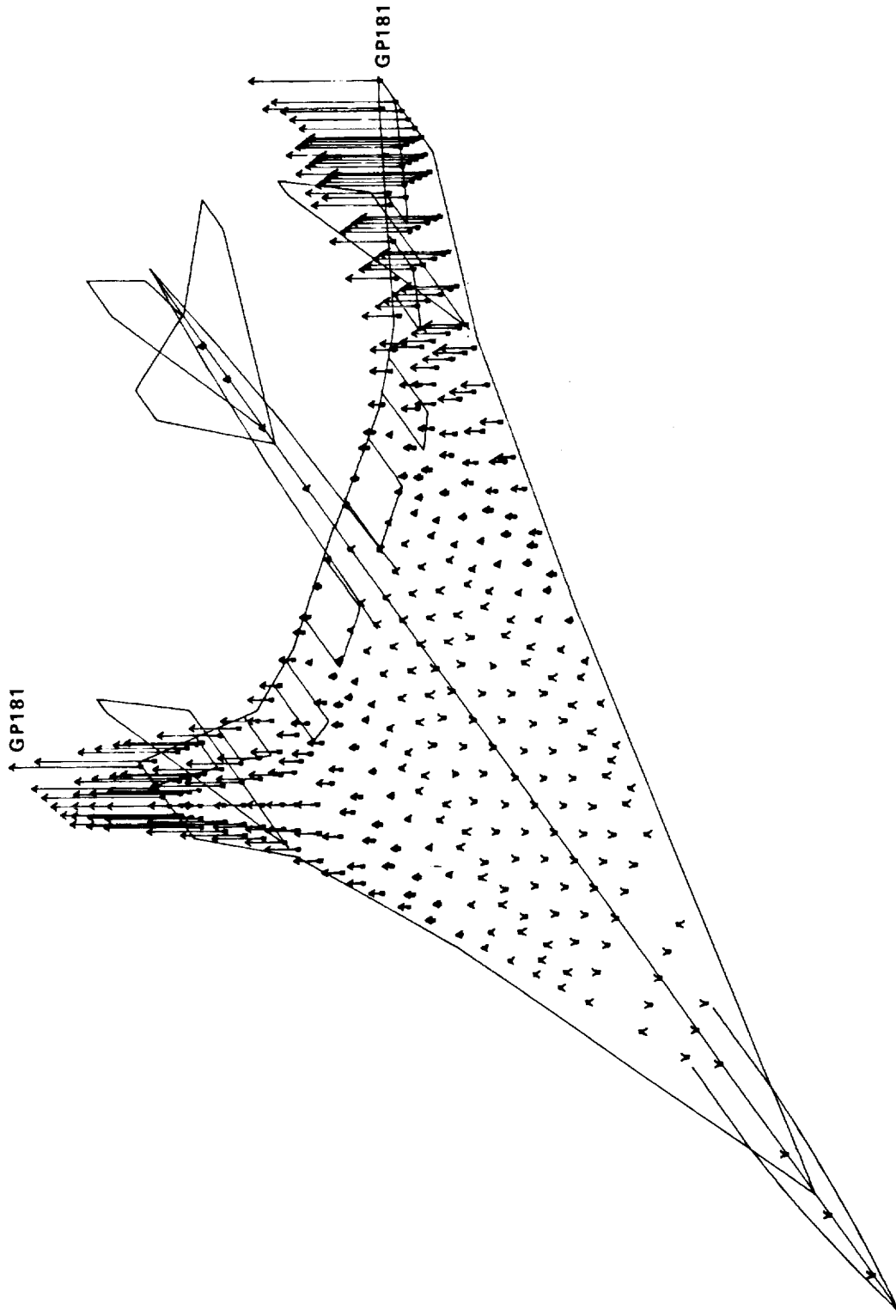
AST TASK IIB FINAL DESIGN LOAD CONDITION DEFLECTIONS - LIMIT  $\Delta Z_{GP 181} = 148$  INCHES

Figure 5-59. Aeroelastic Deflections - Final Design - Condition 20, Mach 2.7  
(Start-of-Cruise) Transient Maneuver



AST TASK I18 FINAL DESIGN LOAD CONDITION DEFLECTIONS - LIMIT  $\Delta Z_{GP181} = 59$  inch (1.50-meter)

Figure 5-60. Aeroelastic Deflections - Final Design - Condition 21, Mach 2.7  
(Mid-Cruise) 1-g Trimmed Flight



AST TASK I18 FINAL DESIGN LOAD CONDITION DEFLECTIONS - LIMIT  $\Delta Z_{GP181} = 373$  INCHES

Figure 5-61. Aeroelastic Deflections - Final Design - Condition 23, Mach 0.90  
Pseudo Gust (Positive)



## REFERENCE

1. Albano, E. and Rodden, W.P., "A Doublet-Lattice Method for Calculation Lift Distributions on Oscillating Surfaces in Subsonic Flows," AIAA Journal, Volume 7, February 1969, pp 279-285, Errata AIAA Journal, Volume 7, November 1969, p. 2192.

1

2

3

4

5

6

SECTION 6  
STRUCTURAL TEMPERATURES  
BY  
D. A. BROGAN

1

2

3

4

5

6

## TABLE OF CONTENTS

<u>Section</u>	<u>Page</u>
INTRODUCTION	6-1
HEAT TRANSFER ANALYTICAL METHODS	6-2
Heat Balance Equations	6-3
Inviscid Flow Field Determination	6-5
Heat Transfer Coefficients	6-6
Thermophysical Properties	6-12
Network Thermal Analysis Techniques	6-17
STRUCTURAL TEMPERATURES - TASK I	6-36
Finite Element Model (2-D NASTRAN)	6-36
Chordwise Stiffened Wing Panels	6-41
Spanwise Stiffened Wing Panels	6-57
Monocoque Wing Panels	6-57
Composite Reinforced Wing Panels	6-64
Fuselage Panels and Frames	6-64
Fuel Thermal Analysis	6-70
Honeycomb Braze Study	6-73
STRUCTURAL TEMPERATURES - TASK II	6-78
Wing Structure Temperatures	6-78
Finite Element Model (3-D NASTRAN)	6-81
Cruise Isotherms - Mach 2.62 (Hot Day)	6-85
STRUCTURAL TEMPERATURES - TASK III	6-95
Wing Structure Temperatures	6-95
Fuselage Temperatures	6-98
Cruise Isotherms - Mach 2.16 (Hot Day)	6-98
REFERENCES	6-103

1

2

3

4

5

6

## LIST OF FIGURES

<u>Figure</u>		<u>Page</u>
6-1	Thermal Properties - Titanium Alloy	6-14
6-2	Thermal Properties - Fiberglass Insulation	6-15
6-3	Thermal Properties - Jet-A Turbine Fuel	6-15
6-4	Turbine Fuel Vapor Pressure	6-16
6-5	Thermal Properties - Graphite/Epoxy Composite	6-18
6-6	Thermal Properties - Boron/Epoxy Composite	6-19
6-7	Thermal Properties - Boron/Aluminum Composite	6-19
6-8	Wing Box Thermal Analyzer Network	6-22
6-9	Network Node Definition, Type-1 Wing Panels	6-22
6-10	Network Node Definition, Type-2 Wing Panels	6-23
6-11	Network Node Definition, Fuselage Panel and Frame	6-23
6-12	Network Node Definition, Submerged Beam Caps	6-25
6-13	Fuel Tank Codes and Locations - Task I	6-29
6-14	Fuel Tank Codes and Locations - Task II	6-29
6-15	Fuel Mass for Tank Combinations - Task I	6-31
6-16	Fuel Height vs Mass for Tank Combinations - Task I	6-32
6-17	Fuel Mass for Tank Combinations - Task II	6-33
6-18	Fuel Height vs Mass, Fuselage Tanks - Task II	6-34
6-19	Fuel Height vs Mass, Forward Wing Tanks - Task II	6-34
6-20	Fuel Height vs Mass, Aft Wing Tanks - Task II	6-35
6-21	Surface Isotherms - Mach 2.7 Cruise	6-37
6-22	Finite Element Model Temperatures - Mach 2.7 Mid-Cruise	6-39
6-23	F. E. Model Temperatures - Chordwise Stiffened - Mach 2.7 Start-of-Cruise	6-43
6-24	F. E. Model Temperatures - Spanwise Stiffened - Mach 2.7 Start-of-Cruise	6-45
6-25	F. E. Model Temperatures - Monocoque - Mach 2.7 Start-of-Cruise	6-47
6-26	Chordwise Stiffened Wing Panel Temperature Histories - 40236 Upper Surface	6-49

LIST OF FIGURES (Continued)

<u>Figure</u>		<u>Page</u>
6-27	Chordwise Stiffened Wing Panel Temperature Histories - 40236 Lower Surface	6-49
6-28	Chordwise Stiffened Wing Panel Temperature Histories - 40316 Upper Surface	6-50
6-29	Chordwise Stiffened Wing Panel Temperature Histories - 40316 Lower Surface	6-50
6-30	Chordwise Stiffened Wing Panel Temperature Histories - 40322 Upper Surface	6-51
6-31	Chordwise Stiffened Wing Panel Temperature Histories - 40322 Lower Surface	6-51
6-32	Chordwise Stiffened Wing Panel Temperature Histories - 40528 Upper Surface	6-52
6-33	Chordwise Stiffened Wing Panel Temperature Histories - 40528 Lower Surface	6-52
6-34	Chordwise Stiffened Wing Panel Temperature Histories - 40536 Upper Surface	6-53
6-35	Chordwise Stiffened Wing Panel Temperature Histories - 40536 Lower Surface	6-53
6-36	Chordwise Stiffened Wing Panel Temperature Histories - 41036 Upper Surface	6-54
6-37	Chordwise Stiffened Wing Panel Temperature Histories - 41036 Lower Surface	6-54
6-38	Chordwise Stiffened Wing Panel Temperature Histories - 41316 Upper Surface	6-55
6-39	Chordwise Stiffened Wing Panel Temperature Histories - 41316 Lower Surface	6-55
6-40	Chordwise Stiffened Wing Panel Temperature Histories - 41348 Upper Surface	6-56
6-41	Chordwise Stiffened Wing Panel Temperature Histories - 41348 Lower Surface	6-56
6-42	Spanwise Stiffened Wing Panel Temperature Histories - 40322 Upper Surface	6-58
6-43	Spanwise Stiffened Wing Panel Temperature Histories - 40322 Lower Surface	6-58
6-44	Spanwise Stiffened Wing Panel Temperature Histories - 40536 Upper Surface	6-59
6-45	Spanwise Stiffened Wing Panel Temperature Histories - 40536 Lower Surface	6-59



LIST OF FIGURES (Continued)

<u>Figure</u>		<u>Page</u>
6-46	Spanwise Stiffened Wing Panel Temperature Histories - 41316 Upper Surface	6-60
6-47	Spanwise Stiffened Wing Panel Temperature Histories - 41316 Lower Surface	6-60
6-48	Monocoque Wing Panel Temperature Histories - 40322 Upper Surface	6-61
6-49	Monocoque Wing Panel Temperature Histories - 40322 Lower Surface	6-61
6-50	Monocoque Wing Panel Temperature Histories - 40536 Upper Surface	6-62
6-51	Monocoque Wing Panel Temperature Histories - 40536 Lower Surface	6-62
6-52	Monocoque Wing Panel Temperature Histories - 41316 Upper Surface	6-63
6-53	Monocoque Wing Panel Temperature Histories - 41316 Lower Surface	6-63
6-54	Composite Reinforced Wing Panel Temperature Histories - 40322 Upper Surface	6-65
6-55	Composite Reinforced Wing Panel Temperature Histories - 40322 Lower Surface	6-65
6-56	Composite Reinforced Wing Panel Temperature Histories - 40536 Upper Surface	6-66
6-57	Composite Reinforced Wing Panel Temperature Histories - 40536 Lower Surface	6-66
6-58	Composite Reinforced Wing Panel Temperature Histories - 41316 Upper Surface	6-67
6-59	Composite Reinforced Wing Panel Temperature Histories - 41316 Lower Surface	6-67
6-60	Bulk Fuel Temperatures in Wing Tanks - Task II	6-72
6-61	Effect of Braze Flow on Honeycomb Panel Temperature Gradient	6-75
6-62	Effective Conductance for Honeycomb Panels	6-77
6-63	Temperatures at Wing Cross Section - Mach 2.62 Start-of-Cruise	6-82
6-64	Temperatures at Wing Cross Section - Mach 2.62 Mid-Cruise	6-83

LIST OF FIGURES (Continued)

<u>Figure</u>		<u>Page</u>
6-65	Temperatures at Wing Cross Section - Mach 1.25 Descent	6-84
6-66	Finite Element Model Wing Temperatures - Mach 2.62 Start-of-Cruise	6-87
6-67	Finite Element Model Wing Temperatures - Mach 2.62 Mid-Cruise	6-89
6-68	Finite Element Model Wing Temperatures - Mach 1.25 Descent	6-91
6-69	External Surface Isotherms - Mach 2.62 Cruise	6-93
6-70	External Surface Isotherms - Mach 2.16 Cruise	6-100

LIST OF TABLES

<u>Table</u>		<u>Page</u>
6-1	Solar Heat Flux vs Altitude	6-7
6-2	Local Flow on a Supersonic Wedge	6-7
6-3	Surface Radiation Properties	6-14
6-4	Temperatures and Gradients for Fuselage Skin Panels - Task I	6-68
6-5	Temperatures and Gradients for Fuselage Frames - Task I	6-69
6-6	Temperatures and Gradients for Wing Structure - Task II	6-79
6-7	Temperatures and Gradients for Wing Structure - Task III	6-96
6-8	Temperatures and Gradients for Fuselage Skin Panels - Task III	6-99
6-9	Temperatures and Gradients for Fuselage Frames - Task III	6-99

1

2

3

4

5

6

7

## LIST OF SYMBOLS

A	area
C	thermal capacity
$C_f$	skin friction coefficient
$c_p$	specific heat at constant pressure
F	radiation geometric view factor
H	enthalpy
h	heat transfer coefficient
k	thermal conductivity
L	length
M	Mach number
P	pressure
Pr	Prandtl number
q	heat flow rate
R	gas constant
r	recovery factor
Re	Reynolds number
S	solar energy flux
St	Stanton number
T	temperature
V	velocity
$\alpha$	radiative absorptivity
$\gamma$	specific heat ratio
$\delta$	solar incidence angle
$\epsilon$	radiative emissivity
$\theta$	time
$\rho$	density
$\sigma$	Stefan-Boltzmann constant

1

2

3

4

5

6

## SECTION 6

### STRUCTURAL TEMPERATURES

#### INTRODUCTION

In establishing the supersonic cruise aircraft structural design, an accurate knowledge of the thermal environment and the response of the structure to this environment is required. Since up to three-fourths of the airframe life will be spent at supersonic cruise, the exterior will be subjected to temperatures in excess of 450K (350 F) for one to three hours per flight. In addition, transients which occur during climb and descent will subject the structures to cyclic variations in thermal gradients and result in differential expansion and thermal stresses.

The generation and analysis of structural temperatures were accomplished to support the design concepts studies. Of primary concern in Task I was to establish the interactions between the thermal environment and the other designing parameters, including the effect of variations in structural arrangement, concepts and materials. Thus, the major effort included:

- Establishment of analytical methods for detail thermal analysis of candidate structural design concepts.
- Generation of element temperatures for the two-dimensional structural models (i.e. chordwise stiffened, spanwise stiffened, monocoque).
- Development of structural temperature histories for the basic 4200 n. mile design flight profile for candidate structural concepts.
- Evaluation of thermal protection concepts for fuel tankage systems.
- Determination of the thermal effects of braze material flow into the honeycomb core of monocoque panels.

A more detailed representation of the structural elements of the hybrid structural approach selected for the engineering design and analysis effort of Task II was determined using the established methodology. The specific Task II effort thus included:

- Development of structural temperatures and thermal gradients for the aircraft incorporating configuration improvements using the selected structural design concepts.
- Generation of element and grid point temperatures for the three-dimensional structural model.

To determine the effect of a reduced thermal environment on the structural arrangement, concepts, material and aircraft mass, the Task III effort was concerned with:

- Generation of structural temperatures and thermal gradients for a Mach 2.2 cruise mission by off-design performance of the baseline (Task II) aircraft configuration.

#### HEAT TRANSFER ANALYTICAL METHODS

The analytical methods used to determine the heat loads, temperature histories, and thermal gradients for the airframe structure are described in this section. The thermal analysis of an aircraft subject to aerodynamic heating can be divided into five steps:

1. Determination of the nonviscous flow field about the aircraft. This step requires the selection of a flight profile and a design atmosphere which, along with vehicle configuration, yields the ambient air properties at the outer edge of the boundary layer.
2. Selection of an appropriate expression for the rate of thermal energy transferred to the skin from the hot gases in the boundary layer (i.e., determination of the aerodynamic heat transfer coefficient).

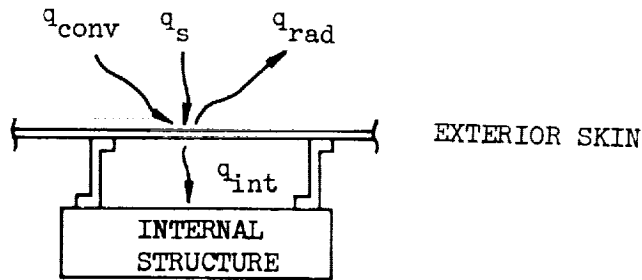


3. Establishment of structural component thermophysical properties.
4. Selection of a mathematical model describing the heat flow paths within the structure.
5. Determination of transient temperature histories for structural components by solving the mathematical model for the selected flight profile.

Details of the first four steps are presented in the following subsections. The structural temperature histories for various design concepts are presented in the appropriate task subsections.

#### Heat Balance Equations

The thermal energy balance at a typical segment of aircraft structure is presented below to show the heat transfer parameters which describe an aircraft thermal analysis and to preface the sections which describe how these parameters were obtained. A sketch of an elementary structural segment is:



The heat balance equation at the surface is

$$q_{\text{conv}} + q_s - q_{\text{rad}} - q_{\text{int}} = C_{\text{skin}} \frac{dT_w}{d\theta}$$

where

- $q_{conv}$  = heat input from aerodynamic heating
- $q_s$  = heat input from solar radiant energy
- $q_{rad}$  = heat lost to exterior by radiation
- $q_{int}$  = heat lost to interior structure
- $C_{skin}$  = thermal capacity of the skin element
- $T_w$  = skin temperature
- $\theta$  = time

The heat balance equation can be expanded (assuming the heat lost to the interior is by radiation and conduction only) to:

$$hA (T_r - T_w) + \alpha_s AS \cos \delta - \epsilon FA \sigma (T_w^4 - T_{ext}^4) - \mathcal{F}_{int} A \sigma (T_w^4 - T_{int}^4) - \frac{kA_c}{L_c} (T_w - T_{int}) = C_{skin} \frac{dT_w}{d\theta}$$

where

- $h$  = aerodynamic heat transfer coefficient
- $k$  = thermal conductivity of conduction path to interior component
- $A$  = area of the skin element
- $A_c$  = area of the conductive path
- $L_c$  = length of the conduction path
- $S$  = solar energy flux
- $\alpha_s$  = solar absorptivity
- $\epsilon$  = emissivity of the skin exterior (in the infrared)
- $F$  = view factor to space

$F_{int}$  = overall radiation interchange factor between the skin and interior component

$T_r$  = recovery temperature

$T_{ext}$  = environment temperature

$T_{int}$  = temperature of the interior structure

$\sigma$  = Stefan-Boltzmann constant

Additional terms to account for internal convection (fuel or boundary layer leakage) can be added if required. The solar energy flux,  $S$ , is a function of altitude due to atmospheric attenuation. Table 6-1 shows the flux values (corrected for an average incidence angle of 15-degrees) used for this analysis. Thermal conductivity, solar absorptivity, infrared emissivity, and thermal capacity are functions of the materials used and are presented in the Thermo-physical Properties section. The sink temperature for radiation relief is generally the average temperature of the surroundings. For surfaces viewing the sky at altitudes above 6 kilometers (20,000 feet), a sink temperature of 35 K (-400 F) is assumed. View factors, area, and lengths are determined by the details of the thermal analysis technique (network analysis) described in a section to follow. The development of aerodynamic heating coefficients and recovery temperatures are discussed in the following two sections.

#### Inviscid Flow Field Determination

Local flow properties (pressure, temperature, velocity) at all examined locations on the airplane external surface are calculated by the equations of compressible flow theory as in Reference 1. Freestream air properties are obtained from the vehicle flight profile and from the United States Standard (1962) Atmosphere tables (Reference 2). The "hot day" condition for these analyses is defined as an ambient temperature 8K above standard day temperature.

The specification of flow properties at the boundary layer edge requires knowledge of either the local flow deflection angle or the local pressure coefficient. Local flow angles are obtained from airplane configuration drawings, and provide, with the vehicle angle of attack, a fairly good approximation of local flow properties at the boundary layer edge. More precise flow definition is obtained with the use of local pressure coefficients, which can account for wing twist, surface irregularities, etc. Pressure coefficients are obtained from aerodynamic load calculations for various Mach numbers and angles of attack for a grid of surface points on the airplane.

A typical calculation procedure for local flow properties is shown in Table 6-2. The equations are for a wedge (flat plate) in supersonic flow, and are applicable to all wing, fin, and fuselage areas (excluding conical sections at nose and tail). Temperature dependence of air properties is included in all calculations. Real gas effects are included for all supersonic flow field calculations and for heat transfer calculations above Mach 3. The air property charts of Reference 3 and 4 are used, either in tabular form for interpolation or as functional curve fits.

#### Heat Transfer Coefficients

The following procedures are used to calculate heat transfer coefficients for aerodynamic heating:

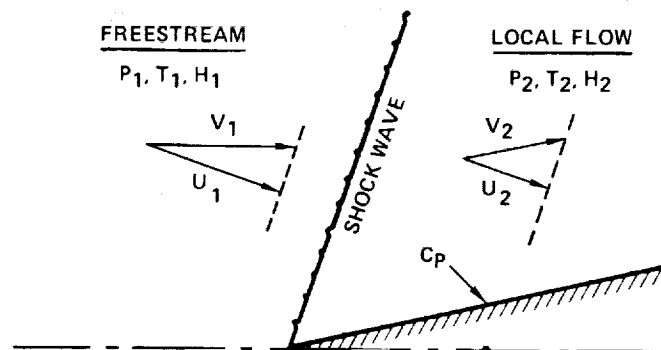
- Laminar flow heat transfer is computed using the Blasius skin friction formula with the Eckert reference enthalpy formula to calculate reference conditions and the Colburn-Reynolds analogy to obtain the heat transfer coefficient.
- Turbulent flow heat transfer is computed using the Spalding and Chi skin friction theory, with a linear Crocco integration through the boundary layer to account for real gas effects in the compressible transformation, and the Colburn-Reynolds analogy to obtain the heat transfer coefficient.

TABLE 6-1. SOLAR HEAT FLUX VS ALTITUDE

ALTITUDE - km (ft)	FLUX - W/m <sup>2</sup> (BTU/hr-ft <sup>2</sup> )
0 (0)	790 (250)
6 (20,000)	1040 (330)
12 (40,000)	1285 (407)
18 (60,000) AND ABOVE	1340 (425)

TABLE 6-2. LOCAL FLOW ON A SUPERSONIC WEDGE

SKETCH:



NOTE:

1. SUBSCRIPT (1) INDICATES FREESTREAM; (2) INDICATES BOUNDARY LAYER EDGE
2.  $f_n(X, Y)$  ARE CURVE FIT OR TABULATED FUNCTIONS FOR THE GIVEN AIR PROPERTY VERSUS THE VARIABLES X AND Y

GIVEN:

- P<sub>1</sub> FREESTREAM PRESSURE
- T<sub>1</sub> FREESTREAM TEMPERATURE
- M<sub>1</sub> VEHICLE MACH NUMBER
- C<sub>p</sub> LOCAL PRESSURE COEFFICIENT
- R AIR GAS CONSTANT

**FREESTREAM:**

- $\rho_1 = P_1 / (R \cdot T_1)$  DENSITY
- $\gamma_1 = f_1(T_1, P_1)$  SPECIFIC HEAT RATIO
- $V_1 = M_1 \cdot \sqrt{P_1 / (\gamma_1 \cdot \rho_1)}$  VELOCITY
- $H_1 = f_2(T_1, P_1)$  ENTHALPY

**LOCAL:**

- $\xi = P_2/P_1 = 1 + \frac{\gamma_1}{2} C_p M_1^2$  STATIC PRESSURE RATIO
- $U_1 = V_1 \cdot \sqrt{(6\xi + 1) / (7M_1^2)}$  NORMAL VELOCITY COMPONENT
- $U_2/U_1 = 1 + \frac{P_1}{\rho_1 U_1^2} (1 - \xi)$  NORMAL VELOCITY RATIO
- $P_2 = \xi \cdot P_1$  LOCAL STATIC PRESSURE
- $H_2 = H_1 + \frac{1}{2} (U_1^2 - U_2^2)$  LOCAL STATIC ENTHALPY
- $T_2 = f_3(H_2, P_2)$  LOCAL STATIC TEMPERATURE
- $V_2 = \sqrt{V_1^2 - U_1^2 + U_2^2}$  LOCAL VELOCITY

Flow transition is assumed to occur at a local Reynolds number of one million, which for the present configuration and flight profile means that turbulent flow exists over all surfaces but the first foot or two of the fuselage nose and wing leading edge.

The calculation procedures for heat transfer coefficient have been included in computer subroutines for direct callout in the temperature calculation program. Use is made of standard atmosphere tables, the vehicle flight profile, and tabulated pressure coefficient data to calculate automatically the local flow field and the heat transfer coefficient at the airplane surface point being analyzed.

The local convective heat flow to the skin is

$$\frac{q_{\text{conv}}}{A} = h(T_r - T_w)$$

where  $h$  is the heat transfer coefficient,  $T_w$  is the skin temperature, and  $T_r$  is the recovery temperature. The recovery temperature, also called the adiabatic wall temperature, is the temperature the skin would reach in the absence of any other heat transfer at the surface. Recovery temperature is determined for real gas calculations from the recovery enthalpy,  $H_r$ , defined as

$$H_r = H_2 + \left( r \frac{V_2^2}{2} \right)$$

$H_2$  and  $V_2$  are evaluated at the boundary layer edge during the local flow calculation. The recovery factor,  $r$ , is defined as the ratio of recovery enthalpy increase (over local static enthalpy) over the total enthalpy increase, or

$$r = \frac{H_r - H_2}{H_T - H_2}$$

The recovery factor is approximated well by the square root of Prandtl number for laminar flow, and by the cube root of Prandtl number for turbulent flow.  $T_r$  is found from real gas tables as a function of  $H_r$  and the local static pressure,  $P_2$ .

The term "reference condition" refers to evaluation of a property at a reference temperature,  $T^*$  or "T-star", and the local static pressure,  $P_2$ .  $T^*$  is determined for these analyses by the Eckert reference enthalpy method (Reference 5), which defines a reference enthalpy as

$$H^* = .5 \times H_w + .28 \times H_2 + .22 \times H_r$$

$H_w$  is evaluated at  $T_w$  and  $P_2$ .

The heat transfer coefficient is evaluated through calculation of a local Stanton number,  $St$ , defined as

$$St = \frac{h}{\rho c_p V_2}$$

Density,  $\rho$ , is evaluated at the reference condition for the Eckert reference enthalpy method (laminar flow), and at the local boundary layer edge condition for the Spalding and Chi method (turbulent flow). Specific heat,  $c_p$ , is evaluated for real gas effects by substitution of a ratio of enthalpy difference to temperature difference, or

$$c_p = \frac{H_r - H_w}{T_r - T_w}$$

The procedure to determine the local Stanton number involves calculation of the local skin friction coefficient,  $C_f$ , and use of a modified Reynolds analogy of the form

$$St = \frac{C_f}{2} R_{AF}$$

where  $R_{AF}$  is the Reynolds analogy factor. The  $R_{AF}$  selected for both laminar and turbulent flow is the Colburn-Reynolds analogy factor,

$$R_{AF} = (Pr^*)^{-2/3}$$

where  $Pr^*$  is the Prandtl number evaluated at the reference condition. Reference 6 found this form of the Colburn-Reynolds analogy to give the best prediction of heat transfer when the Spalding and Chi theory is used for turbulent flow.

The skin friction coefficient for laminar flow is based on the Blasius equation,

$$C_f = .664/(Re^*)^{0.5}$$

The Reynolds number,  $Re^*$ , for this equation is the local Reynolds number based on distance from the leading edge, with air properties evaluated at the reference condition.

The skin friction coefficient for turbulent flow is based on a numerical curve fit of the incompressible flow formulas of Spalding and Chi (Reference 7) performed by White and Christoph (Reference 8),

$$C_{f, inc}(Re_x) = 0.225/(\log_{10} Re_x)^{2.32}$$

which agrees with the Spalding and Chi formulas within 0.5 percent.  $Re_x$  is the local Reynolds number based on distance from start of turbulence. The transformation to compressible flow is made by use of the transformation functions,  $F_C$  and  $F_{Rx}$ , or



$$F_C C_f = C_{f, inc} (F_{Rx} Re_x)$$

The Spalding and Chi expressions for the transformation functions are

$$F_C = \left[ \int_0^1 \left( \frac{\rho}{\rho_2} \right)^{0.5} d \left( \frac{V}{V_2} \right) \right]^{-2}$$

$$F_{Rx} = \left( \frac{T_2}{T_w} \right)^{.702} \left( \frac{T_r}{T_w} \right)^{.772} / F_C$$

For a perfect gas, the ratios  $\rho/\rho_2$  and  $V/V_2$  may be expressed in compatible terms and the integral solved for an explicit definition of  $F_C$  (see References 7 and 8). For a real gas, Pearce (Reference 9) recommends substitution of enthalpy for temperature in the  $F_{Rx}$  equation,

$$F_{Rx} = \left( \frac{H_2}{H_w} \right)^{.702} \left( \frac{H_r}{H_w} \right)^{.772} / F_C$$

and definition of enthalpy variation through the boundary layer based on a linear form of the Crocco expression, or,

$$H = H_w + (H_r - H_w) x (V/V_2) - (H_r - H_2) x (V/V_2)^2$$

The density variation,  $\rho(H, P)$ , is obtained from real gas curves, and the integral in the  $F_C$  expression is evaluated by a five-point Gaussian quadrature.

The resulting compressible, turbulent skin friction coefficient is used directly in the Stanton number equation to determine the local turbulent heat transfer coefficient.

## Thermophysical Properties

The material properties required for these thermal analyses are accumulated in this section to provide a consistent set of basic data and a record of the assumptions made for continuing analyses. The basic thermophysical properties recorded in this section include:

- $k$ , thermal conductivity             $W/(m \cdot K)$  or  $Btu/hr-ft-F$
- $c_p$ , specific heat capacity         $J/(kg \cdot K)$  or  $Btu/lbm-F$
- $\rho$ , density                             $kg/m^3$  or  $lbm/ft^3$
- $\epsilon$ , emissivity (infrared)        - -
- $\alpha_s$ , absorptivity (solar)        - -

Much of the property data was selected from studies performed for the L-2000-7A SST and reported in Reference 10. Other major references include MIL-HDBK-5 (Reference 11) for titanium properties and a comprehensive composite materials report (Reference 12) for composite properties.

Table 6-3 presents a list of surface radiation properties used for the materials considered in this analysis. Values for emissivity and solar absorptivity are assumed constant for the temperature range of interest (250 to 550 K). Composite materials are based on averages of test data reported in Reference 12. Organic matrix composites (epoxies, polyimides) exhibit high emissivities typical for non-metallic surfaces. Metal matrix composites (boron/aluminum) generally show the same radiation characteristics as the outermost metallic layer (in this case, aluminum).

The radiation properties presented are considered adequate for preliminary thermal analyses and for many types of comparative design studies. For extremely detailed analyses requiring precise radiation heat transfer calculations, however, tabulated property data may be inadequate. The magnitude, the angular distribution, and the wavelength dependence of radiation properties are extremely sensitive to surface conditions, which

include factors like roughness, oxide layers, and physical and chemical contamination. The qualitative description of a surface by terms such as "smooth", "polished", "rough", and "oxidized" are highly subjective and broadly interpretable, and generally insufficient for accurate specification of radiation properties. It is probable, then, that tabulated radiation data, although extensive, will not apply with precision to a particular surface under study. The situation is especially unsatisfactory with respect to emissivities for metallic surfaces; large errors for dielectric materials are less likely. The conclusion is that property measurements on particular surfaces of interest are a necessary prerequisite to the execution of highly precise radiation heat transfer calculations. In the absence of particular data, temperatures based on tabulated radiation data should generally be considered preliminary.

Figures 6-1 through 6-3 present conductivity and heat capacity data for titanium, fiberglass insulation, and jet fuel. Linear curves are assumed for most properties as a function of temperature in the range 250 to 550 K. Titanium properties are based on the values for Ti-6Al-4V alloy in Reference 11. Insulation properties are obtained as an average through the data scatter obtainable for 16 kg/m<sup>3</sup> fiberglass. Fuel properties are obtained from Reference 13 for a Jet A type fuel.

Figure 6-4 shows vapor pressure variation for common turbojet fuels as a function of bulk temperature. Vapor pressure is a good indicator of the critical boiling point as shown by the match with temperature range for initial boiling of Jet-A fuel at sea level. The probable minimum tank pressure is marked on the curve to indicate a practical temperature limit to prevent fuel boiling. The typical fuel temperature curve drawn from later analyses (given versus tank pressure) shows that the boiling limit may be approached, but only during the final drawdown stages when only residual fuel would remain in the tank. Further discussion of fuel temperatures is presented in the Task I results subsection.

TABLE 6-3. SURFACE RADIATION PROPERTIES

MATERIAL	ENVIRONMENT	$\epsilon$	$\alpha_s$
<b>METALS</b>			
ALUMINUM	POLISHED	0.1	0.3
	COMMERCIAL SHEET	0.2	0.5
STEEL	OXIDIZED	0.8	
INCONEL	ENGINE COMPARTMENT	0.6	
TITANIUM	EXTERNAL (CLEAN)	0.3	0.65
	INSIDE WING	0.4	
	FUEL-CONTAMINATED	0.5-0.6	
<b>PAINTS</b>			
C 116 WHITE	NORMAL USE	0.8	0.4
54-29C BLACK	NORMAL USE	0.9	0.9
<b>COMPOSITES</b>			
GRAPHITE/EPOXY	NORMAL USE	0.85	0.92
BORON/EPOXY	NORMAL USE	0.95	0.91
BORON/ALUMINUM	NORMAL USE (ESTIMATED)	0.2	0.5

$\epsilon$  = INFRARED EMISSIVITY

$\alpha_s$  = SOLAR ABSORPTIVITY

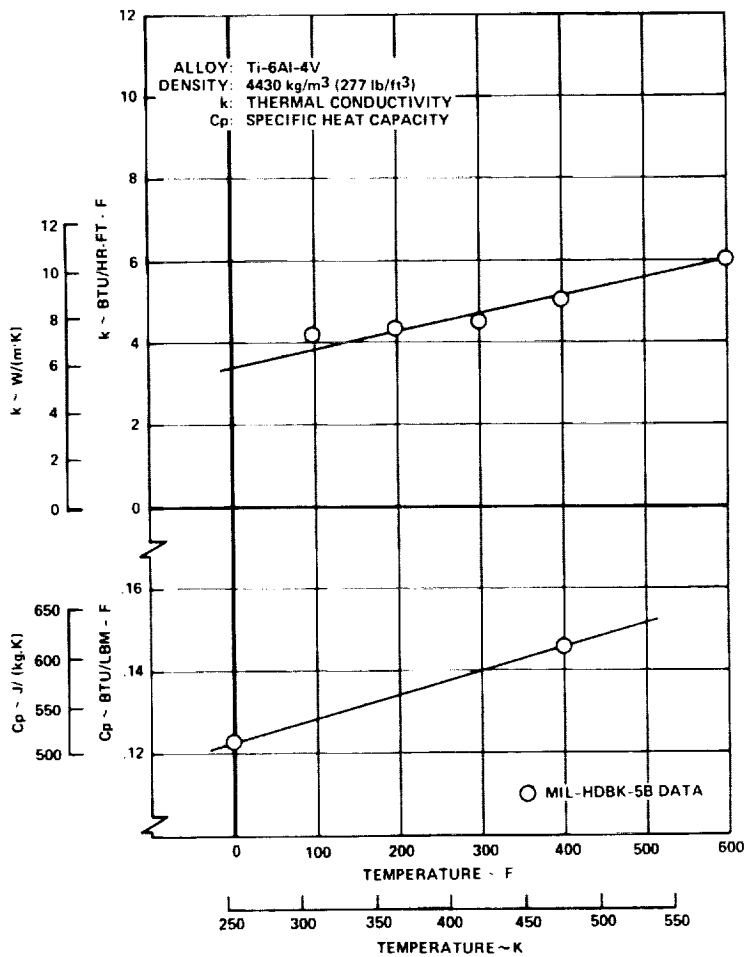


Figure 6-1. Thermal Properties - Titanium Alloy

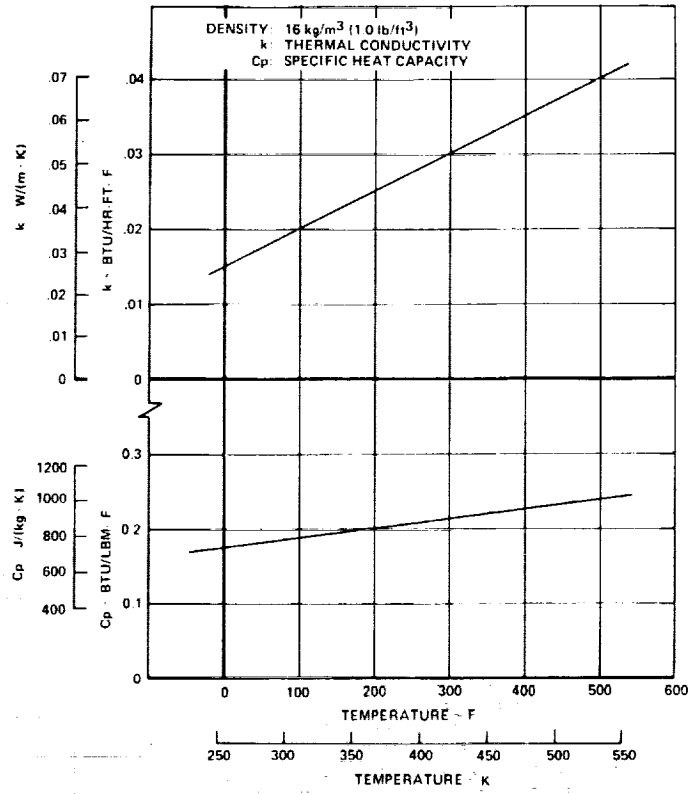


Figure 6-2. Thermal Properties - Fiberglass Insulation

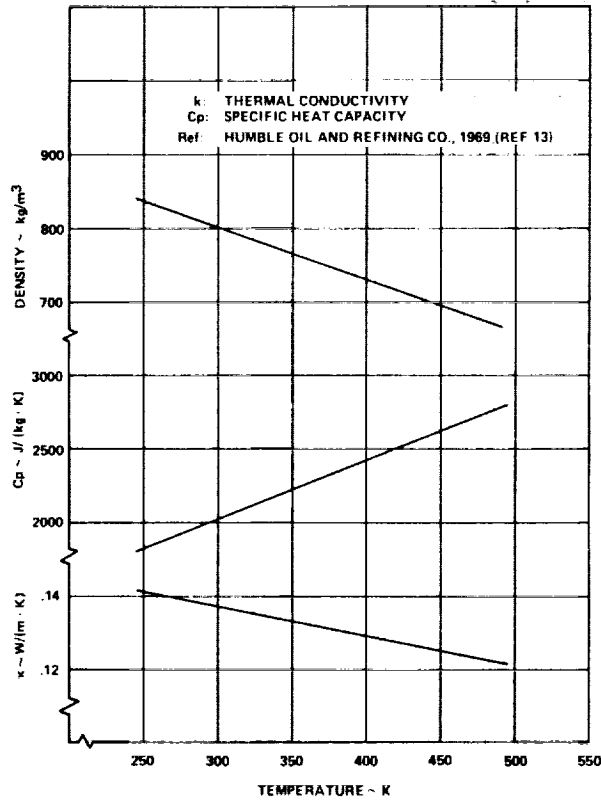


Figure 6-3. Thermal Properties - Jet-A Turbine Fuel

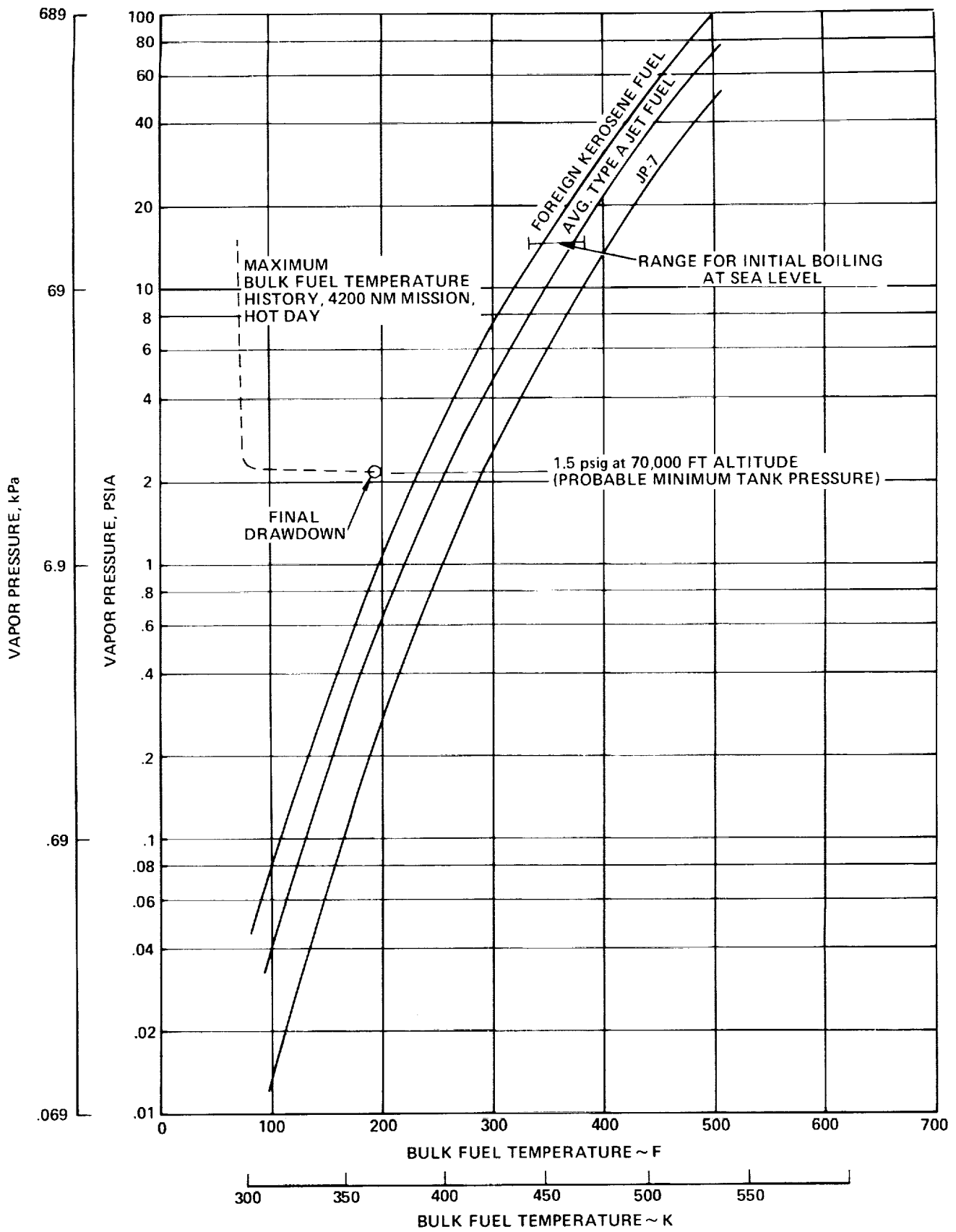


Figure 6-4. Turbine Fuel Vapor Pressure

Figures 6-5 through 6-7 present thermal data for three composites: a graphite/epoxy, a boron/epoxy and a boron/aluminum. Thermal properties for composite materials are difficult to specify because of the relative scarcity of test data compared to the ever increasing varieties of promising composites undergoing development. In addition, thermal conductivity of such materials can depend on factors like composition percentage, void content, and wettability between fiber reinforcement and matrix material, which can vary from sample to sample as well as among material formulations. Fortunately, simplifying assumptions based on valid testing can be made (Reference 14) which may expand the applicability of test data:

- High temperature epoxies and the polyimide laminates exhibit similar thermal properties, justifying the use of epoxy data for polyimide matrix composites.
- Heat capacity data was found to agree with the mixing rule of thermodynamics (volume fraction averaging), indicating a valid method for estimating heat capacity from material content.

The properties shown in the figures for composite materials are based on a comprehensive study (Reference 12) and are considered adequate for preliminary, comparative thermal analyses as performed in this design study.

#### Network Thermal Analysis Techniques

The objective of the thermal analysis techniques described in this section is to establish mathematical models representing physical structure to the degree of detail required for meaningful temperature distributions. For example, in Task I the requirements include sufficient detail to specify the average temperature difference (thermal gradient) from outer surface to innermost element of various structural panel concepts. A breakdown of wing panel structure into four separate elements (nodes) was found sufficient to specify the average thermal gradient through the panel.

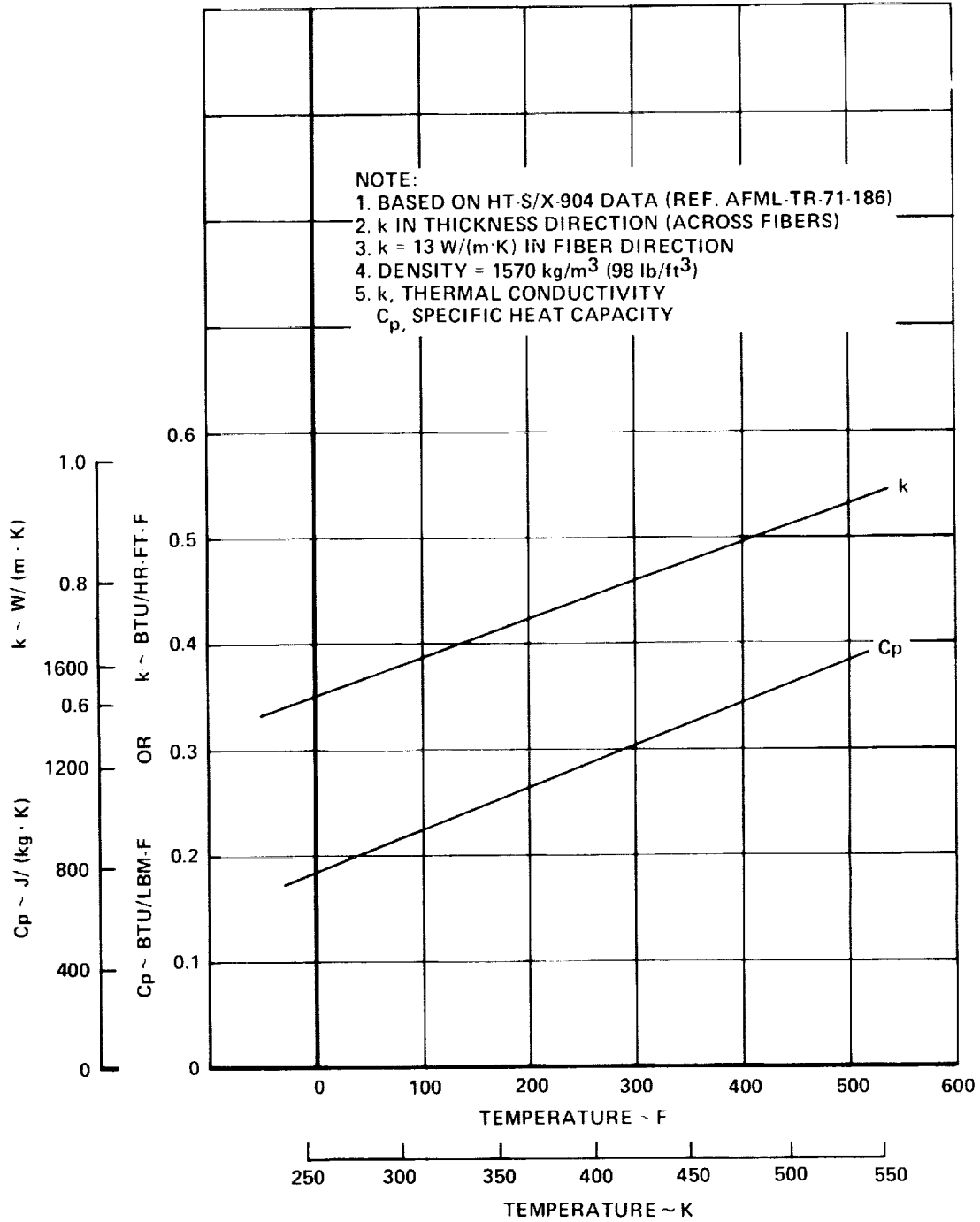


Figure 6-5. Thermal Properties - Graphite/Epoxy Composite



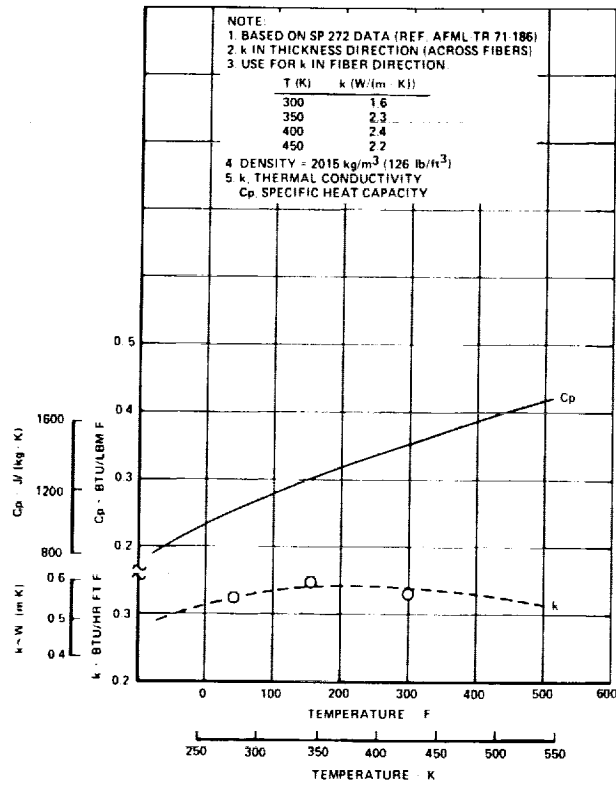


Figure 6-6. Thermal Properties - Boron/Epoxy Composite

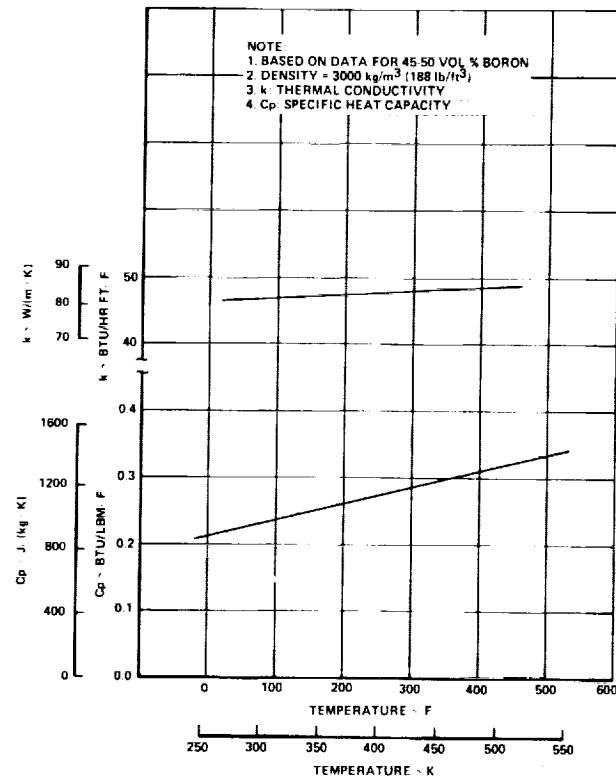


Figure 6-7. Thermal Properties - Boron/Aluminum Composite

The mathematical models for this analysis consist of networks of structural nodes interconnected by heat flow paths and set up for solution using Lockheed's Thermal Analyzer computer program (Reference 15). The solution method is analogous to the solution of voltage distribution in an electrical resistor-capacitor network: current (heat) flows through electrical (thermal) resistors as a function of the voltage (temperature) potential between connected points, and is stored as electrical (thermal) energy in components called capacitors (structural mass) at a rate that is a function of the electrical (heat) capacity of that component. Lockheed's Thermal Analyzer is a completely general and versatile computer program, permitting specification of any type of temperature-or time-dependent heat flow, including conduction, convection, radiation, and variable heat storage. An additional capability allows reconnection of network elements during run time, permitting solution of complex problems such as exposure of fuel tank structure to interior radiation as fuel is drained from the tank.

The thermal networks for this study are generalized to accept arbitrary dimensional data for applicability to similarly shaped structures. Detail dimensions are supplied as standard input data and the actual resistor and capacitor values calculated automatically for each case. This technique eliminates the need for minor network revisions each time a dimension is changed, and saves significant programming time.

All Thermal Analyzer networks were set up to compute in a transient mode. The flight profile for a "hot day" (standard plus 8K) international mission is used to determine aerodynamic heating and altitude effects. Cases are run from takeoff roll to climb, through cruise, and descent to loiter before landing.

Node Definitions. - Heat transfer in the interior of the wing is determined by setting up a wing box network. The network (Figure 6-8) includes sets of nodes for the upper and lower panels, plus one node each for the four vertical webs (to form a rectangular box). The shape of the box is determined by panel size (spanwise by chordwise dimensions) and by wing

depth obtained from wing contour drawings. All node areas are normalized with reference to one square foot of panel surface area to facilitate resistor and capacitor calculations. Heat transfer within the wing box includes radiation exchange, convection to boundary layer air when leakage is a factor, and, for fuel tank areas, convection to fuel and fuel vapor.

Two sets of nodal representations for panels are derived for inclusion in the wing box network. The first set (type-1) is for corrugation or hat-section stiffened panels. The second set (type-2) is for honeycomb panels. The node definitions for corrugation and hat-section panels, which are topologically similar and, therefore, definable as a single network type, are shown in Figure 6-9. Note that node 3 includes both side portions of the stiffener, which should be at identical temperatures. Node 2 thickness includes the cross-section-area-weighted average of skin thickness and stiffener flange thickness (attached to the skin). Heat transfer within the panel includes conduction (nodes 1-2, 2-3, and 3-4) and radiation (nodes 1-3, 1-4, and 3-4). Nodes 1 and 2 are involved in external surface heat transfer; nodes 2, 3, and 4 are exposed to heat transfer within the wing box.

Figure 6-10 shows the node definitions for honeycomb (type-2) panels. Nodes 2 and 3 are defined as the outer and inner halves of the core, respectively. Nodes 1 and 4 include thermal capacity of the braze material. Heat transfer within the panel includes conduction (nodes 1-2, 2-3, and 3-4) and radiation (nodes 1-2, 1-3, 1-4, 2-3, 2-4, and 3-4). To reduce network complexity and computer running time, all braze material was assumed to remain in contact with the face sheets. This assumption yields the most conservative values for maximum thermal gradients through the core. The effect of braze flow onto the core surfaces is examined with a parametric analysis described in a section to follow.

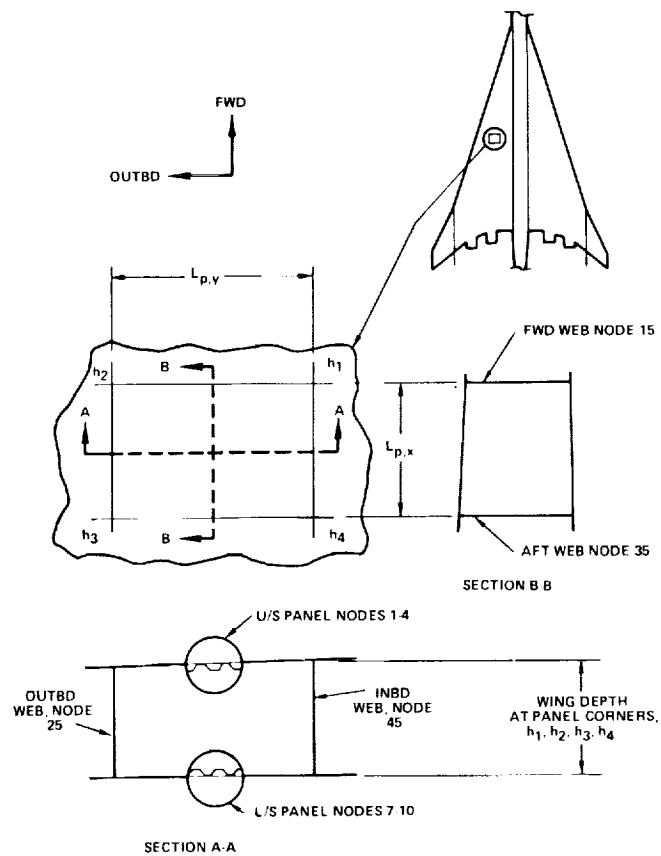
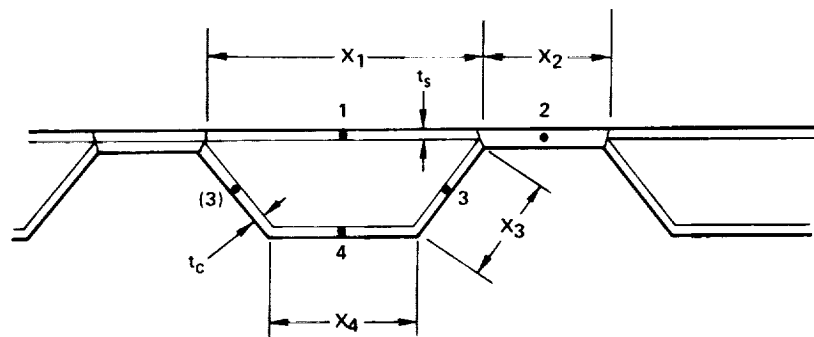


Figure 6-8. Wing Box Thermal Analyzer Network

CORRUGATION PANEL



HAT-SECTION PANEL

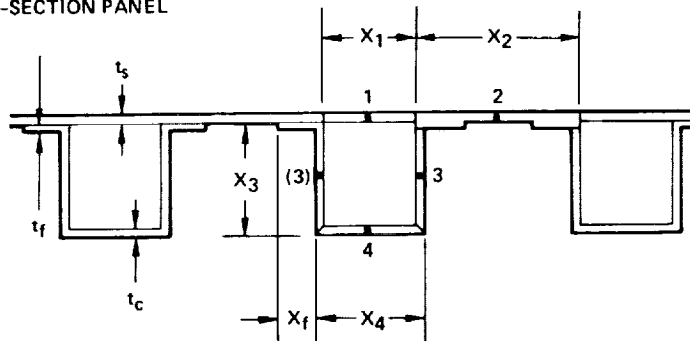
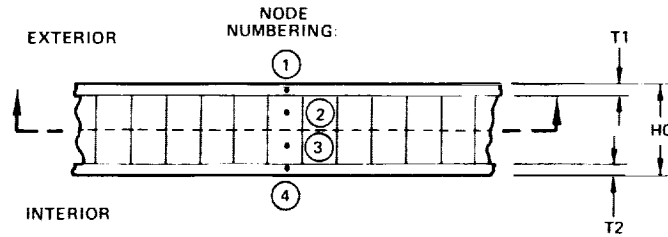
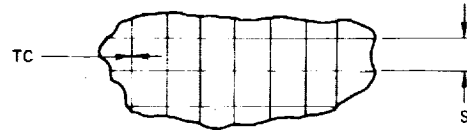


Figure 6-9. Network Node Definition, Type-1 Wing Panels



CORE CROSS SECTION:



DIMENSIONAL DATA:

HC	PANEL THICKNESS
T1	EXTERIOR FACE SHEET THICKNESS
T2	INTERIOR FACE SHEET THICKNESS
S	CORE CELL SIDE
TC	CORE FOIL THICKNESS

ADDITIONAL DATA:

WB	BRAZE WEIGHT/AREA
----	-------------------

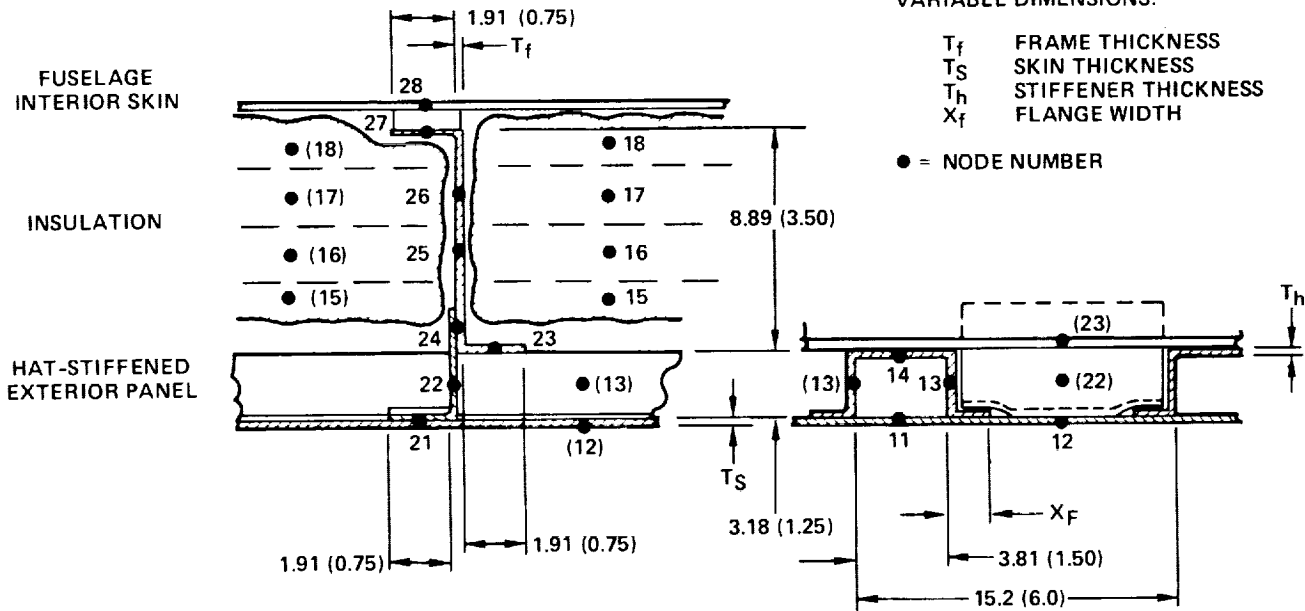
Figure 6-10. Network Node Definition, Type-2 Wing Panels

DIMENSIONS IN CM (IN.)

VARIABLE DIMENSIONS:

$T_f$	FRAME THICKNESS
$T_s$	SKIN THICKNESS
$T_h$	STIFFENER THICKNESS
$X_f$	FLANGE WIDTH

● = NODE NUMBER



NOT TO SCALE  
 CURVATURE NOT SHOWN FOR  
 SKIN PANEL CROSS SECTION

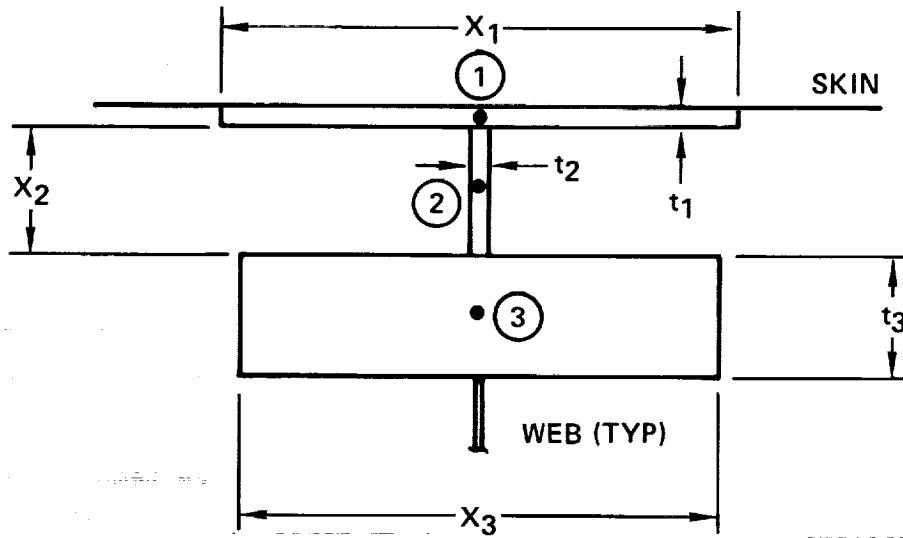
Figure 6-11. Network Node Definition, Fuselage Panel and Frame

Node definitions for the fuselage frame network are shown in Figure 6-11. This network is set up to determine the variation in average skin panel and frame temperatures around the circumference of the fuselage. Hat-section skin stiffeners are assumed, and skin-panel heat transfer is identical to that for type-1 wing panels. Heat transfer to the frame is by conduction and radiation from the skin panels, and by conduction from the surrounding insulation. Conduction through the insulation to the inner skin is included. Boundary conditions on the inner surface of the fuselage wall include a low convection rate to cabin air and radiation to cabin interior. The network at F.S. 750 is adjusted to simulate zee-section stiffeners with the hat-section model. The given frame model may not be valid at F.S. 3000 because this location is behind the pressurized bulkhead, and, unless cooled electronic equipment is located there, insulation may be thinner or nonexistent. Lower surface structures at F.S. 2000 and F.S. 2500 are located in fuel tanks, shielded by the lower fairing, and remain at fuel temperatures.

Temperature input for the three-dimensional finite element model (Task IIB) requires detailed thermal definition of interior load-carrying structure in addition to exterior panels. Figure 6-12 shows node definitions used for 'submerged' beam caps in the wing area. Metallic caps are defined with 3 nodes, composite-reinforced caps (of this configuration) with 8 nodes. Conduction, radiation, and convection are included for these models similarly to methods used for wing panels exposed to exterior and interior heat transfer. Dimensional data used for analysis of these caps are presented in Section 12.

Heat Flow Paths. - Heat flow paths are defined by thermal resistors connected between nodes representing structure or between nodes and given boundary condition temperatures. Heat flows directly into a node may also be defined explicitly. The Thermal Analyzer network details describing the various types of heat flow paths used in these analyses are given in the following paragraphs:

METALLIC SUBMERGED CAPS



COMPOSITE-REINFORCED SUBMERGED CAPS

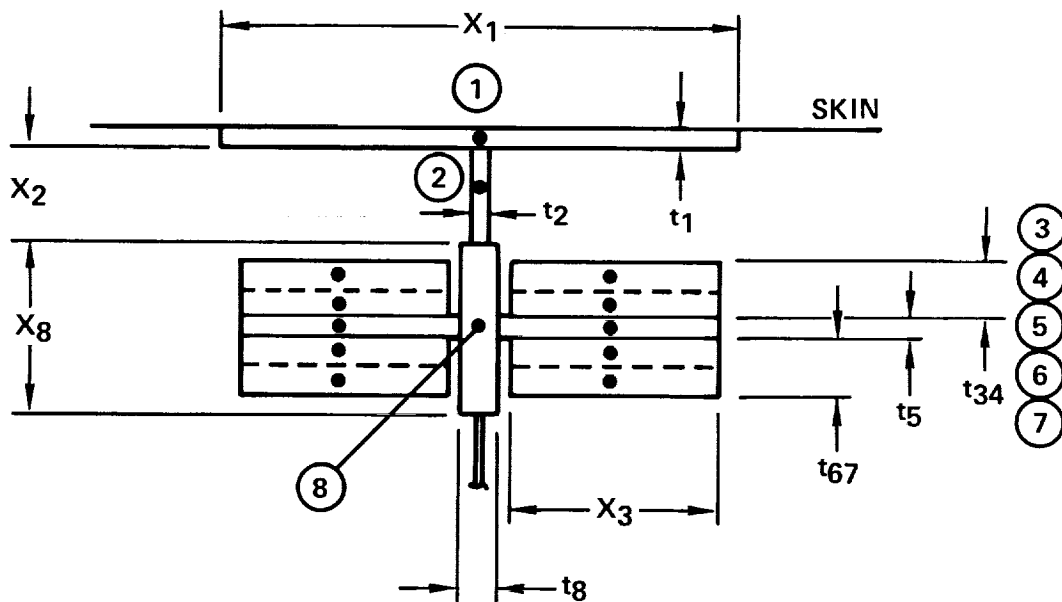


Figure 6-12. Network Node Definition, Submerged Beam Caps

External Convection. - Aerodynamic heating is applied to all exposed surfaces (nodes 1 and 2 of type-1 panels, node 1 of type-2 panels) through a resistor between the surface node and a boundary node set equal to the local recovery temperature. The resistor value is determined from exposed surface area and the local heat transfer coefficient, which is updated every calculation cycle.

Internal Convection. - Three sources of internal convection are considered: boundary layer air leakage, fuel, and fuel vapor (or ullage gases). For wing areas likely to experience boundary layer air leakage, a direct heat input ( $q$ ) is applied to internal exposed surfaces at the rate of  $6.5 \text{ W}/(\text{m}^2 \cdot \text{K})$  ( $1.0 \text{ Btu}/\text{hr}\text{-ft}^2\text{-F}$ ). This rate is adjusted for altitude by the 0.6 power of normalized ambient pressure. Recovery temperature is assumed as the source temperature, based on analysis correlation with some F-12 series aircraft flight test data. For fuel areas, a convection resistor is used between all internal surfaces and either fuel or vapor. A fuel liquid convection rate of  $260 \text{ W}/(\text{m}^2 \cdot \text{K})$  ( $40 \text{ Btu}/\text{hr}\text{-ft}^2\text{-F}$ ) and a vapor convection rate of  $13 \text{ W}/(\text{m}^2 \cdot \text{K})$  ( $2 \text{ Btu}/\text{hr}\text{-ft}^2\text{-F}$ ) are assumed. These values are also based on F-12 series aircraft correlations.

Conduction. - All frames, panels, and caps defined by multiple nodes have conduction resistors connecting the nodes. The resistors are defined from material thickness, cross-section area, and temperature-dependent thermal conductivity. Care is exercised in node and resistor selection to avoid extremely small RC products (the "time constant" of the node) which result in excessive computer run times. Conduction resistance between the surfaces of thin gage material and contact resistance at metal-to-metal and metal-to-composite joints are assumed negligible.



External Radiation. - External radiation includes radiation relief from hot surfaces to a cooler environment and solar irradiation on upward facing surfaces. Radiation relief assumes a net heat transfer determined by the surface emissivity in the infrared range and the local view factor to the surroundings. A radiation resistor is defined between surface nodes and an environment boundary node such that the net exchange is proportional to the difference between the fourth powers of the surface temperature and the environment temperature. For upward facing surfaces, 35 K (53 R) is assumed for "space" temperature; for side and bottom surfaces, local ambient temperature is assumed for the environment. Net solar irradiation is proportional to the local radiation intensity, to the surface absorptivity in the visible light range, and to the view factor toward the sun. Since the solar view factor normally changes throughout a flight, an average value for solar irradiation was used by assuming a constant irradiation incidence angle of 15 degrees from zenith for all upward facing surfaces. Solar heating is input as a direct heat source ( $q_s$ ).

Internal Radiation. - All surfaces exchanging thermal radiation within an enclosure are assumed to emit and reflect radiation diffusely and in a wavelength range for which surface emissivity may be assumed constant (gray-body assumption). Interreflections among surfaces are accounted for by a radiosity matrix solution method after Hottel (reference 16). This method is employed by generating a matrix of geometric view factors for all surfaces within the enclosure, then solving for the effective view factor,  $\mathcal{F}$ , between each pair of surfaces. These factors are constant for a given geometry and surface condition, and are used directly each computing cycle to calculate an updated, temperature-dependent value for each radiation resistor. Storage space for the required matrices and factors is allocated in the input data, and resistors are computed automatically in the Thermal Analyzer program.

Thermal Capacity. - Thermal capacity of a node determines its transient response to applied changes in temperature potential (heating or cooling). Capacity is of primary importance during the transient portions of flight (climb and descent), affecting the maximum temperature gradients between the external and internal surfaces of a structure. Capacity is determined for each node as a product of the mass of the material represented by the node and the temperature-dependent specific heat value for the material.

The presence of fuel in a wing box requires consideration of the variation in thermal capacity for fuel and for the webs as the fuel level decreases. For analytic simplicity, fuel height is updated every minute (maximum use rate is slightly over 2.5 cm or one-inch per minute). Fuel thermal capacity is then calculated as the product of normalized volume (one square foot (.0929 m<sup>2</sup>) surface by fuel height) and temperature-dependent density and specific heat. Exposed web areas are adjusted at the same time and web thermal capacities recalculated for the additional mass. The portion of web submerged in fuel is assumed at fuel temperature and not included in the wing box heat balance. However, as fuel level drops, and a new portion of web is added to the exposed web node, an additional heat flow term is included for the web node to account correctly for the mass addition at a lower temperature. This procedure tends to smooth out the thermal response of the web to the step changes in capacity caused by decreasing fuel levels in a tank.

Fuel Tank Model. - Representation of fuel levels in the wing tanks requires definition of tank locations and fuel usage schedules. Fuel tank locations are based on the aircraft configuration used for each Task and are shown schematically in Figure 6-13 (Task I) and Figure 6-14 (Tasks II, and III).

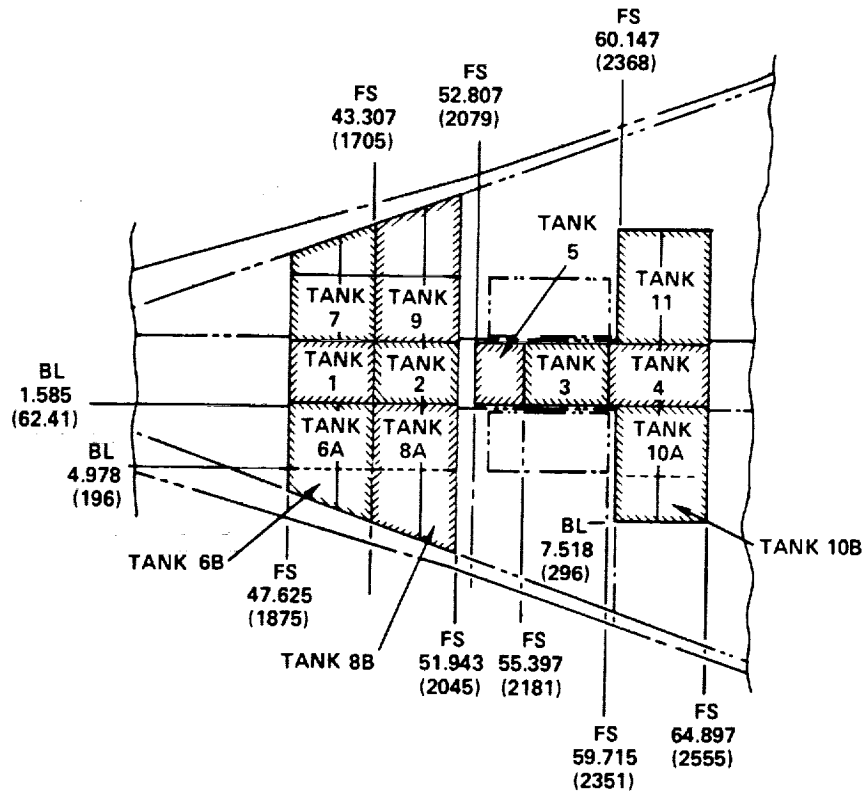


Figure 6-13. Fuel Tank Codes and Locations - Task I

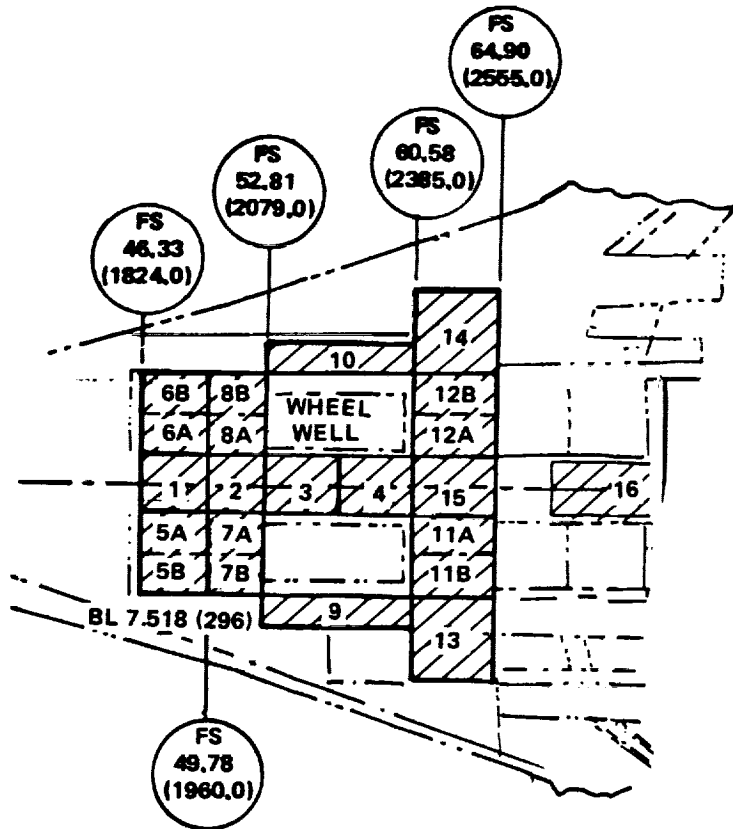


Figure 6-14. Fuel Tank Codes and Locations - Task II

For Task I, the wing tanks are separated for modeling purposes into an inboard and an outboard section at BL 196 to obtain a more accurate definition of local average fuel height. Fuel usage schedules are based on a 340,000 kg (750,000 pound) gross takeoff mass and the hot day 4200 nautical mile international mission flight profile. Figure 6-15 shows tank fuel mass vs. total airplane mass and also vs. flight profile time. Tank mass presented in this figure are for combinations of tanks which are expected to be drained simultaneously. Average heights of fuel for the various tank sections are presented in Figure 6-16 as functions of total fuel mass for the corresponding tank combinations (for example, fuel height in tank section 10B as a function of total fuel mass in Tanks 10 and 11).

For Task II and Task III, the inboard wing tanks (numbered 5, 7, and 11 on left side) are separated for the model at BL 145 into inboard and outboard sections ('A' and 'B'). Fuel usage schedules are based on the Task II optimized configuration, with tank sequencing determined by center of gravity limit requirements. Figure 6-17 shows tank fuel mass versus total airplane mass for single (fuselage) tanks and for the right-left (wing) tank combinations. Average fuel height versus fuel mass is presented in Figures 6-18, 6-19, and 6-20 for the fuselage tanks, forward wing tanks, and aft wing tanks, respectively. Fuel heights for the sectioned tanks are presented for each section versus fuel mass for the whole tank, as explained above for Task I.

The curves in the above figures are input into the data section of the Thermal Analyzer program to provide a simple calculation of fuel height in a given tank for any time point in the given flight profile. During computation, the fuel height is updated every (flight) minute, and capacitors, radiation view factors, and supplementary heat flows are adjusted. Fuel is assumed to empty from the tank immediately after reaching two percent of maximum level, and the computations are allowed to proceed with internal convection only to the remaining fuel vapor.

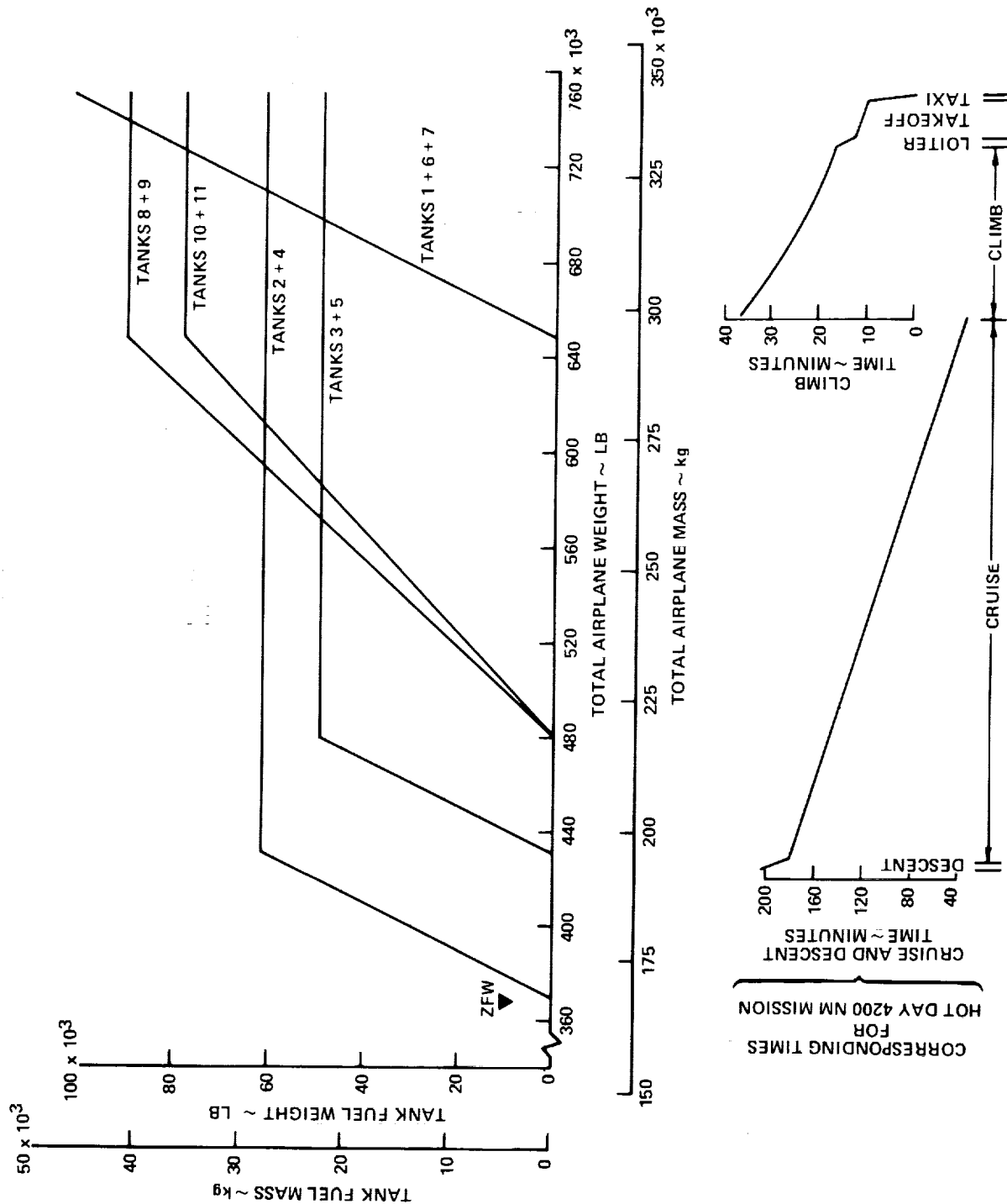


Figure 6-15. Fuel Mass for Tank Combinations - Task I

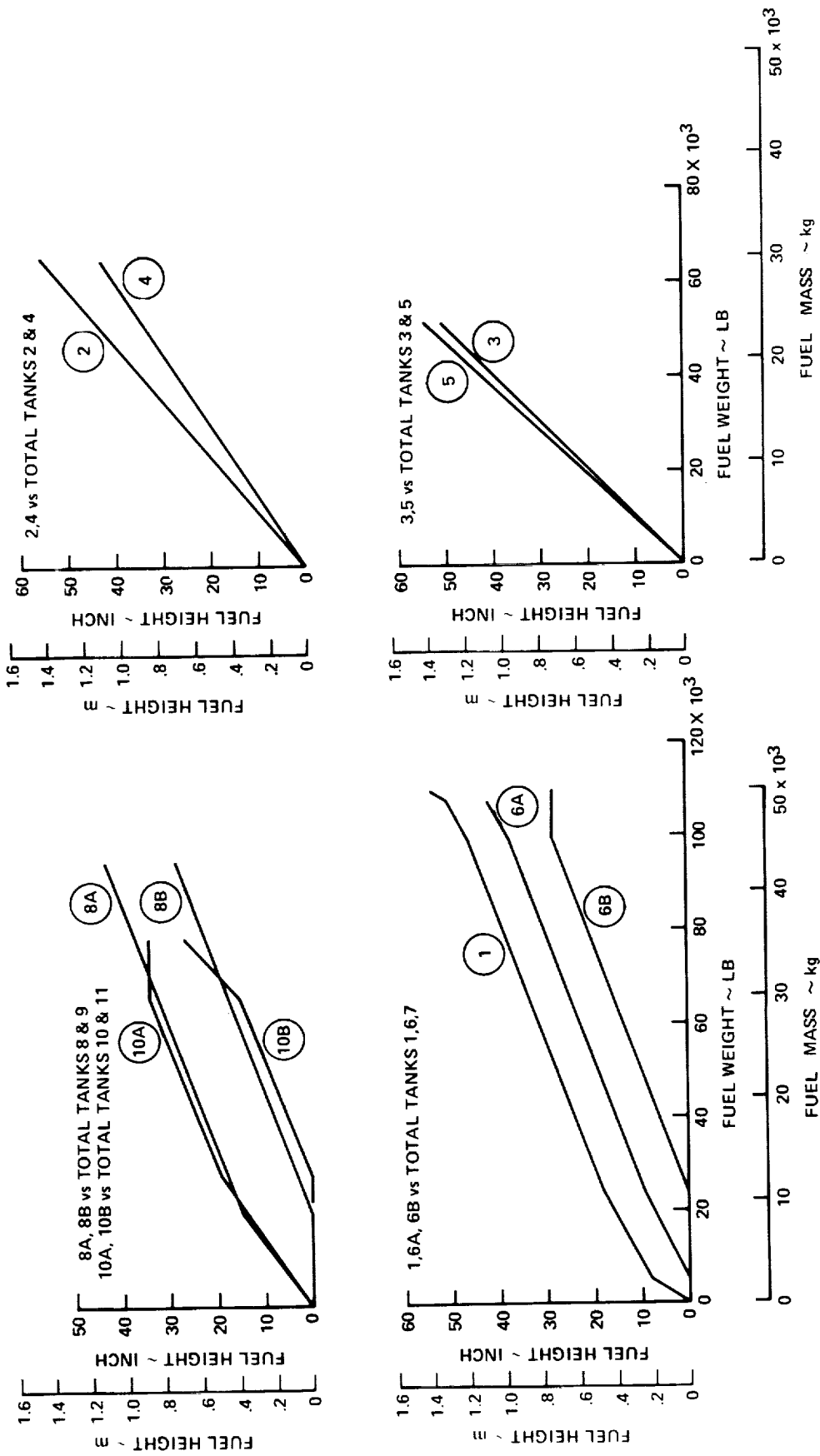


Figure 6-16. Fuel Height vs Mass for Tank Combinations - Task I

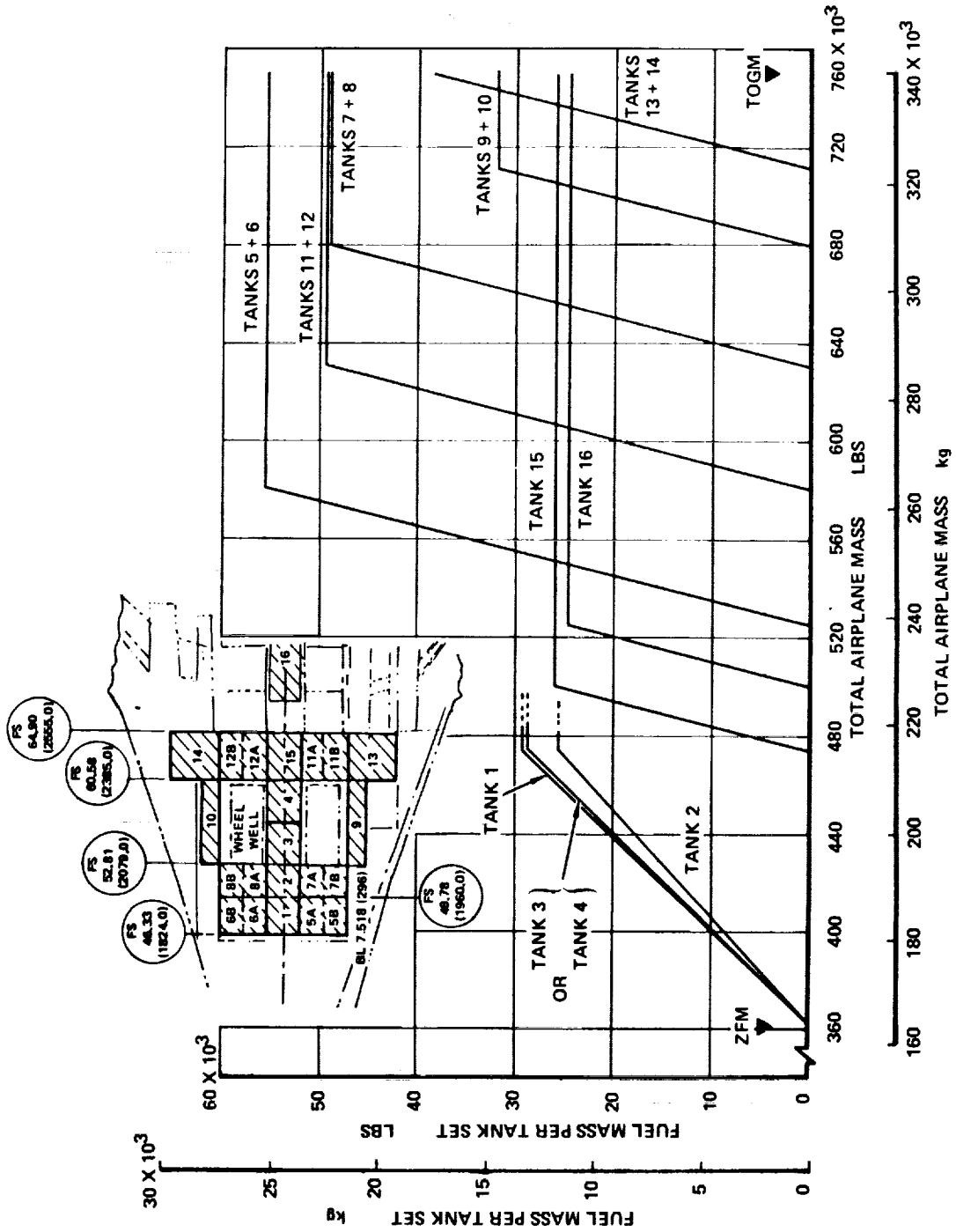


Figure 6-17. Fuel Mass for Tank Combinations - Task II

ORIGINAL PAGE IS  
OF POOR QUALITY

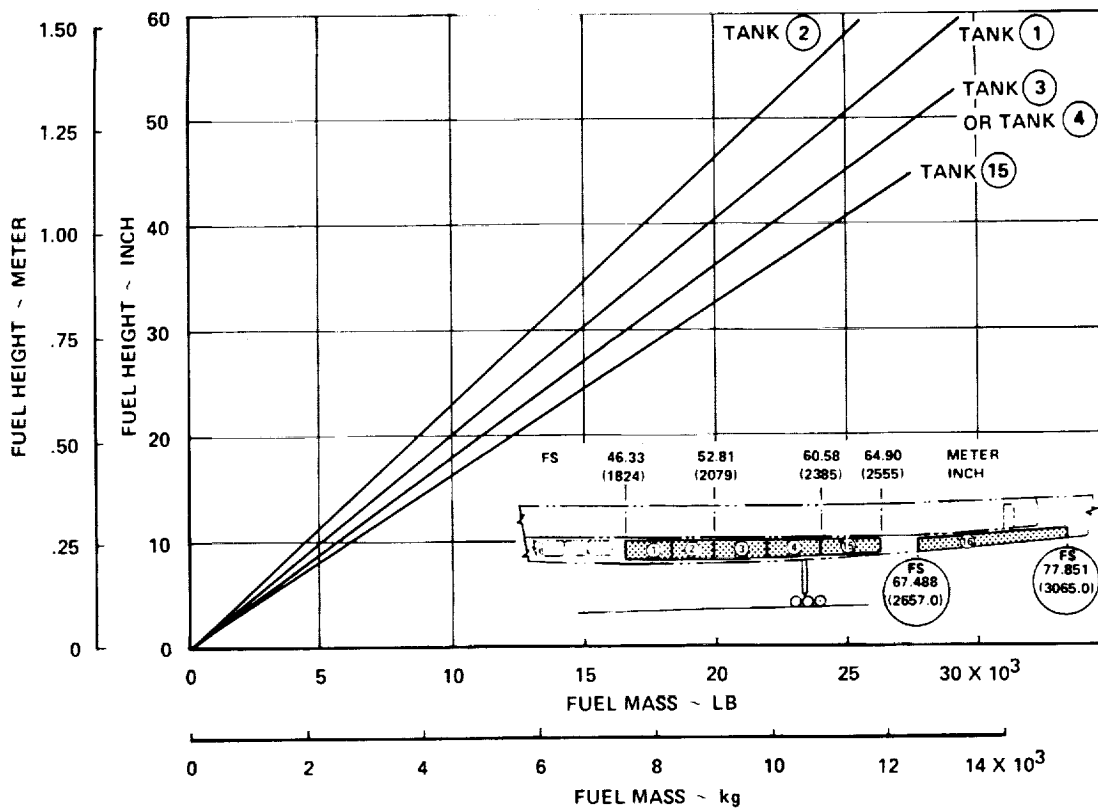


Figure 6-18. Fuel Height vs Mass, Fuselage Tanks - Task II

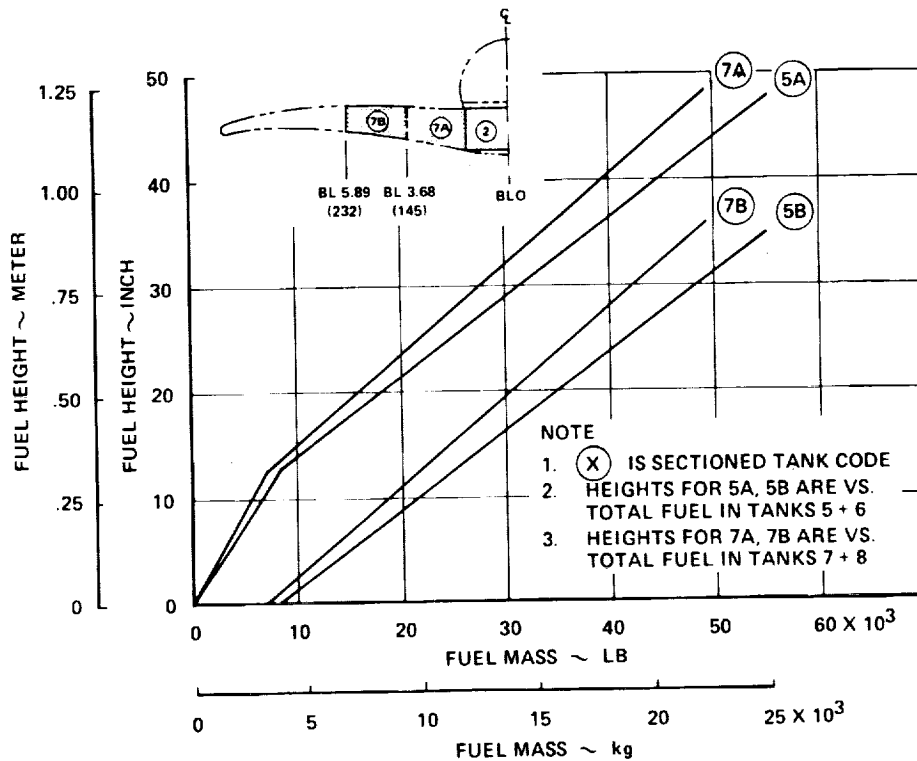
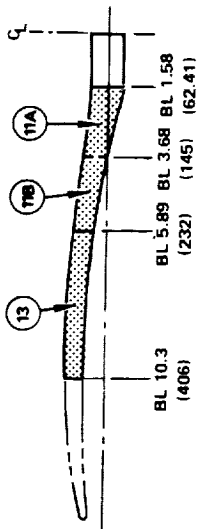


Figure 6-19. Fuel Height vs Mass, Forward Wing Tanks - Task II





- NOTE
1. (X) IS TANK CODE
  2. HEIGHT FOR TANK 9 VS. TOTAL FUEL IN TANKS 9 + 10
  3. HEIGHT FOR TANK 13 VS. TOTAL FUEL IN TANKS 13 + 14
  4. HEIGHT FOR TANK 11A AND 11B VS. TOTAL FUEL IN TANKS 11 + 12

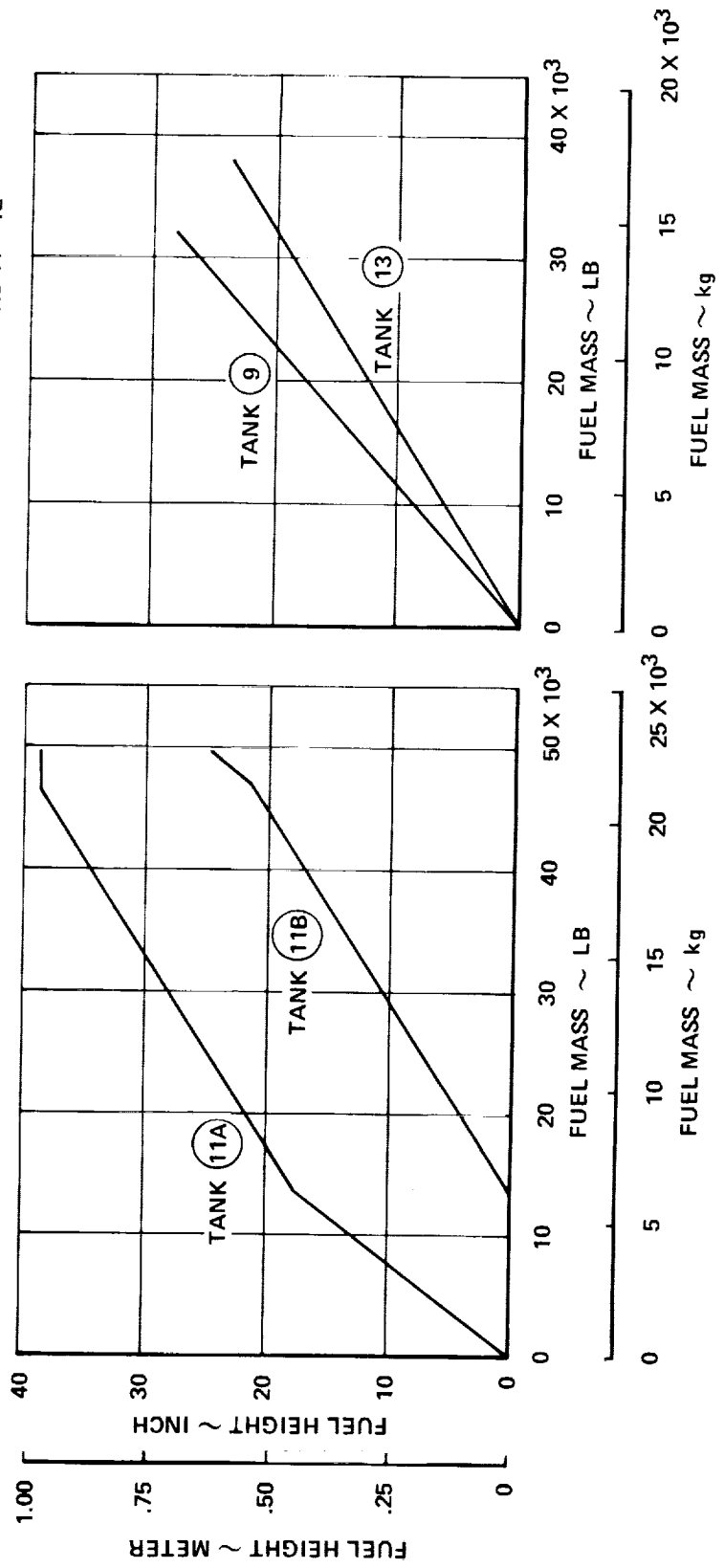


Figure 6-20. Fuel Height vs Mass, Aft Wing Tanks - Task II

## STRUCTURAL TEMPERATURES - TASK I

The structural temperatures developed for the candidate structural concepts are presented in this section. The first subsection describes the technique used to develop initial element temperatures for the two-dimensional finite element model, as required for initial generation of internal structural loads. The next four subsections present temperature histories for selected wing panels for the three structural arrangements (chordwise-stiffened, spanwise-stiffened, and monocoque), and for a composite-reinforced concept. The remaining subsections present temperature results for fuselage panels and frames, a thermal evaluation of the fuel tank system, and the determination of braze effects on honeycomb panels.

### Finite Element Model (2-NASTRAN)

Structural element temperatures were developed for input to the two-dimensional finite element models. Temperatures were estimated without extensive analyses by adapting results from previous SCAT-15F (Reference 17) and L-2000-7 (Reference 10) analyses. These data were used to determine steady-state external surface temperatures (cruise isotherms) for the Arrow-Wing model for a Mach 2.7 hot day (1962 U. S. Standard + 8K) cruise condition. The resulting isotherm map is presented in Figure 6-21.

The extensive thermal gradient studies performed for the L-2000-7 were then utilized to estimate structural element temperatures for the following flight conditions:

- Mach 1.2      Ascent-to-Cruise
- Mach 2.7      Start-of-Cruise
- Mach 2.7      Mid-Cruise
- Mach 1.2      Descent-from-Cruise

Element temperatures derived for the mid-cruise condition (Figure 6-22) were based on the referenced cruise isotherms with corrections applied for areas of abnormal heating or cooling (engines, fuel tanks, main landing gear compartments).

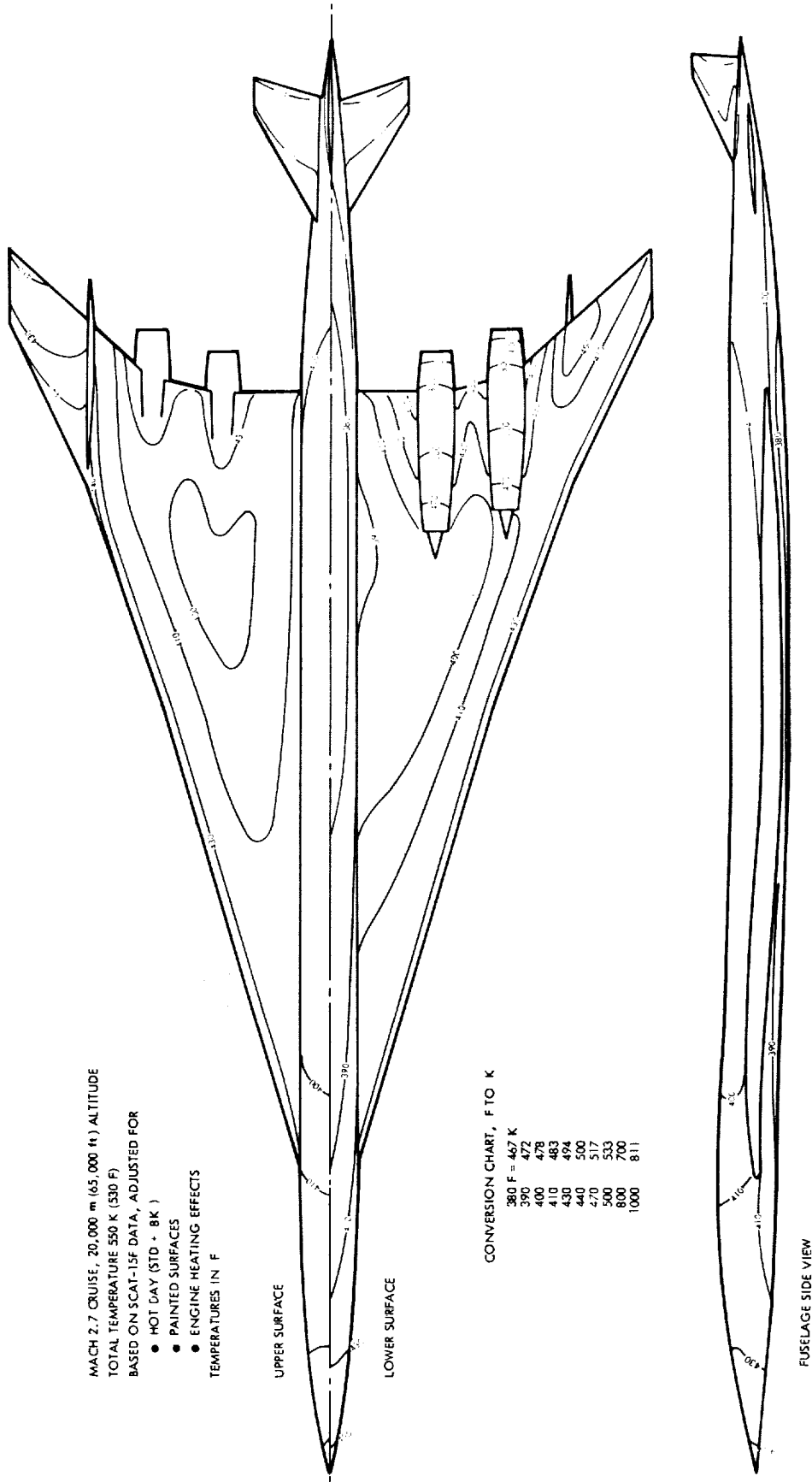


Figure 6-21. Surface Isotherms - Mach 2.7 Cruise

1

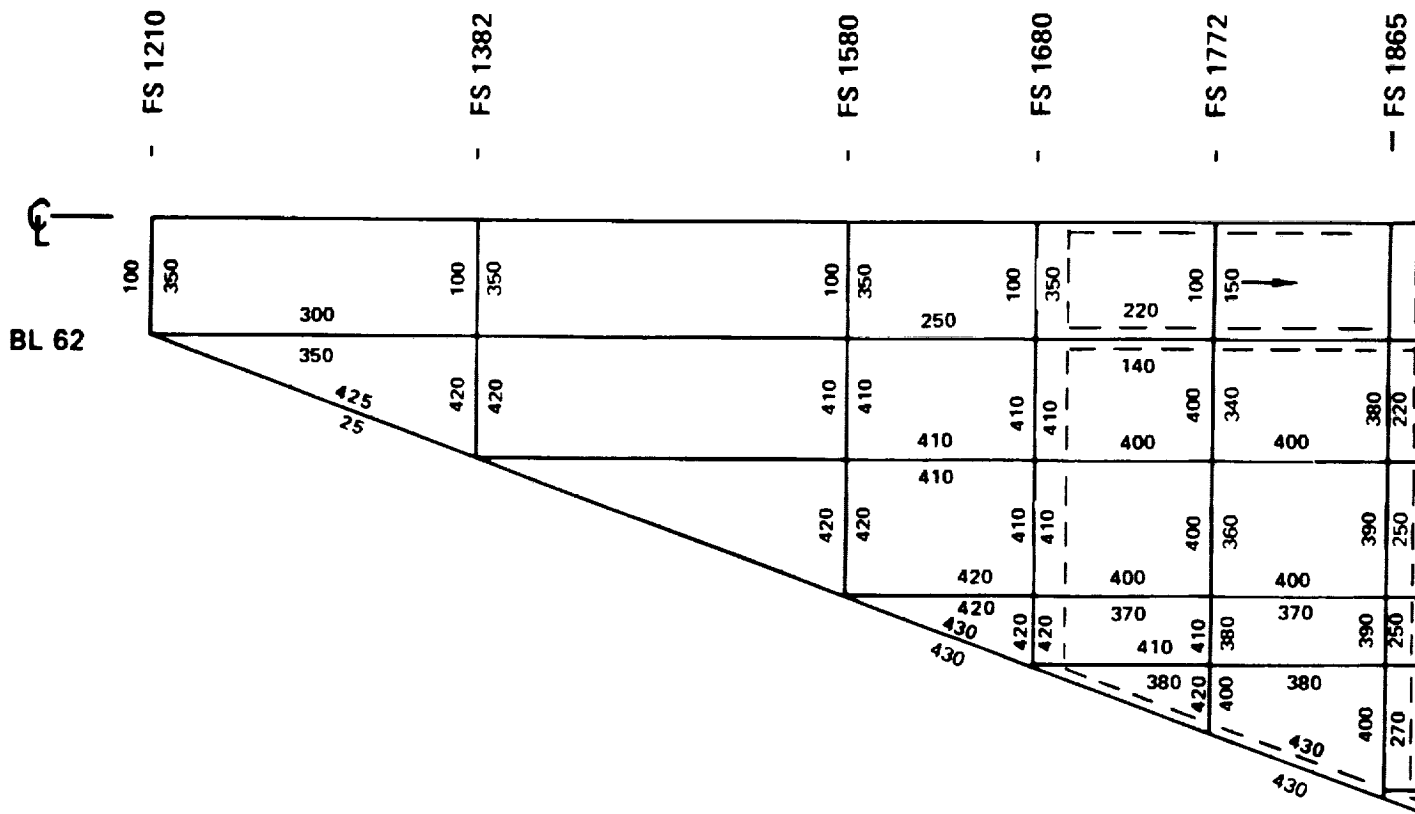
2

3

4

5

6



**CONDITION: MACH 2.7 MID-CRUISE (HOT DAY)**

**XXX = UPPER SURF F** \_\_\_\_\_ **ELEMENT**  
**YYY = LOWER SURF F**

~~X~~ USE  $\frac{370}{150}$  (FU)

**INTERPOLATE FOR MISSING TEMPERATURES**

CONVERSION TABLE	
F	K
100	311
200	367
300	422
400	478
500	533

PRECEDING PAGE BLANK NOT FILMED

FOLDOUT FRAME /



- FS 1955

- FS 2045

- FS 2145

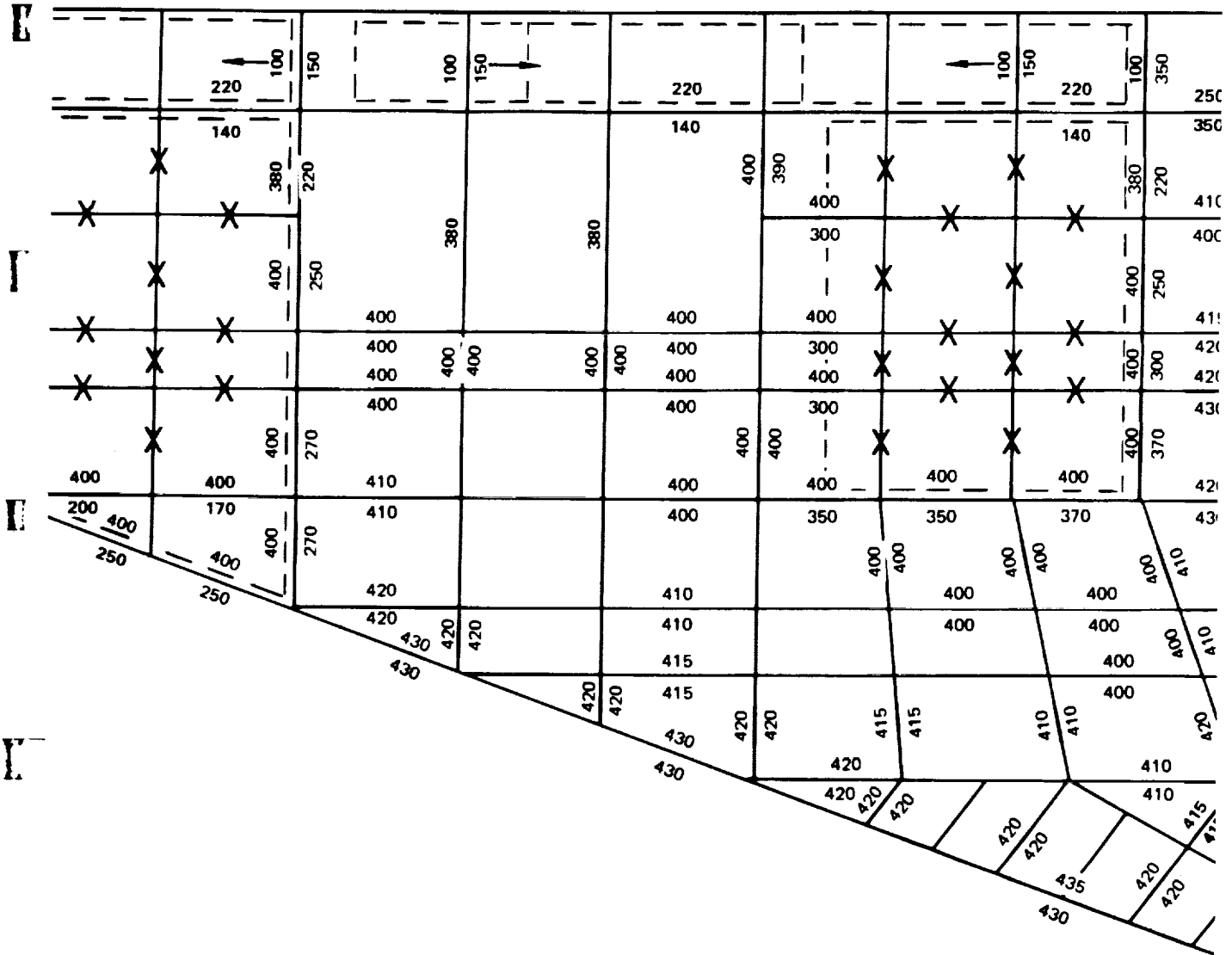
- FS 2235

- FS 2330

- FS 2405

- FS 2485

- FS 2565



FOLDOUT FRAME 2





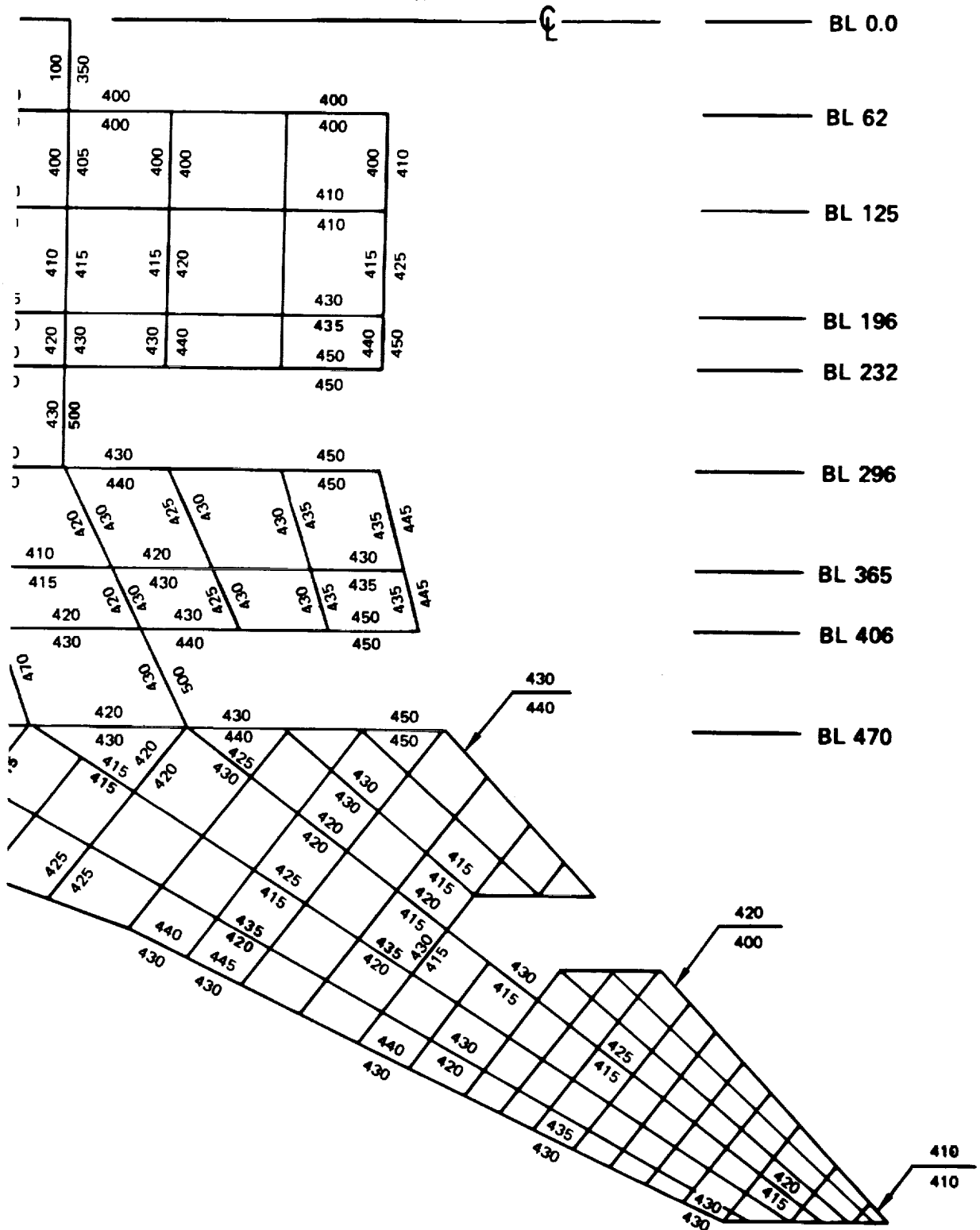


Figure 6-22. Finite Element Model Temperatures-Mach 2.7 Mid-Cruise



Temperatures for the Mach 1.2 ascent condition were assumed to average near 290K (62F) since the cumulative effect of aerodynamic heating is negligible at this point in the flight profile.

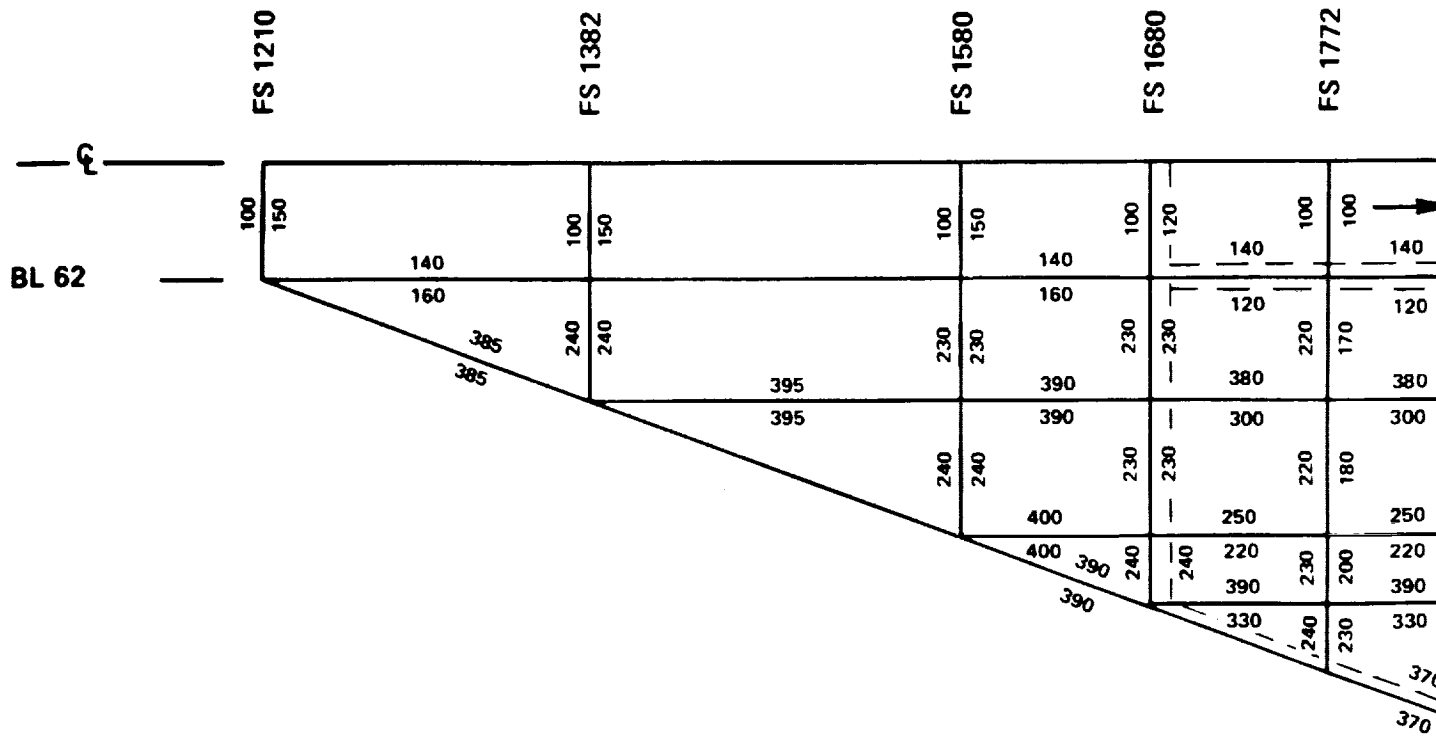
The start-of-cruise and the descent conditions are the most thermally critical transient conditions because the maximum negative and positive (respectively) thermal gradients occur for interior structure (referenced to outer skin). Element temperatures for these conditions were based on the maximum thermal gradients (negative and positive) calculated in the referenced study. Actual structure represented by the Arrow-Wing model element was matched with similar structure in the L-2000-7 study, and the corresponding thermal gradient was applied to determine a mean element temperature. Element temperatures for the start-of-cruise condition are shown in Figures 6-23, 6-24 and 6-25 for the chordwise stiffened, spanwise stiffened and monoque arrangements; respectively

#### Chordwise-Stiffened Wing Panels

Temperature histories for upper and lower surface wing panels at eight point design regions are presented in Figures 6-26 through 6-41. The panels use concave-beaded skin with corrugation stiffening. Three of the panel sets are located in fuel tanks (40322, 40236, 40536); the remainder, in dry bays. Fuel tank locations and the flight profile are based on the Baseline Configuration - Task I.

Temperature histories are presented for the outer skin at the center of the bead, for the corrugation stiffener at the inner face, and for the difference between the inner and outer face, which represents the maximum gradient across the panel. For all panels, temperature gradients reach peak values near the start of cruise (at approximately 30 minutes) and during transonic descent (approximately 190 minutes in flight profile). For fuel tank areas, the temperature difference across the panel maintains a high value until fuel is drained from the tank. The apparent temperature inversion (hotter inside temperature) noted for dry bay panels during cruise is the result of including internal leakage convection in the analysis, and is not inconsistent with some observed results in supersonic cruise aircraft.





**CONDITION: M 2.7 START-OF-CRUISE (HOT DAY)**

XXX = UPPER SURF OF \_\_\_\_\_ ELEMENT  
 YYY = LOWER SURF OF \_\_\_\_\_ ELEMENT

INTERPOLATE ALONG ELEMENTS

CONVERSION TABLE	
F	
100	
200	
300	
400	
500	

PRECEDING PAGE BLANK NOT FILMED

FOLDOUT FRAME /









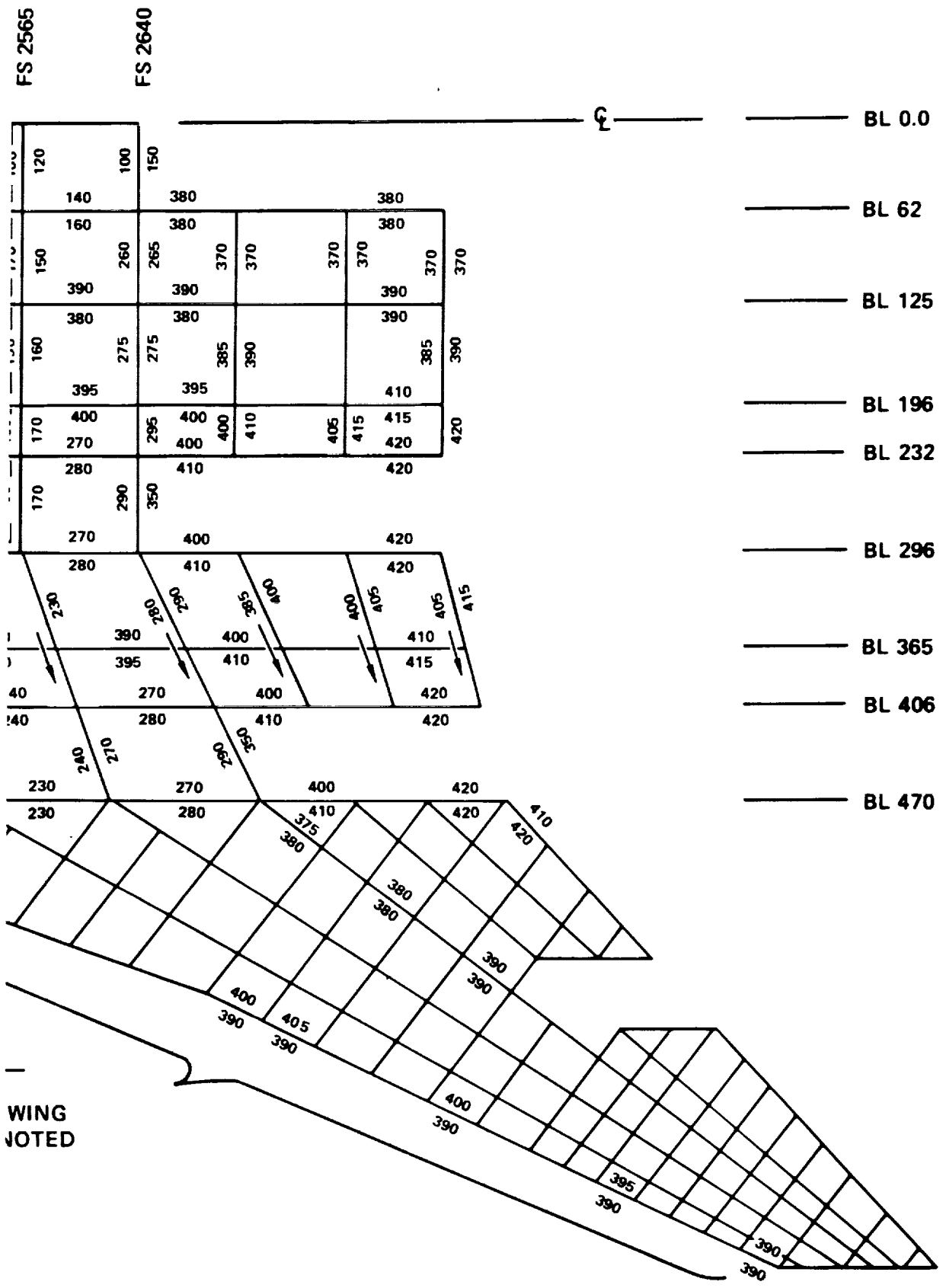
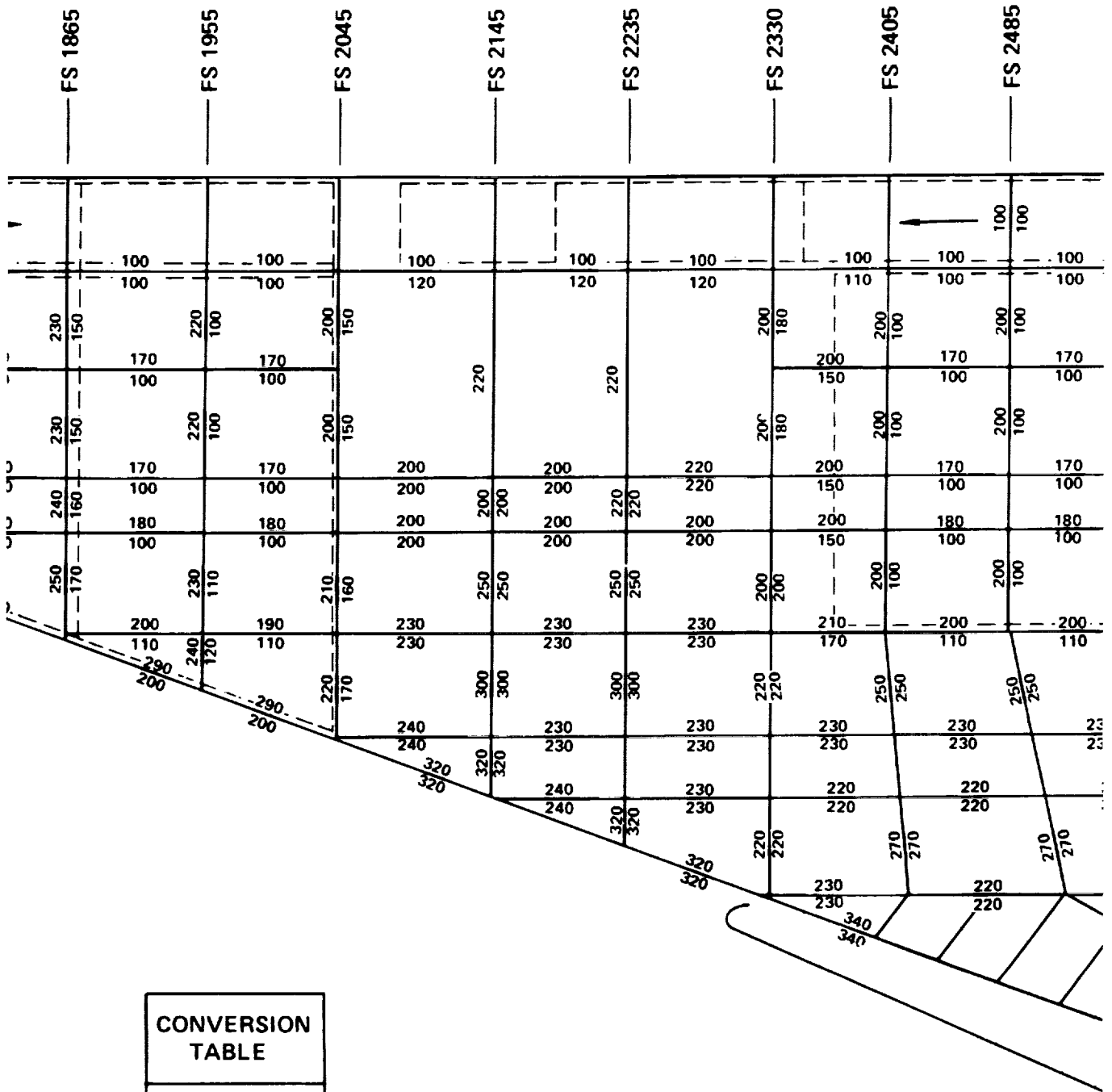


Figure 6-23. Finite Element Model Temperatures-  
Chordwise Stiffened-Mach 2.7 Start-of-Cruise









CONVERSION TABLE	
C	K
100	311
200	367
300	422
400	478
500	533

USE  $\frac{390}{390}$

FOR OUTER WALLS  
EXCEPT AS NOTED



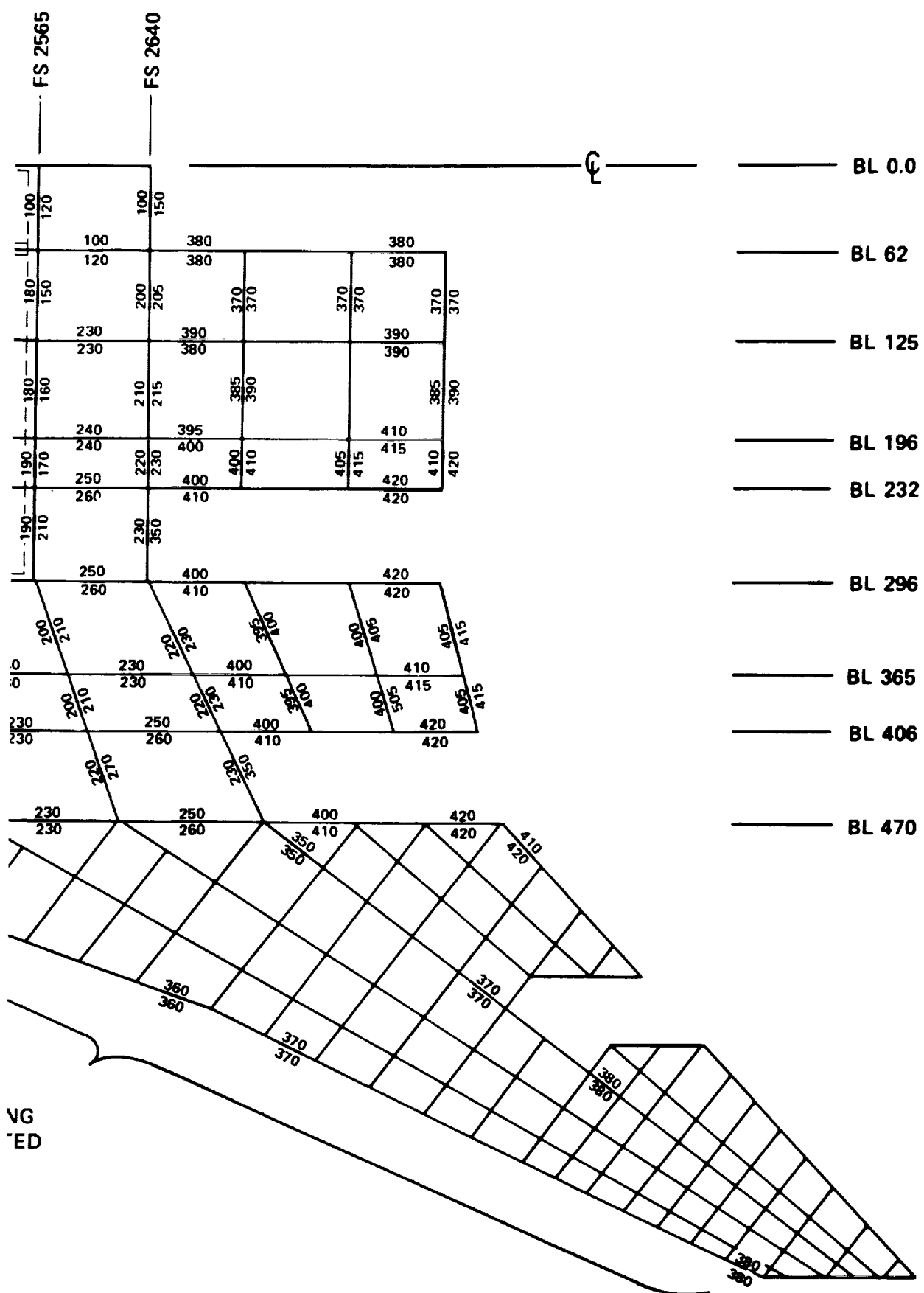


Figure 6-24. Finite Element Model Temperatures-  
Spanwise Stiffened-Mach 2.7 Start-of-Cruise









FS 1865

FS 1955

FS 2045

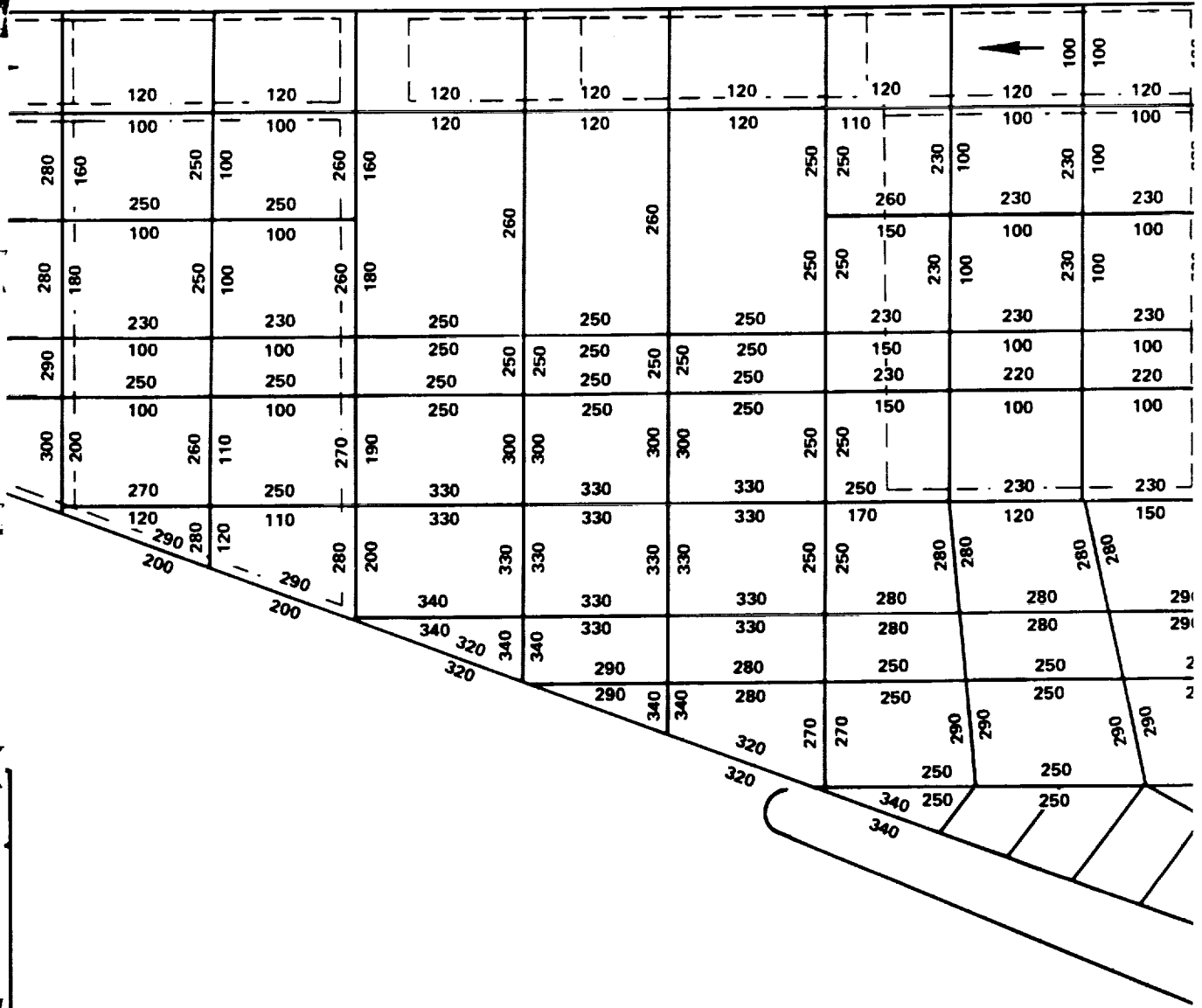
FS 2145

FS 2235

FS 2330

FS 2405

FS 2485



USE -  
FOR C  
EXCE

FOLDOUT FRAME 2







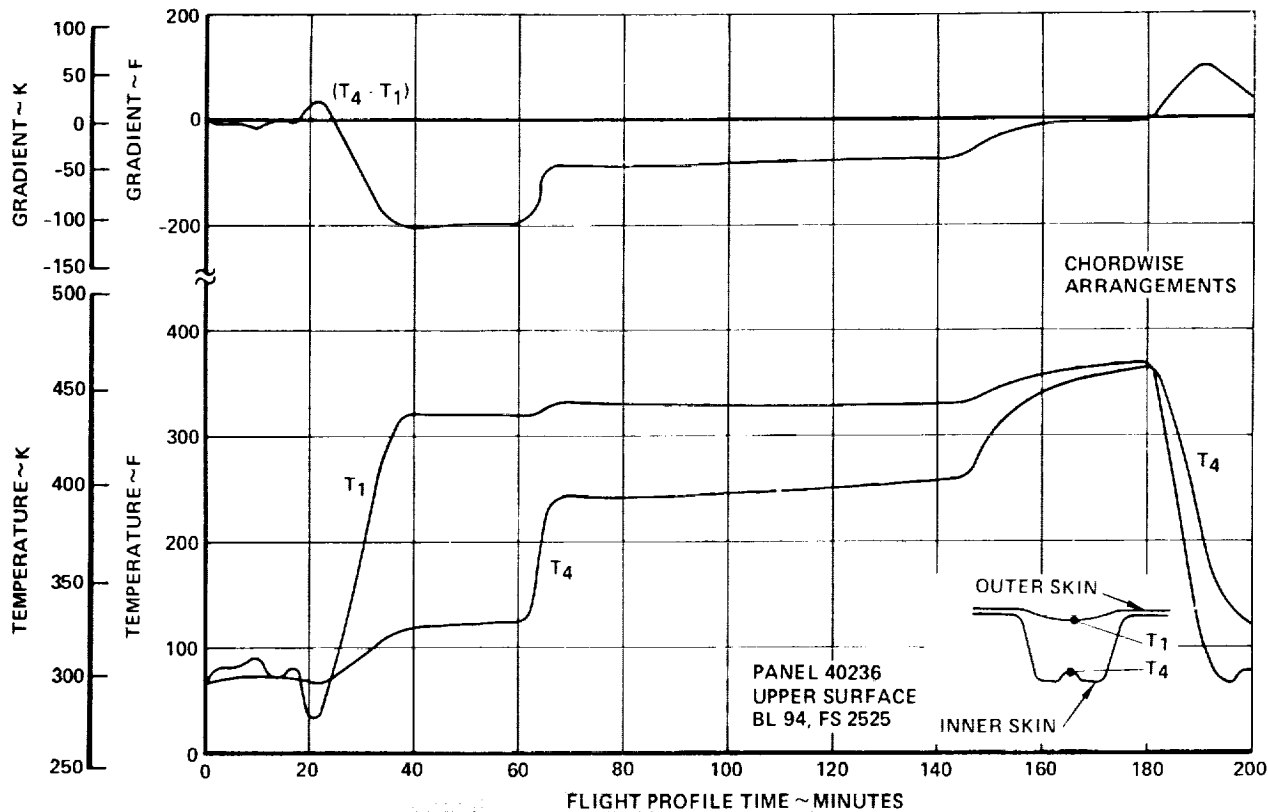


Figure 6-26. Chordwise Stiffened Wing Panel Temperature Histories - 40236 Upper Surface

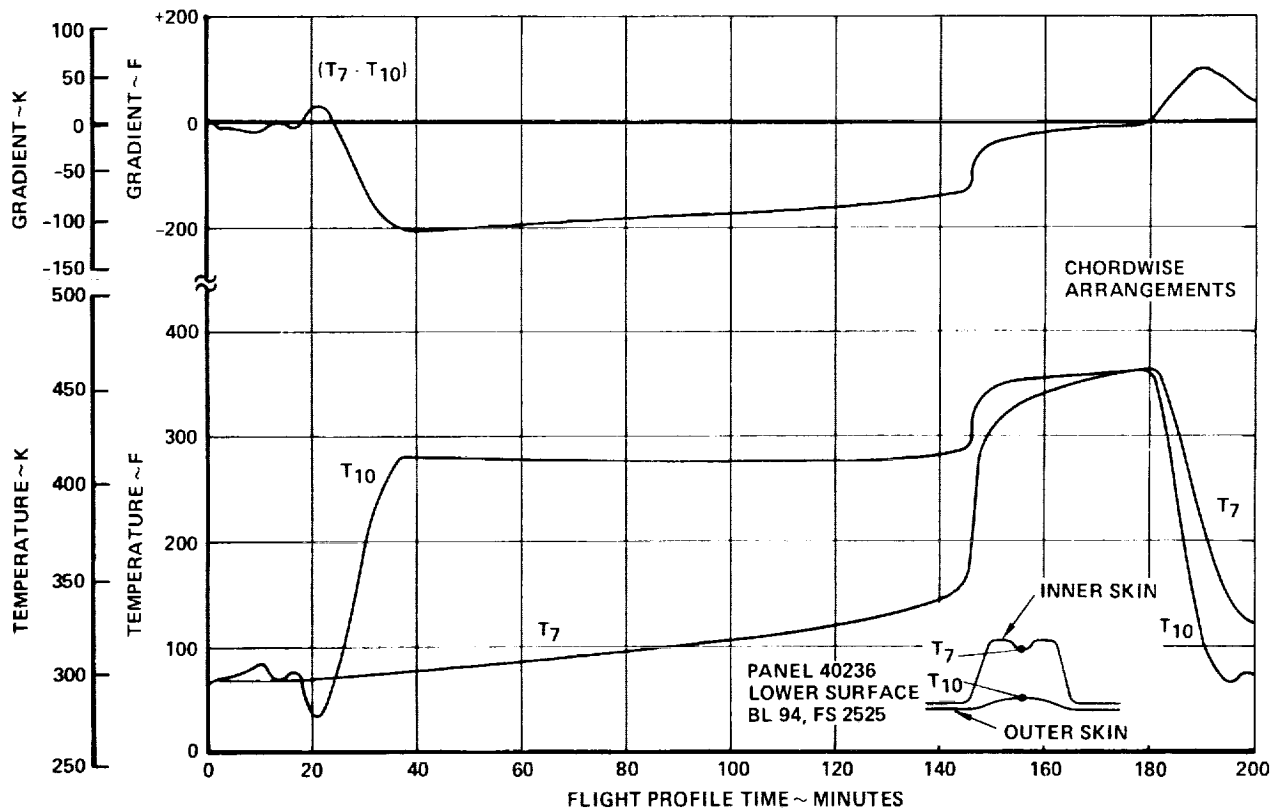


Figure 6-27. Chordwise Stiffened Wing Panel Temperature Histories - 40236 Lower Surface

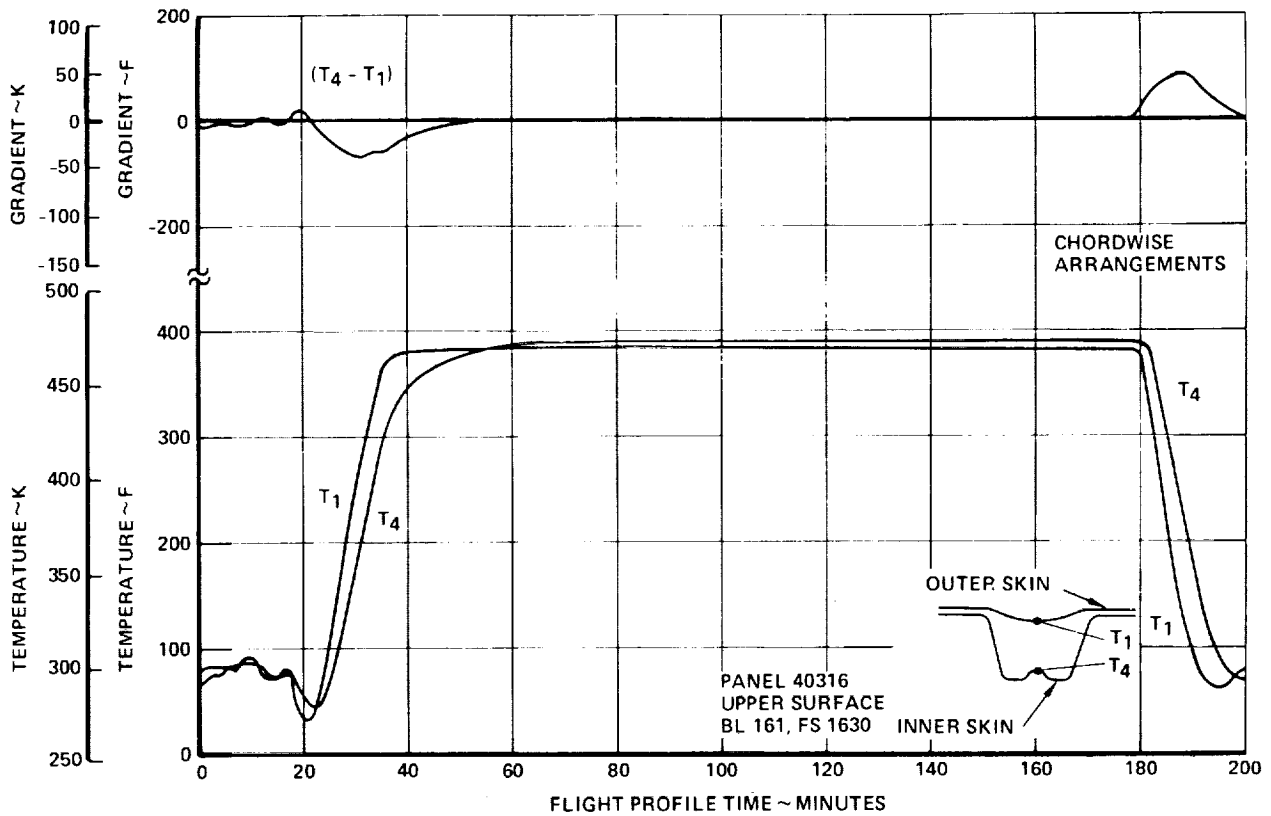


Figure 6-28. Chordwise Stiffened Wing Panel Temperature Histories - 40316 Upper Surface

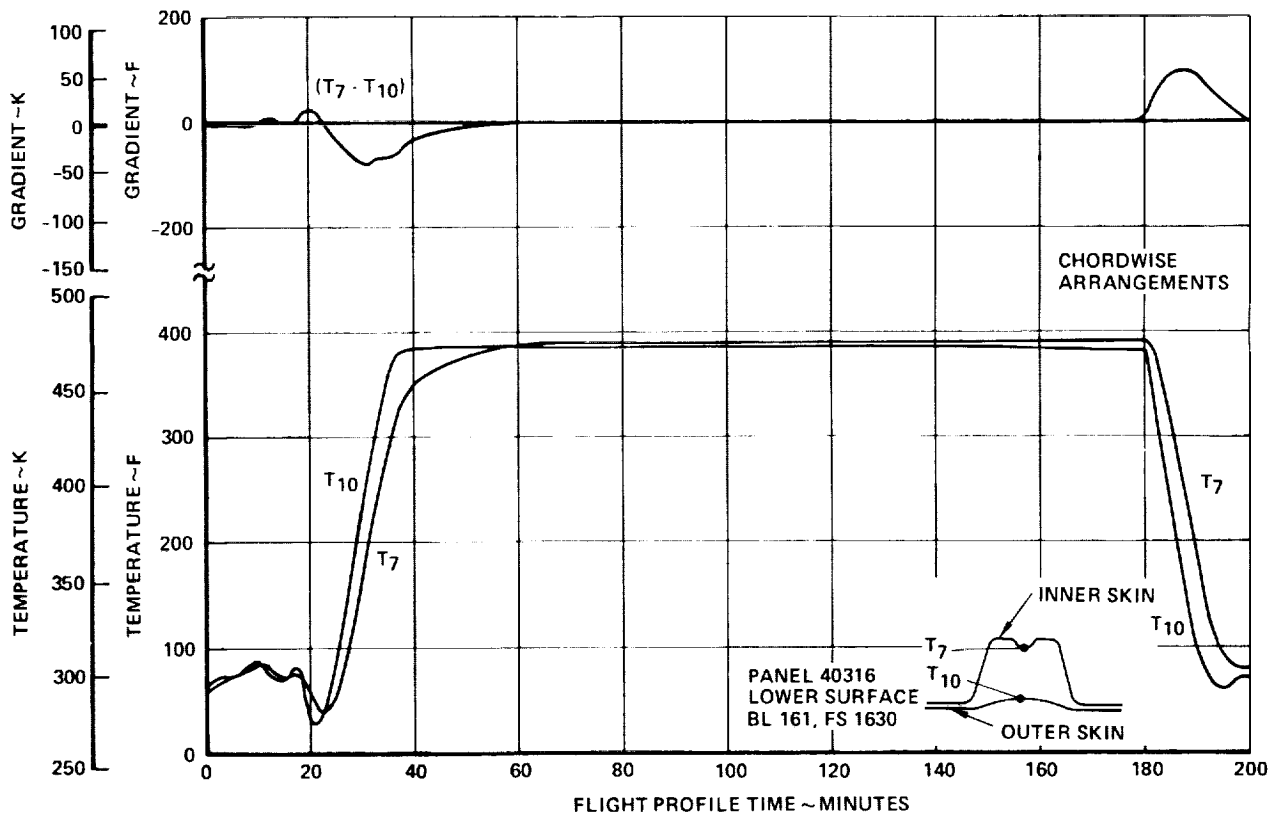


Figure 6-29. Chordwise Stiffened Wing Panel Temperature Histories - 40316 Lower Surface



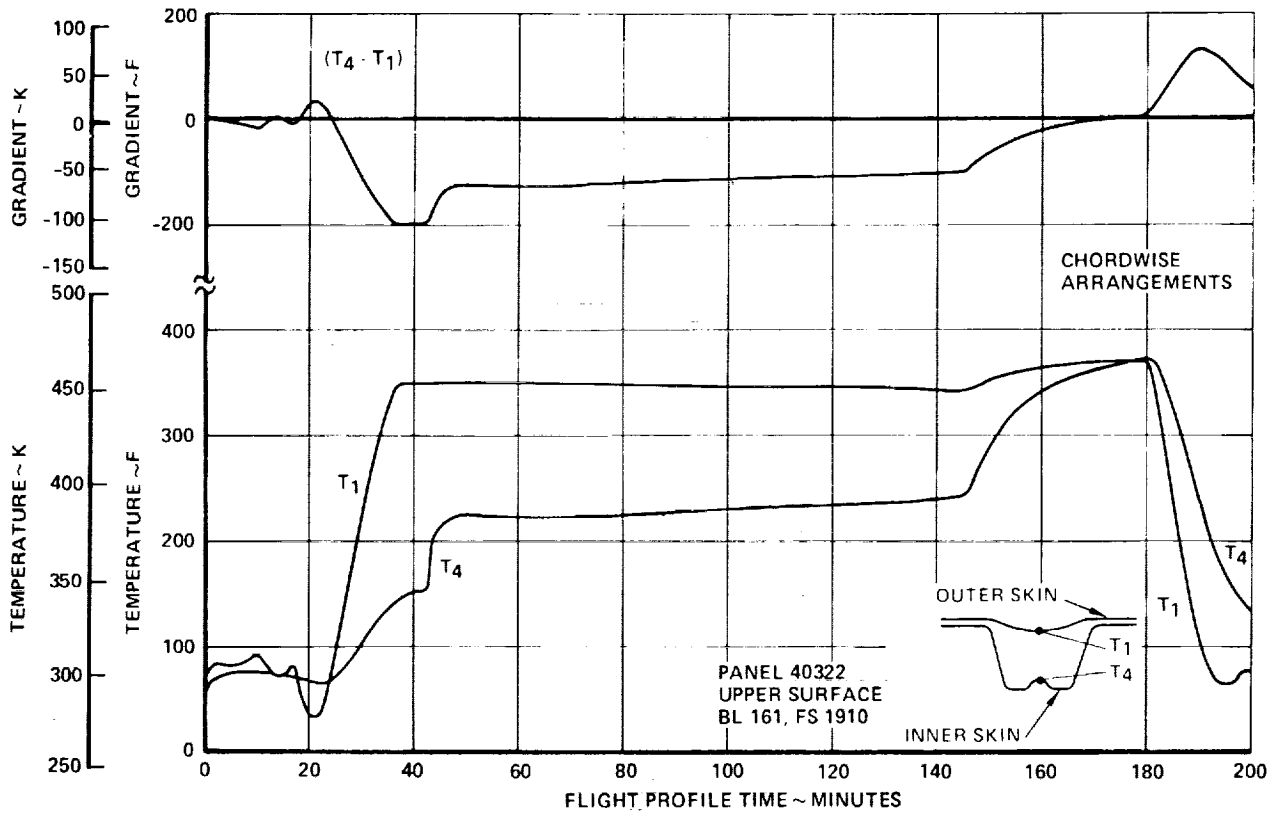


Figure 6-30. Chordwise Stiffened Wing Panel Temperature Histories - 40322 Upper Surface

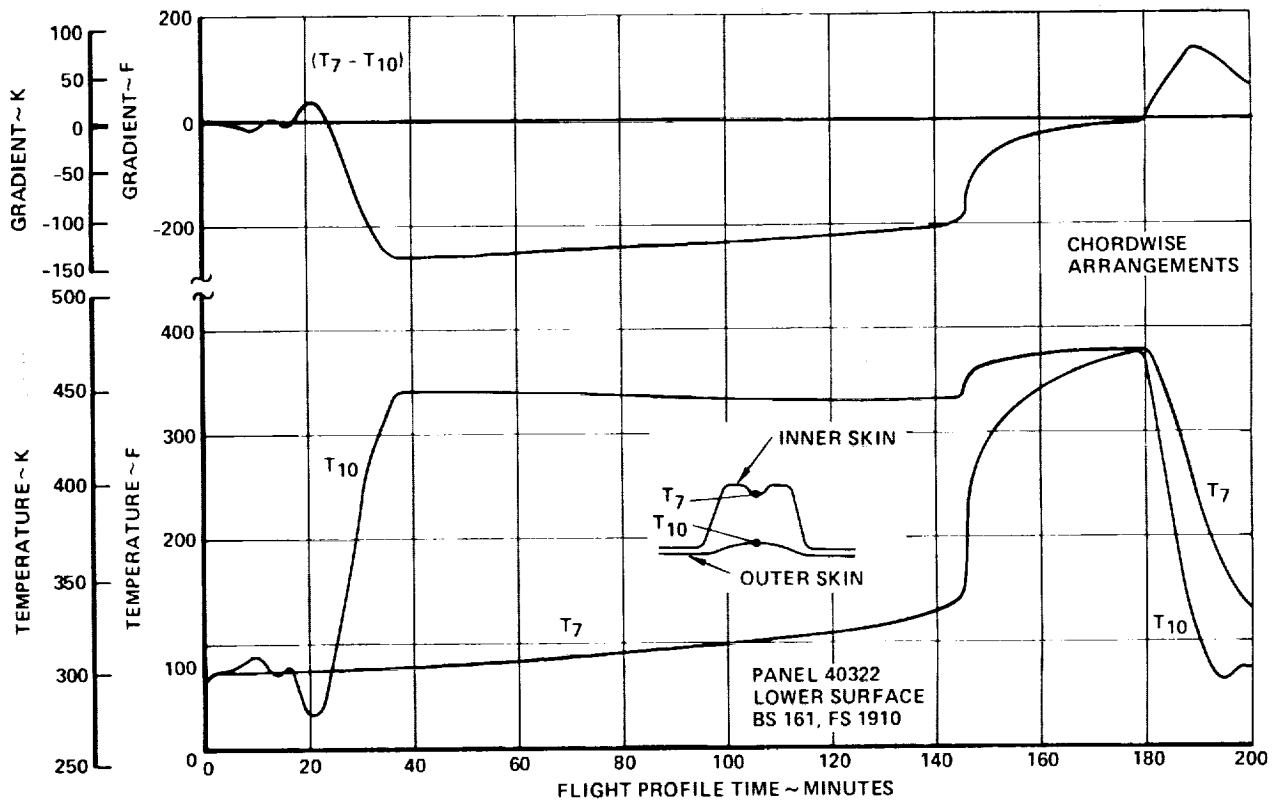


Figure 6-31. Chordwise Stiffened Wing Panel Temperature Histories - 40322 Lower Surface

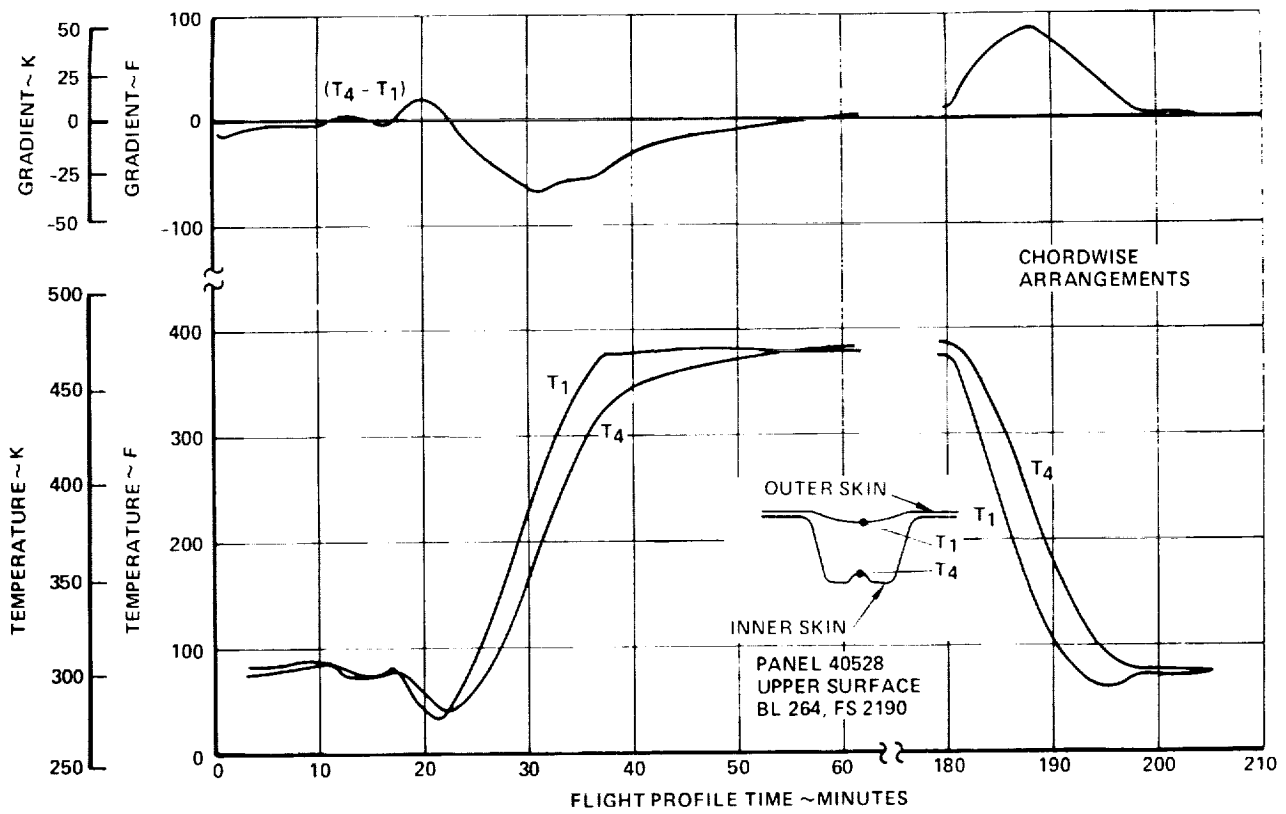


Figure 6-32. Chordwise Stiffened Wing Panel Temperature Histories - 40528 Upper Surface

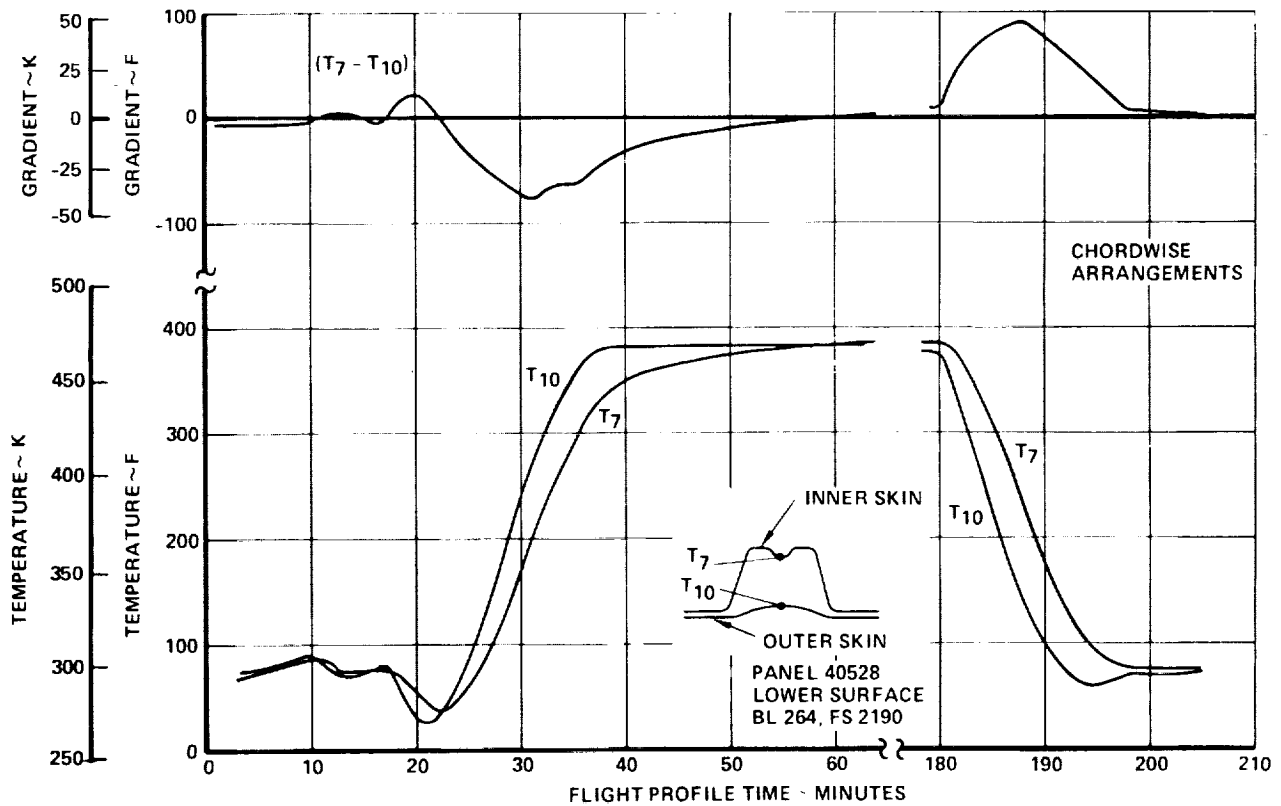


Figure 6-33. Chordwise Stiffened Wing Panel Temperature Histories - 40528 Lower Surface

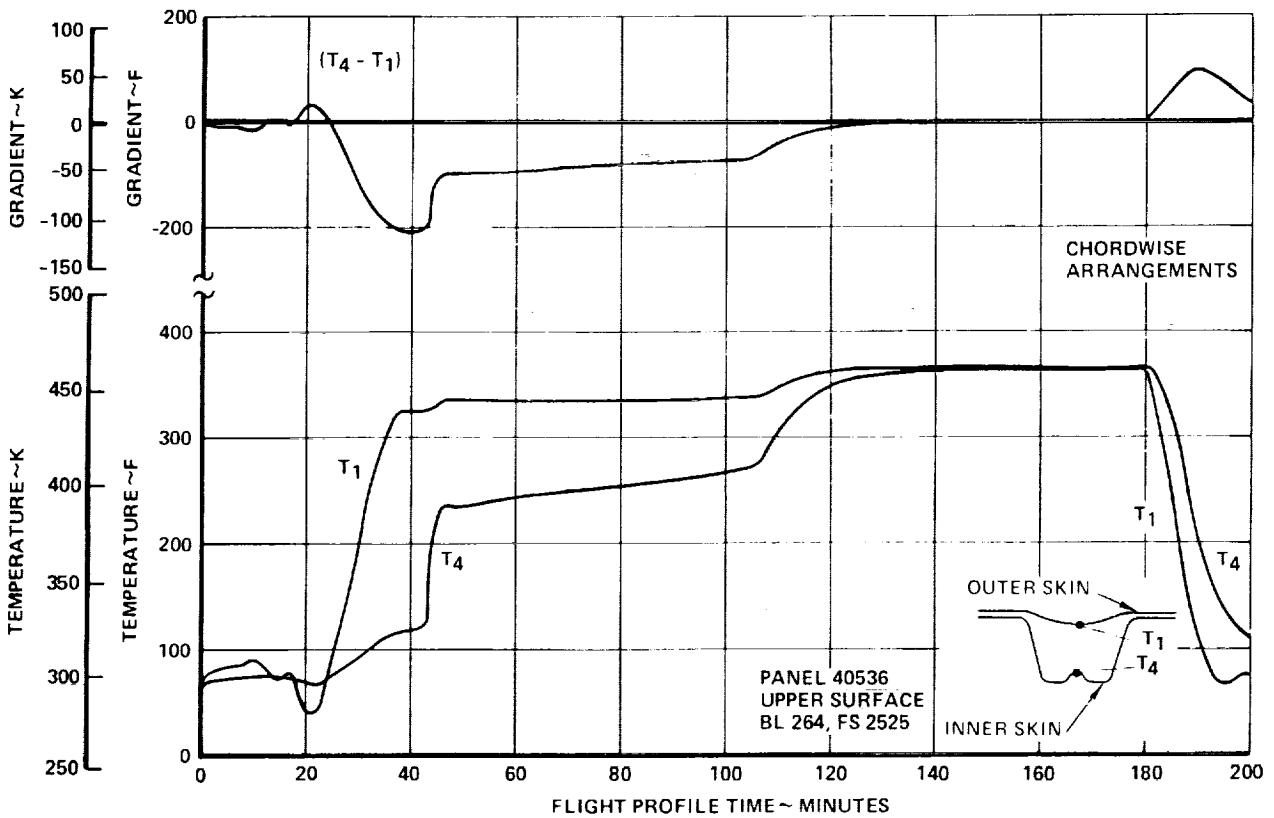


Figure 6-34. Chordwise Stiffened Wing Panel Temperature Histories - 40536 Upper Surface

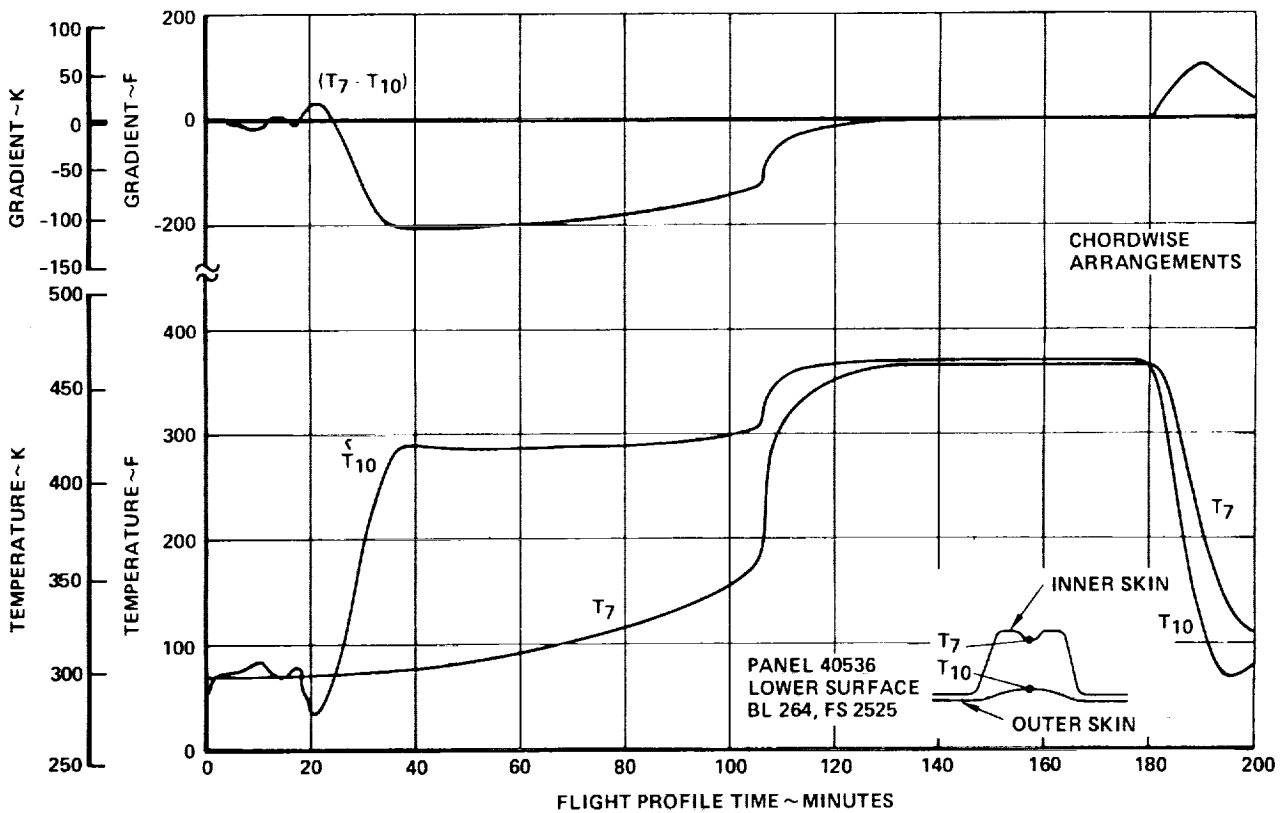


Figure 6-35. Chordwise Stiffened Wing Panel Temperature Histories - 40536 Lower Surface

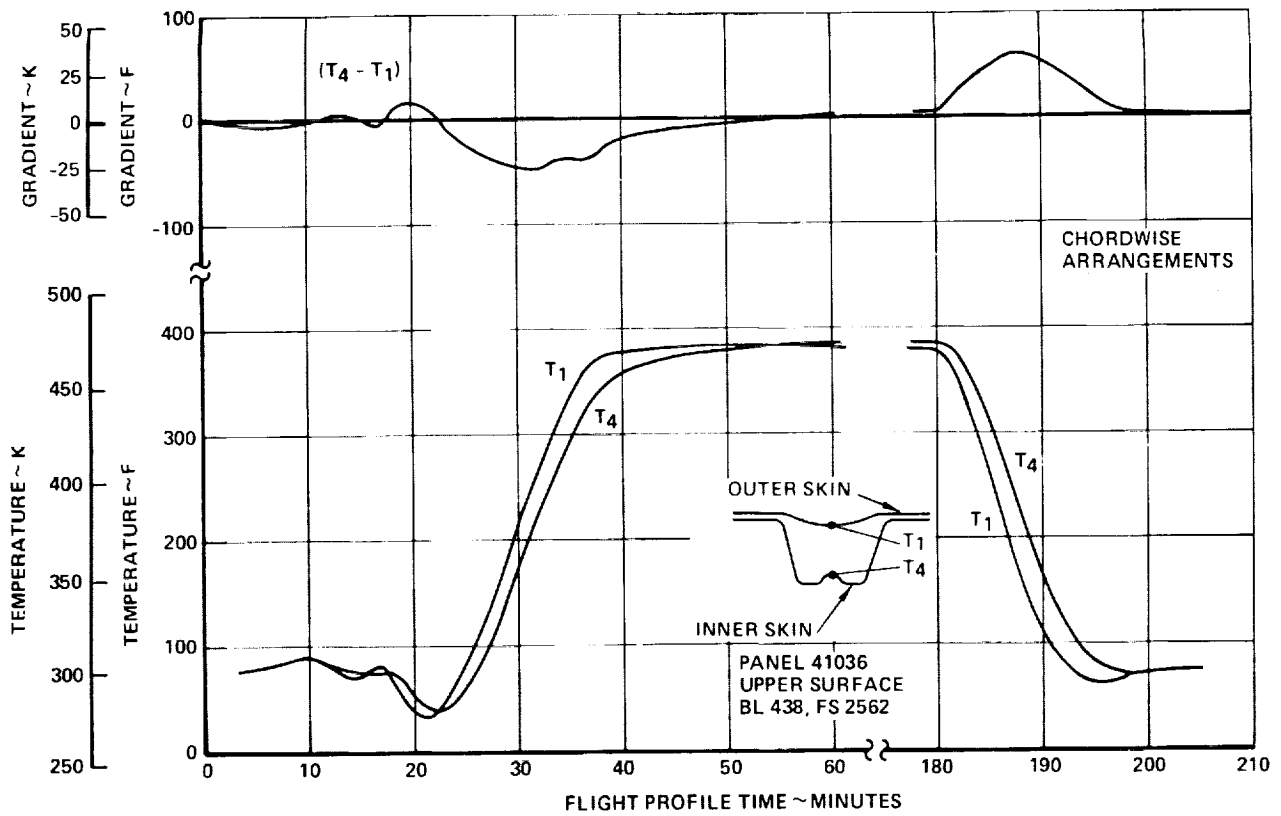


Figure 6-36. Chordwise Stiffened Wing Panel Temperature Histories - 41036 Upper Surface

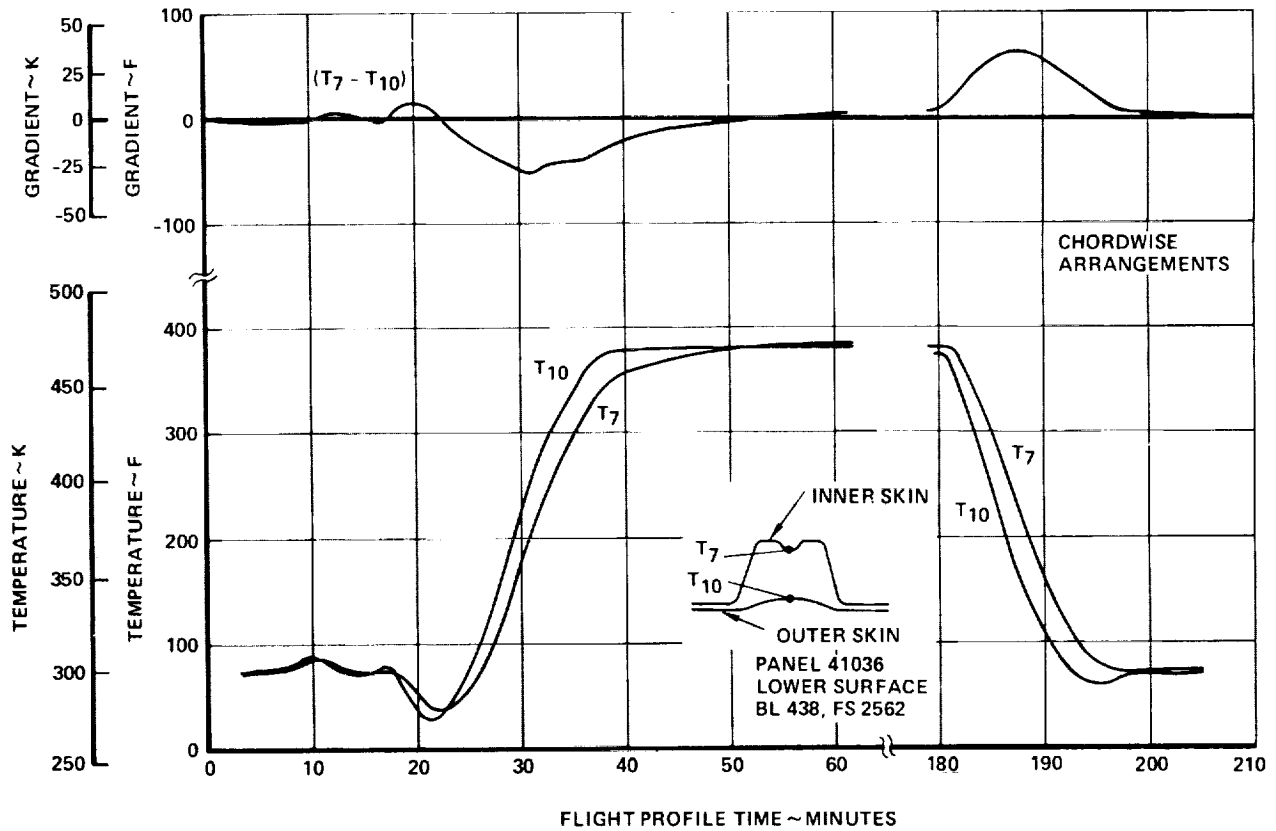


Figure 6-37. Chordwise Stiffened Wing Panel Temperature Histories - 41036 Lower Surface

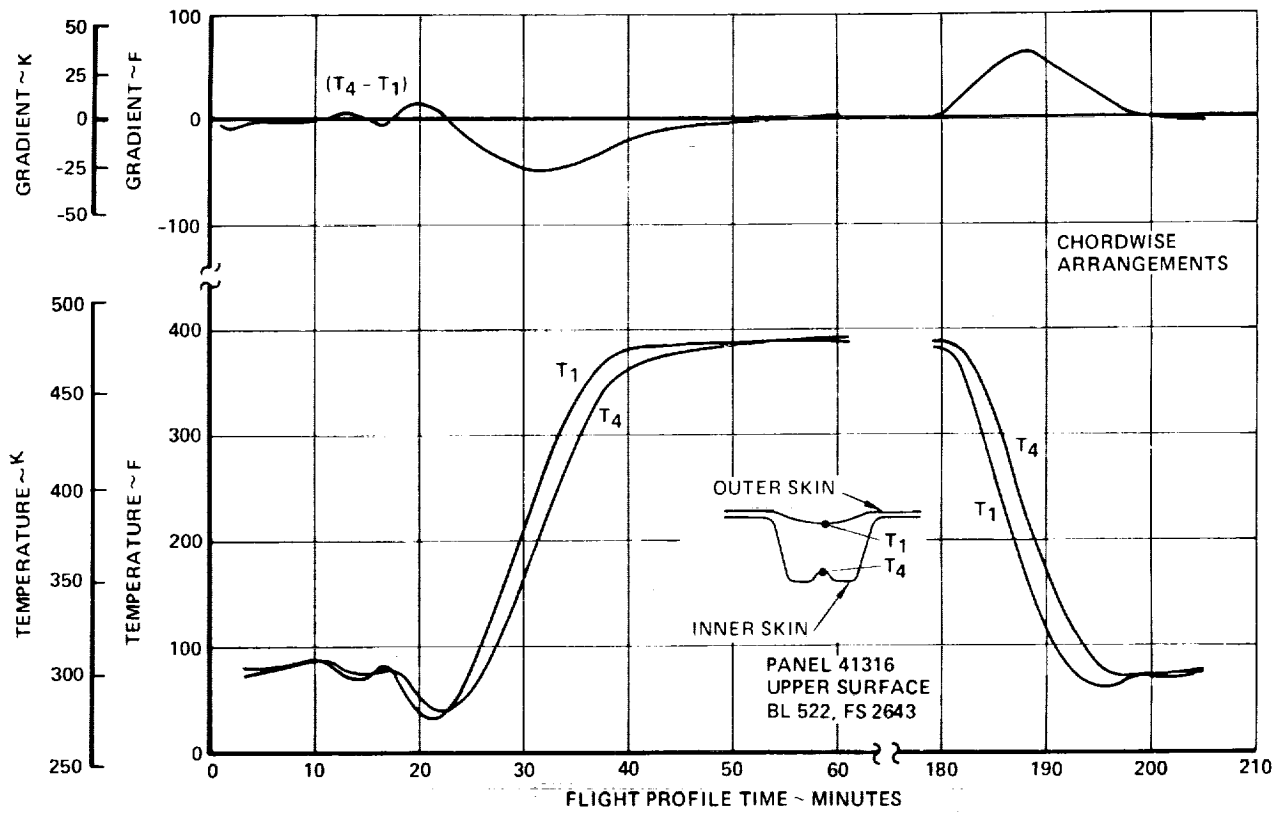


Figure 6-38. Chordwise Stiffened Wing Panel Temperature Histories - 41316 Upper Surface

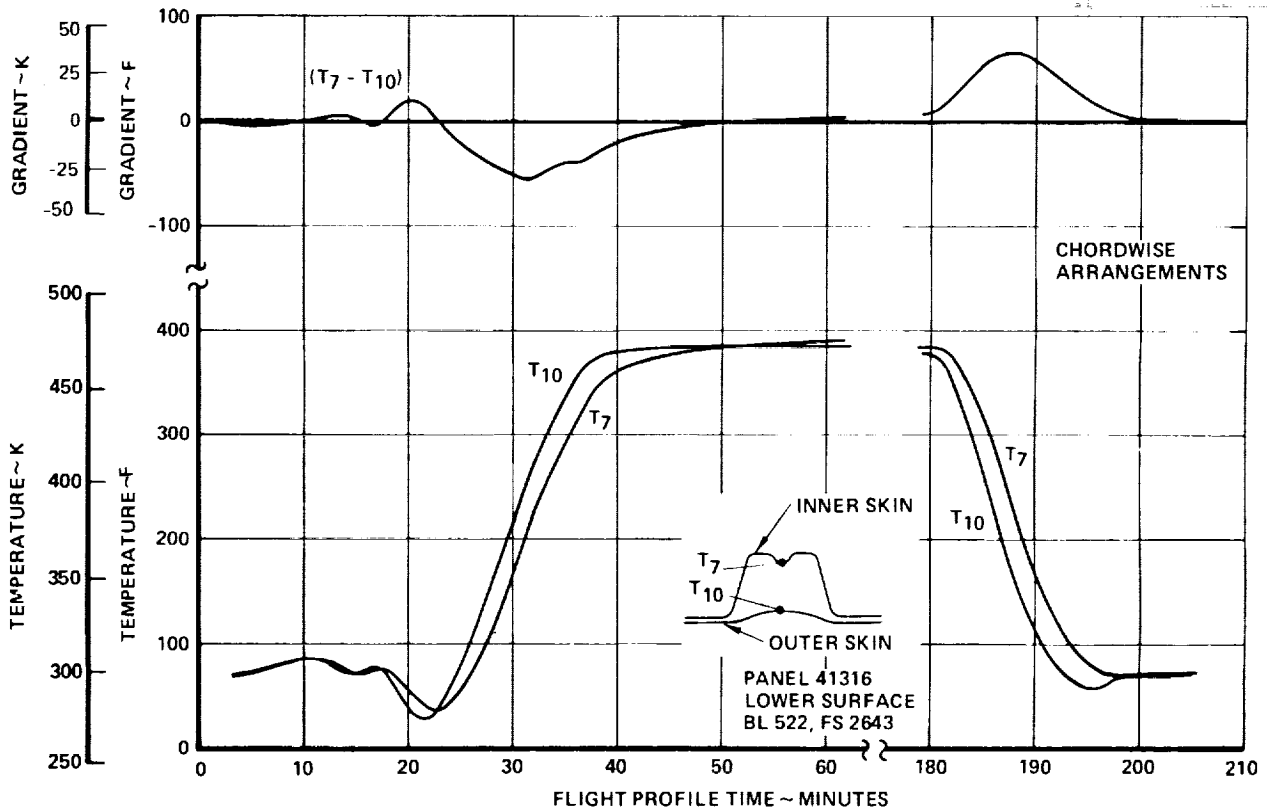


Figure 6-39. Chordwise Stiffened Wing Panel Temperature Histories - 41316 Lower Surface

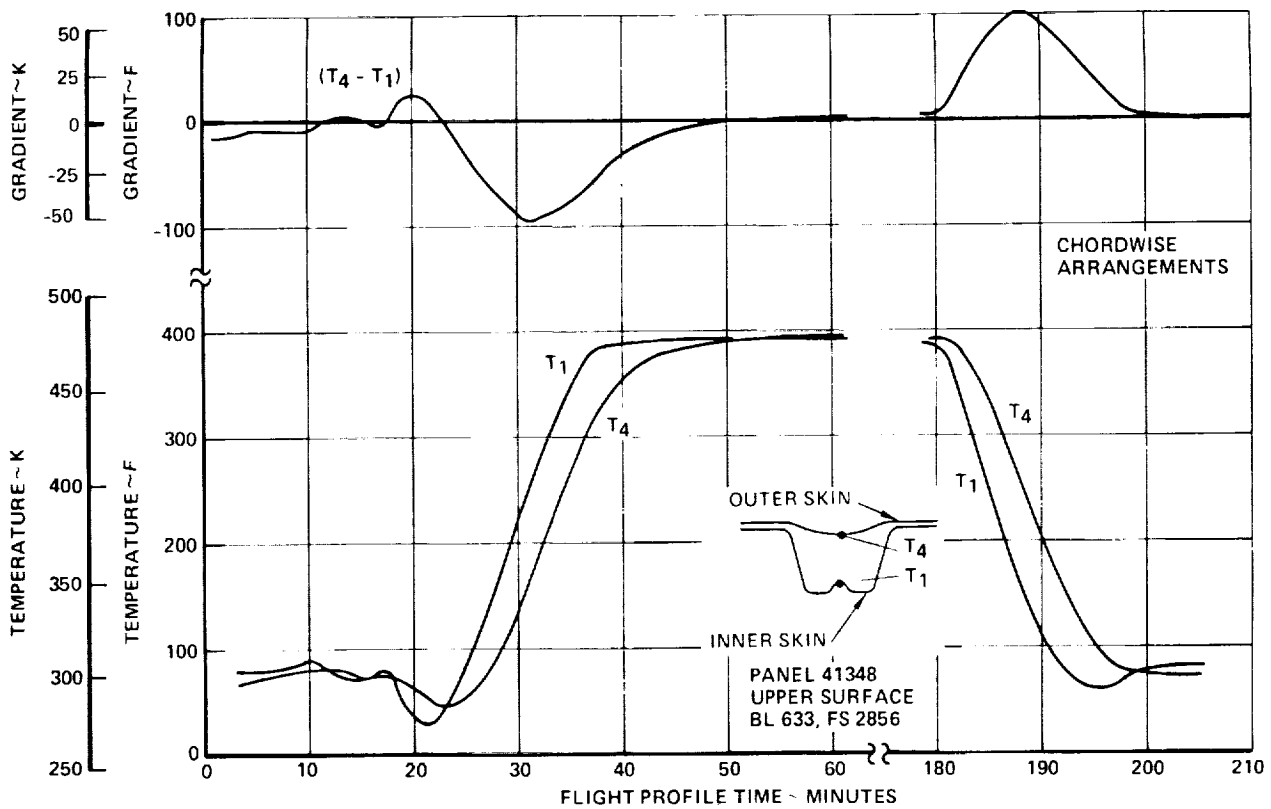


Figure 6-40. Chordwise Stiffened Wing Panel Temperature Histories - 41348 Upper Surface

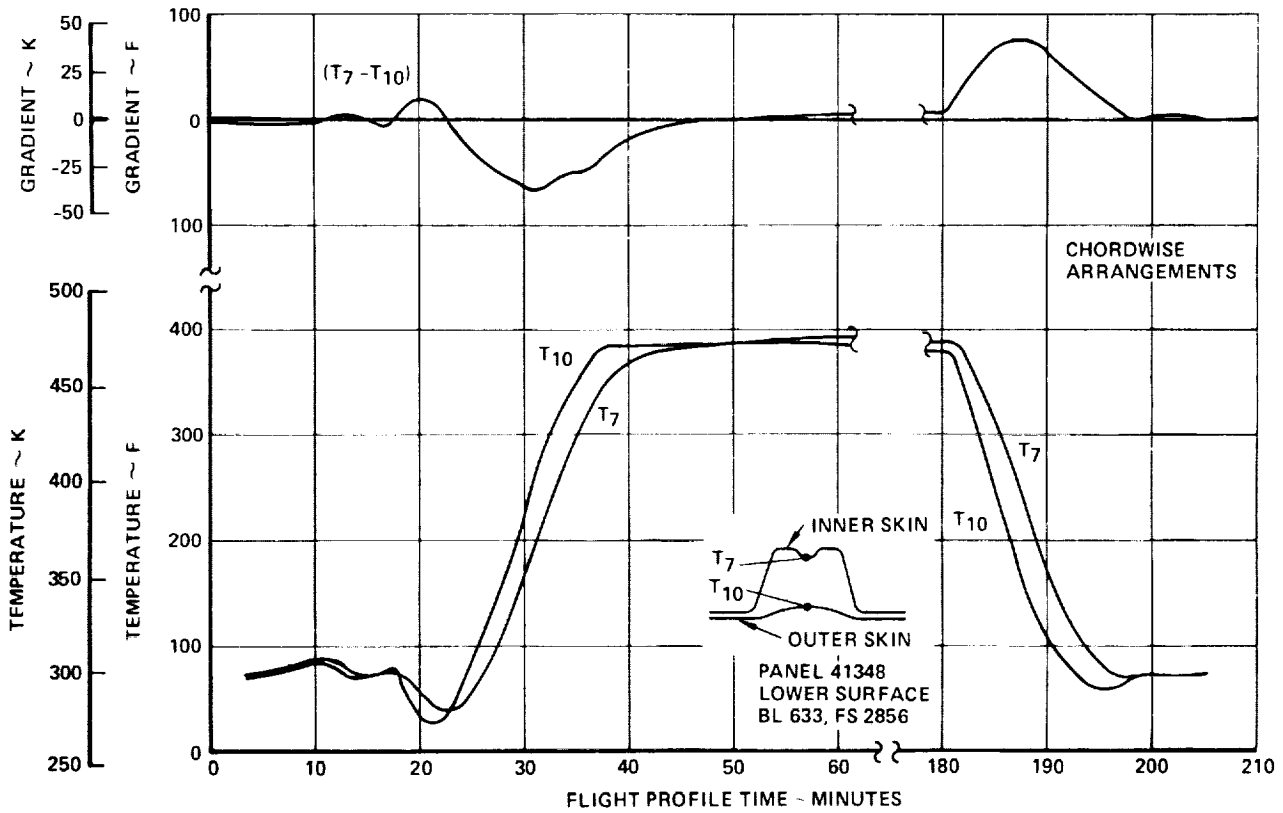


Figure 6-41. Chordwise Stiffened Wing Panel Temperature Histories - 41348 Lower Surface

The results of these analyses are used to define further the material gage and dimensional requirements of wing panels for the chordwise-stiffened design concept.

#### Spanwise-Stiffened Wing Panels

Structural temperature histories for upper and lower wing panels at three point design regions for the spanwise-stiffened arrangement are presented in Figures 6-42 through 6-47. The panels are (spanwise) hat-stiffened with a smooth outer skin. Two panel sets are located in fuel tanks (40322, 40536); the third, in a dry bay (41316). The Task I Baseline configuration is assumed.

Temperature histories are presented for the outer skin above the hat stiffener, for the inner face of the hat stiffener, and for the difference between panel thickness extremities. These results, plus temperature histories developed for four other point design regions not shown, are used to define further the material gage and dimensional requirements of wing panels for the spanwise-stiffened design concept.

#### Monocoque Wing Panels

Figures 6-48 through 6-53 present temperature histories for upper and lower wing panels at three point design regions. The panels are brazed honeycomb with square cell cores. Two panel sets are in fuel tanks (40322, 40536); the third is in a dry bay (41316). The Task I baseline configuration is assumed.

Temperature histories are presented for the outer and inner face sheets, and for the difference between them. No braze material was assumed to flow into the core during the brazing process for this analysis, to obtain the maximum thermal gradient across the panel. These results, plus temperature histories for four other point design regions not shown, are used to define further the material gage and dimensional requirements of wing panels for the monocoque design concept.

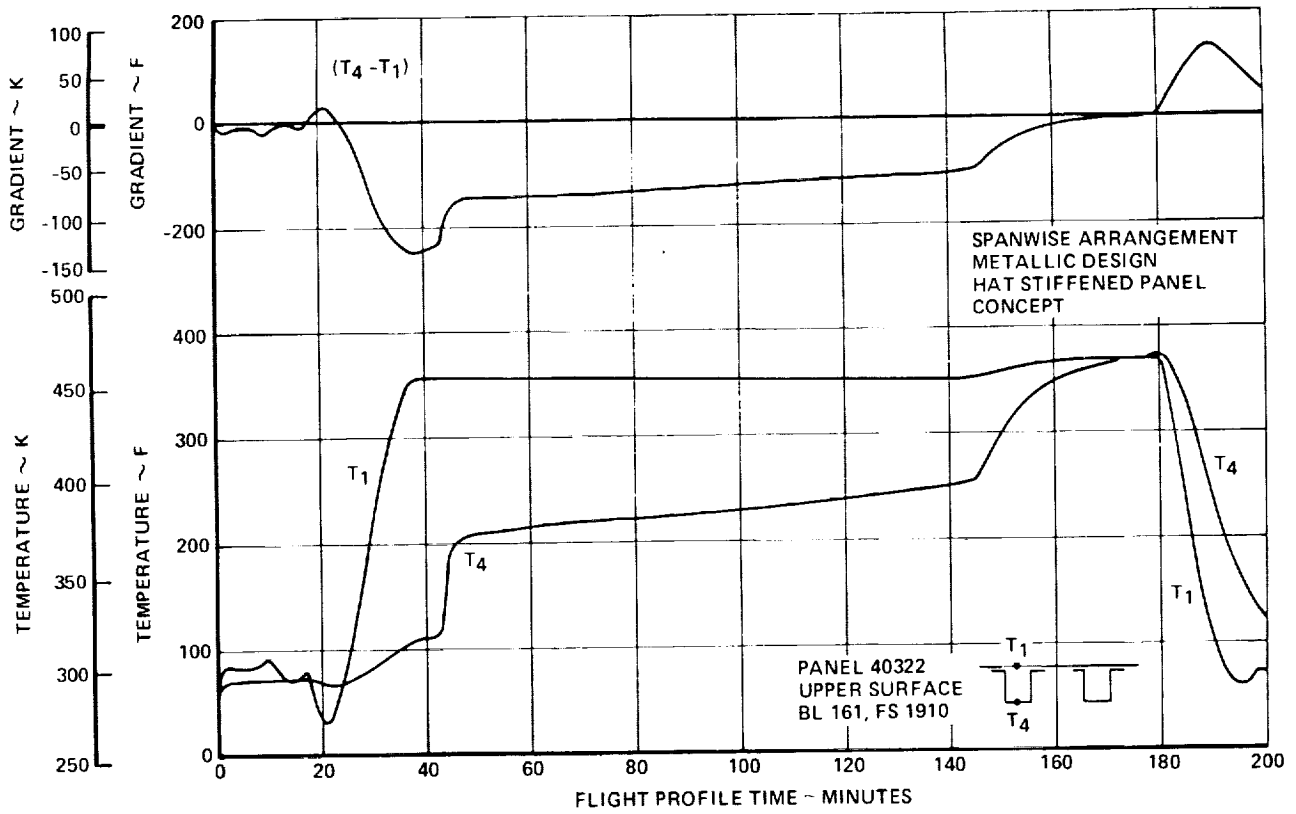


Figure 6-42. Spanwise Stiffened Wing Panel Temperature Histories - 40322 Upper Surface

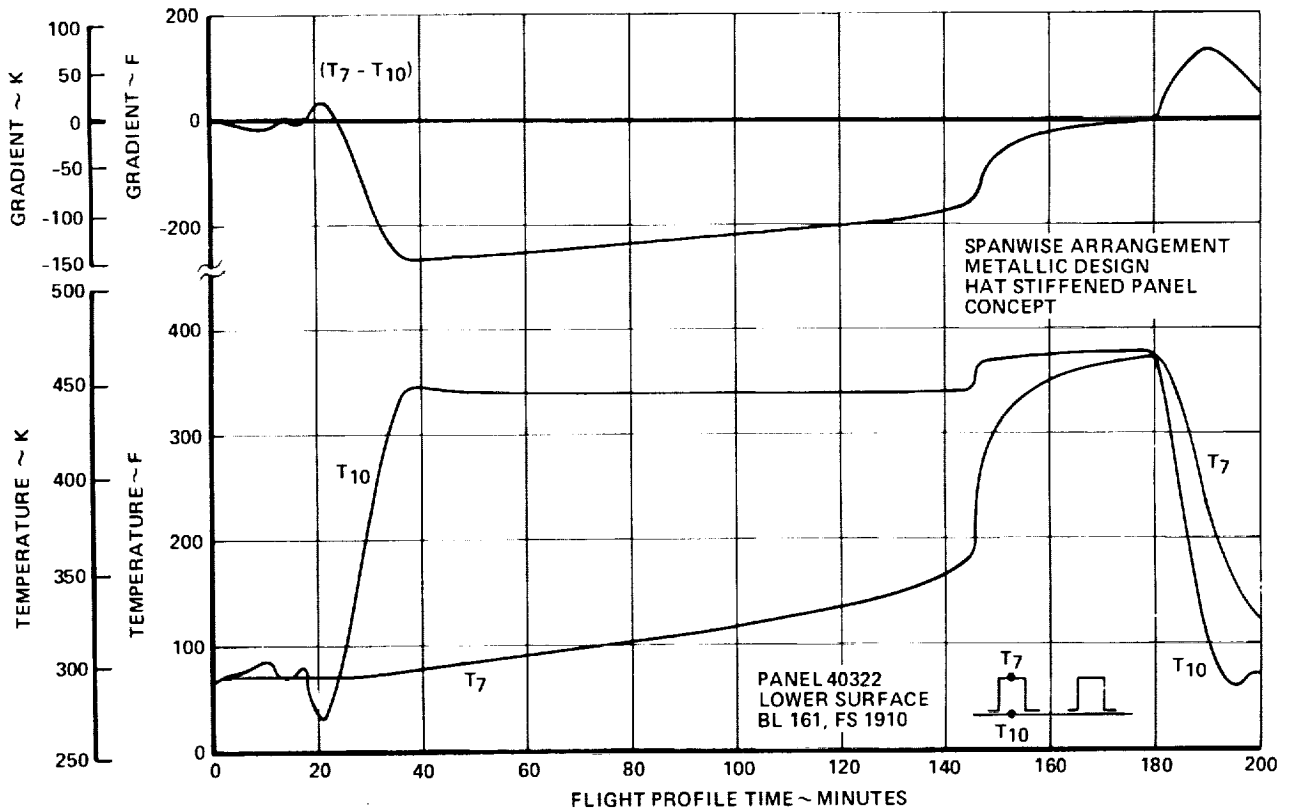


Figure 6-43. Spanwise Stiffened Wing Panel Temperature Histories - 40322 Lower Surface



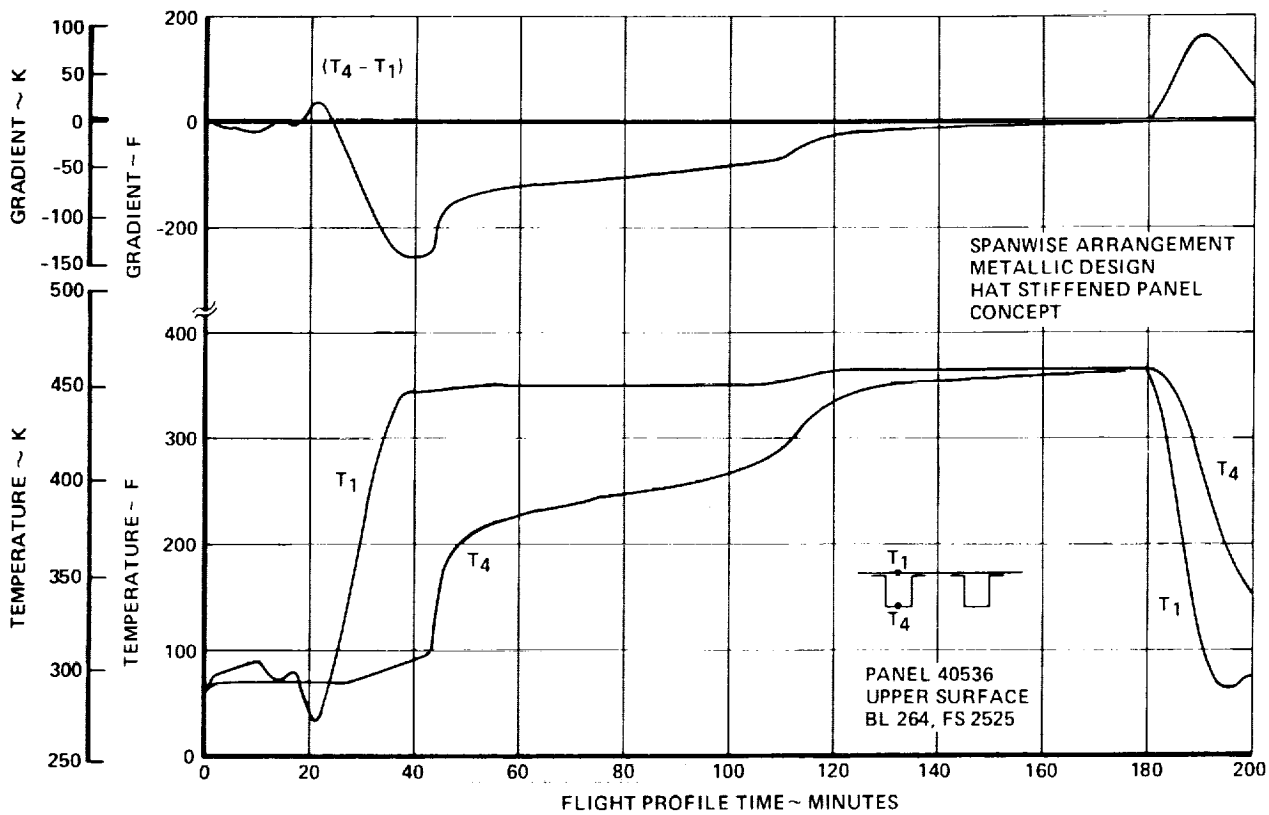


Figure 6-44. Spanwise Stiffened Wing Panel Temperature Histories - 40536 Upper Surface

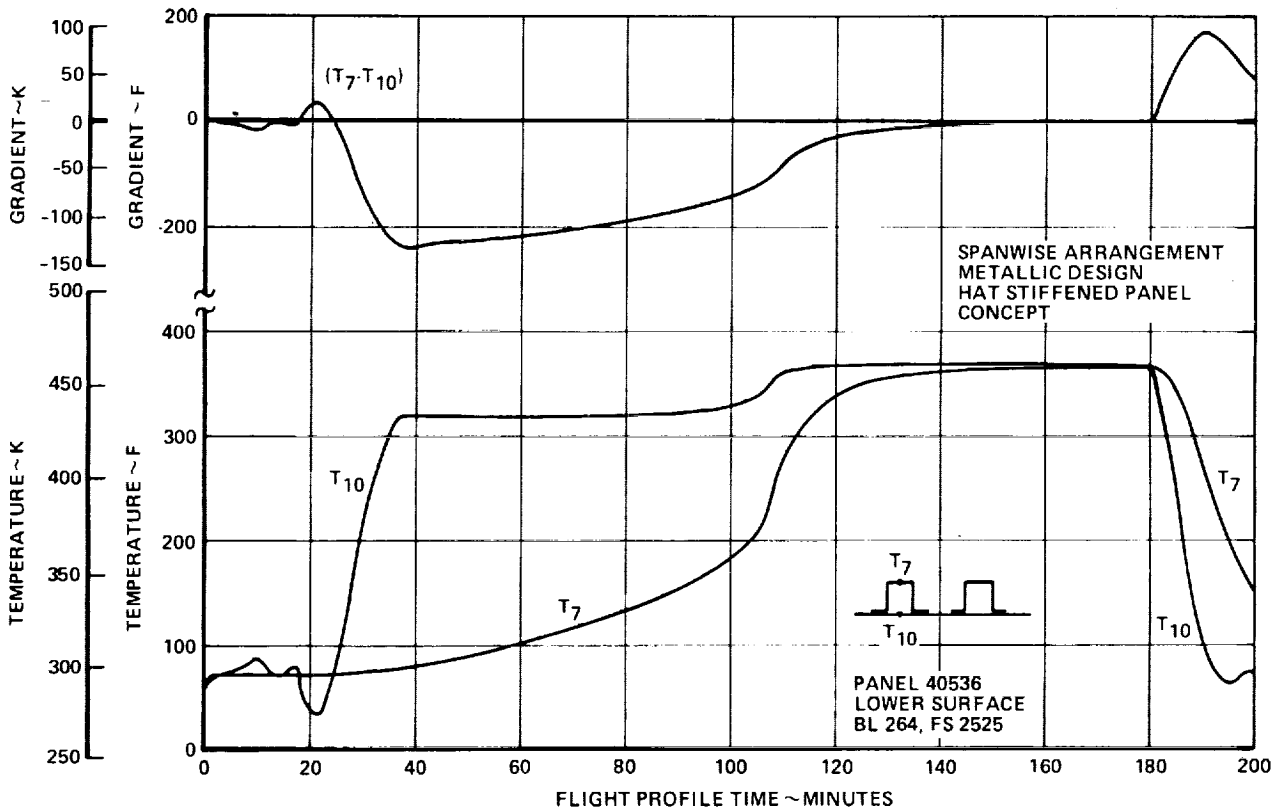


Figure 6-45. Spanwise Stiffened Wing Panel Temperature Histories - 40536 Lower Surface

C.5

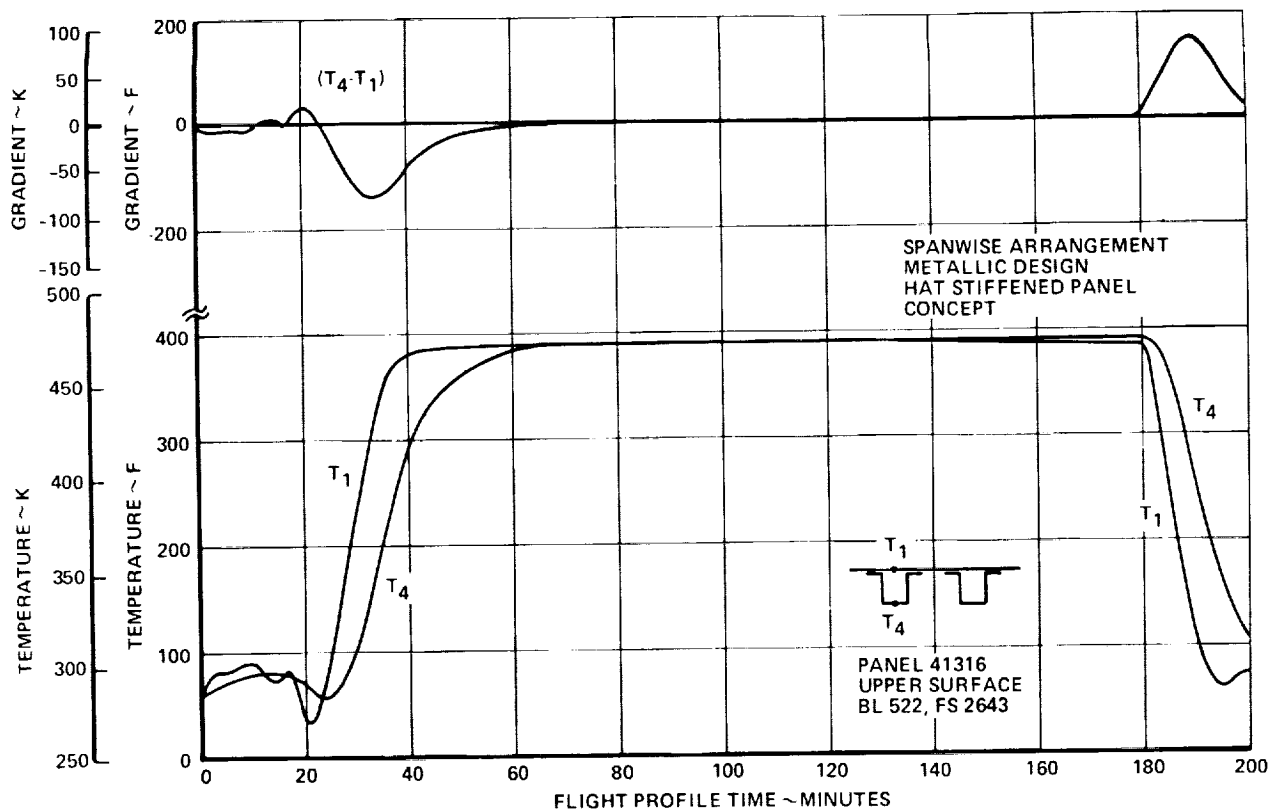


Figure 6-46. Spanwise Stiffened Wing Panel Temperature Histories - 41316 Upper Surface

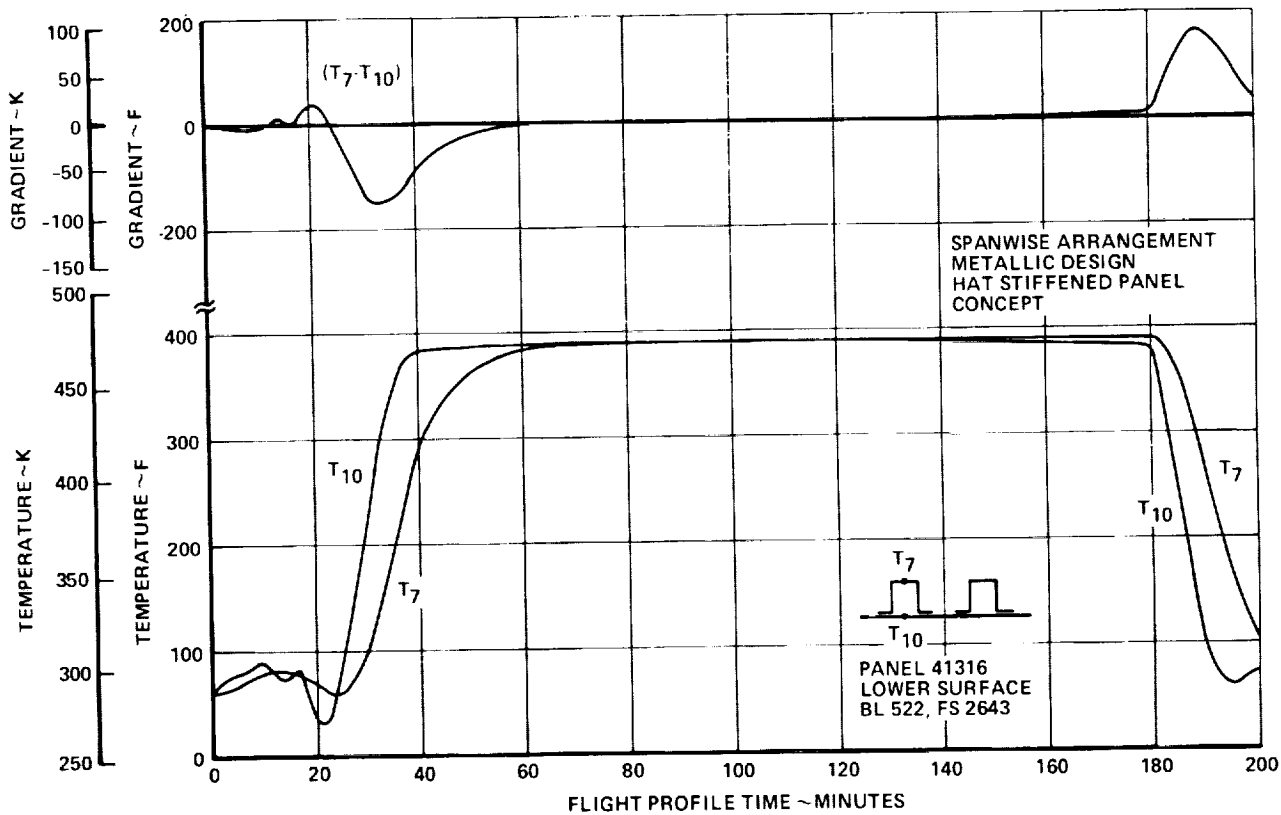


Figure 6-47. Spanwise Stiffened Wing Panel Temperature Histories - 41316 Lower Surface

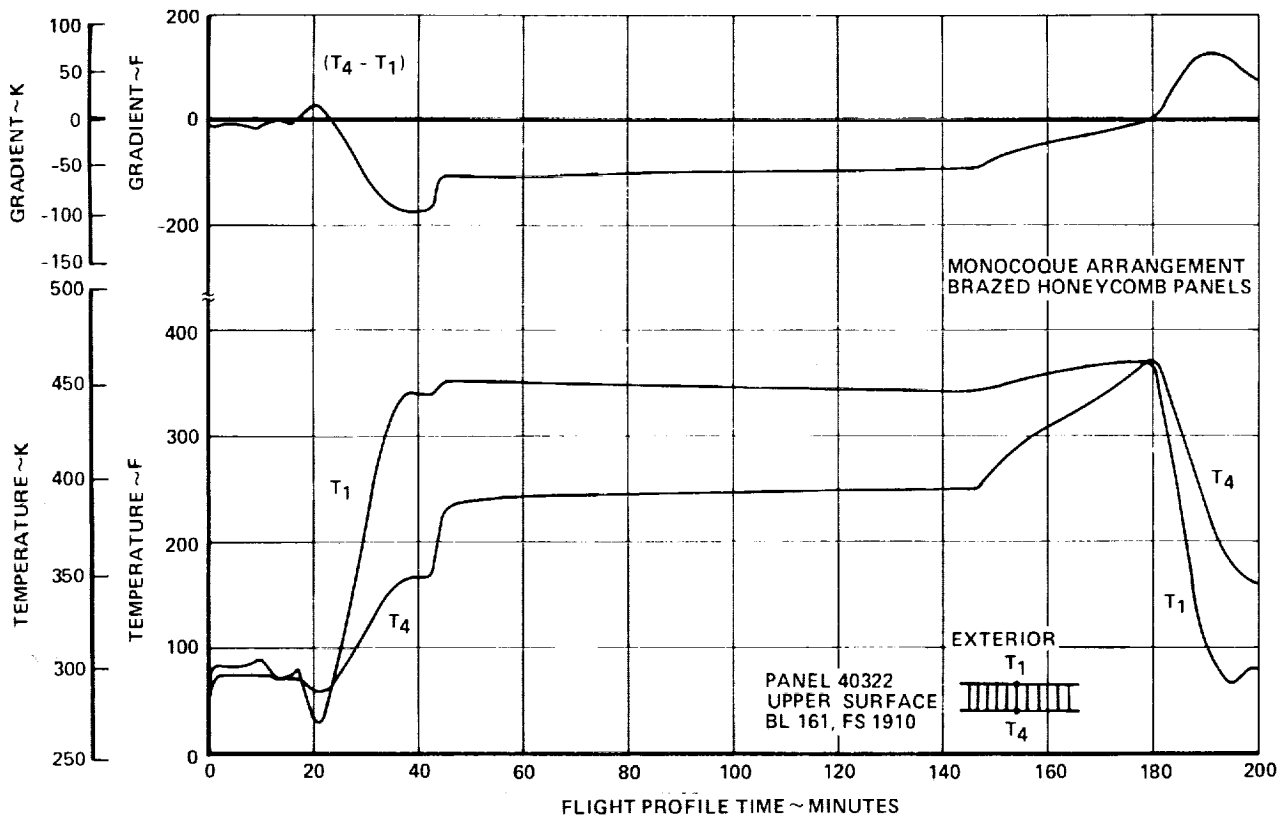


Figure 6-48. Monocoque Wing Panel Temperature Histories - 40322 Upper Surface

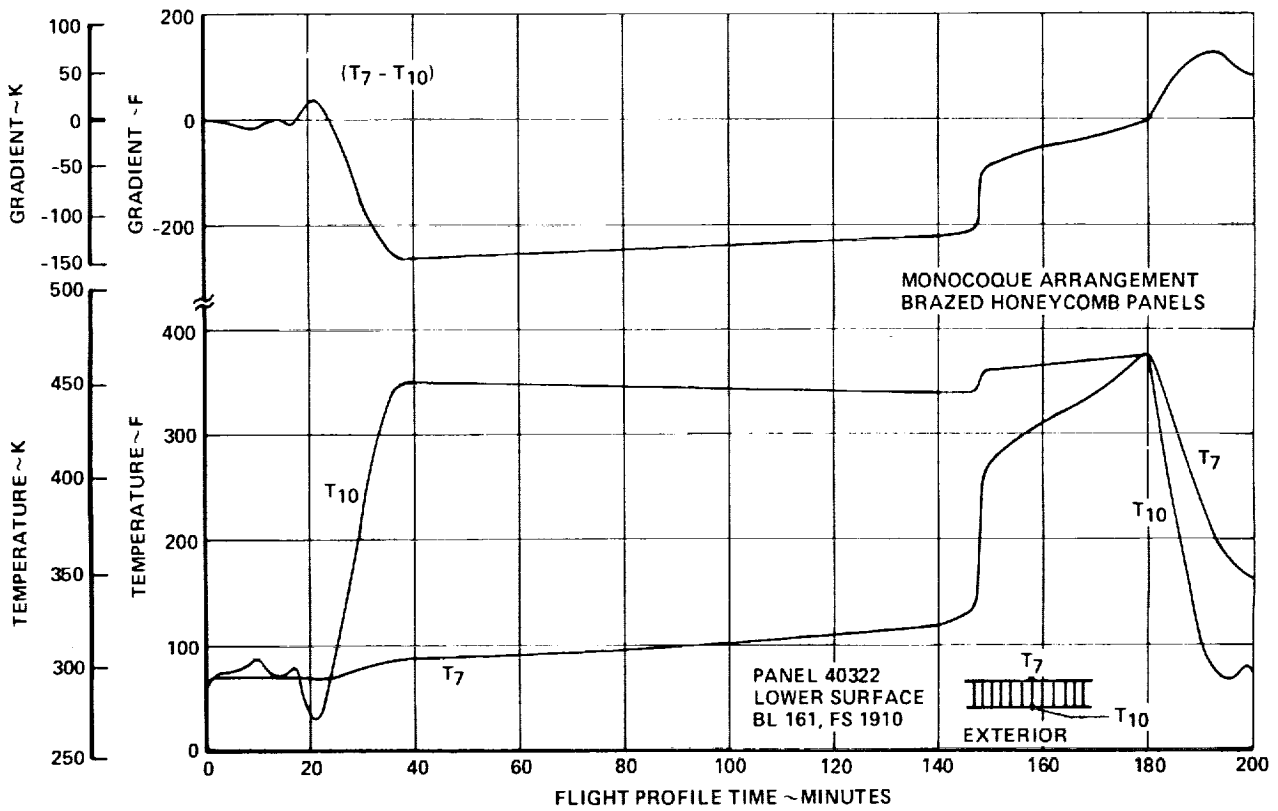


Figure 6-49. Monocoque Wing Panel Temperature Histories - 40322 Lower Surface

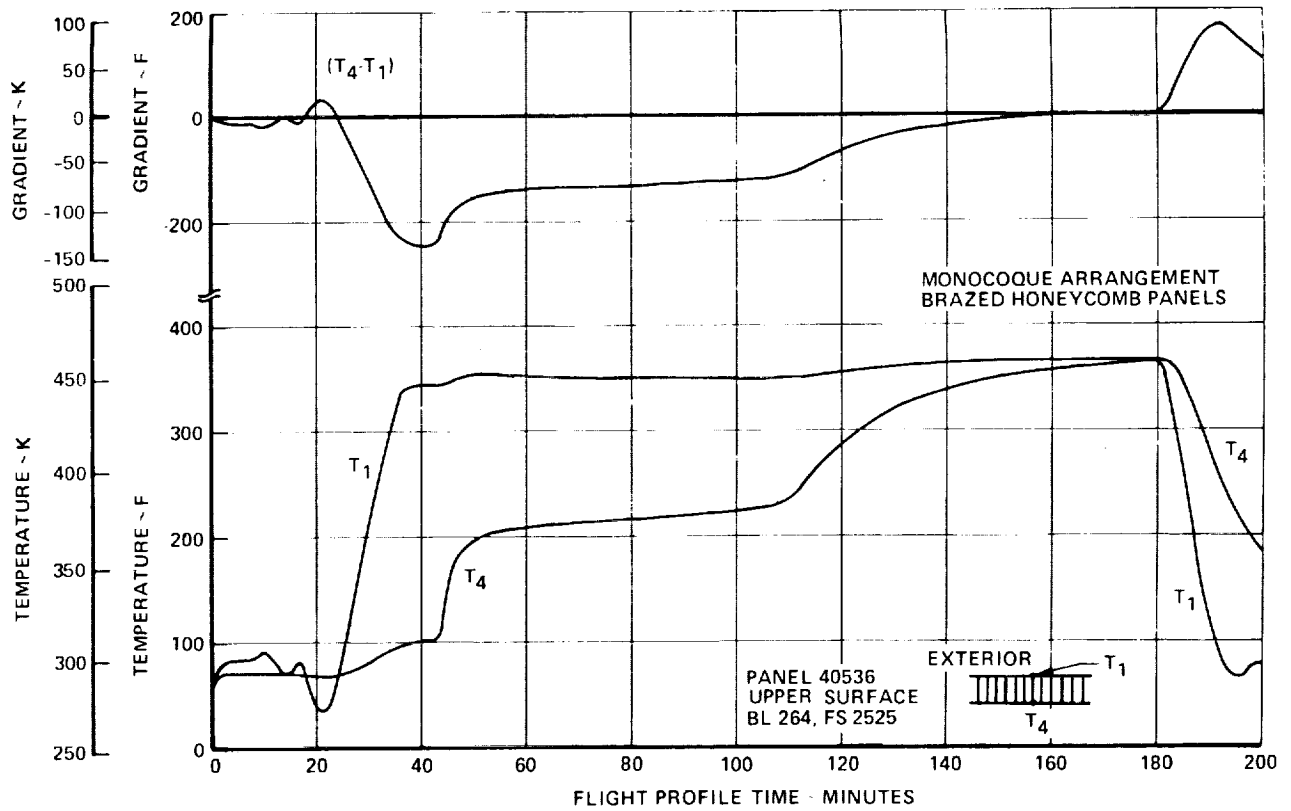


Figure 6-50. Monocoque Wing Panel Temperature Histories - 40536 Upper Surface

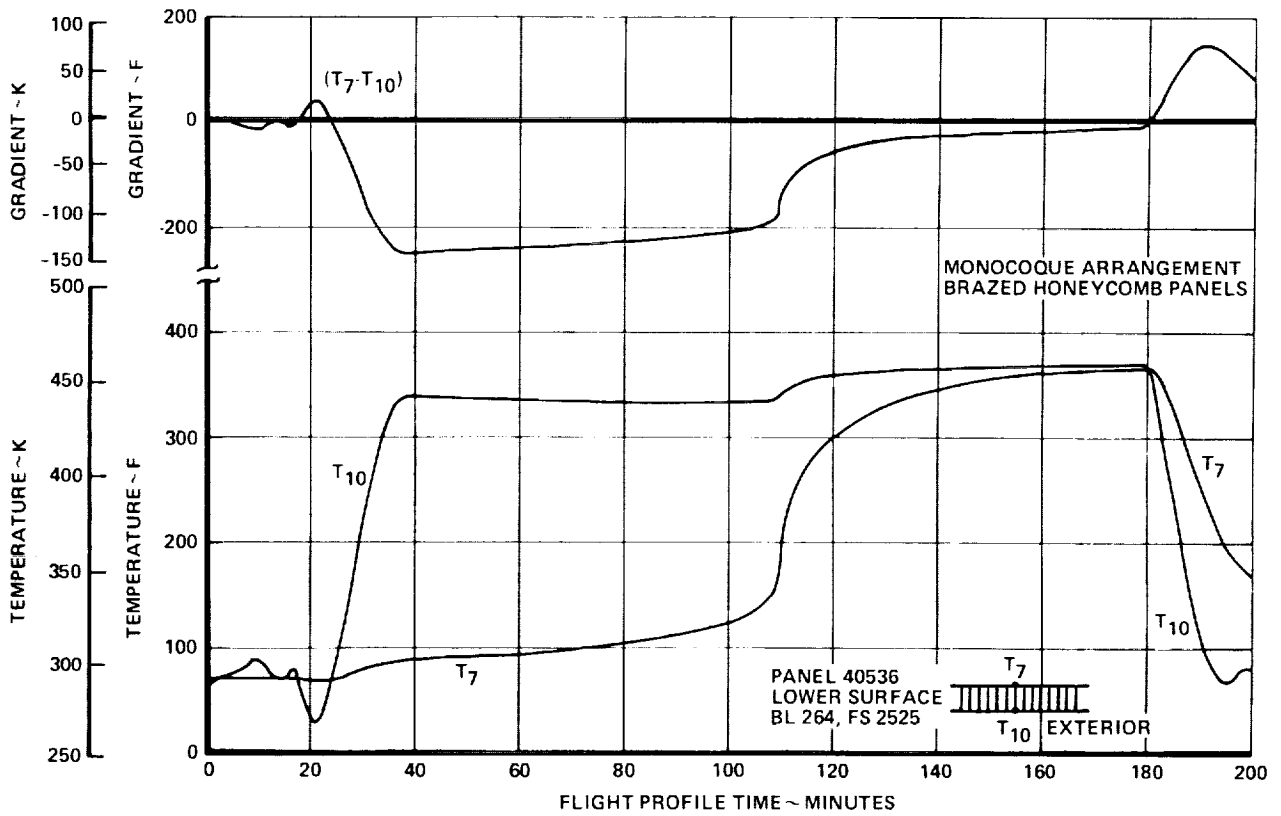


Figure 6-51. Monocoque Wing Panel Temperature Histories - 40536 Lower Surface

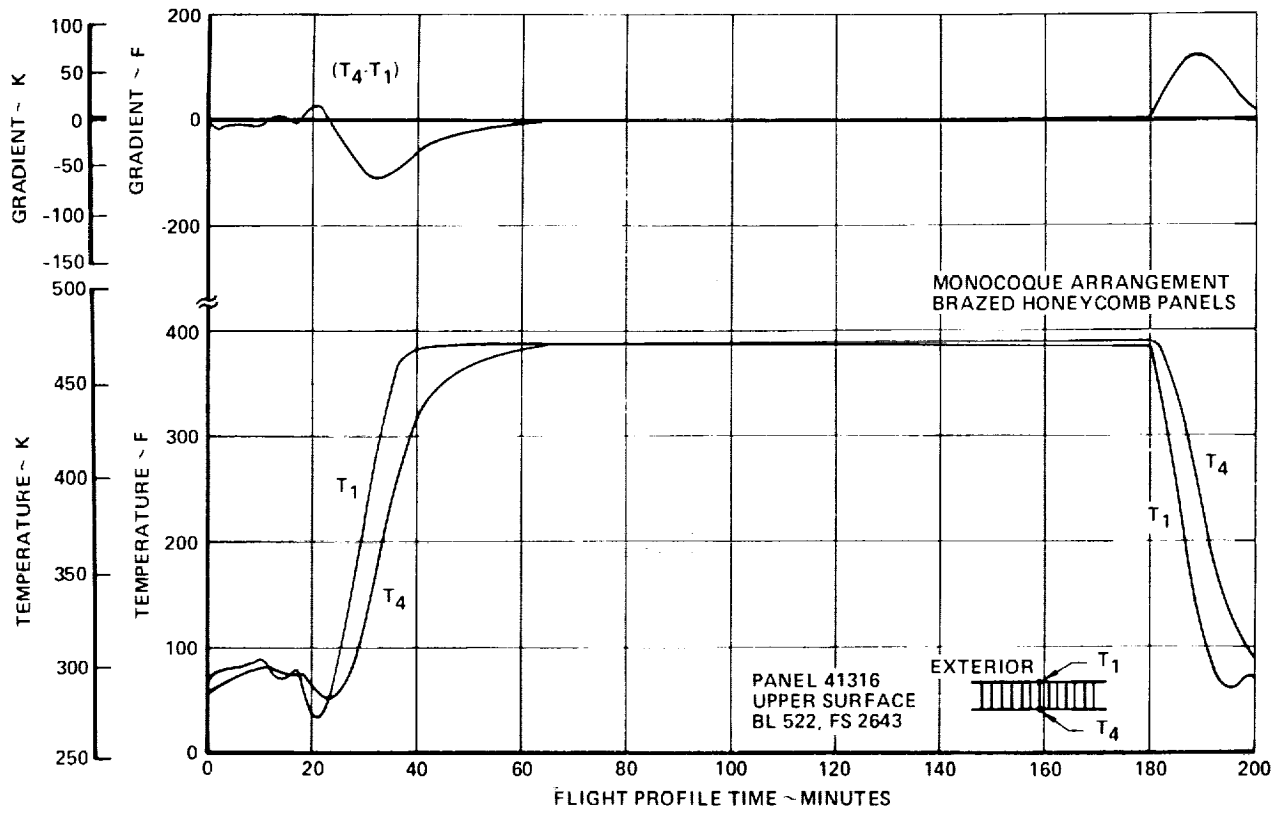


Figure 6-52. Monocoque Wing Panel Temperature Histories - 41316 Upper Surface

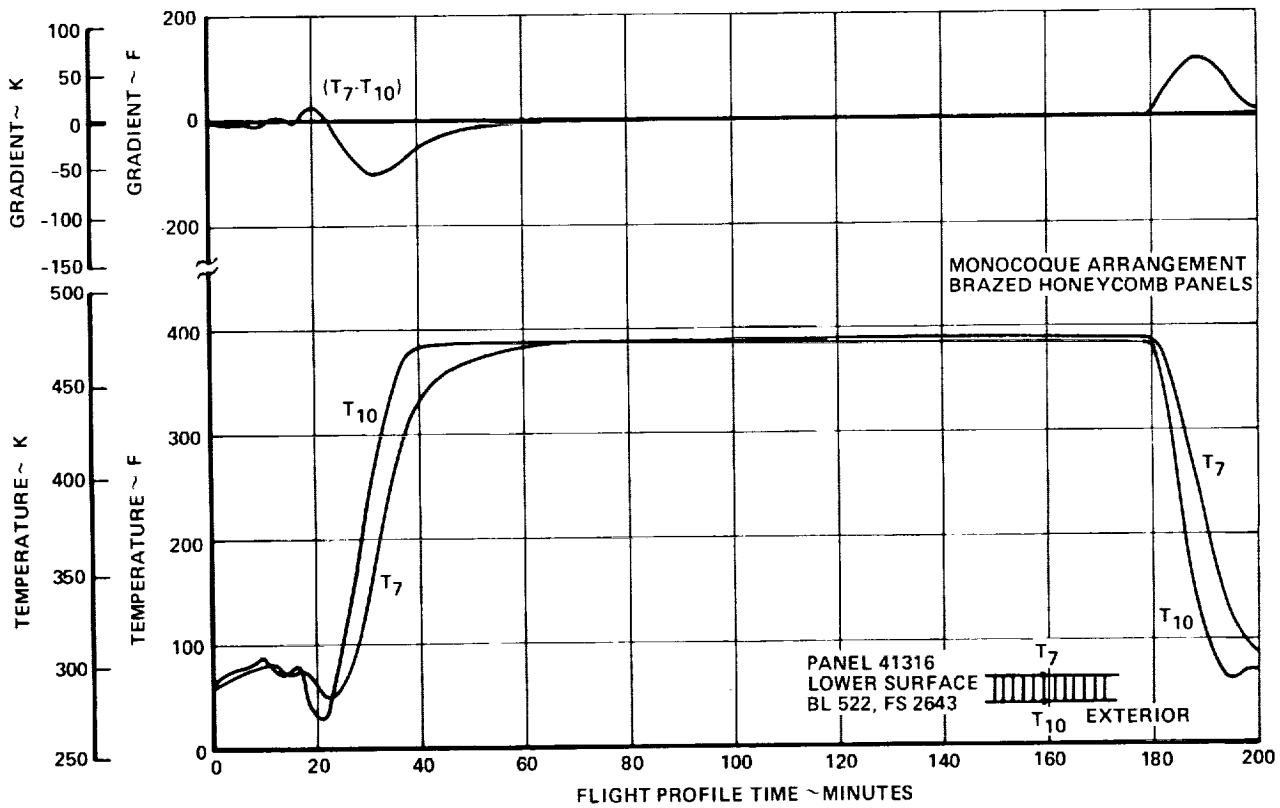


Figure 6-53. Monocoque Wing Panel Temperature Histories - 41316 Lower Surface

## Composite-Reinforced Wing Panels

Figures 6-54 through 6-59 present temperature histories for upper and lower wing panels at three point design regions. The panels are (chordwise) hat-stiffened with boron-polyimide composite reinforcement bonded to the crown (most interior face) of the hat section. Two panel sets are in fuel tanks (40322, 40536); the third is in a dry bay (41316). The Task I airplane configuration is assumed.

Temperature histories are presented for the outer skin above the hat stiffener, for the composite-reinforced face of the hat stiffener, and for the difference between them. Peak panel gradients for this design concept are greater than for the metallic chordwise concept and for the spanwise hat-stiffened concept, principally because of the greater mass concentration at the hat crown and the correspondingly slower response to a changing thermal environment. These results, plus temperature histories at three other point design regions not shown, are used to define further the material gage and dimensional requirements for composite-reinforced chordwise-stiffened wing panels.

## Fuselage Panels and Frames

Temperature histories were developed for fuselage skin panels and circumferential frames using the network analysis method described earlier and the Task I baseline configuration. Results are presented in Tables 6-4 and 6-5 for 10 fuselage locations at four flight conditions: Mach 1.2 climb, start of cruise, mid-cruise, and Mach 1.2 descent. Table 6-4 shows mass-averaged temperatures for skin panels and temperature differentials between outer skin and stiffener crown. Table 6-5 shows mass-averaged frame temperatures and differentials between outer and inner flanges of the frame.

Results of this analysis are used to define further the material gage and dimensional requirements for the fuselage structural concept. In addition, since changes to fuselage structure were not thermally significant during

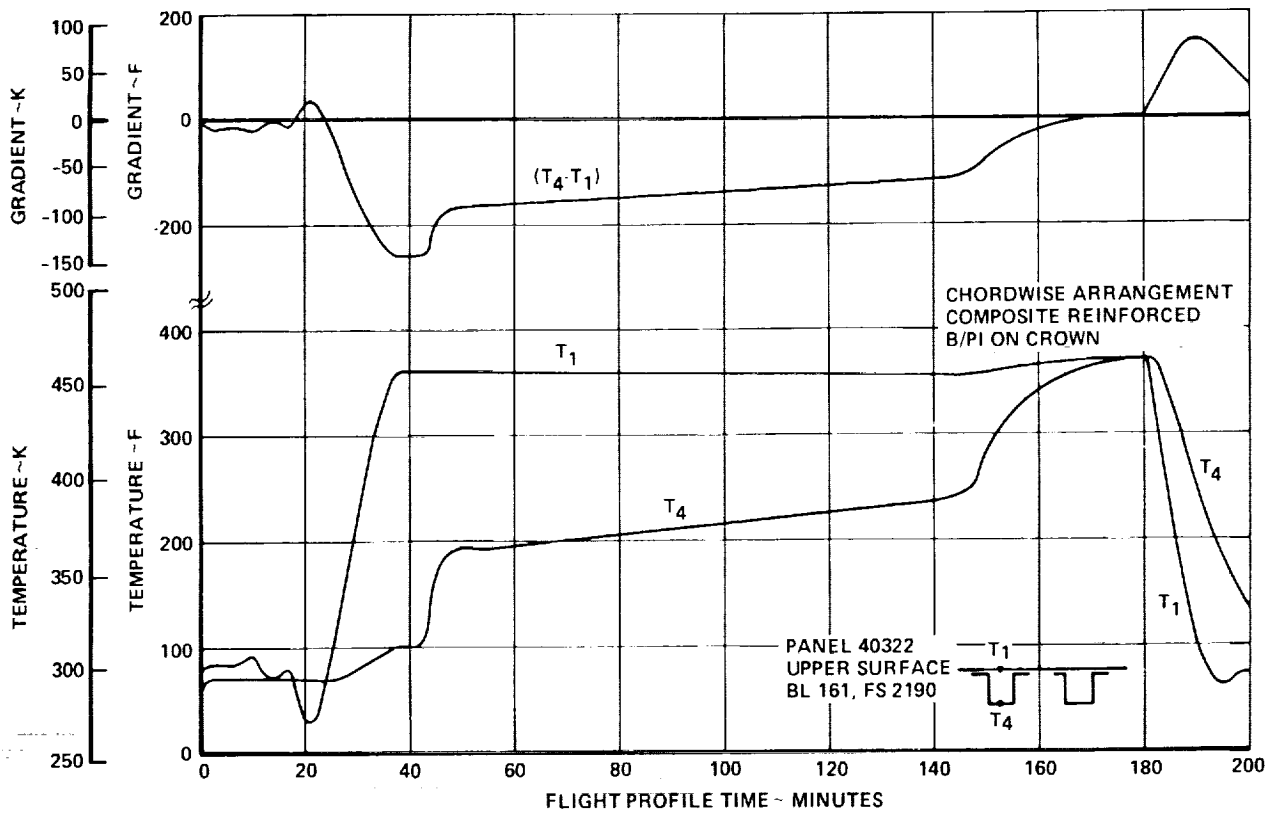


Figure 6-54. Composite Reinforced Wing Panel Temperature Histories - 40322 Upper Surface

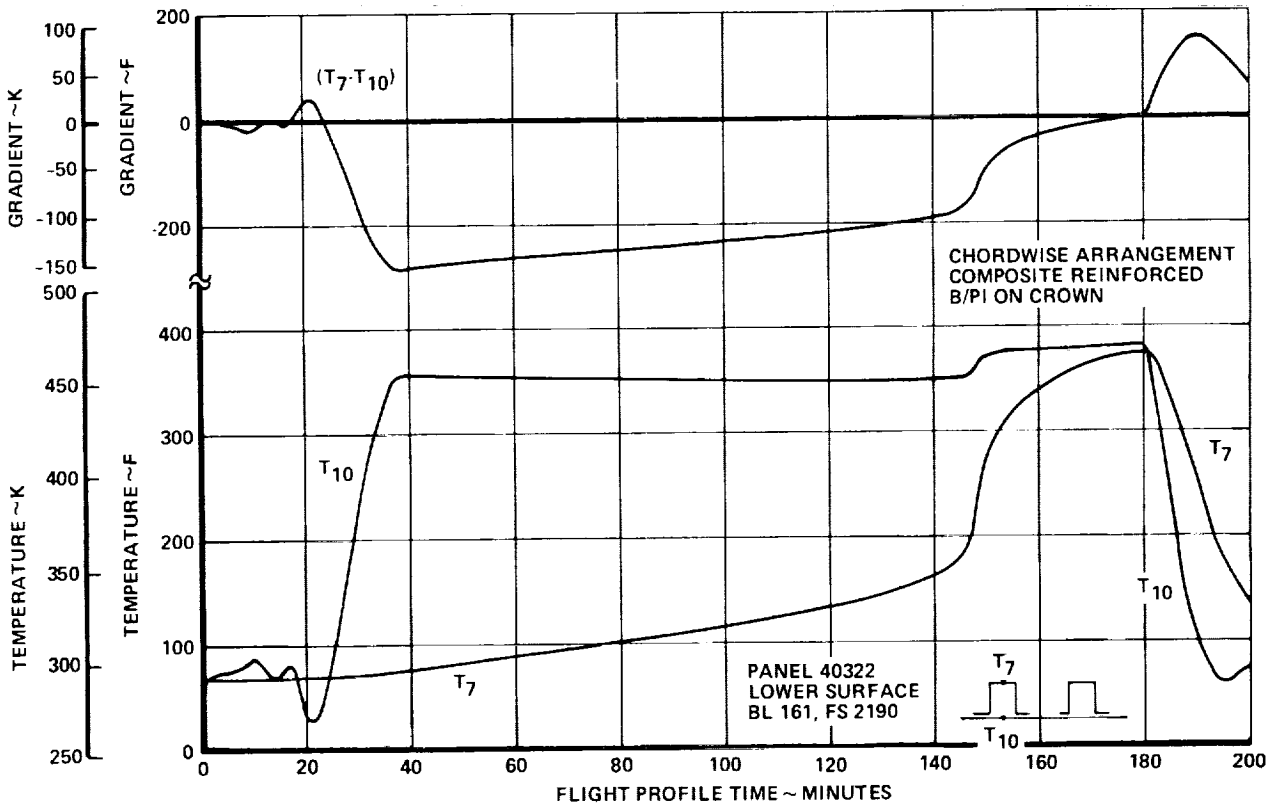


Figure 6-55. Composite Reinforced Wing Panel Temperature Histories - 40322 Lower Surface

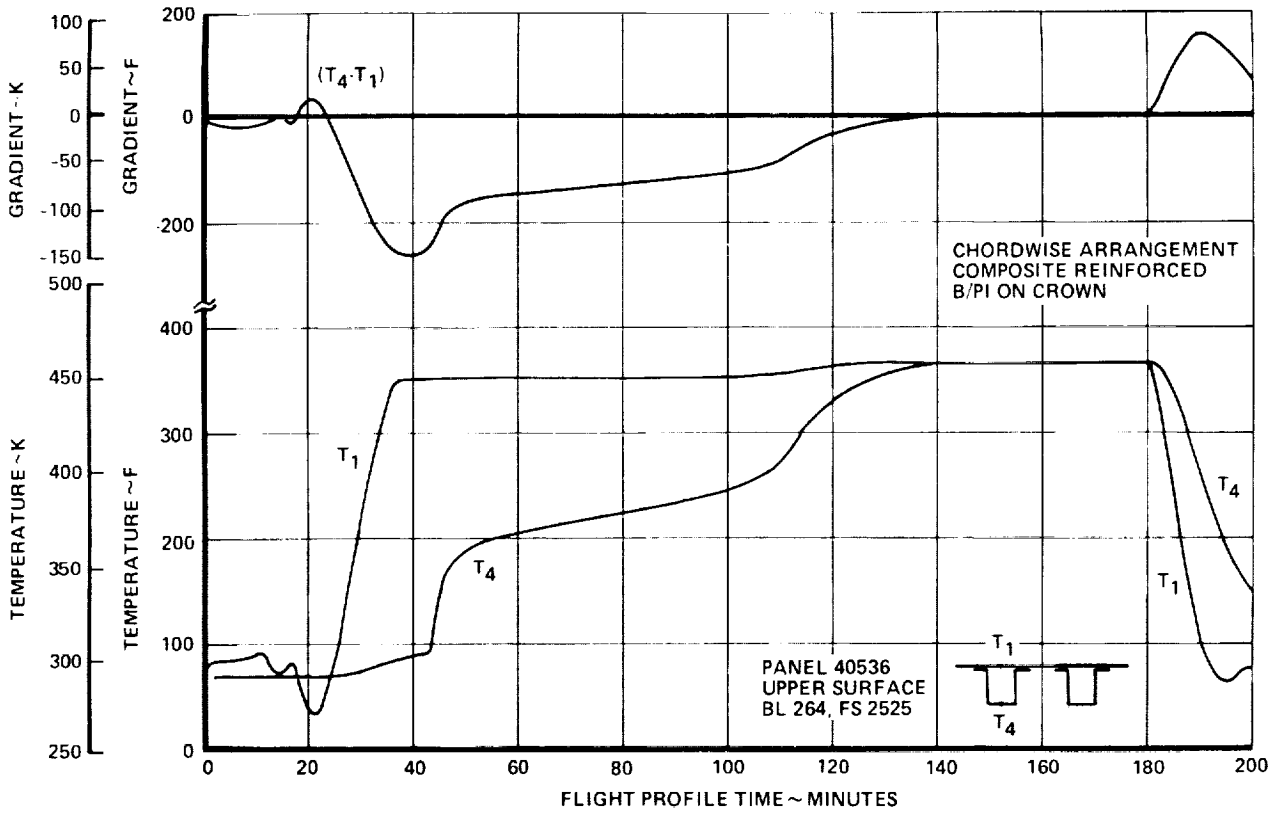


Figure 56. Composite Reinforced Wing Panel Temperature Histories - 40536 Upper Surface

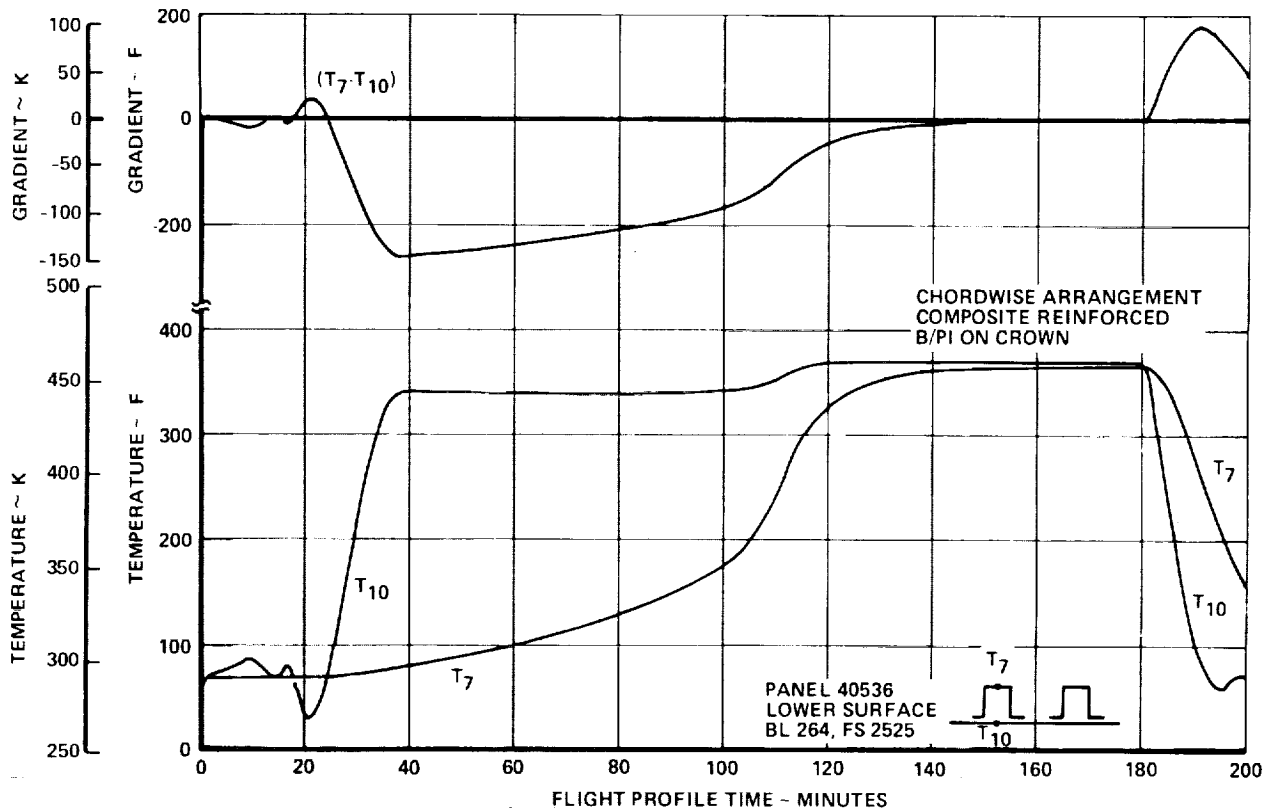


Figure 6-57. Composite Reinforced Wing Panel Temperature Histories - 40536 Lower Surface



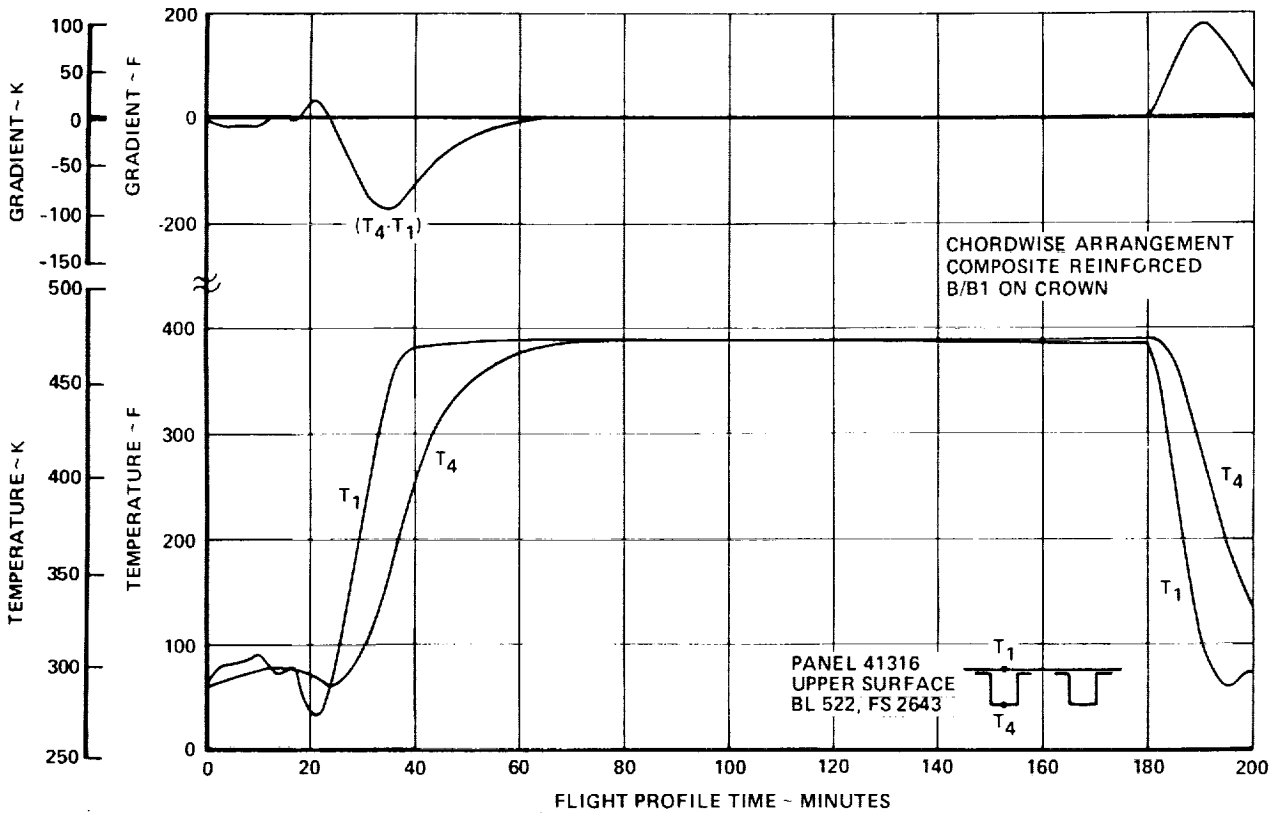


Figure 6-58. Composite Reinforced Wing Panel Temperature Histories - 41316 Upper Surface

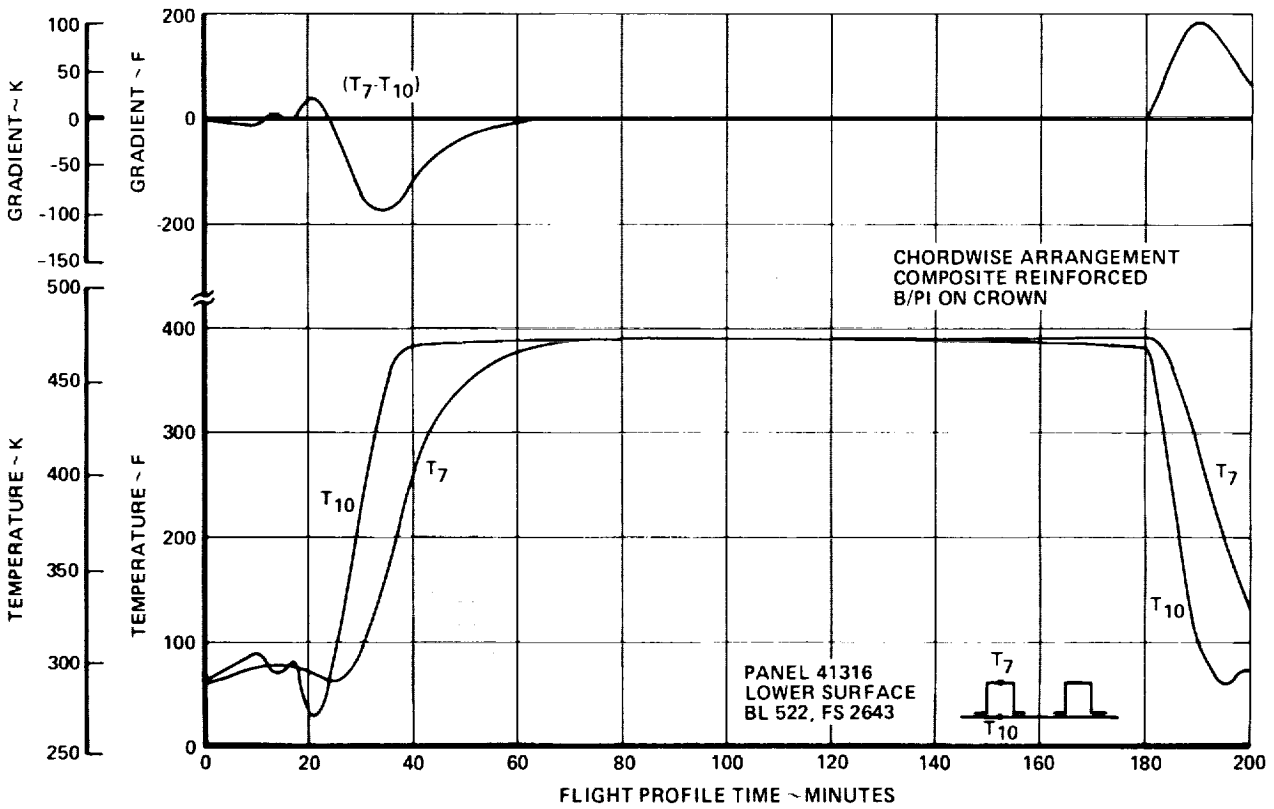


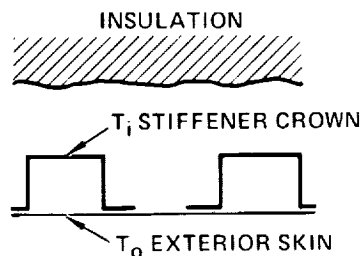
Figure 6-59. Composite Reinforced Wing Panel Temperature Histories - 41316 Lower Surface

TABLE 6-4. TEMPERATURES AND GRADIENTS FOR FUSELAGE SKIN PANELS - TASK I

NOTES:

1. BASED ON HOT DAY (STD+8K)  
4200 n. mi FLIGHT PROFILE.
2. HAT-STIFFENED PANELS,  
EXCEPT ZEE-STIFFENED  
AT FS 750.
3. 'TOP', 'BOTTOM' AT  $\phi$ ;  
'SIDE' AT 90° OR ABOVE WING.

PANEL SCHEMATIC



TEMPERATURES IN F

LOCATION	FLIGHT CONDITION							
	MACH 1.2 CLIMB		START OF CRUISE		MID TO END OF CRUISE		MACH 1.2 DESCENT	
	$T_i - T_o$	$T_{AVG}$	$T_i - T_o$	$T_{AVG}$	$T_i - T_o$	$T_{AVG}$	$T_i - T_o$	$T_{AVG}$
<u>TOP</u>								
FS 750	+ 9	55	-105	342	-11	380	+111	114
2000	+23	53	-175	295	-11	374	+171	144
2500	+24	54	-186	281	-11	372	+181	156
3000	+23	53	-174	292	-11	371	+170	145
<u>SIDE</u>								
FS 750	+12	49	-106	332	-11	369	+109	108
2000	+21	50	-157	324	-11	394	+156	129
2500	+22	50	-171	311	-11	393	+170	139
3000	+23	47	-147	301	-11	358	+142	122
<u>BOTTOM</u>								
FS 750	+12	50	-106	333	-11	370	+109	109
3000	+28	47	-177	278	-10	360	+171	141

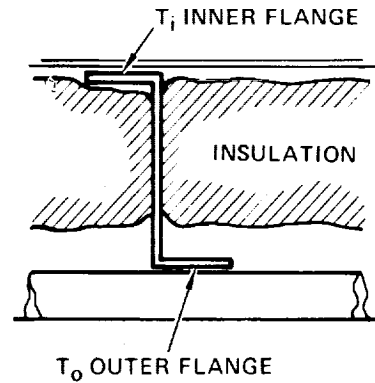
TEMPERATURES IN K

LOCATION	FLIGHT CONDITION							
	MACH 1.2 CLIMB		START OF CRUISE		MID TO END OF CRUISE		MACH 1.2 DESCENT	
	$T_i - T_o$	$T_{AVG}$	$T_i - T_o$	$T_{AVG}$	$T_i - T_o$	$T_{AVG}$	$T_i - T_o$	$T_{AVG}$
<u>TOP</u>								
FS 750	+6	296	-74	336	-103	409	-31	368
2000	+3	296	-41	319	- 89	409	-42	385
2500	+3	296	-35	316	- 82	408	-40	390
3000	+3	296	-41	319	- 89	408	-42	384
<u>SIDE</u>								
FS 750	+8	295	-70	333	- 99	405	-29	364
2000	+4	296	-50	323	- 95	417	-37	388
2500	+4	296	-42	319	- 88	417	-36	393
3000	+5	295	-44	319	- 84	403	-34	376
<u>BOTTOM</u>								
FS 750	+7	295	-70	333	-100	405	-29	364
3000	+4	296	-35	315	- 86	403	-42	381

TABLE 6-5. TEMPERATURES AND GRADIENTS FOR FUSELAGE FRAMES - TASK I

NOTES:

1. BASED ON HOT DAY (STD + 8K)  
4200 n mi FLIGHT PROFILE
2. 'TOP', 'BOTTOM' AT  $\phi$ ;  
'SIDE' AT 90° OR ABOVE WING
3. DATA AT FS 3000 (AFT OF  
PRESSURE BULKHEAD) ASSUMED  
INSULATION—MAY NOT BE VALID



TEMPERATURES IN F

LOCATION	FLIGHT CONDITION							
	MACH 1.2 CLIMB		START OF CRUISE		MID TO END OF CRUISE		MACH 1.2 DESCENT	
	$T_i - T_o$	$T_{AVG}$	$T_i - T_o$	$T_{AVG}$	$T_i - T_o$	$T_{AVG}$	$T_i - T_o$	$T_{AVG}$
<u>TOP</u>								
FS 750	+11	73	-133	145	-186	277	-56	202
2000	+ 6	74	- 74	115	-161	276	-76	233
2500	+ 5	74	- 63	109	-148	274	-72	242
3000	+ 6	74	- 73	114	-160	274	-76	232
<u>SIDE</u>								
FS 750	+14	71	-126	140	-179	269	-53	196
2000	+ 8	73	- 90	121	-171	291	-66	238
2500	+ 7	73	- 76	114	-158	291	-64	248
3000	+ 9	72	- 79	115	-152	266	-61	217
<u>BOTTOM</u>								
FS 750	+13	72	-126	140	-180	270	-53	196
3000	+ 8	73	- 63	108	-154	265	-76	226

TEMPERATURES IN K

LOCATION	FLIGHT CONDITION							
	MACH 1.2 CLIMB		START OF CRUISE		MID TO END OF CRUISE		MACH 1.2 DESCENT	
	$T_i - T_o$	$T_{AVG}$	$T_i - T_o$	$T_{AVG}$	$T_i - T_o$	$T_{AVG}$	$T_i - T_o$	$T_{AVG}$
<u>TOP</u>								
FS 750	+ 5	286	- 58	445	-6	466	+ 62	319
2000	+13	285	- 97	419	-6	463	+ 95	335
2500	+13	285	-103	411	-6	462	+101	342
3000	+13	285	- 97	418	-6	461	+ 94	336
<u>SIDE</u>								
FS 750	+ 7	283	- 59	440	-6	460	+ 61	315
FS 2000	+12	283	- 87	435	-6	474	+ 87	327
2500	+12	283	- 95	428	-6	474	+ 94	333
3000	+13	281	- 82	423	-6	454	+ 79	323
<u>BOTTOM</u>								
FS 750	+ 7	283	- 59	440	-6	461	+ 61	316
3000	+16	281	- 98	410	-6	455	+ 95	334

optimization to the Task II configuration, these temperatures were used directly for input to the three-dimensional finite element model and for composition of the Mach 2.62 cruise isotherm map.

### Fuel Thermal Analysis

The design of fuel storage and thermal protection systems for a supersonic cruise aircraft must reflect consideration of the following objectives:

- Maintenance of heat sink capability (for air conditioning, hydraulic cooling)
- Minimization of fuel vaporization (boiloff)
- Retardation of gum and residue formation during cruise heating of residual fuel.
- Inhibition of thermochemical reaction of fuel vapor in hot tanks
- Maintenance of tank sealant integrity

Design concepts for the Arrow-Wing study accounted for the above by utilizing fuel system concepts developed and tested for the L-2000-7 supersonic transport proposal and for the F-12 series supersonic cruise aircraft.

Fuel heat sink capability is roughly determined by the difference between fuel temperature limit at the engine and bulk fuel temperature in the feed tanks. This capability is optimized for the Arrow-Wing study by using fuel placement and scheduling similar to the L-2000-7:

- All fuel feed tanks are located in the fuselage, protected from aerodynamic heating from above by the passenger area and from below by a fuselage-wing fairing which acts as a heat shield.
- Fuel from the wing tanks is pumped into the feed tanks for mixing with the cooler fuel before subsequent use.

- The shallowest (outboard) wing tanks are used first well before start of cruise, to minimize fuel heating where surface area is high compared to fuel volume.

For the L-2000-7 system, satisfactory cooling capacity was maintainable even under severe operating conditions and with a 317 K (110F) fuel supply temperature. This was accomplished without insulating the tanks or providing active cooling. Additional studies also showed a possible 30 percent reduction in fuel heat sink requirements (hence a higher feed tank temperature limit) through use of advanced environmental control system components.

Bulk fuel temperature histories for the Arrow-Wing study wing tanks (Task II configuration) are shown in Figure 6-60. Temperatures are shown for each sectioned tank from start at 294K (70F) until the tank fuel level has dropped to two percent of the original value (assumed useable limit). This fuel is pumped to the cool fuselage tanks before subsequent use. The wing tank temperatures are significantly below boiling temperature (Figure 6-4) and will inhibit fuel evaporation while fuel is being drawn from each tank. Under extreme conditions (overspeed), spot areas in the tank may become hot enough to produce local nucleate boiling, but experience with L-2000-7 development testing (Ref. 18) showed no fuel degradation upon exposure to hot structure (475-500K, or 395-440F) while bulk fuel temperature remains low.

Once all useable fuel has been drawn from a wing tank during flight, the residual fuel and vapor in the tank will heat up to near external skin temperature. At the maximum exterior temperature of 475K (395F) (for Mach 2.62, hot day cruise), most of the residual fuel will have vaporized. The primary concern then becomes protection of the fuel tanks from residue buildup, vapor reactions, and sealant deterioration at the steady-state temperature of the empty tank. Vapor reaction refers to the 'mild reaction' condition characterized by a slow, glowing oxidation exhibiting slight pressure (1700 Pa, 0.25 psi) and temperature (22K, 40F) surges. The condition is possibly self-sustaining and definitely undesirable.

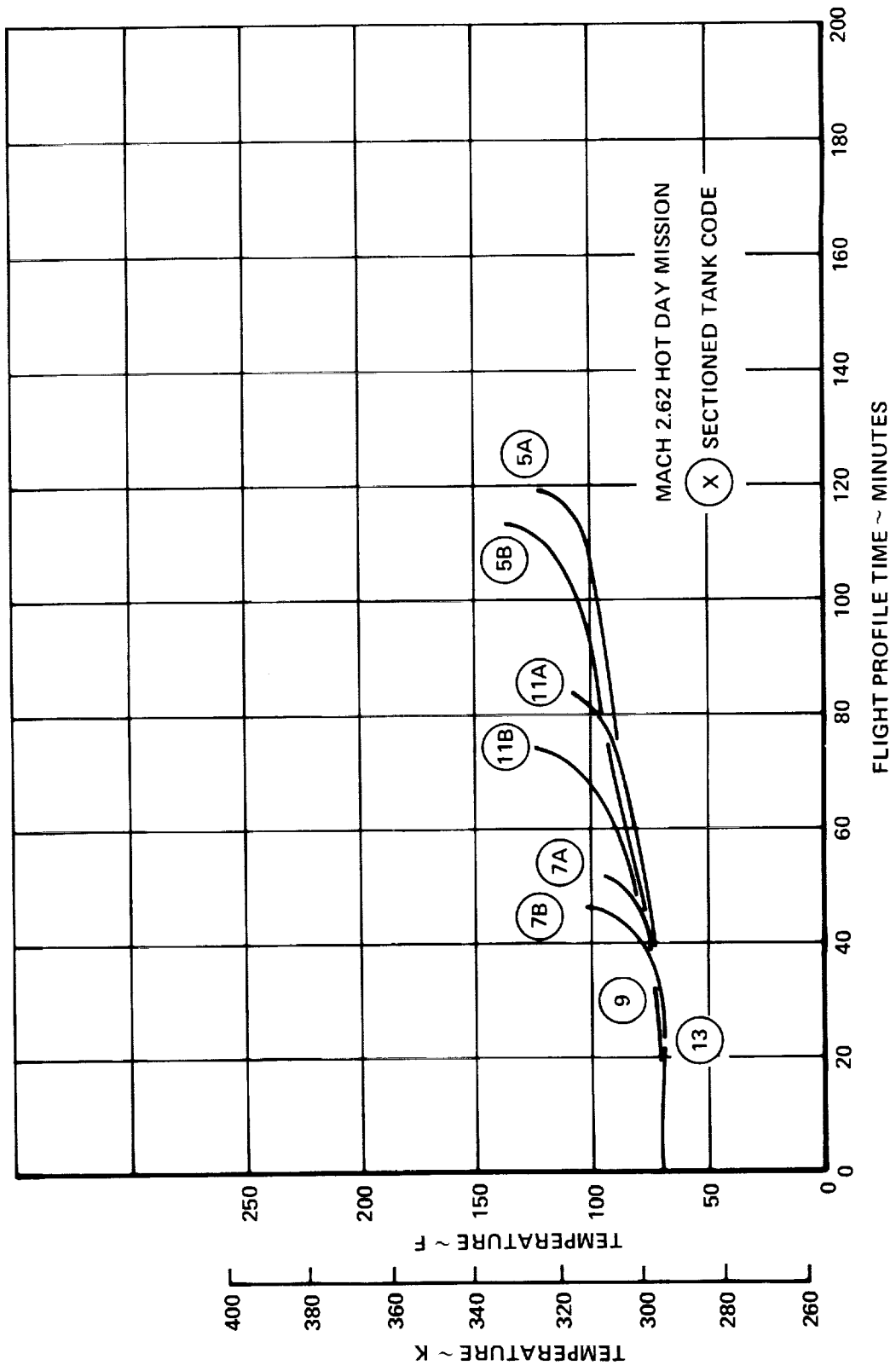


Figure 6-60. Bulk Fuel Temperatures in Wing Tanks - Task II

Tests performed during development of the L-2000-7 airplane design examined the effects of high temperatures on tanks containing residual aviation fuel. Residue buildup during 500 simulated flight cycles at temperatures up to 500K (440F) was deemed unobjectionable and filterable when the tanks were pressurized with air, and practically non-existent when nitrogen gas pressurization was used. Vapor reactions were not detected for air pressurization (up to 30 percent oxygen) at temperatures of 505K (450F), and for nitrogen-purging (under 5 percent oxygen) at much higher temperatures. The results of these tests plus observation of F-12 series aircraft fuel tanks (nitrogen-purged) subject to higher temperatures indicate that a nitrogen purge/pressurization system satisfying requirements for fuel tank inerting will provide effective inhibition of vapor reaction and residue formation for the Arrow-Wing design.

Additional L-2000-7 tests and experience with F-12 series aircraft indicate that current fuel tank sealants retain effectiveness up to temperatures of at least 500K (440F). In eliminating the requirement for fuel tank insulation, the Arrow-Wing fuel system design assures easy access and maintenance when tank sealants must be repaired or replaced. The problem of fuel absorption in porous insulations in the event of slight seepage is also eliminated.

#### Honeycomb Braze Study

The analysis of brazed honeycomb panels described earlier assumed all braze material remains in contact with the panel face sheets and does not flow into the core. This assumption results in the lowest value for effective panel conductance and yields the most conservative estimates for maximum thermal gradient across the panel.

Examination of currently manufactured brazed panels indicates, however, that some amount of braze material-flow into the core is unavoidable. To assess the effects of braze flow, an analytical method was devised to examine the variation in panel thermal gradient with the amount of braze material flow into the core. The analytical method utilized calculation of an overall

conductance between the panel face sheets as a function of the fraction of core surface covered by the flowing braze material.

The factors contributing to overall conductance include:

- conduction through the core material
- radiation interchange among all walls of the core cell enclosure resulting in net radiative transfer between face sheets
- conduction into the core through the 'heat short' of highly conductive braze material.

The fraction of core coverage by braze material was varied from zero to one-hundred percent. Braze thickness was assumed to spread uniformly over covered surfaces.

Figure 6-61 shows the effect on maximum panel gradient of varying the fraction of core coverage. Maximum temperature differential is shown for fuel tank and dry bay panels. The shapes of the curves are fairly consistent for wet or dry, thick or thin panels. As the braze flow from both face sheets approaches complete contact (100 percent coverage), the high conductivity of the aluminum braze material becomes the dominant heat flow mechanism and reduces the maximum thermal gradient significantly.

A braze flow fraction of 0.75 was selected for further honeycomb panel analyses to yield a conservative value for panel thermal gradient, and a realistic value for effective panel conductance. At 0.75, peak gradients are not reduced drastically from theoretical maximums, and panel conductance values show reasonable agreement with published values for typical honeycomb panels. Also, since no honeycomb panels are located in fuel areas for baseline configuration for Task II and III, it was not necessary to examine the adverse effect on fuel temperatures of highly conductive (full braze flow) panels.



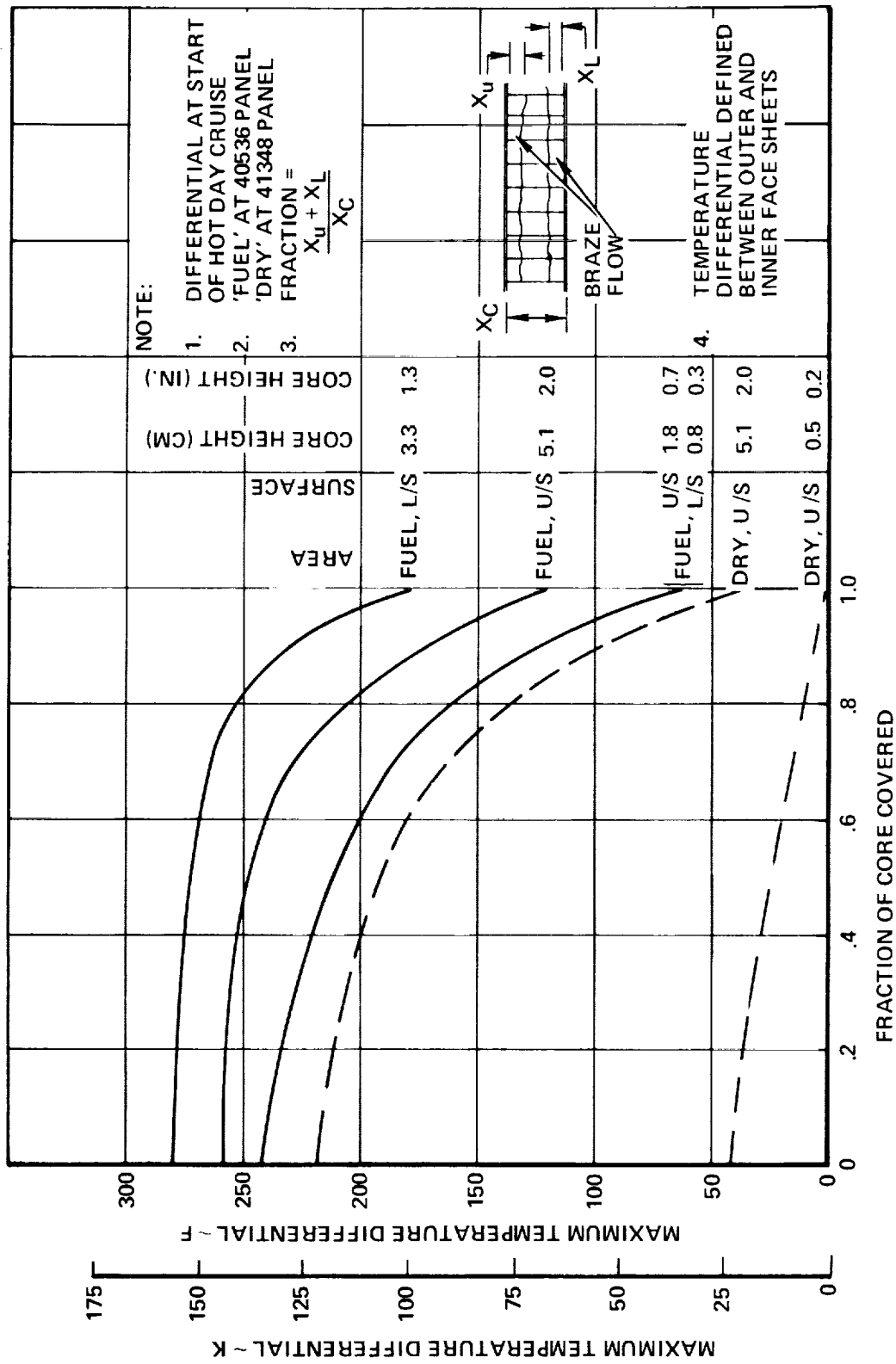


Figure 6-61. Effect of Braze Flow on Honeycomb Panel Temperature Gradient

Figure 6-62 shows the effective conductance calculated for some typical outboard wing panels using a braze flow fraction of 0.75. Conductance is presented as a function of average temperature between inner and outer face sheets. The figure shows the expected trends of inverse proportionality to core thickness and moderate dependence on temperature. The increase in radiative transfer and material conductivity results in about a 50 percent increase in panel effective conductance at cruise temperature (475 K, 395 F) compared to room temperature.

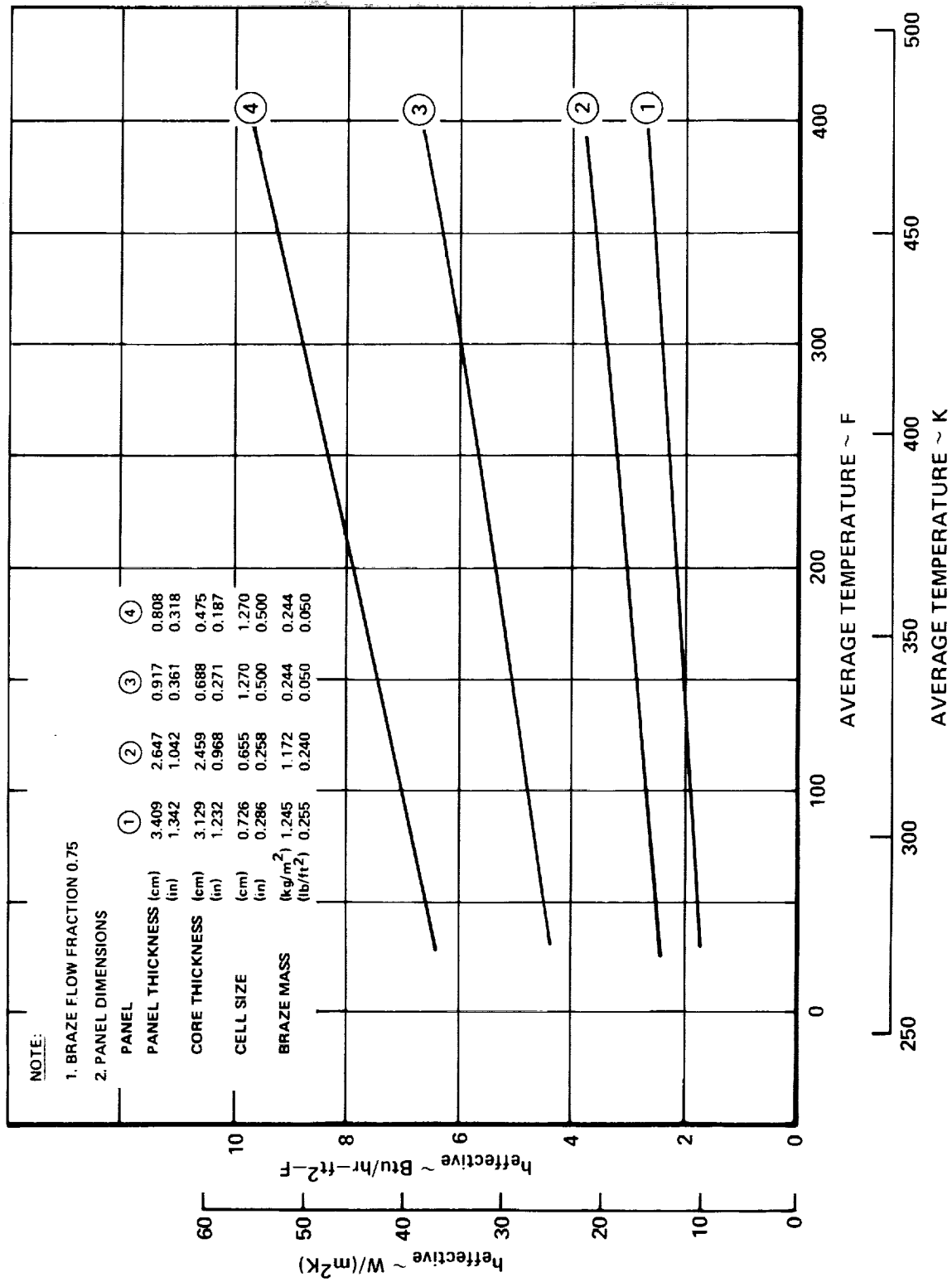


Figure 6-62. Effective Conductance for Honeycomb Panels

## STRUCTURAL TEMPERATURES - TASK II

This section presents temperatures developed for the hybrid structural approach defined by the Task II baseline configuration. The first subsection presents wing structure temperatures for selected point design regions at several structurally important time points in the flight profile. The second subsection presents discussion and selected results from the development of grid point and element temperature sets for the three-dimensional finite element model. The final subsection presents an isotherm map showing the temperature distribution over the entire external surface of the airplane at the middle of cruise.

### Wing Structure Temperatures

Temperature histories were developed for the wing structure at 14 design point regions using wing panels and beam caps defined by the Task II baseline configuration. The flight profile defined for the Task II analysis was assumed.

Table 6-6 presents temperatures for six selected panels at the following five flight conditions:

- Mach 0.90 climb
- Mach 1.25 climb
- Mach 1.25 descent
- Mach 2.7 start of cruise
- Mach 2.7 mid-cruise

Temperatures for the nominal Mach 2.7 conditions are obtained from analysis at the Mach 2.62, hot day (standard +8K) cruise profile. Subscripted temperatures in the table are defined as follows:

- T<sub>1</sub> upper surface panel outer skin
- T<sub>4</sub> upper surface panel inner skin
- T<sub>7</sub> lower surface panel inner skin
- T<sub>10</sub> lower surface panel outer skin

TABLE 6-6. TEMPERATURES AND GRADIENTS FOR WING STRUCTURE - TASK II

POINT DESIGN REGION	UPPER SURFACE PANEL				LOWER SURFACE PANEL				WEB		UPPER CAP		LOWER CAP		FUEL	
	T <sub>1</sub> (F)	T <sub>a</sub> (F)	T <sub>AVG</sub> (F)	Δ T (T <sub>a</sub> - T <sub>1</sub> )	T <sub>7</sub> (F)	T <sub>10</sub> (F)	T <sub>AVG</sub> (F)	Δ T (T <sub>7</sub> - T <sub>10</sub> )	T <sub>WEB</sub> (F)	T <sub>B</sub> (F)	T <sub>R</sub> (F)	T <sub>B</sub> (F)	T <sub>R</sub> (F)	Z <sub>F</sub> (INCH)	T <sub>F</sub> (F)	
<b>MACH 0.9 (CLIMB)</b>																
40322	32	69	47	+ 37	70	29	52	+ 41	70	69	37	70	55	35.30	70	
40236	32	69	47	+ 37	70	29	53	+ 40	70	65	37	70	56	38.60	70	
40536	33	64	45	+ 30	65	29	45	+ 36	68	66	38	70	38	0	-	
41036	35	62	48	+ 27	49	34	41	+ 15	68	70	55	68	50	-	-	
41316	35	62	48	+ 27	49	34	41	+ 15	68	70	70	70	70	-	-	
41348	34	54	44	+ 20	39	31	33	+ 8	67	70	70	70	70	-	-	
<b>MACH 1.25 (CLIMB)</b>																
40322	61	70	63	+ 8	70	58	65	+ 11	70	66	54	70	65	35.30	70	
40236	60	69	62	+ 9	70	56	64	+ 14	70	65	52	70	65	38.60	70	
40536	58	57	57	- 1	56	56	56	0	63	65	51	69	49	0	-	
41036	56	52	54	- 3	41	50	46	- 10	62	67	60	66	55	-	-	
41316	56	52	54	- 3	41	50	46	- 10	61	65	65	65	65	-	-	
41348	57	46	52	- 11	42	51	49	- 9	59	65	65	65	65	-	-	
<b>MACH 1.25 (DESCENT)</b>																
40322	86	260	163	+ 174	261	84	154	+ 177	305	307	103	314	101	0	-	
40236	86	240	153	+ 154	248	84	154	+ 164	292	345	110	348	106	0	-	
40536	88	243	148	+ 155	239	84	150	+ 155	289	338	113	342	106	0	-	
41036	94	214	152	+ 120	141	95	117	+ 46	286	310	150	315	130	-	-	
41316	94	214	152	+ 120	141	95	117	+ 46	276	200	200	165	165	-	-	
41348	91	162	127	+ 72	111	87	92	+ 24	261	175	175	140	140	-	-	
<b>MACH 2.0 (START OF CRUISE)</b>																
40322	362	81	246	- 281	77	367	203	- 290	74	124	329	73	164	35.30	74	
40236	353	83	243	- 270	76	348	185	- 272	73	81	313	72	148	38.60	73	
40536	355	219	298	- 136	225	367	303	- 142	164	90	314	90	332	0	-	
41036	361	265	315	- 96	321	357	340	- 36	173	150	290	140	310	-	-	
41316	361	265	315	- 96	321	357	340	- 36	182	265	265	290	290	-	-	
41348	380	320	350	- 60	349	373	367	- 24	208	300	300	320	320	-	-	
<b>MACH 2.7 (MID-CRUISE)</b>																
40322	356	203	281	- 154	108	357	215	- 249	155	191	344	99	173	15.47	106	
40236	361	302	332	- 59	300	361	333	- 61	276	210	340	155	337	0	-	
40536	367	359	364	- 8	360	370	365	- 10	353	325	360	315	362	0	-	
41036	382	382	382	0	382	382	382	0	380	365	365	395	365	-	-	
41316	386	384	385	- 2	384	385	385	- 1	380	375	375	375	375	-	-	
41348	397	396	396	- 1	388	388	388	- 0	392	385	385	375	375	-	-	

ORIGINAL PAGE IS  
OF POOR QUALITY

TABLE 6-6. TEMPERATURES AND GRADIENTS FOR WING STRUCTURE - TASK II (cont'd)

POINT DESIGN REGION	UPPER SURFACE PANEL			LOWER SURFACE PANEL			WEB	UPPER CAP		LOWER CAP		FUEL	
	T <sub>1</sub> (K)	T <sub>4</sub> (K)	T <sub>AVG</sub> Δ T (K) (T <sub>4</sub> -T <sub>1</sub> )	T <sub>7</sub> (K)	T <sub>10</sub> (K)	T <sub>AVG</sub> Δ T (K) (T <sub>7</sub> -T <sub>10</sub> )		T <sub>WEB</sub> (K)	T <sub>B</sub> (K)	T <sub>R</sub> (K)	T <sub>B</sub> (K)	T <sub>R</sub> (K)	Z <sub>F</sub> (M)
<b>MACH 0.9 (CLIMB)</b>													
40322	273	294	281 + 21	294	271	284 + 23	294	294	276	294	286	0.90	294
40236	273	294	281 + 21	294	271	285 + 22	294	294	276	294	286	0.98	294
40536	274	291	280 + 17	291	271	280 + 20	293	292	276	294	276	0	-
41036	275	290	282 + 15	283	274	278 + 8	293	294	286	293	283	-	-
41316	275	290	282 + 15	283	274	278 + 8	293	294	294	294	294	-	-
41348	274	285	280 + 11	277	273	274 + 4	293	294	294	294	294	-	-
<b>MACH 1.25 (CLIMB)</b>													
40322	289	294	290 + 4	294	288	291 + 6	294	292	285	294	291	0.90	294
40236	289	294	290 + 5	294	286	291 + 8	294	291	284	294	291	0.98	294
40536	288	287	287 - 1	286	286	286 + 0	290	291	284	294	283	0	-
41036	286	284	285 - 2	278	283	281 - 6	290	293	289	292	286	-	-
41316	286	284	285 - 2	278	283	281 - 6	289	291	291	291	291	-	-
41348	287	281	284 - 6	279	284	283 - 5	288	291	291	291	291	-	-
<b>MACH 1.25 (DESCENT)</b>													
40322	303	400	346 + 97	400	302	341 + 98	425	426	313	430	311	0	-
40236	303	389	340 + 86	393	302	341 + 91	418	447	316	449	314	0	-
40536	304	390	338 + 86	388	302	339 + 86	416	443	318	445	314	0	-
41036	308	374	340 + 67	334	308	320 + 26	414	428	339	430	328	-	-
41316	308	374	340 + 67	334	308	320 + 26	409	366	366	347	347	-	-
41348	306	345	326 + 40	317	304	306 + 13	400	353	353	333	333	-	-
<b>MACH 2.7 (START OF CRUISE)</b>													
40322	456	300	392 - 156	298	459	368 - 161	296	324	438	296	346	0.90	296
40236	451	301	390 - 150	298	449	358 - 151	296	300	429	295	338	0.98	296
40536	453	377	421 - 75	380	459	424 - 79	346	305	430	305	440	0	-
41036	456	403	430 - 53	434	454	444 - 20	351	339	416	333	428	-	-
41316	456	403	430 - 53	434	454	444 - 20	356	403	403	416	416	-	-
41348	466	433	450 - 33	449	463	459 - 13	371	422	422	433	433	-	-
<b>MACH 2.7 (MID-CRUISE)</b>													
40322	453	368	411 - 86	315	454	375 - 138	341	361	446	310	351	0.39	314
40236	456	423	440 - 33	422	456	440 - 34	409	372	444	341	443	0	-
40536	459	455	458 - 4	455	461	458 - 6	451	436	455	430	456	0	-
41036	468	468	468 - 0	468	468	468 - 0	466	468	458	453	458	-	-
41316	470	469	469 - 1	469	469	469 - 1	466	464	464	464	464	-	-
41348	476	475	475 - 1	471	471	471 - 0	473	469	469	464	464	-	-

$T_{WEB}$  average for beam webs or trusses  
 $T_B$  average for spar caps  
 $T_R$  average for rib caps  
 $T_F$  fuel temperature

$Z_F$  is the average fuel depth at the panel location.  $T_B$  defines submerged spar cap temperatures for the inboard wing panels, and surface cap temperatures for the outer wing (honeycomb) panels (41316, 41348).

Results of the wing analysis were extrapolated to the entire wing structure at certain flight conditions to provide complete temperature inputs for the finite element structural analysis model. Extrapolations were based on similarity of physical structure, location, and thermal environment. Examples at three flight conditions are shown in Figures 6-63, 6-64, and 6-65 for a vertical cross section through the fuselage and wing in the aft box area. The flight conditions are start of cruise, mid-cruise, and Mach 1.25 descent, respectively. Average temperatures are shown for panels, spar caps, rib caps, webs, fuselage panels and frames, and fuel.

#### Finite Element Model (3-D NASTRAN)

Grid point and element temperatures were developed for inclusion in the three-dimensional finite element structural analysis. Temperatures for the wing, fuselage, control surfaces, and engine support structure were provided. Wing temperatures were based on the extrapolation of point design region analyses described above. Fuselage temperatures were obtained directly from the Task I analysis and were extrapolated from the 10 basic locations. Vertical and horizontal control surface temperatures were obtained through similarity with wing structure by matching leading edge distance and material gage data. Engine support structure temperatures were adopted from L-2000-7 data.

Input for the finite element model includes temperature definition at model grid points and, optionally, on model elements. Grid point temperature supposedly represents an average value for all structural elements connected at that point. Temperature dependent properties of a structural element can then be

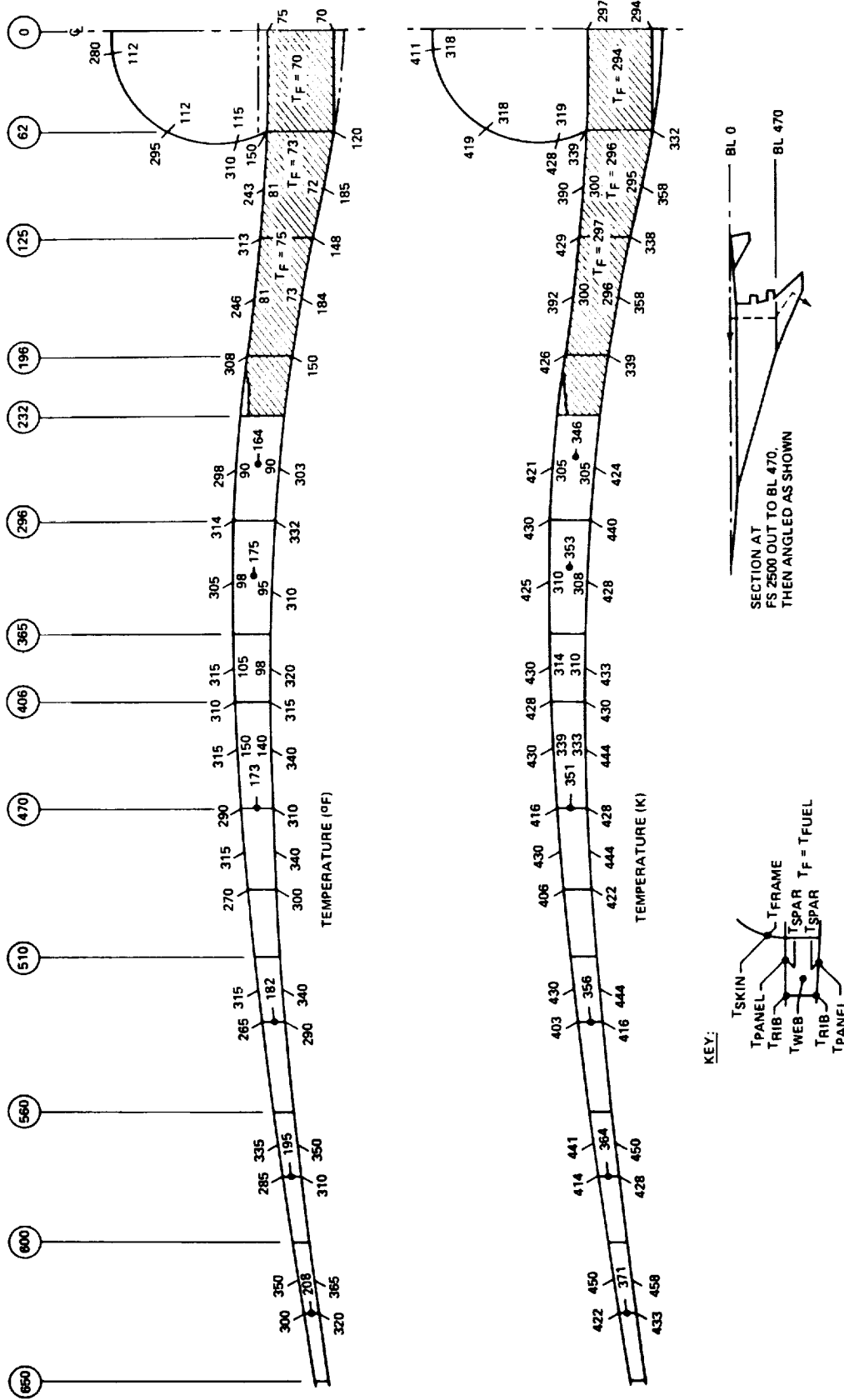


Figure 6-63. Temperatures at Wing Cross Section - Mach 2.62 Start-of-Cruise

ORIGINAL PAGE IS  
OF POOR QUALITY



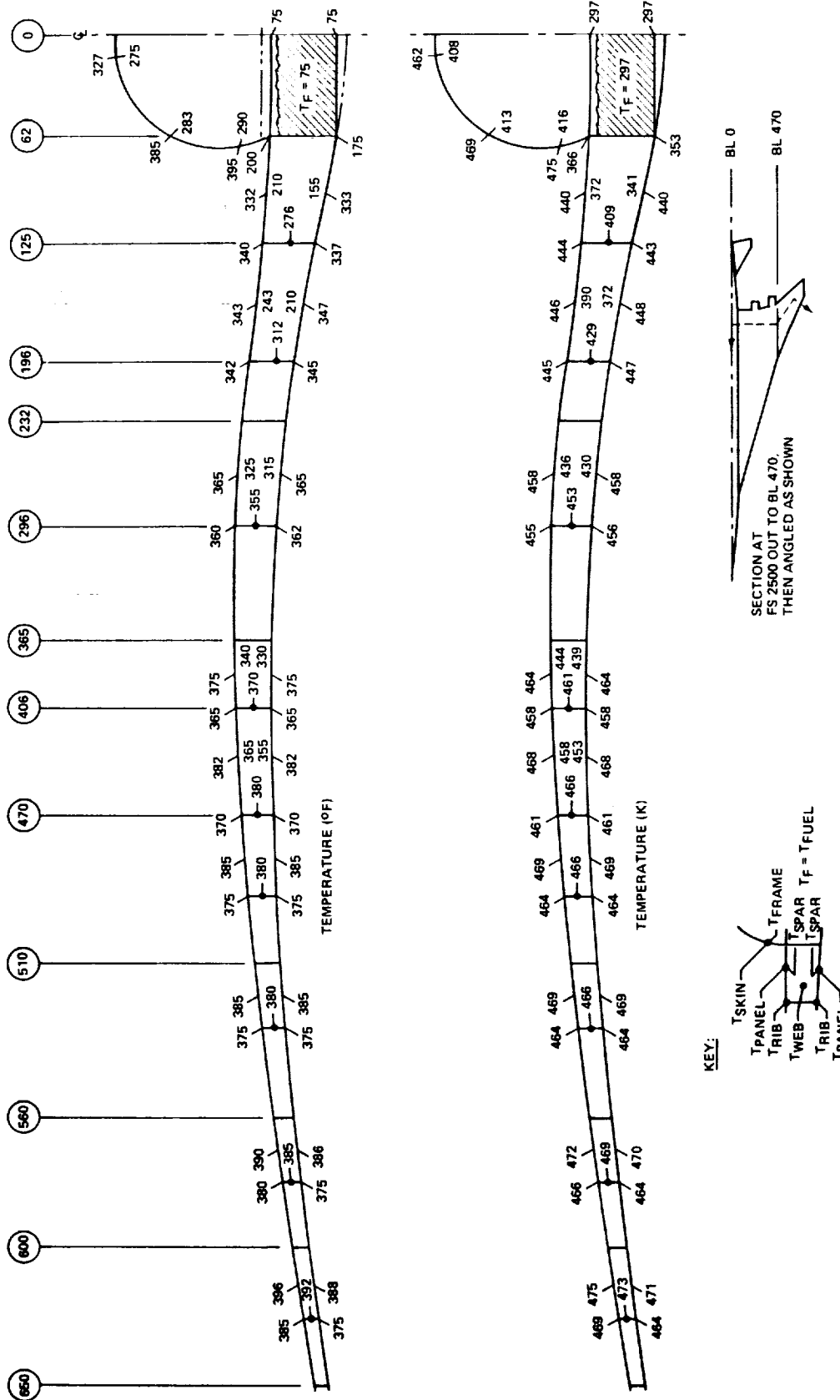


Figure 6-64. Temperatures at Wing Cross Section - Mach 2.62 Mid-Cruise

ORIGINAL PAGE IS  
OF POOR QUALITY

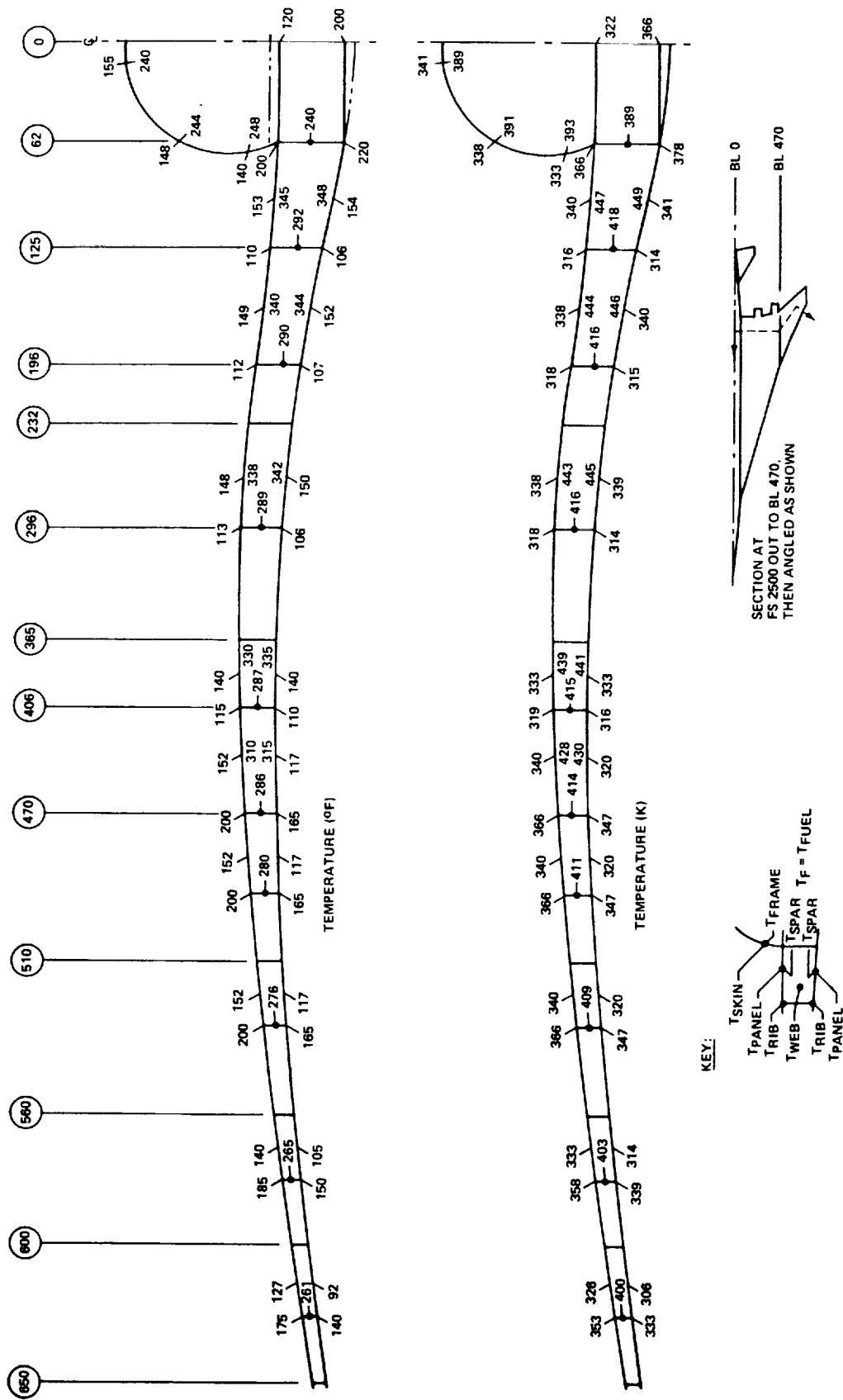


Figure 6-65. Temperatures at Wing Cross Section - Mach 1.25 Descent

estimated by averaging temperatures of its connected grid points. For the Arrow Wing, however, elements of significantly different thermal environment, and hence temperature, are connected at single grid points, so that an averaged grid point temperature is not valid for either element. Examples include the intersection of frames and skin panels on the fuselage, and the intersection of submerged spar caps and surface rib caps in the wing. The problem was resolved by reserving grid point temperatures for primary load-bearing structure, then separately specifying element temperatures where corresponding grid point temperatures are not valid. Thus, wing grid point temperatures reflect values derived for the spar beam caps, and temperatures for elements representing surface rib caps and panels are specified separately. For the fuselage, grid point temperatures represent skin panel temperatures so that the effects of longitudinal thermal expansion can be included directly; temperatures for elements representing fuselage frames are specified separately.

Figures 6-66, 6-67, and 6-68 present wing grid point and element temperature layouts for start-of-cruise, mid-cruise, and Mach 1.25 descent flight conditions, respectively. Not shown are similar temperature layouts for the fuselage, vertical wing, and engine support structure. The wing drawings show upper and lower surface grid point temperatures, and also element temperatures where grid point temperature averaging is not valid. Note that in the outboard wing area (honeycomb panels), spar and rib caps see essentially the same thermal environment (surface exposure), so that grid point temperatures are valid for all connected elements.

#### Cruise Isotherms - Mach 2.62 Hot Day

A map of external surface isotherms (lines of constant temperature) for the entire airplane at a Mach 2.62, hot day (standard +8K) cruise condition is presented in Figure 6-69. Temperature lines are given in 5K (9F) increments except where temperatures change radically due to extraneous heat transfer, near engines, and fuel.

I

E

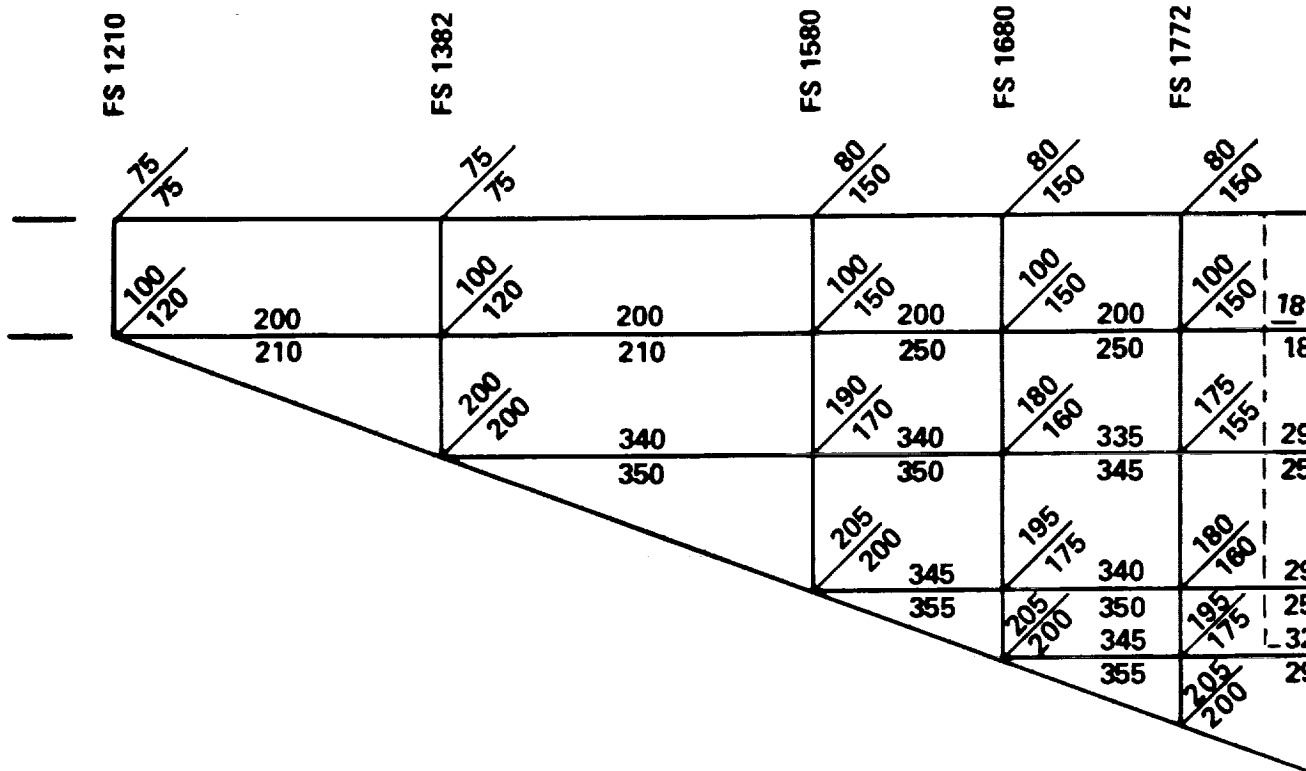
E

Y

W

Y

Y



**NOTES**

1. HOT DAY 4200 N. MILE FLIGHT PROFILE
2. WING STRUCTURE ELEMENT ARRANGEMENT SHOWN
3. GRIDPOINT TEMPERATURES GIVEN AT ELEMENT INTERSECTIONS
4. CIRCLED GRIDPOINT TEMPERATURES TYPICAL FOR REGIONS SHOWN
5. ELEMENT TEMPERATURES GIVEN WHERE INTERPOLATION BETWEEN GRIDPOINT TEMPERATURES IS NOT VALID.
6. TEMPERATURE CODING:

$$\frac{XXX}{YYY} = \frac{\text{UPPER SURFACE (F)}}{\text{LOWER SURFACE (F)}}$$

PRECEDING PAGE BLANK NOT FILMED

FOLDOUT FRAME /









FS 2640

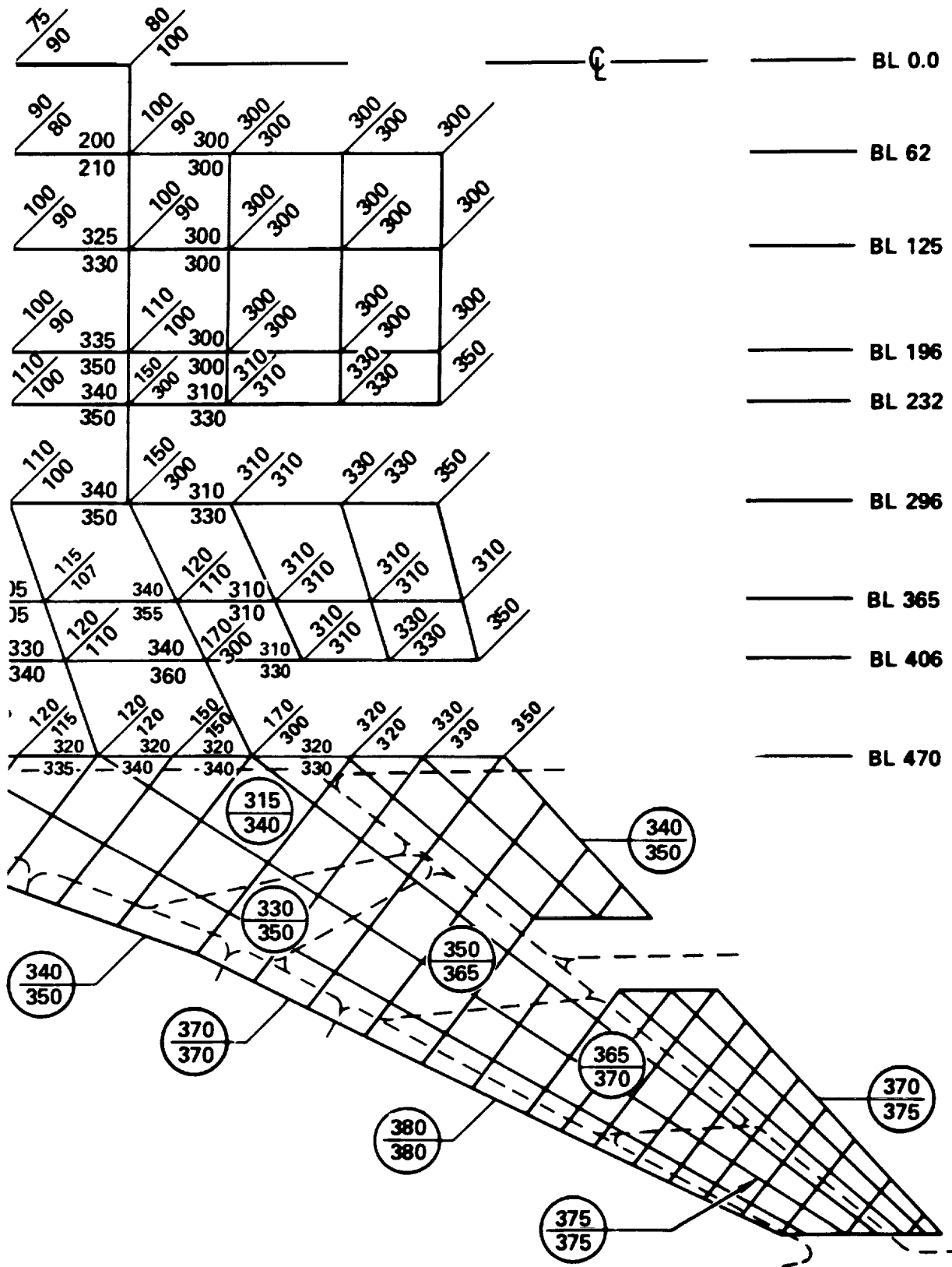
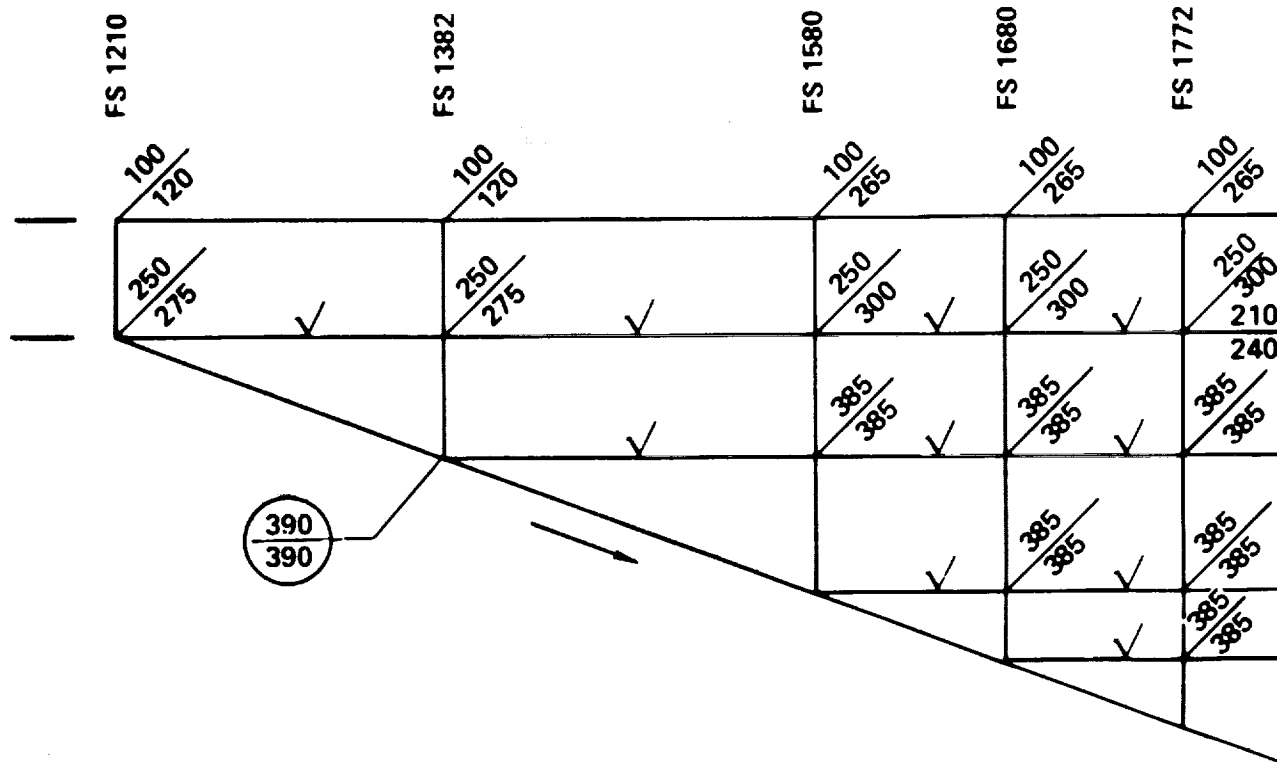


Figure 6-66. Finite Element Model Wing Temperatures - Mach 2.62 Start-of-Cruise





**NOTES**

1. HOT DAY 4200 N. MILE FLIGHT PROFILE
2. WING STRUCTURE ELEMENT ARRANGEMENT SHOWN
3. GRIDPOINT TEMPERATURES GIVEN AT ELEMENT INTERSECTIONS
4. CIRCLED GRIDPOINT TEMPERATURES TYPICAL FOR REGIONS SHOWN
5. ELEMENT TEMPERATURES GIVEN WHERE INTERPOLATION BETWEEN GRIDPOINT TEMPERATURES IS NOT VALID.
6. TEMPERATURE CODING:

$$\frac{XXX}{YYY} = \frac{\text{UPPER SURFACE (F)}}{\text{LOWER SURFACE (F)}}$$

$\checkmark$  = INTERPOLATE GRIDPOINT TEMPERATURES

PRECEDING PAGE BLANK NOT FILMED

FOLDOUT FRAME /







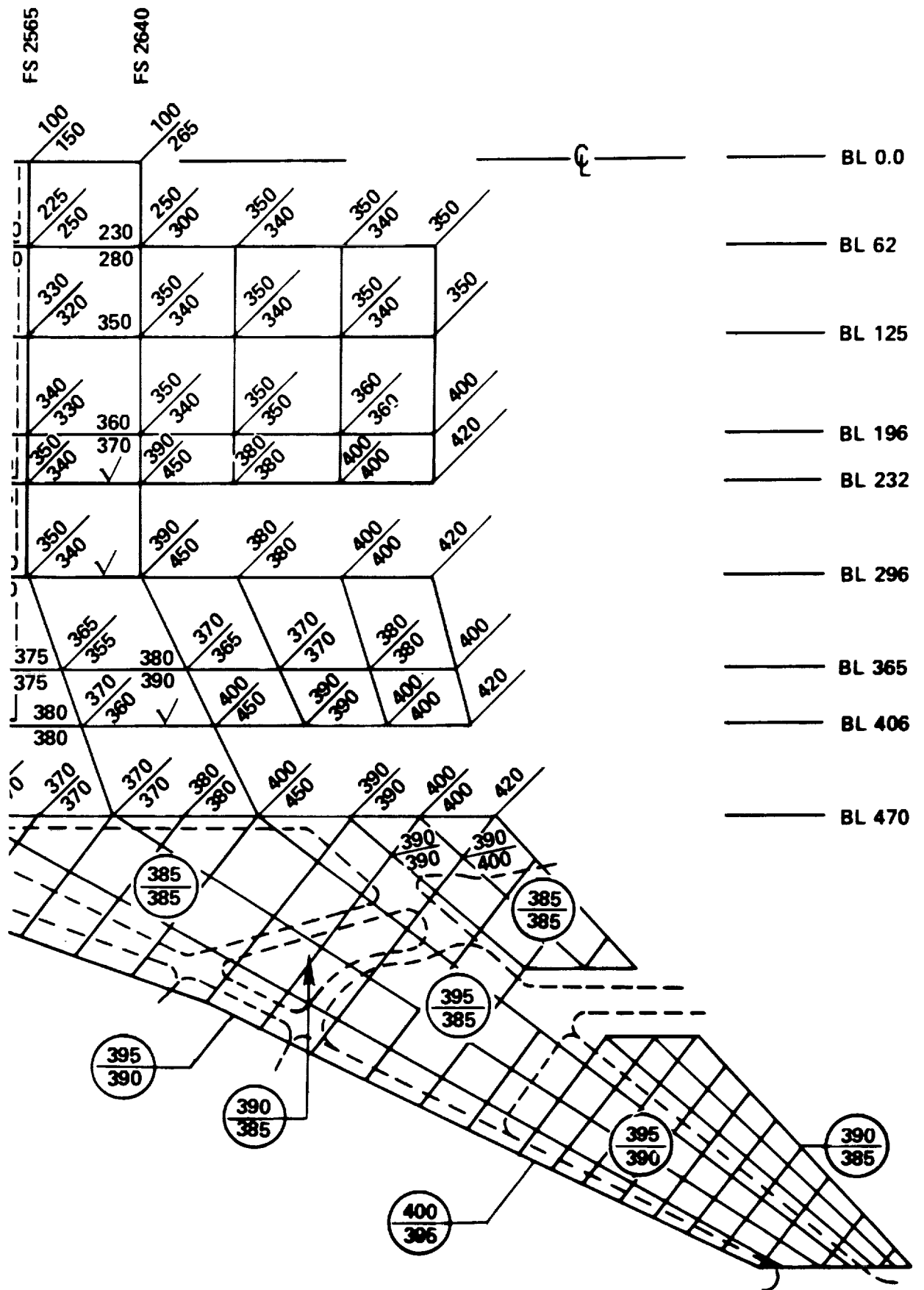
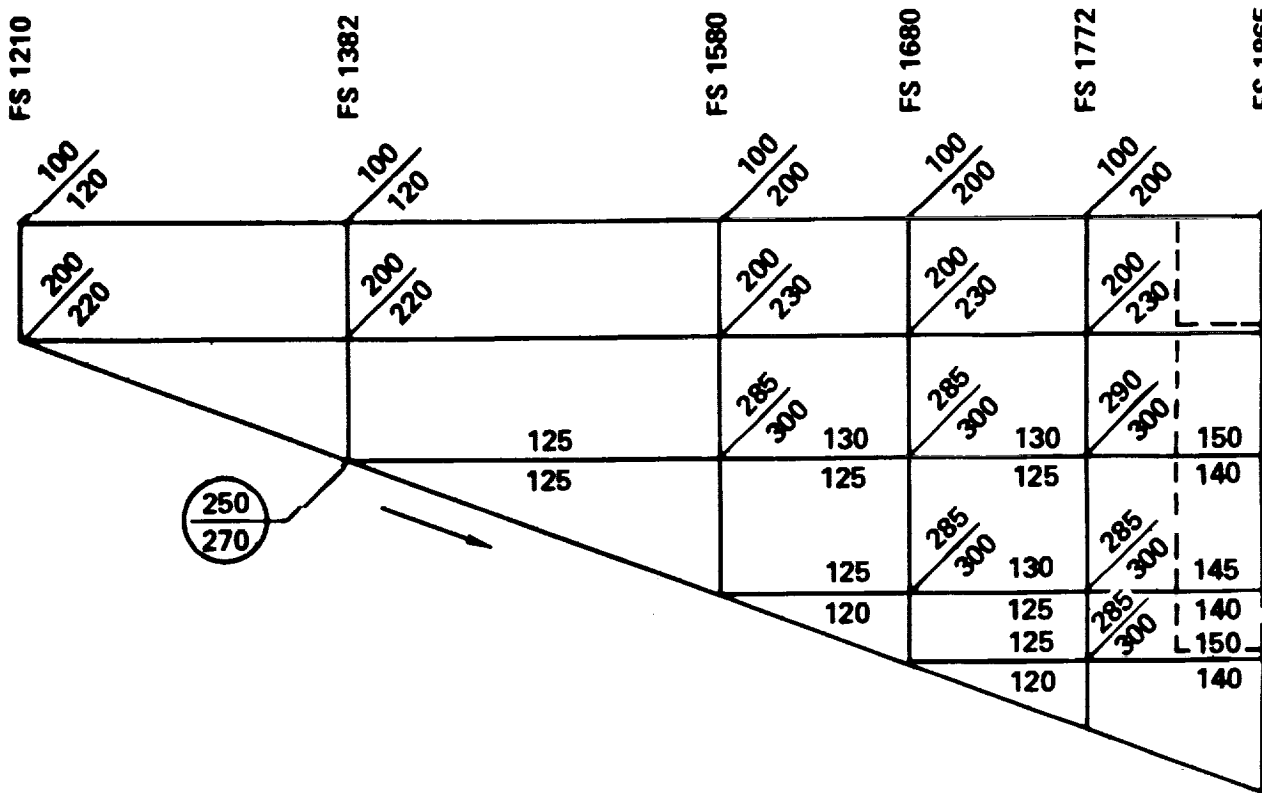


Figure 6-67. Finite Element Model Wing Temperatures - Mach 2.62 Mid-Cruise







**NOTES**

1. HOT DAY 4200 N. MILE FLIGHT PROFILE
2. WING STRUCTURE ELEMENT ARRANGEMENT SHOWN
3. GRIDPOINT TEMPERATURES GIVEN AT ELEMENT INTERSECTIONS
4. CIRCLED GRIDPOINT TEMPERATURES TYPICAL FOR REGIONS SHOWN
5. ELEMENT TEMPERATURES GIVEN WHERE INTERPOLATION BETWEEN GRIDPOINT TEMPERATURES IS NOT VALID.
6. TEMPERATURE CODING:

$$\frac{XXX}{YYY} = \frac{\text{UPPER SURFACE (F)}}{\text{LOWER SURFACE (F)}}$$

PRECEDING PAGE BLANK NOT FILMED

FOLDOUT FRAME /







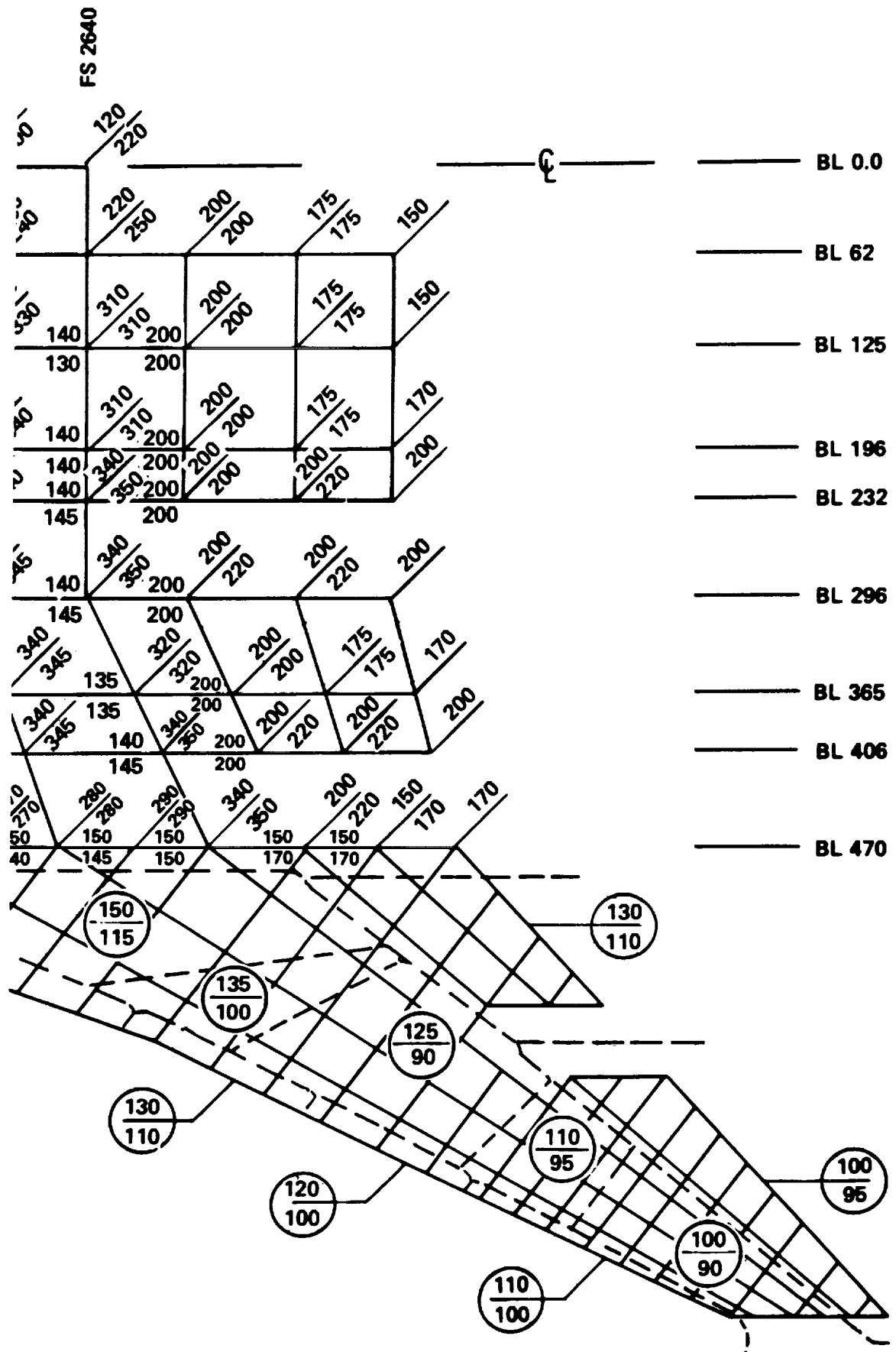


Figure 6-68. Finite Element Model Wing Temperatures - Mach 1.25 Descent





The temperatures shown are derived from the above described analyses at 10 fuselage and 14 wing locations and from some L-2000-7 data. The temperatures represent averages for surface panel structure. Except in fuel tank regions, surface temperatures are nearly identical to average panel temperatures during this part of cruise because the panel thermal gradients induced during the climb portion of flight have become negligible. Large panel gradients in the fuel tank areas are maintained by direct exposure to fuel on the interior and direct exposure to aerodynamic heating on the exterior.

The figure indicates the cooling effect of fuel tanks and landing gear compartment on panel average temperatures. Temperature depressions are noted at the forward wing tanks (number 5 and 6), which are about half full, and at the aft wing tanks (number 11 and 12), which have recently emptied. A cooling effect of about 10K (18F) is noted at the main landing gear area. Surface heating effects from nacelle radiation from nacelle and wing vertical shock impingement are also indicated. These are generally estimated from previous analyses performed for the L-2000-7.



## STRUCTURAL TEMPERATURES - TASK III

The structural temperatures developed to determine the effect of a reduced thermal environment on the structural arrangement, concepts, material and aircraft mass are presented in this section. Temperatures were developed by using the thermal analysis networks and structural data of the Task II configuration and performing the airplane over a Mach 2.16 cruise flight profile. The following subsections summarize temperature and gradient data developed for the wing and for the fuselage, and present an isotherm map of external surface temperatures for a mid-cruise condition.

### Wing Structure Temperatures

Temperature histories were developed for the wing structure at 14 design point regions. Structure was defined by the Task II configuration, but the flight profile for the Task III analysis was assumed.

Table 6-7 presents temperatures for six selected panels at the following five flight conditions:

- Mach 0.90 Climb
- Mach 1.25 Climb
- Mach 1.25 Descent
- Mach 2.2 Start-of-Cruise
- Mach 2.2 Mid-Cruise

Temperatures for the nominal Mach 2.2 conditions are obtained from analysis at the Mach 2.16, hot day (standard +8K) cruise profile. Table column headings are as defined for Table 6-6 (the corresponding table for the nominal Mach 2.7 flight profile).

TABLE 6-7. TEMPERATURES AND GRADIENTS FOR WING STRUCTURE - TASK III

POINT DESIGN REGION	UPPER SURFACE PANEL			LOWER SURFACE PANEL			WEB T <sub>WEB</sub> (F)	UPPER CAP		LOWER CAP		FUEL	
	T <sub>1</sub> (F)	T <sub>4</sub> (F)	T <sub>AVG</sub> Δ T (F) (T <sub>4</sub> -T <sub>1</sub> )	T <sub>7</sub> (F)	T <sub>10</sub> (F)	T <sub>AVG</sub> Δ T (F) (T <sub>7</sub> -T <sub>10</sub> )		T <sub>B</sub> (F)	T <sub>R</sub> (F)	T <sub>B</sub> (F)	T <sub>R</sub> (F)	Z-F (INCH)	T <sub>F</sub> (F)
<b>MACH 0.9 (CLIMB)</b>													
40322	32	69	48 + 37	70	30	52 + 40	70	69	37	70	55	35.30	70
40236	33	69	47 + 36	70	30	53 + 40	70	65	38	70	56	38.60	70
40536	34	64	45 + 30	64	29	45 + 35	68	66	39	70	39	0	-
41036	36	62	48 + 26	49	34	41 + 14	67	66	55	70	55	-	-
41316	36	62	48 + 26	49	34	41 + 14	67	60	60	60	60	-	-
41348	34	54	44 + 20	40	32	33 + 8	66	60	60	60	60	-	-
<b>MACH 1.25 (CLIMB)</b>													
40322	58	70	62 + 11	70	55	63 + 15	70	66	52	70	64	35.30	70
40236	57	69	61 + 12	70	52	62 + 18	70	65	50	70	63	38.60	70
40536	56	57	55 + 1	56	52	53 + 4	63	65	49	69	46	0	-
41036	53	51	52 - 1	39	47	43 - 8	62	65	55	69	55	-	-
41316	53	51	52 - 1	39	47	43 - 8	60	60	60	60	60	-	-
41348	54	45	49 - 9	40	48	46 - 8	58	60	60	60	60	-	-
<b>MACH 1.25 (DESCENT)</b>													
40322	71	199	129 + 128	200	70	121 + 130	229	231	91	234	88	0	-
40236	72	187	122 + 115	192	69	122 + 124	221	245	96	246	91	0	-
40536	75	192	121 + 117	189	69	121 + 120	221	246	100	245	91	0	-
41036	83	181	130 + 98	129	84	106 + 45	218	215	140	218	120	-	-
41316	83	181	130 + 98	129	84	106 + 45	217	180	180	155	155	-	-
41348	78	146	113 + 68	102	76	82 + 26	211	160	160	130	130	-	-
<b>MACH 2.2 (START OF CRUISE)</b>													
40322	255	75	181 - 179	73	253	152 - 180	71	90	231	71	130	35.30	71
40236	250	76	180 - 174	72	243	141 - 171	71	71	222	70	121	38.60	71
40536	250	135	203 - 115	138	253	202 - 114	100	72	220	75	228	0	-
41036	247	155	203 - 92	201	239	221 - 38	103	110	185	110	200	-	-
41316	247	155	203 - 92	201	239	221 - 38	106	150	150	170	170	-	-
41348	257	196	226 - 61	230	252	247 - 22	115	175	175	200	200	-	-
<b>MACH 2.2 (MID CRUISE)</b>													
40322	253	148	203 - 105	93	247	159 - 154	118	144	246	87	136	24.15	92
40236	253	197	227 - 56	194	248	224 - 54	173	141	242	105	235	0	-
40536	258	242	251 - 15	242	255	249 - 13	237	240	251	225	248	0	-
41036	264	261	263 - 3	259	260	260 - 1	255	245	255	240	250	-	-
41316	265	265	265 - 0	261	260	260 + 1	266	255	255	250	250	-	-
41348	269	269	269 - 0	263	261	261 + 1	268	260	260	250	250	-	-

TABLE 6-7. TEMPERATURES AND GRADIENTS FOR WING STRUCTURE - TASK III(cont'd.)

POINT DESIGN REGION	UPPER SURFACE PANEL				LOWER SURFACE PANEL				WEB T <sub>WEB</sub> (K)	UPPER CAP		LOWER CAP		FUEL	
	T <sub>1</sub> (K)	T <sub>4</sub> (K)	T <sub>AVG</sub> (K)	Δ T (T <sub>4</sub> - T <sub>1</sub> )	T <sub>7</sub> (K)	T <sub>10</sub> (K)	T <sub>AVG</sub> (K)	Δ T (T <sub>7</sub> - T <sub>10</sub> )		T <sub>B</sub> (K)	T <sub>R</sub> (K)	T <sub>B</sub> (K)	T <sub>R</sub> (K)	ZF (M)	TF (K)
MACH 0.9 (CLIMB)															
40322	273	294	282	+ 21	294	272	284	+ 22	294	293	276	294	286	0.90	294
40236	274	294	281	+ 20	294	272	285	+ 22	294	291	276	294	286	0.98	294
40536	274	291	280	+ 17	291	271	280	+ 19	293	292	277	294	277	0	-
41036	275	290	282	+ 14	283	274	278	+ 8	293	292	286	294	286	-	-
41316	275	290	282	+ 14	283	274	278	+ 8	293	289	289	289	289	-	-
41348	274	285	280	+ 11	278	273	274	+ 4	292	289	289	289	289	-	-
MACH 1.25 (CLIMB)															
40322	288	294	290	+ 6	294	286	290	+ 8	294	292	284	294	291	0.90	294
40236	287	294	289	+ 7	294	284	290	+ 10	294	291	283	294	290	0.98	294
40536	286	287	286	+ 1	286	284	285	+ 2	290	291	283	294	281	0	-
41036	285	284	284	- 1	277	281	279	- 4	290	291	286	294	286	-	-
41316	285	284	284	- 1	277	281	279	- 4	289	289	289	289	289	-	-
41348	285	280	283	- 5	278	282	281	- 4	288	289	289	289	289	-	-
MACH 1.25 (DESCENT)															
40322	295	366	327	+ 71	366	294	323	+ 72	383	384	306	385	304	0	-
40236	295	359	323	+ 64	362	294	323	+ 69	378	391	309	392	306	0	-
40536	297	362	323	+ 65	360	294	323	+ 67	378	392	311	391	306	0	-
41036	301	356	328	+ 54	327	302	314	+ 25	376	375	333	376	322	-	-
41316	301	356	328	+ 54	327	302	314	+ 25	376	355	355	341	341	-	-
41348	299	336	318	+ 38	312	298	301	+ 14	373	344	344	328	328	-	-
MACH 2.2 (START OF CRUISE)															
40322	397	297	356	- 99	296	396	340	- 100	295	305	384	295	328	0.90	295
40236	394	298	355	- 97	295	390	334	- 95	295	295	379	294	323	0.98	295
40536	394	330	368	- 64	332	396	368	- 63	311	295	378	297	382	0	-
41036	393	341	368	- 51	367	388	378	- 21	313	316	358	316	366	-	-
41316	393	341	368	- 51	367	388	378	- 21	314	339	339	350	350	-	-
41348	398	364	381	- 34	383	395	393	- 12	319	353	353	366	366	-	-
MACH 2.2 (MID CRUISE)															
40322	396	338	368	- 58	307	393	344	- 86	321	335	392	304	331	0.61	306
40236	396	365	381	- 31	363	393	380	- 30	351	334	390	314	386	0	-
40536	399	390	395	- 8	390	397	394	- 7	387	389	395	380	393	0	-
41036	402	400	401	- 2	399	400	400	- 1	397	391	397	389	394	-	-
41316	403	403	403	0	400	400	400	+ 1	403	397	397	394	394	-	-
41348	405	405	405	0	401	400	400	+ 1	404	400	400	394	394	-	-

ORIGINAL PAGE IS  
OF POOR QUALITY

## Fuselage Temperatures

Temperature histories were developed for fuselage skin panels and circumferential frames using the Task II airplane configuration with the Task III flight profile. Results are presented in Tables 6-8 and 6-9 for 10 fuselage locations at four flight conditions: Mach 1.2 climb, start-of-cruise, mid-cruise, and Mach 1.2 descent. Table 6-8 shows mass-averaged temperatures for skin panels and temperature differentials between outer skin and stiffener crown. Table 6-9 shows mass-averaged frame temperatures and differentials between outer and inner flanges of the frame.

### Cruise Isotherms - Mach 2.16 (Hot Day)

A map of external surface isotherms (lines of constant temperature) for the entire airplane at a Mach 2.16, hot day (standard +8K) cruise condition is presented in Figure 6-70. Consistent with the Mach 2.7 data the temperature lines are given in 5K (9F) increments except where temperatures change radically due to extraneous heat transfer, near engines and fuel.

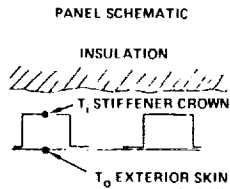
The temperatures shown are derived from the above described analyses at 10 fuselage and 14 wing locations and from some L-2000-7 data. The temperatures represent averages for surface panel structure. Except in fuel tank regions, surface temperatures are nearly identical to average panel temperatures during this part of cruise because the panel thermal gradients induced during the climb portion of flight have become negligible. Large panel gradients in the fuel tank areas are maintained by direct exposure to fuel on the interior and direct exposure to aerodynamic heating on the exterior.

The figure indicates the cooling effect of fuel tanks and landing gear compartment on panel average temperatures. Temperature depressions are noted at the forward wing tanks (number 5 and 6), which are about half full, and at the aft wing tanks (number 11 and 12), which have recently emptied. A cooling effect of about 5K (9F) is noted at the main landing gear area. Surface heating effects from nacelle radiation from nacelle and wing vertical shock impingement

TABLE 6-8. TEMPERATURES AND GRADIENTS FOR FUSELAGE SKIN PANELS - TASK III

FUSELAGE SKIN PANELS  
MAXIMUM THERMAL GRADIENTS & TEMPERATURES

- NOTES
1. BASED ON HOT DAY (STD + 8K) MACH 2.16 CRUISE FLIGHT.
  2. HAT STIFFENED PANELS, EXCEPT ZEE STIFFENED AT FS 750.
  3. 'TOP', 'BOTTOM' AT  $\phi$ ; 'SIDE' AT  $90^\circ$  OR ABOVE WING.



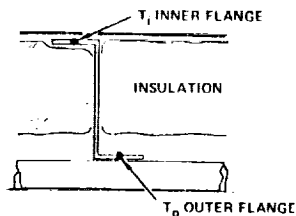
TEMPERATURES IN F

LOCATION	FLIGHT CONDITION							
	MACH 1.2 CLIMB		START OF CRUISE		MID TO END OF CRUISE		MACH 1.2 DESCENT	
	T <sub>i</sub> , T <sub>o</sub>	T <sub>Ave</sub>	T <sub>i</sub> , T <sub>o</sub>	T <sub>Ave</sub>	T <sub>i</sub> , T <sub>o</sub>	T <sub>Ave</sub>	T <sub>i</sub> , T <sub>o</sub>	T <sub>Ave</sub>
<b>TOP</b>								
FS 750	+ 4	56	-115	232	-8	259	+108	102
2000	+18	54	-144	201	-7	256	+133	127
2500	+19	55	-148	192	-7	255	+137	136
3000	+18	54	-143	200	-7	255	+132	128
<b>SIDE</b>								
FS 750	+ 7	50	-114	223	-8	246	+105	95
2000	+16	51	-140	216	-9	262	+129	114
2500	+18	52	-145	207	-8	261	+135	121
3000	+19	48	-132	204	-8	239	+118	107
<b>BOTTOM</b>								
FS 750	+ 7	51	-114	224	-8	247	+106	96
3000	+24	48	-140	189	-7	241	+127	123

TABLE 6-9. TEMPERATURES AND GRADIENTS FOR FUSELAGE FRAMES - TASK III

FUSELAGE FRAMES  
MAXIMUM THERMAL GRADIENTS & TEMPERATURES

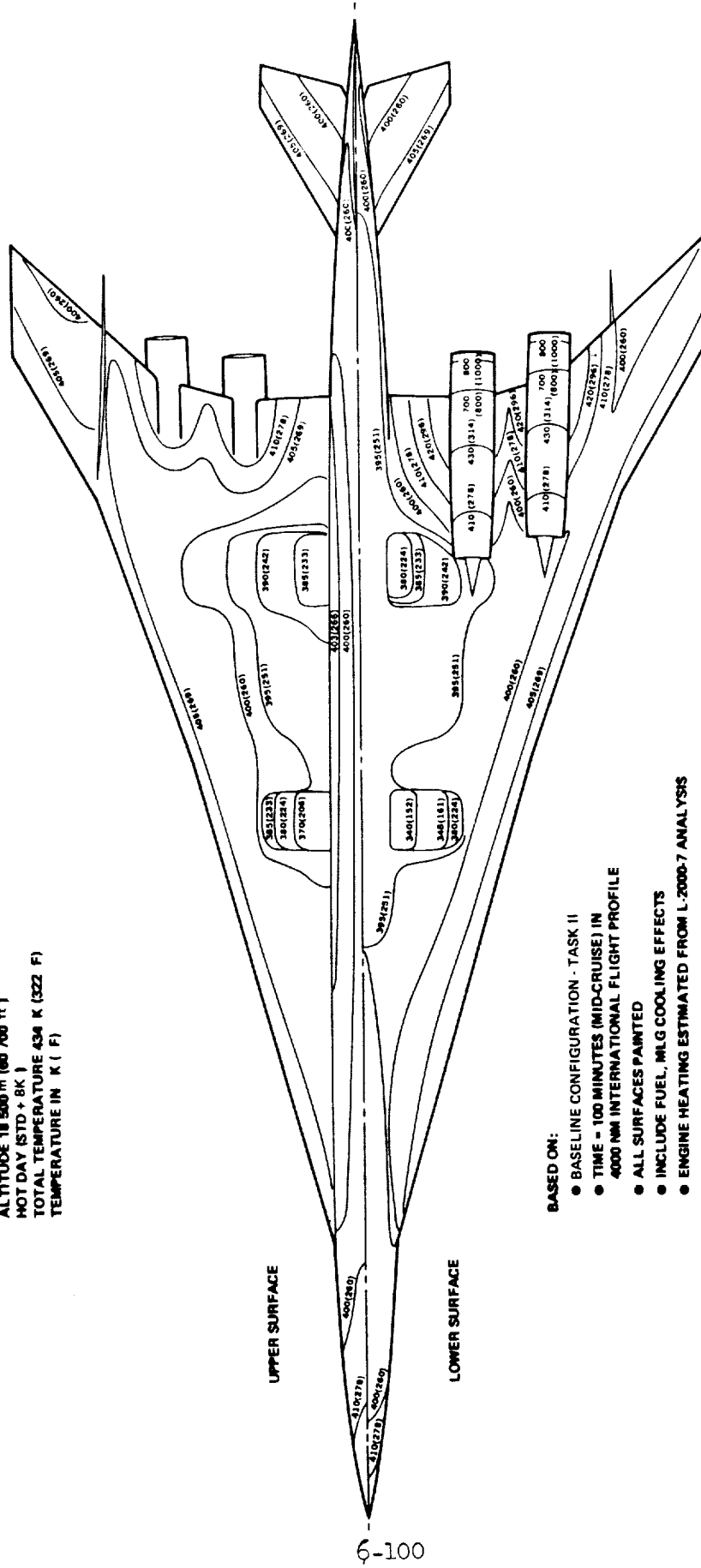
1. BASED ON HOT DAY (STD + 8K) MACH 2.16 CRUISE FLIGHT
2. 'TOP', 'BOTTOM' AT  $\phi$ ; 'SIDE' AT  $90^\circ$  OR ABOVE WING
3. DATA AT FS 3000 (AFT OF PRESSURE BULKHEAD) ASSUMED INSULATION MAY NOT BE VALID



TEMPERATURES IN F

LOCATION	FLIGHT CONDITION							
	MACH 1.2 CLIMB		START OF CRUISE		MID TO END OF CRUISE		MACH 1.2 DESCENT	
	T <sub>i</sub> , T <sub>o</sub>	T <sub>Ave</sub>	T <sub>i</sub> , T <sub>o</sub>	T <sub>Ave</sub>	T <sub>i</sub> , T <sub>o</sub>	T <sub>Ave</sub>	T <sub>i</sub> , T <sub>o</sub>	T <sub>Ave</sub>
<b>TOP</b>								
FS 750	+13	72	-46	97	-109	192	-57	168
2000	+ 8	74	-21	85	-93	196	-66	183
2500	+ 7	73	-17	83	-84	198	-62	187
3000	+ 8	74	-20	85	-92	195	-66	183
<b>SIDE</b>								
FS 750	+16	70	-41	93	-100	183	-52	161
2000	+10	72	-24	86	-95	199	-62	184
2500	+ 8	72	-20	83	-87	201	-59	189
3000	+11	71	-20	83	-83	183	-55	170
<b>BOTTOM</b>								
FS 750	+15	71	-42	93	-101	184	-53	162
3000	+ 9	72	-15	82	-85	185	-62	175

**MACH 2.16 CRUISE**  
**ALTITUDE 18 500 m (60 700 ft.)**  
**HOT DAY (STD + 8K)**  
**TOTAL TEMPERATURE 434 K (322 F)**  
**TEMPERATURE IN K ( F)**



- BASED ON:**
- BASELINE CONFIGURATION - TASK II
  - TIME - 100 MINUTES (MID-CRUISE) IN 4000 NM INTERNATIONAL FLIGHT PROFILE
  - ALL SURFACES PAINTED
  - INCLUDE FUEL, MILG COOKING EFFECTS
  - ENGINE HEATING ESTIMATED FROM L-2000-7 ANALYSIS

Figure 6-70. External Surface Isotherms - Mach 2.16 Cruise

are also indicated. These are generally estimated from previous analyses performed for the L-2000-7.

1

2

3

4

5

6



## REFERENCES

1. "Equations, Tables, and Charts for Compressible Flow", NACA Report 1135, 1953
2. "U.S. Standard Atmosphere, 1962", U.S. Government Printing Office, Washington, D. C., December 1962
3. Hansen, C. F., "Approximations for the Thermodynamic and Transport Properties of High Temperature Air", NASA TR R-50, 1959
4. Keenan, J. H., and Kaye, J., "Gas Tables", Wiley & Sons, 1945
5. Eckert, E. R. G., "Survey of Boundary Layer Heat Transfer at High Velocities and High Temperature", WADC TR 59-624, 1960
6. Johnson, C. B., and Boney, L. R., "A Simple Integral Method for the Calculation of Real-Gas Turbulent Boundary Layers with Variable Edge Entropy", NASA TN D-6217, 1971
7. Spalding, D. B. and Chi, S. W., "The Drag of a Compressible Turbulent Boundary Layer on a Smooth Flat Plate With and Without Heat Transfer", J. Fluid. Mech., Vol. 18, pt 1, January 1964, pp 117-143
8. White, F. M., and Cristoph, G. H., "A Simple New Analysis of Compressible Turbulent Two-Dimensional Skin Friction Under Arbitrary Conditions", AFFDL-TR-70-133, 1971
9. Pearce, B. E. "Method of Spalding and Chi Modified for Real Gas Effects and Determination of a Virtual Origin", Aerospace Corp., 1969
10. "Supersonic Transport Development Program", Phase III Proposal, FA-SS-66-7 Volume II-C Airframe Design Report, Section 5, Lockheed-California Company, September 1966
11. "Military Standardization Handbook - Metallic Materials and Elements for Aerospace Vehicle Structures", MIL-HDBK-5B, September 1971
12. Hertz, J., et al, "Advanced Composite Applications for Spacecraft and Missiles, Phase I Final Report", Convair Aerospace Division, AFML-TR-71-186, Vol. II, March 1972
13. "Data Book for Designers - Fuels, Lubricants, and Hydraulic Fluids", Humble Oil and Refining Co., April 1969
14. Kim, D. H., "The Thermophysical Properties of Fiber Reinforced Plastics", AIAA Paper No. 72-366, April 1972
15. Schultz, H. D., "Thermal Analyzer Computer Program for the Solution of General Heat Transfer Problems", Lockheed-California Company Report LR 189C2, 1965
16. McAdams, W. H., "Heat Transmission", McGraw-Hill Book Co., Inc., 1954



REFERENCES (Continued)

17. Fahlbush, H., "CL 938-15.F Flight and Aeromechanics Data for Structural Design, Part II (u)", Lockheed Report LR 18774-II, 1965, (C)
18. "Supersonic Transport Development Program", Phase III Proposal, FA-SS-66-7 Volume II-E Airframe Design Report, Section 5, Lockheed-California Company, September 1966



E

F

W

K

V